Proceedings of the 2003 WJTA American Waterjet Conference

August 17-19, 2003

Adam's Mark Hotel
Houston, Texas

The 2003 WJTA American Waterjet Conference is sponsored by the

WJTA
WaterJet Technology Association

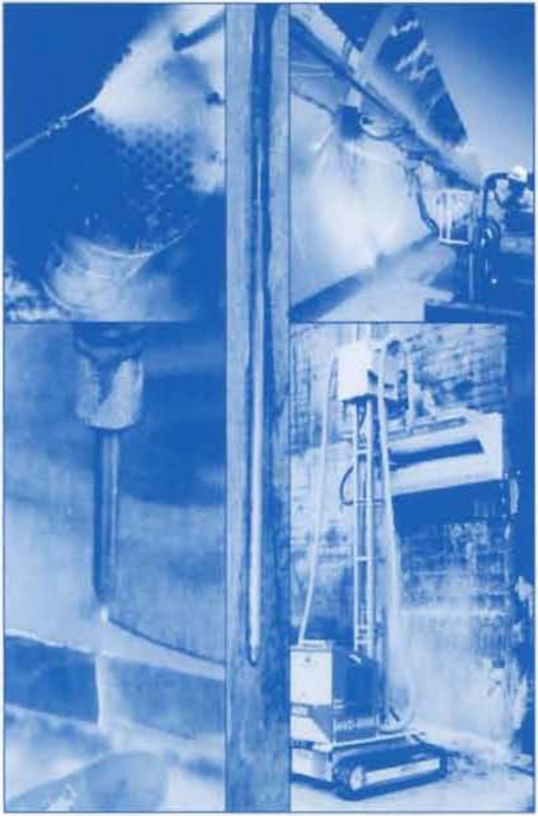

WaterJet Technology Association

The WaterJet Technology Association (WJTA) was created in 1983 at the 2nd U.S. Water Jet Conference, held on the campus of the University of Missouri-Rolla, by members of the waterjet industry acting in concert with university and government officials. The major impetus to the creation of the Association was to provide a means of service and communication within the industry, as epitomized by the biennial waterjet conferences.

Formal objectives of the Association have been adopted as follows:

- To provide a means of cooperation between government, industry, university, and research institutions on all matters of fluid jets, including waterjets and abrasive jets for jet cutting, industrial cleaning, and other uses in the manufacturing, mining, construction, and process industries.
- To foster domestic and international trade in jet cutting and jet cleaning, products and services.
- To promote in general the interests of the jet application industry in all branches, including establishment of recommended practices.
- To promote the mutual improvement of its members, and the study and advancement of the arts and sciences connected with jet cutting and industrial cleaning.

In regard to the third objective, it should be noted that at the 3rd U.S. Water Jet Conference held on the campus of the University of Pittsburgh in May of 1985, the Association adopted the first ***Recommended Practices for the Use of Manually Operated High Pressure Water Jetting Equipment.***

The *Recommended Practices* are revised and updated periodically, the most recent revision being published in April 1999.

WJTA Administration

John Wolgamott
Chairman of the Board
StoneAge, Inc., Durango, Colorado

George A. Savanick, Ph.D.
President
Apple Valley, Minnesota

Lydia M. Frenzel, Ph.D.
Vice President
Advisory Council, San Marcos, Texas

Andrew F. Conn, Ph.D.
Secretary
Conn Consulting, Inc., Baltimore, Maryland

Larry Loper
Treasurer
High Pressure Equipment Co., Erie, Pennsylvania

2003 WJTA Conference Committee

Pat DeBusk
Chairman
Houston, Texas

Craig Anderson
Parker Polyflex
Stafford, Texas

Randy Kruger
Onyx Industrial Services
Baytown, Texas

Jack Russell
Dow Chemical Company
Freeport, Texas

David Summers, Ph.D.
Proceedings Editor
University of Missouri-Rolla
Rolla, Missouri

Andrew F. Conn, Ph.D.
Conn Consulting, Inc.
Baltimore, Maryland

Lydia M. Frenzel, Ph.D.
Advisory Council
San Marcos, Texas

Mohamed Hashish, Ph.D.
Flow International Corporation
Kent, Washington

George A. Savanick, Ph.D.
Apple Valley, Minnesota

International Advisors

Franz H. Trieb, Austria
Leo Kosowan, Canada
Jaroslav Vasek, Ph.D., Czech Republic
Pekka Patjas, Finland
Daniel Weber, France
Frank Pude, Germany
O.V. Krishnaiah Chetty Ph.D., India
Giancarlo Franchini, Italy
Ryoji Kobayashi, Ph.D., Japan
Ronald Saliba, Malta
Joost Ballieux, Netherlands
Gensheng Li, Ph.D., PR China
Won Ho Kang, Republic of Korea
Christian Öjmertz, Ph.D., Sweden
Philippe Meyer, Switzerland
Brian Storie, United Kingdom

WaterJet Technology Association
917 Locust Street ● Suite 1100 ● St. Louis, MO 63101-1419
Telephone: (314)241-1445 ● Fax: (314)241-1449
Email: wjta@wjta.org ● Web Site: www.wjta.org

Foreword

These are difficult economic times. Waterjetting enterprises need to work efficiently in order to prosper in a slow economy. Waterjetters should be aware of the latest advances in waterjet technology because this knowledge can lead to new products or result in lowering the cost of production of waterjet products or services.

The WaterJet Technology Association (WJTA) exists to disseminate the latest information relating to the state-of-the-art of waterjet technology. WJTA spreads the word through publications, including the periodical, *Jet News*; codes of practices, such as *Recommended Practices For The Use Of Manually Operated High Pressure Waterjetting Equipment*, instructional videotapes and compact disks; and a series of biennial waterjet conferences.

This publication is a record of the *Proceedings* of the 2003 Waterjet Conference – the 11th in a series of waterjetting conferences initiated in 1983. During this Conference, 44 papers were presented on a variety of subjects ranging from firefighting to the cutting of sandwiches. Copies of these papers are included in this publication.

In addition to the research and development papers presented at the Conference, contractor's roundtable discussions were held in which technology and safety issues facing waterjet contractors were discussed. An exhibition was held wherein the largest number of companies in the history of the WJTA Conferences exhibited the latest equipment and supplies. Live demonstrations of waterjetting equipment were presented in the parking lot of the Adam's Mark Hotel. Nine companies demonstrated practical waterjet cutting and cleaning with commercial equipment.

WJTA hereby thanks the organizing committee and its chairman, Pat DeBusk, for lending their expertise in planning this Conference and to Dr. David Summers for editing these *Proceedings*.

— George A. Savanick, Ph.D.
President

Once again I have the pleasure of being a part of WJTA's efforts to advance the knowledge and cooperation in our industry. We all spend the majority of our time intensely involved in solving the particular problems our jobs present to us. It is beneficial, therefore, to occasionally come together with others who have similar challenges, to share what we have learned, and what we still strive to improve. I know that my own company has benefited enormously from the conference proceedings and attendance at these gatherings. I give humble thanks to the authors for making the effort and taking the time to share with us their knowledge and experience. Their labors help to improve our industry and our profession.

— John Wolgamott
Chairman of the Board,
WaterJet Technology Association

Preface

About five years ago I was asked if there was anything that waterjets would NOT be used for at some time in the future. After a brief thought I suggested that they were unlikely ever to be used for cutting sandwiches, and that the knife still had a future. I refer you to Franz Trieb's paper on that subject in these *Proceedings* to show that waterjets have proved to be more effective than I had anticipated.

Twenty years ago, when the second Conference was held on the University of Missouri-Rolla campus, the WaterJet Technology Association (WJTA) was formed. At that time we had only hopes for the future, although the 118 delegates heard some 42 papers on topics, as now, that ranged from theoretical analysis to practical use. For those who have an interest, those papers are now freely available through the WaterJet Technology Association web page, together with papers from the other early Conferences.

In the intervening years the size and strength of the industry has grown considerably, so that we now routinely divide the papers in the conference into separate groups to address, for example, the differing needs of those more interested in cleaning as opposed to those who use ultra-high pressure systems for cutting and fabrication. The papers provide only a basis for the transfer of knowledge that is a main purpose for these biennial events. The fellowship and exchanges, the exhibition booths and demonstrations and the discussions and questions are other major parts, and I encourage you to take advantage of these opportunities.

I would like to thank the authors who have submitted papers, and who have again provided a very interesting and exciting snapshot of the current directions in which the industry is moving. Our thanks should also go to the local hosts for this meeting – Pat DeBusk, chairman; Craig Anderson; Randy Kruger and Jack Russell. The paper review committee included Dr. Andrew Conn, Dr. Lydia Frenzel, Dr. Mohamed Hashish and Dr. George Savanick, and their help is gratefully acknowledged.

These conferences are successful because of the support that the WJTA receives from Birenbaum and Associates, who make all the arrangements for its organization and operation. I am particularly grateful to Dr. Mark Birenbaum, Ken Carroll and LeAnn Hampton for their skills in ensuring the Conference success, and to Jan Tubbs, whose indefatigable efforts have ensured that the papers were received, reviewed, sorted, printed and organized into this volume.

This has been an exciting 20 years, may the next two decades bring even more success and excitement to you all, as this dynamic technology becomes an even greater contributor to the industries of the 21st Century.

— David Summers, Ph.D.
Editor

Proceedings of the 2003 WJTA American Waterjet Conference

August 17-19, 2003 • Houston, TX

TABLE OF CONTENTS

Proceedings of the 2003 WJTA American Waterjet Conference

Session A: Ultra-High Pressure Cutting And Surface Preparation

1-A **"Cutting Mechanism and Cutting Efficiency for Water Pressures Above 600 MPa,"** *H. Louis, M. Mohamed and F. Pude*

2-A **"Feasibilities of Abrasive Water Jet Multipass Cutting Technique,"** *B. Jurisevic. K.C. Heiniger, A. Schuetz and M. Junkar*

3-A **"Modelling of Wear Mechanisms at the Abrasive Waterjet Cutting Front,"** *Axel Henning and Engelbert Westkämper*

4-A **"Physical Basis of High-Pressure Hybrid Water-Abrasive-Ice Jet Application for Surface Treatment,"** *P. Borkowski*

5-A **"An Analytical Model for Prediction of Residual Stresses in Water Jet Peening,"** *N. Ramesh Babu and G. Vikram*

6-A **"Mathematical Modeling of Ultra High Pressure Waterjet Peening,"** *S. Kunaporn, M. Ramulu and M. Hashish*

Session B: Putting A System Together

1-B **"Pipe Threads – What is the Limit?,"** *D. Wright, J. Wolgamott and G. Zink*

2-B **"Recommended Practices for the Use of High Pressure Hose,"** *Paul Webster and Stephen Johns*

3-B **"Acoustic Emission of Plain Water Jets,"** *A. Bortolussi, R. Ciccu, W. Cuccu, A. Marcus, G. Massacci, and S. Usala*

4-B **"Waterjet Nozzle Material Types,"** *D. Wright, J. Wolgamott and G. Zink*

Session C: Cutting Stone And Other Uses

1-C **"Some Aspects of Hydroabrasive Suspensive Jet Cutting of Marble,"** *A. Perec*

2-C **"Erosion of Natural Stone by Abrasive Grains,"** *M. Monno, W. Polini, C. Ravasio and S. Turchetta*

3-C **"Modeling Jet Cutting of Oil Sands,"** *J.T. Bartley and B. Singh*

4-C **"Waterjet Researches at São Paulo University: Part 3 Waterjet Methods of Cutting Dimensional Stone,"** *Guillermo Ruperto Martín Cortés, Carlos Tadeu Lauand, and Wildor Theodoro Hennies*

"Waterjet Researches at São Paulo University: Part 4 Dimension Stone Exploitation with High-Pressure Waterjets," *Guillermo Ruperto Martín Cortés, Carlos Tadeu Lauand, Alexandre Sant' Anna and Wildor Theodoro Hennies*

5-C **"Comparative Performance Study of Polyacrylamide and Xanthum Polymer in Abrasive Slurry Jet,"** *S.V. Chacko, A. Gupta and D.A. Summers*

6-C **"Investigation of the High-Speed Water Slugs,"** *O. Petrenko, V. Samardzic, E.S. Geskin, G.A. Atanov, B. Goldenberg and A. Semko*

Session D: Advances In Industrial Cutting

1-D **"Inside AWJ Nozzles,"** *Mohamed Hashish*

2-D **"Quantitative Study of Abrasive Contamination in a Ductile Material During Abrasive Aqua Jet Machining (AAJM),"** *K. Patel and F. Chen*

3-D **"Potential of Polymeric Additives for the Cutting Efficiency of Abrasive Waterjets,"** *H. Louis, F. Pude and Ch. von Rad*

4-D **"Bending Radius Dependence in AWJ Machining of Stone Free-Form Profiles,"** *L. Carrino, M. Monno, W. Polini and S. Turchetta*

5-D **"Advanced Error Correction Methodology Applied to Abrasive Waterjet Cutting,"** *J. Olsen, J. Zeng, C. Olsen and B. Guglielmetti*

Session E: Cleaning Surfaces

1-E **"WJ Decoating,"** *M. Annoni and M. Monno*

2-E **"Radiological Decontamination of Armored Personnel Carriers with Continuous and Pulsed Waterjets at Umea, Sweden,"** *W. Yan, A. Tieu, B. Ren, M. Vijay, D.S. Haslip, T. Cousins, D. Estan, T. Jones, E.J. Waller, B.E. Sandström, K. Lidström, T. Ulvsand and G. Ågren*

3-E **"Formation and Application of a Rectangular Jet,"** *E.S. Geskin and B. Goldenberg*

4-E **"Manufacturing Case Study Involving Major Oil Company,"** *Michael T. Gracey and R.O. Berry Jr.*

5-E **"Development of Airport Runway Rubber Glue Removing Vehicle in China,"** *Shengxiong Xue, Zhengwen Chen, Haojun Peng, Yibin Fan, Yongqiang Wang, and Xu Zuo*

Session F: Industrial Cutting Considerations

1-F **"Development of a Production Line for Packaging with Waterjets,"** *Axel Henning, Bernd Biesinger, Peter Willems, Wolfgang Rauh and Horst Ranke*

2-F **"Pure Waterjet for Sandwiches – The Second Step,"** *Franz H. Trieb*

3-F **"Abrasive Waterjet Used as a Tool for Producing Materials Test Specimens,"** *U. Andersson, G. Holmqvist and K.M.C. Öjmertz*

4-F **"A Study of Abrasive Waterjet Machining of Kevlar Composite,"** *Rahmah Bte Abdullah, Ahsan Ali Khan and M. Ramulu*

5-F **"Developments in Abrasive Waterjets for Micromachining,"** *D.S. Miller*

6-F **"Application of Abrasive Waterjet Machining in Undergraduate Engineering Courses,"** *D.G. Taggart, D. Chelidze, W.J. Palm, B.E. Stucker and T.J. Kim*

7-F **"Pure Water-Jet Cutting of Fresh Meat Reduces the Risk of Contamination,"** *M. Alitavoli*

Session G: Research Into Cutting

1-G **"Abrasive Waterjet Machining of Aerospace Structural Sheet and Thin Plate Materials,"** *I. Conner, M. Ramulu and M. Hashish*

2-G **"Measurement of Particle Velocities in High Speed Waterjet Technology,"** *Anuja Dorle, L. John Tyler,and David A. Summers*

3-G **"Monitoring of the AWJ Cutting in the Submerged Conditions,"** *Andrej Lebar, Bostjan Jurisevic and Mihael Junkar*

4-G **"Study of Ice Particle Production Using Experimental and Computational Fluid Dynamic Methods,"** *D.K. Shanmugam and Y. Morsi*

5-G **"Modulation of Cutting Operation With Abrasive Waterjets,"** *Axel Henning and Engelbert Westkämper*

Session H: New Uses For Equipment

1-H **"An Abrasive Suspension Waterjet for Drilling Small-Diameter Holes,"** *P.W. Johnson, A.J. Graettinger and C.H. Sewell*

2-H **"A Method for Suppression of Building Fires, While Providing Access for Interrogative Equipment,"** *Samir Dorle, D.A. Summers, and A. Gupta*

3-H **"WJ Forming: A New Opportunity,"** *E. Grossi, M. Monno and A. Vergari*

4-H **"Improvements in a Multi-Use Waterjet Tool for Humanitarian Demining,"** *R.D. Fossey, D.A. Summers, J.G. Blaine, G. Galecki and S. Dorle*

5-H **"A Mobile Waterjet Training Module,"** *Gary W. Toothe*

6-H **"Formation and Application of Fine Ice Abrasive,"** *K. Kluz, E.S. Geskin, D.V. Shishkin, B. Goldenberg and O. Petrenko*

2003 WJTA American Waterjet Conference
August 17-19, 2003 ● Houston, Texas

Paper 1-A

CUTTING MECHANISM AND CUTTING EFFICIENCY FOR WATER PRESSURES ABOVE 600 MPA

H**.** Louis, M. Mohamed, F. Pude
Institute of Materials Science
University of Hannover
Germany

ABSTRACT

An increase in pressure above 400 MPa up to a level of 900 MPa gives the potential to:

increase cutting efficiency with pure waterjets
increase efficiency with water abrasive jets
increase the field of application of pure waterjet for cutting purposes even into the cutting of metallic materials.

The mechanism of abrasive waterjet use for cutting materials has been well examined and is understood. In contrast to pure waterjet cutting, the cutting mechanism with the AWJ is quite different. This paper describes the cutting equipment, the possibility of reduction of abrasive material and ability to cut smaller radius curves in the case of abrasive as well as in the case of pure waterjets and finally intensively discusses the mechanism of the material removal process when using plain waterjets for cutting metallic materials.

Organized and Sponsored by the WaterJet Technology Association

1. INTRODUCTION

In recent years, high-pressure waterjet technology has become extensively used in many areas of industry. The maximum working pressure is currently limited to 400 MPa, at the state-of-the art, but recent researchers have proposed an extension of the useful range of this technology by increasing the working pressures above 400 MPa [1-6]. This increase of pressure has the potential to:

- Increase efficiency of waterjets and abrasive waterjets
- Reduce abrasive consumption
- Cut thin metal plates using only high pressure water

Cutting ability is directly related to the velocity of the waterjets. By increasing the velocity of the jet (which is raised by increasing pump pressure), the typical effect is a linear increase in cutting efficiency for both waterjets and abrasive waterjets. In the case of abrasive waterjets, the water mainly acts to accelerate the abrasive particles and does not work directly in cutting the material except in the case of soft material; cutting comes from the kinetic energy of the water which is transferred to the abrasive particles. Increasing the velocity of the water will also lead to an increase in the particle velocity. This gives a higher efficiency in cutting with abrasive particles. The effect of pressure on the depth of cut at different traverse rates for aluminum materials is shown in **figure 1**. It can be seen that the depth of cut depends on the pressure in an almost linear manner for all the traverse rates that were tested.

Figure 2 shows a comparison of abrasive consumption at a kerfing depth of 30 mm, test parameters are an orifice diameter of 0.25 mm, focus tube diameter of 1.2 mm, traverse rate of 100 mm/min and a standoff distance of 2 mm. Under these working conditions the abrasive consumption decreases to 42% at a pressure of 300 MPa in comparison with that required when cutting at 240 MPa.

The influence of pressure on the depth of cut for aluminum materials at different standoff distance using a traverse rate of 1.69 mm/s and a nozzle diameter 0.178 mm is shown, as an application of pure waterjets in cutting thin metal plate, in **figure 3**. The figure shows that with increasing pressure a shorter standoff distance is more effective, [1].

2. PRESSURE GENERATION SYSTEM

In order to obtain these higher pressures with pumps suitable for waterjet machining, three different kinds of pump systems can be used.

2.1. Conventional Intensifier Pump

The output pressure of the intensifier pump is determined by the inlet hydraulic oil pressure and the pressure intensification ratio. This ratio is defined as the area of the oil – side piston divided by the area of the pressurized water side plunger, **figure 4a**. Normally this ratio is 20. It was [1, 2] reported that, an intensification ratio of 33:1 has been used in a 690 MPa intensifier pump.

2.2. Modified Autofrettage Pump

Pressure-controlled pumps are normally used for waterjet cutting. Autofrettage pumps are flow controlled. In [5-6], a modified autofrettage pump (1000 MPa) with a pressure intensification ratio of 50:1 was used.

2.3. Multi-Stage (Intensifier) Pump

An increase in water pressure can be obtained by increasing the inlet pressure of the intensifier pump. This can be achieved by an additional, pre-aligned, plunger pump as shown in **figure 4b** or by using multi-stage intensifier pumps. By using two intensifier pumps with a transmission ratio of 20:1, a 690 MPa intensifier pump [2] was developed.

All these systems were used for laboratory investigation and are in the early stages of introduction for practical industrial use. Pressures above 400 MPa can be considered as a challenge for the materials and component designs of these systems.

3. THERMODYNAMIC BEHAVIOUR OF WATER AT HIGHER PRESSURE

To handle water at high pressure in the range of 900 MPa, three physical aspects should be taken into consideration. These aspects are the phase diagram of ice, the compressibility, and the adiabatic heating of the fluid.

3.1 Phase Diagram of Ice

When working at high pressure (900 MPa) it is necessary to look at the fundamentals of the water-phases at different conditions. The understanding of phase diagrams for water is extremely important to define the limits of working pressure. For example at the high pressure of 1000 MPa liquid water is expected to freeze at room temperature. All of the natural ice on earth is hexagonal ice (Ice I). Ice I is the normal form of ice made by freezing water at atmospheric pressure. In contrast when water is frozen in other cicumstances the resulting substance displays a multi-faceted range of solid phases, and all of these are referred to as forms of ice. Most of these phases can be produced by the application of high pressures. The first high pressure phase was discovered a century ago [8] in a programmed study of the pressure-volume-temperature relationships of various materials and these phases were named as Ice II and Ice III. This discovery was extended in experiments [7-10] carried out at pressure up to 2 GPa and led to the discovery of Ices V and VI. The phase diagram of ice is shown in **figure 5**.

3.2 Compressibility of Water

In physics liquids are normally considered to be incompressible media. This simplification can be used for most technical applications. But this simplification is not practicable in the field of high pressure applications (> 100 MPa). The phase diagram of water shows that pressure has an essential greater influence on density than temperature [8]. Therefore, density is handled in the following considerations as a pure function of pressure. There are two different equations to calculate the density form. The first equation is:

$$\frac{dp}{E} = \frac{d\rho}{\rho} \quad \rightarrow \qquad (1)$$

where E is the modulus of compressibility [11]. This state equation reads, after integration,

$$\rho = \rho_o \left(\frac{p + E}{p_o + E} \right)^{\frac{1}{n}}$$

The second equation is [12]:

$$\rho = \rho_o e^{p/E} \rightarrow \qquad (2)$$

where the constant factors are E = 3.047 10^8 N/m^2 (ρ_o=1.02 103 kg/m^3 and n= 7.15). **Figure 6** shows the density of water versus pressure for two different equations [11, 12].

3.3 Adiabatic Heating

The heating of water under adiabatic compression will increase the temperature of water by approximately 3°C/100 MPa, where the initial temperature level impacts the slope of the temperature curves. The rise in temperature during adiabatic compression for water of different temperatures is shown in **figure 7**, [13]. This adiabatic heating decreases the risk of ice formation. In practical applications even when the water temperature at the inlet is at room temperature friction in the intensifier, couplings and hoses will cause the temperature to rise, this means that the risk of freezing at 900 MPa with inlet water at ambient temperature is not great.

4. EXPERIMENTAL SETUP

4.1 900 MPa Cutting Systems

The system used in these experiments consists of an inlet pressure pump feeding water from tap water at maximum permissible pressure of 1.0 MPa at +20^0 C to the filtration system. The filters are followed by a pressure intensifier that supplies a water flow rate up to 0.5 l/min with a maximum pressure of 1,000 MPa with an intensification ratio of 1:63 (BÖLHER HOCHDRUCKTECHNIK Model CP 1000-0.5). To provide greater safety, the high pressure pump was kept in a separate room, while the pump control unit was installed near the CNC control unit in another room, where the experiments were carried out. A video camera was used to monitor and record the cutting process. The movement of the work piece is numerically controlled, where the guiding system consists of a two NC controlled axes, while the Z-axis is manually adjustable. The experimental apparatus is shown in **figure 8.**

4.2 An alternative system for Fundamental Investigations

The selection of the nozzle diameter depends on both the flow rate and the pressure of the fluid. Based on the technical specifications of the pump described in 4.1, where the flow rate was 0.5 l/min, the maximum nozzle diameter that could be selected was 0.12 mm. For this reason when nozzle diameters above 0.12 mm were tested an alternative pump system was used for the fundamental investigations.

A conventional cutting table, manufactured by Steiner-Moser Company, Austria was used in this program. The high pressure water was generated depending on flow rates either by a plunger pump (WOMA, 150 MPa, 40 l/min) or by intensifier pumps (UHDE 400 MPa / 3.8 l/min or FLOW 415 MPa / 7.6 l/min).

5. RESULTS

The effect of pressure on the depth of cut in an aluminum work piece at pressures up to 900 MPa, with a traverse rate of 10 mm/min, and a 0.1 mm diameter diamond nozzle is shown in **figure 9**. It is clear, that with increasing pressure the depth of cut increases due to increased hydraulic power. The depth of cut increased from 1.4 mm at a pressure of 300 MPa to 8.2 mm at 900 MPa pressure. The effect of pressure on the depth of cut for a 0.08 mm diameter sapphire nozzle with the same working conditions is shown in **figure 10**. The depth of cut increased with the larger nozzle diameter. This is due to increased hydraulic power and jet stability with the diamond nozzle when compared to the sapphire nozzle. The effect of the traverse rate on the depth of cut under these working conditions, (pressure 900 MPa, 0.08 mm diameter sapphire nozzle in aluminum) is shown in **figure 11**. It is clear that with increasing traverse rate the cut depth decreases. The depth of cut increased from 4.7 mm at a traverse rate of 20 mm/min to 8.3 mm at a rate of 5 mm/min.

6. CUTTING MECHANISM FOR WATERJETS

6.1 Effect of Standoff Distance

Figure 12 shows the influence of standoff distance on the depth of cut in aluminium using a 200 mm/min traverse rate, 0.3 mm nozzle diameter and a 300 MPa jet pressure. It is clear from the figure that the standoff distance represents a fairly effective cutting tool control, changing the type of loading applied by pure waterjets. Interpolation of this figure indicates that there is an optimum standoff distance, where the depth of cut is a maximum. It seems that this optimum is related to the properties of the material, pressure, nozzle type and size. The depth of cut was increased by increasing the standoff distance to a certain value because of a change in loading from stagnation to impact pressure and was then decreased by further increasing the standoff distance, due to an increased jet dispersion and a reduction of energy because of friction with the surrounding medium (air). **Figure 13** shows photomicrographs at different standoff distances for polished aluminium using a traverse rate of 300mm/min, a nozzle diameter of 0.2 mm and a pressure of 50 MPa.

6. 2. Effect of Loading Time

The effect of loading time on the volume of material removed from the test aluminium was measured in the current work by changing the traverse rate (300, 500, 800 and 1000 mm/min). Photomicrographs of the wear tracks at a pressure of 50 MPa and a standoff distance of 50 mm are shown in **figure 14**. When the details of the formed craters are closely examined it can be seen, that at a traverse rate of 300 mm/min the degree of plastic deformation is relatively high. Water droplets impact the stress free surface and form indentation craters, which look like small pits of 15 – 20 µm, plowing craters with deformed ridges that surround the circumference of a central depression, a result of the shear stress caused by tangential water flow. As the traverse rate is increased to 500 mm/min, the plastic deformation of the deformed craters decreased and the diameter of the indentation craters decreased to 10 – 15 µm. At 800 mm/min, the cavities vanished and the grain boundaries became delineated, coarse slip bands were developed across the width of the grains and the grains became increasingly undulated. At 1000 mm/min, only grain boundaries were observed, without any cavities.

6.3 Topography of Jet Generated Surface

An inspection of the worn surface can reveal the cutting mechanism of the waterjet. The wear track caused by the waterjet in cutting aluminum (pressure 100 MPa, traverse rate 40 mm/min, standoff distance $300d_n$ and nozzle diameter 0.2 mm) is shown in **Figure 15 (a, b, c and d)**. In figure15 (b), it can be seen that the severity of wear is greatest in the center of the wear track and decreases towards the sides. The distortion that occurred in the surface depends on the diameter of the water drops, not on the grain size of the worn surface. Plastic deformation is clearly shown on the worn surface. Figure15 (d) shows a higher magnification of the worn surface. The erosive action of the water drops is clearly shown, forming a series of holes and cavities. The diameter of the holes and cavities is relatively fine (ranging form 5 to 10 µm). The direction of impact of the water drops varied due to the irregularity of the severely deformed surface. The material around the holes shows relatively greater deformation due to the ductility of the material tested.

6.4 Effect of Material Types

The materials tested were selected to represent two extreme types of crystal structure in relation to ductility. The tested materials were aluminum as a ductile, face centered cubic material, (fcc) and zinc with a closest packed hexagonal structure (hcp). The wear track caused by the 100 MPa waterjet, with a traverse rate of 40 mm/min, standoff distance 10 mm and a nozzle diameter of 0.2 mm is shown in **figure 16**. The width of the wear track exceeded 400 µm. The damage to the aluminum is in the form of small depressions over the whole area of the wear track and erosion occurred by ductile removal of the material constituting the rim.

Zinc exhibits crack initiation and growth rather than simple ductile shearing off of small particles where deformation and crack growth can be facilitated. Initial depressions grow but do not form craters, the material is lost by removal of large pieces of the grains through transcrystalline fracture. Wear grooves formed by the erosion of zinc test specimens by waterjet attack under the same conditions as above are shown in figure 16. The edge of the wear groove is corrugated indicating brittle failure. The wear debris for aluminum and zinc is shown in **figure 17**.

6.5 Cutting Mechanism for Waterjets and Abrasive Waterjets

Figure 18 compares the micro-structural variations found in the cutting area when cutting AlZnMgCu 1.5 with an abrasive waterjets (AWJ) (nozzle diameter 0.25 mm, abrasive focus tube diameter 0.9 mm, pressure 240 MPa, traverse rate 100 mm/min, abrasive cutting flow rate 8 g/s) in comparison with pure waterjet (WJ) cutting of AlMgSi0.5 (sapphire nozzle diameter 0.08 mm, pressure 900 MPa, traverse rate 10 mm/min, standoff distance 10 mm). The microstructure differs due to the change in material removal mechanisms between a waterjet and an abrasive waterjet. The surface finish was found to become worse with an increase in the depth cut, as it does for AWJ cutting. The mechanism of the jet cutting process generally depends on the process parameters. In the case of AWJ, in the first stage of cutting the abrasive particles strike the surface at a shallow angle producing a relatively smooth surface. The material removal phenomenon associated with this process of cutting is called the cutting wear mechanism. A secondary region, which displays unsteady cutting with striation marks is called the deformation cutting zone. The traces of micro-grinding as the basic cutting mechanism can be seen over the whole cutting area. In the case of WJs, the mechanism of waterjet cutting is erosion caused by localized failure that occurs due to the localized fluid pressure (impact pressure). This pressure exceeds the strength of the target material leading to a plastic deformation, material flow and material removal. The dynamic loading by waterjets leads in principle to the same structure as that which can be seen in section 6.2, 6.3 and 6.4.

7. CONCLUSIONS

We can summarise the conclusions as follows:

- Increasing the pressure of the water leads to an increase in cutting efficiency of waterjets and abrasive waterjets
- Flow rates for water and especially for abrasives can be reduced
- Sheet metal can be cut to a certain extent (thickness, hardness) with waterjets only
- The surface structure generated by the waterjet is different when abrasive waterjet cutting because of the change in cutting mechanism.
- Different types of pump systems are available
- Loading system components above 500 MPa has a negative influence on their lifetime

8. ACKNOWLEDGEMENTS

The authors are scientists of the Waterjet Laboratory Hannover (WLH) in the Institute of Materials Science, University of Hannover and members of the German Working Group of Waterjet Technology (AWT). The experimental equipment has been kindly supported by a 1000 MPa intensifier pump from Böhler Hochdrucktechnik GmbH.

9. REFERENCES

1. Hashish, M: Cutting and Drilling at 690 MPa; Proceedings of the 10th American Waterjet Conference, Houston 1999, pp. 137-152.
2. Rhagavan, C.; Ting, E.: Hyper Pressure Waterjet Cutting of Thin Sheet Metal; Proceedings of the 6th American Waterjet Conference, Houston 1991, pp. 493-504.
3. Imanaka.O, Fujino S.,Shinohara K., Kawate Y."Experimintal Study of Machining Characteristics by Liquid Jets of High Power Density up to 1018Wcm-2" first international symposium on Jet Cutting Technology 5-7 april, 1972, G3-25 –G3-35.
4. Oweinah, H.: Leistungssteigerung des Hochdruckwasserstrahlsschneidens durch Zugabe von Zusatzstoffen; Dissertation Techn. Hochschule Darmstadt, 1989.
5. Trieb, F. and Zamazal, K.:waterjet Cutting 300 MPa High Pressure to 800 MPa Ultra High Pressure; 6th Pacific Rim International Conference on Water Jetting Technology, Sydney Australia 9-11 October, (2000)
6. Trieb, F. and Zamazal, K.:800MPa Pure Waterjet and Abrasive Waterjet Cutting-Whats Next; Proceedings of the 2001 WJTA American Waterjet Conference, August 18-21,2001,pp. 797-807
7. Victor, F.; Robert W.:Physics of Ice. Oxford University Press Inc,New York, 1999.
8. Bridgman, P.: The Phase Digram of water to 45,000 kg /cm2. Journal of Chemical Physics (1937) Vol.5, Nr.1-12, S.964/966.
9. Wagner, W.; Saul, A.; Pruß,A.:International Equations for the Pressure along The melting and along the Sublimation Curve of Ordinary Water Substance. Journal Physics Chemical Reference data, 1994, Vol. 23, No.3,S.515/525.
10. Heide Koch: Einfluß von Hochdruck auf Phasenübergänge Wasser-Eis und dessen Nutzung zur Konservierung in der Lebensmittel- und Biotechnologie. DKV-Tagungsbericht, 20-22. Nov, 1996,S 141/160
11. Truckenbrodt, E: Strömungsmechanik. Berlin, Heidelberg, New York, Springer Verlag 1968.
12. Tait, P.G.: Report on some of the physical properties of fresh water and sea water; Phys. Chem. Z., 1888.
13. Bridgman. P. W.:Thermodynamic Properties of Liquid Water to 80° and 12000 KGM.; Proceedings of the American of Arts and Science, Vol. XLVIII. No.9, 1912.

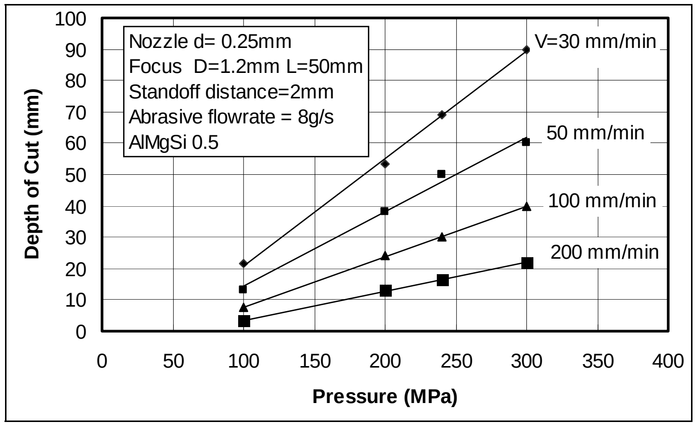

Figure 1. Influence of pressure on the depth of cut at different traverse rates

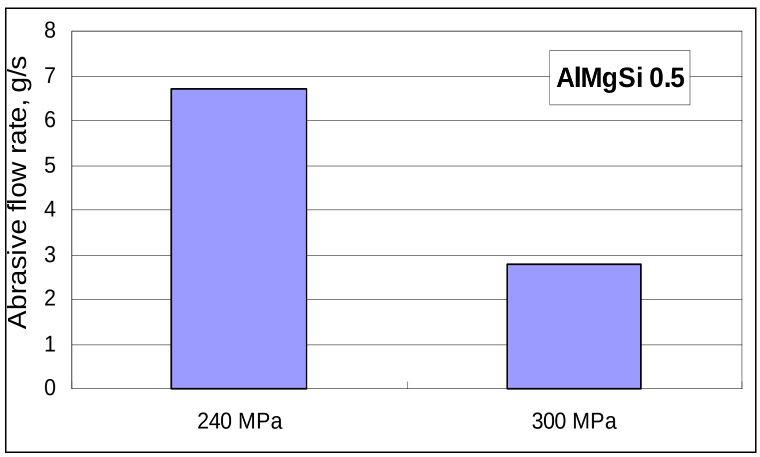

Figure 2. Comparison of abrasive consumption to achieve equal cutting depth

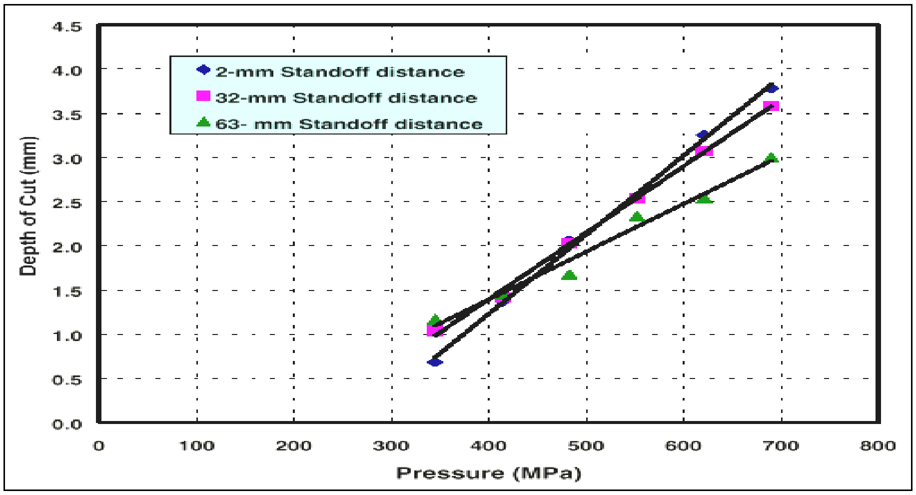

Figure 3. Effect of pressure and standoff distance on waterjet cutting of thin (1.6 mm) aluminum, [1].

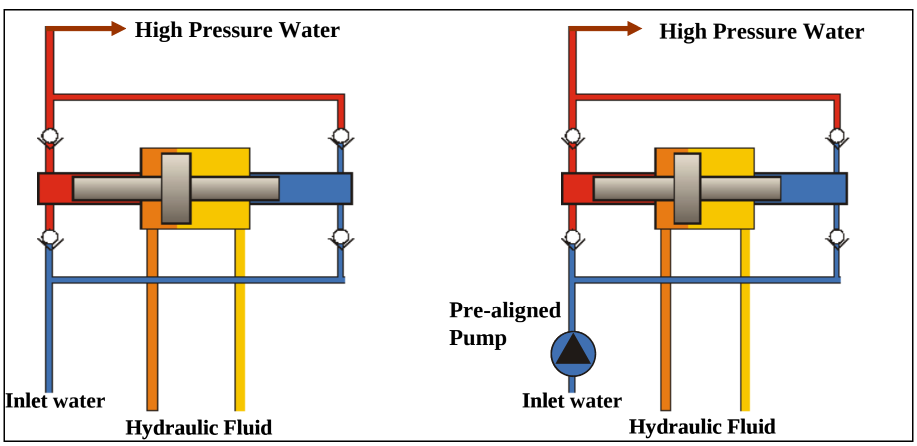

Figure 4a. Intensifier pump **Figure 4b.** Intensifier pump with a pre-aligned pump

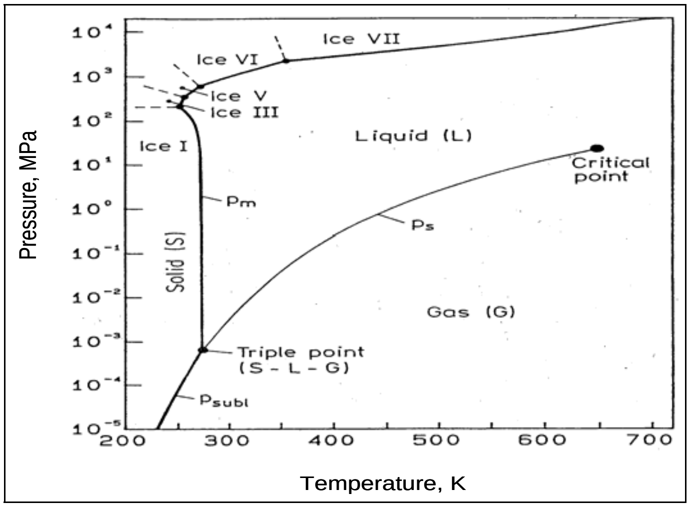

Figure 5. The phase-boundary curves of water in a pressure-temperature diagram, [9].

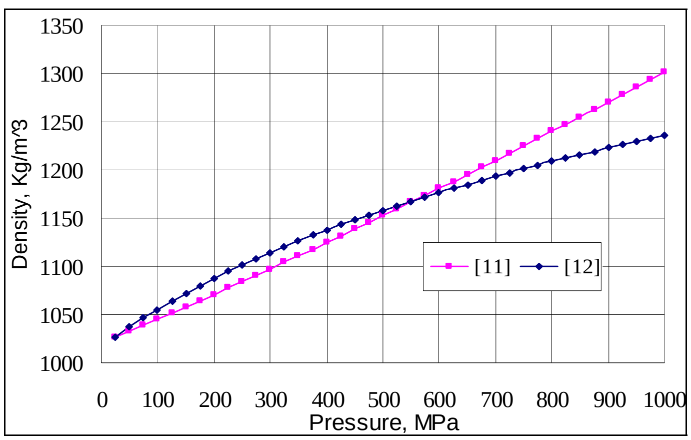

Figure 6. Dependence of density of water on pressure

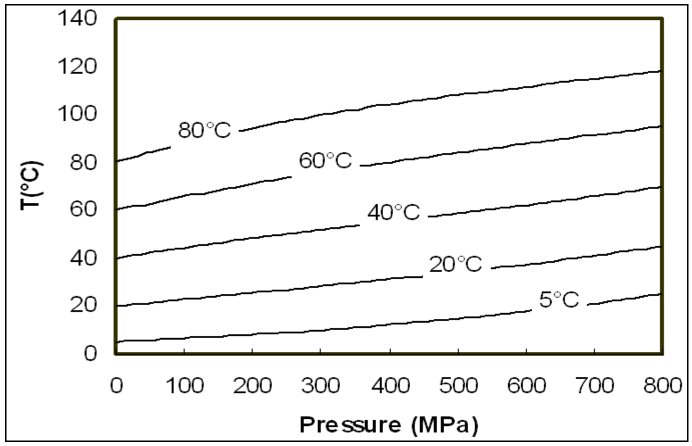

Figure 7. Temperature rise during adiabatic compression of water, [13].

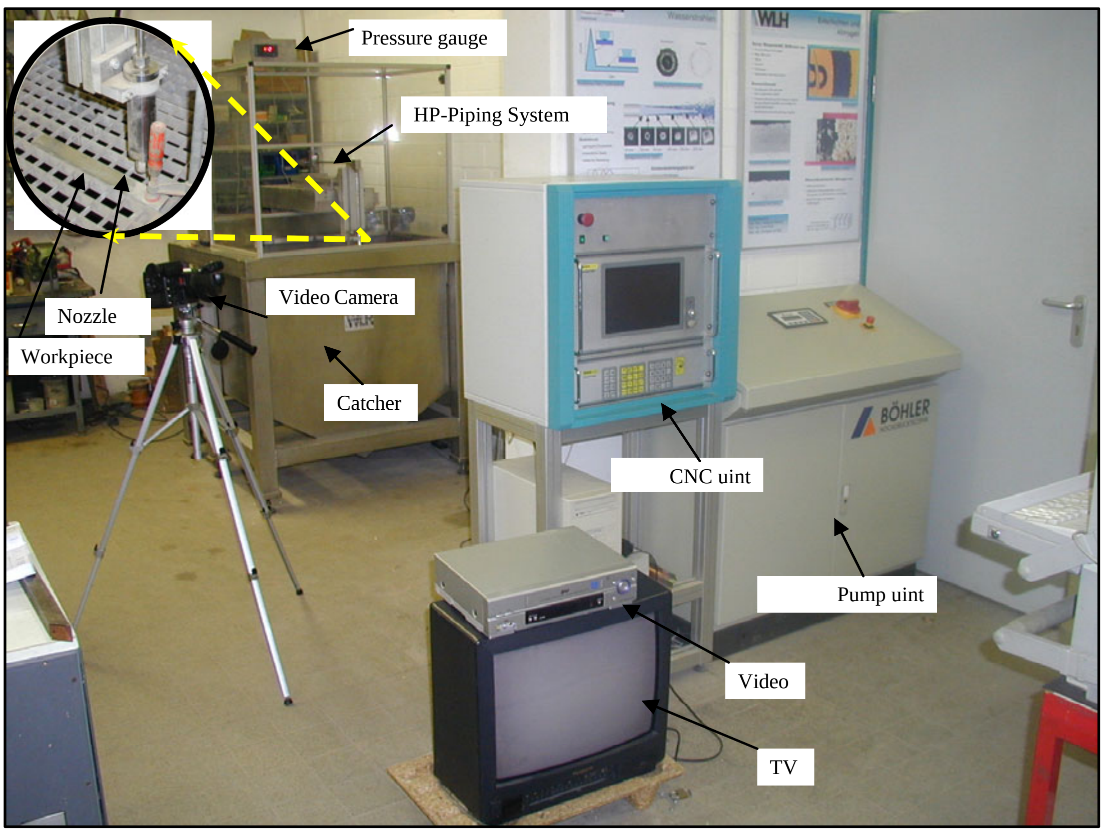

Figure 8. Experimental setup (cutting cell, data acquisition)

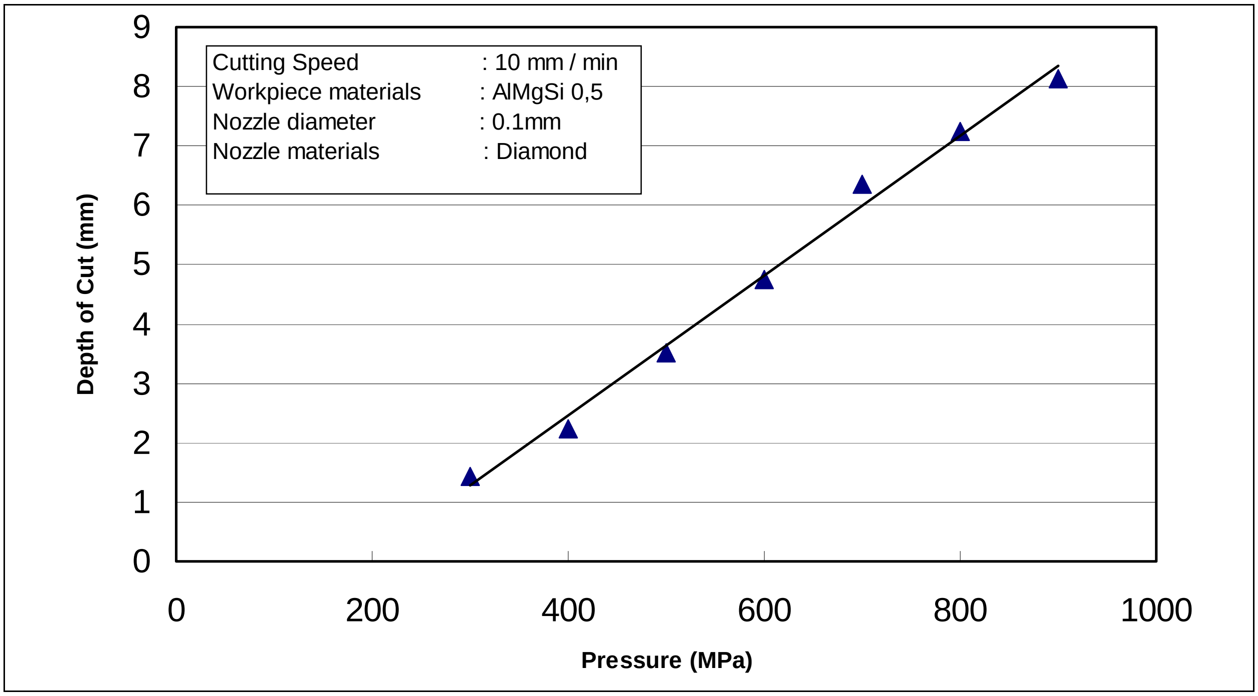

Figure 9. Effect of pressure on depth of cut at a nozzle diameter of 0.1 mm

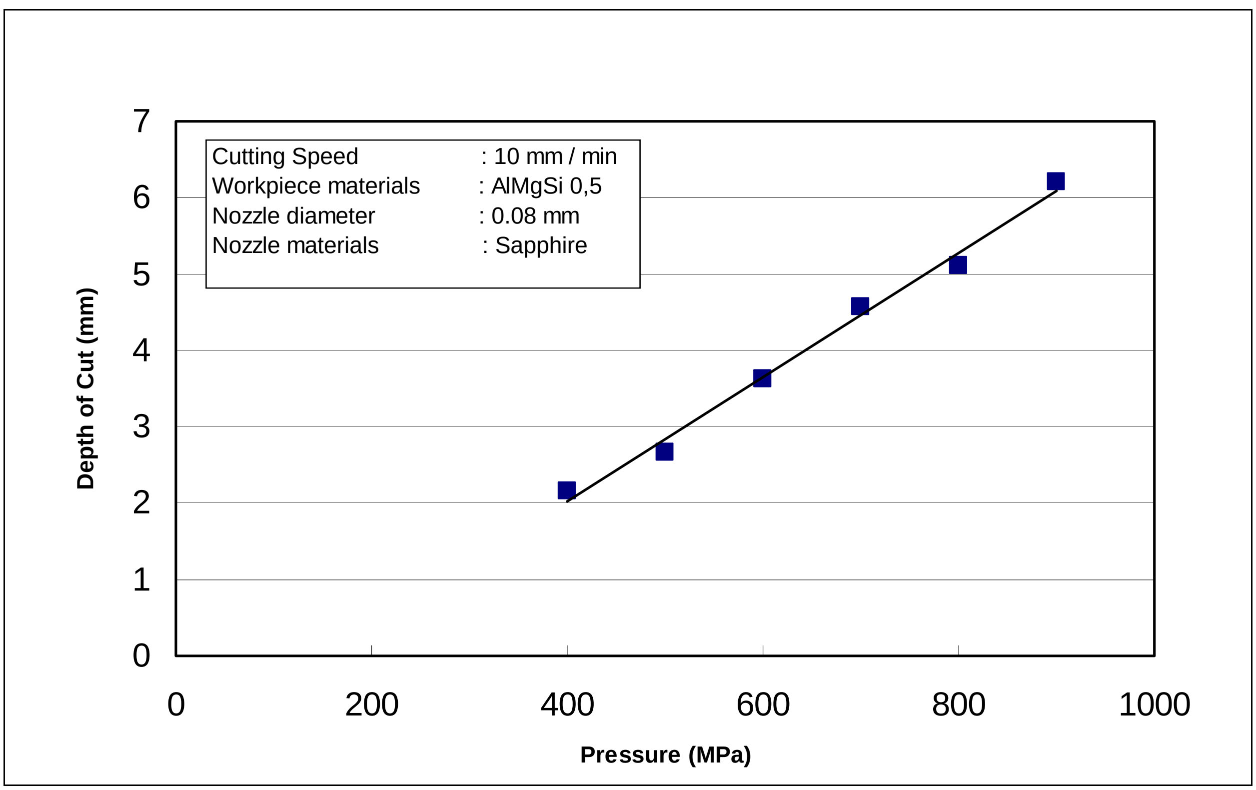

Figure 10. Effect of pressure on depth of cut at a nozzle diameter of 0.08 mm

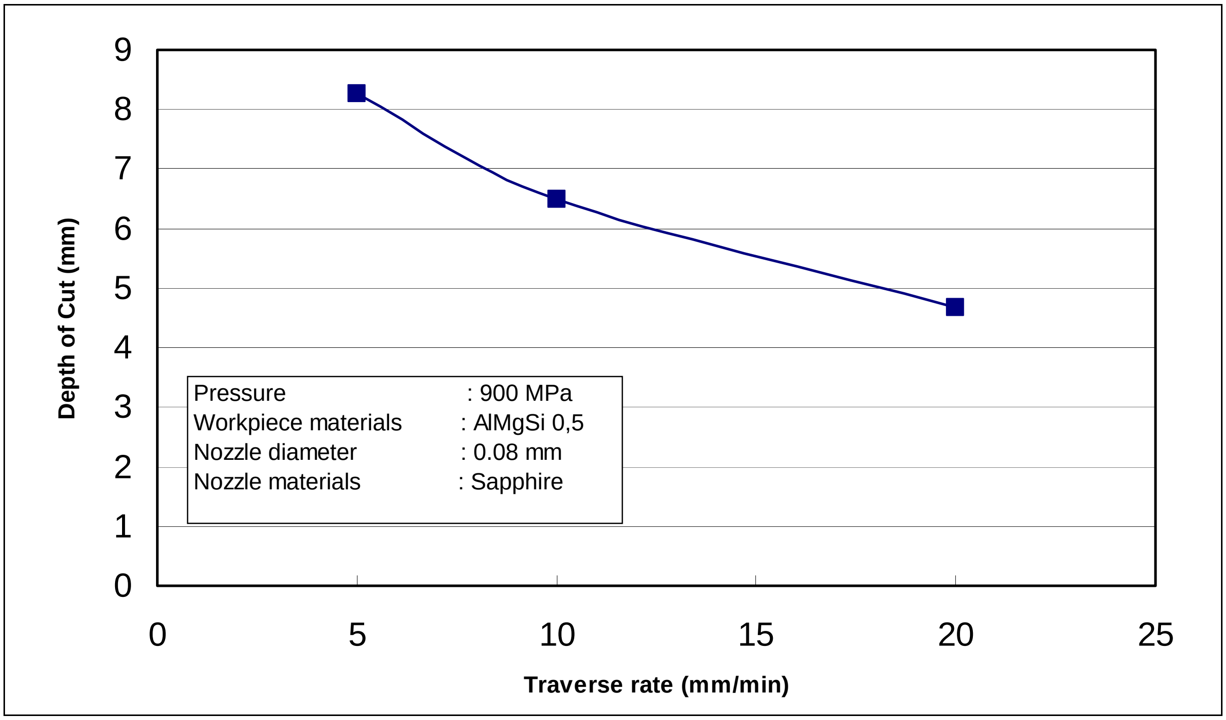

Figure 11. Effect of traverse rate on the depth of cut at 900 MPa working pressure.

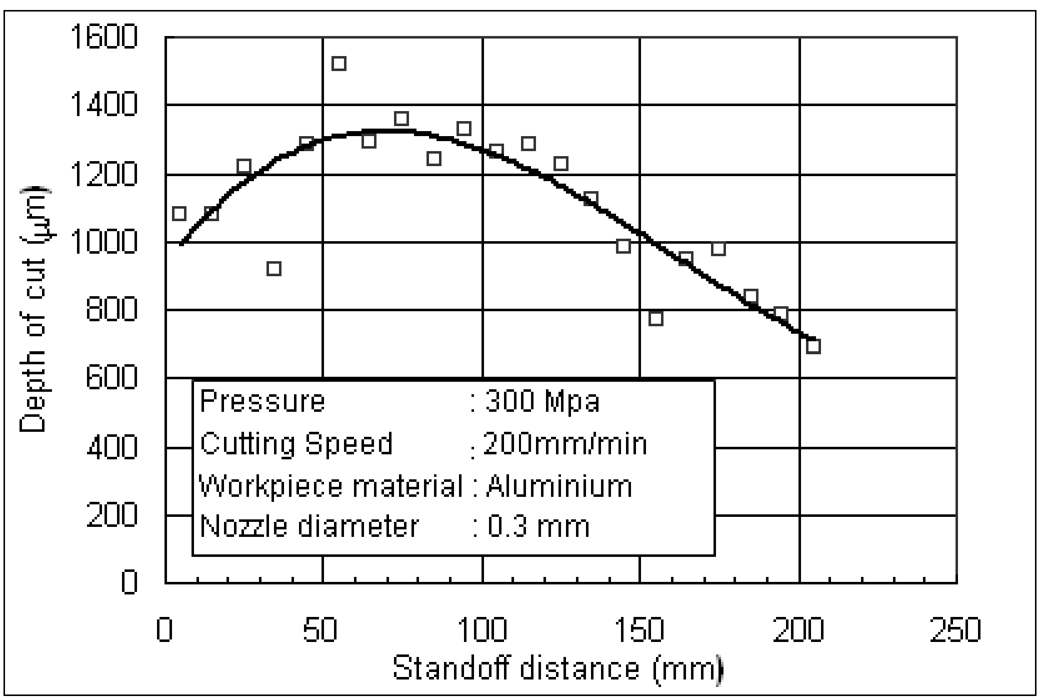

Figure 12. Effect of standoff distance on the depth of cut

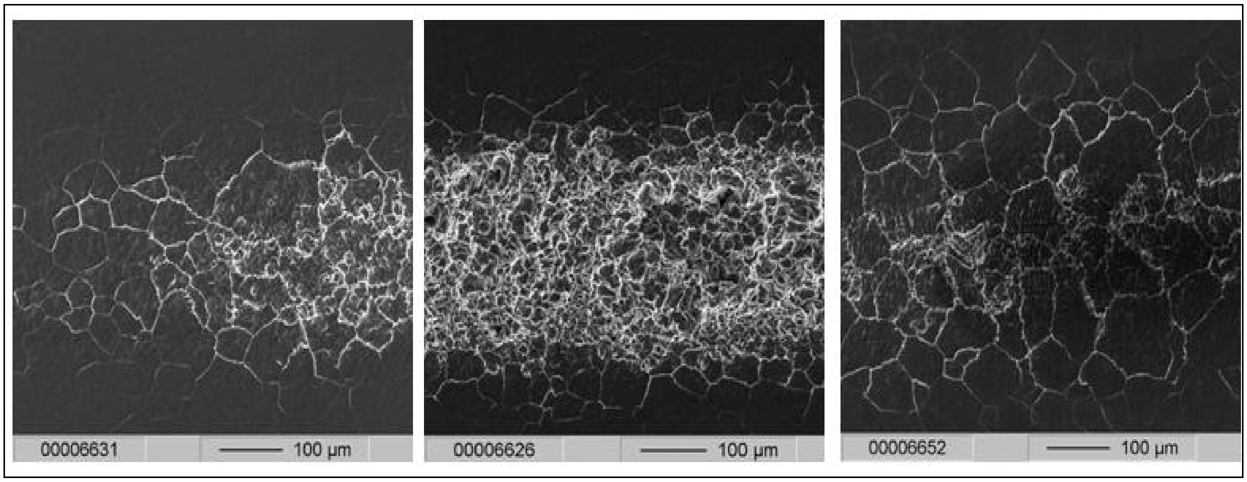

s = 150 d_n s = 300 d_n s = 500 d_n

Figure 13. Topography of jet generated surface at different standoff distances

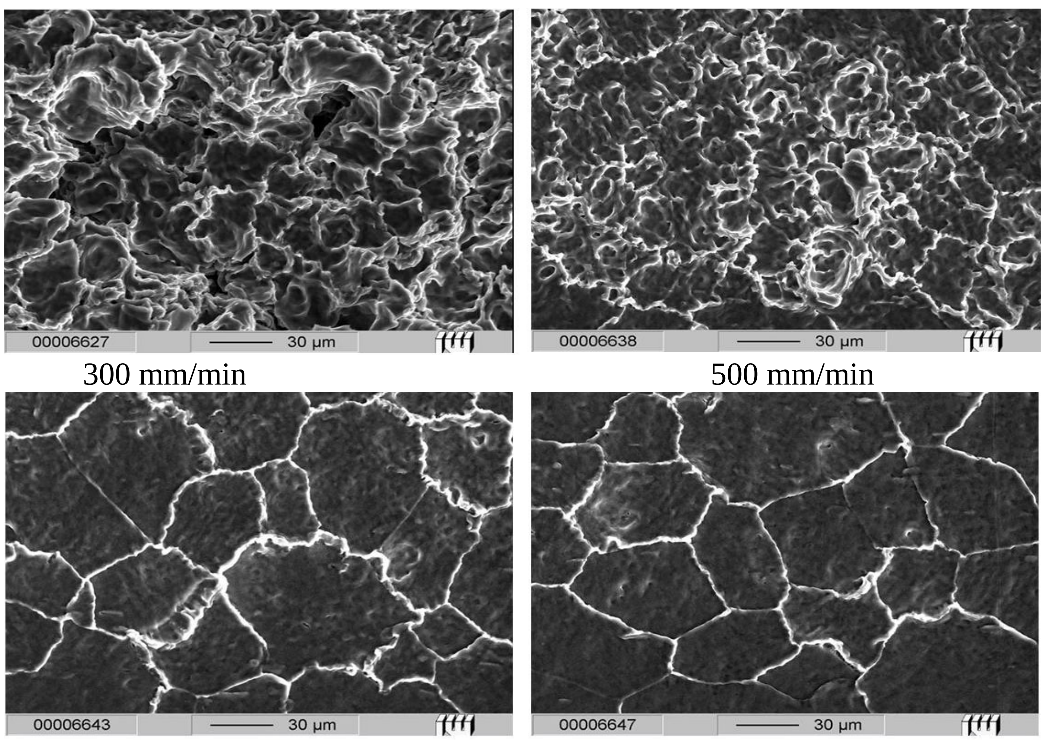

Figure 14. The effect of loading time on aluminium at a standoff distance 50 mm

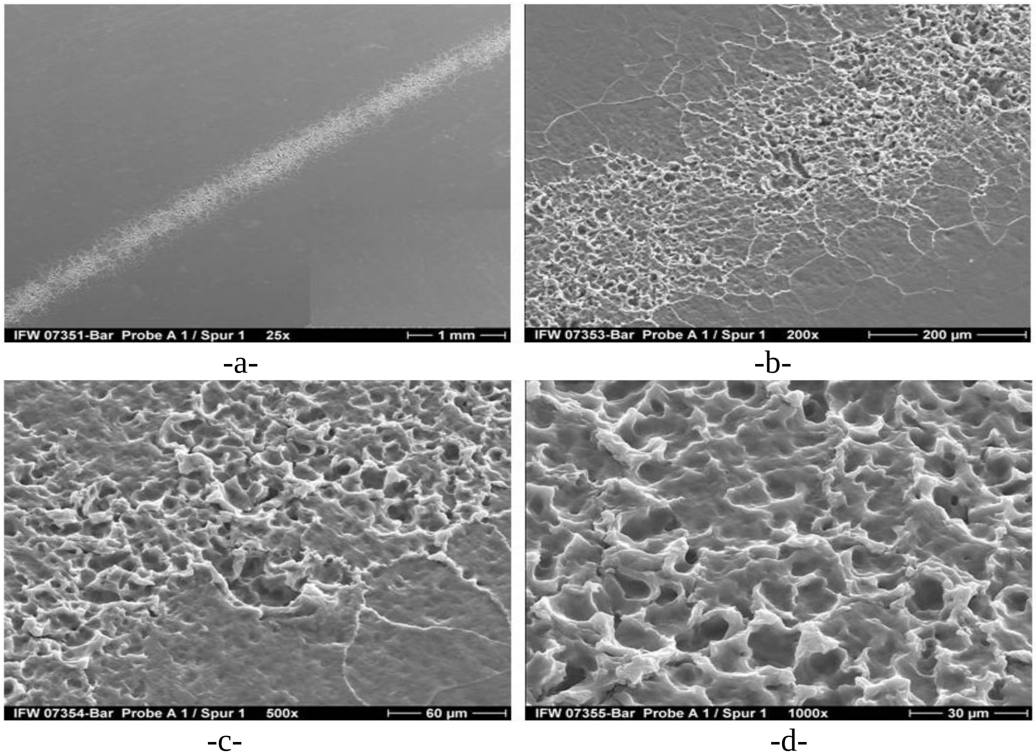

Figure15. Topography of jet generated surface.

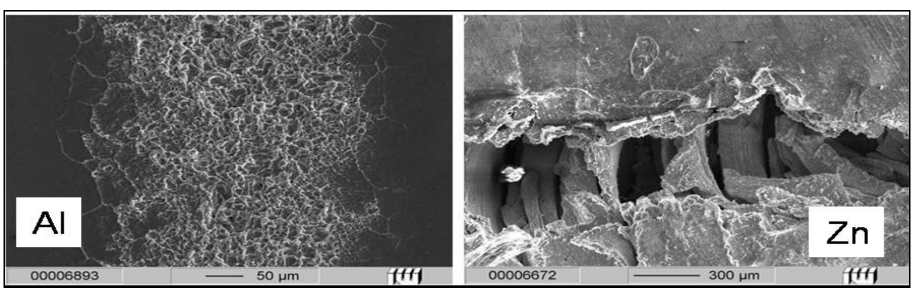

Figure 16. Wear track caused by waterjet for aluminum and zinc

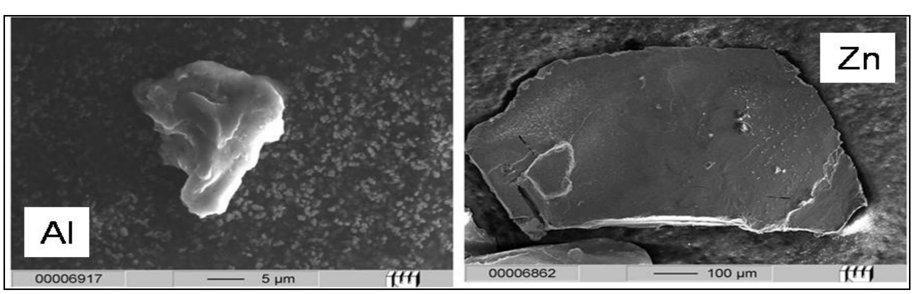

Figure 17. Wear debris caused by waterjet impact on aluminum and zinc

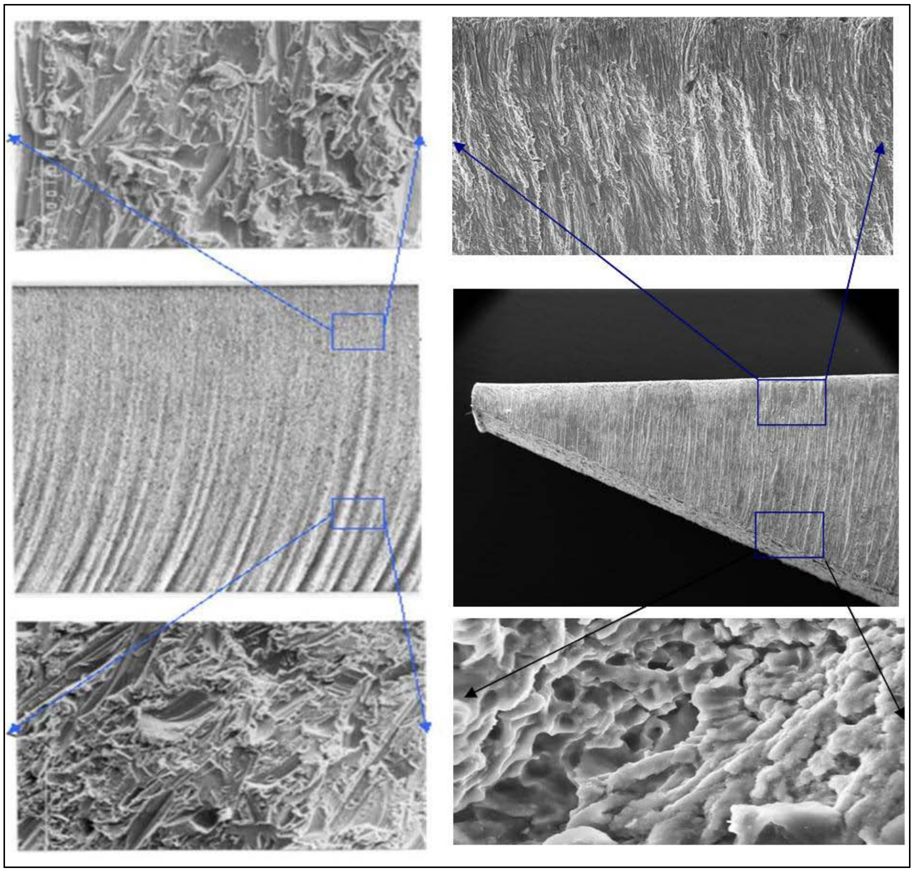

Figure 18. Surface Topography of samples cut with AWJ and WJ

2003 WJTA American Waterjet Conference
August 17-19, 2003 • Houston, Texas

Paper 2-A

FEASIBILITIES OF ABRASIVE WATER JET MULTIPASS CUTTING TECHNIQUE

B. Jurisevic, K.C. Heiniger, A. Schuetz
Swiss Competence Centre of Water Jet Technology
University of Applied Sciences, Aargau
Windisch, Switzerland

M. Junkar
Laboratory for Alternative Technologies
University of Ljubljana
Ljubljana, Slovenia

ABSTRACT

Abrasive Water Jet (AWJ) machining is a well-established manufacturing process in several fields of production. Currently, it is also one of the fastest growing technologies. Usually, AWJ machining is used for contour cutting in a single plane. Many possibilities exist to improve the process in order to improve the machining quality and energy efficiency and to reduce the machining time and costs, all at the same time.

Because the cutting surface quality decreases along the depth of cut, the AWJ must have a threshold cutting capability to reach the demanded machining quality over all the depth of the cut. Part of the AWJ energy is lost because it’s not involved in the cutting process. A certain number of abrasive particles don’t take part in the material removal process.

In our research we explore the feasibility of a multipass cutting technique in case of an industrial material such as an aluminum alloy. We look for the optimal cutting head traverse rate for the single passes and the cutting conditions in which the multipass technique still is superior compared to single pass cutting.

Our objectives are to reduce the energy used for cutting, reduced the machining time and increase the quality of the cutting surface. In achieving these objectives the production costs will be reduced as well.

1 INTRODUCTION

In several cases of 2D contour cutting operations it was showed that using an Abrasive Water Jet (AWJ) instead of alternative manufacturing procedures the machining time and especially the costs could be drastically decreased while still achieving the demanded quality. In these cases the AWJ reduces the machining costs so much, that there is no motivation for further optimization of the process. Nevertheless, since more products are machined using the AWJ, the need for process optimization in terms of time/costs reduction and machining quality improvement arises.

In the field of AWJ cutting, one possibility to improve the machining performance is the use of a multipass cutting technique, where instead to cut through the workpiece along the contour in one pass, a higher traverse rate is used what automatically implies a higher number of passes along the contour in order to cut through the whole workpiece thickness. When the jet exits from the workpiece in single pass cutting, it still has a substantial amount of energy, which is lost in the catcher. In multipass cutting this occurs only at the last pass (or at last few passes), but because the traverse rate is higher than in single pass cutting the amount of the total lost energy during the whole cutting process is smaller. If we make a simple energy balance we can see that during multipass cutting, more energy available in the jet is actually used for the cutting process comparing with single pass cutting. A better surface quality in multipass cutting can be attributed to the higher concentration of jet energy in the material removal zone due to a higher traverse rate what implies a shorter exposure time. Using a multipass cutting technique, the uncut part, which takes place at the exit of the jet from the workpiece, can be avoided or at least substantially minimized.

In the present research, we first give an overview of the available literature on the AWJ multipass cutting technology, which is presented, in the next chapter. The experiments are divided in two parts. In the first part we analyze the influence of the traverse rate on the material removal rate for a single pass. To compare the performance of the multipass with single pass cutting we observe the surface roughness, taper of the cut and the cutting time. The results obtained from the experiments are graphically represented and discussed in chapter 5. In the last chapter we present our conclusions and anticipate further research in the domain of AWJ multipass cutting.

2 LITERATURE OVERVIEW

One of the first investigations, where the multipass cutting was investigated was made by Hashish [1, 2] in the early 80's. It was found out that the traverse rate and number of passes should be as high as possible in order to achieve the highest depth of cut until the hydrodynamic mode of penetration is present [1]. During experiments on plexiglass it was shown that the multipass cutting is more effective compared to the single pass with smaller abrasive flow rates [2]. In the same study it was also observed that in the case of plain water jet, the cutting results always improve at higher number of passes. AWJ multipass milling tests were performed on aluminum, glass, titanium, graphite composites and mild steel [3]. In the case of mild steel multipass milling, the highest material removal rate was obtained at a traverse rate of 250 mm/s, but the smallest depth non-uniformity was obtained at the traverse rate of 420 mm/s. During experiments made on glass, Lexan and Lucite samples it was observed that the kerf created by the previous passes keep the jet coherent what leads to a greater depth of cut [4]. Other researches show the economical superiority of AWJ multipass cutting [5, 6]. Bortolussi and Ciccu analyze the multipass cutting of thick steel plates, where they observe an absence of waviness and constant cut quality over the entire cut area, improvement of the cutting quality and a substantial decrease in cutting costs per unit length comparing with single pass cutting [5]. Agus et al. observed that cutting costs decrease with the increase of traverse rate up to an optimal value during the multipass cutting experiments on marble, granite, plexiglass and aluminum [6]. In a recent research Wang and Guo analyze the cutting performance of multipass AWJ on industrial ceramics [7]. According to their observation from experiments made on 87% aluminum ceramics the smooth cutting zone increases with using higher number of passes. Comparing to single pass cutting, the same surface quality can be obtained by multipass cutting in less cutting time. By increasing the number of passes, better quality can be obtained with multipass cutting in the same cutting time comparing to single pass cutting. If all the passes in multipass cutting are made in the same direction instead of altering the cutting direction, the smooth cutting zone increases by 4 to 20% [7].

3 OBJECITVES

In the presented work we explore the feasibility of AWJ multipass cutting technique and compare its performance with single pass cutting in order to:

1. Increase the material removal rate m_R (smaller cutting time and costs)
2. Increase the machining quality (smaller surface roughness and taper of the cut)
3. Obtain a more uniform surface quality along the whole depth of the cut

The used criteria to compare multipass with single pass cutting were the surface roughness (Ra), taper of the cut (T_R) and cutting time (t_C). Beside that also the quality along the depth of the cut (h_C) was observed.

4 EXPERIMENTAL WORK

The experimental work was divided in two parts. First, we look for a traverse rate, which enables the highest material removal rate. In the second part we compare multipass and single pass cutting by measuring the surface roughness and taper of the cut. All the experiments were performed on an AlMgSi1 (6082) aluminum alloy samples with the properties listed in Table 1.

For the experiment we used a AWJ test installation composed by a Bystronic BJD 50 hydraulic intensifier with water pressure (p_W) up to 400 MPa and water volume flow (V_W) up to 5 l/min, a Stäubli RX 130 robot, a cutting head with abrasive feeding system mounted on a fix support and a catcher tank. During all experiments the parameters listed in Table 2 were kept constant.

4.1 Optimal traverse rate for the highest material removal rate

In order to find the optimal traverse rate (v_C), which produces the highest material removal rate, we carried out several series of experiments. A wide range of traverse rates from 2 up to 400 mm/s was observed as listed on Table 3.

For each traverse rate five kerfs of 50 mm length were made 6 mm apart from each other on an aluminum sample shown on Figure 1. The first three sets were repeated three times each, while the fourth set was made in four repetitions.

The material removal rate (m_R) in g/s is calculated using Equation 1, by weighting the samples before and after each set of experiments using a Mettler AT261 Delta Range scale with a resolution of 0.01 mg.

$$m_R = \frac{\Delta m}{L_C} \cdot v_C \tag{1}$$

In Equation 1 Δm is the removed workpiece material in grams during the observed cut of length L_C in mm using the traverse rate v_C expressed in mm/s.

4.2 Optimal multipass cutting strategy

In order to compare the performance of multipass with single pass cutting, a wide range of experiments was made on AlMgSi1 (6082) aluminum alloy of three different thicknesses (T_S), namely 5, 10 and 20 mm.

The surface roughness was measured at three points at three different depths of the cut surface in the case of the samples of thickness 5 and 10 mm, while on 20 mm thick samples it was measured at one position at each depth as showed on Figure 2. A Mitutoyo SJ-201 measuring instrument with a resolution of 0.08 μm and measuring range between 0.01 and 75 μm was used for the surface roughness measurements.

The influence of the number of passes (n_P) on the material removal rate (m_R) was observed by making three passes at seven different traverse rates (7, 8, 10, 20, 30 and 40 mm/s). The removed material was measured by weighting the samples between each pass, as described in the previous section.

5 RESULTS ANALYSIS AND DISCUSSION

The presented results indicate that in AWJ multipass cutting two optimal traverse rates exist. One enables the highest material removal rate and the other the better surface quality expressed in surface roughness and taper of the cut. From Figure 3 it can be observed that an optimal range of traverse rates exists between 3 and 10 mm/s, where the highest material removal rate takes place. Analyzing the results obtained from the comparison between the single pass and multipass cutting, it can be observed that the surface roughness and taper improve using a traverse rate, which is higher that the optimal traverse rate. The optimal traverse rate is that at which the highest material removal rate is obtained in case of AlMgSi1 (6082) aluminum alloy used in our investigations.

The first three sets of experiments concerning multipass cutting, were made on 5 mm thick samples using three different abrasive mass flows. It can be seen from Figure 4, Figure 5 and Figure 6, with abrasive mass flow (m_A) of 30, 60 and 90 g/min respectively, that the smallest surface roughness is obtained at the highest abrasive mass flow rate of 90 g/min. Since the surface roughness decreases with an increase of the abrasive flow, for all the further experiments this parameter was set to 90 g/min. In the fourth set of multipass cutting experiments the traverse rate was extended up to 60 mm/s as shown on Figure 7. In the fifth set the traverse rate was increased up to 160 mm/s and the stand-off distance (h_{SO}) reduced from 4 down to 2 mm. The surface roughness measurement results of this series are shown on Figure 8. Two sets of experiments were performed at greater sample thicknesses, as namely 10 and 20 mm. In these cases the traverse rate was increased up to 400 mm/s, while the other process parameters were kept unchanged. The results of the surface roughness measurements are given on Figure 9 and Figure 10 for the sample thicknesses 10 and 20 mm, respectively. It can be observed that the roughness and cutting time decreases to a certain level after which the roughness is more or less constant while the cutting time starts to increase at higher traverse rates. Nevertheless, it can be observed form Figure 9 and especially from Figure 10 that using a multipass cutting technique instead of single pass, the quality of the cut can be improved and the cutting time reduced in the case of greater workpiece thicknesses.

The taper of the cut was calculated using Equation 2 by measuring the top (b_T) and the bottom width of the cut (b_B) in the forth and fifth series of experiments and the results are shown on Figure 11 and Figure 12 respectively.

$$T_R = \frac{b_T}{b_B} \tag{2}$$

The influence of the number of passes on the material removal rate was observed at six different traverse rates (7, 8, 10, 20, 30 and 40 mm/s) for three passes. The results are shown on Figure 13, where can be observed that the material removal rate is more or less constant for the second and third pass.

In order to have a better representation of the ratio between the traverse rate (v_C), number of passes (n_P) and cutting time (t_C), these values are listed in Tables 5-9.

6 CONCLUSIONS

From the presented research of multipass performance on AlMgSi1 (6082) aluminum alloy it can be seen that using an appropriate traverse rate which is higher than the one used in single pass cutting, the cutting time can be reduced and the cutting quality improved. There exist two optimal traverse rates. Using the first one the highest material removal rate can be achieved, while the second traverse rate permits a reduction in the surface roughness and taper of the cut using multipass cutting technique.

Summarizing the results, some general trends can be plotted as shown on Figure 14. The portion of the jet energy involved in the material removal process increases at elevated traverse rates, because less energy is dissipated in the jet catcher beyond the workpiece. In the same figure it can be observed that the cutting time decreases with the increase of the traverse rate and starts to increase in the multipass region. It was also observed, that the best quality of the cut doesn't coincide with the smallest cutting time. There exists a region where the optimization of multipass cutting has to be done depending on which machining attribute is more relevant in the given case, either the cutting time or the quality of the cut.

The proposed experimental methodology can easily be applied to define the multipass cutting performance on other workpiece materials. In further research the performance of multipass cutting on hard-to-machine material like tool steel and ceramics will be explored. Another important point is the machining of complicated contours where the effect of multipass cutting in the corners has to be analyzed. Defining the optimal process parameters in multipass cutting in order to machine the sharp corners or small radii, the quality at these points can be improved compared to single pass cutting where the effect of jet lag in the workpiece decrease the quality of the cut, especially its geometry.

7 REFERENCES

[1] Hashish, M.: "Critical and Optimum Traverse Rates in Jet Cutting." Proceedings of the First U S. Water Jet Conference, p.p. 66-82, Golden, CO, 7-9 April 1981, Colorado School of Mines.

[2] Hashish, M.: "Experimental Studies of Cutting with Abrasive Waterjets." Proceedings of the Second U S. Water Jet Conference, p.p. 402-416, Rolla, MO, 24-26 May 1983, University of Missouri-Rolla.

[3] Hashish, M.: "Milling with Abrasive-Waterjets: A Preliminary Investigation." Proceedings of the Fourth U S. Water Jet Conference, p.p. 1-11, Berkeley, CA, 26-28 August 1987, The American Society of Mechanical Engineers, ASME.

[4] Hashish, M.: "Visualization of the Abrasive-Waterjet Cutting Process." Experimental Mechanics, 28: 159-169, 1988.

[5] Bortolussi, A., Ciccu, R.: "Contour Cutting of Thick Steel Plates." Proceedings of the 14th International Conference on Water Jetting, p.p. 273-284, Brugge, Belgium, 21-23 September 1998, BHR Group.

[6] Agus, M., et.al.: "Multi-pass Abrasive Waterjet Cutting Strategy." Proceedings of the 16th International Conference on Water Jetting, p.p. 242-257, Aix-en Provence, France, 16-18 October 2002, BHR Group.

[7] Wang, J., Guo, D., M.: "The Cutting Performance in Multipass Abrasive Waterjet Machining of Industrial Ceramics." Journal of Material Processing Technology, 6546: 1-7, 2003, Article in Press.

8 NOMENCLATURE

m_R	material removal rate [g/s]	l_F	focusing tube length [mm]
t_C	cutting time [s]	$\#_A$	abrasive mesh [1]
Ra	surface roughness [mm]	d_A	abrasive particle size [mm]
T_R	taper of the cut [1]	Δm	removed material [g]
h_C	depth of the cut [mm]	L_C	length of cut [mm]
p_W	water pressure [MPa]	T_S	sample thickness [mm]
V_W	water volume flow [l/min]	n_P	number of passes [1]
v_C	traverse rate [mm/s]	m_A	abrasive mass flow [g/min]
ρ_M	material density [kg/m^3]	h_{SO}	stand-off distance [mm]
d_O	orifice diameter [mm]	b_T	top width of the cut [mm]
d_F	focusing tube diameter [mm]	b_B	bottom width of the cut [mm]

9 TABLES

Table 1. Workpiece material properties

property	**value**
material designation DIN / AA	AlMgSi1 / 6082
density (ρ_M)	2700 kg/m^3
maximum strain stress (R_m)	275÷350 MPa
plasticity threshold ($R_{p,\ 0.2}$)	240÷310 MPa
Brinell hardness (HB)	84÷105 HB
Elastic module (E)	96 000 MPa

Table 2. Fixed process parameters during all the experiments

parameter	**value**
orifice diameter (d_O)	0.15 mm (0.006”)
focusing tube diameter (d_F)	0.50 mm (0.02”)
focusing tube length (l_F)	76 mm (3”)
abrasive type	Garnet
abrasive mesh ($\#_A$) / particle size (d_A)	120 / 0.125 mm

Table 3. Observed traverse rates to define at which the highest material removal rate is obtained

set of exp.	**cutting head traverse rate [mm/s]**									
1	40	80	120	160	200	240	280	320	360	400
2	2	3	4	5	10	20	30	40	-	-
3	4	5	6	8	10	-	-	-	-	-
4	5	6	7	8	9	-	-	-	-	-

Table 4. Process parameters used for multipass cutting experiments

set of experiment	m_A [g/min]	h_{SO} [mm]	T_S[mm]	results shown on	observed attribute
1	30	4	5	Figure 4.	roughness
2	60	4	5	Figure 5.	roughness
3	90	4	5	Figure 6.	roughness
4	90	4	5	Figure 7.	roughness
5	90	2	5	Figure 8.	roughness
6	90	2	10	Figure 9.	roughness
7	90	2	20	Figure 10.	roughness
8	90	4	5	Figure 11	taper
9	90	2	5	Figure 12	taper

Table 5. Traverse rate (v_C), number of passes (n_P) and cutting time (t_C) for the first three sets of multipass cutting experiments, which results are shown on Figure 4-6 respectively

set	1 (Figure 4)			2 (Figure 5)				3 (Figure 6)			
v_C [mm/s]	2	7	8	2	7	8	10	2	7	8	10
n_P [1]	1	2	2	1	2	2	2	1	2	2	2
t_C [s]	25.0	14.3	12.5	25.0	14.3	12.5	10.0	25.0	14.3	12.5	10.0

Table 6. Traverse rate (v_C), number of passes (n_P) and cutting time (t_C) for the fifth set of multipass cutting experiments, which results are shown on Figure 7

v_C [mm/s]	3	4	5	6	15	20	30	40	50	60
n_P [1]	1	1	1	2	2	3	4	5	7	8
t_C [s]	16.7	12.5	10.0	16.7	6.7	7.5	6.7	6.3	7.0	6.7

Table 7. Traverse rate (v_C), number of passes (n_P) and cutting time (t_C) for the sixth set of multipass cutting experiments, which results are shown on Figure 8

v_C [mm/s]	2	3	4	5	7	8	10	12	15
n_P [1]	1	1	1	1	2	2	2	2	2
t_C [s]	25.0	16.7	12.5	10.0	14.3	12.5	10.0	8.3	6.7
v_C [mm/s]	20	40	60	80	100	120	140	160	
n_P [1]	3	5	7	12	17	26	32	37	
t_C [s]	7.5	6.3	5.8	7.5	8.5	10.8	11.4	11.6	

Table 8. Traverse rate (v_C), number of passes (n_P) and cutting time (t_C) for the seventh set of multipass cutting experiments, which results are shown on Figure 9

v_C [mm/s]	1	2	4	8	20	50	80	100
n_P [1]	1	1	2	3	5	13	31	46
t_C [s]	50.0	25.0	25.0	18.8	12.5	13	19.4	23.0
v_C [mm/s]	120	140	160	180	200	300	400	
n_P [1]	60	72	82	90	104	159	214	
t_C [s]	25.0	25.7	25.6	25.0	26.0	26.5	26.8	

Table 9. Traverse rate (v_C), number of passes (n_P) and cutting time (t_C) for the eighth set of multipass cutting experiments, which results are shown on Figure 10

v_C [mm/s]	0.5	50	100	200	300	400
n_P [1]	1	36	100	223	346	464
t_C [s]	100.0	36.0	50.0	55.8	57.7	58.0

10 FIGURES

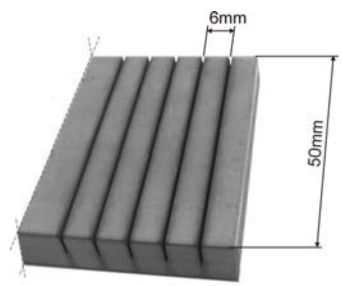

Figure 1. Aluminum samples used to define the optimal traverse rate

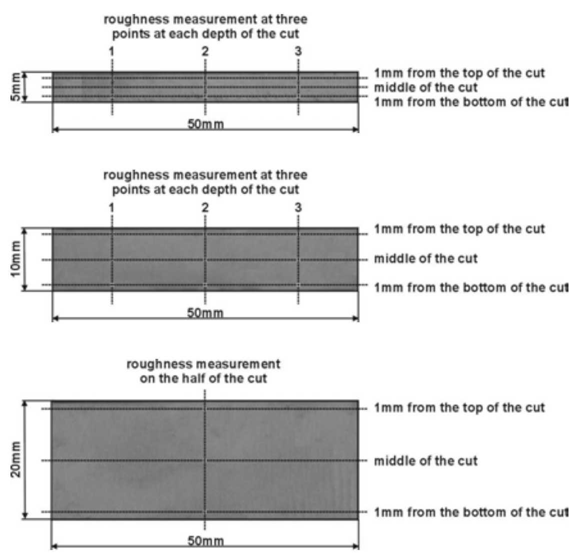

Figure 2. Surface roughness measurement positions on the cut surface

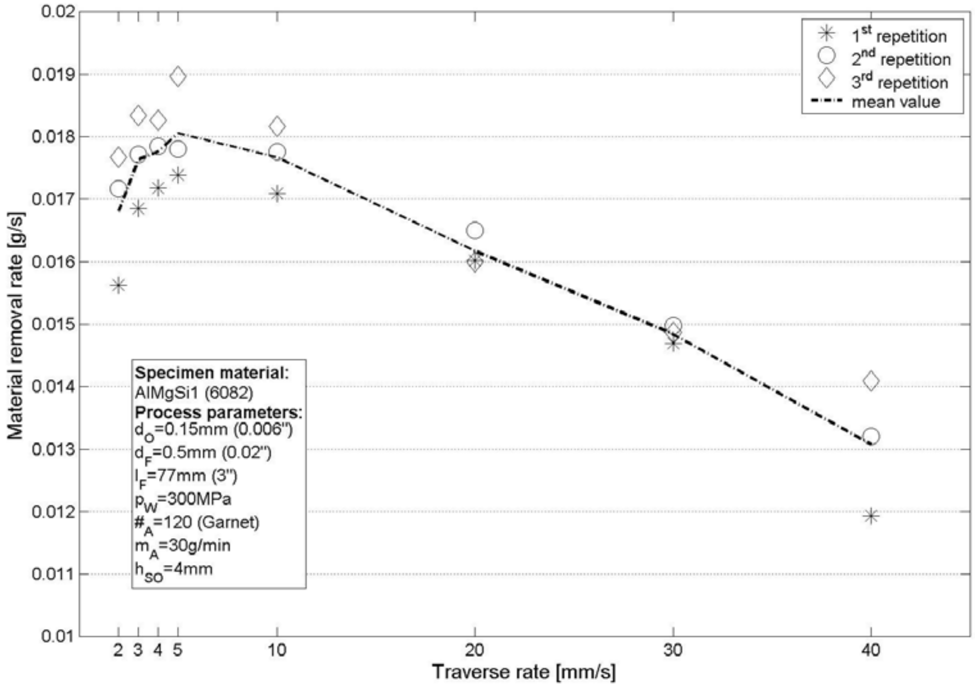

Figure 3. Optimal traverse rate to achieve the highest material removal rate

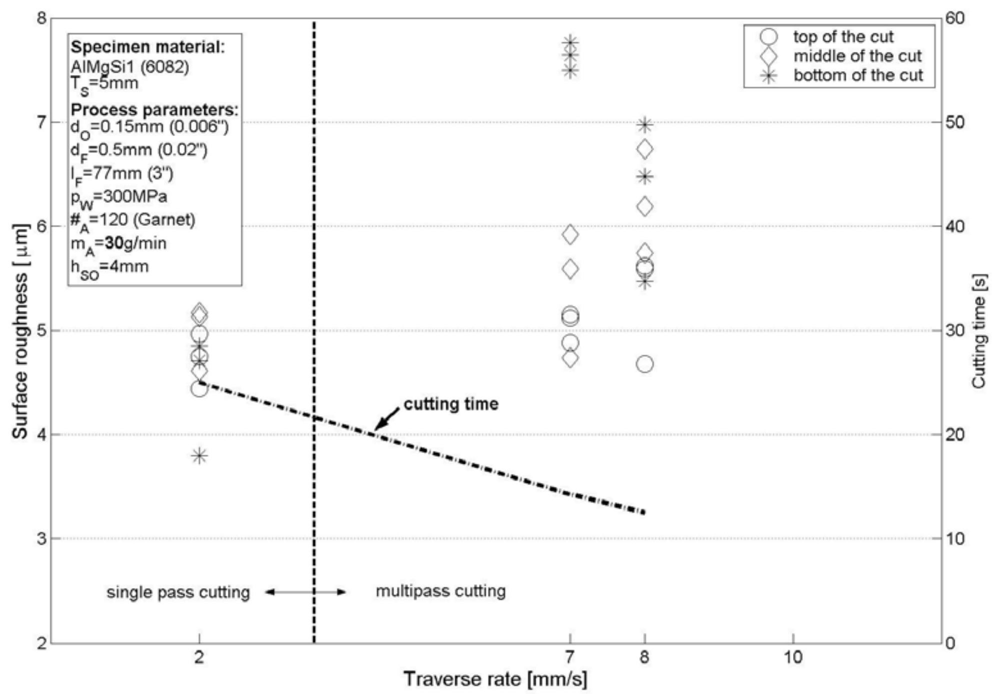

Figure 4. Surface roughness measurements on 5 mm thick specimens, m_A=30 g/min

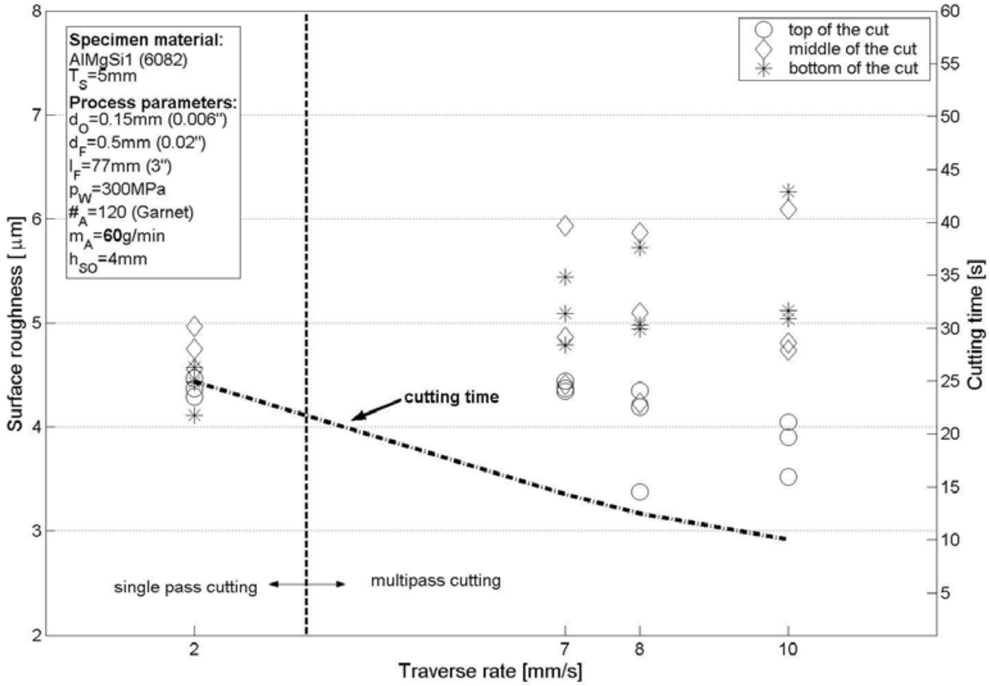

Figure 5. Surface roughness measurements on 5 mm thick specimens, m_A=60 g/min

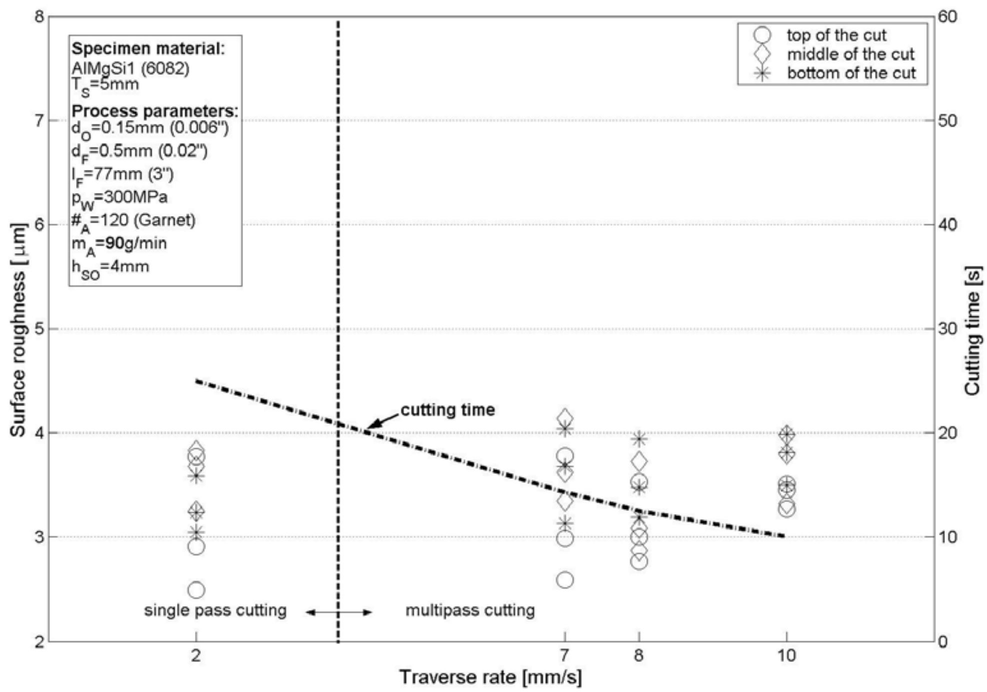

Figure 6. Surface roughness measurements on 5 mm thick specimens, m_A=90 g/min

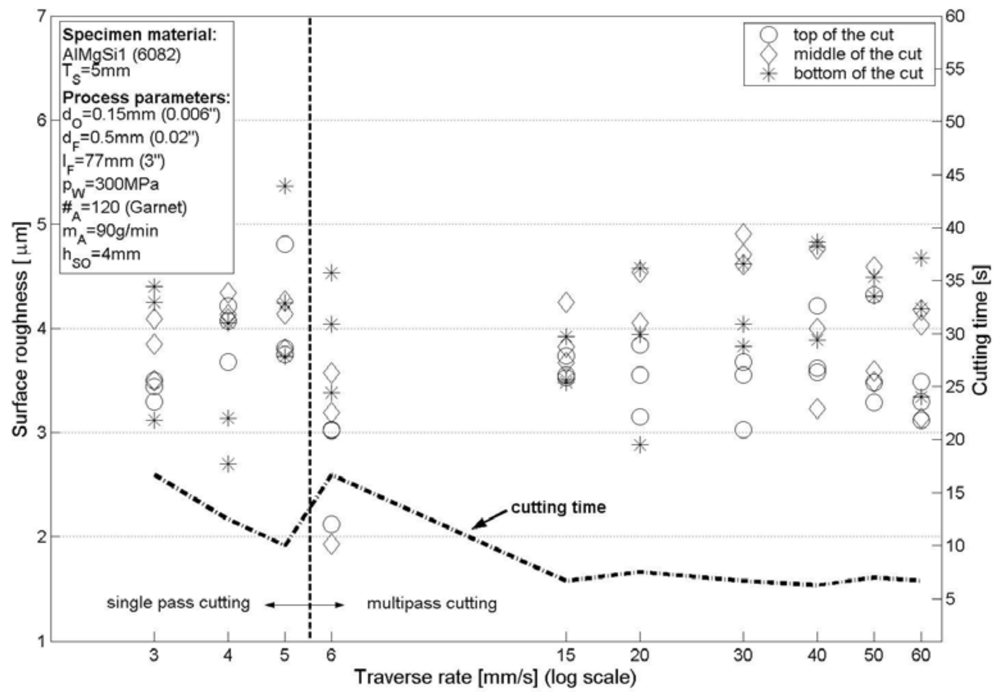

Figure 7. Surface roughness measurements on 5 mm thick specimens

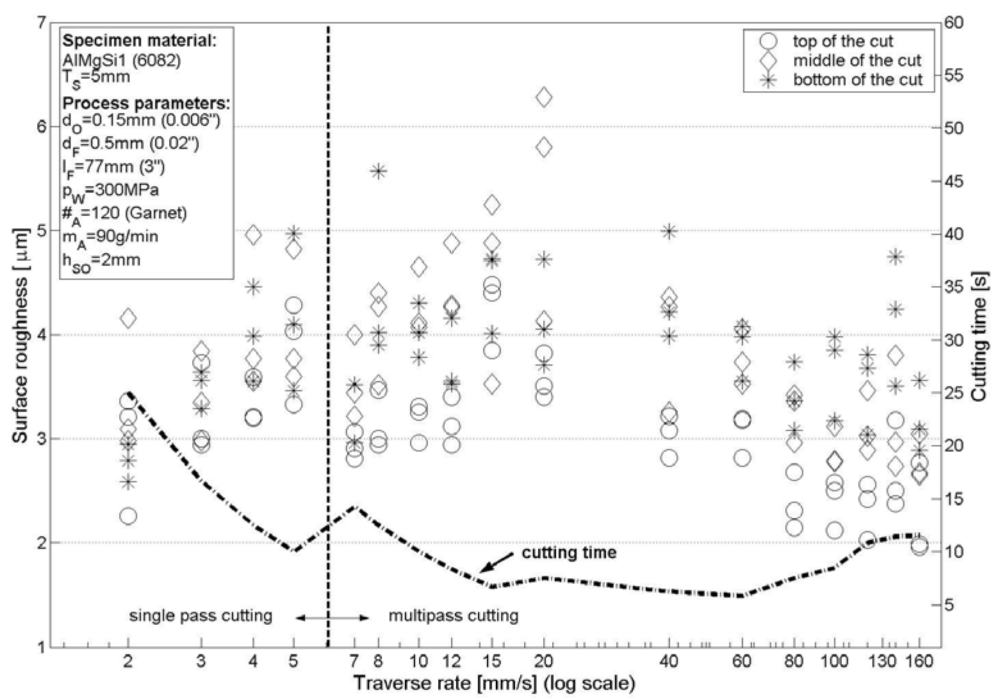

Figure 8. Surface roughness measurements on 5 mm thick specimens

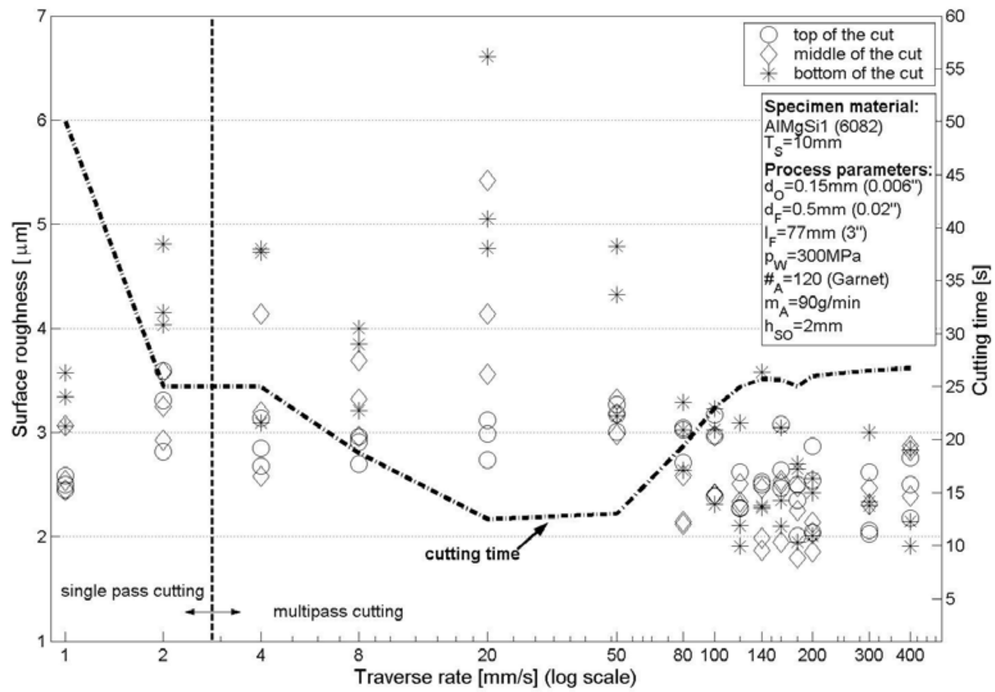

Figure 9. Surface roughness measurements on 10 mm thick specimens

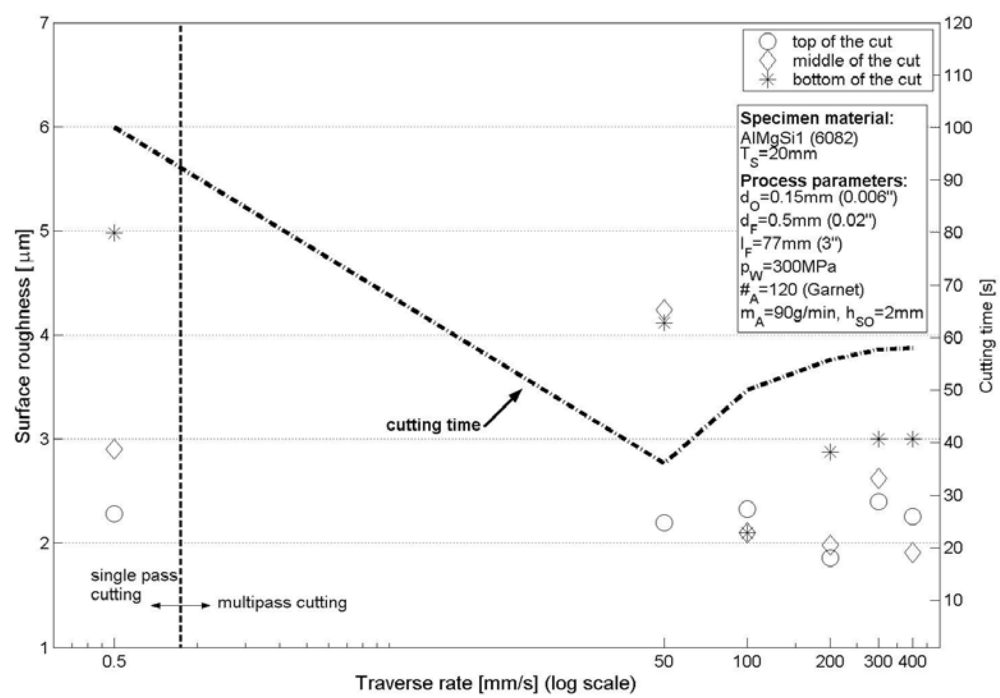

Figure 10. Surface roughness measurements on 20 mm thick specimens

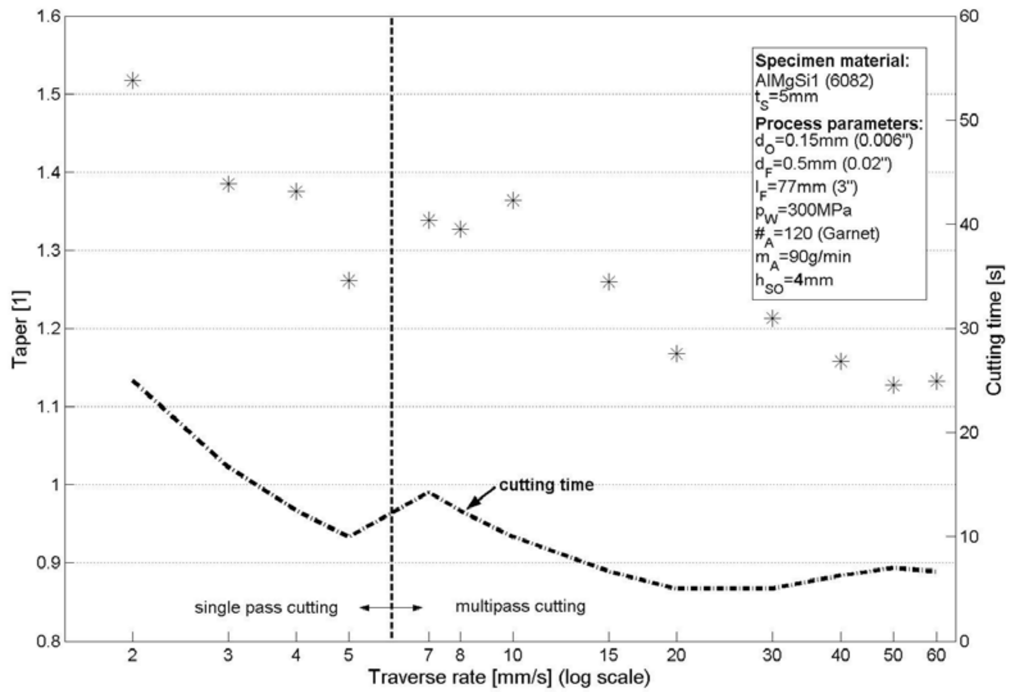

Figure 11. Taper measurements on 5 mm thick specimens with stand-off distance set at 4mm

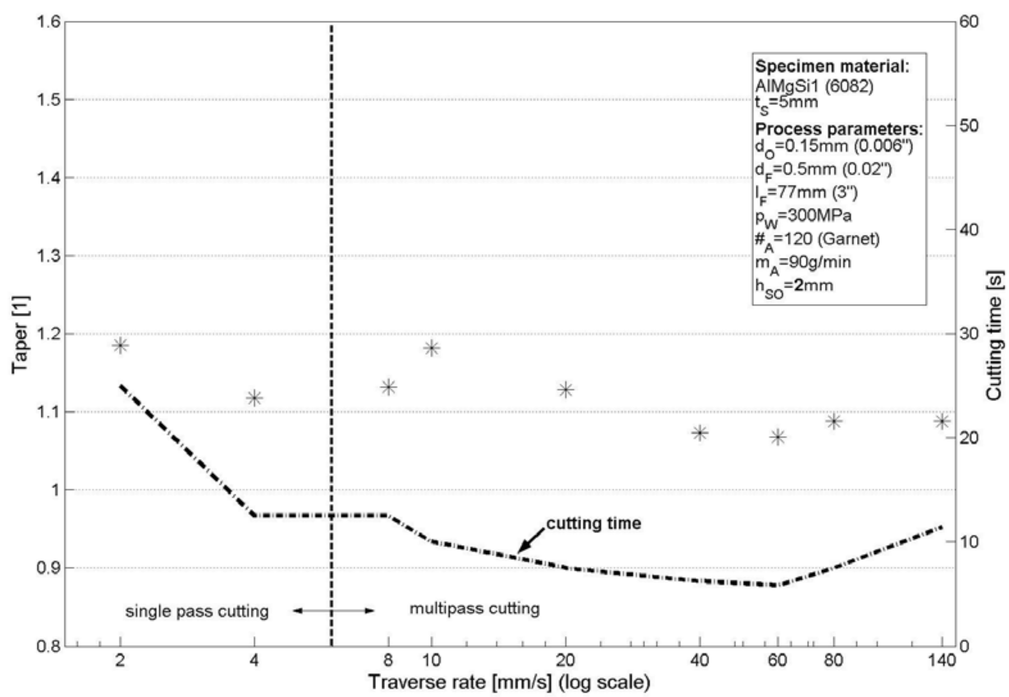

Figure 12. Taper measurements on 5 mm thick specimens with stand-off distance set at 2mm

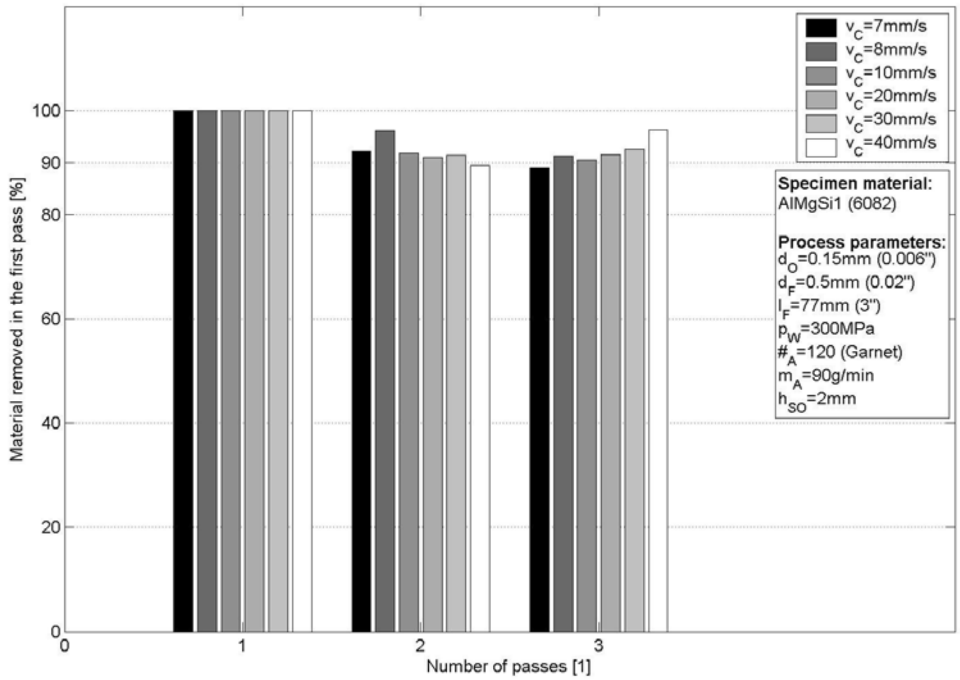

Figure 13. Influence of the number of passes on the material removal rate

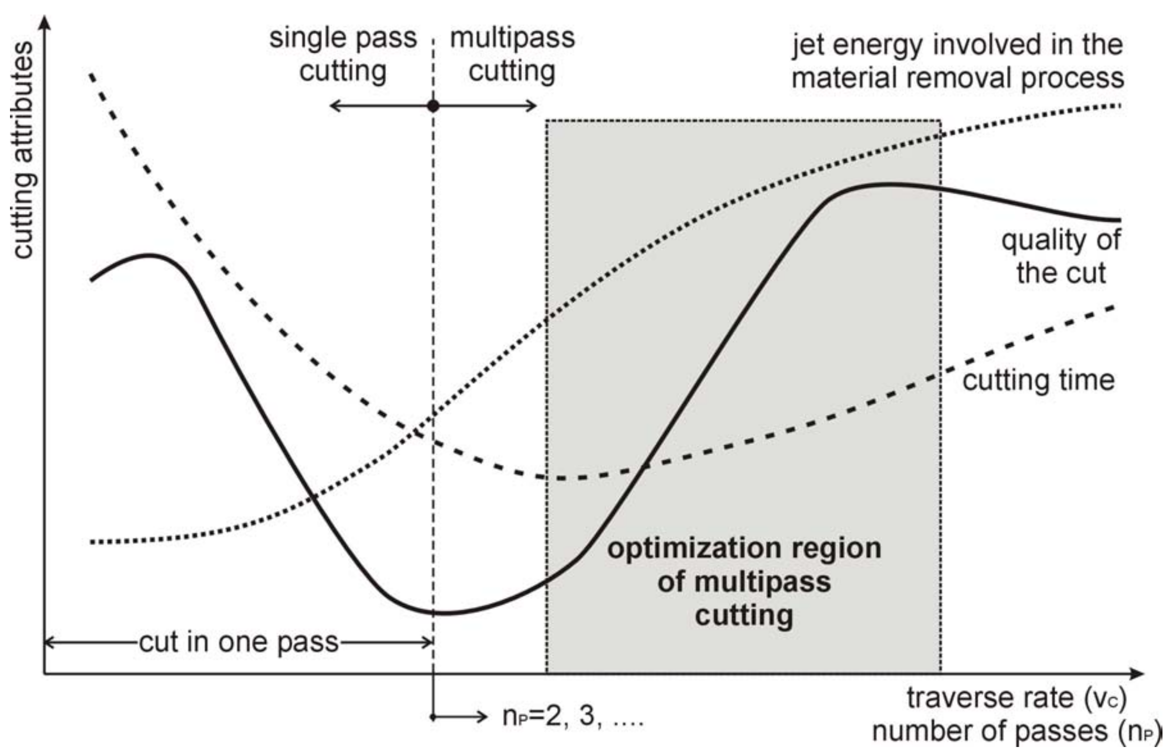

Figure 14. Trends of the observed cutting attributes as function of the traverse rate and number of passes for a given workpiece thickness

2003 WJTA American Waterjet Conference
August 17-19, 2003 • Houston, Texas

Paper 3-A

MODELLING OF WEAR MECHANISMS AT THE ABRASIVE WATERJET CUTTING FRONT

Axel Henning, Engelbert Westkämper

Fraunhofer Institute for Production Engineering and Automation

Nobelstr. 12, 70569 Stuttgart, Germany

henning@ipa.fhg.de

ABSTRACT

The usage of abrasive waterjet has been established in many fields of industrial production. Limitations in performance and surface quality hinder a wider distribution of applications. Especially the formation of structures at the cutting edge has been identified as a major limiting factor. Better understanding may here result in control and optimal usage of the immanent physical processes and may lead to higher cutting efficiency.

In this paper new approaches to modeling the abrasive waterjet cutting process are elaborated. Starting with the particle impact zone the geometrical constraints of the process were analyzed and the primary impact zone was simulated. After the first impact the particles flow along the curve of the leading cutting front. The processes that are involved in the secondary impact zone at the cutting front were analyzed by simulating the motion of the particles along the curve. From this new information about the active erosion processes could be derived. With this a better understanding of the participating processes new approaches to modeling the abrasive waterjet can be initiated resulting in optimization of the overall outcome in regard of surface quality and cutting performance.

1 INTRODUCTION

Cutting with abrasive waterjet has become a widely used tool in machining special and innovative materials. For meeting the specific demands of industrial production it is essential to optimize the process in regards of both quality of the cutting edge and cutting performance. For this a thorough understanding of the processes that are involved in the generation of the cutting edge surface is necessary.

Modelling of the process behavior plays an important role for the industrial use of the technique. With the information jet parameters can be chosen and adapted to the actual cutting task. Also for integration in CAM systems process modelling is necessary. With the strongly growing distribution of this technique and demands for higher precision and performance the control of the process and the knowledge of geometry which can be expected become more and more important. Because of the very complex and often nonlinear behavior of the cutting contour for modelling the cutting process is mostly reduced to few significant parameters with limited range. There are three basic approaches to modelling of the cutting contour: functional, analytical, and phenomenological (Westkämper, 1999). Functional models reduce the process to a functional relationship between input and output data with empirically determined factors and exponents (Kovacevic (1994), Hashish (1988), Kim&Zeng (1992)). Analytical approaches describe the effect of the impact of single particles on the cutting contour. The distribution and the energy of the particles is calculated from hydraulic parameters and flow patterns of the jet (e.g. Kovacevic, 1996). Analytical and functional models are good for quantitative description of the process outcome but do not describe the geometrical behavior of the process. Phenomenological models put an emphasis on the proceeding of the process. Here cyclic step formation could be found resulting in lateral and transversal propagation of the process (e.g. Hashish, 1988, Henning (2001)).

First descriptions of the dynamic process were given by phenomenological models (e.g. Hashish (1988), Blickwedel (1990), Guo (1994)). According to those the quasi-stable and approximately cyclic progress of the cutting process the cutting plane is formed by step propagation. By the use of high-speed cameras (Figure 1) first detailed information about the process and the step propagation could be gathered (e.g. Hashish (1985), Ohlsen (1995)). A complete understanding of the processes that are involved in particle- workpiece- interaction is not provided yet.

2 ABRASION PROCESSES

Analytic approaches to understanding of the workpiece-particle interaction describe the qualitative effect of individual abrasive particle impacts at the workpiece. From hydraulic parameters the energy distribution and thus the erosion effect of particles is calculated (e.g. Niu, 1997, Fukunishi, 1995). With this complex system however only few of the relevant parameters are considered. With the help of time discrete simulation of the erosion process the process is represented qualitatively and adapted quantitatively with processing and mateMost approaches to modeling the erosion effects and wear characteristics are based on early works of Finnie (1959, 1972, 1995) and Bitter (1963). Based on experiments and theoretical considerations the wear behavior of particle impacts was evaluated. In principle they agree on different erosion mechanisms to take part in the overall process: Deformation and Cutting wear.

Neilson and Gilchrist (1968) simplify the equations to

Cutting wear:
$$W_C = \tfrac{1}{2} m \frac{(v \cdot \cos\theta)^2 - v_P^2}{\Phi} \tag{1}$$

$$W_{C1} = \frac{m}{2\Phi} v^2 \cdot \cos^2\theta \cdot \sin\left(\frac{\pi}{2} \cdot \frac{\theta}{\theta_0}\right) \quad \text{for } \theta_0 \le \theta \tag{2}$$

Deformation wear:
$$W_D = \tfrac{1}{2} m \frac{(v \cdot \sin\theta - K)^2}{\varepsilon} \tag{3}$$

Where K is the velocity component normal to the surface below which no erosion takes place and v_P is the residual parallel component of particle velocity at small angles of attack respectively. With the factor v_P the steep rise of the wear characteristic is described resulting in zero erosion at parallel impact ($\theta=0°$) and maximum erosion at θ_0. The factors Φ and ε represent the energy needed for removal of one mass unit of the bulk material for either mechanism. These factors of course strongly depend on material and particle properties and have to be experimentally evaluated (Figure 2As it is shown in Figure 2 and Figure 3 in erosion of materials mostly different mechanisms take place simultaneously. According to the specific material properties the weighting of the different mechanisms differ. Microcracking occurs when highly concentrated stresses are imposed by abrasive particles, especially in the surface of brittle or quasi-brittle materials. Large debris are detached from the surface due to crack formation and propagation. Microploughing and microcutting are the dominant mechanisms in more ductile materials. The proportion of wear groove volume deformed and built up on the sides, i.e. the ratio between microcutting and -ploughing depends on the attack angle of the abrasive particle. Below a specific attack angle and for softer material only microploughing occurs (see Figure 3a/b). (zum Gahr, 1987)

3 PRIMARY IMPACT SIMULATION

With abrasive waterjet cutting the abrasive particles are accelerated in the mixing chamber and focussing tube onto a flat surface. Previous studies (Ojemertz (1993), Henning (2000)) have shown that the distribution of particle effects on the workpiece can be described with a gaussian bell function.

$$J(x,y) = \frac{N}{\sqrt{2\pi\sigma^2}} \cdot e^{-\frac{(x^2+y^2)}{2\sigma^2}} \tag{4}$$

With this function the jet can be divided into different concentric areas. Within the inner circle of a radius of the size of the variance $r=\sigma$ 68% of the jet effect takes place. Within a radius of $r=2\sigma$ the accumulated effect is 95% and within $r=3\sigma$ more than 99% of the effect takes place. These are displayed in the figures as crosshair circles on the probe.

As described above the wear effect does strongly depend on the angle of impact $F(\theta)$. With the surface being subject to temporal change with the advancing process and a linear movement of the jet with the federate u the process can be described with

$$\frac{\partial}{\partial t} S(r,t) + u \cdot \frac{\partial S(r,t)}{\partial x} = J(r) \cdot F(\theta) \qquad (5)$$

In the simulation we used three different functions for the effect of the impact angle:

1. no effect of impact angle:	$F_1(\theta) \equiv 1$	(6)
2. brittle behavior:	$F_2(\theta) = \sin^2 \theta$	(7)
3. ductile behavior:	$F_3(\theta) = \cos^2 \theta$	(8)
4. ductile behavior (Finnie with θ_0=18,34°):	$F_4(\theta \geq \theta_0) = \cos^2 \theta + \frac{1}{3} \sin^2 \theta$ $F_4(\theta < \theta_0) = \sin(2\theta) - 3 \sin^2 \theta$	(9)

With each of these functions the impact of a normal distributed jet was simulated. It appeared that the choice of function had a strong impact on shape and depth of the primary kerf. With this simulation any effect of curvature and secondary impacts was neglected.

From the simulated surface (Figure 4a) the angle of impact (Figure 4b) and the spatial curvature (Figure 4c) can be derived. The colors of the surface in Figure 4b and c represent the impact angle and the curvature. It can be seen that the impact angle takes values above 30° only at the outer rim of the kerf, where little interaction takes place. The curvature is positive at the upper leading edge and becomes negative at the bottom.

With the application of the different functions of the impact angle at the primary impact simulation a quite differentiated picture is drawn. With such the material properties do not only have an effect on the depth of the primary kerf but also on its shape.

In Figure 5a in the left pictures the simulated impact angle is displayed for different angular functions. As could be seen in Figure 6 large impact angles only occur at the outer rim of the cutting edge, which had been referred to as initial damage zone in previous studies (see Momber, 1997). For all three different types of simulation the impact angles within the inner two circles where the most effect of the jet is active the impact angles were 20° and lower. Within the inner circle the impact angle was lower than 5°. In Figure 5b the curvature is shown. It changes from large positive values at the leading cutting edge to large negative values at the rear position. This area of negative curvature is of most interest when evaluating the secondary impact situation.

For all different simulations on ductile behaving materials the overall effective impact angle was very small so that rolling and sliding of the particles must be considered as the consecutive wear mechanism.

4 GEOMETRICAL CONSIDERATIONS

The very process of structure and thus striation formation has a major effect on the outcome of the geometry of the cut and on the quality of the cutting edge. So far deepest insights could be gained with the visualization of the cutting front in transparent material (e.g. Hashish, 1986). It could be found that the process of structure formation seems to be very stable so that even after disturbances (e.g. abrasive mixing problems) the structure comes back to its steady state. These structures remain the same over long cutting distances, only depending on external parameters (hydraulic, material, etc.). Therefore it is the aim of this approach to gain a better understanding about the mechanisms that take place in the secondary impact zone.

When taking a look at the behaviour of curvature of any function that fulfils the constraints for cutting fronts/ striation patterns as we know it from experiments we can see interesting features. As a set of functions we evaluate polynominal functions with $y(0)=0$ and $y'(0)=0$ resulting in

$$\begin{aligned} y(z) &= \frac{a}{n}\cdot z^{n} \\ y'(z) &= a\cdot z^{n-1} \\ y''(z) &= \frac{a}{n-1}\cdot z^{n-2} \end{aligned} \tag{10}$$

The curvature is the change of direction of the tangent vector over the arc length

$$\kappa = \lim_{P_2 \to P_1} \frac{\theta(P_2)\text{-}\theta(P_1)}{\overset{\frown}{P_2 P_1}} \tag{11}$$

It can also be calculated from the inverse of the radius of the curve with the derivatives of the function over z.

$$k = \rho^{-1} = \frac{y''}{(1+(y')^2)^{3/2}} \tag{12}$$

Here the curvature is

$$\kappa = \frac{\frac{a}{n-1} z^{n-2}}{\left(1+a^2\cdot z^{2n-2}\right)^{3/2}} \tag{13}$$

In Figure 9 the curvature, its slope over the arc length and the change of slope is displayed. It becomes clear that for the exponent n=2 the curvature decreases in linear manner. With other exponents that would fulfil the constraints as well the curvature shows a curved behaviour and also positive values for n<1 that would cause the particles to leave the cutting edge. For the whole (unified) arc length of the cutting edge the slope of curvature is almost constant (Figure 9b) and the change of slope changes from positive to negative values at the exponent n=2 (see Figure 9c).

The curvature is a measure for the difference between the impacting angle θ_1 and the exiting angle θ_1 for all contacts of particles with the workpiece in the cutting front (see Figure 8). Linear decrease of the curvature can thus be interpreted as a change of impacting conditions that lead to reduced exiting angles at which further erosion on this part of the cutting front is not likely to occur and the particles flow further down the cutting front without loosing much of their energy.

In experiments of previous works (Henning, 2001) and from other authors (see Momber, 1997) a second order parabolic shape of the cutting front has been identified before (see also Figure 1). When analyzing the shape of striation a linear behaviour of the striation displacement could be found in the secondary impact zone (Figure 7) crossing a threshold value kc. This threshold value kc was experimentally detected in modulated cutting (Ditzinger, 2000). In conventional cutting the leading angle of the primary profile is very small, so that kc can be neglected there (z->z*).

$$\frac{\Delta y(z)}{\Delta z} = 2c_1 \cdot (z - k_C) + c_2 \quad \Delta z = 2\text{mm} \tag{14}$$

With integration over z*=z-kc we get the shape of the cutting front:

$$\begin{aligned} &\text{Curve:} && y(z^*) = c_1 (z^*)^2 + c_2 (z^*) + c_3 \\ &\text{Slope:} && \frac{dy}{dz} = c_1 \cdot z^* + c_2 \\ &\text{Change of slope:} && \frac{d^2y}{dz^2} = c_1 \end{aligned} \tag{15}$$

with $y(0) = 0$ and $y'(0) = 0$ the constants c_1=c_2=0. The curvature k of the cutting front is the change of the angle of the tangent to the curve over the arc length and not over the cutting depth.

$$k = \frac{c_1}{(1 + (c_1 z + c_2)^2)^{3/2}} \tag{16}$$

With the slope of the curve being the tangent of the angle of the curve $y'(z) = \tan\theta(z)$ and $\cos\theta = (1 + \tan^2\theta)^{-0.5}$ one can write for k for monoton rising functions with $y''(z) \equiv c_1$

$$k(\theta) = c_1 \cdot \cos^3\theta(z) \tag{17}$$

Thus the curvature of the cutting front decreases with the arc length of the cutting front. The curvature strongly correlates with the curve angle of the cutting front. In many works (e.g. Guo (1994), Kim& Zeng (1992)) it has been reported that the exit angle is typical for every cutting condition. With this analysis it can be stated that there is with this characteristic exit angle also a lower limit of curvature for the secondary impact zone. After reaching this curvature within the limit cycle the type of volume removal mechanism of the particles most likely changes again. For further investigation of this the movement and the energy of the particles has to be analysed.

5 PARTICLE MOVEMENT

The shape of the cutting front and its extend implies that the process of abrasive waterjet cutting is subject to multiple action of the particles. The area of jet lag cannot result from primary impacts only. In previous studies different approaches to modelling the processes in the secondary impact zone have been addressed (Momber, 1997). Due to the nature of the process a closed modelling of the process is not possible because of turbulence within the acceleration process and because of a wide distribution of particle sizes and shapes. Also the trajectories of the particles cannot be described discretely. In general there are two different physical mechanisms for particles to cause wear on a surface. They can either impact like in the primary zone or slide on the surface. In the real process it will always be a combination of small angle impact and sliding wear. In the following simulation the particles are considered of spherical shape and a uniform diameter.

Both the angle of impact and the rotational speed of the particles play an important role on the amount of wear at the cutting edge. For the simulation full contact at the whole cutting front was assumed leading to pure friction on the surface. With such the curvature of the curve plays a most important role. The normal forces that cause the particle to act on the surface is the centripetal force $F_N = k \cdot m \cdot v^2$ resulting in a tangential friction force $F_R = \mu \cdot F_N$.

With the curvature k=k(s) and the velocity v=v(s) being subject to change over the arclength of the curve s. With the angular momentum one can write for the rotational velocity

$$\omega = \frac{r}{\Phi} \int \frac{F_R}{v - \omega r} ds \tag{18}$$

The frictional work along the arc length of the cutting front is

$$W_{Friction} = \int \frac{F_R (v - \omega r)}{v} ds \tag{19}$$

This leads with the energy conservation

$$W_{kin\,0} = W_{Translation} + W_{Rotation} + W_{Friction} \tag{20}$$

to the differential equation for the contact situation

$$\frac{m}{2}\left(v_0^2 - v(s)^2\right) = \frac{\mu^2 r^2 m}{2\Phi}\left[\int \frac{k(s)^2 \cdot v(s)^2}{v(s) - \omega(s) r} ds\right]^2 + 2\mu \int k(s) \cdot v(s) \cdot (v(s) - \omega(s) r) \cdot ds \tag{21}$$

In Figure 10 the numerical solution of this differential equation is displayed for an initial velocity of the particle of v_0=400m/s and no initial rotational speed ω_0=0. A parabolic shape as described in the previous chapter is assumed. The kinetic energy of the particle is transformed into rotational energy and energy loss due to friction (Figure 10a). With this the velocity of the particle is reduced while the rotational speed increases until the difference between the circumferential speed becomes very small (Figure 10b). In this situation the particle rolls over the surface without significant friction. After that point wear through friction is unlikely to occur- a different mechanism of wear has to come into action here going along with a change in surface structure visible on the cutting edge.

6 DISCUSSION AND CONCLUSION

Understanding of the mechanisms that lead to the formation of the cutting edge and the striation patterns is an essential part for further optimisation of the cutting process and thus improvement of both cutting quality and performance.

In the first part of this paper the focus was laid on the primary impact situation where accelerated particles first impact on the workpiece. Based on erosion analysis from literature the qualitative effect of the jet could be simulated. It could be shown that for most particle-workpiece interactions the impact angle is very small resulting in a steep top part of the cutting front. The shape of the cutting front – and here especially the medium angle- depends on material properties (brittle/ductile, hardness, yield stress, etc). This complies on the one hand with many experimental and phenomenological studies of the cutting front and striation structures. On the other hand this suggests that not micro-cracking and -cutting, but ploughing is the dominant wear mechanism in this process zone. This shallow angle impact has also a large effect on consecutive processes. Large angle impact more likely cause deformation and cracking at the impact with most energy transferred to the workpiece. The particles deflect at large exit angles with small amount of residual energy and will most likely not cause any consecutive abrasion. With small angle impact most of the kinetic energy remains with the particle in translatoric and rotatoric energy. Depending on the impact situation (angle, curvature, roughness, etc.) a part of the kinetic energy is used by friction between workpiece and particle resulting in accelerated rotation and erosion. Since most of the kinetic energy remains with the particle it can cause multiple shallow angle impacts when flowing down the cutting edge. A most important factor of particle-workpiece interaction here is the curvature of the cutting front. At high curvature the normal load on the particle is higher resulting in accelerated abrasion e.g. at steps. At negative curvature the particles loose contact with cutting edge and leave the process zone.

With all contacts the particles are subject to friction and therefore will be rotationally accelerated. At every contact the particles change their direction resulting in a curved cutting front. If for all contact situations the impact and exit angle would be the same the cutting front would have same curvature from top to bottom. As both velocity and rotational speed of the particle change the exit angle changes to smaller values resulting in a monotone decrease of curvature. The second order parabolic shape of the cutting front that has been observed in many studies before offers best constraints with a linear decrease of curvature.

The amount of frictional work depends on the contact length and therefore on the difference between the translatorical velocity and the circumferential velocity. At pure rolling behavior the difference is zero resulting in minimal friction and therefore minimal abrasion of the particle. At this point the particle can not transfer any energy through tribological mechanisms even though the kinetic energy may still be very high. At this point a second bifurcation of the abrasive cutting process is most likely to occur and boring processes that are known from phenomenological studies are initiated.

With these new modelling approaches new insights in the participating processes of abrasive waterjet cutting could be gained. Further analytical and experimental work is necessary here in order to apply the new approaches to different materials and cutting situations and to transform the qualitative description of mechanisms to quantitative models of the cutting process. With this new understanding of the processes new approaches to improve both the quality of the cutting edge and the cutting performance may be possible qualifying this brilliant technique for even more innovative applications.

7 ACKNOWLEDGEMENT

We gratefully acknowledge the support of the Volkswagen Foundation in this project.

8 REFERENCES

Bitter, J.G.A. (1963) A Study of Erosion Phenomena, Part I & II, Wear 6, 5-21, 169-190

Blickwedel, H. (1990) Erzeugung und Wirkung von Hochdruck-Abrasivstrahlen. Fortschrittsberichte VDI - Reihe 2, Nr. 206. Düsseldorf, VDI-Verlag 1990 Zugl. Dissertation, Universität Hannover, 1990

Ditzinger, T.; Friedrich, R.; Henning, A.; Radons, G. (1999): Non-Linear Dynamics in Modeling of Cutting Edge Geometry. Proceedings of the 10th American Waterjet Conference, Houston, USA, S. 15-32

Engel, P A, Impact wear of materials, Amsterdam-Oxford-New York 1976

Finnie, I. (1959); An experimental study of erosion, Wear, Volume 3, Issue 1, Page 76

Finnie, I. (1972); Some observations on the erosion of ductile metals, Wear, Vol. 19, Issue 1

Finnie, I. (1995), Some reflections on the past and future of erosion, Wear 186-187 (1995)

Friedrich, R., Radons, G., Ditzinger, T., Henning, A. (2000)." Ripple formation through a convective instability from moving and erosion sources", Physical review letters 85, 4884

Fukunishi, Y. et. al. (1995) ;Numerical simulation of striation fornations on waterjet cutting surface, In: Proceedings of the 8th American Waterjet Conference 1995, Houston Texas

Guo, N.S. (1994), Schneidprozess und Schnittqualität beim Wasserabrasivstrahlschneiden. VDI-Fortschritt-Berichte, Reihe 2, Nr. 328,

Hashish, M. (1988), „Visualization of the abrasive waterjet cutting processes," Experimental mechanics 45, 159 (1988), 159-169.

Henning, A. (1998) ;Cutting edge quality improvements through geometrical modelling, 14th International Conference on Jetting Technology, Brugge, Belgium.

Henning, A.; Anders, S. (1998): Cutting-edge quality improvements through geometrical modelling. In: Papers presented at the 14th International Conference on Jetting Technology, Brugge, Belgium, pp.321-328

Henning, A.; Westkämper, E. (2000) Modelling of contour generation in abrasive water-jet cutting. In: Jetting Technology : Papers presented at the 15th International Conference on Jetting Technology, Ronneby, Sweden, 6-8 September 2000, S. 309-320

Hutchings, I M (1976), Some Comments on the theoretical treatment of erosive particle impacts, Proc. 5th Int. Conf. On Erosion by Solid and Liquid impact, 36.1-6

Zeng, J; Kim, T. (1992) Development of an abrasive waterjet kerf cutting model for brittle materials, in Proceedings of the 11th International Conference on Jet Cutting Technology 1992, pp. 483-501.

Kovacevic, R. ; Yong, Z. (1996) ;Modelling of 3D abrasive waterjet machining; 13th International Conference on Jetting Technology; Oct. 29-31, 1996 ; Sardinia, Italy

Kovacevic, R.; Fang, M. (1994) ;Modelling of the influence of the abrasive waterjet cutting parameters on the depth of cut based on fuzzy rules, International Journal Machine Tools Manufacturing, vol. 34, no. 1, 1994, pp. 55-72.

Hashish, M. (1984) On the modelling of abrasive waterjet cutting, in Proceedings of 7th International Symposium on Jet Cutting Technology 1984, Ottawa Canada, pp. 249-265.

Hashish, M. (1988) Visualization of the abrasive waterjet cutting processes, Experimental mechanics, Jun. 1988, pp. 159-169.

Momber, AW, Kovacevic, R. (1997) Principles of Waterjet Cutting, Springer Verlag, Berlin

Neilson, J H and Gilchrist, A, Erosion by a stream of solid particles, Wear, II (1968) ,111-122

Niu, M. ; Fukunishi, Y. ; Kobayashi, R. (1997) Experimental and numerical studies on the mechanism of abrasive jet cutting ; 9th American Waterjet Conference ; August 23-26 ; 1997 ; Dearborn, Michigan

Öjmertz, C (1993), Abrasive waterjet milling: An experimental investigation; 7. American Waterjet Conference, 1993, Houston

Rumpf, H, Beanspruchungstheorie der Prallzerkleinerung, Chemie-Ingenieur-Technik 31 (1959), Nr. 5, 323-337

Sawamura,T., Fukunishi, Y. (1998) Study of the abrasive waterjet structure by measuring water and abrasive velocities separately

Sheldon, G L, Finnie, I. (1966), I, On the Ductile Behavior of Nominally Brittle Materials During Erosive Cutting, Journal of Engineering for Industry, pp. 387-392

Tilly, G P (1969), Erosion caused by airborne particles, Wear, 14 (1969), 63-79

Uetz, H. (1986) Abrasion und Erosion. Carl Hanser Verlag München, Wien, 1986.

Westkämper, E.; Henning, A.; Radons, G.; Friedrich, R.; Ditzinger, T. (2000): Cutting Edge Quality through Process Modeling of the Abrasive Waterjet; Proceedings of 2nd CIRP International, Capri, Italy, S. 179-188

Winter, R E and Hutchings I M (1974), Solid particle erosion studies using single angular particles, Wear, 29 (1974), 181-194

Zeng, J. and Kim, T. (1992). „Development of an abrasive waterjet kerf cutting model for brittle materials," in Proceedings of the 11th International Conference on Jet Cutting Technology

Zum Gahr, K H, Microstructure and wear of materials, Amsterdam-Oxford-New York-Tokyo, 1987

9 FIGURES

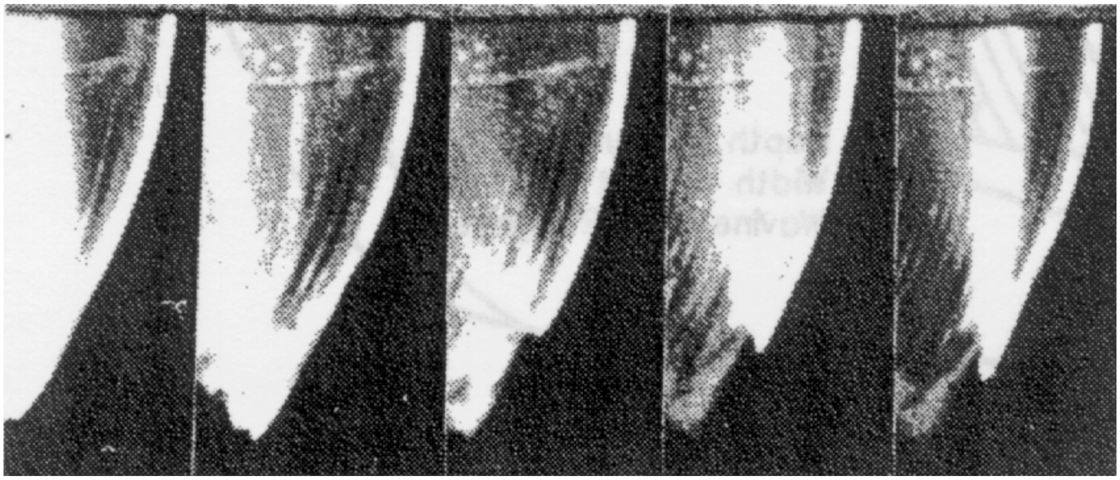

Figure 1: Visualization of step propagation with high speed cameras (Hashish, 1985)

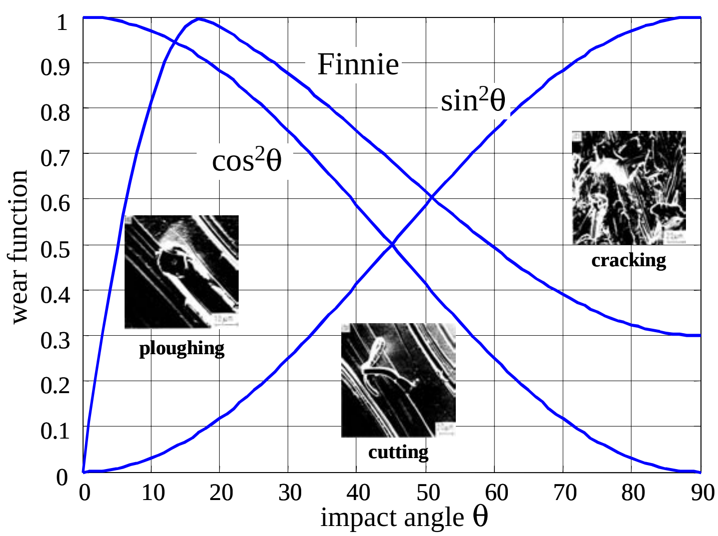

Figure 2: Wear functions for different materials (REM from Gahr, 1987)

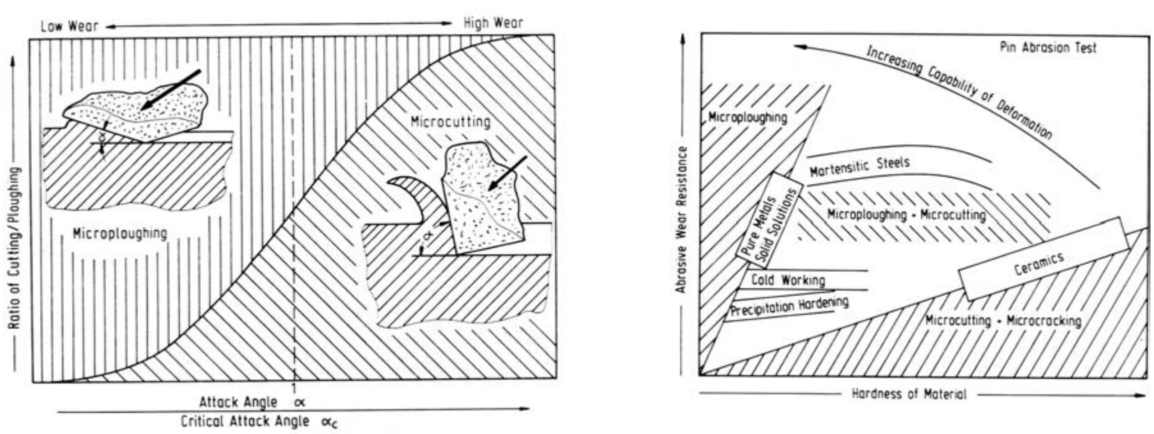

Figure 3: Ploughing, cutting and cracking in abrasive erosion (from Gahr, 1987)

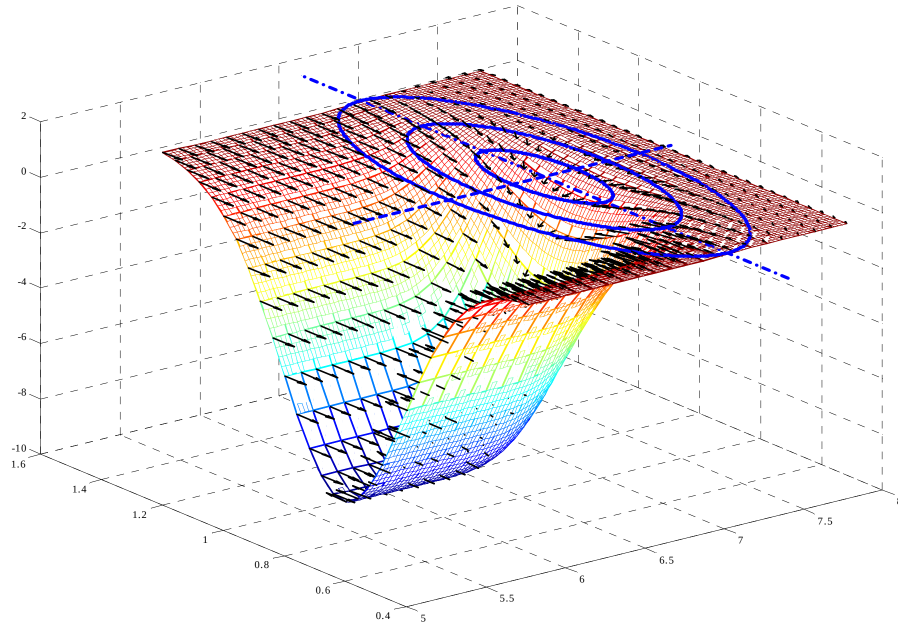

a) Geometry of Simulation

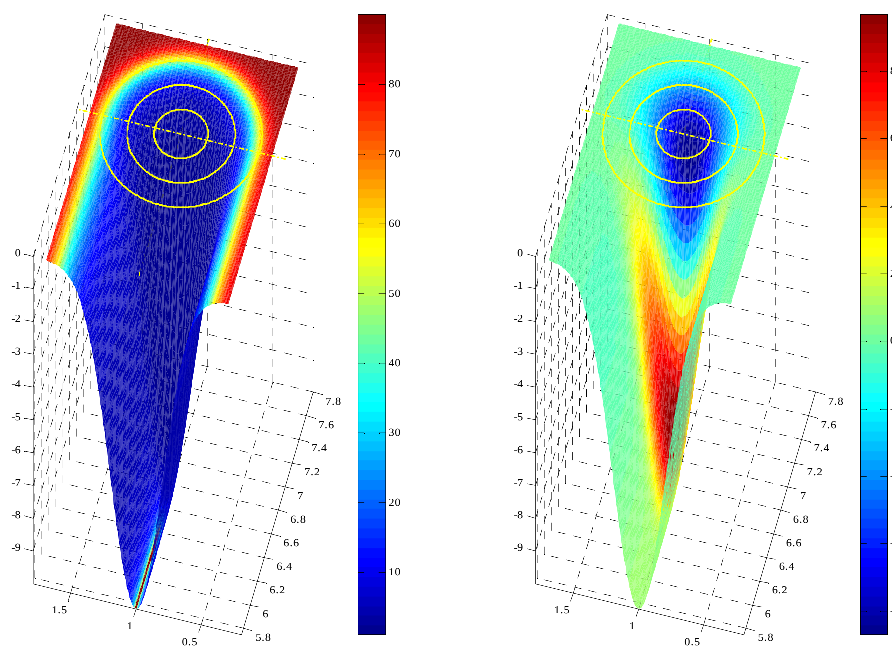

b) Geometry with impact angle shading **c) Geometry with spatial curvature shading**

Figure 4: Simulation of primary impacts

Simulation with no effect of impact angle

(Gaussian shape only)

Simulation with ductile behavior ($\cos^2\theta$)

Simulation of ductile behavior (Finnie equation)

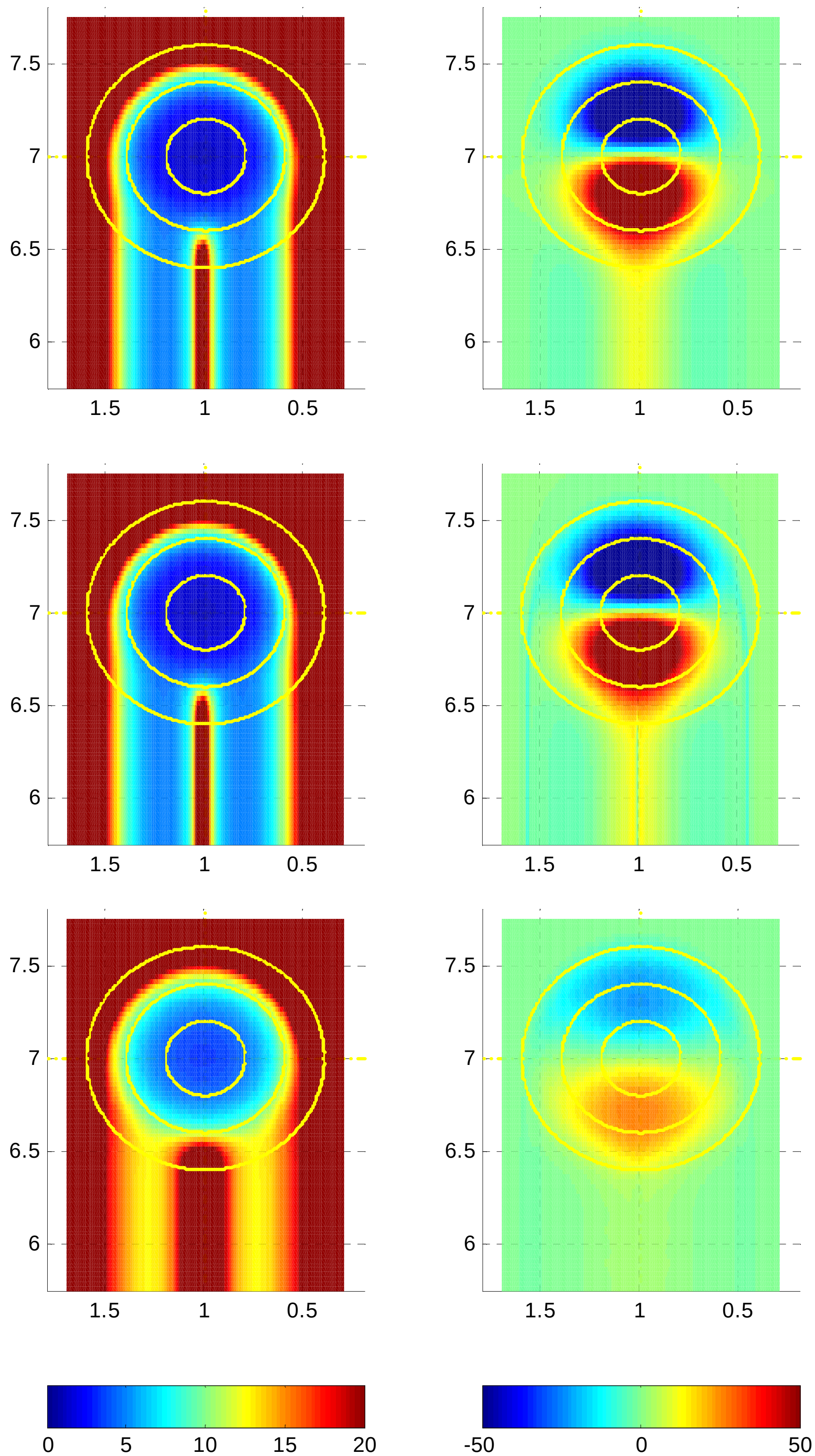

a) impact angle in Degrees **b) curvature in mm^{-2}**

Figure 5: Effect of different materials on primary kerf

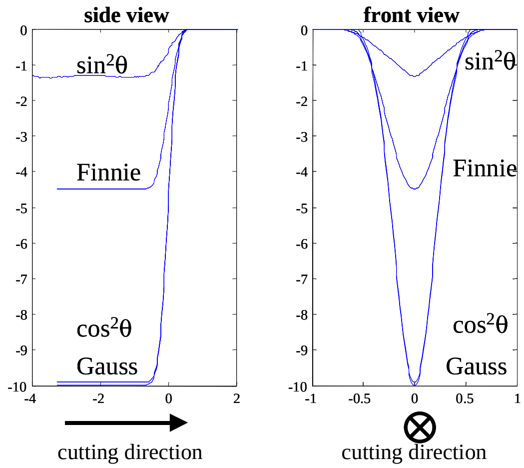

Figure 6: Primary profiles with different material properties

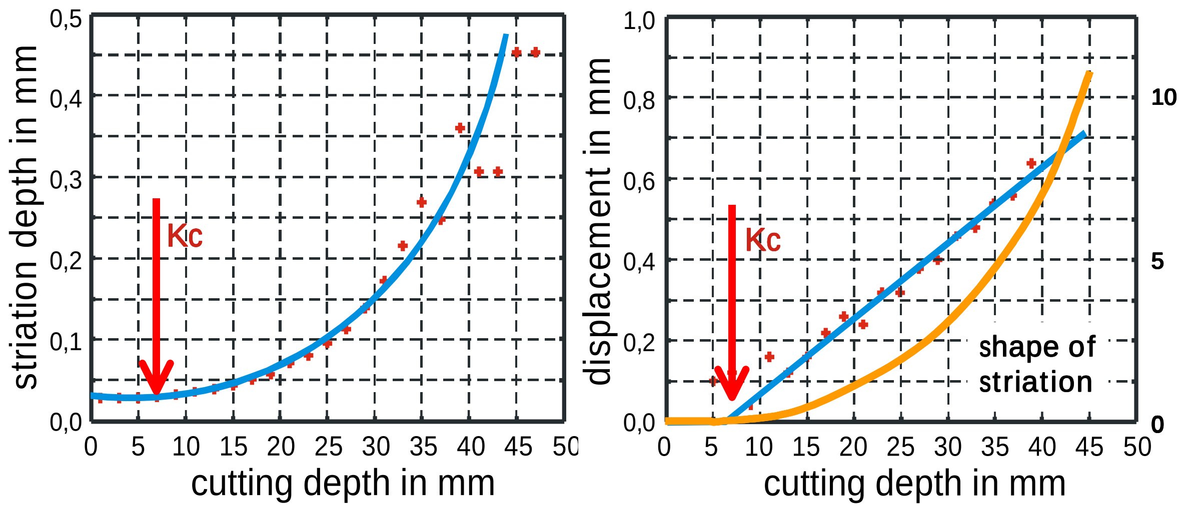

Figure 7: Analysis of striation depth and shape
a) striation depth b) displacement and jet lag

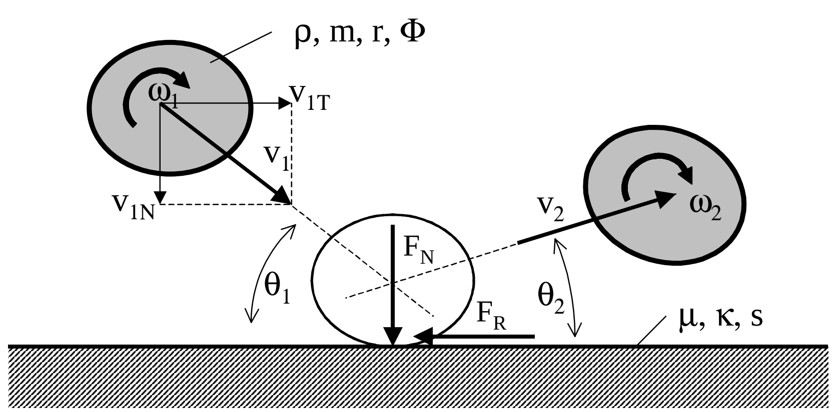

Figure 8: Parameters at impact/ sliding situation

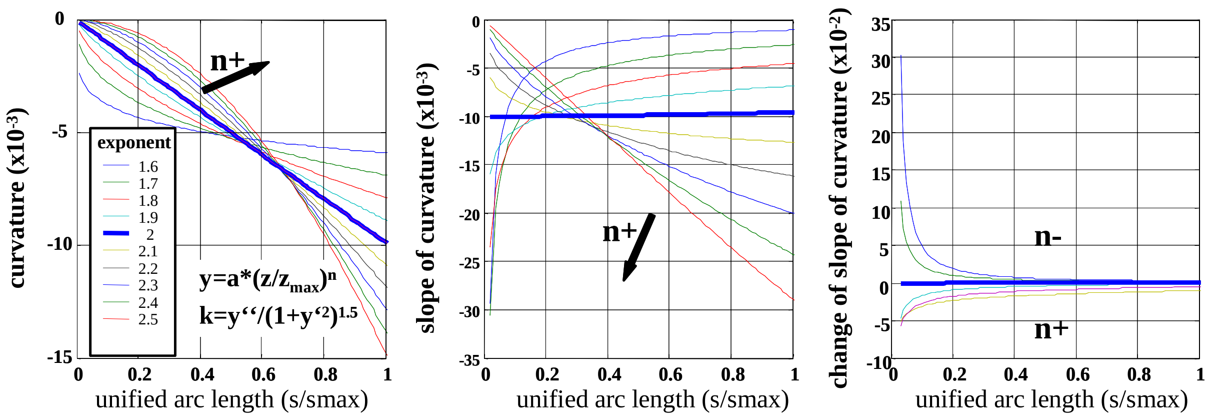

Figure 9: Discussion of curvature at the cutting front

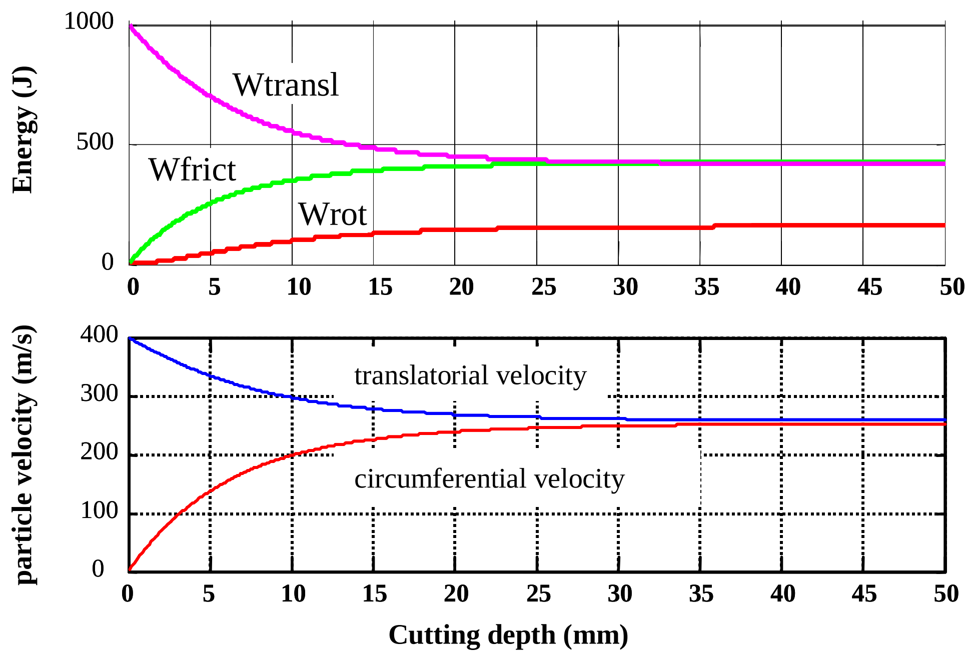

Figure 10: Simulation of particle work and velocity

2003 WJTA American Waterjet Conference
August 17-19, 2003 • Houston, Texas

Paper 3-A

PHYSICAL BASIS OF HIGH-PRESSURE HYBRID WATER-ABRASIVE-ICE JET APPLICATION FOR SURFACE TREATMENT

P. Borkowski
Technical University of Koszalin
Koszalin, POLAND

ABSTRACT

The high-pressure hybrid water-abrasive-ice jet treatment is a new technology that has grown in popularity lately. Such technology is based on a high-pressure abrasive-water jet with addition of dry-ice pellets CO_2. Theoretical basis, including velocity and kinetic energy distributions of solid particles also with thermodynamical ice particles state during hybrid jet creation are discussed in. Using theoretical results, it was build the experimental plant accompanied with suitable equipment. It enables adequate research to achieve that makes possible to determine that very complicated and specific jet erosion mechanism. Tests on a high-pressure hybrid water-abrasive-ice jet are aimed at creation of a good water jet tool used for surface treatment.

Organized and Sponsored by the WaterJet Technology Association

1. INTRODUCTION

Surface treatment using the high-pressure hybrid water-abrasive-ice jet consists in bulk micro-treatment the surface with abrasive grains and ice particles transported with a water jet. Due to high rate of this jet, often aerated to considerable degree, the solid particles obtain the energy necessary to perform a treatment operation. A number of the surface processing technologies based on above have been previously suggested. Another, the adoption of the ice jet technology is determined by the adequate proportion of abrasive and ice particles characterized by specific usable properties.

The firs component of that hybrid jet, which are an abrasive grains, is used for almost a quarter century as an abrasive-water jet and for this reason these problems are well known (Summers D. A., 1995) (Momber A. W., Kovacevic R., 1998) (Borkowski P., 2002**) (Borkowski J., Borkowski P., Kowalewski A., 2001). Thus a noticeable interest in high-pressure cryogenic jets (Hashish M., Miller P., 2000) (Liu H. T., Fang S., Hibbard C., Maloney J., 1999) (Truchot P., Mellinger P., Duchamp R., Kim T. J., Ocampo R., 1991) (Borkowski P., 2001*), abrasive-cryogenic jets (Dunsky C. M., Hashish M., 1996) (Hashish M., Dunsky C. M., 1998) (Borkowski P., 2002*) and ice jets (Galecki G., Vickers G. W., 1982) (Borkowski P., 2003*), has been aroused in recent years. A high-pressure ice jet is created by ice particles driven by a stream of air (Geskin E. S., Goldenberg B., Shishkin D., Babets K., Petrenko K. 2000) (Geskin E. S., Shishkin D., Babets K., 1999), other gas or water (Borkowski J., Borkowski P., 2001) displaced with a great velocity. Ice particles applied to them are produced by freezing of water droplet (Kiyohashi H., Hanada K., 1999) or by crushing the larger ice particles (Shishkin D. V., Geskin E. S., Goldenberg B., 2001) (Liu B.-L., Liu L.-H., Wu L., 1998) or are obtained from dry-ice pellets CO_2 (Spur G., Uhlmann E., Elbing F., 1999). Exactly this technology of ice generation has been wide spread lately. Usually dry-ice pellets are accelerated by compressed air. Owing to that, components of this ice jet escape into the atmosphere leaving merely particles of disposable impurities. In such conditions, the sublimation of CO_2 gas has no influence on erosion mechanism. While hybrid jet treatment, where acceleration medium is a stream of water, such a sublimation process is of great importance (Borkowski J., Borkowski P., at all, 2003).

It is possible to increase the efficiency of surface treatment with a hybrid jet including dry-ice pellets CO_2. It is of great importance especially when fairly hard impurities are to be disposed of. Thus this paper is devoted to investigations on the physical basis of a high-pressure hybrid water-abrasive-ice jet.

2. HIGH-PRESSURE HYBRID JET CREATION

It is possible to assess the phenomena occurring in the process of surface treatment with the high-pressure hybrid water-abrasive-ice jet and determine its physical principles analyzing the quantities describing dynamics of individual solid particles which is a spherical shape. Therefore, the present theoretical analysis of solid particles behavior during their acceleration and interaction with the material was designed for such the sprinkler with a concentric nozzle (Borkowski P., 1997) (Borkowski P., 2001**). Abrasive and ice particles kinetics in the high-pressure hybrid jet and their thermodynamic state and ice (CO_2) sublimation analyses that decide of the ice grain quality as an erosive particle are required.

2.1. Sprinkler building and jet creation

The sprinkler (**Figure 1**) could be adequate equipment that offers such good conditions, which is a countershaft mounted on the typical high-pressure pistol outlet. A sprinkler body 1 with situated inside a concentric nozzle 2 and a tube 3, whereas the adequate pipe stubs are connected with a water inlet and an abrasive inlet. After turning water on, elementary jets flow out through little holes drilled in the front nozzle flange and interfere with each other in the tube 3 sucking in the air which flows through the centre nozzle hole and transport the abrasive from the container. In the sprinkler tube 3 a resultant abrasive-water jet is created, which is a very efficient tool for abrasive-water jet surface treatment (Borkowski P., 2001[***]) (Borkowski P., 2003[**]). During initial testing it turned out that the most important part in high pressure abrasive-water jet creation plays such a concentric nozzle and its tube. The moultioutlet concentric nozzle is a double flange pipe with a few water holes drilled in one of these flanges. It became fundamental to develop optimal constructions of a multioutlet concentric nozzle and a tube that are adapted to a standard abrasive-water sprinkler and enables maximum surface treatment efficiency (Borkowski P., 2001[**]). All examinations gave a lot of results, which most spectacular are connected with cost. This takes into consideration not only technical but also economical aspects of surface treatment process. On the basis of these results it possible to assume that optimized nozzle (Borkowski P., 1997) and tube (Borkowski P., 2001[**]) construction.

2.2. Kinetics of high-pressure water-ice jet

In order to create the high-pressure hybrid water-abrasive-ice jet with high-quality erosion properties it is necessary to know the solid particle behaviour. Therefore it is important to know abrasive and ice particles velocity in the sprinkler outlet, especially in the erosion area and its kinetic energy.

2.2.1. Velocity of abrasive and ice particles

Theory supported on fluid mechanics laws was used to determine the length of solid particles acceleration. Under steady-state conditions of fluid flow, the thrust force of a jet counterbalances the aerodynamic resistance of ice particles causing its acceleration. On that basis (Borkowski P., 2001[*]) (Borkowski P., 2003[*]) it is possible to establish expression describing the maximum velocity of particles in a steady-state jet:

$$v = \left(\frac{u^2 t}{ut + K}\right) \cdot \left(\frac{D_o}{D_x}\right)^2 \eta \qquad (1)$$

It is possible to determine quantities D_o, D_x, η included in these formulas only by the experimental method (Borkowski P., 1997) (Borkowski P., 2001[*]). Considering the above relationship (1) the appropriate calculations of the solid particles flow-velocity in steady-state conditions were carried out. Example results of flow-velocity calculations for abrasive and ice particles in the erosion area 250 mm distant from the sprinkler tube outlet ($\nu_{0.25}$) are presented in **Figure 2**. It is evident that an increase in the sprinkler tube length and water pressure causes an increase in the solid particles velocity.

A crucial conclusion was drawn from these investigations that the abrasive and ice particles velocity both at the sprinkler tube outlet and the erosion area is the fact that abrasive grains velocity is in the range of approximately 30% - 50% higher than ice particles, that all affect on their crush. High-pressure water-abrasive-ice jet created in the cryo-sprinkler with the concentric nozzle (Borkowski P., 1997) inside depends on water pressure and is hardly sensitive for jet aeration. Therefore it is advisable for water-abrasive-ice jet creation to use the sprinkler tube with the length of L_t = 125÷150 mm.

2.2.2. Kinetic energy of abrasive and ice particles

Making use of the above specified abrasive and ice particles flow-velocity it is possible to calculate their kinetic energy E_K in the cutting zone as well, according to the following expression:

$$E_K = \frac{2}{3}\pi \cdot r^3 \rho_o v^2 \ . \tag{2}$$

Diagrams of kinetic energy for abrasive and ice particles in the erosion area 250 mm distant from the sprinkler tube outlet ($v_{0.25}$) are presented in **Figure 3**. As shown in the illustrations, an increase in the sprinkler tube length and the water pressure causes an intensive increase in the kinetic energy of abrasive and ice particles. The above results revealed that, for different dimension of abrasive grains (SiO_2 #60) and dry-ice pellets (CO_2) and consequently their different density, the kinetic energy of dry ice pellets is 300÷500 times higher than the abrasive particles.

2.3. Thermodynamics of dry-ice pellets (CO_2)

2.3.1. The end temperature of ice particles

To evaluate the suitability of ice particles for cleaning one has first of all to get to know a temperature which will have they at respective stages of the process creating the water-abrasive-ice jets. A model of a thermal transient conduction in a system of weak thermal resistance was used to determine a temperature of ice particles.

To obtain an equation allowing calculating the end temperature of ice particles, on the basis of well known Newton’s heat equation, the energy balance should be drawn up. After transformation of the energy balance and calculation of end temperature of ice particles after “heating up” by air during its transport from a container to a sprinkler and with high-pressure water jet, it is possible to determine (Borkowski J., Borkowski P., Chomka G., 2002) (Borkowski P., Chomka G., 2002) the following equation:

$$T_{ie} = T_w - \left[\left(T_w - T_a\right) + \left(T_a - T_i\right) \cdot e^{\frac{-\alpha S}{c\rho V}t} \right] \cdot e^{\frac{-\alpha S}{c\rho V}t} \tag{3}$$

Taking this equations (3) into consideration a series of calculation of ice particles therodynamical states were made which enable to determine suitability of ice particles in the process of cleaning as it is shown on exemplary **Figure 4**.

On the basis of above graphs analyses one can state that the initial temperature of ice grain is a factor strongest affecting the end temperature of ice grain. The next factor regarding their intensive influence on the end temperature of ice grain is their size and a distance between a water-ice jet outlet form a sprinkler tube and the work material. A slighter influence on the end temperature exerts a temperature of water and the next after is water pressure which has the effect on a jet rate and therefore its time of “heating up” of ice particles. A temperature of air has a little influence on the end temperature of ice and the slightest effects exerts the suction pipe length. All that is essential for appropriate construction of the necessary experimental plant.

2.3.2. Problem of ice particles sublimation effect

Dry ice pellets CO_2 accelerated in a high-pressure water jet collide each other and with internal surfaces of pipes and a sprinkler and are impinged by abrasive grains as well. Dry ice pellets CO_2 in consequence of all these collisions undergo a partial sublimation, and therefore such the high-pressure hybrid jet “smokes” with gas CO_2. However, the most intensive sublimation of dry ice pellets CO_2 occurs in an erosion zone because of the collision with the work surface. Thus, the prominent deformation ice-pellet volumes or their disintegration causes that the process of sublimation is taking its course very rapidly, usually nearly explosive in character. The impetuosity of this process results from the fact that gaseous CO_2 is 800 times larger in volume than when it is in the form of dry ice pellets (Borkowski P., 2003[*]) (Borkowski J., Borkowski P., at all, 2003).

Considering this specific character of the ductile impingement of dry ice pellets CO_2 onto the work surface one can assume that kinetics energy of that pellet is totally transformed into the energy of the ice sublimation. That makes it possible to determine the sublimated volume of dry-ice pellets in the course of that collision. It is expressed by the following relation:

$$z = \frac{E_k}{c_s m} \tag{4}$$

Regarding the above, it was found that depending on the pressure of water the volume of dry-ice pellets was sublimated within 1.4 ÷ 7.3%. Then, the volume of gas CO_2 received from a sublimated dry-ice pellet is expressed by the following formula:

$$V_g = \frac{V\,E_k}{c_s m}\delta \cdot w \tag{5}$$

The results of calculations made on the basis of the above relation are presented in a diagram (**Figure 5**). Such the great volume of gas CO_2 generated rapidly in the contact area of dry-ice pellets with the work surface produces a very dynamic increase in the gas pressure. It makes the cracks existing in the surface layer of the workpiece grow and disrupt.

3. HIGH-PRESSURE HYBRID JET STRUCTURE

3.1. Pressure distribution in a jet

The high-pressure water jet structure depends on total-pressure (Matsuyama K., Ueno S., Masutani T., Nishiguchi K., 1995) and abrasive-grain distribution (Mazurkiewicz M., Olko P., Jordan R., 1987). The research on the water jet pressure distribution was carried out using a special piezoelectric dynamometer (Borkowski P., 1997) (Borkowski P., 2003[**]).

It results from the measurements that the high-pressure hybrid abrasive-ice-water jet forms a coating in the shape of a tube with significantly increased water concentration in its external layers. The spatial pressure distribution (**Figure 6**) shows distinct preferred directions, where the hybrid-water jets have the highest pressure. The number of such elementary jets is equal to the number of water holes arranged in sprinkler nozzles. A few times lower pressure prevails between these preferred directions in external layers of the jet. However, the definitely lowest pressure occurs in internal layers of hybrid abrasive-ice water jets.

3.2. Solid particles distribution in a jet

The second very important factor that determines the high-pressure hybrid jet structure is abrasive and ice particles distribution. The abrasive grain distribution in a cross-section of the jet was examined by adequate counting of scratches made by grains remaining on the workpiece surface treated with the abrasive-water jet. It is the latest ten-circular stratified-cellular method (Borkowski P., 2002[**]), which is an update of the previous ten-circular stratified method (Mazurkiewicz M., Olko P., Jordan R., 1987) developed by M. Mazurkiewicz and his coworkers and its upgrade referred to earlier own works (Borkowski P., 1997).

Some examples of experimental results are presented in **Figure 7**. It results from these spatial plots that the highest number of abrasive grains flows along the axis of an abrasive-water jet where the lowest total pressure prevails. Whereas, on increasing the distance from the axis, the flow rate of abrasive grains was decreased. The lowest number of grains was present in external jet layers where the highest pressure prevailed. Definitely, the highest density of solid particles distribution is characteristic for the internal layers of a hybrid jet, where the water pressure is the lowest one. It was also confirmed that an increase in the number of water holes in a sprinkler nozzle leads to an increase in flow rates of solid particles.

On the basis of pressure distribution in a hybrid jet analysis, it is expected that dry-ice pellets distribution CO_2 are similar to abrasive grains (**Figure 8**). However, taking into consideration ice grains dimension (size), their number is considerably smaller than for abrasive once. For example, in practical conditions of a hybrid jet formation, the abrasive grains consumption is in the range of 100 kg/h and 150 kg/h of dry-ice particles respectively. In such conditions, for one ice grain erosion accompany of approximately 70 abrasive grains. Therefore all that proportions are important for treatment mechanism.

4. HIGH-PRESSURE HYBRID JET INFLUENCE ON WORKPIECE

4.1. Experimental plant and equipment

Taking into consideration above theoretical analysis results it was build the suitable experimental plant, exemplified by **Figure 9**, is to be applied. This plant includes a valve 1 supplying municipal water to a cooler 2 where it is pre-cooled. A high pressure pump 3 enables to obtain a water jet at adequate pressure which is stabilized by a control system 4. This jet is once again cooled in a cooler 5 than it flows to a high pressure spray gun 6 and a cryo-sprinkler 7. This sprinkler is different in design from the previous one (Borkowski P., 1997) (Borkowski P., 2001[**]) mainly due to characteristics of the concentric nozzle and external and internal insulating inserts. A high pressure water jet flowing through a cyro-sprinkler 7 produces a negative pressure in a tube 9 sucking in ice particles from a container 10 situated in a room at a controlled temperature. Abrasive and ice particles sucked up from a container 10 and 11 respectively to a nozzle of a cryo-sprinkler 7 get accelerated by a high pressure water jet and formed in a hybrid water-abrasive-ice jet sprayed on a workpiece 8. Earlier experiments (Borkowski J., Borkowski P., 2001) (Borkowski P., 2001[*]) let to establish that the best building of cryo-sprinkler is equipped with a four-outlet concentric nozzle with water jets d_w=1.2mm in diameter and a tube D_t=22 mm in diameter and L_t= 150 mm in length.

The high-pressure hybrid water-abrasive-ice jet configured in this way was used for processing about a dozen different types of material such as metal plates (steel, aluminum, copper and lead), plastics, PVC materials, plexiglass, glass, ceramics, different rock materials, rubber etc. Surfaces of the above materials differed in quality because apart from their natural state they had surfaces passivated, corroded and also coated with brittle layers of vitreous enamel and elastic paint or asphalt (izohan type), either rubberized or glue spread etc. Lead, aluminum and cupper, which are distinguished by high ductility, were most often used for testing the course of erosion mechanism with this sort of hybrid water-abrasive-ice jet.

Quality and a degree of surface erosion of processed materials were assessed with different measuring instruments, including:

- scanning electron microscope JEOL 5500LV,
- TalyScan 150 Dual Gauge System of Taylor-Hobson.

4.2. Mechanism of surface treatment

Analyses of interaction between the abrasive-ice grains and workpiece should be carried out regarding that the total jet pressure and the flow rate of such kind grains exert the most marked influence on the errosiveness of a hybrid jet. Thus, the abrasive and ice jet distribution determines the performance and quality of surface treatment. A significant pressure prevailing in external layers of hybrid jet, despite a low concentration of solid particles, results in intensive treatment of material surfaces. Then, the internal jet layers caused the eroded surface to become smooth leaving a great number of small scratches made by abrasive and ice grains at the lowest pressure (**Figure 10**). These processes were evident especially while treatment of rather soft materials. During hybrid jet treatment it was also found the wavy characteristic of the surface, that is similar to other jet kind (Borkowski P., 2003[*]) (Borkowski P., 2003[**]) (Borkowski P., 2001[*]). However the waviness of surface treated is more intensify for small angles of spraying (than for larger ones). These investigations did not confirmed the essential effect of cryogenic shrinkage of coatings, which could intensify the decoating process.

Details of treated surface with high-pressure hybrid jet comprising abrasive grains and ice particles are shown in SEM micrographs (**Figure 11**). Abrasive grains hitting surface causes erosion of small chips (**Figure 11a**) resulting in numerous pits and cracks (**Figure 11b**). Besides, the impact of ice particles is characterized by a great area of its hit and is significantly mild than abrasive grains. These ice grains partially sublimate causing a great volume of condensate gas CO_2, that effect violently on obtained cracks penetration, which are caused of abrasive grains hits. Such an explosive influence of ice gas CO_2 and water drops affecting on grow of small cracks (**Figure 11 c**) and sometimes even extract of a new chips (**Figure 11 d**). All that causes that the treatment mechanism is very complicated.

4. 3. Model of surface erosion using high-pressure hybrid water-abrasive-ice jet

It was found on the basis of thorough analysis of the process of erosion on the surface treated with a high-pressure hybrid water-abrasive-ice jet that the physical mechanism of the treatment was very complicated and specific. A simplified version of such the model of erosion is illustrated diagrammatically in **Figure 12**. It was revealed that the big dry-ice pellet 1 impinging onto the work surface 2 makes it deformed squeezing out the flashes 3 around the crater. This great caving includes the great number of marks 4 produced by relatively fine abrasive grains. This impingement made the part of the dry-ice pellet undergo the sublimation and generate the gas CO_2 with the volume 800 times larger. Due to the explosive character of the generation of that gas, the cracks and gaps 5 were growing under the influence of previous collisions of abrasive grains. Consequently, the particles 6 detached from the workpiece took the form of new characteristic chips (**Figure 11 d**).

Sudden character of that process is nearly explosive, while the treatment zone is smoggy caused of condensate CO_2 gas. Water plays also important part in this process revealing its effects not only in the form of cavitational erosion, but also as a medium penetrating the cracks obtained, causing disaggregation of the material. This mechanism generally results in uniform spalling of particles splitted off the workpiece surface. Such an erosion mechanism is especially favorable for decoating of brittle layers from material surface.

5. CONCLUSIONS

Theoretical analysis of problems connected with the solid particles motion in the high-pressure hybrid water-abrasive-ice jet and the effects of their action on the workpiece allowed formation of a few conclusion of more general character:

- Hybrid jet erosion efficiency, created by means of the sprinkler with the optimized 4 holes construction nozzle, like all the above discussed quantities undergo a distinctive increase along with an increase in the water pressure and the sprinkler tube length, whereas an influence of the jet aeration ratio is rather insignificant.
- The maximum velocity of abrasive grains at the sprinkler outlet reaches values close to the flow velocity of water jet carrying them, however these grains at the erosion area with the workpiece reaches the velocity exceeding 270 m/s while for dry-ice pellets such velocity is smaller in the range of approximately 30% - 50%. Owing to this area, the abrasive grains reveal kinetic energy close to $1x10^{-3}$ J, while the kinetic energy of dry ice pellets is 300÷500 times higher.
- Effectiveness of surface treatment with the hybrid jet depends on the quality of ice particles. For this reason it is recommended to use the ice of the highest quality and also possibly the lowest temperature of a high-pressure water jet so that the quality of ice particles accelerated with it declined as low as possible.
- The lowest pressure occurs in internal layers of hybrid jets, whereas much more higher pressure is characteristic for external layers with clear separated elementary jets which number is equal to the number of water holes arranged in sprinkler nozzles.
- The highest number of solid particles flows along the axis of hybrid jet whereas the lowest ones in external layers of the jet where prevailed the highest pressure.
- The flow rate of abrasive grains (#36) during such high-pressure hybrid jet treatment reaching the range of 90,000 - 150,000 grains per second while the ice pellets number is 70 times lower. It

is very important for the grains distribution characteristic and erosion mechanism, also for surface treatment intensity.

● The hybrid jet structure determines the performance and quality of surface treatment. A significant pressure prevailing in external layers of hybrid jets results in intensive treatment of material surfaces whereas the internal jet layers caused the treated surface to become smooth.

● This kind treatment makes possible to obtain considerably high smoothness of surface, which can be obtained by precise grinding. However, the heterogeneity of the hybrid jet structure could cause the wavy effect on surface.

● The mechanism of the erosion process on the surface treated with a high-pressure hybrid water-abrasive-ice jet is very complicated and specific because a large number of small size abrasive grains are accompanied with large particles of dry-ice pellets. Therefore impingement made the part of the dry-ice pellet undergo the sublimation and generate the gas CO_2 with the volume 800 times larger. Due to the explosive character of the generation of that gas, the cracks and gaps were growing under the influence of previous collisions of abrasive grains. Consequently, the particles detached from the workpiece took the form of new chips.

6. REFERENCES

Borkowski P. “Basis of highpressure water-ice jet creation and application for surface treatment”. Surface Treatment VI. *Computer Methods and Experimental Measurements for Surface Treatment Effect*. Greece, pp. 85-96, 2003*.

Borkowski P. “Fundamentals of surface treatment with high-pressure abrasive-water jet”. 7th Pacific Rim International Conference on Water Jetting Technology. Jeju, Korea, 2003**.

Borkowski J., Borkowski P., at all. “Chosen aspects of high-energy hybrid abrasive jet”. *Sci. Publ. Mech. Eng. Dept*. Techn.Univ. Koszalin, 2003.

Borkowski P. “Chosen problems of surface machining with high pressure hydrojetting technology”. *7th Meeting of Machinery Construction Committee PAN* (Polish Academy of Science). *Sci. Publ. Mech. Eng. Dept*. Techn.Univ. Koszalin, No. 30, pp. 139-152, 2002*.

Borkowski P. “High-pressure abrasive-water jet surface treatment”. (in Polish). Center of Pro-Ecological Technologies, Koszalin, 2002**.

Borkowski P., Chomka G. “Thermodynamics and kinetics aeration of high-pressure water-ice jet”. *7th Meeting of Machinery Construction Committee PAN* (Polish Academy of Science). *Sci. Publ. Mech. Eng. Dept*. Techn.Univ. Koszalin, No. 30, pp. 127-138, 2002.

Borkowski J., Borkowski P., Chomka G. “Thermodynamical aspects of high-pressure water-ice jet formation”. *Archives of Civil and Mechanical Engineering*. Polish Academy of Science-Wroclaw Branch, Vol. II, No. 1, pp. 35-46, 2002.

Borkowski P. “Physical basis of surface treatment with high-pressure cryogenic multiphase liquid jet”. *Archives of Civil and Mechanical Engineering*. Polish Academy of Science-Wroclaw Branch, Vol. I, No. 1, pp. 19-37, 2001*.

Borkowski P. “The sprinkler optimization used for highpressure hydroabrasive cleaning”. *Modern Techniques and Technologies. Sci. Publ. Mech. Eng. Dept*. Techn.Univ. Koszalin. No. 29, pp. 27-38. 2001**.

Borkowski P. “Selection of peripheral equipmen for small vessels corroded surface cleaning by high-pressure hydroabrasive jet”. *Int. Conf. Water Jet Machining WJM 2001*, Cracow, pp. 149-158, 2001***.

Borkowski J., Borkowski P. “Chosen issues of creation and application of high-pressure water-ice jet”. *2nd Int. Conf. Water Jet Machining WJM 2001*, Cracow, pp. 127-140, 2001.

Borkowski J., Borkowski P., Kowalewski A. “Principles of modeling of the surface machining by highpressure abrasive water jet with genetic algorithm using”. *Archives of Civil and Mechanical Engineering*. Polish Academy of Science-Wroclaw Branch, Vol. I, No. 1, pp. 7-18. 2001.

Borkowski P. “Multioutlet concentric nozzle optimization in aspect of useful properties of highpressure hydroabrasive jet”. Ph. D - thesis. Techn. Univ. of Koszalin. 1997.

Dunsky C. M., Hashish M. “Observations on cutting with abrasive-cryogenic jets”. *13th Int.Conf. Jetting Technology – Applications and Opportunities*. Sardinia, pp. 679-690. 1996.

Galecki G., Vickers G. W. “The Development of Ice-Blasting for Surface Cleaning”. *6th Int. Symp. Jet Cutting Technology*. Surrey, U.K., Paper B-3, pp. 59-78, 1982.

Geskin E. S., Goldenberg B., Shishkin D., Babets K., Petrenko K. “Ice based decontamination of sensitive surfaces”. *15th Int. Conf. Jetting Technology*. Ronneby, pp. 219-228, 2000.

Geskin E. S., Shishkin D., Babets K. “Application of ice particles for precision cleaning of sensitive surfaces”. *10th American Waterjet Conf.* Vol. 1, Houston, pp. 315-333, 1999.

Hashish M., Dunsky C. M. “The formation of cryogenic and abrasive-cryogenic jets”. *14th Int. Conf. Jetting Technology*. Brugge, pp. 329-343, 1998.

Hashish M., Miller P. “Cutting and washout of chemical weapons with high-pressure ammonia jets”. *15th Int. Conf. Jetting Technology*. Ronneby, pp. 81-92, 2000.

Kiyohashi H., Hanada K. “A study of production of ice particles by the heat of vaporization of cryogenic liquefied fuels and their application in ice jets, and so on”. *Int. Symp. New Appl. of Water Jet Techn.* Ishinomaki, pp. 51-60. 1999.

Liu B.-L., Liu L.-H., Wu L. “Research on the preparation of the ice jet and its cleaning parameters”. *14th Int. Conf. Jetting Technology*. Brugge, pp. 203-210, 1998.

Liu H. T., Fang S., Hibbard C., Maloney J. “Enhancement of ultrahigh-pressure technology with LN_2 cryogenic jets”. *10th American Waterjet Conf.* Vol. 1, Houston, pp. 297-313, 1999.

Matsuyama K., Ueno S., Masutani T., Nishiguchi K. “Observation of water jet structure with a cantilever method for measurement of total pressure distribution”. *4th Pacific Rim Int. Conf. Water Jet Technology*. Shimizu, pp. 127-138. 1995.

Mazurkiewicz M., Olko P., Jordan R. “Abrasive particle distribution in a high pressure hydroabrasive jet”. *Int. Waterjet Symp*. Beijing, pp. 4.1-4.10. 1987.

Momber A. W., Kovacevic R. “Principles of abrasive water jet machining”. Springler-Verlag. London, 1988.

Shishkin D. V., Geskin E. S., Goldenberg B. “Development of a technology for fabrication of ice abrasives”. *2001 WJTA American Waterjet Conf. Minneapolis,* Paper No. 27, 2001.

Spur G., Uhlmann E., Elbing F. “Dry-ice blasting for cleaning: process, optimization and application”. *Wear*. (233-235), pp. 402-411, 1999.

Summers D. A. *Waterjetting Technology*. 1st ed. Chapman & Hall. New York, 1995.

Truchot P., Mellinger P., Duchamp R., Kim T. J., Ocampo R. “Development of a cryogenic waterjet technique for biomaterial processing applications”. *6th American Water Jet Conf.*, Houston, pp. 473-480, 1991.

7. ACKNOWLEDGEMENTS

I would like to thank my father, Professor DSc., PhD, MSc. Jozef Borkowski, for scientific discussion in initial phase of this work and The Polish National Science Foundation (KBN) for their support (Research Grant No. 8 T07D 027 20).

8. NOMENCLATURE

c - specific heat of ice,
c_s - sublimation heat of CO_2,
d - diameter of a spherical grain model ($d=2r$),
d_w – diameter of water hole of concentric nozzle,
m - solid particle weight,
n_a - flow-rate of abrasive grains,
n_i - flow-rate of dry-ice pellets CO_2,
n_u - unit number of abrasive grains,
p - water pressure,
r - radius of a spherical grain model,
t - time of flowing through the sprinkler tube,
u - high-pressure water jet velocity $u=(2p/\rho_o)^{0,5}$,
v - solid particle velocity in a stream,
$v_{0,25}$ - solid particle velocity in a stream distant 0,25m from sprinkler tube outlet,
w - coefficient of multiplying gas-solid CO_2 volume,
z - coefficient of sublimated ice pellets piece volume,
C_D - discharge coefficient of solid particles moving in a water jet,
D_n - diameter of concentric nozzle hole,
D_o - jet diameter at a sprinkler outlet,
D_t - diameter of sprinkler tube,
D_x - jet diameter at a cross-section under consideration,
E_k - kinetic energy of solid particle,
K - constant $K=(8r\rho):(3C_D\rho_w)$,
L - length of suction hose,
L_s - distance from the outlet of nozzle,
L_t - length of sprinkler tube,
R_w - radius of water hole position in nozzle,
S - surface of ice-grain,
T_a - temperature of air,
T_i - initial ice temperature,
T_{ie} - end temperature of ice particle,
T_w - temperature of water,
V - volume of dry-ice pellets CO_2,
V_g - CO_2 gas volume of sublimation process,
α - coefficient of heat absorption,
δ - effectiveness of sublimation process,
ε - angle of water hole inclination in concentric nozzle,
η - coefficient of jet efficiency,
κ - angle of jet spraying,
ρ - ice density,
ρ_o - solid particle density,
ρ_w - water density.

9. GRAPHICS

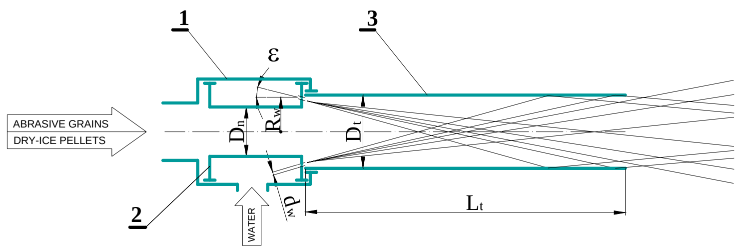

Figure 1. Schema of sprinkler geometry and characteristics

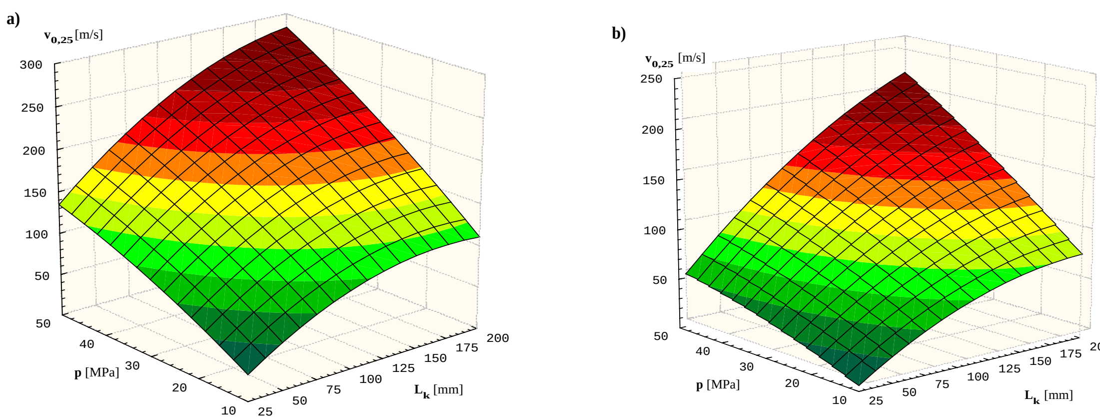

Figure 2. Influence of the sprinkler tube length and water pressure on the velocity in the erosion area for solid particles moving in jet of 10% water content. a - sand quartz #36, b - dry-ice pellets CO_2.

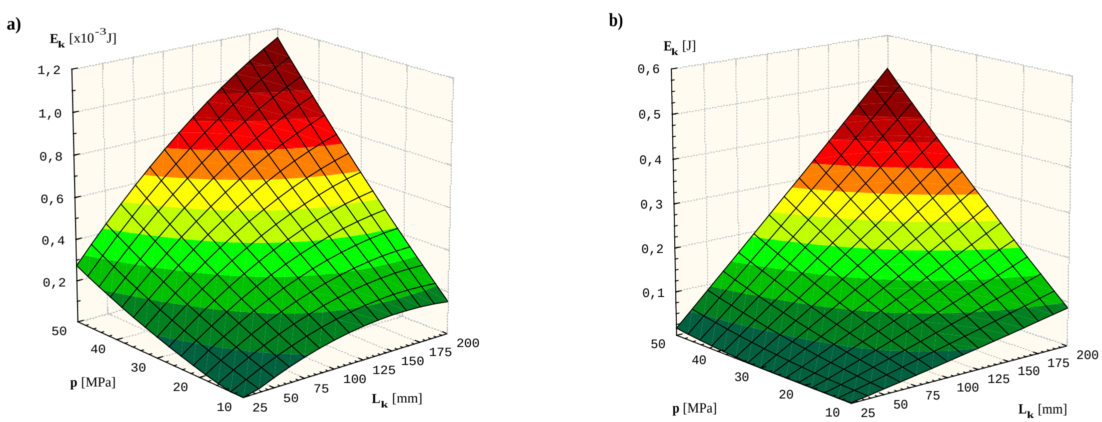

Figure 3. Influence of the sprinkler tube length and the water pressure on the kinetic energy for solid particles carried by jet of 10% water content, a - sand quartz #36, b - dry-ice pellets CO_2

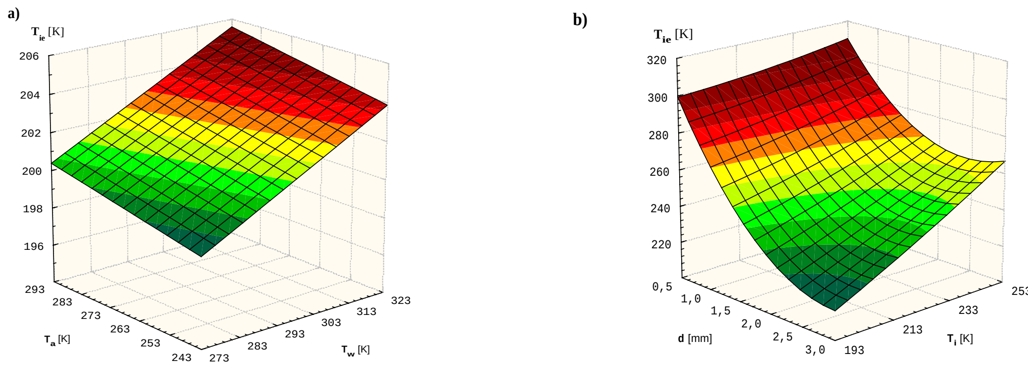

Figure 4. The end temperature of dry-ice pellets CO_2 vs.: a - temperature of air and water; b - initial ice temperature and ice particles diameter. Work conditions: p = 20 MPa, L=5 m, L_s = 250 mm

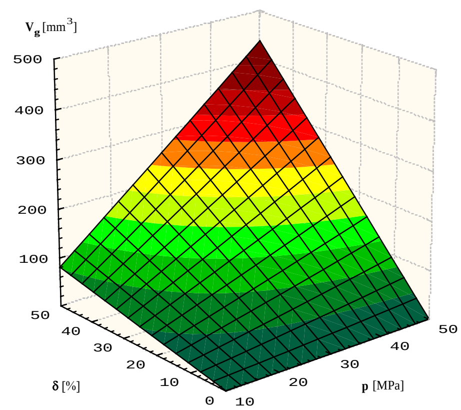

Figure 5. Gas volume of dry-ice pellets CO_2 sublimation vs. water pressure and effectiveness of sublimation process.

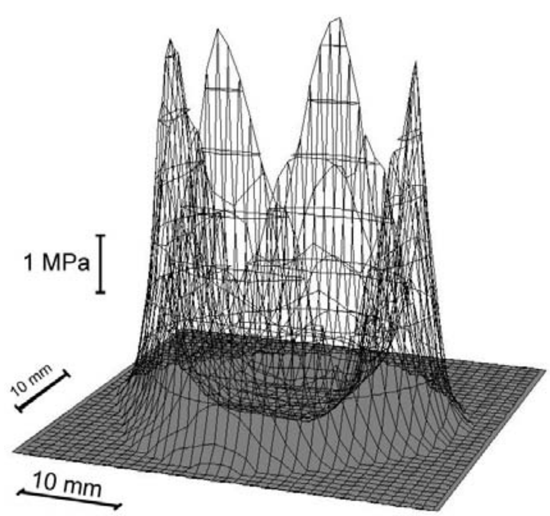

Figure 6. Total pressure distribution in hybrid jet. Spray gun equipped with 4 holes nozzle. Work conditions: p_n=25MPa, sand quartz #36, dry-ice pellets CO_2, L_s=200mm

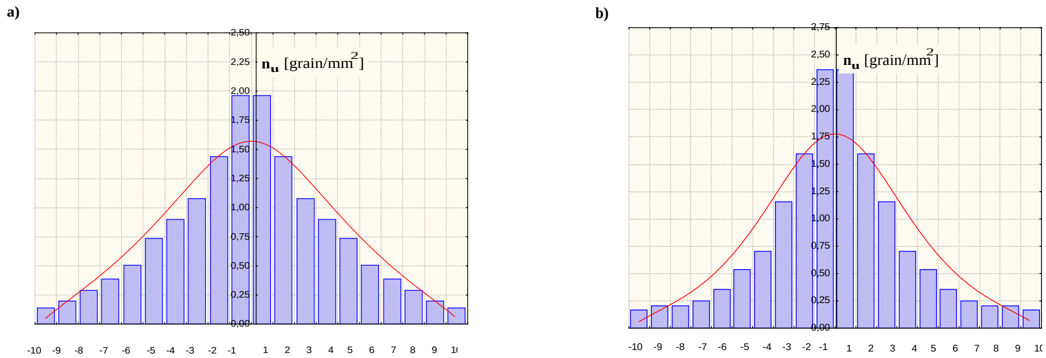

Figure 7. Abrasive grains distribution in the hybrid jet created in concentric nozzle for: a - 4 holes; b - 6 holes. Work conditions: p=25MPa, sand quartz #36, dry-ice pellets CO_2

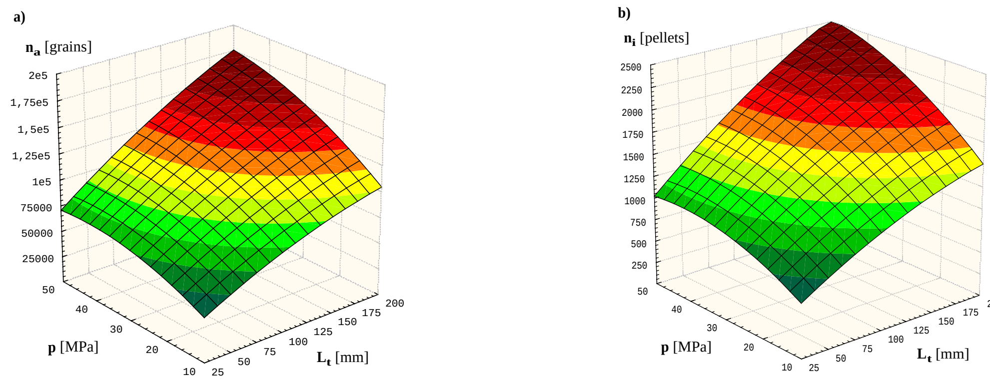

Figure 8. Relationship of the solid particles flow-rate through the sprinkler of the water pressure and the sprinkler tube length for: a - sand quartz #36, b - dry-ice pellets CO_2.

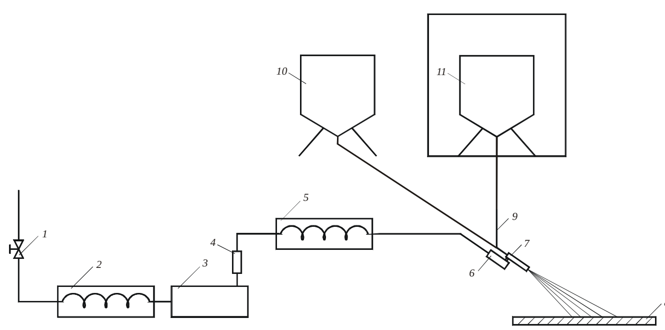

Figure 9. Sample test-stand for creation high-pressure hybrid water-abrasive-ice jet

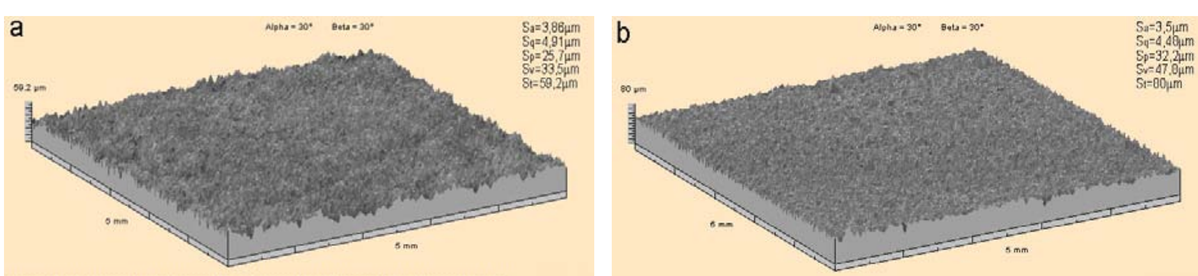

Figure 10. Exemplary effects of brass metal sheet treatment with hybrid water-abrasive-ice jet. Work conditions: p_n=20MPa, L_s=200mm, $\kappa=45^0$, dry ice pellets CO_2, a - garnet #90; b - corundum #90

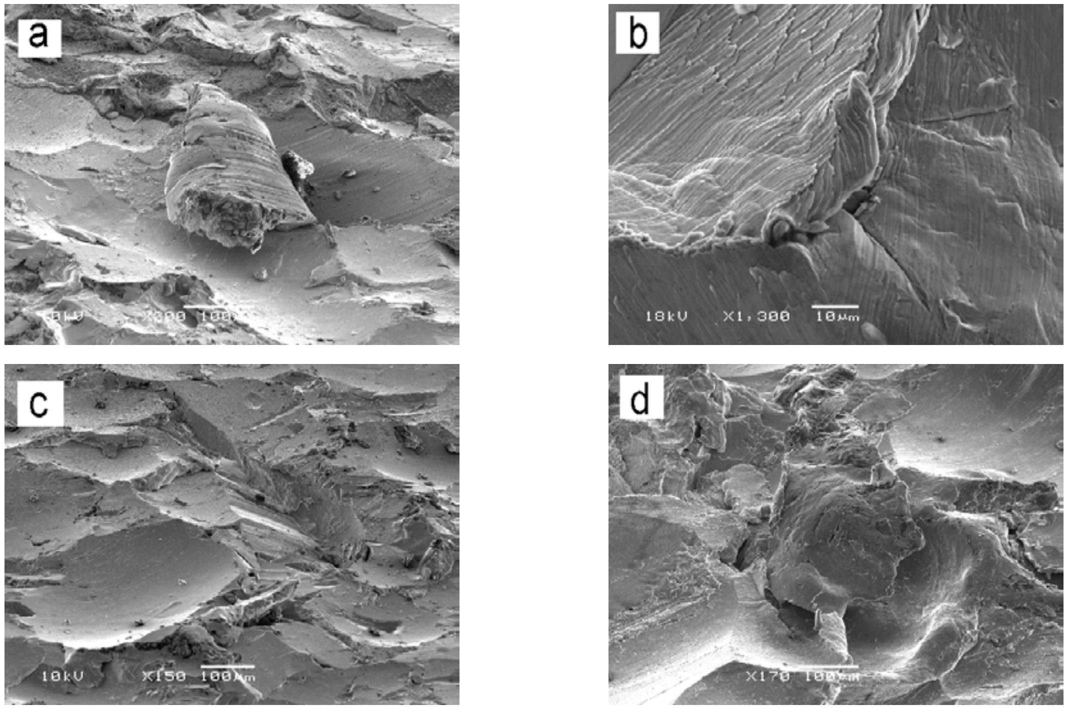

Figure 11. Surface of the brass treated by high-pressure hybrid jet with exposed: a- typical chip, b – small pits and cracks, c – cracks enlarged by sublimated gas CO_2, d – chip created as a effect of sublimated gas CO_2

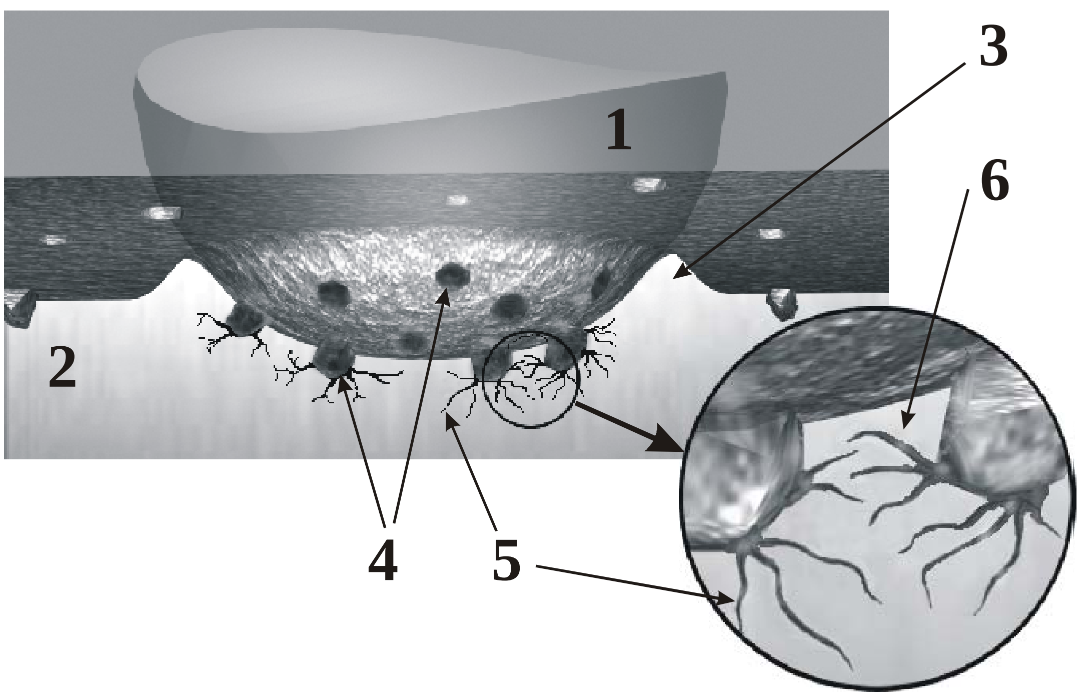

Figure 12. Model of surface erosion using hybrid water-abrasive-ice jet (transparent ice model)

2003 WJTA American Waterjet Conference
August 17-19, 2003 Houston, Texas

Paper 5-A

AN ANALYTICAL MODEL FOR PREDICTION OF RESIDUAL STRESSES IN WATER JET PEENING

G. Vikram and N. Ramesh Babu
Indian Institute of Technology Madras
Chennai, India

ABSTRACT

In the present work, an analytical approach is proposed to estimate the residual stresses induced on the surface of a material treated by water jets. The dynamic response of material to jet impact, assuming elastic behavior of the material, is determined using the Navier's equation. Owing to the axi-symmetry of the jet loading, the equations are transformed into Hankel space using zero and first order Hankel transforms and are solved. Due to the absence of a closed form expression for the Inverse-transform of the solution, suitable engineering approximations are made to solve this problem. The results thus obtained are used to determine the strain field, which in turn is used to determine the zone of plastic deformation. Using von Mises yield criterion and assuming kinematic hardening of the material, the residual stresses on the surface of the material are evaluated. The predicted stresses are compared with the results published in the literature.

Organized and Sponsored by WaterJet Technology Association

1. INTRODUCTION

Most of the machine components operating under cyclic loading are susceptible to fatigue. The fatigue life of the component can be improved by introducing compressive residual stress on the surface of the component, which increases the time for crack propagation. This compressive residual stress can be introduced with the aid of a variety of techniques such as shot peening, surface rolling, presetting etc. One of the recently emerging techniques is water jet peening.

The most widely used technique to introduce residual stresses on the surface of the material is by shot peening. However, water jet peening, though similar to shot peening, has several advantages over it. A water jet peened surface has an improved surface finish, which increases the crack initiation time. Water jet peening also enables complete and uniform coverage of the given surface area and results in a more uniformly induced residual stresses in the subsurface.

Experimental and theoretical attempts are made to predict the magnitude, depth and gradient of residual stress induced on the surface of the material with water jet peening. The experimental methods [1] are tedious, cumbersome and time consuming. The theoretical attempts are limited to a few numerical models. Recently, attempts are being made to employ suitable finite element methods for predicting the residual stresses induced on a surface treated with a stationary jet [2]. The aim of the present work is to develop an analytical model that can predict the residual stresses quickly and will be useful in determining the optimum working parameters for water jet peening.

2. METHODOLOGY

The flow charts below briefly indicate the peening process and the various steps involved in determining the residual stresses induced on the surface using water jet peening. The various steps involved in the determination of residual stresses are

1. Governing equations and boundary conditions.
2. Solving these equations by transformation into Laplace-Hankel space
3. Inverse Transformation of the solution using suitable engineering approximations.
4. Evaluation of strain and stress fields and determining the residual stresses.

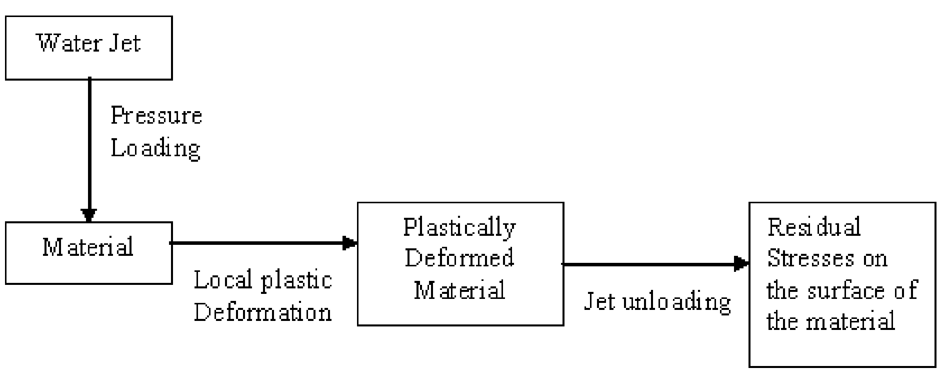

Penning process

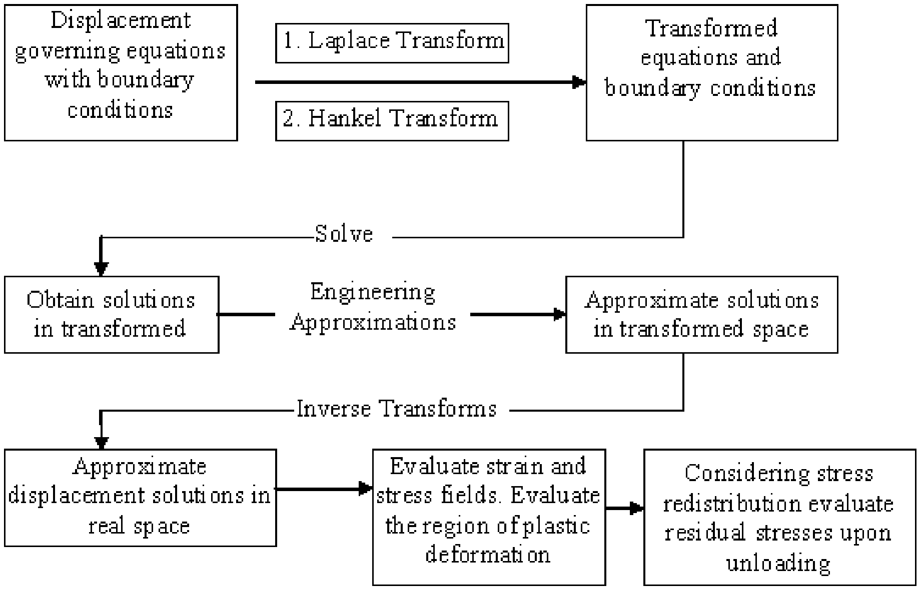

Different steps involved in evaluating the residual stresses induced on the surface of a material using the present model.

2.1 Governing Equations

The governing equations for the material response are determined using the equilibrium equations. Substituting for strains in terms of displacements into the equilibrium equations, the Navier's equations of motion are obtained, which can be represented in Einstein's notation as

$$(\lambda+\mu)u_{j,ji}+\mu u_{i,jj}+\rho f_i=\rho\ddot{u}_i \tag{1}$$

In vector notation, the above equation can be written as

$$(\lambda+\mu)\nabla\nabla.\vec{u}+\mu\nabla^2\vec{u}+\rho f_i=\rho\ddot{\vec{u}} \tag{2}$$

This complex displacement equation can be reduced to a simple set of equations by introducing scalar and vector potentials. By Helmholz theorem, a vector field can be resolved into the gradient of a scalar and the curl of a zero-divergence vector. Considering ϕ and $\overline{H}$ as scalar and vector potentials, the displacement field can be expressed as

$$\vec{u}=\nabla\varphi+\nabla x\overline{H} \qquad \nabla.H=0 \tag{3}$$

Substituting for displacement in terms of the potentials, the equation (2) reduces to the following set of equations in the absence of body forces

$$\begin{aligned}(\lambda+2\mu)\nabla^2\varphi&=\rho\ddot{\varphi}\\ \mu\nabla^2H&=\rho\ddot{H}\end{aligned} \tag{4}$$

2.1.1 The axi-symmetric case of water jet peening

The jet impingement on a thin specimen can be considered as a problem similar to axi-symmetric pressure loading on semi-infinite media. Since the jet is axi-symmetric, the azimuthal displacement component, u_θ, is absent. Hence, the displacement field can be represented in terms of its components as

$$\vec{u}(r,z,t) = u_r \vec{e}_r + u_z \vec{e}_z$$

In terms of scalar and vector potentials

$$\vec{u} = \nabla\varphi + \nabla x(H_\theta e_\theta) \quad (5)$$

The required governing equations in terms of ϕ and H_θ are obtained by substituting the above displacement field in the equation (2), and can be written as

$$\nabla^2\varphi = \frac{1}{c_1^2}\frac{\partial^2\varphi}{\partial t^2} \quad (6a)$$

$$\nabla^2 H_\theta - \frac{1}{r^2}H_\theta = \frac{1}{c_2^2}\frac{\partial^2 H_\theta}{\partial t^2} \quad (6b)$$

where c_1 and c_2 are the propagation velocities of dilatational and distortional disturbances .

Equation (6b) can be reduced to a scalar wave equation by defining a scalar function $\psi = -\int H_\theta \, dr$ and substituting for H_θ in the equation (6b). The equations after substitution are obtained as

$$\nabla^2\varphi = \frac{1}{c_1^2}\frac{\partial^2\varphi}{\partial t^2} \quad (7a)$$

$$\nabla^2\psi = \frac{1}{c_2^2}\frac{\partial^2\psi}{\partial t^2} \quad (7b)$$

The displacements and stresses in terms of ϕ and ψ are obtained as

$$u_r = \frac{\partial\varphi}{\partial r} + \frac{\partial^2\psi}{\partial r\partial z}, \qquad u_z = \frac{\partial\varphi}{\partial z} + \frac{\partial^2\psi}{\partial z^2} - \frac{1}{c_2^2}\ddot{\psi}, \qquad u_\theta = 0 \quad (8)$$

$$\tau_{zz} = \lambda\nabla^2\varphi + 2\mu\frac{\partial}{\partial z}\left(\frac{\partial\varphi}{\partial z} + \frac{\partial^2\psi}{\partial z^2} - \frac{1}{c_2^2}\ddot{\psi}\right), \qquad \tau_{rz} = \mu\frac{\partial}{\partial r}\left(2\frac{\partial\varphi}{\partial z} + 2\frac{\partial^2\psi}{\partial z^2} - \frac{1}{c_2^2}\ddot{\psi}\right) \quad (9)$$

2.2 Boundary Conditions

Figure 1 shows the velocity profiles of a propagating jet in different regions. The jet the exit of the nozzle has a uniform distribution of velocity. As the jet propagates in air, the resistance offered by the atmosphere on the jet periphery decelerates the jet and the spatial distribution of velocity changes to a gaussian distribution. When the shear forces exerted on the periphery of the jet become high, the jet disintegrates into droplets. This droplet region is very useful and is found to induce maximum residual stresses [1]. When a water jet impinges on any surface, it exerts a hydrostatic pressure equivalent to impact pressure, which is sustained for a short duration. In the droplet region, the droplets strike the surface randomly and the time of impact of each droplet is very low. Hence, in the droplet region, the impact pressure is maintained all the time due to the discrete nature of the particles striking the surface and this impact pressure exerted by the jet can be considered as a step input. Since the velocity of jet exhibits a radial variation, the pressure exerted by the jet also varies along the radius. This variation can be approximated as

$$P(r) = P_o(1-r^2) \tag{10}$$

where P_o is the peak pressure considering the impact nature and 'r' the non-dimensional number representing the radial distance. Hence the boundary conditions for the jet loading can be written down as

$$\tau_{zz} = P_o(1-r^2)\ U(t) \qquad \text{at } z = 0 \tag{11a}$$

$$\tau_{rz} = 0 \qquad \text{at } z = 0 \tag{11b}$$

where U(t) represents a unit step input.

As there is time dependency and radial symmetry in the above equations, it will be convenient to work in transformed coordinates rather the real space time coordinates [3]. It was shown by Graff that by applying the Laplace and Hankel transforms to axi-symmetric problems, the governing differential equations can be reduced into simple forms. Owing to the radial symmetry, the Hankel transform reduces the governing equations to a set of wave equations with single variable dependency in the transformed space.

2.3 Transformations

(a) Laplace transform of governing equations and boundary conditions:

Let the Laplace transform of the variables be represented as

$$\varphi^1(r,z,s),\psi^1(r,z,s),u^1(r,z,s),\tau^1(r,z,s) = L\{\varphi(r,z,t),\psi(r,z,t),u(r,z,t),\tau(r,z,t)\}$$

The transformed governing equations are

$$\nabla^2\varphi^1 = \frac{s^2}{c_1^2}\varphi^1 \tag{12a}$$

$$\nabla^2\psi^1 = \frac{s^2}{c_2^2}\psi^1 \tag{12b}$$

The transformed displacement relations and stress boundary conditions are

$$u_r^1 = \frac{\partial\varphi^1}{\partial r} + \frac{\partial^2\psi^1}{\partial r\partial z}, \qquad u_z^1 = \frac{\partial\varphi^1}{\partial z} + \frac{\partial^2\psi^1}{\partial z^2} - \frac{s^2}{c_2^2}\psi \tag{13}$$

$$\tau_{zz}^1 = \lambda\nabla^2\varphi^1 + 2\mu\frac{\partial}{\partial z}\left(\frac{\partial\varphi^1}{\partial z} + \frac{\partial^2\psi^1}{\partial z^2} - \frac{s^2}{c_2^2}\psi^1\right) = \frac{P_o}{s}(1-r^2) \quad \text{at } z = 0 \tag{14}$$

$$\tau_{rz}^1 = \mu\frac{\partial}{\partial r}\left(2\frac{\partial\varphi^1}{\partial z} + 2\frac{\partial^2\psi^1}{\partial z^2} - \frac{s^2}{c_2^2}\psi^1\right) = 0 \qquad \text{at } z = 0$$

(b) Hankel Transform:

To take advantage of the radial symmetry, Hankel transform of the above equations is taken. Let the Hankel transform of the preceding equations be represented as follows.

$$\varphi^{l,h}(\xi,z,s),\psi^{l,h}(\xi,z,s),u^{l,h}(\xi,z,s),\tau^{l,h}(\xi,z,s) = H\{\varphi^{l}(r,z,s),\psi^{l}(r,z,s),u^{l}(r,z,s),\tau^{l}(r,z,s)\}$$

By taking a zero order Hankel transform of ϕ^1 and ψ^1, the governing equations reduce to a set of wave equations with derivates with respect to only the z coordinate

$$\frac{d^2\varphi^{l,h}}{dz^2} - (\xi^2 + \frac{s^2}{c_1^2})\varphi^{l,h} = 0 \tag{15a}$$

$$\frac{d^2\psi^{l,h}}{dz^2} - (\xi^2 + \frac{s^2}{c_2^2})\psi^{l,h} = 0 \tag{15b}$$

For transforming the displacement and stress relations, a zero order Hankel transform is applied for components where derivatives with respect to r are absent. For terms where derivates are present, a first order Hankel transform is chosen because of the way the transform operates on the derivatives. The displacement and stress relations in the transformed state are estimated as

$$u_r^{l,h} = -\xi(\varphi^{l,h} + \frac{d\psi^{l,h}}{dz}) \tag{16a}$$

$$u_z^{l,h} = \frac{d\varphi^{l,h}}{dz} + \frac{d^2\psi^{l,h}}{dz^2} - \frac{s^2}{c_2^2}\psi^{l,h} \tag{16b}$$

$$\tau_{zz}^{l,h} = \lambda\frac{s^2}{c_1^2}\varphi^{l,h} + 2\mu(\frac{d^2\varphi^{l,h}}{dz^2} + \frac{d^3\psi^{l,h}}{dz^3} - \frac{s^2}{c_2^2}\psi^{l,h}) = \frac{2P_o}{s\xi^3}[2J_1(\xi)\text{-}\xi J_o(\xi)] \qquad \text{at } z = 0 \tag{17a}$$

$$\tau_{rz}^{l,h} = -\mu\xi(2\frac{d\varphi^{l,h}}{dz} + 2\frac{d^2\psi^{l,h}}{dz^2} - \frac{s^2}{c_2^2}\psi^{l,h}) = 0 \qquad \text{at } z = 0 \tag{17b}$$

2.4 Solution in transformed space

Solving the equations (15a) and (15b) with the boundary conditions given in the equation (17a) and (17b), the Laplace-Hankel transformed solutions for displacement are given by

$$u_r^{l,h} = \frac{2P_o}{s\mu\xi^2}[\xi J_o(\xi)\text{-}2J_1(\xi)]\frac{[(2\xi^2 + \frac{s^2}{c_2^2})e^{-z(\xi^2+\frac{s^2}{c_1^2})^{\frac{1}{2}}} - 2(\xi^2 + \frac{s^2}{c_1^2})^{\frac{1}{2}}(\xi^2 + \frac{s^2}{c_2^2})^{\frac{1}{2}}e^{-z(\xi^2+\frac{s^2}{c_2^2})^{\frac{1}{2}}}]}{[(2\xi^2 + \frac{s^2}{c_2^2})^2 - 4\varepsilon^2(\xi^2 + \frac{s^2}{c_1^2})^{\frac{1}{2}}(\xi^2 + \frac{s^2}{c_2^2})^{\frac{1}{2}}]} \tag{18a}$$

$$u_z^{l,h} = \frac{2P_o}{s\mu\xi^3}[\xi J_o(\xi)\text{-}2J_1(\xi)]\frac{[-(\xi^2+\frac{s^2}{c_1^2})^{\frac{1}{2}}(2\xi^2+\frac{s^2}{c_2^2})e^{-z(\xi^2+\frac{s^2}{c_1^2})^{\frac{1}{2}}}+2\xi^2(\xi^2+\frac{s^2}{c_1^2})^{\frac{1}{2}}e^{-z(\xi^2+\frac{s^2}{c_2^2})^{\frac{1}{2}}}]}{[(2\xi^2+\frac{s^2}{c_2^2})^2\text{-}4\varepsilon^2(\xi^2+\frac{s^2}{c_1^2})^{\frac{1}{2}}(\xi^2+\frac{s^2}{c_2^2})^{\frac{1}{2}}]} \quad (18b)$$

Though the solution of the displacement field is obtained, it is in the transformed coordinates. To arrive at the solution in the real space, Inverse-Laplace followed by Inverse- Hankel transform of the preceding expressions must be evaluated. As can be seen, the solution is too complex and a closed form solution does not exist. However, the solution is relatively simple on the surface i.e. z = 0 and can be obtained using some engineering approximations. The displacement field on the surface can be determined by,

$$u_r^{l,h} = \frac{2P_o}{s\mu\xi^2}[\xi J_o(\xi)\text{-}2J_1(\xi)]\frac{[(2\xi^2+\frac{s^2}{c_2^2})\text{-}2(\xi^2+\frac{s^2}{c_1^2})^{\frac{1}{2}}(\xi^2+\frac{s^2}{c_2^2})^{\frac{1}{2}}]}{[(2\xi^2+\frac{s^2}{c_2^2})^2\text{-}4\varepsilon^2(\xi^2+\frac{s^2}{c_1^2})^{\frac{1}{2}}(\xi^2+\frac{s^2}{c_2^2})^{\frac{1}{2}}]} \quad (19a)$$

$$u_z^{l,h} = -\frac{2P_o s[\xi J_o(\xi)\text{-}2J_1(\xi)][(\xi^2+\frac{s^2}{c_1^2})^{\frac{1}{2}}]}{\mu c_2^2\xi^3[(2\xi^2+\frac{s^2}{c_2^2})^2\text{-}4\varepsilon^2(\xi^2+\frac{s^2}{c_1^2})^{\frac{1}{2}}(\xi^2+\frac{s^2}{c_2^2})^{\frac{1}{2}}]} \quad (19b)$$

2.5 Engineering approximations and Laplace Inversion

To transform the displacement solution from the transformed space into the real space, some engineering approximations are made. While taking an Inverse-Laplace transform, a closed form solution cannot be obtained due to the presence of square roots. To obtain a closed form solution, the product of the 2 terms, $(\xi^2+\frac{s^2}{c_1^2})(\xi^2+\frac{s^2}{c_2^2})$ is approximated to a perfect square given by $[\xi^2+\frac{1}{2}(\frac{s^2}{c_1^2}+\frac{s^2}{c_2^2})]^2$. This approximation calls for a change in the coefficients of terms involving‘s’. This induces an error in the spatial domain as well in the frequency domain. To investigate the error introduced due to this approximation, the solution in transformed space before and after the approximation is plotted. It can be seen from figures 2 and 3 that there is no perceptible difference and the error due to the approximation is calculated to be less than 10%. To evaluate the error in the real space, the error surface is numerically integrated. To evaluate the error exactly, the error surface must be integrated in a complex domain parallel to the jω axis for evaluating the Inverse-Laplace transform and in the real domain to evaluate the Inverse Hankel transform. It can be shown that all the singularities of the error function lie on the jω axis. Hence the integration is performed along a line parallel to the jω axis displaced by a very small value, δ.

The numerically evaluated value of the error is found to be less than 8% for most of the region. By considering this approximation to be valid, the closed form solution for the Inverse-Laplace transform for $c_1 = 2c_2$ is obtained as

$$u_r^h = \frac{P_o}{3\mu\xi^5}[2J_1(\xi)\text{-}\xi J_o(\xi)][-1+\cos(\frac{\sqrt{6}}{2}\xi c_2 t)] \tag{20a}$$

$$u_z^h = \frac{2P_o}{\mu\xi^4}[2J_1(\xi)\text{-}\xi J_o(\xi)][\frac{2}{3}\{1\text{-}\cos(\frac{\sqrt{6}}{2}\xi c_2 t)\} + \frac{1}{\sqrt{6}}\sin(\sqrt{6}\xi c_2 t)] \tag{20b}$$

$$\frac{du_z^h}{dz} = \frac{P_o}{3\mu\xi^4}[2J_1(\xi)\text{-}\xi J_o(\xi)][1+\frac{1}{2}\cos(\sqrt{6}\xi c_2 t)] \tag{20c}$$

2.6 Hankel Inversion

The solution in the real space is obtained by evaluating the Inverse-Hankel transform of the preceding expressions. The desired displacement field in the real space is given by

$$u_r = \int_0^\infty u_r^h \xi J_1(\xi r) d\xi$$

$$u_z = \int_0^\infty u_z^h \xi J_0(\xi r) d\xi$$

The above integrals are evaluated by numerical integration. The resulting solution is the time varying displacement field. This gives the dynamic response of the material to the jet loading under elastic behavior. Using this, the stress and strain fields are evaluated under elastic conditions.

2.7 Stress-strain fields

The displacement strain relations in cylindrical coordinates are given by the following set of equations.

$$e_{rr} = \frac{\partial u}{\partial r},\ e_{\theta\theta} = \frac{1}{r}\frac{\partial u}{\partial \theta} + \frac{u_r}{r} \quad = \quad \frac{u_r}{r} \text{ (axi-symmetric)}, \quad e_{zz} = \frac{\partial u}{\partial z}$$

$$e_{r\theta} = \frac{1}{2}(\frac{1}{r}\frac{\partial u_r}{\partial \theta} + \frac{\partial u_\theta}{\partial \theta} - \frac{u_\theta}{r}) \qquad e_{rz} = 0 \ e_{\theta z} = 0 \text{ (axi-symmetric)}$$

By substituting the displacement fields from the expressions given in the section 2.6, the strain fields can be determined. The strain field thus calculated is time dependent. However, since only the maximum strain is of importance in this analysis, this is determined by considering the maximum strain in the time history at every point in the domain. Subsequently the stress field can be determined through the stress-strain relations for an isotropic material. The stress and strain fields calculated are based on the assumption that the material is elastic. But the stresses in water jet peening are large enough to cause plastic deformation. It is due to this plastic deformation that the material will be unable to go back to its original state upon unloading thus inducing residual stresses on the surface of the material.

2.8 Estimation of residual stress on a water jet peened surface

The residual stresses induced after unloading of the jet are determined by modeling the specimen as an elastic-perfectly plastic material. The Yield criterion chosen is the von Mises criterion. In the present case, the determination of residual stresses is rather simple compared to a general case due to the nature of the solution. Though the results of modeling are discussed in the next section, it can be seen from figures 6 and 7 that the predicted radial and hoop stresses are almost equal and the normal stress is greater than both of them by a factor. This is valid for almost 50% of the region under jet loading and more importantly valid in the region where plastic deformation is most likely. Using this fact, the residual stresses are determined with ease. The stress field follows the relation

$$\sigma_{rr} = \sigma_{\theta\theta} = K\sigma_{zz} \tag{21}$$

where K is a constant. Using the von Mises criterion the values of each of the stress components at which the plastic deformation occurs can be determined. This is possible as the stress components are related to each other by the above relation. Using the von Mises criterion

$$(\sigma_{rr}-\sigma_{\theta\theta})^2+(\sigma_{rr}-\sigma_{zz})^2+(\sigma_{zz}-\sigma_{\theta\theta})^2 \le 2S_y^2 \tag{22}$$

Substituting the relation from equation (21) in the above equation,

$$\sigma_{zz} \le \frac{S_y}{1-K} \qquad \sigma_{rr}, \sigma_{\theta\theta} \le \frac{S_y K}{1-K} \tag{23}$$

All the three stress components attain their maximum at the same loading condition and any further increase of load will cause the material to plastically deform. Since we are assuming an elastic-perfectly plastic material behavior, the stress field taking into account the plastic behavior can be obtained as follows. From the stress field predicted in the previous section (assuming elastic behavior), the stress components beyond the elastic region are replaced by the upper bounds specified in the equation (23). This will cause a redistribution of the stress in the surrounding region, which is taken care during modeling. After determining the stress field taking into account the plastic nature, the residual stresses are obtained by reverse loading the specimen with the same load.

3. RESULTS AND DISCUSSION

The effectiveness and accuracy of the proposed approach is demonstrated by solving the classical problem of uniform pressure distribution in a circular domain on an elastic half-space. The results predicted by the proposed model are compared with the solution given by Timoshenko [4]. The stress values predicted by the proposed theory at the centre point of loading are, $\sigma_{rr} = \sigma_{\theta\theta} = 0.82\sigma_{zz}$, which closely agrees with the theoretical solution.

In order to validate the proposed model in predicting residual stress, the results obtained for a given set of parameters are compared with the results obtained using finite element methods which are available in the literature [2]. A 140 MPa (20 ksi) stationary water jet with 1mm jet diameter, impinging on the surface of an annealed 1100 series aluminum which has low yield strength (55 MPa) is considered. Though the pressure of water jet is 140 MPa, considering the effects of divergence of the jet and water hammer effect, the value of peak pressure 'P_o', is estimated to be close to 450 MPa. Considering the specimen to be elastic-perfectly plastic material, the proposed analysis is carried out with the final objective of determining the variation of different components of residual stresses.

Figure 4 and 5 shows the time varying displacement field evaluated using the proposed methodology. It can be observed from figure 4 that the radial displacement is maximum near the periphery of the jet. This result is physically perceivable as the material, which is beneath the jet is pushed out and the radial displacement at the periphery is a cumulative effect of this. This figure also clearly depicts the propagation of the wave on the surface of the material.

From the displacement field, the strain field and the stress field are evaluated assuming elastic nature of the material. Figures 6 to 8 show the variation of stresses as a function of distance from the loading axis. To account for the plastic deformation, and to predict the residual stresses induced upon unloading, the procedure outlined in the section 2.8 is used. The value of axial stress component (σ_{zz}) at which the material starts to deform plastically is evaluated from the von Mises criterion and is obtained as 310 MPa. It can be seen from figures 9 and 10 that the magnitude and nature of residual radial and hoop stresses predicted are in good agreement with those predicted using finite element methods. The magnitude of residual stresses predicted is slightly higher than that estimated using finite element methods. This may be due to the fact that the present analysis considers dynamics response of material where as the finite element solutions are obtained for static cases.

The results obtained by using finite element methods predict the surface residual radial and hoop stresses are said to be identical [2]. Contrary to this, the proposed method reveals that the surface radial and hoop stresses though close to each other in magnitude and variation, are not the same. Figures 9 and 10 show that residual radial stress approaches zero asymptotically from the negative side where as the residual hoop stress approaches zero from the positive side.

4. CONCLUSIONS

In this work, an analytical model to predict the residual stresses in water jet peening is outlined. The material response to jet loading in terms of displacements is estimated using the Navier's equation. To take advantage of the axial symmetry in the problem, the equations are transformed and solved in the transformed space. It is shown that a Laplace transform followed by a Hankel transform of appropriate order can be used to reduce the complex governing equations into wave equations with a single variable dependency. To counter the problem of non existence of closed form solutions for Inverse-transforms, engineering approximations to the solution are made. It is shown that the error associated with this approximation is less than 10%. The analysis showed that this approximation introduces a greater error in the frequency component than in the magnitude of the solution and that there is no associated error in the steady state solution. Hence it is concluded that the approximation will not alter the predicted residual stresses to a considerable extent.

The displacement field thus obtained is used to estimate the maximum values of strains and stresses in the given domain assuming the material to be elastic in nature. The stress field accounting for the plastic nature of the material is determined using the von Mises yield criterion and stress field predicted from the displacements. Finally, the residual stresses induced on the surface are estimated by superimposing a reverse load of equal magnitude and determining the resultant stress. The proposed approach gave results, which are in good agreement with the results predicted using finite element methods. This approach gives the advantage of reduced computational time along with good accuracy of prediction in comparison to the finite element approaches.

In order to model the process more accurately for utilizing it to predict the optimal water jet peening parameters, attempts are being made to account for the energy loss in plastic deformation. It is also proposed to extend the model to a moving jet in further work.

5. ACKNOWLEDGEMENTS

We would like to acknowledge the guidance and help we received form Dr. M. S. Sivakumar, Dr. C. Lakshmana Rao and Dr. Krishnan Balasubramanian from IIT Madras in some of the technical issues of the work.

6. REFRENCES

1. Tönshoff H.K., Kroos F. and Hartmann M., "Water Peening- An advanced application of Water Jet Technology", *Proceedings of 8th American Water Jet Conference*, pp.473-484, Houston, 1995.

2. Daniewicz S. R., Cummings S. D., "Charecterization of a water peening process", *ASME Journal of Engineering Materials and Technology*, Vol. 121, pp. 336-340, 1999.

3. Graff K. F., "Wave Motion in Elastic Solids", Dover, New York, 1991.

4. Timoshenko S. P. and Goodier J. N., "Theory of Elasticity", McGraw-Hill, 1984.

7. NOMENCLATURE

c_1	propagation velocity of dilatational waves in the material	(mm/s)
c_2	propagation velocity of distortional waves in the material	(mm/s)
e	strain field	
f	body force per unit volume (N/m^3)	
H	Hankel transform; $H_o(g(r)) = \int_0^\infty \xi\, J_o(\xi r)\, g(r)\, dr$	
J_o	Bessel function of order zero	
J_1	Bessel function of first order	
L	Laplace transform; $L(g(t)) = \int_0^\infty e^{-st} g(t)\, dt$	

P_o	peak impact pressure	(Mpa)
r	radial distance	(mm)
s	parameter in Laplace transform	
u	displacement field	
ξ	parameter in Hankel transform	
S_y	yield strength	
λ , μ	lame's constants	
σ	normal stress components	
τ	shear stress components	

8. FIGURES

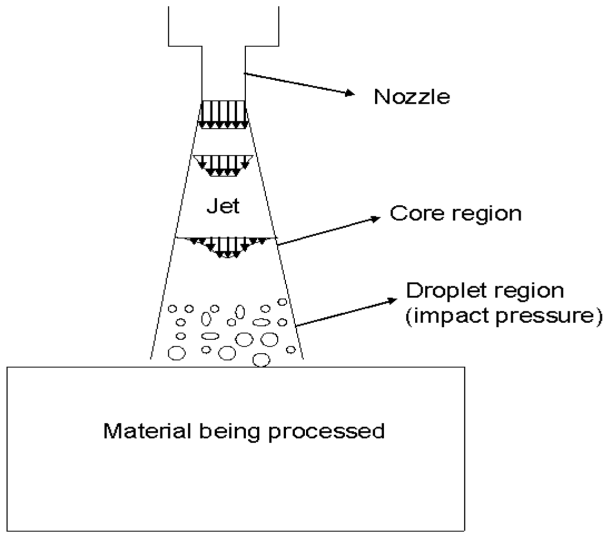

Figure 1: Schematic sketch of the peening process

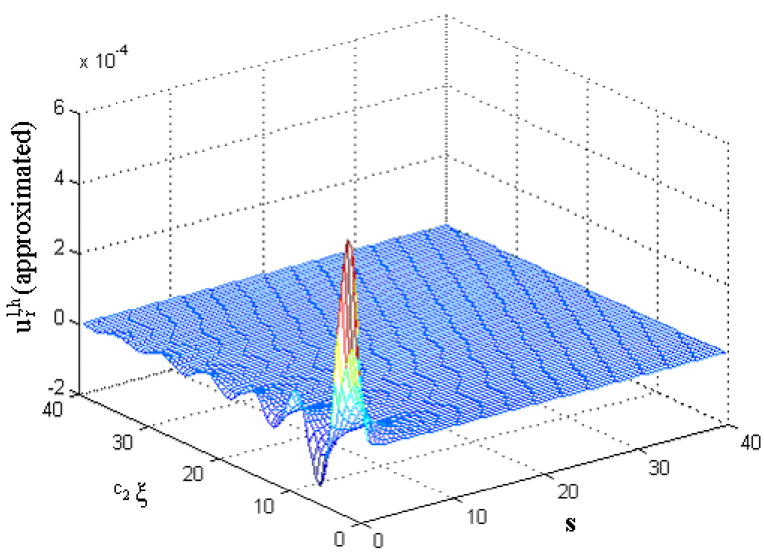

Figure 2: Approximated solution of radial displacement in transformed space.

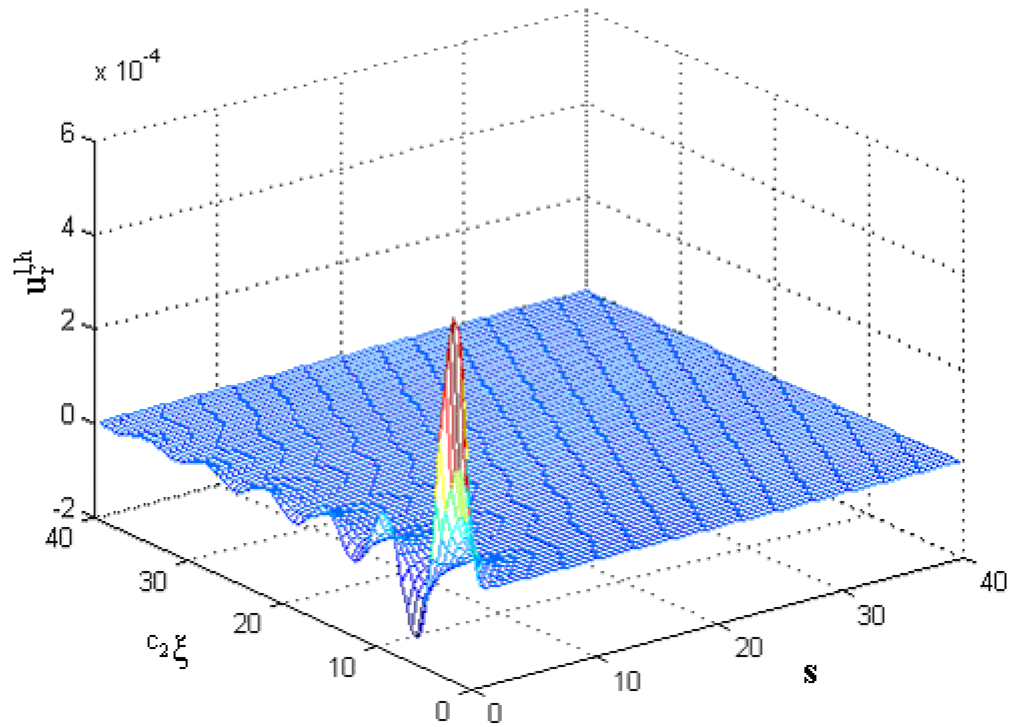

Figure 3: Actual solution of radial displacement in transformed space

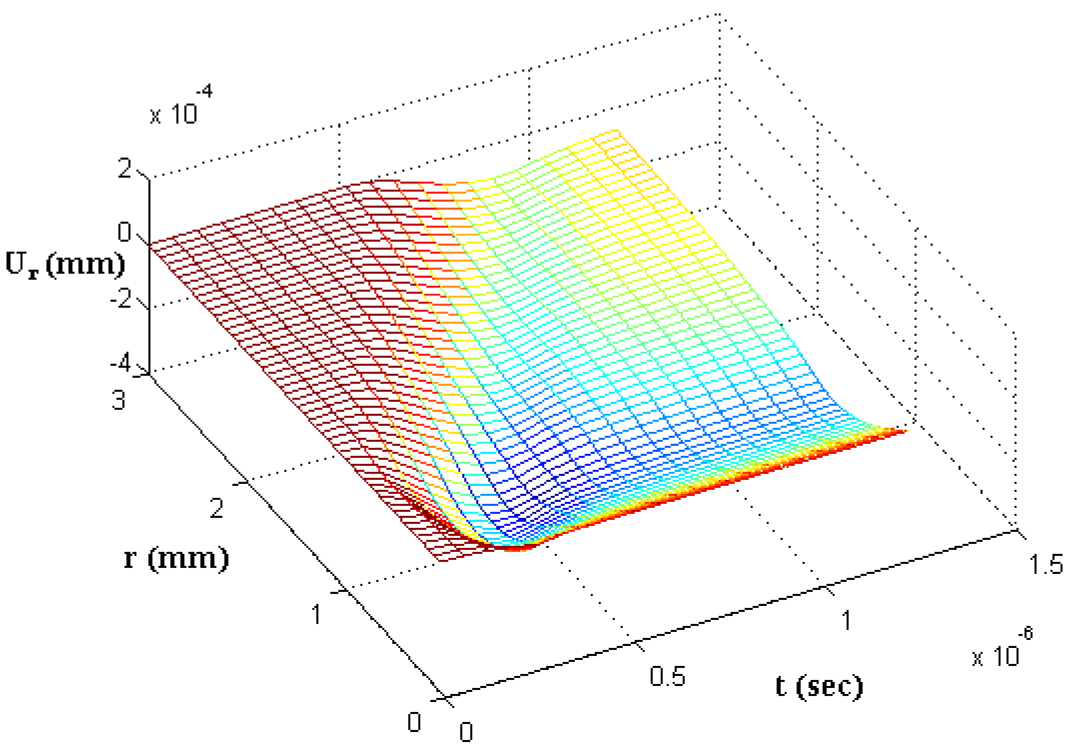

Figure 4: Time varying radial displacement predicted using the proposed model

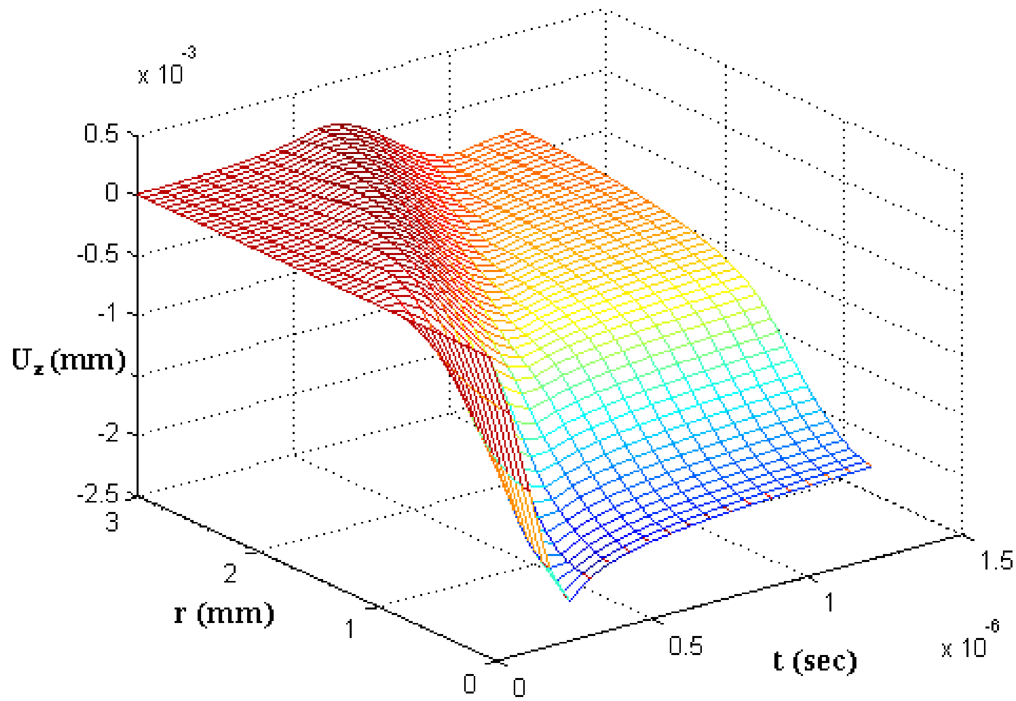

Figure 5: Time varying axial displacement predicted using the proposed model

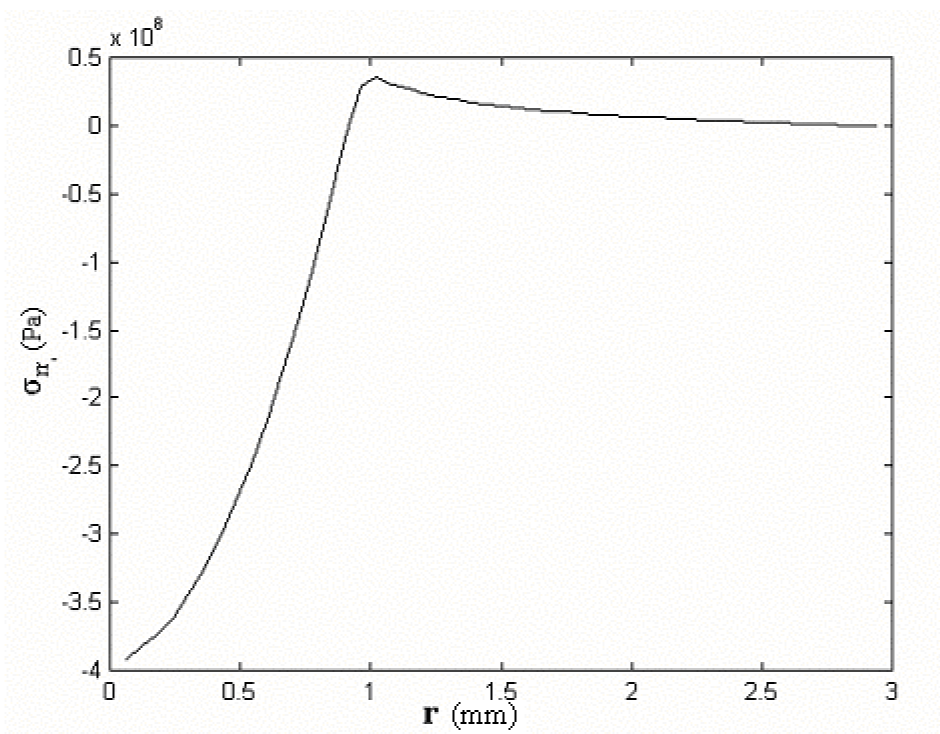

Figure 6: Radial stress variation as a function of radial distance

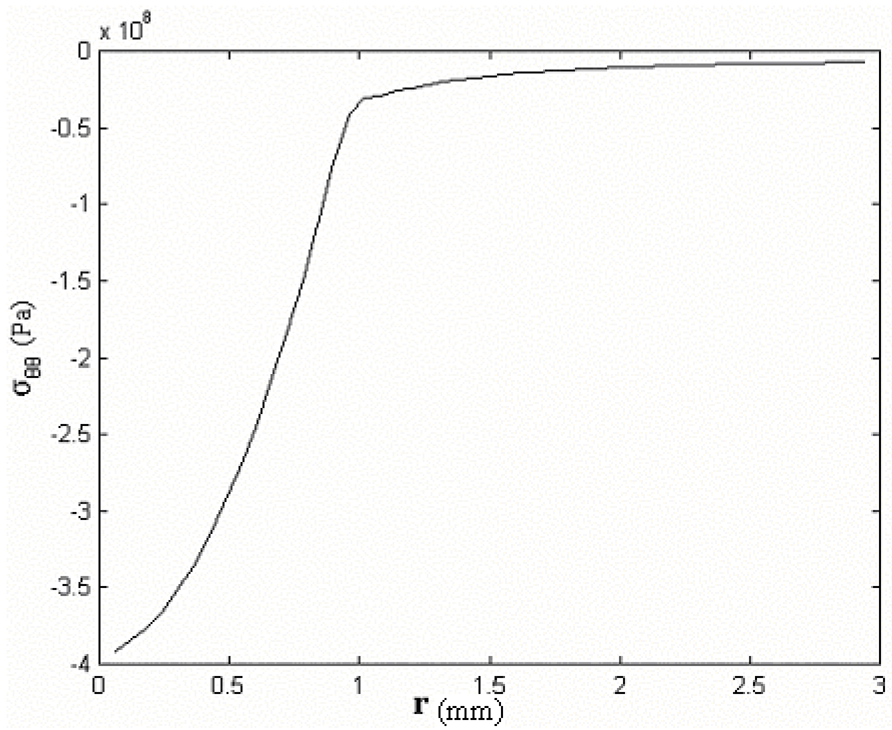

Figure 7: Hoop stress variation as a function of radial distance

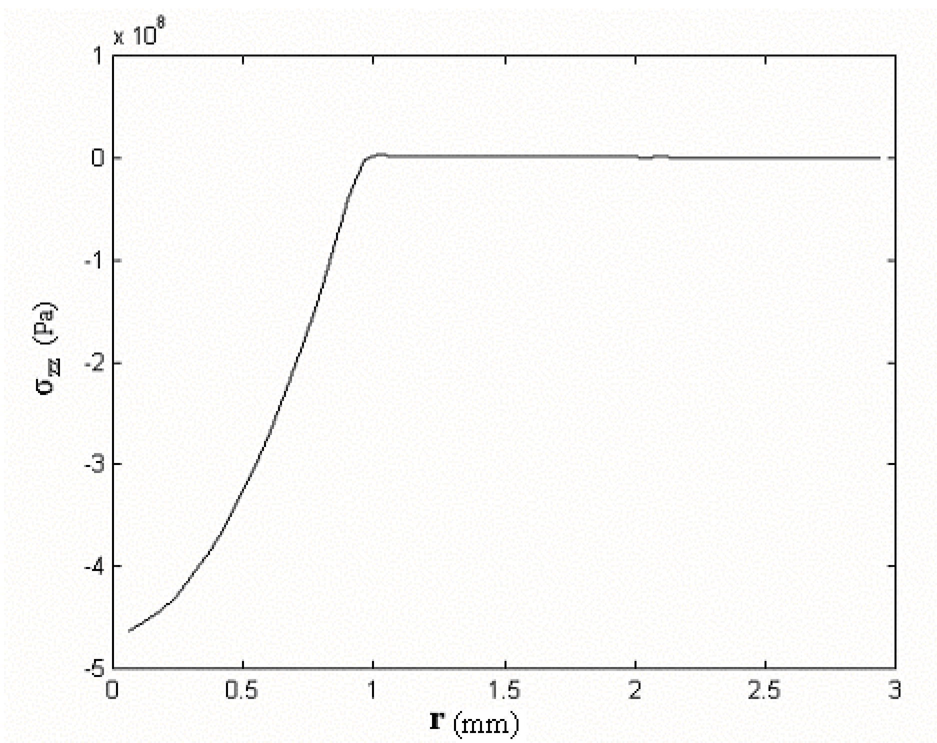

Figure 8: Axial stress variation as a function of radial distance

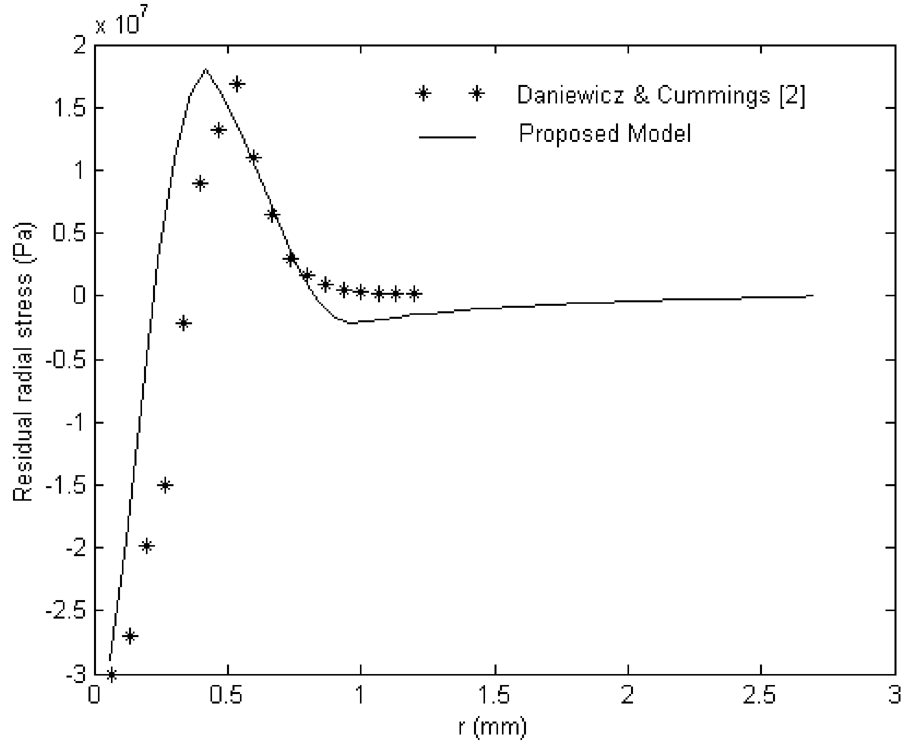

Figure 9: Residual radial stress variation as a function of radial distance

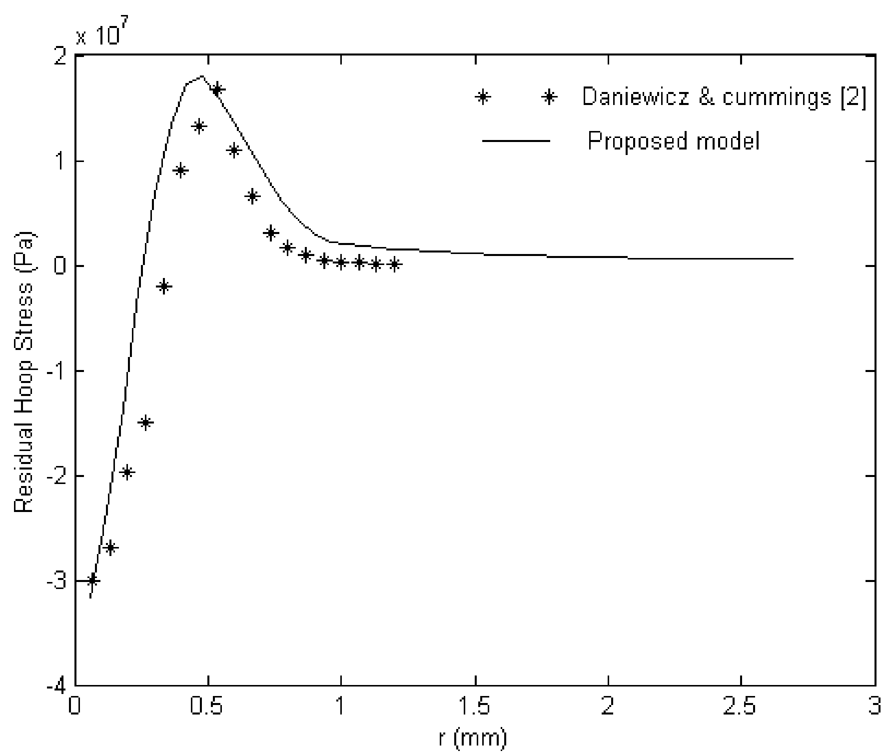

Figure 10: Residual hoop stress variation as a function of radial distance

2003 WJTA American Waterjet Conference
August 17-19, 2003 • Houston, Texas

Paper 3-A

MATHEMATICAL MODELING OF ULTRA HIGH PRESSURE WATERJET PEENING

S. Kunaporn
Walailuk University
Nakhonsithammarat, Thailand

M. Ramulu
University of Washington
Seattle, Washington, USA

M. Hashish
Flow International
Kent, Washington, USA

ABSTRACT

Waterjet peening is a recent promising method in surface treatment. It has potential to induce compressive residual stresses that benefit the fatigue life of materials similar to the conventional shot peening process. However, there are no analytical models that incorporate process parameters, i.e. supply pressure, jet exposure time, and nozzle traverse rate etc., to allow predicting the optimized peening process. Mathematical modeling of high pressure waterjet peening was developed in this study to describe the relation between the waterjet peening parameters and the resulting material modifications. Results showed the possibility of using the proposed mathematical model to predict an initial range for effective waterjet peening under the variation of waterjet peening conditions. The high cycle fatigue tests were performed to validate the proposed model and fatigue test results showed good agreement with the predictions.

1. INTRODUCTION

Effects of the impacting high pressure waterjet on the solid target have been of interest among researchers [1-13] not only to understand the mechanisms associated with jet material interface but also to apply waterjet in material removal processes such as cleaning, cutting, and paint removal etc. An additional application of the high-pressure waterjet to surface treatment was realized as early as 1984 in inducing compressive residual stress to enhance fatigue strength [1]. The process now is known as water peening. Water peening is similar to shot peening except it uses high-pressure droplets that are disintegrated in the waterjet flow field instead of solid shots. Fig. 1 illustrates the schematic of changes in jet structure with distance from the nozzle. The high-velocity droplets that benefit for peening are typically found in the transition region of jet structure.

In shot peening, the contact pressure resulting by the impact of the solid shot is represented in a form of a Hertzian pressure distribution [14-15]. The Hertzian pressure distribution was used in a numerical analysis as an interfacial load on to a material's surface to evaluate shot peening performance. Waterjet peening is still lacking for theoretical developments if compared to shot peening. The criteria for peening for any applied peening conditions on a specific target material have not yet well defined. This might due to the complexity of the jets in the waterjet peening operation, which involves many variables and conditions. However, some studies have been experimentally and numerically performed to describe the effects of waterjet on the material target. For example, Leach and Walker [16], and Rehbinder [17] presented the pressure distribution across the jet stream in parabolic and exponential forms, respectively. Powell and Simpson [18] subsequently employed the Leach and Walker parabolic pressure distribution to predict the residual stress state of the elastic half-space due to the impinging jet for a rock cutting application. Most recently, Daniewicz *et al.* [7] attempted to predict the material response in waterjet peening by using finite element analysis. The jet was assumed to be stationary with the impact pressure equal to the stagnation pressure, calculated by neglecting process parameters that were involved in the waterjet peening process such as standoff distance, nozzle feed rate etc. Results in their study showed under prediction of compressive residual stress in the material target compared to experiments.

This paper presents the results of recent study on waterjet peening of 7075-T6 aluminum alloy using ultra high-pressure waterjet. The study aimed at formulating the mathematical model of waterjet peening for evaluating the effects of high impact jet on material as well as optimizing the process. The analytical study of the waterjet peening process is presented and results are discussed and verified with experiments.

2. MATHEMATICAL MODELING OF WATERJET PEENING

In this study, we have assumed the moving jet in the waterjet peening operation (Fig. 2) as a stationary jet to avoid the complications of the effects of shear pressure that are possibly induced by the movement of the jet along the surface. Therefore, the simplified stationary jet imposes only a normal pressure onto the contact area. The approach used for the modeling of moving jet in waterjet peening is based on an understanding of a basic knowledge of a jet structure for peening in relations to the concept of elastic-plastic response of material to the impact jet. The magnitude of the interfacial impact pressure resulting from waterjet on the material is derived. The predicted impact pressure is subsequently used to predict the initial effective range for peening. The initial range defined by the model is the range of applied peening conditions that is sufficient to initiate yielding on the target but does not cause surface erosion.

Based on an elastic-plastic theory, the material will initiate yielding when the interfacial pressure is equal to $C \cdot S_y$, where C is a constant value that depends upon the geometry of the contact and the yield condition and S_y is the yield strength of the material. For Poisson's ratio ν = 0.3, the constant values C for the onset of yielding was found to be 1.59 and 1.51 under the Hertz pressure and the uniform pressure acting on a semi-infinite body, respectively [19]. Therefore, following this concept, the minimum compact pressure, that is sufficient to induce plastic deformation in the target, can be estimated if the properties of the target and the geometry of the impact pressure are known.

Considering the jet structure from Fig. 2, it was assumed that the momentum of a liquid jet outflow from the nozzle remained constant between the nozzle and the point of the impact. A change of momentum, M, with the control volume, cv, is equal to the impulse force, F, acting normal to the target surface. The momentum, . is given as $\int_{cv} V\rho V \cdot dA$, where V is the velocity and dA is the element area on a plane perpendicular to the direction of the velocity. The momentum conservation of the jet from the jet nozzle exit (1) to the contact area (2) gives

$$\left(\int V\rho V \cdot dA\right)_1 = \left(\int V\rho V \cdot dA\right)_2 \tag{1}$$

Assuming the jet velocity at the nozzle, V_1, exit as V_e, and V_2 is the impact velocity at the target defined as V_{im}, thus Eq. (1) is written as:

$$V_e^2\left(\frac{\pi}{4}d_n^2\right) = V_{im}^2\left(\frac{\pi}{4}d_{im}^2\right) \tag{2}$$

where d_{im} and d_n are the diameter of the waterjet at the point of the impact and at the nozzle exit, respectively. The droplet diameter at the point of the impact, d_{im}, is denoted in this model as the equivalent droplet d_{eq}. From Eq. (2), d_{eq} is then given as:

$$d_{eq} = \frac{V_e}{V_{im}}d_n = \sqrt{\frac{2p_s}{\rho}}\left(\frac{d_n}{V_{im}}\right) \tag{3}$$

where p_s is the pump pressure releasing from nozzle exit.

During the peening operation, it is assumed here that the motion of the jet produces uniform pressure across the contact area. Therefore, the impinging normal point force acting on the surface due to each droplet is calculated in relation to the pressure as:

$$F_d = p_c \frac{\pi d_{eq}^2}{4} \tag{4}$$

where p_c is the collapse pressure.

Substituting Eq. (3) into Eq. (4), we obtain

$$F_d = p_c \frac{\pi d_n^2}{4}\left(\frac{V_e}{V_{im}}\right)^2 = p_c A_n \left(\frac{V_e}{V_{im}}\right)^2 \tag{5}$$

where A_n is the cross sectional area of the nozzle and is equal to $\frac{\pi}{4} d_n^2$.

To consider the phenomena of the full stream of the jet, we assume that the surface is repeatedly struck by multiple impacts of single droplet. As a result, the exposure time of solid target under repeated impacts needs to be obtained. By considering the jet structure as shown in Fig. 2, the exposure time will be designated by t_p and it is the time of the jet over the contact area, 2*a*, which is given as $t_p = \frac{2a}{u}$, where u is the nozzle traverse speed and 2*a* is the contact diameter, which is equal to $d_n + 2SOD\,tan\frac{\alpha}{2}$ for this jet structure. Note that the impact area, 2a, used in this model is considered as an equivalent area similar to the area resulting by the round jet. The contact areas resulting from using different jet types (as shown in Fig. 3) will be simply considered as the equivalent area similar to the round jet in the model. With this exposure time, the total volume of liquid, V_L, coming out form the nozzle is $V_L = A_n V_e t_p$, where A_n is the nozzle area, V_e is the jet velocity at the nozzle exit.

In the view of the full stream jet, the number of the droplets in the total volume of the jet, defined as the droplet intensity, *I*, is equal to the ratio of the total waterjet volume, V_L, to the volume of a single equivalent droplet, $V_{d_{eq}}$. Then *I* is obtained by

$$I = \frac{V_L}{V_{d\,eq}} = \frac{A_n V_e t_p}{\frac{\pi}{6} d_{eq}^3} \text{ droplets in the jet} \tag{6}$$

The term "site" is introduced in this model as an area on the surface that is equal to the cross-sectional area of one equivalent droplet as graphically shown in Fig. 2. Therefore, a number of sites per contact area on the surface, A^*, is $A^* = \frac{A_a}{A_{d_{eq}}}$, where A_a and $A_{d_{eq}}$ are the cross-section of the contact surface of the jet and the cross section of the equivalent droplet that is given in Eq. (3).

From the assumption that the droplet distribution is uniform over the contact area and all droplets have the same diameter and are in the spherical shape, the number of impacts of the droplets per contact area, *N*, is defined by

$$N = \frac{I}{A^*} = \frac{I}{A_a / A_{d_{eq}}} = \left(\frac{A_n V_e t_p}{\frac{\pi}{6} d_{eq}^3} \right) \div \frac{A_a}{A_{d_{eq}}} = \left(\frac{A_n V_e t_p}{\frac{\pi}{6} d_{eq}^3} \right) \div \left(\frac{\frac{\pi}{4} (2a)^2}{\frac{\pi}{4} d_{eq}^2} \right) \quad (7)$$

The number of impacts of the droplets per contact area, *N*, can be simplified to

$$N = \frac{3}{2} \frac{d_n V_{im}}{(2a) u} \quad (8)$$

Considering the full stream of the jet, the total impact force due to the stream of the jet onto material surface is equal to the resulting force of each single droplet multiplied by the total number of the impacts, *N*. As a result, the total impact force, F_{impact}, can be calculated by

$$F_{impact} = N \cdot F_d = N \cdot \frac{\pi}{4} p_c d_{eq}^2 \quad (9)$$

By knowing the impact force, the impact pressure due to the impact of the stream jet is then obtained by assuming that the jet movement across the contact area produces a uniform pressure. Thus the impact pressure of waterjet can be given as:

$$P_{impact} = \frac{F_{impact}}{A_a} = \frac{N \cdot \frac{\pi}{4} p_c d_{eq}^2}{\frac{\pi}{4} (2a)^2} \quad (10)$$

Substituting Eq. (3), and Eq. (8) into Eq.(10), the impact pressure can be expressed as:

$$P_{impact} = \frac{3}{2u} \left(\frac{d_n}{2a} \right)^3 V_e^2 \frac{p_c}{V_{im}} = 3 \left(\frac{d_n}{2a} \right)^3 \cdot \left(\frac{p_s}{\rho \cdot V_{im}} \right) \cdot \left(\frac{p_c}{u} \right) \quad (11)$$

From the perspective of the collapse pressure under the impact of the high velocity jet, the magnitude of the pressure developed by an imploding droplet on the target is a highly localized water-hammer pressure [20-23]. This high magnitude of the water hammer pressure is assumed to be responsible for the plastic deformation at the point of the impact, which influences the residual stress and strength properties. Therefore, it is used as the collapse pressure to characterize the pressure and the force at the interface. The water- hammer pressure, p_w, was given as [20]:

$$p_w = \rho C_o V_o \tag{12}$$

where is the fluid density, C_o is the compressive wave velocity of the liquid, and V_o is the collapse velocity of the jet. If we substitute Eq. (12) into Eq. (11), the impact pressure can be finalized in terms of the major peening parameters as:

$$P_{impact} = 3C_o\left(\frac{d_n}{2a}\right)^3 \frac{p_s}{u} = 3C_o\left(\frac{d_n}{d_n + 2SOD\,tan\frac{\alpha}{2}}\right)^3 \frac{p_s}{u} \tag{13}$$

The mathematical model of the impact pressure (Eq.13) is used to further predict the final standoff distance for waterjet peening that can initiate yielding in a material. Based on the theory of elasticity as discussed previously, the minimum impact pressure required to initiate yielding of a material under the impact of the jets, P_y, is defined as when it is equal to $C \cdot S_y$. If this value is substituted into Eq. (13), a final standoff distance, SOD_f, meaning the largest standoff distance that gives the interface pressure at the threshold of plastic deformation can be estimated as follows:

$$SOD_f = \frac{d_n}{2\,tan\frac{\alpha}{2}}\left(\left(\frac{3C_o}{P_y}\frac{p_s}{u}\right)^{1/3} - 1\right) = \frac{d_n}{2\,tan\frac{\alpha}{2}}\left(\left(\frac{3C_o}{C \cdot S_y}\frac{p_s}{u}\right)^{1/3} - 1\right) \tag{14}$$

The constant C is a value depending on the geometry of the interfacial pressure based on elastic theory, which can be estimated by FEA. With the known C value, the final standoff distance, SOD_f, can be estimated for any given waterjet peening condition by the proposed mathematical model.

The variation of all process parameters, p_s, d_n, u and . will give the level of impact pressure that can be used to estimate the standoff distance at which the jet has no effects on the material target. . A schematic representation is plotted in Fig. 4 to describe how each parameter relates to the predicted final standoff distance, SOD_f. As follows from the figure, SOD_f increases as $\frac{p_s}{u}$ and p_s increase, and u and . decrease.

As previously discussed, the constant value C is dependent on the geometry of the interfacial pressure and properties of the target body. In order to estimate the SOD_f using the proposed Eq. 14, it is necessary to define C. Previous study has been performed to define the constant value C using finite element analysis [24-25]. Results showed that the constant C value of 1.59

given for the surface loading of the theoretical Hertzian pressure could be initially used for the prediction of an effective peening range by Eq. 14.

3. EXPERIMETAL VERIFICATION

3.1 Experimental Setup: High Cycle Fatigue Testing

The test specimens were fabricated into hour glass, circular cross section fatigue life rotating bending test specimens (Fig. 5). After fabrication, the gage section of each test specimen was surface treated by waterjet peening under conditions. To verify how peening conditions affects the fatigue limit of Al7075-T6, tests with different variations of p_s and *SOD* for waterjet peening on the test specimens were made. These variations were chosen such that the proposed mathematical model used to predict the peening range could be verified. The peening conditions were listed in Tables 1. The waterjet peening system employed a high-pressure pump with control unit, capable of generating pump pressures, p_s, up to 400 MPa. The pressurized water was controlled and directed through a 0.3-mm sapphire orifice before entering a nozzle specially designed for the purpose of waterjet peening. The nozzle was oriented perpendicular to the surface of the test specimen. With the test specimen fixed in a holder, the nozzle was moved and adjusted to obtain an appropriate nozzle-to-surface standoff distance, SOD (Fig. 2).

Both peened and unpeened hour-glass, circular cross section fatigue life test specimens were fatigue life tested in completely reversed rotating bending (R= S_{min}/S_{max} = -1) until fracture. A commercial R.R. Moore rotating bending fatigue test machine (4-point flexure) was used at rotational speeds up to 10,000 RPM at alternating stress, *S*, that ranged from 200 to 430 MPa. The number of cycles to fracture, along with corresponding applied stress amplitude were recorded for each test for later analysis.

3.2 Results of High Cycle Fatigue Testing

It is apparent that the degree of fatigue improvements is strongly dependent on peening conditions as observed in the S-N curves Fig.5 to Fig.7. The fatigue improvement was found under some peening conditions (e.g. SK-F1-FT1-1 for p_s of 103 MPa, SK-F1-FT2-1 for p_s of 207 MPa, and SK-F1-FT3-1 for p_s of 310 MPa). The maximum degree of fatigue improvement was about 20%-25% as compared to the unpeened condition. For each applied supply pressure in this waterjet peening study, the variation of standoff distance has an effect on the degree of fatigue improvement. Fatigue endurance limit of was found to decrease with increasing standoff distances.

According to the proposed mathematical model developed based on the multiple impacts of the droplets as previously given in Eq. 14, the SOD_f or the maximum standoff distance at which waterjet peening can induce plastic deformation was estimated for the applied peening conditions as listed in Table 1. For u = 12.7 mm/s, d_n = 0.33 mm, and . = 20°, the proposed mathematical model predicted that SOD_fs for three different supply pressures of 103, 207, and 310 MPa were 33mm, 42 mm, and 48 mm, respectively. Observations from fatigue testing results showed that the specimens waterpeened at the standoff distances less than the predicted SOD_f, did show an improvement of fatigue life in a comparable amount to that of shot peening. The conditions that showed the improvement of fatigue limits were SK-F1-FT1-1 for p_s of 103 MPa, SK-F1-FT2-1 for p_s of 207 MPa, and SK-F1-FT3-1 for p_s of 310 MPa.

In contrast, the conditions that applied standoff distances greater than the predicted SOD_f showed no or slight improvement of fatigue limits. Such conditions were SK-F1-FT1-2 and SK-F1-FT1-3 (p_s of 103 MPa) and SK-F1-FT2-2 and SK-F1-FT2-3 (p_s of 207 MPa), and SK-F1-FT1-3 (p_s of 310 MPa). The roughness measurement of these fatigue test specimens showed no apparent changes in surface roughness parameters. Therefore, it is possible that the waterjet under these conditions might not induce sufficient plastic deformation at the surface to improve its fatigue limit. This observation is in agreement to the prediction from the proposed mathematical model. However, it is important to note that the number of fatigue tests for some conditions are small that might not be enough to establish the fatigue test results for such conditions. However, the deduction of the fatigue results might be possible from the tendency that was observed in their S-N curves.

4. CONCLUSION

The mathematical modeling based on the multiple impacts of the jets has been proposed to estimate the contact pressure and the feasible peening range. Fatigue results showed that the proposed mathematical model might be a practical tool to predict the initial waterjet peening range since results showed some agreement between the fatigue study and the proposed model. Fatigue life improvement by waterjet peening was observed in the specimen waterpeened under the effective conditions predicted by the proposed model. Fatigue results did show that the viability of the proposed mathematical model that predicted the effective range for waterjet peening. With this observation, the proposed mathematical model could be used as the initial means to find out the optimal range for waterjet peening. However, more studies on other metals are necessary to perform in order to validate the model.

5. REFERENCES

1. Salko, D., “Peening by Water”, Proceedings of 2nd International Conference on Shot Peening, ICSP-2, Chicago, Illinois, 14-17 May 1984, Edt. Fuchs, H.O., American shot peening Society, New Jersey, pp. 37-38.
2. Blickwedel, H., Haferkamp, H., Louis, H. and Tai, P.T., “Modification of Material Structure by Cavitation and Liquid Impact and Their Influence on Mechanical Properties,” Erosion by Liquid and Solid Impact, Proc. 7th International Conference on Erosion by Liquid and Solid Impact, 7-10 September 1987, pp.31.1-31.6.
3. Mathias, M., Gocke, A. and Pohl, M., “The residual stress, texture and surface changes in steel induced by cavitation”, Wear, Vol. 150, 1991, pp. 11-20.
4. Yamauchi, Y., Soyama, H., Adashi, Y., Sato, K., Shindo, T., Oba, R., Oshima R., and Yamabe, M., “Suitable Region of High-Speed Submerged Water Jets for Cutting and Peening,” *JSME International Journal*, Series B, Vol.8, No.1, 1995, pp.31-38.

5. Tonshoff, H.K., Kross, F. and Marzenell, C., "High-pressure water Peening – a New Mechanical Surface-Strengthening Process", Annals of the CIRP Vol. 46, No. 1, 1997, pp 113-116.
6. Hirano, K., Enmoto, K., Hayashi, M., Oyamada, O., Hayashi, E., and Shimizu, S., "Stress Corrosion Cracking Mitigation by Water Jet Peening", PVP, Plant System/Components Aging Management, ASME 1997, Vol. 349, pp.89-93.
7. Daniewicz, S.R., and Cummings, S.D., "Characterization of Water Peening Process", Transaction of the ASME, Vol. 121, July 1999, pp. 336-340.
8. Krull, P., Nitschke-Pagel, Th., and Wohlfahrt, H., " Stability of Residual Stresses in Shot Peened and High Pressure Water Peened Stainless Steels at Elevated Temperature", The 7th International Conference on Shot Peening, Warsaw, Poland, 1999.
9. Soyama, H., "Improvement in Fatigue Strength of Silicon Manganese Steel SUP7 by Using a Cavitating Jet", JSME International Journal, Series. A, Vol. 43, No.2, 2000, pp173-177.
10. Colosimo, B.M., Monno, M., and Semeraro, Q., " Process Parameters Control in Water Jet Peening", International Journal of Material and Product Technology, Vol. 15, No. ½, 2000, pp.10-19.
11. Ramulu, M., Kunaporn, S., Jenkins, M.G., Hashish, M., and Hopkins, J., " Fatigue Performance of High Pressure Waterjet peened Aluminum Alloy", 2000 ASME Pressure Vessels and Piping Conference, Seattle, WA, July 23-27, 2000.
12. Kunaporn, S, Ramulu, M., Jenkins, M.G., Hashish, M., and Hopkins, J., "Ultra High Pressure Waterjet Peening, Part I: Surface Characteristics", 2001 WJTA American Waterjet Conference, Minneapolis, MN, August 18-21, 2001, paper no 25.
13. Kunaporn, S, Ramulu, M., Jenkins, M.G., Hashish, M., and Hopkins, J., "Ultra High Pressure Waterjet Peening, Part II: Fatigue Performance", 2001 WJTA American Waterjet Conference, Minneapolis, MN, August 18-21, 2001, paper no. 26.
14. Al-Obaid, Y.F., "A Rudimentary Analysis of Improving Fatigue Life of Metals by Shot Peening", Journal of Applied Mechanics, Vol.57, June 1990, pp. 307-312.
15. Al-Hassani, S.T.S., " An Engineering Approach to Shot Peening Mechanics", Proceedings of 2nd International Conference on Shot Peening, ICSP-2, Chicago, Illinois, 14-17 May 1984, Edt. Fuchs, H.O., American shot peening Society, New Jersey, pp. 275-281.
16. Leach, S.J., and Walker, G.L., "The Application of High Speed Liquid Jets to Cutting", Philosophical Transactions, Royal Society of London Series A, Vol. 260, 1966, pp. 295-308.
17. Rehbinder, G, " Some Aspects of the Mechanism of Erosion of Rock with a High Speed Water Jet", paper E1, 3rd International Symposium on Jet Cutting Technology, May, 1976, Chicago, IL, pp. E1-1 to E1-20.
18. Powell, J.H., and Simpson, S.P., "Theoretical Study of the Mechanical Effects of Water Jets Impinging on a Semi-Infinite Elastic Solid", International Journal of Rock Mechanics and Mining Science, Vol.6, 1969, pp. 353-364.
19. Tabor, D., *The Hardness of Metals*, The Clarendon Press, Oxford, 1951.
20. Blowers, R. W., "On the Response of an Elastic Solid to Droplet Impact", Journal of Institute Mathematics Applications (1969), Vol. 5, pp. 167-193.
21. Obara, T., and Bourne, N.K., and Field. J.E., "Liquid-Jet impact on liquid and solid surface," Wear, 1995, Vol. 186-187, pp. 38-394.
22. Johnson, W. and Vickers, G.W., "Transient Stress Distribution caused by Water-Jet Impact", Journal Mechanical Engineering Science, Vol. 15, No.4, 1973, pp. 302-310.

23. Hwang, J.B.G., and Hammitt, F.G., "On Liquid-Solid Impact Phenomena", Journal of Applied Physics, Mar 21-25, 1976, ASME, pp. 24-27. (Cavitations and Phosphate Flow Forum, 1976.
24. Kunaporn, S., "An Experimental and Numerical Analysis of Waterjet Peening of 7075-T6 Aluminum Alloy", Doctoral Dissertation, University of Washington, 2002.
25. Kunaporn, S, Ramulu, M.G., Hashish, M., "Finite Element Analysis of Residual Stress induced by Ultra high Pressure Waterjet", The 16th International Conference on Water Jetting, Aix-en-Provence, France, 16-18 October 2002.

Table 1: Waterjet peening conditions of circular fatigue test specimens.

Test Set	Test Identification	No of. specimens	p_s (MPa)	*Actual SOD* (mm)	u (mm/s)	No. of jet passes	Nozzle Type	*Predicted SOD$_f$* (mm)
FT1	SK-F1-FT1-1	7	103	24	12.7	4	Fan	32
	SK-F1-FT1-2	3		36				
	SK-F1-FT1-3	3		47				
FT2	SK-F1-FT2-1	7	207	36	12.7			42
	SK-F1-FT2-2	3		59				
	SK-F1-FT2-3	3		83				
FT3	SK-F1-FT3-1	9	310	44	12.7			48
	SK-F1-FT3-2	3		77				

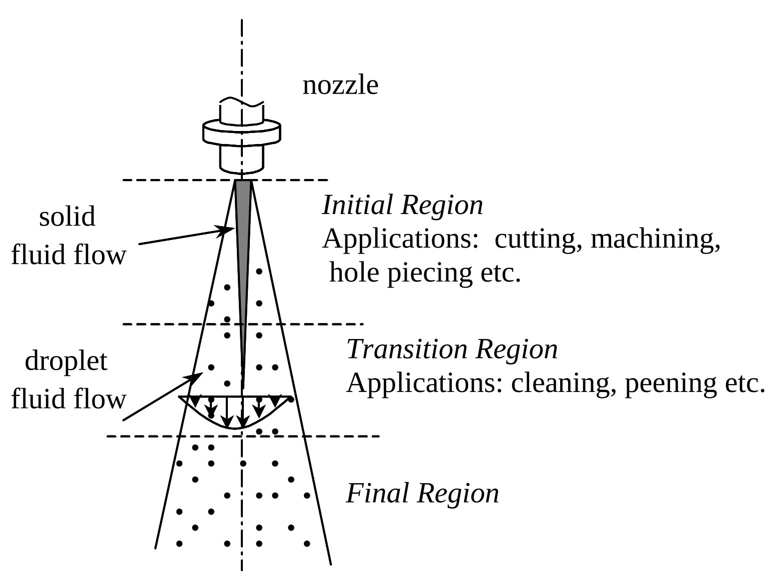

Figure 1: Schematic of changes in jet structure with distance from the nozzle.

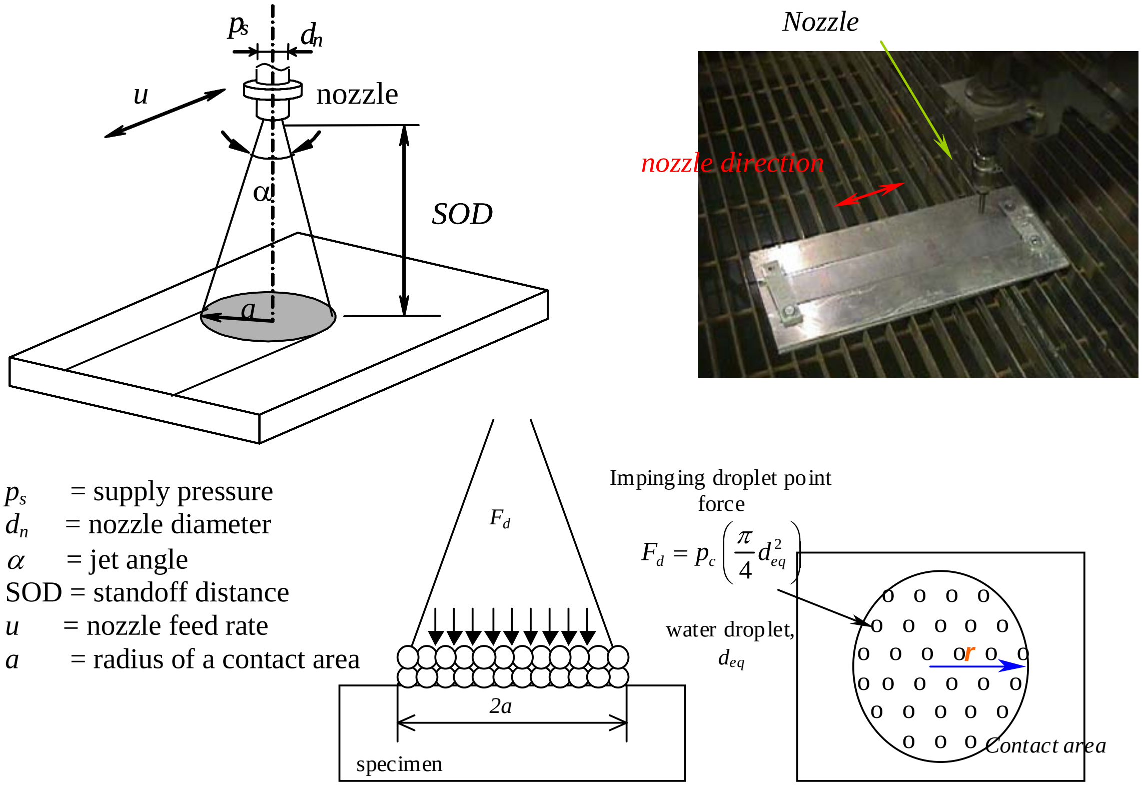

Figure 2: Graphic representation of the waterjet peening process.

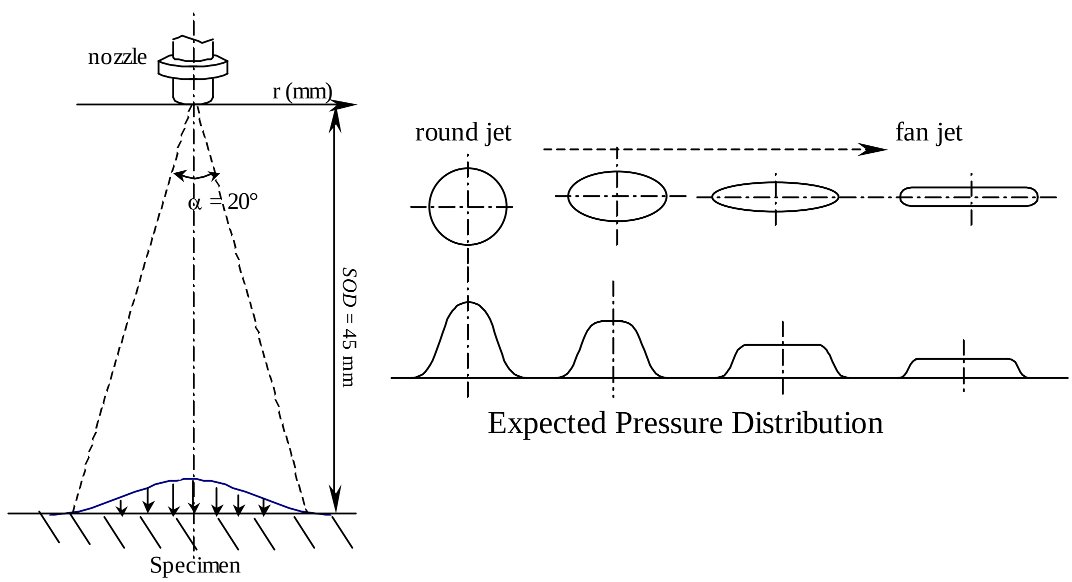

Figure 3: Schematic of pressure profile across a cross section of the jet resulting from using different kinds of nozzles in the waterjet operation

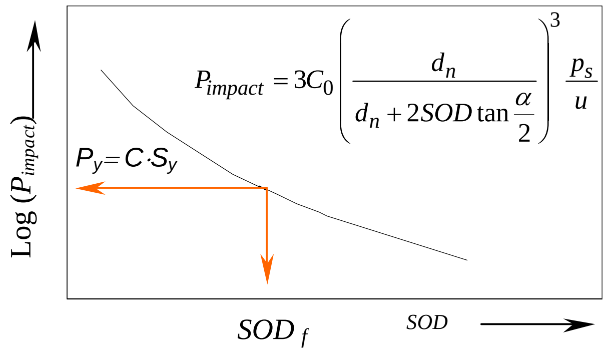

P_y : the minimum pressure distribution at which yielding can be initiated

SOD_f : the maximum SOD that can be used in UHPWJ peening to initiate yielding

Figure 4: Pressure distribution curve.

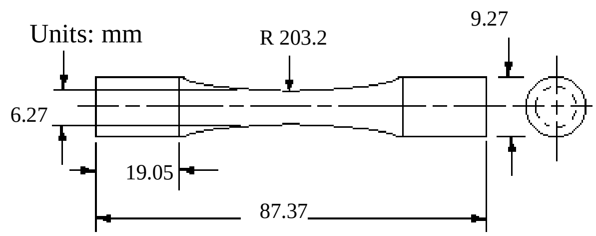

Figure 5: Geometry and Dimensions of Hourglass, Circular Cross-section Fatigue Life Test Specimens

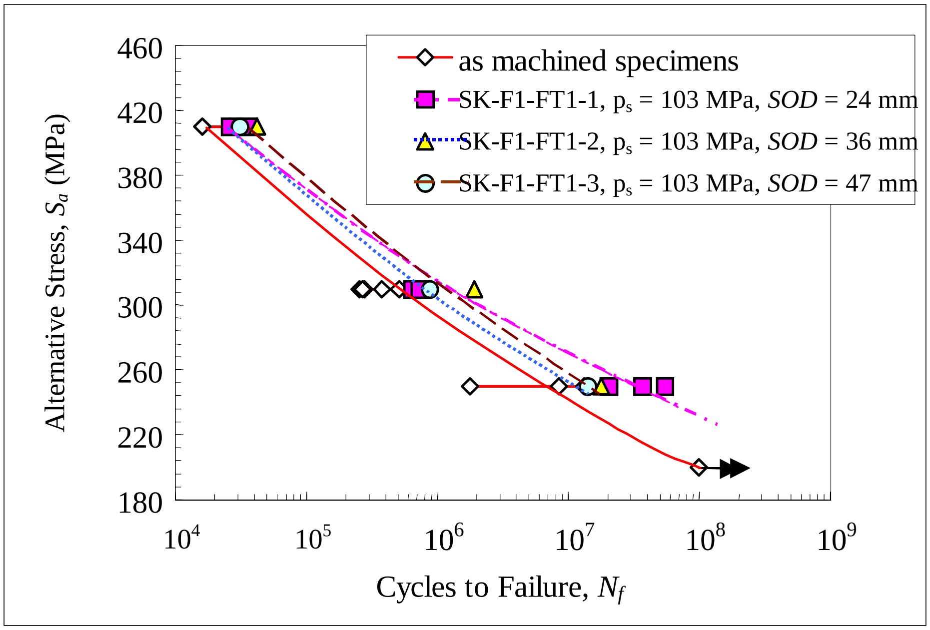

Figure 5: S-N curves for as-machined and waterjet-peened circular cross section fatigue life test specimens set SK-F1-FT1 for p_s = 103 MPa, u = 12.7 mm/s.

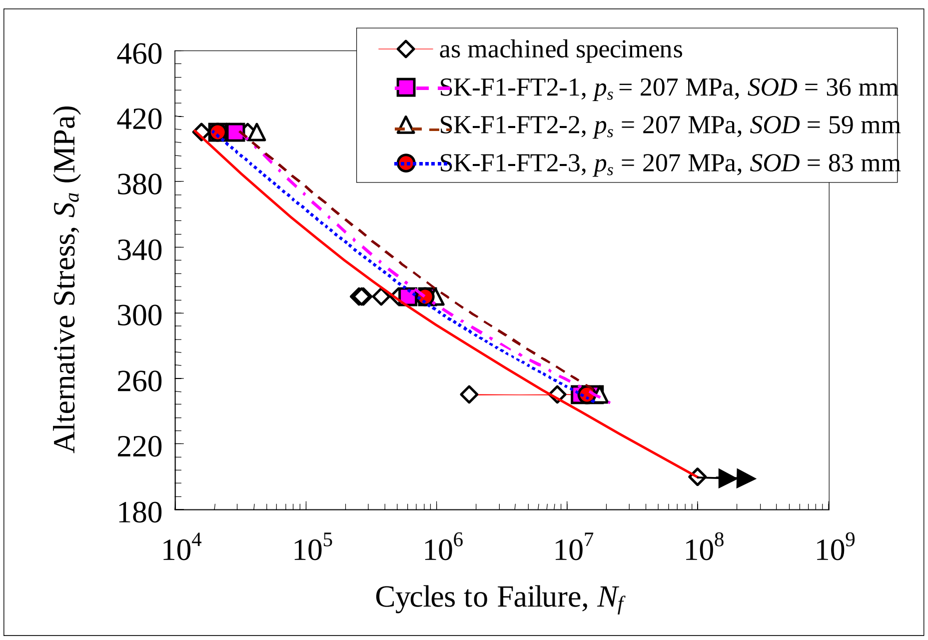

Figure 6: S-N Curves for as-machined and waterjet-peened circular cross section fatigue life test specimens set SK-F1-FT2 for p_s = 207 MPa, u = 12.7 mm/s.

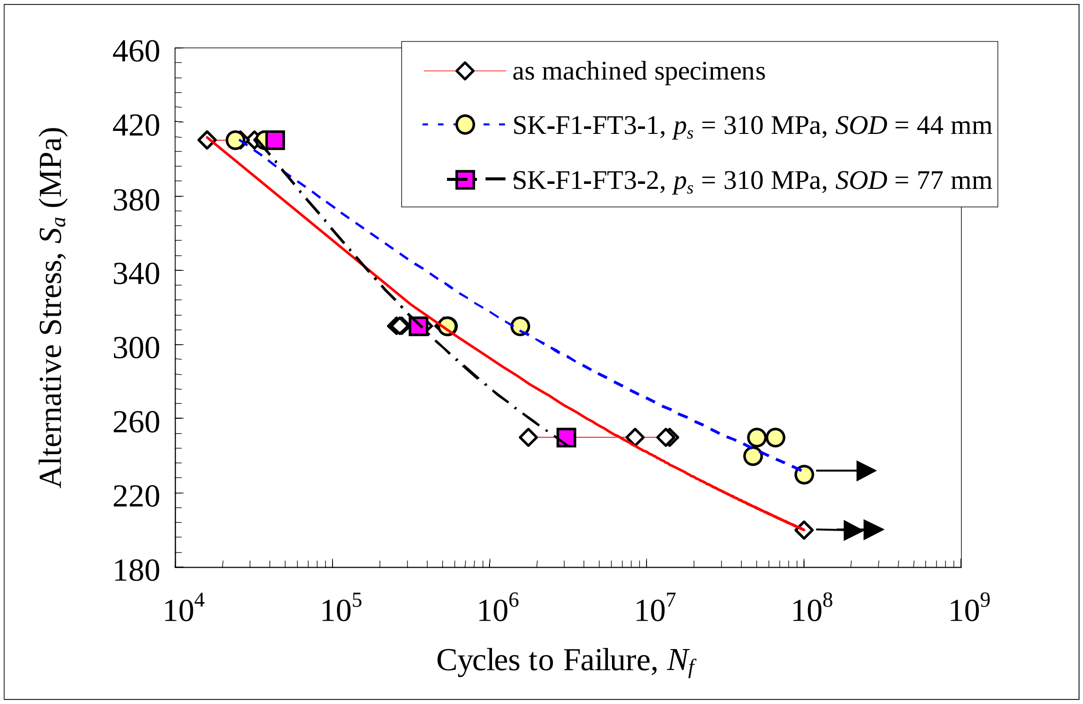

Figure 7: S-N curves for as-machined and waterjet-peened circular cross section fatigue life test specimens set SK-F1-FT3 for p_s = 310 MPa, u = 12.7 mm/s.

2003 WJTA American Waterjet Conference
August 17-19, 2003 · Houston, Texas

Paper 3-A

PIPE THREADS-WHAT IS THE LIMIT?

D. Wright, J. Wolgamott, G. Zink
StoneAge, Inc.
Durango, Colorado, U.S.A.

ABSTRACT

At present there is no established guideline in the waterblast industry regarding the maximum operating pressure of tapered pipe thread connections. This paper presents the results of tests to determine the failure point of tapered pipe threads when internally pressurized.

Male pipe threads machined on short sections of pipe with various inside diameters were tested to burst or thread failure in three stainless steel materials. Female pipe couplings in two stainless steel materials and with various outside diameters were also tested to failure. Pipe thread sizes from 1/8 to 1-1/4 NPT were studied. Variables such as the number of threads engaged and the effect of repeated assembly of pipe thread connections were also tested.

Comparisons between actual failure points and the predictions of common equations were made, in an effort to determine the best fit for making calculations. Hopefully, based on these tests and others, a consensus can be reached regarding the use of pipe threads in the waterblast industry.

1. INTRODUCTION

The purpose of this research was to find through testing at what pressures pipe thread connections fail, and to compare the actual values to predicted values to determine the best equations for calculating burst pressures. These values in combination with a factor of safety can then be used to determine safe operating pressures for these components.

A factor of safety is used to allow for uncertainty in material properties, geometry and the operating environment. Safety factors can be as high as 20 for structures such as dams, to as low as 1.5 for a commercial aircraft, which would not get off the ground if built like a dam, but must be inspected and maintained regularly. The Waterjet Technology Association has specified a safety factor of 2.5 for components used in a system chosen primarily with weight considerations in mind. This means that once the burst pressure of a component is determined by testing or calculation, this value is divided by 2.5 to determine the operating pressure for that component.

The two equations commonly used for calculating the burst pressure of a cylinder are known as Barlow (equation 1) and Lame′ (equation 2). The Barlow equation is used when the cylinder is considered to be thin walled, because it assumes the stress across the wall is constant. Thin walled is defined by the ratio of the inside diameter/wall being greater than ten. For cylinders with this ratio being less than ten, the Lame′ equation should be used, as it allows for decreasing stress values through the wall. All test samples used in these tests had a ratio less than ten.

$$P = 2\ S\ t\ /\ D \qquad (1)$$

$$P = S\ (w^2-1)\ /\ (w^2+1) \qquad (2)$$

Where
P = pressure (burst)
S = tensile strength of material
t = wall thickness
D = outer diameter
w = wall ratio (outer diameter / inner diameter)

The working pressure for the component then becomes P / 2.5 to account for the factor of safety. Variations to these equations account for the reduction of the wall thickness when threads are cut. The thread depth values are shown in Table 1 for each thread size tested. For externally threaded components two times the thread depth is subtracted from the outer diameter, while for internally threaded components two times the thread depth is added to the inner diameter.

2.0 TEST PROCEDURE

Two methods of pressurizing the test samples were used; a single stroke intensifier capable of pressures up to 560 MPa (80,000 psi) and a triplex plunger pump capable of pressures up to 280 MPa (40,000 psi). The intensifier was used where possible, except in cases where the test fittings leaked and the intensifier could not produce enough volume to maintain pressure. Some samples did not fail up to 560 MPa (80,000 psi); actual failure points for these are not known.

The male pipe samples were installed in 17-4 stainless steel test fittings with a calculated wall thickness to allow 560 MPa (80,000 psi) without yield. The female pipe couplings were tested with 17-4 stainless steel male threads. All fittings were assembled with Parker Thread Mate and Teflon tape and tightened to five turns of engagement.

Samples made from 303, 304A bar, 304L seamless schedule 160 pipe and 17-4 H900 stainless steel were tested. The properties of these materials are shown in Table 2; these are the values used for all calculations. All threads were machined, with a standard root radius of .15 mm (.006 in.).

3.0 TEST RESULTS

3.1 Male Pipe

Pipe sizes of 1/8, 1/4, 1/2, 3/4, 1, and 1-1/4 NPT were tested. Table 3 lists each test sample by size, material, type of failure and failure pressure.

Solid plugs of each size were made from 304A hot finished bar and tested to determine where thread failure occurred. The 1/8, 1/4 and 1/2 NPT plugs went to 560 MPa (80,000 psi) without failure, the limit of these tests. The 3/4, 1 and 1-1/4 NPT samples failed by shearing of the threads. The results of the plug tests are shown in Figure 1.

Figures 2 and 3 show the results of 1/8 and 1/4 NPT samples, machined from 304A bar, with two different inside diameters. These results are compared to values calculated with the Lame′, Barlow and Barlow with the thread depth allowance (Barlow-c) equations, using the nominal outer and inner diameters, as well as the calculated results with the thread depth removed from the outer diameter. Both 1/8 NPT samples failed by burst in the wall with the threaded end remaining intact; the burst failure in the thin walled 1/4 NPT sample started at the last thread root. The thick walled 1/4 NPT sample failed by burst in the wall and the threads remained intact. These four pieces are shown in Figure 4.

Three samples of 1/2 NPT 304A bar were machined, with three different inside diameters. The middle size inner diameter matched that of standard 1/2 schedule 160 pipe. In addition, a sample of 304L schedule 160 1/2 pipe was tested. These results are shown in Figure 5, again compared to calculated values. The thin walled sample burst failure started at the last thread root; burst failure occurred in the wall in the other two samples as well as in the pipe sample. Figure 6 shows these pieces.

Similar samples were prepared for 3/4 NPT, machined from bar as well as from 3/4 schedule 160 pipe. The results are shown in Figure 7, and Figure 8 shows these samples. All samples failed by burst, which began in the wall on all of these.

The same series of tests were performed on 1 NPT samples. However, only the thin walled piece machined from bar and the sample of 1 schedule 160 pipe failed by burst. The other two machined pieces failed by thread shear. The results of these tests are shown in Figure 9, and the pieces are shown in Figure 10. Figure 11 shows all the pieces made from schedule 160 304 L pipe as a group; note that every failure occurred in the pipe wall, independent of the pipe threads.

Two samples of 1-1/4 NPT were machined from 304A bar, with two different inside diameters. The thin walled sample failed by burst, beginning at the last thread root. The thick walled sample failed by thread shear. These results and samples are shown in Figures 12 and 13.

Samples of each of the pipe sizes were also made from 17-4, in the H900 condition. These pieces had inside diameters at least as large as standard schedule 40 pipe sizes, as it was desired to have them fail below 560 MPa (80,000 psi). The results of these tests are shown in Figure 14, compared to the calculated values. The 1/8, 1/4 and 1/2 NPT samples failed by burst, shattering into multiple pieces. The 3/4 and 1 NPT samples broke cleanly off at the last exposed thread, while the 1-1/4 NPT sample burst out one side. These pieces are shown in Figure 15.

3.2 Pipe Couplings

Sample pipe couplings were made in both 303 and 17-4 H900 stainless steels, in sizes of 1/4, 1/2, 3/4 and 1 NPT, with two different outside diameters. Table 4 lists each test sample by size, material, type of failure and failure pressure.

The biggest difficulty of testing the couplings was due to yield causing a leak. If this occurred above the 280 MPa (40,000 psi) limit of the triplex pump, the only way to continue with the intensifier was to reassemble and retighten the fittings, which effectively results in more threads engaged, and allows reaching a burst failure if this process is repeated. However, it was found that failure due to thread shear occurred at much lower pressures than burst, as the coupling yielded and reduced the thread contact area. Therefore, when possible, the couplings were taken to failure by yield and thread shear, but in cases where they yielded and leaked suddenly without shear or rupture, this point was taken as the failure pressure.

In the case of 17-4, which has a yield strength very close to the tensile strength, it was possible to reach burst failure without a large leak in some of the couplings. The 1/4 NPT couplings of 17-4 stainless steel yielded and leaked without failing; these values are plotted in Figure 16, and are less than the calculated yield and burst values using the Lame′ equation. The thin walled 1/2 NPT made from 17-4 failed by burst, breaking into several pieces, while the thick walled coupling did not fail at 560 MPa (80,000 psi); Figure 17 shows these values compared to the calculated values. The 3/4 NPT 17-4 thin walled coupling failed by burst, a single split down the side, but the thick walled coupling failed by thread shear. Both failures were greater than that predicted by calculated burst; these values are shown in Figure 18. The thin walled 1 NPT 17-4 yielded and leaked between the calculated values for yield and burst. The thick walled coupling failed by thread shear above that calculated for burst; Figure 19 compares the actual values to the calculated values for burst and yield.

All of the failures in the 303 stainless steel were caused by thread shear as yield progressed. Both of the 1/4 NPT samples yielded and leaked, without our being able to make them fail. Actual values shown in Figure 20 are the points at which this occurred, compared to calculated values using the Lame′ equation for burst and yield. The same results occurred with the 1/2 NPT 303 couplings; these values are shown in Figure 21. The failures in the 1/4 and 1/2 NPT samples occurred close to the calculated burst; well above the calculated yield. Both of the 3/4 NPT couplings failed by thread shear; Figure 22 shows these results versus the calculated values. The 1 NPT samples also failed by thread shear; these results are plotted in Figure 23. The failures in the 3/4 and 1 NPT samples occurred about midway between the calculated yield and burst values.

3.3 Thread Engagement and Multiple Assembly

A series of tests to determine the effect of number of threads engaged was performed using the 3/4 NPT 303 stainless steel couplings with a 44 mm (1.75 in.) outer diameter, which were known to fail by thread shear. These results are shown in Figure 24. The coupling with 6.5 threads of engagement did not fail, but yielded and leaked; this point was used on the plot. Over the range tested, each thread of engagement resulted in a 12 percent difference.

Testing of multiple assemblies took place on a sample of 1/2 NPT 304L pipe and a 3/4 NPT 303 coupling with a 44 mm (1.75 in.) outer diameter. Each sample was assembled and disassembled 100 times. The 1/2 NPT pipe sample failed in the pipe wall, not in the thread. The 3/4 NPT sample failed by thread shear at 248 MPa (35,400 psi), with 5.75 threads engaged, 5 percent less than the value predicted from the thread engagement tests.

4.0 CONCLUSIONS

Figure 25 shows the average difference between the actual failures and the values predicted by the equations used for each material. The testing of the male pipe samples machined from 304A bar resulted in burst failures equal to or greater than values predicted by the Lame′ equation for thick walled cylinders. Failures due to thread shear occurred in the 1 and 1-1/4 NPT heavy walled samples, where the burst pressure exceeded the thread strength. All samples of 304L pipe failed in the pipe wall, at values predicted by the Lame′ equation, with no failures related to the pipe threads.

The 17-4 stainless steel male pipe samples showed some failures occurring at less than the predicted values of the Lame′ equation; it is possible that the actual strength of these pieces was less than used in the calculations. Materials such as 13-8 and 15-5 are known to have better transverse toughness properties than 17-4 and would be recommended in cases where size or weight constraints require designs at the 2.5 times burst limit. Otherwise, with very strong materials such as 17-4, parts can be designed with much higher burst values without much sacrifice in weight.

The testing of the couplings of 303 and 17-4 showed a failure mode of thread shear to be much more likely than failure due to burst. The thread shear failures were caused by yield of the coupling. Actual failures due to yield and thread shear typically occurred above the calculated yield, but below the calculated burst.

1/8 NPT	.635 mm (.025 in.)
1/4 NPT	.973 mm (.038 in.)
1/2 NPT	1.288 mm (.0507 in.)
3/4 NPT	1.288 mm (.0507 in.)
1 NPT	1.590 mm (.0626 in.)
1 NPT	1.590 mm (.0626 in.)

Table 1. Thread depth

Material	Yield Strength	Tensile Strength
303 SS	245 MPa (35,000 psi)	630 MPa (90,000 psi)
304L SS pipe	238 MPa (34,000 psi)	595 MPa (85,000 psi)
304A SS bar	277 MPa (39,600 psi)	640 MPa (91,500 psi)
17-4 H900 SS	1190 MPa (170,000 psi)	1330 MPa (190,000 psi)

Table 2. Material properties

Size	Material	O.D.	I.D.	Failure Pressure	Failure Type
1/8	304A bar	10.3 mm (.405 in.)	Plug	560 MPa (80,000 psi)	No failure
1/8	304A bar	10.3 mm (.405 in.)	4.8 mm (.189 in.)	507 MPa (72,400 psi)	Burst
1/8	304A bar	10.3 mm (.405 in.)	6.6 mm (.260 in.)	294 MPa (42,000 psi)	Burst
1/8	17-4 H900	10.3 mm (.405 in.)	7.4 mm (.290 in.)	444 MPa (63,500 psi)	Burst
1/4	304A bar	13.7 mm (.540 in.)	Plug	560 MPa (80,000 psi)	No failure
1/4	304A bar	13.7 mm (.540 in.)	6.1 mm (.239 in.)	526 MPa (75,100 psi)	Burst
1/4	304A bar	13.7 mm (.540 in.)	8.9 mm (.350 in.)	286 MPa (40,900 psi)	Burst
1/4	17-4 H900	13.7 mm (.540 in.)	9.9 mm (.390 in.)	356 MPa (50,800 psi)	Burst
1/2	304A bar	21.3 mm (.840 in.)	Plug	560 MPa (80,000 psi)	No failure
1/2	304A bar	21.3 mm (.840 in.)	9.7 mm (.380 in.)	518 MPa (74,000 psi)	Burst
1/2	304A bar	21.3 mm (.840 in.)	11.8 mm (.466 in.)	403 MPa (57,500 psi)	Burst
1/2	304L pipe	21.3 mm (.840 in.)	11.8 mm (.466 in.)	313 MPa (44,700 psi)	Burst
1/2	304A bar	21.3 mm (.840 in.)	13.6 mm (.537 in.)	305 MPa (43,600 psi)	Burst
1/2	17-4 H900	21.3 mm (.840 in.)	15.7 mm (.618 in.)	403 MPa (57,500 psi)	Burst
3/4	304A bar	26.7 mm (1.050 in.)	Plug	464 MPa (66,300 psi)	Thread shear
3/4	304A bar	26.7 mm (1.050 in.)	13.3 mm (.525 in.)	394 MPa (56,300 psi)	Burst
3/4	304A bar	26.7 mm (1.050 in.)	15.5 mm (.611 in.)	321 MPa (45,800 psi)	Burst
3/4	304L pipe	26.7 mm (1.050 in.)	16.3 mm (.643 in.)	271 MPa (38,700 psi)	Burst
3/4	304A bar	26.7 mm (1.050 in.)	18.0 mm (.710 in.)	244 MPa (34,800 psi)	Burst
3/4	17-4 H900	26.7 mm (1.050 in.)	21.3 mm (.838 in.)	286 MPa (40,900 psi)	Burst
1	304A bar	33.4 mm (1.325 in.)	Plug	410 MPa (58,500 psi)	Thread shear
1	304A bar	33.4 mm (1.325 in.)	17.4 mm (.688 in.)	360 MPa (51,400 psi)	Thread shear
1	304A bar	33.4 mm (1.325 in.)	20.7 mm (.815 in.)	294 MPa (42,000 psi)	Thread shear
1	304L pipe	33.4 mm (1.325 in.)	20.7 mm (.815 in.)	266 MPa (38,000 psi)	Burst
1	304A bar	33.4 mm (1.325 in.)	24.6 mm (.970 in.)	196 MPa (28,000 psi)	Burst
1	17-4 H900	33.4 mm (1.325 in.)	26.6 mm (1.048 in.)	292 MPa (41,700 psi)	Burst
1-1/4	304A bar	42.2 mm (1.660 in.)	Plug	309 MPa (44,200 psi)	Thread shear
1-1/4	304A bar	42.2 mm (1.660 in.)	24.3 mm (.958 in.)	305 MPa (43,600 psi)	Thread shear
1-1/4	304A bar	42.2 mm (1.660 in.)	33.7 mm (1.328 in.)	170 MPa (24,300 psi)	Burst
1-1/4	17-4 H900	42.2 mm (1.660 in.)	34.0 mm (1.338 in.)	302 MPa (43,100 psi)	Burst

Table 3. List of male pipe samples and test results

Size	Material	O.D.	I.D.	Failure pressure	Failure type
1/4	303	21.3 mm (.840 in.)	11.1 mm (.438 in.)	340 MPa (48,600 psi)	Yield, leak
1/4	303	28.6 mm (1.125 in.)	11.1 mm (.438 in.)	441 MPa (63,000 psi)	Yield, leak
1/4	17-4 H900	16.8 mm (.661 in.)	11.1 mm (.438 in.)	418 MPa (59,700 psi)	Yield, leak
1/4	17-4 H900	18.8 mm (.741 in.)	11.1 mm (.438 in.)	526 MPa (75,100 psi)	Yield, leak
1/2	303	28.4 mm (1.120 in.)	18.3 mm (.719 in.)	232 MPa (33,100 psi)	Yield, leak
1/2	303	31.8 mm (1.250 in.)	18.3 mm (.719 in.)	317 MPa (45,300 psi)	Yield, leak
1/2	17-4 H900	26.1 mm (1.029 in.)	18.3 mm (.719 in.)	541 MPa (77,300 psi)	Burst
1/2	17-4 H900	28.9 mm (1.137 in.)	18.3 mm (.719 in.)	560 MPa (80,000 psi)	No failure
3/4	303	36.8 mm (1.450 in.)	23.4 mm (.922 in.)	178 MPa (25,400 psi)	Thread shear
3/4	303	44.4 mm (1.750 in.)	23.4 mm (.922 in.)	240 MPa (34,300 psi)	Thread shear
3/4	17-4 H900	32.5 mm (1.280 in.)	23.4 mm (.922 in.)	332 MPa (47,500 psi)	Burst
3/4	17-4 H900	36.3 mm (1.430 in.)	23.4 mm (.922 in.)	464 MPa (66,300 psi)	Thread shear
1	303	52.8 mm (2.080 in.)	29.4 mm (1.156 in.)	201 MPa (28,700 psi)	Thread shear
1	303	63.5 mm (2.500 in.)	29.4 mm (1.156 in.)	245 MPa (35,000 psi)	Thread shear
1	17-4 H900	40.7 mm (1.603 in.)	29.4 mm (1.156 in.)	441 MPa (63,000 psi)	Yield, leak
1	17-4 H900	45.4 mm (1.789 in.)	29.4 mm (1.156 in.)	456 MPa (65,200 psi)	Thread shear

Table 4. List of pipe coupling samples and test results

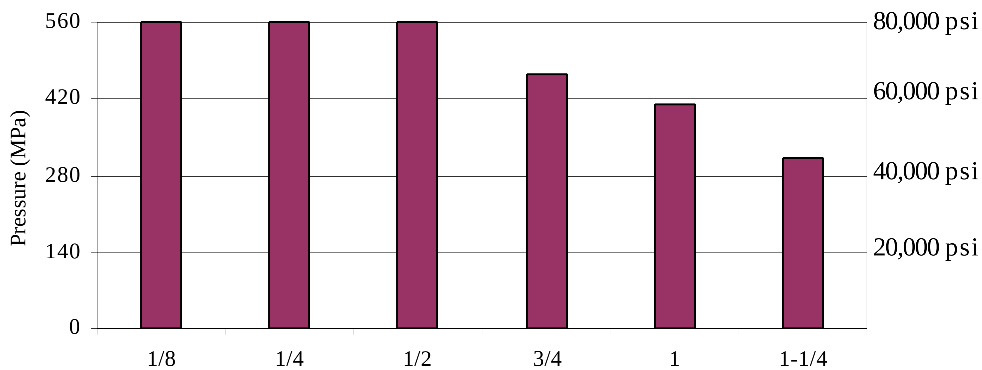

Figure 1. Pipe plug failure pressures, 304 male in 17-4 female

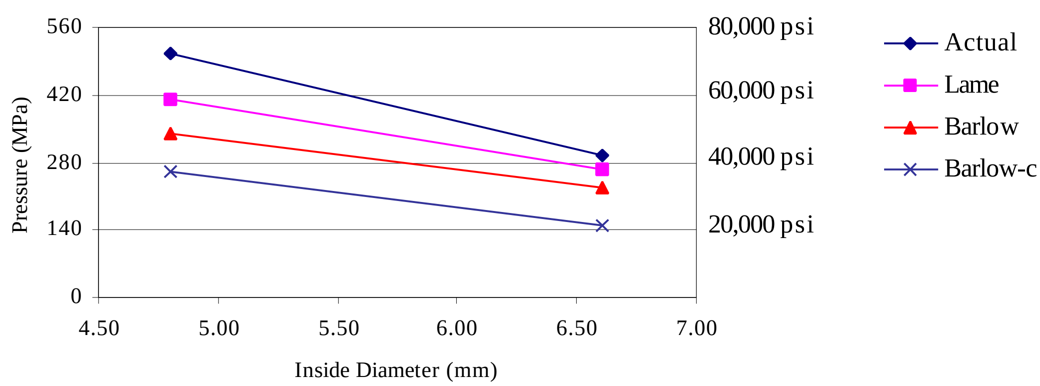

Figure 2. Results of 1/8 NPT 304 samples compared to calculated burst

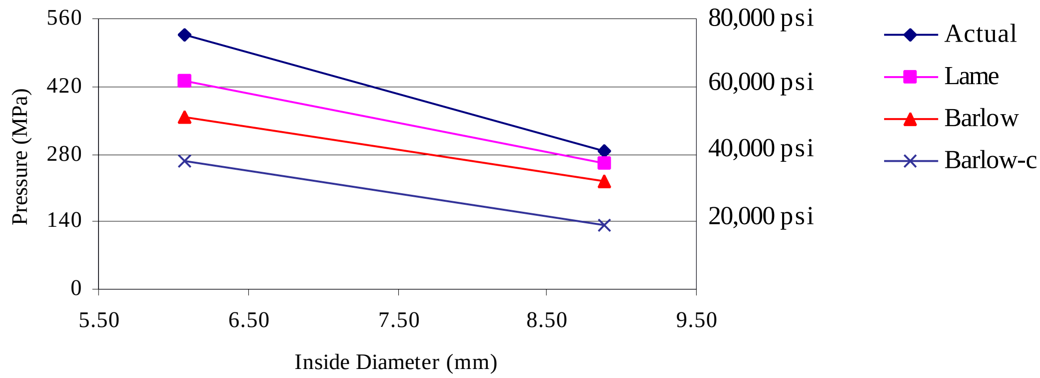

Figure 3. Results of 1/4 NPT 304 samples compared to calculated burst

Figure 4. 1/8 and 1/4 NPT 304 test samples

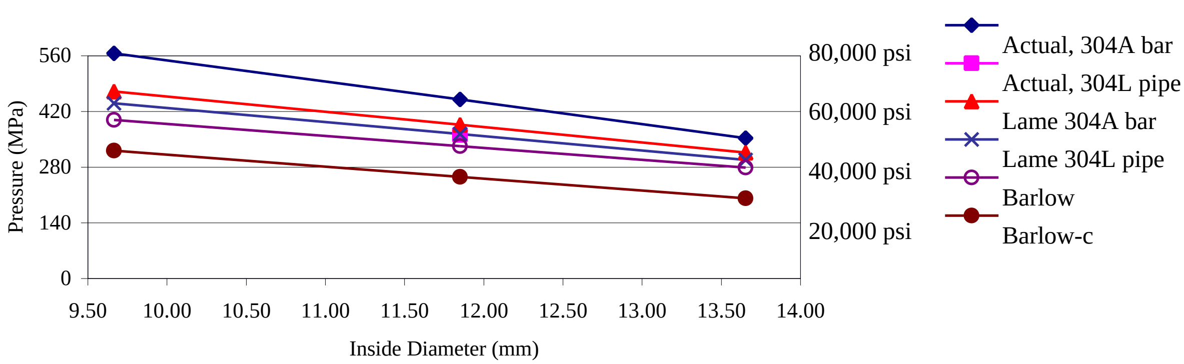

Figure 5. Results of 1/2 NPT 304 samples compared to calculated burst

Figure 6. 1/2 NPT 304 test samples

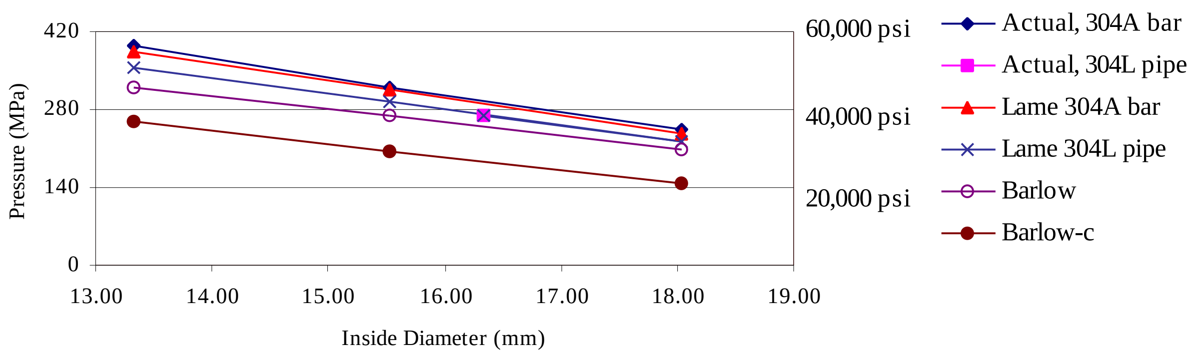

Figure 7. Results of 3/4 NPT 304 samples compared to calculated burst

Figure 8. 3/4 NPT 304 test samples

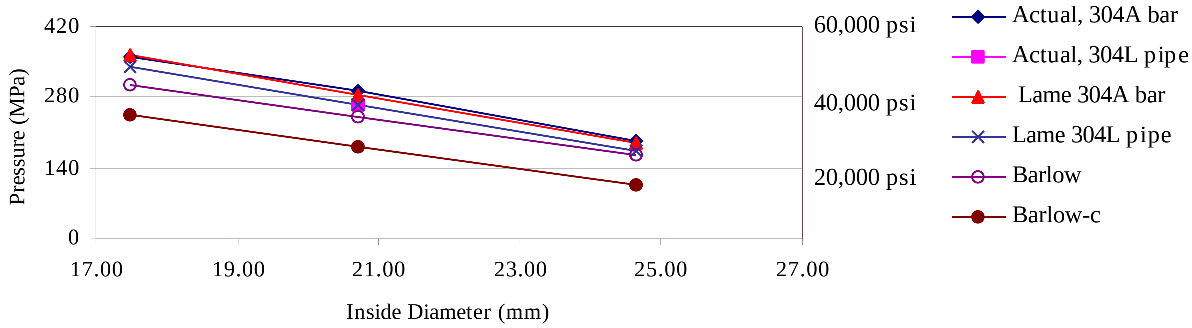

Figure 9. Results of 1 NPT 304 samples compared to calculated burst

Figure 10. 1 NPT 304 test samples

Figure 11. 304L schedule 160 seamless pipe samples (1/2, 3/4, and 1 NPT)

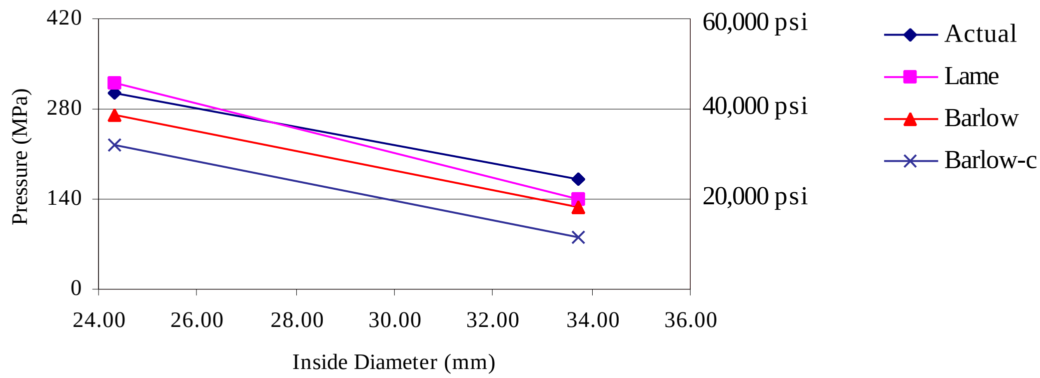

Figure 12. Results of 1-1/4 NPT 304 samples compared to calculated burst

Figure 13. 1-1/4 NPT 304 test samples

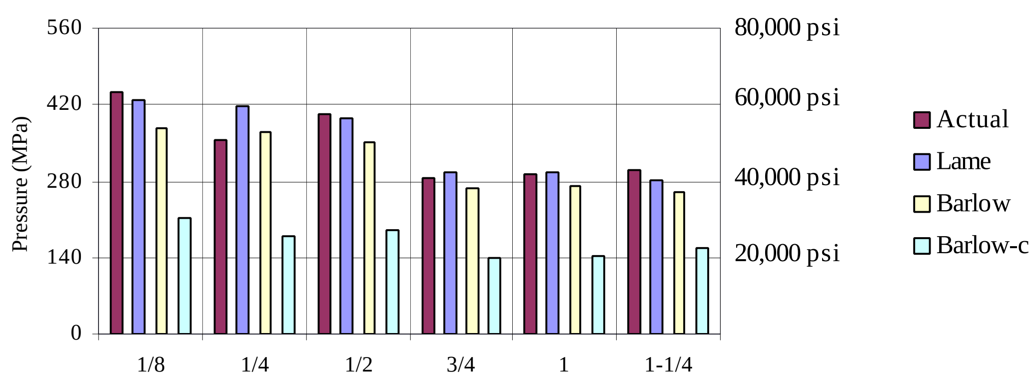

Figure 14. Results of 17-4 samples compared to calculated burst

Figure 15. 17-4 test samples

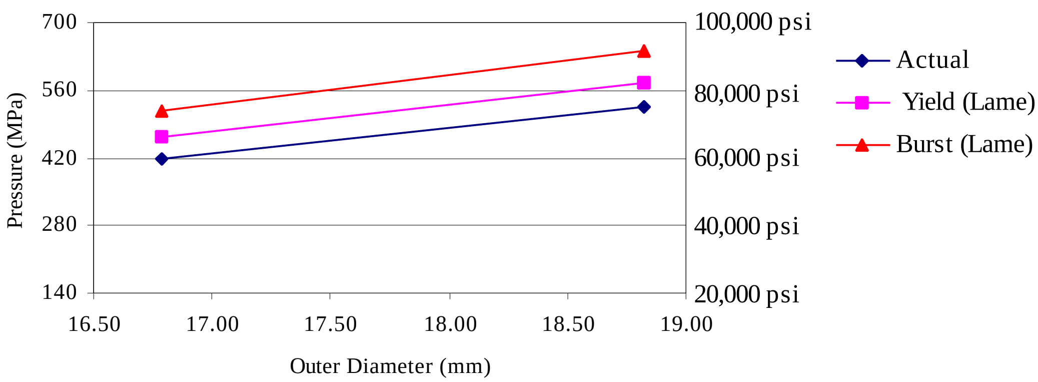

Figure 16. 1/4 NPT couplings, 17-4, failures compared to calculated yield and burst

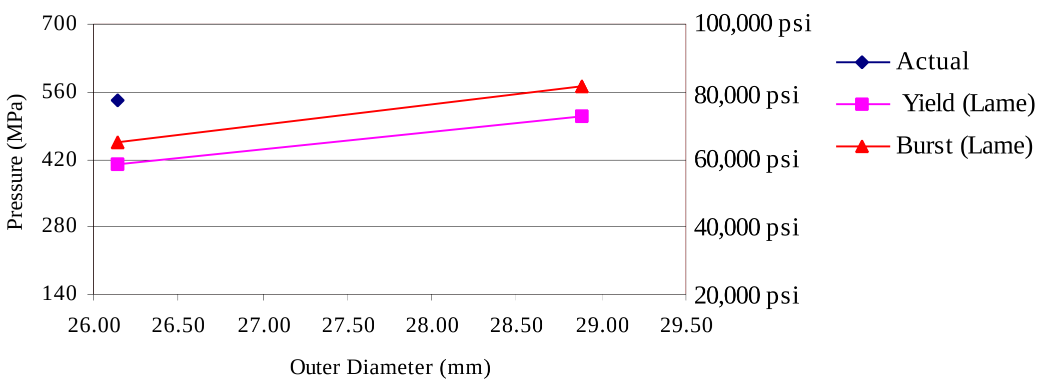

Figure 17. 1/2 NPT couplings, 17-4, failures compared to calculated yield and burst

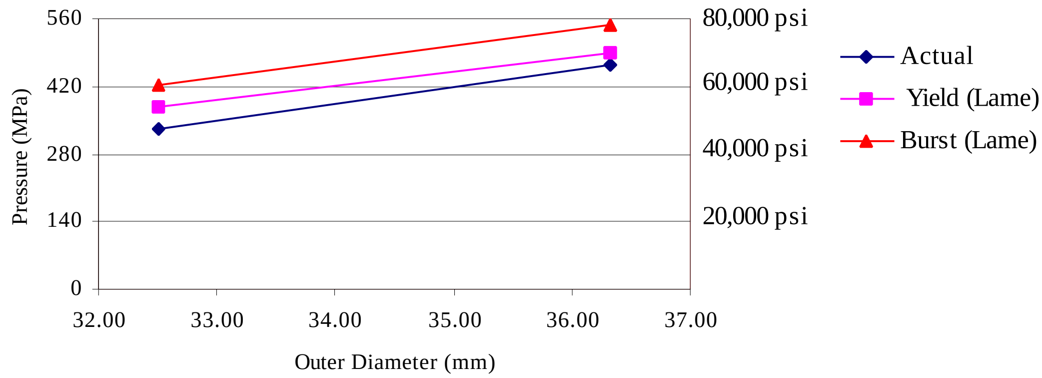

Figure 18. 3/4 NPT couplings, 17-4, failures compared to calculated yield and burst

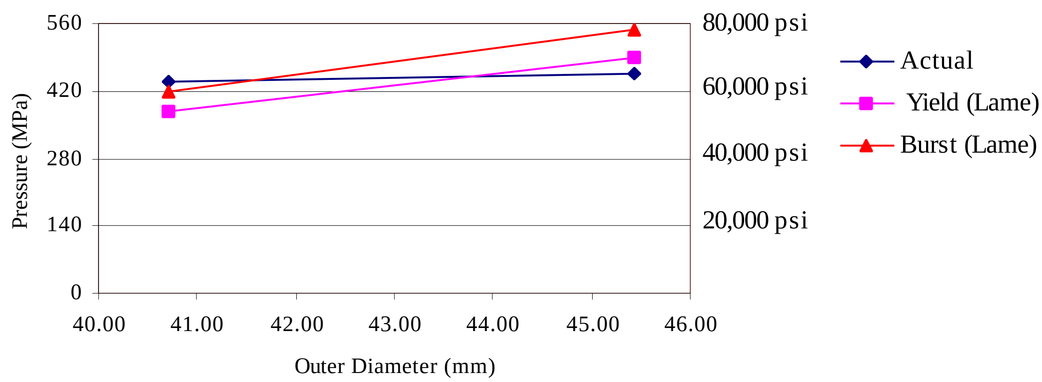

Figure 19. 1 NPT couplings, 17-4, failures compared to calculated yield and burst

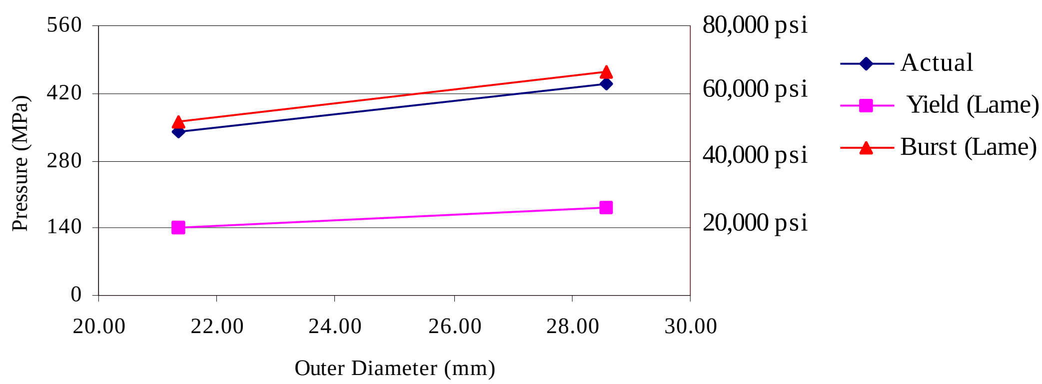

Figure 20. 1/4 NPT couplings, 303, failures compared to calculated yield and burst

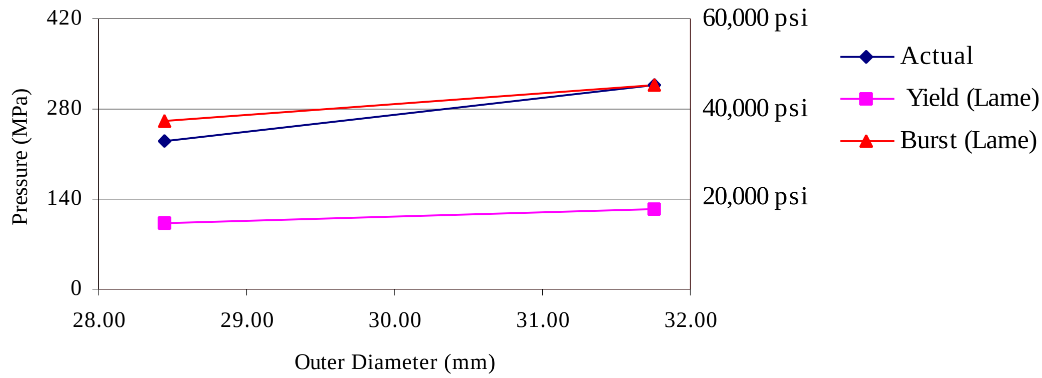

Figure 21. 1/2 NPT couplings, 303, failures compared to calculated yield and burst

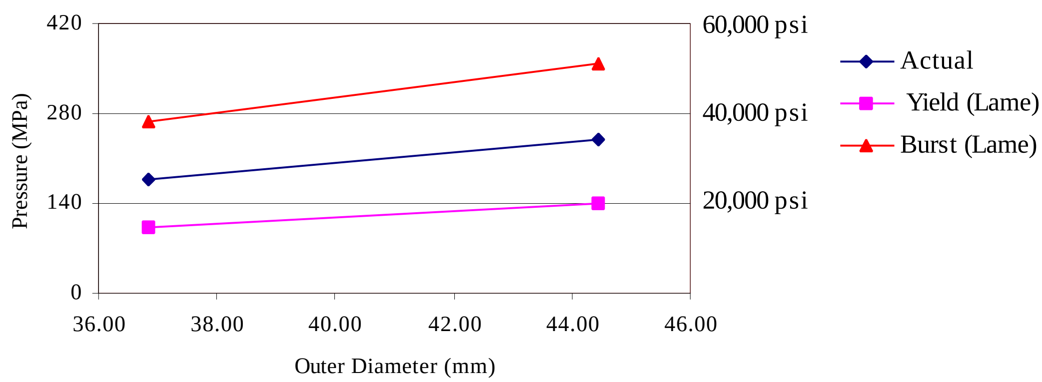

Figure 22. 3/4 NPT couplings, 303, failures compared to calculated yield and burst

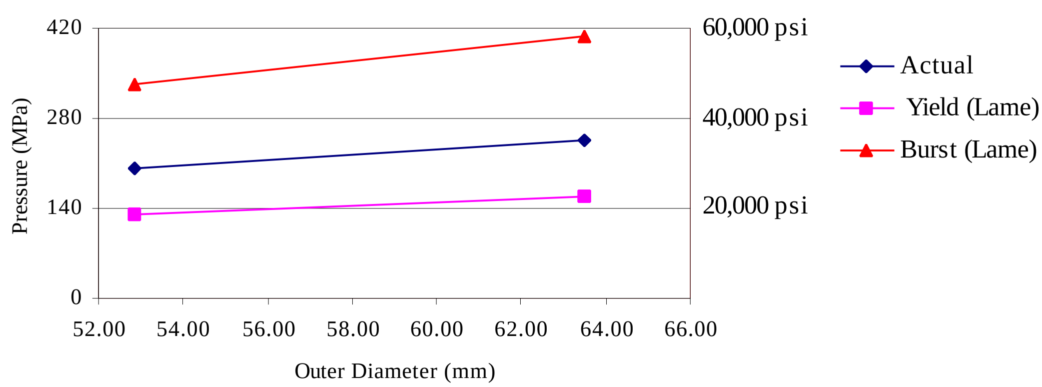

Figure 23. 1 NPT couplings, 303, failures compared to calculated yield and burst

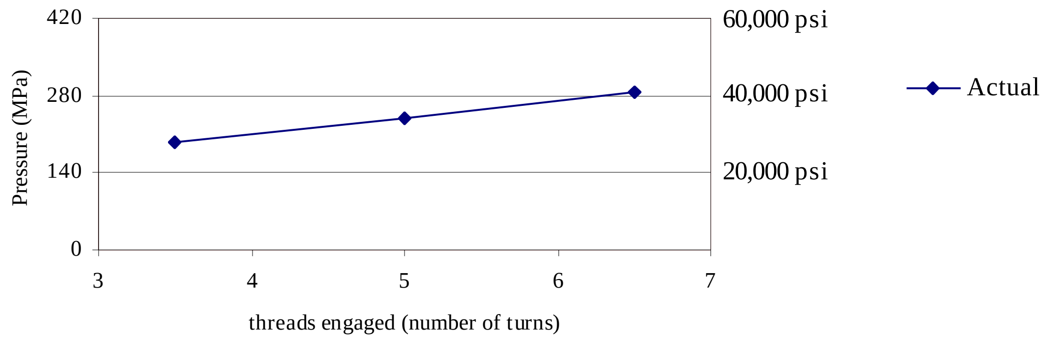

Figure 24. 3/4 NPT couplings, 303, effect of threads engaged

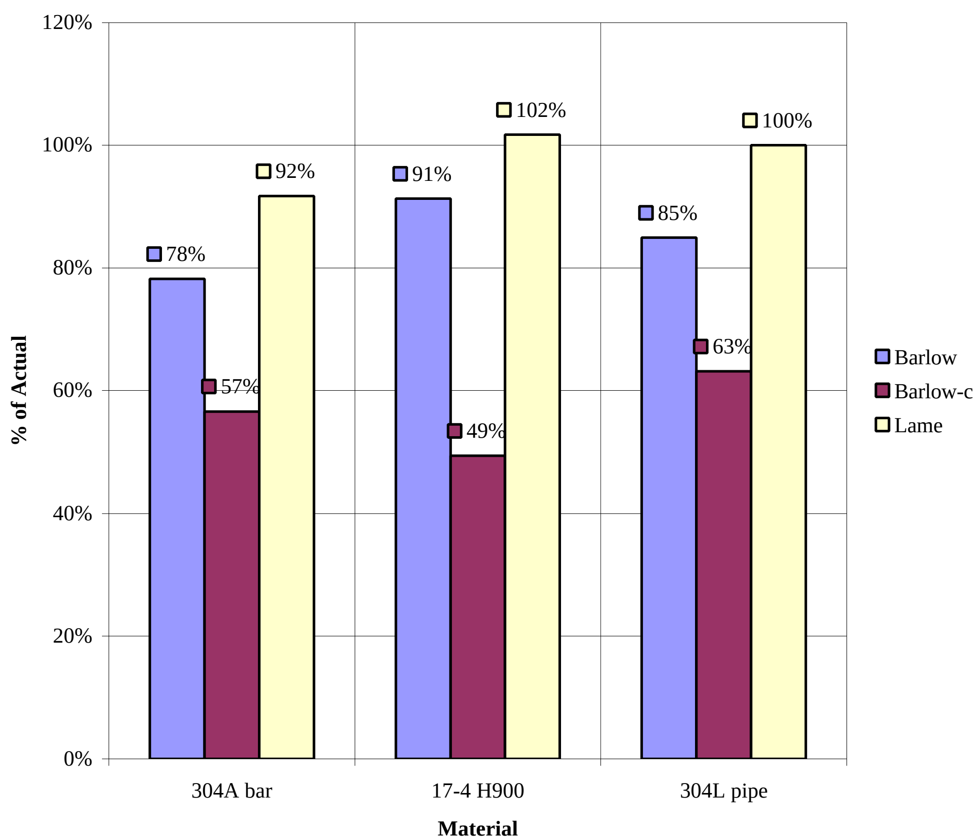

Figure 25. Average of calculated values to actual failures, by material type

2003 WJTA American Waterjet Conference
August 17-19, 2003 ● Houston Texas

Paper 2-B

RECOMMENDED PRACTICES FOR THE USE OF HIGH PRESSURE HOSE

Paul Webster, Stephen Johns
Parker Hannifin Corp., Polyflex Business Unit
Houston, Texas

ABSTRACT

Ultra High Pressure (UHP) hoses are a key component in today's water jetting systems. This paper will present field practices to assist the user in maximizing hose life, determining when a hose should be replaced, along with presenting manufacturing techniques and accessories used to build a safe and reliable product. Many external factors can decrease the life expectancy of a hose assembly. The continued advancement in fitting and hose development enhances connection technology and service life. The use of accessories, including but not limited to bend stiffeners, safety shields, abrasion shields, and containment grips can substantially add to the service life while providing increased safety measures. Daily inspection of hose assemblies is critical to operator safety. Photos of damaged hose, examples of safety devices and test results are included in this paper.

Organized and Sponsored by the WaterJet Technology Association

1. INTRODUCTION

Today 55,000 psi water jetting equipment is fast becoming a reality; therefore, it is more important than ever to follow safety guidelines and practices that extend the life of the high-pressure hose. Working pressures are much higher than 10 years ago when 40,000 psi equipment first became available. Advances in manufacturing techniques and the use of accessories have dramatically increased the life of the hose. Flex lances will also be specifically addressed, since they require the greatest adherence to safety due their close proximity to the operator. This paper will describe:

- Market Trends; The Development of UHP Hose
- Factors that Reduce Hose Service Life
- Practices that Increase Service Life
- UHP Hose Safety
- Evaluation of Hose for Service
- Conclusion
- Illustrations

2. MARKET TRENDS; THE DEVELOPMENT OF UHP HOSE

During the early 1980’s the hydraulic tool industry developed equipment that “pushed the envelope” of technology and accessories to support this industry. The hydraulic hose, being one of these accessories, was not capable of handling the requirements required by this equipment. Dr. John Rogan, an entrepreneur for a product line of bolt tensioners realized the need for a new hose that offered higher operating pressures, increased impulse life and most important lower volumetric expansion that would allow for faster cycle times of the equipment. This state of the art thermoplastic hose exceeded the current market offering. Soon after, Dr. Rogan was supplying hoses not only for his own equipment but realized the market needs for other industry applications, including water blasting, high pressure test equipment replacing steel tubing, and chemically resistant hose for the oil & gas industry. As a result, the UHP hose industry was born.

This ‘new hose’ now commonly referred to as UHP hose was based on a thermoplastic core tube reinforced with very high strength steel wire and jacketed with a thermoplastic outer cover. The performance capabilities of a UHP hose are the result of proprietary methods where the wire reinforcement is “spiralized” onto the core tube. This precise spiralization process allows the hoop stress to be equally distributed throughout the high strength reinforcing layers permitting the hose to function at higher pressures with minimal volumetric expansion and axial movement.

The water blasting industry has been the driving force of hose manufacturers and UHP equipment over the last three decades. The 1980’s forced manufacturers to develop what some would now consider low-pressure equipment. In the early 1990s, pressures increased to 36,000 psi and then 40,000 psi in the later part of the decade.

Historically, an increase in equipment pressure requirements was followed by an increase in flow rates. Thus, a 36,000 psi hose would be developed with a 3/16” ID, then a 3/10” ID and today a ½” ID, 36,000 psi hose is available. In the year 2000, working pressures approached 45,000 psi with new pumps in development designed to operate at 50,000 and 55,000 psi. It has been quite a challenge for manufacturers to develop technology and design equipment because of the stresses exerted on materials at these elevated pressures. In the future, water-jetting pressures may reach 60,000 psi to 65,000 psi; however, significant R&D expenditures will be required in material science, as current practices are reaching their design limits.

3. HOSE ASSEMBLY MAKEUP

3.1 UHP Hose with Safety Shield

In figure 1, a typical UHP hose is shown with a 3/8” high-pressure (HP) tube nipple fitting. The important features illustrated are the stiffener, the safety or abrasion shield and the relief sight holes in the fitting, swivel nut and stiffener. The safety shield may also be referred to as a burst or containment shield. The safety or containment shield is designed to resist a hose burst or pinhole leak at the rated working pressure and offers abrasion resistance to protect the hose from external damage. The stiffener is used to prevent the hose from bending directly behind the fitting, which decreases the stress at the hose/fitting interface. The relief hole is a leak indicator and offers some protection from pressure build up within the fitting or threaded connection. In figure 2, the abrasion shield is clamped directly onto the hose fitting using a retaining sleeve. With the safety shield attached in this manner, additional pressure relief holes are added to the shield to relieve any pressure build up and indicate leakage.

3.2 UHP Hose with Abrasion Shield

Cuts, tears and punctures are common sources of abuse causing premature hose failures. An abrasion shield is a flexible thermoplastic cover designed to prevent these common causes of hose damage. In figure 2, an abrasion shield like the safety shield, is clamped directly onto the hose fitting using a retaining sleeve. An abrasion shield does not have relief holes to vent pressure build up nor does it offer operator protection from high-pressure fluid leakage.

3.3 Flex Lance

Figure 3 illustrates a typical flex lance. Flex lances are rated from 10,000 psi to 30,000 psi. The flex lance fitting is commonly called a ‘ProLance™’ fitting. These are a one-piece welded design and may or may not have a hex. Their short length and small OD profile allow easy passage through small ID tubes found in heat exchangers, P-traps and chemical processing tubes. Flex lances have a tough outer cover and may also have an additional outer stainless steel braid for extra abrasion resistance. In the absence of a fitting hex, the user must grip onto the outside of the hose fitting to attach a nozzle, adapter or stinger, which if done improperly will compromise the integrity of the fitting and hose assembly. Guidelines for attaching jetting components to the hose fitting are covered in section 6.4.

3.4 Hose Fitting Types

UHP fittings come in many connection types and sizes. Illustrated in figure 4 is a 3/8" high-pressure tubing nipple and a Type M fitting. High-pressure tube nipples use a gland nut and collar arrangement. A better gland nut & collar configuration is the anti-vibration type, which prevents the tube from fatiguing at the thread root and the metal-to-metal seal from fretting, cracking and then leaking. The European style high-pressure tubing, gland nut and collar, use metric threads rather than unified threads (UN) found in North America. The Type "M" profile is available in all hose sizes and working pressures up to 55,000 psi. The swivel nut has an internal thread and also protects the male cone so neither can become damaged. The Type M fitting also eliminates the problem of external thread failure common with tubing nipples. The European Type M equivalent uses a metric or a BSPP thread (British Standard Parallel Pipe). Illustrated in figure 5 is the DIN 20 (heavy series) fitting, which is more popular in Europe and Asia. This fitting has a 24-degree male cone with an o-ring and metric swivel nut. These are rated up to 26,090 psi. NPT threads ½" and smaller are typically rated at 15,000 psi and ¾" NPT and above are rated at 10,000 psi. Check with the manufacturer and verify the pressure rating of their adapter or fitting since the strength of the material governs the pressure carrying capabilities. Not all are rated to the same pressure even though the thread form and geometry appear to be similar.

4. FACTORS THAT REDUCE SERVICE LIFE

4.1 Hose Fitting Stress

The most common type of damage is at the fitting since this is the weakest point of the hose assembly. Stiffeners are installed on the hose assembly to reduce the bending moment directly behind the fitting, which reduces stress at the hose and fitting interface and prolongs assembly service life. See figure 6. A stiffener keeps the hose straight behind the fitting and the safety shield acts as a semi stiff bend restrictor to let the hose gradually bend. A general rule of thumb is to keep the hose supported and straight directly behind the fitting for a minimum length of 3 times the hose OD. Figure 7 illustrates a hose attached to a gun in a manner that creates a bending stress at the fitting. Another type of stress at the fitting is axial loading where the hose assembly is stretched or compressed at the fitting. Two cases are given as examples. In the first case, the hose assembly is hanging from scaffolding and stretches or tensile loads the hose at the topside fitting. In the second case, a hose assembly is attached along its length to a cable or other vertical fixture by the use of a tethering device; however, the tethering device slides on the support letting the hose fitting support the weight of the hose and tethering components. Refer to table A for an example of the decrease in service life in these cases.

4.2 Abrasion

Abrasion is regarded as damage to the outer cover and underlying reinforcement. When the outer cover becomes abraded to the extent that the reinforcement is visible, the environment will cause degradation and the reinforcement becomes the acting wear member. All reinforcing layers whether steel or fiber contribute to the strength of the hose. If the reinforcement becomes degraded, hose life will be reduced. The hose should always be visually examined prior to use for signs of abrasion. Refer to figure 8 for an example of a badly abraded flex lance.

4.3 Kinks & Crushes

Kinks and crushes are due to mishandling and improper installation. Several scenarios cause kinking. Dragging the hose around a sharp corner or pulling the hose when it is in a coiled state and not letting the hose naturally un-twist may cause the hose to kink. With a safety shield or abrasion shield, damage is not easily detectable. Crushes may occur if heavy equipment is dropped on the hose assembly or if special clamping accessories are improperly attached to the assembly. Crushes are visibly detected as oval, flattened areas along the length of the hose. Both kinks and crushes will significantly reduce service life or may lead to immediate failure when pressurized.

4.4 Impulse & Flex Fatigue

Hose fatigue is similar to that in high-pressure steel tubing and adapters. The main component that causes hose fatigue is pressure cycling and to a lesser extent hose flexing. The steel wire reinforcement is cold worked every time it is pressurized (stressed) and depressurized (un-stressed). Pumps where pulsation dampeners are not used cause the hose to expand and relax at very high frequencies. The magnitude of pressure change has the most affect on hose reinforcement fatigue since the wire is stressed and un-stressed to a greater degree. If the pressure is constant and offers very little cyclical pulsation, hose service life will increase. High frequency flexing will cause the wire reinforcement to fatigue; however, these cases are very rare and only occur in applications where the hose is under constant flexing. High frequency flexing of UHP hose should be avoided.

4.5 Flex Lance Damage

Flex lance applications demand extraordinary caution due to operator proximity to the waterjet. By far the most common failure is, again like the UHP hose, caused by damage at the fitting and hose interface. Figure 8 shows a typical lance presented for evaluation. The outer cover is missing, the hose is kinked at the fitting and the steel reinforcement is severely damaged. Figure 9 shows a wrinkled outer cover at the fitting. This is a clear sign that the hose assembly has been ‘kinked’ behind the fitting and should be immediately taken out of service. Figure 10 shows a fitting that has been squashed from using a vice or similar clamping device to hold the fitting to facilitate nozzle assembly. Anytime the outer cover is missing, the hose is kinked, crushed, twisted or the fitting is squashed oval the assembly must immediately be taken out of service. Refer to section 6.4 for more information on flex lance fittings.

4.6 Chemical Attack

UHP hoses use very tough materials that resist fatigue and abrasion, but can still suffer chemical attack. In water jetting applications, chlorine and fluorine are the two main chemicals of concern and are present in all city municipalities. If these chemicals are concentrated, then the core tube may experience crazing. Crazing is a condition where the core tube has longitudinal cracks in the core tube. Unfortunately at this time not enough data has been collected to know what concentration levels will chemically attack the tube or what circumstances allow chorine and fluorine to be present in these concentrations. Future tests will help understand this problem and offer guidelines to detect and control chemical attack.

5. PRACTICES THAT IMPROVE SERVICE LIFE

5.1 Hose Fitting Stress

Reduce stress at the fitting by using stiffeners or supporting the hose so it is straight for a minimum length of 3 times the hose OD. Install adapters that let the hose hang straight down as opposed to having the hose exit the pump or gun horizontally and then drooping down to the ground. If the hose is hanging from a great height, use support grips to support the weight of the hose rather than having the fitting support the weight. Do not torque or twist the hose assembly.

5.2 Pressure Spikes and Pulsations

Minimize pressure spikes and pressure pulsations as much as possible. Pressure spikes are internal to water jetting systems and cause internal damage to all working components of the system. Pressure spikes are often created when the gun or lance is pressured up. The release of pressure by the relief valve is not instantaneous so there is a moment when the pressure exceeds the relief set point and creates a pressure spike. Pressure spikes are often higher than the rated working pressure of the hose assembly and overly stresses the hose construction.

UHP hose typically contracts upwards of 2%. For each pressure pulsation, the hose contracts and elongates. Use accumulators or pressure pulsation dampeners, if available from the manufacturer, to smooth out the pressure wave. Operate the pump at the manufacturers recommended RPM. Operators must not decrease the pump speed (RPM) to lower the flow rate, as this will create severe pressure pulsations.

5.3 Flexing and Twisting

UHP hose is designed to bend and flex under high pressure. In one extreme application, the hose is oscillated side to side in a 60-degree arc at frequencies upwards of 60 cycles per minute. The hose performs very well; however, the extreme flexing causes the reinforcement to fatigue. Another hose application is found in boring machines. The hose is rotated to assist in the directional control of the hole being drilled. Please note that service life will be reduced if additional stresses such as flexing and torsion are subjected to the hose. Lab tests show that if a UHP hose is twisted 10 degrees, service life will be reduced. Refer to Table A for results of torsion tests.

5.4 Abrasion

A primary source of hose failure is abrasion resulting from cuts, friction caused by the hose rubbing on the ground or against objects in the operating environment. As previously mentioned, prevention of cover abrasion is critical to hose life. New hoses coming onto the market may have two layers of dissimilar colored covers. When the outer cover is worn down to the sub-layer, the color change becomes evident and immediate action can be taken to prevent further abrasion. Several accessories offer additional protection to the hose cover. Abrasion shields are commonly installed on the hose at the factory to prevent abrasion. Nylon spiral guards, which can be applied in the field, are especially good at preventing initial abrasion or stopping further abrasion once it has begun. Other types of shields can be wrapped around the hose and secured with tie wraps for localized abrasion resistance. Ask your hose supplier what abrasion accessories are available for the hose you are using.

6. UHP HOSE SAFETY

6.1 Safety Shields

As discussed already, safety shields are used to protect the user in the event of a hose fluid leak. In many cases, inadequate shields are used on UHP hoses or abrasion shields are expected to provide operator safety from a high-pressure fluid leak. A properly rated shield will resist a burst and the resultant waterjet at the system's rated working pressure. A safety shield can run the entire length of the hose assembly or it can be a short five to six foot whip that is affixed to one or both fittings. A whip may also serve as a bend restrictor lessening the bending moment behind the fitting. Figure 11 shows a whip being used as opposed to a full-length safety shield. Abrasion shields offer no resistance to a hose burst and are <u>only</u> used to protect the hose from abrasion. Never let the hose come in contact with the any part of the body unless a safety shield is installed on the hose assembly. Make sure the equipment manufacturer has approved the safety shield based on the hose size and working pressure. Do not use an un-approved safety shield or protective shields that have pulled away from the fitting exposing the hose.

6.2 Containment Grips, Support Grips and Bend Restrictors

Containment grips are used to reduce hose "whipping" in the event the hose separates from the fitting under pressure. Additionally, it can act as a support grip. Containment grips bite into the hose as the grip is pulled. The harder the grip is pulled, the tighter it grips the hose. In laboratory tests, the containment grip can crush the hose if pulled with enough force. Like the safety shield, the containment grip must be properly rated to the hose by specifying its breaking strength. For example a ½" ID, 20,000 psi working pressure hose produces a 15,708 lb. end load. A 1.25 design margin is typically used in rating a containment grip; therefore, a breaking strength of 19,635 lbs. is required for the above example.

Support grips are much shorter and have a lower breaking strength than containment grips. They are used to support the weight of the hose assembly such as a hose hanging from scaffolding. They should not be expected to contain whipping of the hose assembly.

Bend restrictors are used to prevent the hose from bending behind the fitting. These are different from the stiffeners illustrated in figure 1. Bend restrictors are semi-ridged and allow the hose to bend gradually. They typically do not offer burst protection. Containment grips, support grips and bend restrictors are shown in figure 12.

6.3 Relief Holes

UHP hose fittings, high pressure adapters and even some quick connect couplers have relief holes. Relief holes are used principally as a leak indicator and to vent fluid leakage. If the leaking fluid is not vented, then pressure may build up in the connection and may cause separation. Relief holes are found on Type M swivel nuts, female high-pressure ports, all large bore UHP hose fittings and 40,000 through 55,000 psi hose fittings. Refer to figure 1 for examples of relief holes. In the case of a swivel nut or a gland nut & collar assembly, simply tightening the fitting may stop the leak. If the male or female cone is too far damaged or worn, then no amount of tightening will stop the leak. At ultra high pressures, even a microscopic leak will quickly wear and become enlarged to the extent that the relief hole may not be able to fully dissipate the fluid and pressure. It is strongly recommended that if a leak is observed at a relief hole, replace the part at once.

6.4 Flex Lances

Flex lances are specifically addressed in this paper due to their close proximity to the user. Reiterating what has already been presented; the most common point of fluid loss is at the fitting. The hose may become kinked or the outer cover is worn away and the wire reinforcement becomes corroded. Corrosion may account for a loss of ½ the hose's rated burst strength given a design factor or 2.5 to 1 (given the burst pressure is 2.5 times the working pressure). Due to the nature of flex lance fittings and their one-piece design, there is no hex or parallel flat to grasp onto to tighten the nozzle, adapter or stinger. Therefore, the common method is to use vice grips, a vise, or a pipe wrench to hold the fitting. Although it is very infrequent, squashing the fitting oval is possible and it is suggested that the user examine the fitting for possible damage after installing the nozzle or adapter. Measure the roundness of the fitting. It should not be out of round more than .010"

The use of tube lancing machines for cleaning tube bundles has become fairly common today. This moves the operator away from the lance and waterjet. Several manufactures offer mechanized lancing machines that increase operator safety, increase the life of the flex lance and are often more productive.

7. EVALUATION OF HOSE FOR SERVICE

Make it standard practice to inspect the UHP hose prior to use. If the assembly is equipped with a burst shield, make sure it has not pulled off of the fitting or out of the stiffener exposing the hose. Look for indications of leaks at relief holes. If the hose has an abrasion shield, inspect for areas that are worn through exposing the hose to abrasion. These areas can be repaired inexpensively. Refer to section 5.4 for quick solutions that can prevent further abrasion. In the case of flex lances, look for exposed wires. This is a serious condition and demands immediate removal from service. Check if the cover is wrinkled behind the fitting, which indicates a kink.

Also look for kinks and crushed areas along the length of the flex lance. Inspect the fitting for damage. It may be oval from improper assembly or the waterjet has begun to wear away the fitting. Check for stiff sections along the length of the hose. This indicates the area is corroded and the hose must be discarded at once. Check the age of the hose assembly. If its age cannot be determined it is safer to not use the flex lance than to risk possible failure.

8. CONCLUSION

Since the initial development of high-pressure hose, many technical advancements have been made. The core tube materials are much tougher, have improved fatigue resistance and new manufacturing methods produce tube of consistent quality. The quality and tenacity of the pressure carrying reinforcement has improved dramatically. This makes for a longer service life and higher rated burst strength. Hose fittings have been engineered to avoid leakage thereby increasing service life. Given these advancements, the end user can expect the same level of performance from each and every hose assembly. Outer covers are tougher and offer greater abrasion resistance and may be extra thick, which may eliminate the need for abrasion shields. These special covers are becoming standard on many of the large bore hoses and have multi-layer covers of different colors. If the outer cover is worn down to the sub-layer then the color change is evident and added protection or hose replacement can be addressed at this point. Further study in chemical attack is planned, as are lighter safety shields. Manufacturers are investing in R&D to increase flow and pressure ratings in larger hose types, which are used as supply hoses. On going technical improvements include, chemical compatibility, weight reducing polymers, increased hose flexibility and higher working pressures. Finally, safety is of utmost concern and manufacturers are actively improving and developing new accessories that will protect the operator and offer a safe product that can be used with the highest confidence.

Table A

55ksi Hose Impulse Test	Test Results
Torsion Test	10 % reduction of impulse life with 10-degree twist.
Bent Fitting Test	63 % reduction of impulse life when bent at minimum bend radius without keeping hose straight behind fitting.
Compressive / Tensile Test	52 % reduction of impulse life with 60 lb. continuous axial compressive or tensile load.

9. ILLUSTRATIONS

Figure 1- Basic design of a 40,000 and 55,000 psi hose assembly with safety (burst) shield and stiffener.

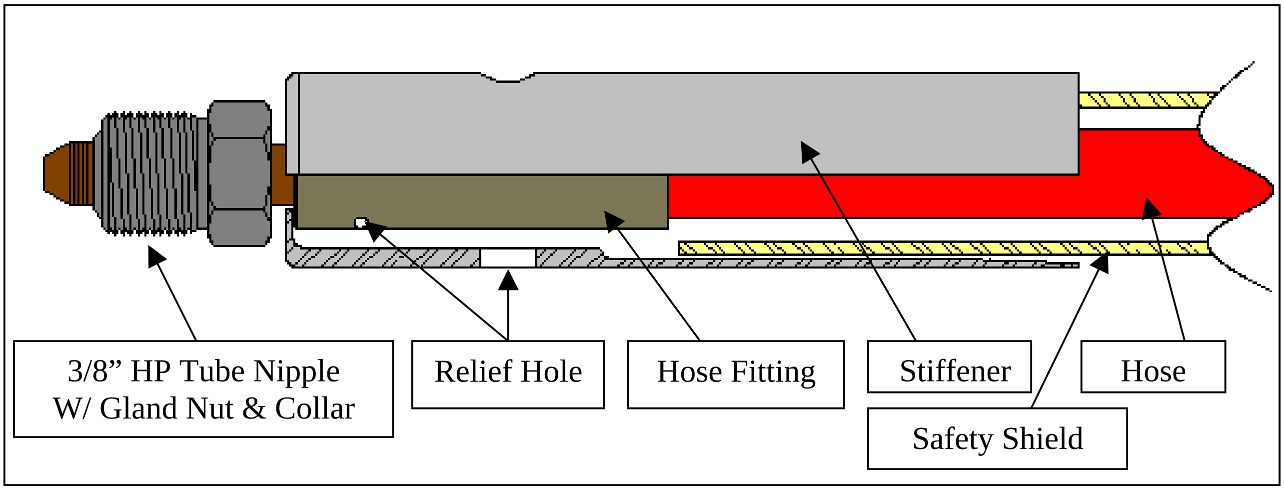

Figure 2 - Basic design of a 40,000 psi hose assembly with safety or abrasion shield without stiffener.

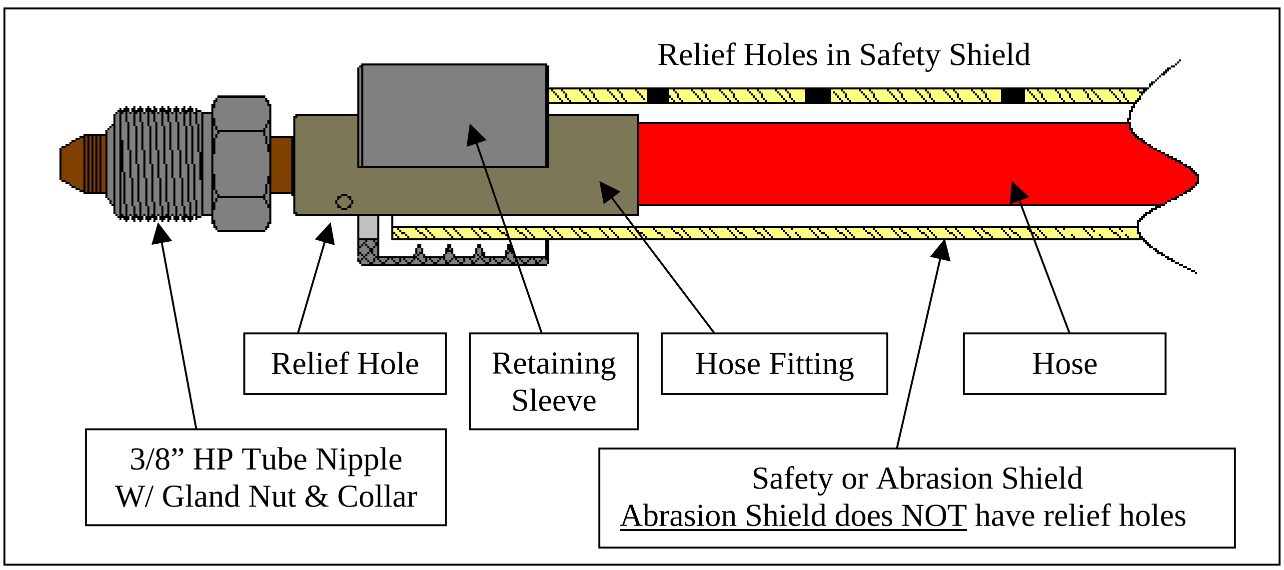

Figure 3 - Basic design of a 10,000 through 30,000 psi flex lance with ProLance™ fitting.

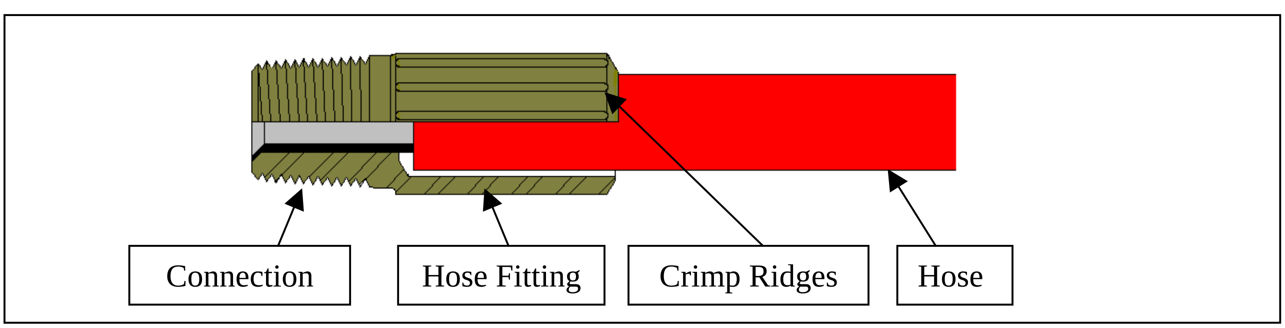

9. ILLUSTRATIONS (continued)

Figure 4 - Basic design of High Pressure (HP) Tube Nipple and Standard Type “M” Fitting

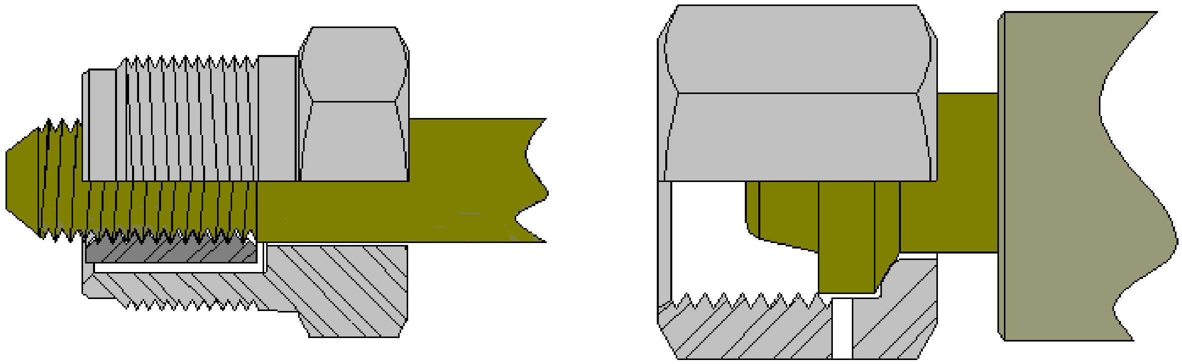

Rated to 55,000 psi
1/4, 3/8, & 9/16” HP Tube Nipple Connection

Rated up to 55,000 psi - Standard Type “M” Connection

Figure 5 - Basic design of European Style DIN 20 (heavy series) Metric O-Ring Fitting

Rated up to 26,090 psi
Metric O-Ring Style Fitting
(Heavy Series)

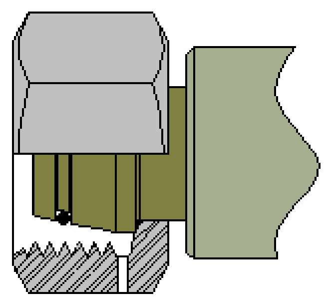

Figure 6 - Kinked 40ksi Hose**.** The hose was supplied with an abrasion shield only. A stiffener or bend restrictor was not used. Note the wrinkled outer cover directly behind the fitting.

9. ILLUSTRATIONS (continued)

Figure 7 – Top two photos show a hose attached to a gun without a burst shield and the hose is stressed at the fitting due to it being attached to the gun improperly.

Figure 7 (continured) - The photo below shows a UHP hose with a burst shield, stiffener, and is properly attached so the hose is not bent at the fitting.

9. ILLUSTRATIONS (continued)

Figure 8 - Flex Lance kinked, wires damaged, and outer cover is worn away.

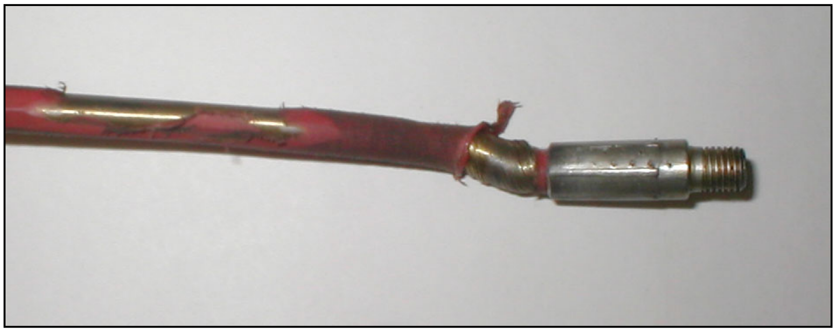

Figure 9 - Flex Lance kinked behind fitting. Note the wrinkled outer cover.

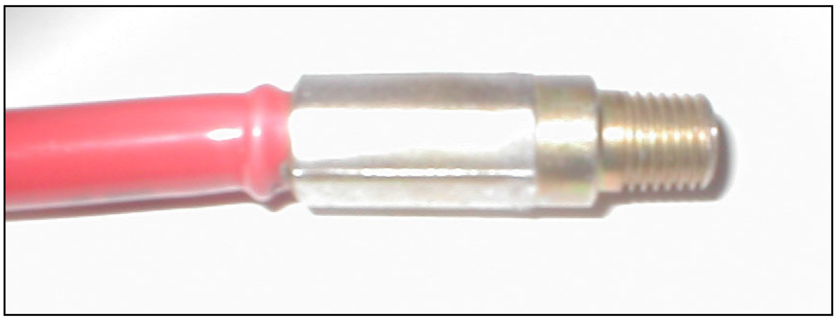

Figure 10 - Flex Lance with Squashed ProLance™ Fitting

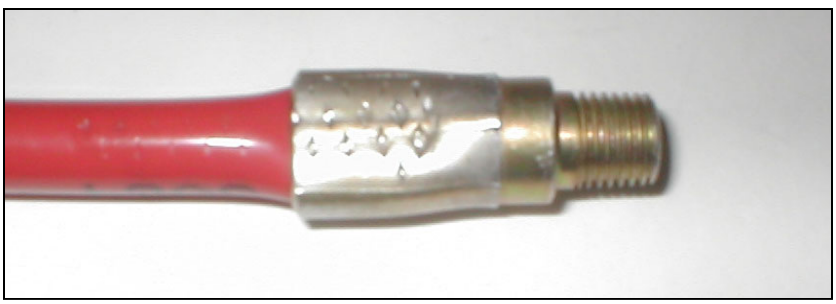

Figure 11 - Hose is shown with whip check as opposed to a full-length safety shield.

9. ILLUSTRATIONS (continued)

Figure 12 - The top photo shows a containment grip, the middle shows a support grip and the bottom photo shows at bend restrictor. All accessories shown are design for UHP Hose.

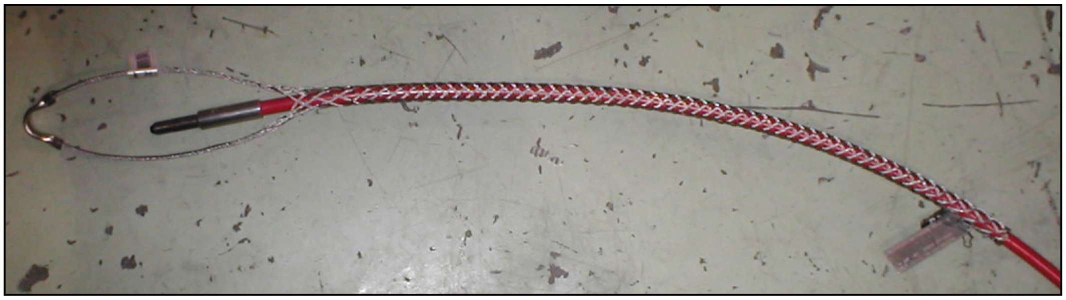

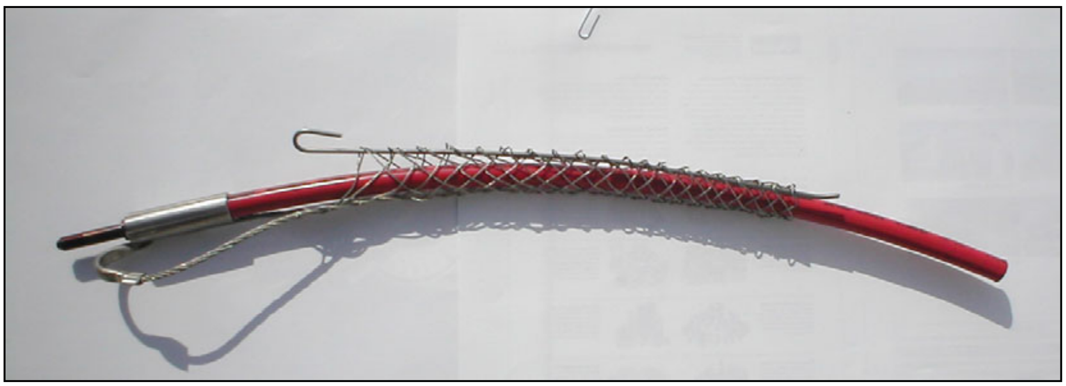

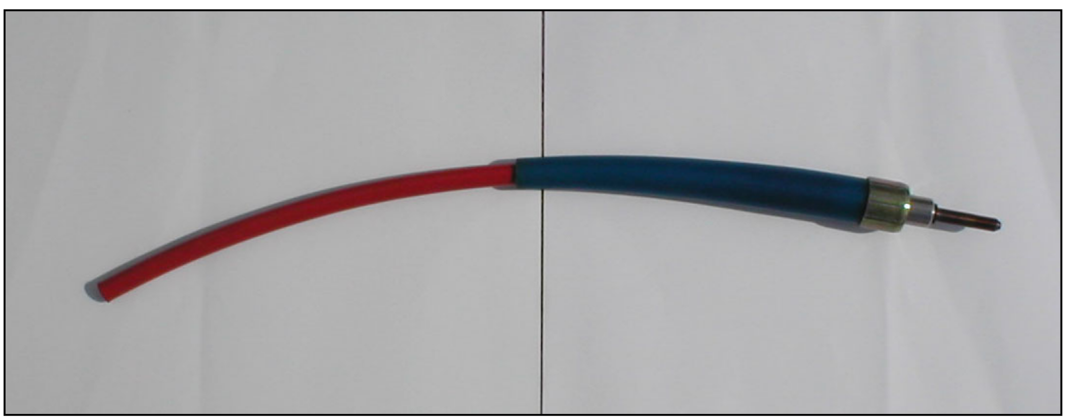

2003 WJTA American Waterjet Conference
August 17-19, 2003 • Houston, Texas

Paper 3-B

ACOUSTIC EMISSION OF PLAIN WATER JETS

A. Bortolussi
CNR - Institute of Environmental Geology and Geo-engineering
Cagliari Department - Italy

R. Ciccu, W. Cuccu, A. Marcus, G. Massacci, S. Usala
Department of Geo-engineering and Environmental Technologies
University of Cagliari – Italy

ABSTRACT

The paper deals with the characteristics of sound emission of plain water jets. Sound power emission has been determined by sound intensity measurements, according to ISO 9614-1, varying the different operative parameters. In particular, 1/3 – octave band sound power spectral levels have been evaluated for two nozzle diameters and four pressure values. The measurements allow identification of the contribution of each 10 cm length of free exposed water jet. Analysis of the results has led to the definition, for different operative conditions, of the maximum water jet free exposed length beyond which an increase in sound power is negligible.

1. INTRODUCTION

The high level of noise produced is one of the most relevant environmental effects connected with the use of water jet technology in general, and to plain water jets in particular. As matter of fact, safe application of such technology always includes for machine operators, and all other personnel operating near the working area, the use of adequate ear protection, the characteristics of which depend upon the kind of application.

A number of studies (1, 2, 3) have been conducted to evaluate the noise level and the corresponding safety measures to be adopted.

The present work examines the correlation between the characteristics of sound emission of plain water jets and the most important operative parameters such as pressure, nozzle diameter and stand-off distance. In particular, sound power emissions have been measured for the whole and for separated sections of an exposed jet. Beside the intrinsic characteristics of sound emission, such a procedure allowed the definition, for different operative conditions, of the contribution of the different jet sections and the minimum length of exposed jet that produces a defined maximum noise level.

2. EXPERIMENTAL PLAN

Sound power emission is the most effective parameter to use in order to instrument a comparison of sound emissions from different sources. In fact sound power emission is an objective descriptor of a sound source, independent of the environmental acoustic characteristics and measurement conditions. This parameter is obtained by elaborate measurements of sound intensity that represents the energy flowing through the unit area during unit time.

The entire procedure to define the sound power emission has been standardised according to ISO 9614-1. The procedure consists of a determination of the energy flowing out from a defined volume by means of punctual surface measurements of sound intensity (4, 5).

In the present work, the reference volume adopted, including the noise source, had the shape of a parallelepiped. The bottom surface of the parallelepiped was covered with a noise reflecting material, allowing the passage of the water jet through a small opening. One of the vertical faces parallel to the jet direction was also reflecting. Sound intensity has been measured perpendicularly to the surface to correspond with the nodes of a grid defined for each of the faces of the parallelepiped. The number of measuring points (four for the smaller faces and six for the larger ones) and the dimensions of the parallelepiped (1 m x 1 m x 1.5 m) have been defined by specific procedures optimising the quality of the results. Figure 1 shows the measurement configuration.

The sound intensity measuring system consists of two microphone sound intensity probes and a dual channel processor. The accuracy of the intensity measurements is strongly dependent upon the phase accuracy between the two measurement channels, including the microphone. Sound intensity measurement systems are classified as Class 1 based upon the pressure-residual-intensity index, which is measured using a residual intensity-testing device (Model CAL291):

- Larson•Davis Model 3200 Multi-channel Real Time Analyzer
- Larson•Davis Model 2260 Sound Intensity Probe
- Larson•Davis Model CAL250 Microphone calibrator
- Larson•Davis Model CAL291 Residual Intensity Calibrator (satisfying the residual intensity test device specification of both IEC 1043:1993(*) and ANSI(**) S1.9-1196)

(*) IEC 1043:1993 Instruments for the measurement of sound intensity - Instruments which measure intensity with pairs of pressure sensing microphones.

(**) ANSI S1.9-1996 Instruments for the measurement of sound intensity.

The combination of the Model 3200 Analyzer and the Model 2260 Sound Intensity Probe meets or exceeds the specifications of the standards for a sound intensity measurement system.

The sound power emission of each of the system settings has been obtained by discrete integration of the single sound intensity measurements on the surface of the reference volume.

The experimental plan is based on the definition of sound power emission for system configurations characterised by different settings of pressure, nozzle diameter and exposed jet length. To evaluate their influence on noise level, the variable parameters have been set at the following values:

- Pressure:	30, 50, 70 and 120 MPa
- Nozzle diameter:	0.5, 1.2 mm
- Exposed Jet Length:	10 – 100 cm, 10 cm step

Different exposed jet lengths have been obtained by changing the length of the jet included in the reference volume, that means changing the distance between the nozzle and the bottom surface of the parallelepiped. The experimental plan is given in Table 1. In the same table, for each combination of pressure and nozzle diameter, the values of flow rate, jet velocity (in the nozzle section) and jet power are given.

3. RESULTS AND DISCUSSION

For each of the system configurations, characterised by a fixed value of pressure, nozzle diameter and exposed jet length, a one third (1/3) octave band sound power spectrum has been acquired. As an example, the graphs of Figure 2 represent the sound power levels measured as a function of frequency bands obtained for a single system configuration. In addition the total sound power level L is reported on the same graphs. The spectrum of Figure 2 (a) gives the values in dBA, corrected to take into account that the human ear has a different sensitivity to each different sound frequency, shown in the following A-weighted sound level, while the spectrum of Figure 2 (b) is relative to the linear dB level (without any correction).

Spectra of Figure 2 are relative to the system configuration at a pressure of 70 MPa, nozzle diameter 1.2 mm and exposed jet length 100 cm.

Considering the graph in Figure 2 it is possible to define a higher sound emission level for frequencies exceeding 1000 Hz. Such a result was confirmed for all the tests conducted and in conclusion it can be reported as a specific characteristic of water jet technology sound emission.

The phenomenon constitutes a disadvantage for this technology. In fact the human ear has a higher sensitivity to the frequencies included between 1000 and 4000 Hz, as shown in the graph of Figure 2 (a), in which the A-weighted level is increased in the range of frequencies between 1000 and 4000 Hz, while it is reduced for the other values of frequency.

In Table 2 the maximum values of the linear sound power total levels and the A-weighted sound power total levels measured for each parameter configuration are reported. In the same table the exposed jet length corresponding to the condition of maximum total level measured is shown.

3.1 Influence of pressure

The influence of pressure can be put evaluated by considering the tests conducted at a nozzle diameter 1.2 mm (pressures 30, 50 and 70 MPa) and 0.5 mm (pressures 70 and 120 MPa) with the same exposed jet length (100 cm).

Linear and A-weighted sound power levels are reported as a function of frequency bands respectively in Figure 3 (a) and (b) for the first series of tests and in Figure 4 (a) and (b) for the second series.

Both graphs of Figure 3 and 4 show that with increasing pressure the sound power level increases for all frequency bands. The increase is not constant but is higher for frequencies exceeding 1000 Hz (about 9 dB for 20 MPa step) and lower for lower frequencies (about 5-6 dB for 20 MPa step). The increase in linear sound power total level is about 9.9 dB (10.6 dBA for the A-weighted value).

Considering Figure 3 (a), at a nozzle diameter of 1.2 mm, it is possible to note that the increase in sound power level follows the described trend in a more consistent way when passing from a pressure of 50 MPa to 70 MPa; in fact when the pressure is increased from 30 MPa to 50 MPa, the increase in sound power level is almost constant over the different frequencies.

Comparing the results obtained using different nozzle diameters, it is interesting to point out that, for a 0.5 mm nozzle diameter, almost the same increase in the sound power level is obtained by passing from a pressure of 70 MPa to 120 MPa, with a step of 50 MPa in comparison with the 20 MPa step adopted for the 1.2 mm nozzle diameter.

The qualitative outline of the curve is similar for all the experimental conditions, showing two maximum points: an absolute maximum at about 2500 Hz and a relative maximum at about 200 Hz.

Increasing the pressure at the same nozzle diameter implies an increase in the fluid velocity and consequently the water flow rate (Table 1). As illustrated, such an increase in velocity produces a higher sound power level especially at higher frequencies. The fact that the expected increase in sound power level is more significant at higher frequencies can be explained by considering that the higher jet velocity has the effect of increasing the turbulence and droplet production, though not their volume but in their rate of formation within almost the same volume. It is also worth noting that, as reported in Table 2, increasing the jet power by about 13.2 kW by increasing the pressure (pressures 30 and 70 MPa at 1.2 mm nozzle diameter), produces corresponding values of A-weighted sound power total level that are increased by 15.4 dBA.

Considering the same Table 2, the relevant influence of pressure is evident: for the configurations at jet power 5.2 kW (1.2 mm, 30 MPa ≡ 10.4 l/min, 238 m/s) and 7.2 kW (0.5 mm, 120 MPa ≡ 3.6 l/min, 475 m/s), which differ only by 2 kW in power but by 90 MPa in pressure (207 m/s in jet velocity), the corresponding values of the A-weighted total sound power levels differ by 14.3 dBA.

3.2 Influence of nozzle diameter

The effect on sound power level is slightly different if the jet power is increased by increasing the nozzle diameter, at constant pressure.

In fact in such a case the higher sound power level is distributed meanly at medium-low frequencies and is less significant at higher frequencies.

The phenomenon is clearly illustrated in the graphs of Figure 5, where sound power levels are reported as a function of frequency for two nozzle diameters.

A probable reason for such behaviour is that, for the same pressure, a larger nozzle diameter implies a higher volume of produced turbulence, while the intensity remains at the same level.

As a result of this, an increase in jet power of 15.5 kW (Table 2: 0.5 mm and 1.2 mm nozzle diameter, 70 MPa pressure), obtained by increasing the flow rate from 2.7 to 15.8 l/min, produces an increase of A-weighted sound power total level of 10.5 dBA, which is lower then the value (15.4 dBA) obtained by increasing the jet power by 13.2 kW by increasing pressure.

Based on these considerations of sound emission, it is clear that, when possible, it is more convenient to increase the jet power by increasing the nozzle diameter at constant pressure (jet velocity).

3.3 Influence of exposed jet length

The effect of exposed jet length represents the influence of stand-off distance. In fact in most cases, after reaching the target material, the jet is immersed in the cut or slot during excavation with a drastic attenuation of the noise; and practically all noise effects are due to that portion of jet that is travelling in free air from the nozzle to the target material.

The correlation between linear sound power total level and exposed jet length is reported in Figure 6 for three levels of et power obtained by a combination of different pressures and nozzle diameters (flow rates).

The graphs of Figure 6 show that by increasing the exposed jet length the linear sound power total level is increased to a limit whose value depends upon the jet power. Such a limit represents the stand-off distance beyond which any increase has no influence from the noise point of view.

In the case of a lower power jet this limit value is lower and it is reached at a shorter exposed jet length.

The graphs of Figure 6 show that such a limit is about 50 cm for a jet power of 2.9 kW, 80 cm for a jet power of 7.2 kW and over 100 cm for a jet power of 18.4 kW.

Considering the same Figure 6, in the case of a 0.5 mm nozzle diameter, it is possible to compare, for different exposed jet lengths, the effect of an increase in pressure on the linear sound power total level and to point out that such a parameter is always increased in value in the range 7 - 10 dB, being higher for higher exposed jet lengths.

It is also interesting to note that for two different values of jet power (7.2 and 18.4 kW) the correlation between the linear sound power total level and the exposed jet length is almost the same, at least up to 100 cm. In spite of the relevant difference in pressure and nozzle diameter, the two jets seem to be characterised by equivalent sound parameters.

In the case of a 18.4 kW jet power, the effect of a higher value of nozzle diameter, 1.2 mm instead of 0.5 mm, corresponds to an increase in flow rate from 3.6 to 15.8 l/min (about 4 times higher), is attenuated by the effect of the lower pressure, 70 MPa instead of 120 MPa, corresponding to a decrease in water velocity in the nozzle section from 475 to 363 m/s (about 1/4 lower).

It seems reasonable to consider that the sound emission of a plain water jet depends mainly on pressure, and then on jet velocity, which is responsible for the intensity of the turbulence generated around the jet, while the nozzle diameter influences the volume affected by such turbulence, which is increased both in diameter and length as the nozzle diameter is increased.

The graphs of Figure 7 show the contribution to the A-weighted sound power total level by different jet portions for different settings of the operational parameters. The contribution of each jet portion has been calculated taking into account the cumulative values of the sound power level for different jet lengths. In some cases it has not been possible to calculate the contribution because there was no difference between the corresponding cumulative values.

Data reported in Figure 7 show that, for the configuration with a 0.5 mm nozzle diameter - 70 MPa pressure, the jet portion that gives the higher contribution to the noise level is included between 20 and 40 cm, while in case of a configuration with a 0.5 mm nozzle diameter - 120 MPa pressure such a jet portion is located between 30 and 50 cm. For the configuration of a 1.2

mm nozzle diameter at 70 MPa pressure, the available data does not allow identification of the jet portion giving the maximum contribution since their values were still increasing.

It seems that there is a jet portion where the turbulence of the jet is at a maximum value, producing higher noise levels, and that the distance of such jet portion from the nozzle depends on the jet parameters, being higher for higher jet power.

All these considerations are evidence of the great influence of stand-off distance, a parameter which it is important to control in order to reduce the sound power level of water jets and to improve the environmental conditions for the operators.

4. CONCLUSIONS

The sound power level of a water jets is one of the parameters that must be taken into account when considering the safety characteristics of that technology. The research conducted has pointed out different aspects related to the influence of some operational parameters. In particular the results have outlined that:

- increase in pressure induces an increase in the sound power levels especially at higher frequencies, in a range where the human ear is more sensitive;
- increase in nozzle diameter produces an increase in sound power levels relevant at medium -lower frequencies, with a relatively lower negative effect on the human ear;
- increase in jet power has a lower effect in terms of A-weighted sound power total level when obtained by increasing nozzle diameter rather than pressure;
- sound power total levels increase up to a limit value when increasing the exposed jet length; such a limit value is reached at lower exposed jet lengths in the case of a lower jet power; as a consequence the negative noise effect due to a high stand-off distance is more relevant with higher jet power and especially with higher jet pressures; the relevant influence of stand-off distance on water jets sound power level is also confirmed by considering the different contribution to the noise of different jet portions.

5. AKNOWLEDGEMENTS

This work was carried out within the framework of research projects supported by MURST and CNR. Many thanks to Mr P. Borghero for his valuable assistance provided during these tests.

6. REFERENCES

1 Atzeri, S., Benedetto, G., Ciccu, R., Massacci, G., Patrucco, M., 1993, “Noise Generated By High Velocity Water Jets: Laboratory Measurements”, Proceedings Of 3rd International Congress on Air and Structure Borne Sound and Vibration. Montreal, Canada, pp. 911-918.

2 Katakura, H., Miyamoto, H., 1997, “Waterjet-Related Noise and its Countermeasures”, Proceedings of 9th American Waterjet Conference, Dearborn, MI, pp.783-797.

3 Munoz, J., Kain, I., 2001, “Abrasive waterjet cutting comparative study between open catcher tank and water catcher tank”, Proceedings of the 2001 WJTA American Waterjet Conference, Minneapolis, USA, pp 153-161.

4 ISO 9614-1, 1993, “Acoustics - Determination of sound power levels of noise sources using sound intensity - Part 1: Measurement at discrete points”, ISO - International Organization for Standardization, Geneve, Switzerland.

5 ISO 9614-2, 1996, “Acoustics - Determination of sound power levels of noise sources using sound intensity - Part 2: Measurement by scanning”, ISO - International Organization for Standardization, Geneve, Switzerland.

7. TABLES

Table 1. Experimental design.

N.	Pressure [MPa]	Nozzle Diameter [mm]	Flow Rate [l/min]	Jet Velocity [m/s]	Jet Power [kW]	Max Exposed Jet Length [cm]	Increasing Step [cm]
1	30	1.2	10.4	238	5.2	100	100 (1 test)
2	50	1.2	13.4	307	11.2	100	100 (1 test)
3	70	1.2	15.8	363	18.4	100	10 - 20 (6 tests)
4	70	0.5	2.7	363	2.9	100	10 (10 tests)
5	120	0.5	3.6	475	7.2	100	10 - 20 (9 tests)

Table 2. Maximum Linear sound power total level and A-weighted sound power total level measured for each parameter configuration.

Pressure [MPa]	Nozzle Diameter [mm]	Jet Power [kW]	Linear sound power total level [dB]	A-weighted sound power total level [dBA]	Corresponding exposed jet length [cm]
30	1.2	5.2	104.8	104.4	100
50	1.2	11.2	112.4	112.5	100
70	1.2	18.4	119.3	119.8	100
70	0.5	2.9	108.7	109.3	50
120	0.5	7.2	118.2	118.7	100

8. GRAPHICS

Figure 1. Sound intensity measurement configuration: reference volume and grids.

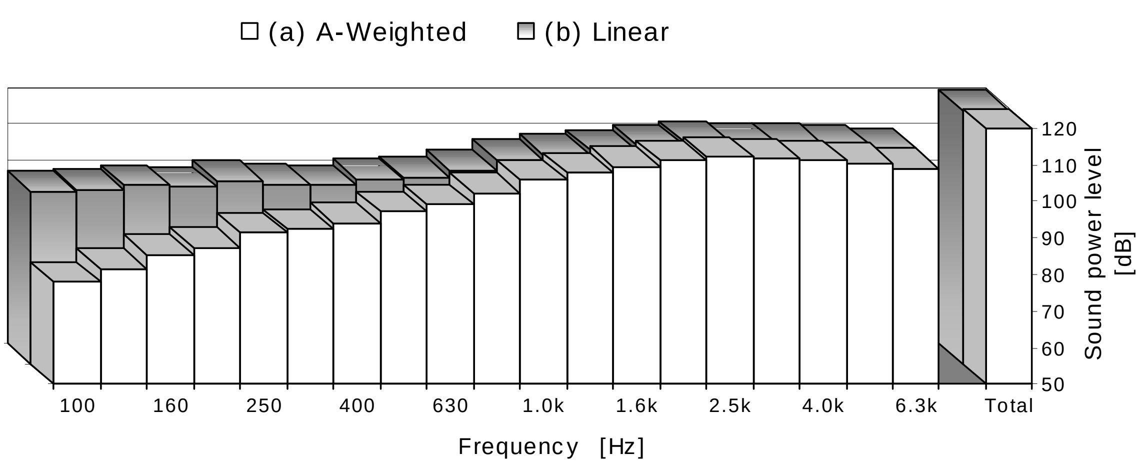

Figure 2. A-weighted (a) and Linear (b) sound power levels measured as a function of frequency bands; pressure 70 MPa, nozzle diameter 1.2 mm, exposed jet length 100 cm.

(a)

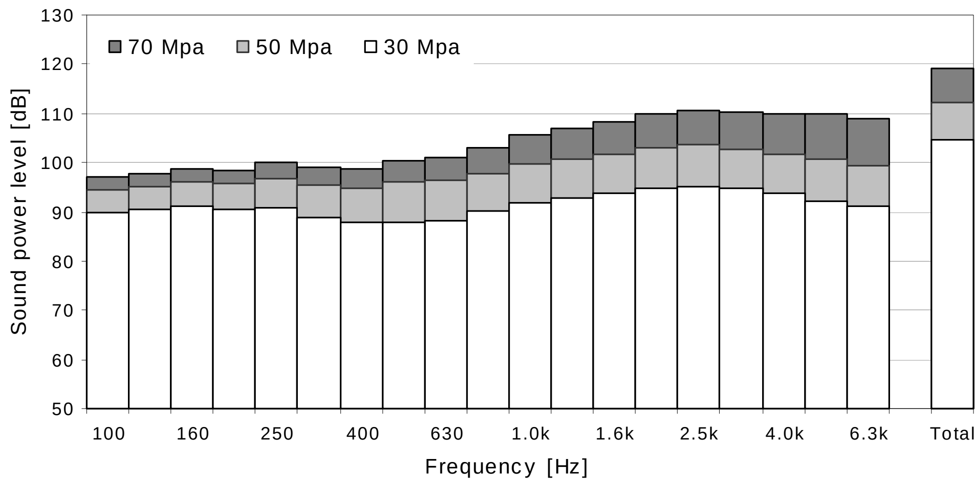

(b)

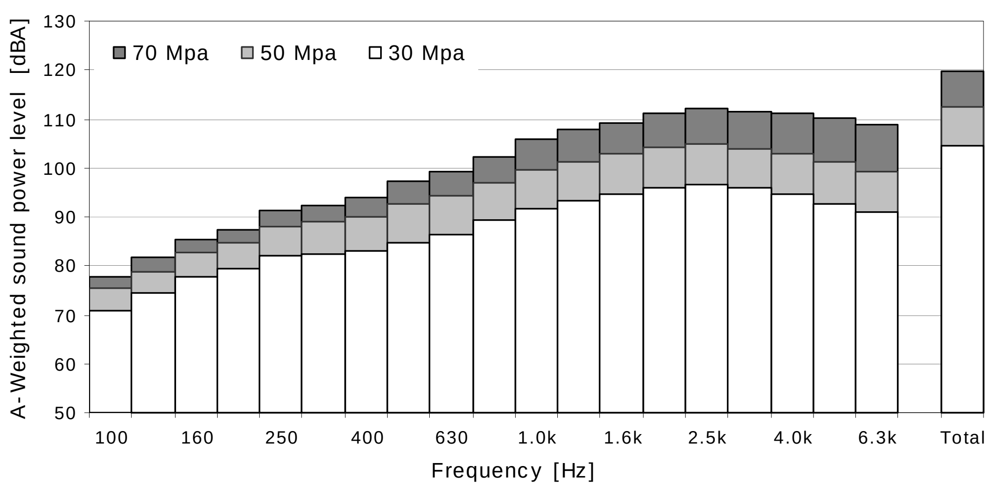

Figure 3. Linear (a) and A-weighted (b) sound power levels as a function of frequency bands for pressures 30, 50 and 70 MPa; nozzle diameter 1.2 mm, exposed jet length 100 cm.

(a)

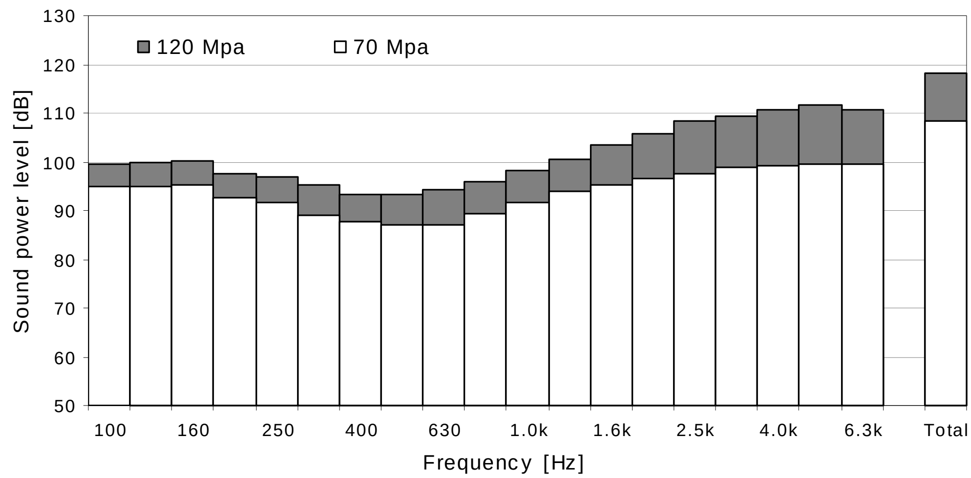

(b)

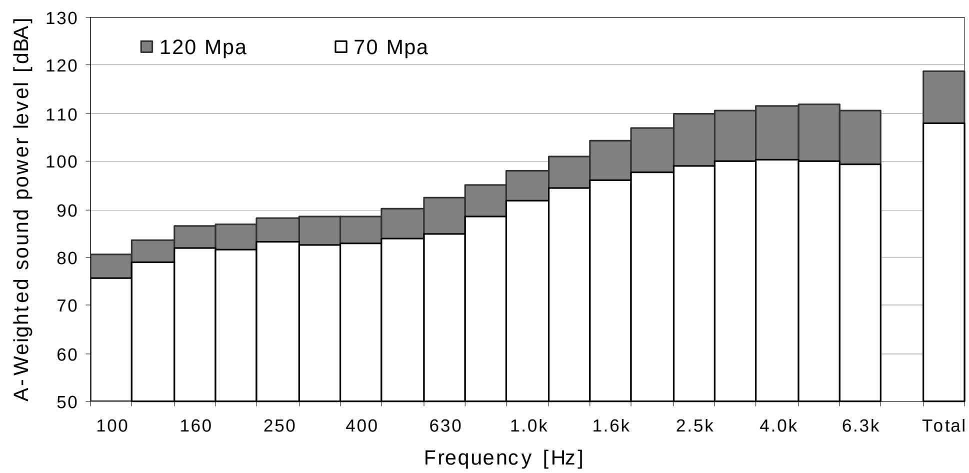

Figure 4. Linear (a) and A-weighted (b) sound power levels as a function of frequency bands for pressures 70 and 120 MPa; nozzle diameter 0.5 mm, exposed jet length 100 cm.

(a)

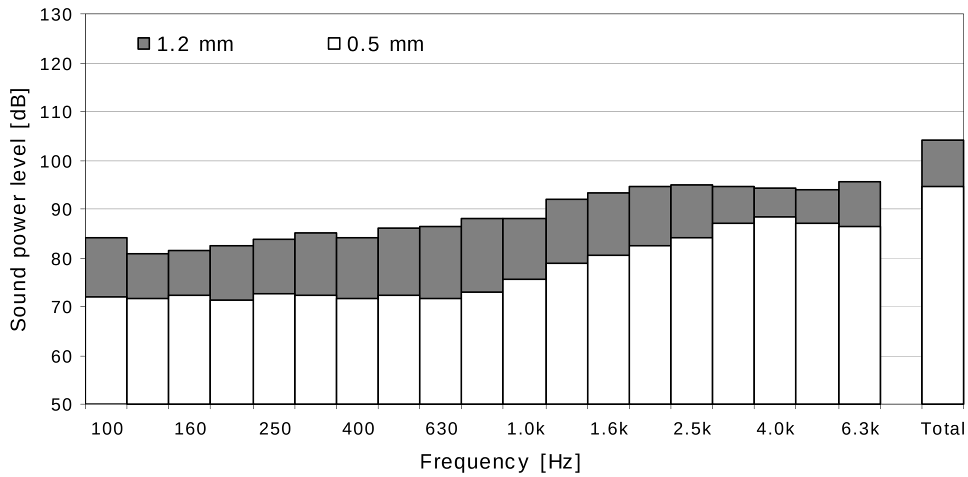

(b)

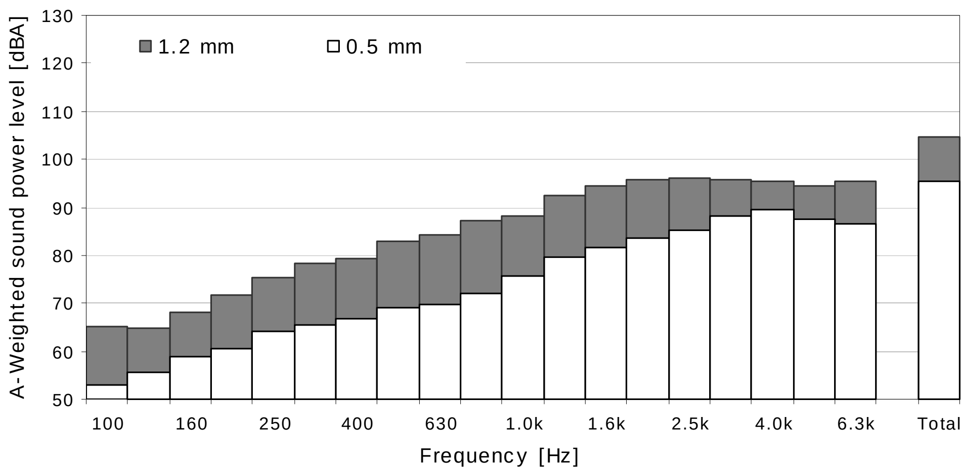

Figure 5. Linear (a) and A-weighted (b) sound power levels as a function of frequency bands for nozzle diameters 0.5 and 1.2 mm; pressure 70 MPa, exposed jet length 10 cm.

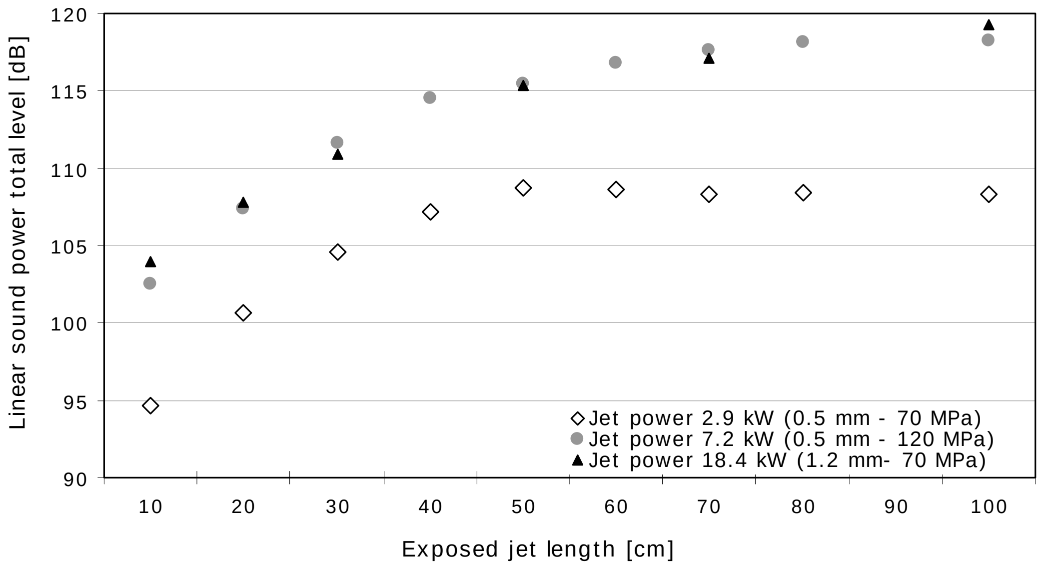

Figure 6. Correlation between linear sound power total level and exposed jet length for different jet power levels.

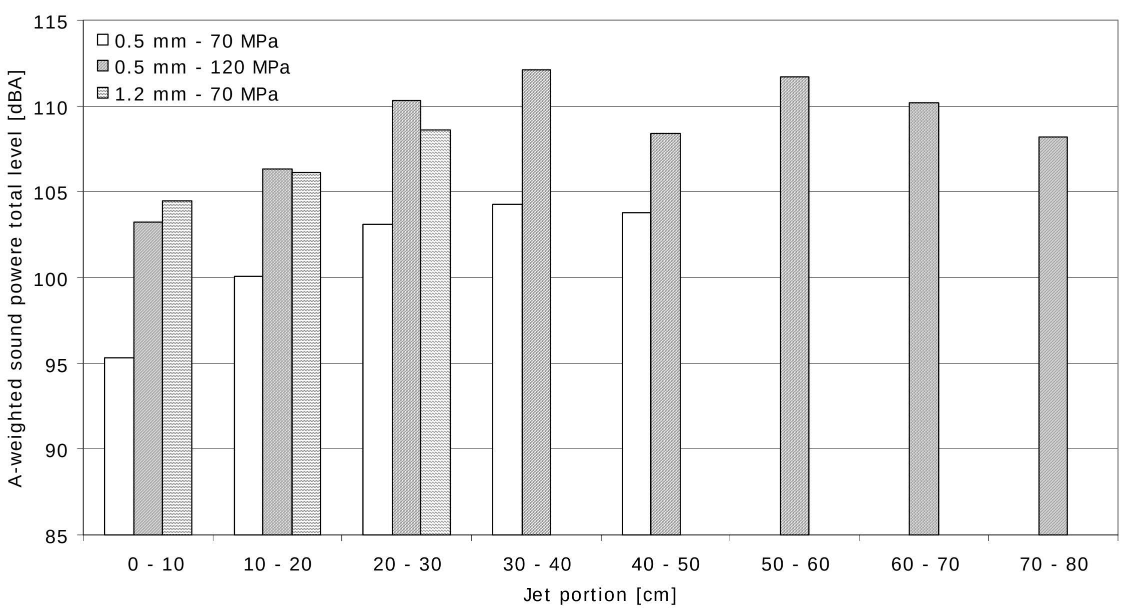

Figure 7. Sound contribution of different portions of the exposed jet length.

2003 WJTA American Waterjet Conference
August 17-19, 2003 • Houston, Texas

Paper 3-A

WATERJET NOZZLE MATERIAL TYPES

D. Wright, J. Wolgamott, G. Zink
StoneAge, Inc.
Durango, Colorado, U.S.A.

ABSTRACT

There are three common nozzle material types used in waterjet cleaning: steel, carbide, and sapphire. Each has advantages in certain applications, while having real limitations in others. Jet quality produced and life expectancy are both critical issues for industrial waterblast nozzles. This paper presents the results of lab testing and field analysis to determine the wear rate and failure modes of each material type. Commercially available examples were tested under typical waterblast operating conditions and wear was determined by measurement of orifice size and visual deterioration of the jet quality. Recommendations are given for nozzle material depending on operating conditions.

1. INTRODUCTION

Nozzles are often the least expensive individual component of a waterblast system, but they can make a difference of two or more times the effectiveness of the most expensive component, the high pressure pump. Initial jet quality of a new nozzle is dependent on the design of the nozzle, and can vary by as much as 60 percent between one type and another.

Through use, all nozzle materials wear and result in deteriorating jet quality and decreasing production rates. Another result of nozzle wear may be decreasing pump pressure; as some nozzle materials wear the orifice size increases, requiring an increase in flow rate to maintain the same pressure. Since waterblast pumps have a fixed output in flow, once their maximum output is reached, the pump pressure decreases as the orifice size increases.

The various nozzle materials wear differently depending on the water quality and chemistry, the operating pressure, and the nozzle design.

2. TESTING

Commercially available nozzles were tested five at a time in a manifold, at pressures between 112 and 126 MPa (16,000 and 18,000 psi). Nozzle orifice size and visual jet quality were compared over operating times up to 40 hours. Tests were conducted with water filtered to 25 micron. Additional information is based on reports from field use.

3. RESULTS

3.1 Carbide Nozzles

Tungsten carbide nozzles are usually considered to be the most durable of all material types. In cases of dirty unfiltered water, they are the most durable. In applications where flow rates exceed 190 lpm (50 gpm) or more, water may not be filtered and these users typically get the longest life from carbide nozzles.

There are conditions where carbide nozzles are not the best type of material to use; at pressures above 10,000 psi and with water filtered to 25 micron or better, the life of a carbide nozzle may be as short as 10 to 20 hours. These nozzles wear by erosion of the material; this wear can be quite uniform, where the orifice size increases uniformly and the nozzle still produces a coherent jet. In these cases, a worn nozzle is defined by being so large that the desired operating pressure cannot be maintained. This problem is most evident with small orifice sizes. For example, if a .7 mm (.028 in.) diameter nozzle is being used, a 0.1 mm (.004 in.) increase in orifice size is a 15 percent change, resulting in a 30 percent change in flow rate. However, if a nozzle size of 2.0 mm (.079 in.) is being used, the 0.1mm increase in orifice size is a difference of only 5 percent in size, causing a 10 percent change in flow rate.

Another failure of carbide nozzles occurs when the erosion does not occur uniformly. There may be a slight change in orifice size, but the big change occurs in the quality of the jet produced. In these cases the evidence of the nozzle being worn is indicated by reduced production rates, with the jet having deteriorated in cutting ability by half or more.

Tungsten carbide is composed of carbide particles cemented together by a binder. Ratios of binder to carbide vary, as well as binder types. Both of these variables affect the toughness as well as the erosion resistance of the nozzle. In our tests, cobalt binder to carbide ratios of 5 percent and 15 percent were tested, and there was a difference in both wear rate and type of wear. The wear mechanism of carbide materials when used as a nozzle material is not well understood; it is likely erosion of the binder, possibly combined with corrosion-erosion.

Figure 1 shows the change in orifice size for the two different carbide types, and Figures 2 and 3 show the jet patterns produced by each type after the tests. The 5 percent binder had a relatively consistent wear around and through the orifice, and is shown in Figure 4. The 15 percent binder did not change in size much but had uneven wear in the form of deep pockets which affected jet quality. Figure 5 shows the effect on pressure with wear of the 5 percent binder carbide nozzle, if the output of the pump's flow rate is constant. Overall, the 15 percent binder material showed the longest life.

De-ionized water will also cause very rapid failure of carbide nozzles. With this type of water condition, the erosion of the orifice size can result in a useful life of less than 10 hours.

3.2 Steel Nozzles

Nozzles made from steel vary widely in design and in quality. They are built as replaceable threaded inserts, or can be made by drilling into a disposable head or bit, as would be used in tube cleaning. Those made as replaceable inserts typically have a better jet quality because the inlet to the nozzle can be formed as desired; holes drilled into a head do not have this option and have the worst quality. The better quality replaceable nozzles usually have longer life as well. With water filtered to 25 micron or better and pressures up to 140 MPa (20,000 psi), properly built steel nozzles can have useable lifetimes of 150 to 200 hours and will outlast carbide nozzles. Figure 6 shows the jet patterns produced after 40 hours by a steel nozzle and two different carbide nozzles. Wear in steel nozzles is defined by degradation of the jet pattern produced; orifice size change does not usually occur.

Steel nozzles wear by two mechanisms: cavitation erosion and abrasive erosion. The rate of cavitation erosion is mostly dependent on the design of the nozzle, while abrasive erosion will occur in all steel nozzles with the presence of abrasive particles in the water. Figure 7 shows a steel nozzle orifice with 50 hours use with recycled, unfiltered water; the wear due to abrasive erosion is very smooth and even. Figure 8 shows a drilled orifice in a head as an example of cavitation erosion in steel. It is rough and uneven, with pockets running across the flow path.

The shape of the inlet to the orifice can affect the rate of cavitation erosion. Figure 9 shows two drilled orifices in a steel head, with the one on the left having a chamfered inlet. Unfortunately, this is often not possible to do, as access to the back side of the orifice is needed to perform this operation. Operating pressure also influences the rate of cavitation erosion; a steel nozzle that might last 150 hours at 140 MPa (20,000 psi) will only last 20 to 30 hours at 250 MPa (36,000 psi).

In the case of the tube cleaning heads, where the nozzles are drilled directly into the head and erosion due to cavitation is the primary mode of failure, life is also dependent on water filtration. Figure 10 shows the average life based on water filtration for heads made of 17-4 stainless steel, at an operating pressure of 70 MPa (10,000 psi).

3.3 Sapphire Nozzles

Sapphire nozzles are most commonly used for operating pressures above 140 MPa (20,000 psi). They produce high quality jets in orifice sizes less than 1 mm (.040 in.) but have poorer quality jets in larger sizes, compared to carbide and good quality steel nozzles. Sapphire nozzles require very clean water, filtered to 10 micron or better. With good conditions, their life can approach 200 hours or more, as the material does not suffer from the erosion problems of carbide or steel nozzles. However, the sapphire material is very brittle, and any tiny chip on the edges of the orifice will destroy the jet quality. Any particles in the water passing through the nozzle will cause these chips, and if a large particle strikes the sapphire it can be instantly cracked. They are also quite easily damaged by rebound of the material being jetted. For these reasons, sapphire is not commonly used in waterblasting operations at pressures below 140 MPa (20,000 psi).

4.0 CONCLUSIONS

There is no single nozzle material that is suitable for all operating conditions. Selection should depend on how well the water will be filtered and on the operating pressure. The nozzle design also has some effect on operating life; the initial jet quality produced is an indication of the quality of the nozzle design. Table 1 lists the nozzle material types discussed in this paper and the recommended conditions for each.

Carbide nozzles outlast all other materials when unfiltered water is used. There are different types of carbide available with variations in type of binder and binder percentage; these factors affect the type of wear and wear rate of carbide nozzles.

Steel nozzles will outlast carbide when water filtered to 25 micron or better is used; this difference in life becomes greater with operating pressures above 70 MPa (10,000 psi). Steel nozzles can wear rapidly with dirty water conditions. The life of a steel nozzle is also dependent on the design of the nozzle; a good design can allow a life of up to 200 hours, while a poorly designed nozzle may have a life of only 40 hours.

Sapphire nozzles require filtration to 10 micron or better to have a reasonable life. They are very fragile, and dirty water can cause instant failure. With properly filtered water, sapphire nozzles can last 200 hours or more.

Recommended Material	Operating Conditions
Carbide	Dirty, unfiltered water; pressures below 140 MPa (20,000 psi)
Steel	Water filtered to 25 micron or better, pressures below 140 MPa
Sapphire	Water filtered to 10 micron or better, pressures above 140 MPa

Table 1. Recommended nozzle materials depending on operating conditions

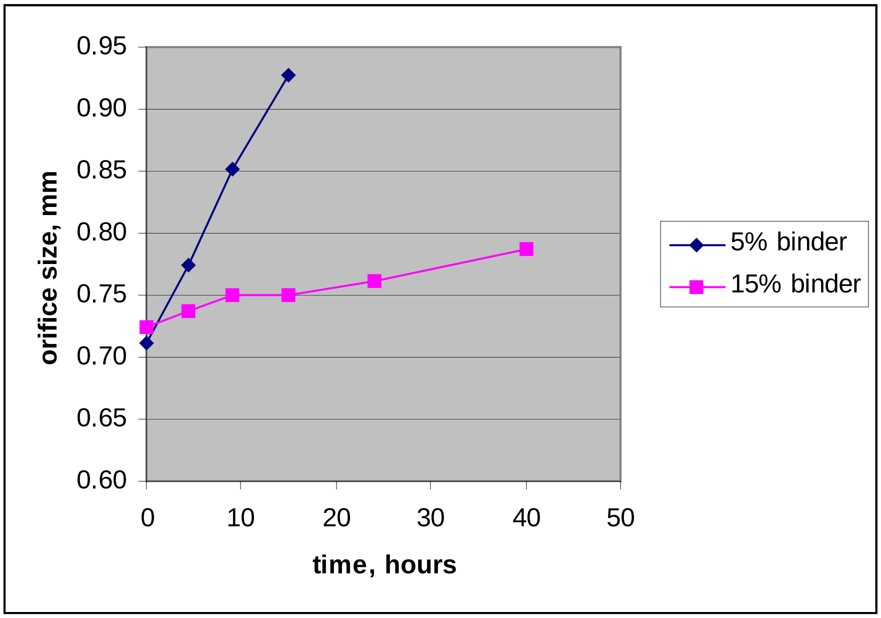

Figure 1. Wear rates in orifice size for two different types of carbide nozzle material

Figure 2. Jet pattern produced by the 5% binder nozzle after 15 hours on the left, compared to new of the same material and design on the right

Figure 3. Jet pattern produced by the 15% binder nozzle after 40 hours on the right, compared to new of same design and material on the left

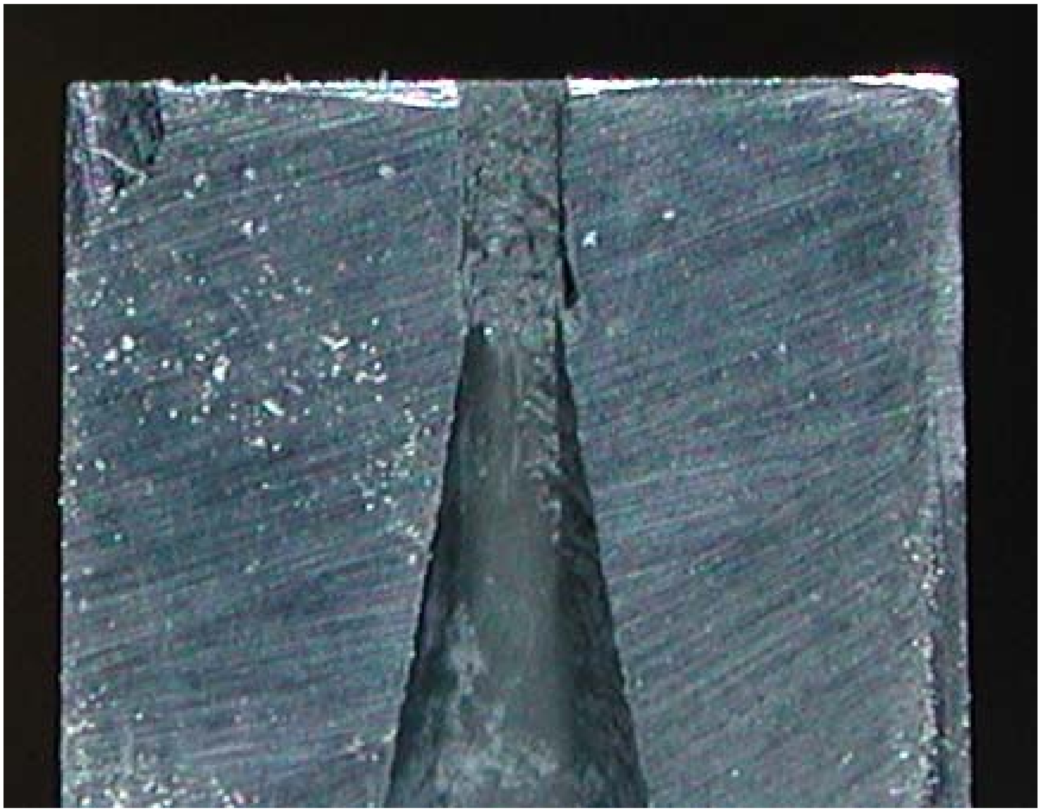

Figure 4. Section of 5% binder carbide nozzle after 15 hours

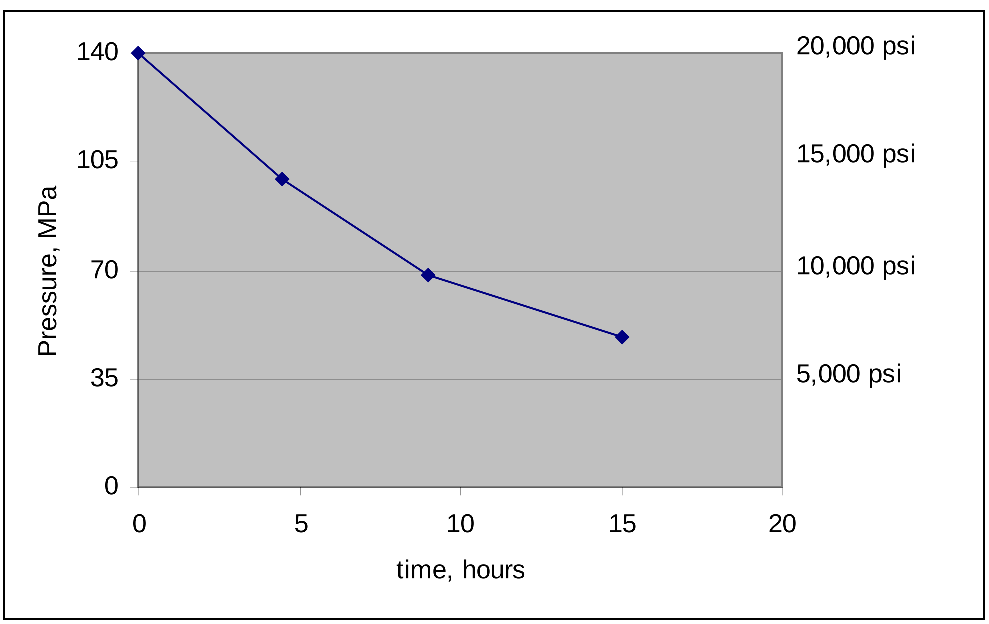

Figure 5. Effect of orifice wear on pump pressure, 5% binder carbide nozzle

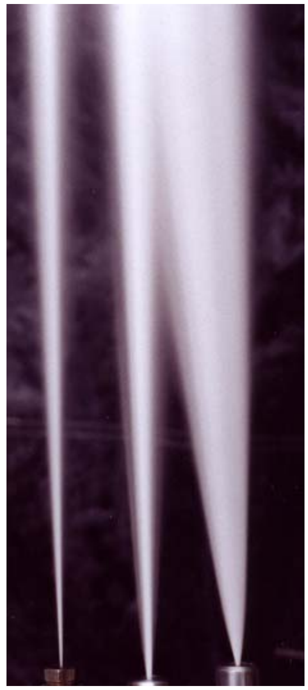

Figure 6. Jet pattern produced by steel nozzle after 40 hours on the left, compared to 5% binder carbide after 10 hours in center, and 15% binder carbide after 40 hours on right

Figure 7. Steel nozzle on the right showing abrasive erosion from very dirty water

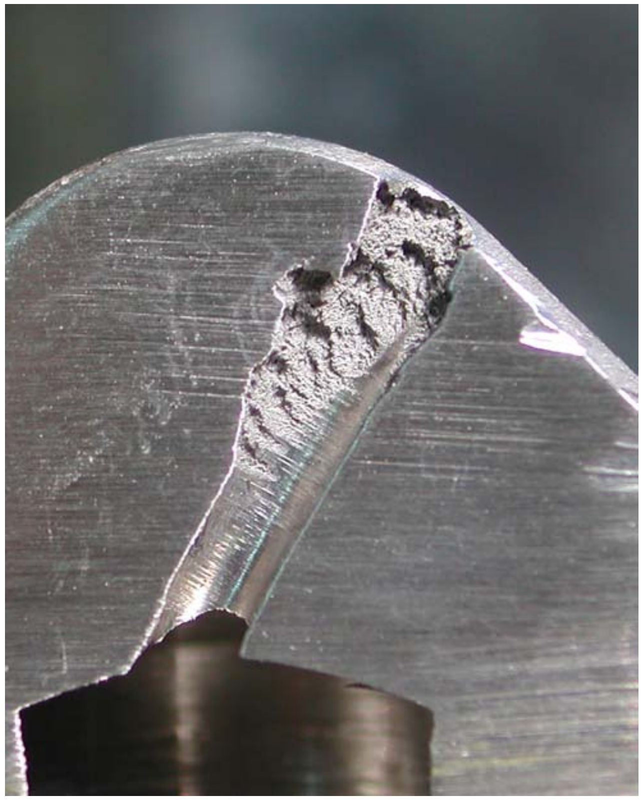

Figure 8. Steel nozzle with cavitation erosion

Figure 9. Steel nozzles, effect of inlet shape to orifice on cavitation erosion

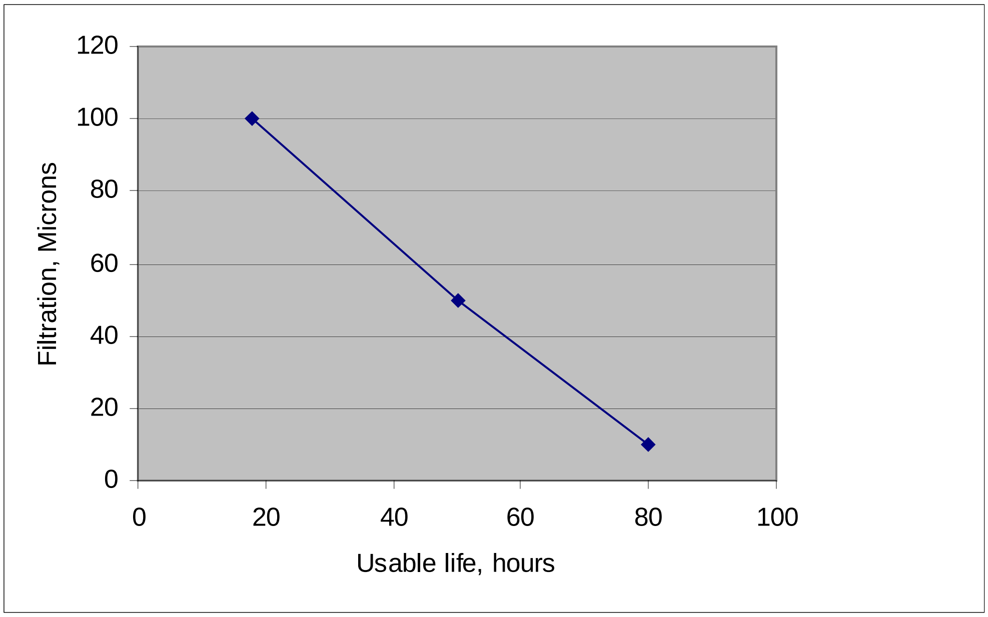

Figure 10. Nozzle life at 70 MPa (10,000 psi), drilled steel nozzle head

2003 WJTA American Waterjet Conference
August 17-19, 2003 Houston, Texas

Paper 3-A

SOME ASPECTS OF HYDROABRASIVE SUSPENSION JET CUTTING OF MARBLE

A. Perec
Management and Economics Faculties
Technical University of Koszalin
Koszalin, Poland

ABSTRACT

The paper presents the results of a complex of studies on the parameters controlling the cutting of marble with a hydroabrasive suspension jet, whose pressure is reduced to 30 MPa. Such a considerable operating pressure reduction is a result of an original and in-house construction of the BORJET 01 appliance, whose advantage comes from the creation of a circuitous liquid motion. The influence of the most important hydraulic and technological parameters on the cutting depth is presented in the paper. In addition, coefficients of erosion and proper energy characterizing the cutting process have been compared. The effectiveness of the suspension jet cutting at a pressure reduced to 30 MPa is compared with conventional hydroabrasive jet cutting at a pressure of 300 MPa.

1. INTRODUCTION

In recent years, high pressure water-jet machining has competed effectively with conventional methods of separation of materials. This is above all because of its universal potential as a means of solving a variety of problems such as blank cutting of complex shapes, cutting various materials or in the possibility of cutting in extreme conditions [2] (where there is a risk of fire or explosion, or to work under water to a depth of 6,000 m, etc.).

The most serious disadvantage of current systems for cutting with a high pressure hydroabrasive jet and working at pressures of 400 MPa, is in the use of an injector mixer to create the jet - due to its low efficiency, especially when there are very large differences in the velocities of the working media. Elimination of the injector mixer and the use of the jet's circumferential motion [1, 7] to create and mix a hydroabrasive stream under high pressure can radically change the situation. Because of this change, similar machining effects can be achieved even though the working pressure has been lowered by an order of magnitude.

2. TEST STAND

A test stand [5] has been constructed using a new concept to create a prototype of the BORJET 01 appliance. It is of a universal nature and allows quick changes to be made in the configuration of the hydraulic connections, which in turns makes it possible to change the method of mixing, the manner in which the abrasive is entrained as well as allowing changes in the water supply, and the way in which the hydroabrasive jet is used.

The BORJET 01 appliance (Figure. 1) has been built from two containers and four independent hydraulic lines, which allow adjustments to be made in the basic flow parameters. Each line consists of the following valves: a cut-off valve, a throttle valve, a non-return valve and a manometer. An overflow valve acts to prevent an excessive increase in pressure. It is set at a pressure of 30 MPa.

A hydraulic monitor of the P26 type is used as the source of high pressure water. It is based on elements from a plunger pump made by the Austrian company WOMA. This unit can produce a maximum pressure of 75 MPa with a water flow of 75 dm^3/min.

3. TEST METHOD

Materials were cut by directing the hydroabrasive jet perpendicular to the machined surface [7], and moving the sample at a rectilinear traverse speed relative to the working nozzle. The thickness of the samples was selected so that, with the most effective machining parameters, through cutting should not occur, since that would make it difficult to correctly determine the depth of the cut.

Marble is a metamorphic (transformed) rock, which has secondarily crystallized at some depth in the ground under considerable pressure and at an elevated temperature. The marble used is characterized by its white color. It is of average crystalline size and is exceptionally resistant to the influence of atmospheric conditions. It takes a very good finish.

4. TEST RESULTS

4.1. Tests of influence of type and size of abrasive

Tests of the influence of the abrasive type and size were carried out to select the most advantageous combination for further tests, based on maximum cutting efficiency and minimal cost.

The tests were carried out with the following parameters: pressure p=28MPa, feed V_p=4mm/s, rate of delivery m_a=70g/s, distance from the nozzle b=6mm, applying a nozzle of l=75mm length and inside diameter Ø=2.0mm. The results of these tests are presented in Figure 2.

The largest depth of cut [2], over 78mm, was achieved while using aloxite #30. This is above all because of the high density of the aloxite, which gives an increase in the kinetic energy of the grains. The isometric shape of the aloxite grains also improves the machining effects.

Another abrasive that produced a large depth of the cut was aloxite#46 and #60. However, because of the high costs of these synthetic abrasives, they cannot commonly be used in high pressure hydroabrasive jet machining research. These abrasives can only be used sporadically for cutting hard to work materials as well as in those cases when the cost of the abrasive does not play a significant part.

Garnet #60 appeared to be the best of the natural abrasives based on the cut depth achieved. The last abrasive material examined was quartz sand, and its low price and free availability, made it attractive in machining with a high pressure hydroabrasive jet. From among the grain sizes tested (#60, #46), quartz sand #46 turned out to be the most effective.

4.2 Influence of traverse speed and pressure

Cutting was conducted with the following constant parameters:

- abrasive: quartz sand #30,
- inside diameter of nozzle Ø=2.0mm,
- length of hydroabrasive nozzle l=50mm,
- distance nozzle – material b=6mm,
- abrasive flow rate m_a=60g/s.

The largest depth of cut h=48.51 was obtained with the slowest traverse speed V_p=1mm/s and the highest working pressure p=28MPa (Figure 3). When the pressure was lowered to 16MPa, the cut depth decreases and, at the same traverse speed, reached a value of h=38.83mm. when the traverse speed was raised to Vp=6mm/s, the cut depth decreases at all pressure levels and reached a value h=13.73mm at a pressure of 16MPa.

4.3. Influence of abrasive flow rate and pressure

Cutting tests were carried out with the following parameters held constant:

- abrasive: quartz sand #30,
- traverse speed Vp=4mm/s,
- inside diameter of nozzle Ø=2.25mm,
- length of hydroabrasive nozzle l=50mm,
- distance nozzle – material b=6mm.

The effects of cutting marble are illustrated in Figure 4. The largest cut depth h=40,06mm was obtained at the highest working pressure p=28MPa and abrasive flow rate m_a=70g/s. A decrease in the depth of the cut over the whole range of working pressures occurred with change in the abrasive feed rate. As working pressure decreased depth of cut also fell. The smallest cut depth exceeding h=6mm was obtained with the greatest abrasive flow rate and the lowest pressure p=16MPa.

4.4. Influence of abrasive flow rate and sizes of nozzles

In order to determine the influence of abrasive flow rate and nozzle size on the depth of cut in steel a decision was made to make test cuts with nozzles having the following geometry:

- length l=50, 75 and 100mm,
- diameter Ø=2.0; 2.25; 2.5 and 2.75mm.
-

The remaining parameters for the cutting process were as follows:

- abrasive: quartz sand #30,
- traverse speed Vp=4mm/s,
- distance nozzle – material b=6mm,
- working pressure p=28MPa.

4.4.1. Influence of abrasive flow rate and nozzle diameter with a nozzle length of 50 mm

The depth of cut in marble (Figure 5) was less dependent on the abrasive flow rate and the nozzle diameter, and for most parameters ranged from 24 to 32mm. The largest cut depth was obtained while machining with a nozzle diameter Ø=2.25mm, reaching a maximum of 40mm with an abrasive flow rate m_a=70g/s. The smallest cut depth over h=20,14mm was obtained with the minimum abrasive flow rate and with the smallest diameter nozzle used.

4.4.2 Influence of abrasive flow rate and nozzle diameter with a nozzle length of 75 mm

Typical cutting effects are given in Figure 6. The deepest cut in the marble, h=55.3mm, was with a nozzle diameter of Ø=2.25mm at the highest abrasive feed rate. Reducing both the nozzle diameter and the abrasive feed rate decreased the cutting depth. The poorest machining efficiency was seen when the abrasive feed rates lay between 50 and 70g/s with the largest nozzle diameters. The cutting depth in this range did not exceed 31mm.

4.4.3 Influence of abrasive flow rate and nozzle diameter with a nozzle length of 100mm

For marble cutting with a 100 mm long nozzle, the deepest cut, h=37,5mm , (Figure 7) was achieved at the 70g/s abrasive flow rate with a nozzle diameter of Ø=2.25mm. As the abrasive flow changed , so the cutting depth decreased also, and this was the case for all working diameters. The largest cutting depth decrease occurred when the hydroabrasive jet diameter was reduced below 2.0 mm. Lowering the abrasive flow rate resulted in a shallower cutting depth, as well. The lowest value, 27.23mm, was, similar to earlier results, at the smallest abrasive flow rate, with the smallest diameter nozzle.

5. STATE OF THE MATERIAL SURFACE AFTER MACHINING

In order to assess the condition of the cut surface, examinations of the surface microstructure were carried out and roughness measurements were made.

5.1. Surface microstructure

The microstructure was examined by means of a scanning microscope. Figure 8 illustrates the image, which was subject to an analysis using a JEOL type JSM1 scanning microscope. The surface of the marble was examined at a magnification of 300x. The surface that has been cut is dull and rough. Processing marks are not very visible and the traces of the cut are almost straight. This is the result of the great susceptibility of marble to high-pressure hydro-abrasive jet processing.

5.2. Surface roughness

The roughness of the lateral surface of the cut material was measured to find the erosive influence of the hydroabrasive jet. The roughness of the material cut with the hydroabrasive jet was defined with a parameter R_a, determined by measuring roughness over a system of lines M (the arithmetic mean then giving a deviation R_a of the average line profile).

Figure 9 shows the amplitude of the marble indentations relative to the position along the length of the traverse measured. The average surface roughness value is R_a=5,25μm.

6. ENERGY CONSUMPTION OF THE PROCESS

A vital issue in the assessment of the efficiency of the machining process is the determination of its energy consumption (specific energy). Specific energy is a calculated value of the amount of energy consumed to remove unit volume of material [10]:

$$E_a = 2.12 \cdot 10^6 \frac{p^{15} d^2}{S \upsilon_p \rho^{0.5}} \qquad (1)$$

The erosion coefficient E_R is determined by the volume of material removed by a unit volume of the abrasive material. This is expressed by the following relationship:

$$E_R = \frac{S \upsilon_p}{m_a} \qquad (2)$$

Figure 10 shows the dependency of the specific energy on the traverse speed and the pressure when cutting marble. The specific energy reaches its greatest values at a pressure of 28MPa and a traverse speed of 1mm/s. The smallest values of the energy are reached for both materials when cut at the highest pressures and the smallest traverse speeds.

Figure 11 illustrates the dependency of the erosion coefficient on traverse speed and the working pressure when cutting marble. The greatest values of the erosion coefficient are reached at the highest traverse speed and the largest nozzle diameter. The smallest erosion coefficient values were obtained at the lowest jet pressure and, as a result of this, the smallest nozzle diameter.

7. SUMMARY

- From the abrasives examined, aloxite appears to be the best abrasive with regard to cutting efficiency.
- Conversely, in terms of reduced wear of nozzles, garnet and quartz sand are the best abrasive.
- The best results can possibly be achieved by using larger grains, e.g. #30.
- The influence of traverse speed is inversely proportional to the depth of the cut, irrespective of the remaining parameters of the process.
- The working pressure has a direct influence on the depth of the cut and, in most cases, the highest possible pressures should be used.

The test results allows one to define the best machining parameters for marble without the need to conduct additional tests, and this undoubtedly plays a part in a better understanding of the hydroabrasive cutting process in conditions where a reduced working pressure can be used, which will contribute to its wider application.

Further laboratory studies of this technique for separating materials should be carried out with the aim of increasing the working pressure, since at lower values the jet is not possible to achieve the high machining efficiency, which has been achieved by high-pressure jets created with traditional injection mixers.

In order to reduce the costs of hydroabrasive cutting, studies on decreasing both water and abrasive flow rates should be carried out.

Owing to such procedures, the efficiency of the cutting process should be ever higher, as a result of which there may be a wider practical application of this most interesting technology.

8. REFERENCES

[1] Borkowski J., Perec A., 1995, Wplyw warunków kreacji wysokoenergetycznej strugi hydrosciernej o obnizonym cisnieniu na efektywnosc obróbki metali. XVIII Naukowa Szkola Obróbki Sciernej. Wroclaw - Szklarska Poreba.

[2] Brandt C., Louis H., Meier G., Tebbing G., 1994, Abrasive Suspension Jet at Working Pressure up to 200 MPa. 12th Int. Symposium on Jet Cutting Technology. Rouen.

[3] Chudy J., Perec A.., 2001, Energetyczne aspekty intensyfikacji obróbki wysokocisnieniowa struga hydroscierna i struga hydroscierna o obnizonym cisnieniu. 2-nd Int. Conf. on Water Jet Machining WJM 2001. Cracow, pp. 159-168.

[4] Perec A.., Some aspects of hydroabrasive suspensive jet cutting of aluminum alloy. 7th Pacific Rim International Conference on Water Jetting Technology. Jeju, Korea.

[5] Perec A.: 1998, Badania skutecznosci przecinania wapienia wysokoenergetyczna struga hydroscierna o obnizonym cisnieniu. International Conference on Water Jet Machining, Kraków.

[6] Perec A.., 2001, Badania skutecznosci przecinania stali konstrukcyjnej wysokoenergetyczna struga hydroscierna o obnizonym cisnieniu. 2-nd International Conference. on Water Jet Machining WJM 2001. Cracow, pp. 209-218.

[7] Perec A., 1995, Influence of conditions highpressure, suspensive, hydroabrasive jet creation onto cutting materials parameters in lower working pressure aspect.(In Polish). Doctor trial.Technical University of Koszalin.

[8] Perec A.., 2001, Wlasnosci powierzchni materialów konstrukcyjnych przecinanych wysokocisnieniowa struga hydroscierna. XXIV NSzOS. Lopuszna, pp.137-144.

[9] Vijay M.M., 1989, Evalution of abrasive-entreined water jets for sloting hard rocks. 5th American Water Jet Conference. Toronto, pp. 333-342.

[10] Yazici S. Summers D. A.., 1989, The inwestigations of DIAJET cutting of granite. 5th American Water Jet Conference. Toronto, pp. 346-350.

9. NOMENCLATURE

E_a - specific energy [MJ/m^3]
d – nozzle diameter [cm],
S – cross sectional area [cm^2],
υ_p – traverse speed [cm/min],
p – pressure [MPa],
ρ- mass denisity water,
Er – erosion efficiency [cm^3/g],
m_a – abrasive flow rate [g/s].

10. GRAPHICS

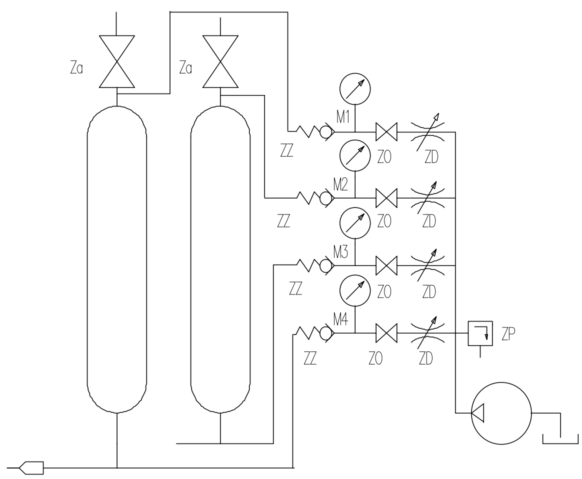

Figure 1. Hydraulic diagram for a prototype model of the BORJET 01

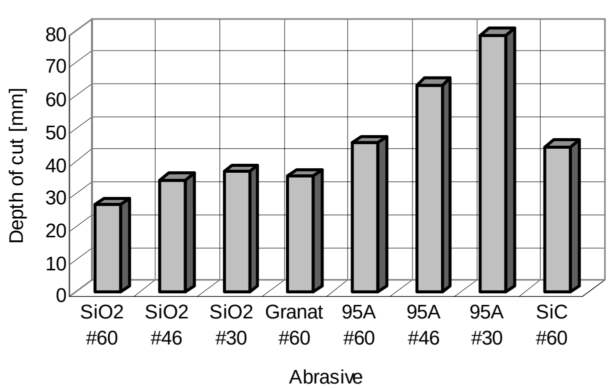

Figure 2. The effect of abrasive type and size on the depth of cut

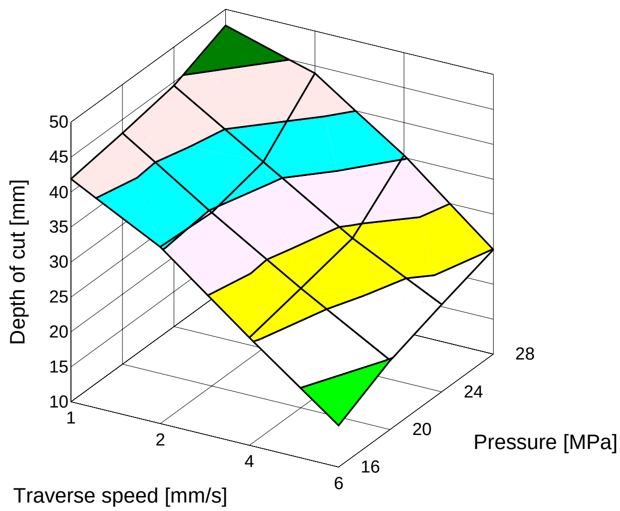

Figure 3. Influence of traverse speed and pressure on depth of cut

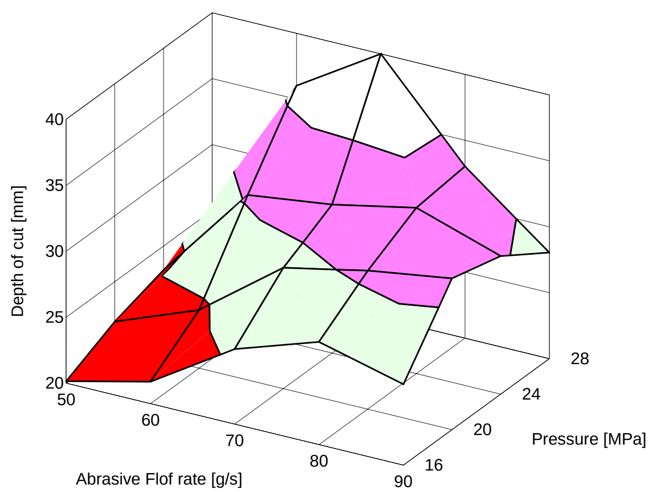

Figure 4. Influence of abrasive feed rate and pressure on depth of cut

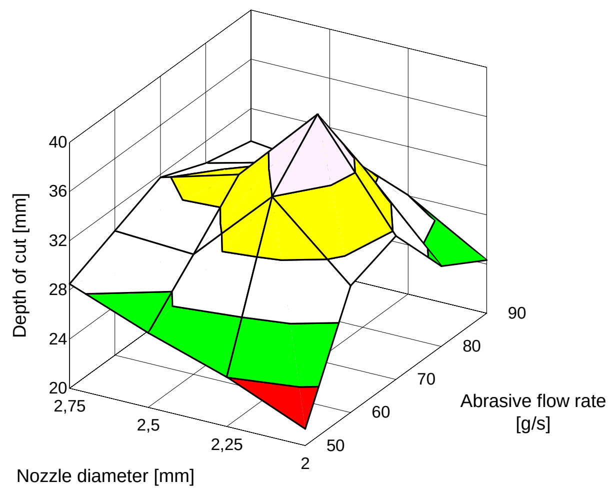

Figure 5. Influence of abrasive feed rate and nozzle diameter at a nozzle length of 50mm on depth of cut

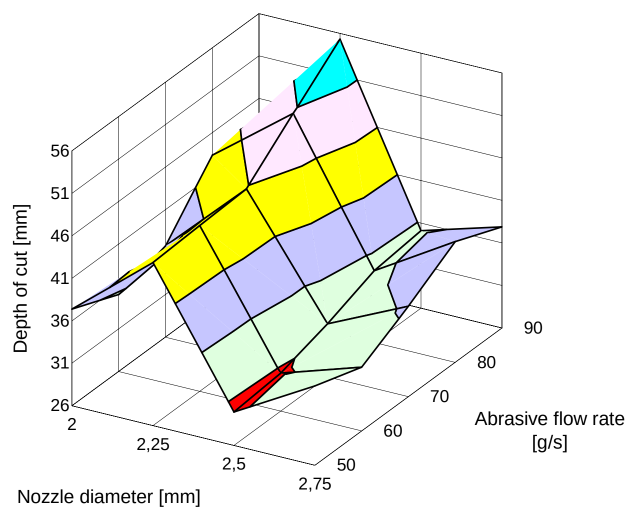

Figure 6. Influence of abrasive feed rate and nozzle diameter at a nozzle length of 75mm on depth of cut

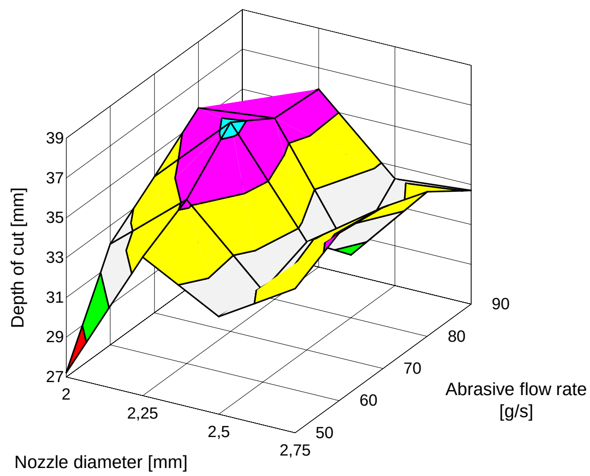

Figure 7. Influence of abrasive feed rate and nozzle diameter At a nozzle length of 100mm on depth of cut.

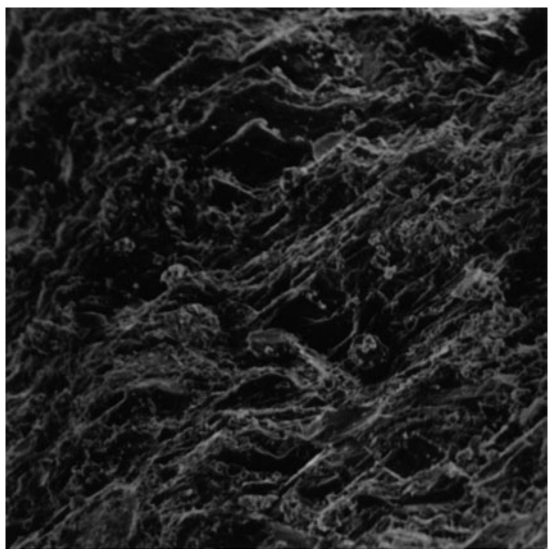

Figure 8. Microstructure of the cut surface (300x)

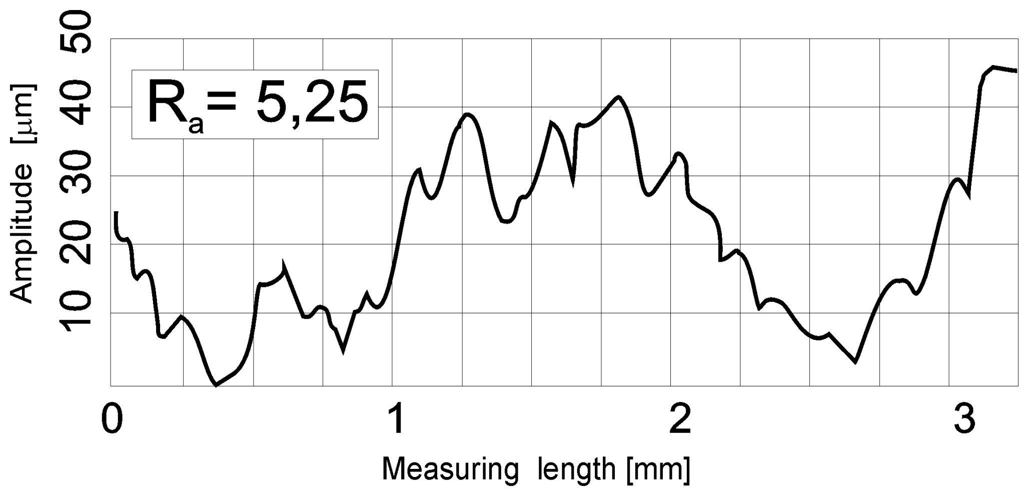

Figure 9. Profile of the roughness amplitude of the cut surface

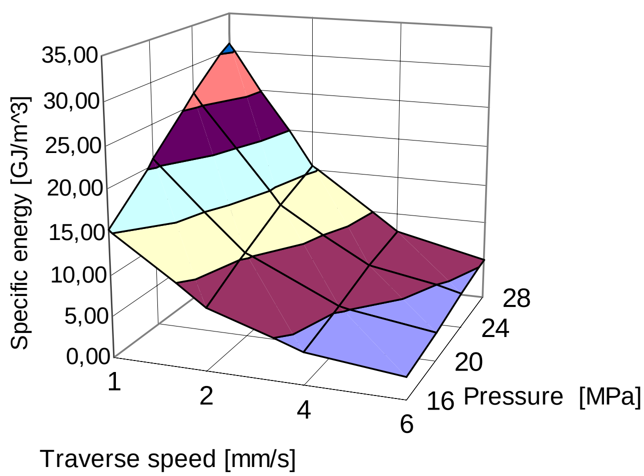

Figure 10. Dependency of specific energy on traverse speed and jet pressure

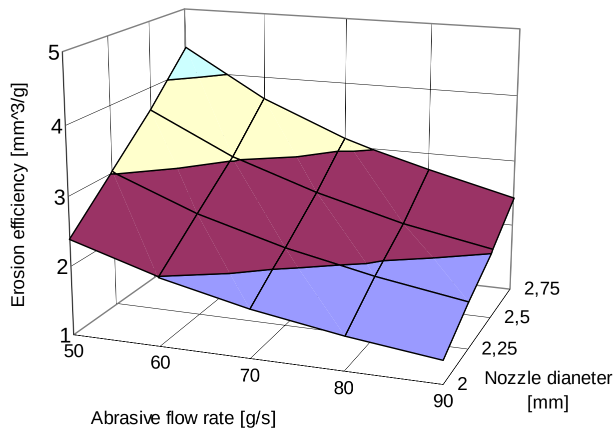

Figure 11. Dependency of erosion efficiency on traverse speed and pressure

2003 WJTA American Waterjet Conference
August 17-19, 2003 • Houston, Texas

Paper 2-C

EROSION OF NATURAL STONE BY ABRASIVE GRAINS

M. Monno, C. Ravasio
Dipartimento di Meccanica, Politecnico di Milano
Milano, Italy

W. Polini, S. Turchetta
Dipartimento di Ingegneria Industriale, Università degli Studi di Cassino
Cassino (FR), Italy

ABSTRACT

Abrasive waterjet technology has assumed a considerable importance in the cutting of natural stone, offering numerous advantages in comparison with conventional methods.

Natural stone removal by an abrasive water jet involves mainly erosion by the abrasive particles impacting on the cutting surface at high angles. The craters formed are due to brittle fractures.

The present work describes a new test apparatus to study erosion due to the impact of a small quantity of abrasive particles on a marble surface. The testing machine is made up of a tube through which a compressed-air flow at 10 bar pressure accelerates a small amount of abrasive particles towards a marble surface. In this way the action of the abrasive particles has been separated from that of water during marble cutting. By adjusting the values for both the pressure and the flow rate of the air it is possible to change the speed of the impinging particles. A pair of position transducers allow the indirect measurement of the abrasive grain speed.

This work is addressed toward the analysis of the influence of both abrasive and impact angle on the erosion of White Carrara marble using this new test equipment.

1. INTRODUCTION

In recent years, high pressure water jet cutting has shown a significant improvement in performance and a substantial widening of its applications: It represents, in fact, an interesting alternative to some traditional technologies both for solving specific technical problems and for improvements in the industrial production processes.

A considerable contribution to the improvement of the process can be attributed to the intense activity of international research groups into water jet technology, carried out by the manufacturing companies, research institutes and by end-users of this technology.

WJ/AWJ technology shows interesting characteristics in comparison with other cutting processes. In fact, it represents a “cold” cut, applicable to a wide range of materials of industrial interest, with a low environmental impact. Such characteristics have favoured, particularly in recent years, the development and spreading of this technology into many industrial areas.

The main advantages of the AWJ, compared with conventional methods where a sharp-edged tool engraves the surface of the material, are (1):

- extended tool life;
- process automation;
- complex free-form profile cutting.

Due to its flexibility in workpiece materials and cutting path geometry, the AWJ technology constitutes nowadays an interesting alternative to conventional marble and stone cutting processes.

The traditional technologies, in fact, suffer from limitations due to the brittleness and the hardness of such materials and to the impossibility of shaping curvilinear or particular geometric shaped cuts.

With the introduction of abrasive water jet cutting of ceramics, marble and other natural stones for particular applications, such as the production of pavements, engraving, etc., the study of erosion by abrasive particles on materials that display brittle behaviour is continuously gaining importance.

An analysis of experimental work found out in the literature on this subject, emphasises the influence of the abrasive granulometry, the abrasive mass flow rate and effect of its fluctuations on the performances obtained by the AWJ, in terms of cutting kerf depth and surface finish (2-3). Abrasive particle effects are influenced not only by jet velocity, standoff distance and water-abrasive ratio in the jet but also by the target material. Three types of interaction mechanism can be observed from the point of view of the target material (4):

- interaction with metal or plastic material (steel, aluminum, copper, etc.);
- interaction with brittle material without oriented cleavage (glass,ceramics, etc.);
- interaction with material consisting of mineral grains (stone, granite, etc.).

If the target materials are brittle materials such as glass and ceramics without oriented cleavage, the mechanism of interaction depends upon the relative strength, hardness and fracture toughness of the abrasive particles and the target material. The main mechanism of interaction is the impact of particles on the material, creating microcratering and the formation of very small chip-like glass or ceramic particles that also act as new abrasive particles (5).

For carbonate marbles or sedimentary carbonates, which consist only of monomineral grains or crystals of calcite or dolomite, the main mechanisms of interaction are microcratering, cutting of carbonate grains with plastic deformation, and tearing up some small parts of the carbonate crystal along well-developed carbonate cleavage planes.

However, in the literature, an analysis of the erosion of brittle materials by abrasive particles could not be found. Thus, the hardness, brittleness and in-homogeneity characteristics of such natural materials needs to be studied to allow more complete theoretical and experimental modelling efforts.

The aim of this study is the analysis of the erosion caused by a small quantity of abrasive particles on the surface of stone materials, estimating the erosion rate and analysing the variation of the morphology of impact craters for comparison with existing theories in the literature.

Attention has been focused on an abrasive water jet machine suitable for stone cutting, in particular using Barton Garnet. The effect of this abrasive on White Carrara marble has been studied. By means of these damage tests (erosion and abrasion) carried out using a new testing equipment, useful indications of the behaviour of different abrasives and granulometries used in the AWJ process and, particularly, in marble cutting have been obtained.

2. STATE OF THE ART

In recent years the study of the erosion of brittle materials under abrasive particle impact has assumed an increased importance with the introduction of abrasive water-jet technology into the working of ceramic, marble and other natural stones.

Erosion is the progressive loss of original material from the surface of a solid, due to the relative motion between a solid and a fluid in contact. If the fluid contains solid particles, the phenomenon is called abrasive erosion when the relative motion is approximately parallel to the surface of the solid, or erosion when the impact is approximately perpendicular to the surface.

For brittle materials erosion mechanisms and models have been proposed for impacts normal to the surface, based on the hypothesis that the erosion is the result of cumulative damage due to the impact of single particles, which do not interact.

Finnie considers that the kinetic energy possessed by the eroding particles is the main factor in volume removal (6). The author only considers normal impact to the surface. Considering that the Hertzian contact stress generated at the moment of the impact triggers microfissures that form from pre-existing discontinuities and cause them to propagate, he proposed the following relationship:

$W = k\, r^{a}\, v^{b}$

Where:
r: dimension of the particles
a, b: parameters of the shape of the particles
v: speed of impact
W: eroded volume
k: a dimensional coefficient influenced mainly by the shape and type of the abrasive used.

This equation shows that the erosion of brittle materials is approximately inversely proportional to the square of the bending stress while the dependency on elastic module is smaller.

Bitter in (7) proposed an elasto-plastic model to calculate the total volume removed by a single particle impact. The volume removed by plastic flow was evaluated as

$$W = \frac{M(v\sin\alpha - K)^2}{2\varepsilon}$$

where:
M: the mass of abrasive particle
v: velocity of impact
α: impact angle
K: the threshold velocity of impact at which the elastic limit is just reached
ε: the energy required to remove one unit volume of material.

In order to test the equation proposed by Bitter, experiments were carried out using small steel balls. These balls were dropped onto slabs of glass from various heights and with various impact angles . It was concluded that, under an impact angle of 19°, erosion becomes negligible.

An erosion model was developed by Ruft and Wiederhorn based on elasto-plastic theory in (8). This assumed that the dimensions of the lateral fissure were proportional to the radial ones and the depth of the lateral fissure was proportional to the maximum indentation distance achieved by the particle. The volume removed is given by

$$W = \alpha \cdot K_c^{-4/3} \cdot r^{11/3} \cdot v^{22/9} \cdot H^{1/9}$$

where:
v: velocity of impact
r: a dimension of the particle
Kc: fracture toughness of the eroded material
H: hardness of the eroded material

Hashish in (9) in considering material that cannot be cut with a pure water jet, focused his attention on the cutting groove formed using an AWJ.

He considered Finnie's studies, in which there was no direct calculation of the shape and density of the abrasive particle. He changed the system particle-material target from a two-dimensional situation to a three-dimensional one. These modifications were included in equations for the motion of the particle.

The material removal in AWJ is a complex erosion process. Two mechanisms have been identified as dominant ways for material removal. These are the cutting wear which occurs at low impact angles and the deformation wear at high impact angles. The material properties associated with these two types of wear can be connected to dynamic fracture, to toughness and to the hardness of the target.

Mazurkiewicz in (10) considered that the weight loss was overestimated in Finnie and Bitter’s theories. In fact some particles are crushed and others hit and bounce off without cutting.

Gorham in (11) carried out experiments where small tungsten carbide spheres are supported on glass surface; subsequently an increasing load is applied, in a similar way to a normal hardness test. This is a static test and therefore does not show a direct dependency between the erosion and the kinetic energy of the eroding media. For low loads a Hertzian fracture with an overturned truncated cone shape was observed. Increasing the applied load, led to he formation of micro-fractures in the walls of the cone. The volume removed is estimated as follows:

$$a^3 = \frac{3}{8} PR \left[\frac{(1-v_1)}{G_1} + \frac{(1-v_2)}{G_2} \right]$$

where:
a: radius of the contact area
P: the applied load
R: radius of the sphere
v_1 and v_2: Poisson's ratio of the glass plate and the indenter respectively
G_1 and G_2: shear moduli of the target material and abrasive particle.

The experiments showed that as the removal mechanism grows it increases the size of the primary and secondary fracture cones.

Raissi (12) applied these proposed models to AWJ cutting, considering a large abrasive flow rate moved by the high pressure waterjet stream.

In this work some hundreds of abrasive particles normally used for AWJ cutting are accelerated by compressed air, and they are used to separate out the high pressure water erosion component.

3. EXPERIMENTAL PROCEDURE

3.1. Test material

These experimental investigations were carried out on a stone material, known as White Carrara marble. Carrara marble is among the best known of Italian minerals (Figure 1). What characterises this material is the perfection of the shape of the crystals, and their transparency and sharpness. In the best pieces of this stone there are also perfectly shaped quartz crystals. The beauty of these minerals is highlighted also by the white marble matrix that increases and amplifies the colours and the shape of the minerals.

The mechanical properties of the marble are described in Table 1. In general, stone materials have a hardness that makes them difficult to machine, and a very low thermal expansion coefficient, which makes them suitable for external applications.

The most common usage of stone is for outside and inside flooring, outside and inside domestic coverings, and urban furnishings, house building and sacred art. AWJ technology represents an effective alternative for dealing with marble’s brittle properties. It is commonly used to produce decorations or ornamental products.

3.2. Testing system

A new testing system has been developed for evaluating the damage produced by the impact of a very few abrasive particles on a sample surface. In this way the action of the abrasive particles has been separated from that of the water during marble cutting. This process uses very few abrasive particles, thus the collisions between abrasive particles are negligible. Figure 2 shows the operating principle of the test system.

The device is made up of an accelerating tube where, under the action of a 10 bar pressurised air flow, abrasive particles reach a designated speed and are thrown onto the target surface. Setting values for both pressure and air flow rate controls the speed of the impinging particles.

The speed of the abrasive particles is measured by two pairs of optical fibre sensors (OMRON-E32-TC200), each pair comprising an emitter and a receiver, located in sequence along the particle path. A continuous light infrared beam is established between each emitter and receiver,. The two sensors detect when this beam is interrupted by the passage of an object (in this case, a particle) and send an electric signal to the oscilloscope at the times that the two beams are broken t_1 and t_2; the oscilloscope displays these interruptions. The speed of the particles is then calculated, knowing the distance between the two sensors,. The position of the sensor pairs has been optimized to ensure that the abrasive particle trajectory always runs through the optical axis of both sensors. The speed of the particles, at the exit of the tube, is about 100 m/s. The value obtained is the average speed of the flow in a particular test; the influence of air resistance has been neglected.

The marble sample is inserted into an aluminium slab, shaped to hold the sample in the sample table. The loading device (Figure 3) is made up of an aluminium cylinder with a horizontal through hole coaxial with the acceleration tube. The load capacity depends on the type of abrasive and it is about 0,8 g for Barton Garnet.

The impact angle of the single particles onto the target surface is varied by orienting the testing sample to the desired angle, and the results obtained are then analysed under a microscope.

Figure 4 shows a block diagram of the testing system as it was built.

The sequence of events during an impact test are:

- introduction of the abrasive particles into the loading device;
- introduction of the loading device into the firing device;
- introduction of the sample into the aluminum slab;
- selection of the impact angle;
- opening of the solenoid valve;
- expulsion of the abrasive particles;
- speed measurement;
- recovery of the sample.

3.3. Abrasive material

The abrasive used for the experiments is Barton Garnet, mesh 30 and mesh 50, a size which is widely used for AWJ machining.

The garnet group contains closely related, isomorphous minerals that may intergrow or contain a slight percentage of another element found in a different garnet member replacing one of its own.

Garnets are isostructural, meaning that they share the same crystal structure. This leads to similar crystal shapes and properties.

The common garnets can be divided into two basic subgroups: the Almandine and the Andradite subgroup.

There are additional minerals included in the garnet group, such as goldmanite, calderite, knorringite, schorlomite, etc. but they are very rare, and they are not used in waterjet technologies.

Almandine is the iron aluminium garnet. Magnesium can substitute for the iron and become more like pyrope, the magnesium aluminium garnet. Almandine is usually found either as a rock forming mineral in magmatic and metamorphic acid rocks and in other alluvial deposits.

Industrial abrasive made from garnet almandine is the prevalent abrasive used in AWJ cutting.

Andradite is the calcium-iron garnet or rarely calcium-aluminium. Industrial abrasive products based on andradite are used mainly for air blasting and cleaning (cleaning of metal surfaces, paint removal, etc.). Tests of andradite abrasive in AWJ cutting have given a lower performance when compared to that of almandine garnet (4).

Table 2 shows the physical properties of Barton garnet. The mass of the abrasive volume used in a single shot is, on average, 0.8g.

3.4. Experimental procedure

The study of the weight loss of natural stone under AWJ attack has been carried out using an experimental approach according to a factorial experimental plan, that is shown in Table 3.

The impact distance, the mass of the abrasive volume in a shot and the speed of the particles can, to a close approximation, be considered fixed.

The abrasive mesh size and the impact angle have been varied.

The mass loss of the sample, from before and after particle impact, has been measured by a precision balance.

Figure 5 shows the shape of a crater on the sample surface scraped by the abrasive particles, as seen under an optic microscope. The shape and the dimensions of the craters in a single sample are almost all different and therefore it is impossible to define a correlation between geometric parameters of the craters (shape and dimensions) and process parameters of the test (impact angle and mesh) (13).

3.5. Evaluation procedure

The analysis of variance (ANOVA) model has been implemented to determine the influence of abrasive mesh and impact angle on mass loss. The fundamental hypotheses to apply an ANOVA model (that are the normality and the homogeneity of the variance of the residuals) have been verified. Moreover, the response trend (increase or decrease) vs. both abrasive mesh and impact angle has been evaluated by using Main Effect Plots.

4. DISCUSSION OF RESULTS

The results of the ANOVA analysis shows that the impact angle is the major influence on the mass loss, while the abrasive mesh seems to be less significant. Moreover, an increase in the mesh size implies a decrease in the chip mass removed from the sample (see Figure 6), since a larger mesh number corresponds to a smaller particle dimension. An increase in the impact angle induces an increase in the mass loss (see Figure 6), since the kinetic energy of the abrasive mass in a shot is transferred more effectively to the marble sample as the mass impacts perpendicular to the sample surface.

5. CONCLUSIONS

The present study has used a new testing system that has been developed to evaluate the damage produced by the impact of very small number of abrasive particles on a sample surface. Such a device is composed of an acceleration tube where, under the power of a 10 bar pressurized air flow, abrasive particles reach the required speed and are thrown onto the target surface.

The testing system has been used to evaluate the mass loss of White Carrara Marble due to the impact of a known volume of Barton Garnet. Different values of abrasive mesh size and impact angle have been considered. It has been found that the impact angle is the major influence on mass loss, while the abrasive mesh size seems to be less significant. An increase of both the mesh and the impact angle implies a decrease in the marble mass removed from the sample.

The results are in line with the theory of brittle materials:

- erosion takes place through the formation and propagation of cracks;
- brittle materials are affected by repeated deformations, that decrease as the impact angle decreases.

The results obtained provide a basis for modelling the relationship between mass loss and both mesh size and impact angle. Such a model can be very effective in understanding the phenomena that occur at the interface between an abrasive waterjet and marble during cutting.

6. ACKNOWLEDGMENTS

This work has been carried out with the funds received by the Italian M.I.U.R. (Ministry of Instruction, University and Research) within the project entitled "Stone manufacturing technologies" (COFIN01).

7. REFERENCES

(1) Carrino L., Monno M., Polini W., Turchetta S., *Surface processing of natural stones through AWJ*, 16th International Conference on Water Jetting Technology, October 2002, Aix en Provence – France

(2) Bortolussi A., Manca M.G., *Surface finishing of marble with abrasive waterjet*, 16th International Conference on Water Jetting Technology, October 2002, Aix en Provence – France

(3) Carrino L., Monno M., Polini W., Turchetta S., *Study of cutting quality and efficiency in stone production*, Proceedings 15th International Symposium on Jetting Technology, September 2000, Ronneby - Sweden

(4) Institute of Geonics, Academy of sciences of the Czech Republic, Ostrava - *Abrasive for AWJ Cutting*, 2002

(5) Zeng J., Kim T.J., *Development of an abrasive waterjet kerf cutting model for brittle materials*, 11th International Conference on Water Jetting Technology, St. Andrews, 1992

(6) Finnie I., *The mechanism of erosion of ductile metals*, Proc. 3rd U.S. Nat. Congr. Appl. Mech.,ASME,1958

(7) Bitter J.G.A., A study of erosion phenomena, part I-II. Wear 6: 1963

(8) Ruft A.W., Wiederhorn S.M., *Erosion by solid particle impact*, Treatise on Materials Science and Technology, 1979

(9) Hashis M., *Pressure effects in abrasive waterjet machining*, Journal of Engineering Materials and Technology, July 1989

(10) Mazurkiewicz M., *A study of a leading edge profile for a slot formed during hydro-abrasive cutting*, Proc. 6th Amer. Water Jet Conf., Water Jet Techn. Ass., St. Louis, 1991

(11) Gorham D.A., Salman, *Indentation fracture of glass and mechanism of material removal*, Wear 233, 1999

(12) Mabrouki T., Raissi K., Cornier A., *Numerical simulation and experimental study of the ineraction between a pure high-velocity waterjet and targets*, Wear 239, 2000

(13) Miranda R.M., Kim T.J., *Abrasive waterjet cutting of marble and calcerous stones: a phenomenological study*, 1996, Proceedings of the 13th International Symposium on Jet Cutting Technology, Bedford, England

8. TABLES

Table 1. Mechanical properties of White Carrara marble

Density [kg/m^3]	2705
Water absorption [%]	0.06
Compressive strength [MPa]	131
Compressive strength to ageing by frost [MPa]	126
Young modulus [MPa]	75000
Flexural strength [MPa]	16.9
Abrasion resistance	0.52
Impact resistance [cm]	61
Knoop hardness [MPa]	1463

Table 2. Physical properties of Barton Garnet

Toughness	brittle
Hardness (mohs)	6.5 - 7.5
Density [g/cm^3]	4.1 - 4.3

Table 3. Experimental plan

Fixed factors	**Levels**
Abrasive kind	Barton Garnet
Impact distance [mm]	40
Abrasive quantum mass [g]	0.8
Speed of the particles [m/s]	100
Variable factors	
Abrasive mesh	30 - 50
Impact angle	90 - 80 - 70 - 60 - 50

9. GRAPHICS

Figure 1. White Carrara marble quarry

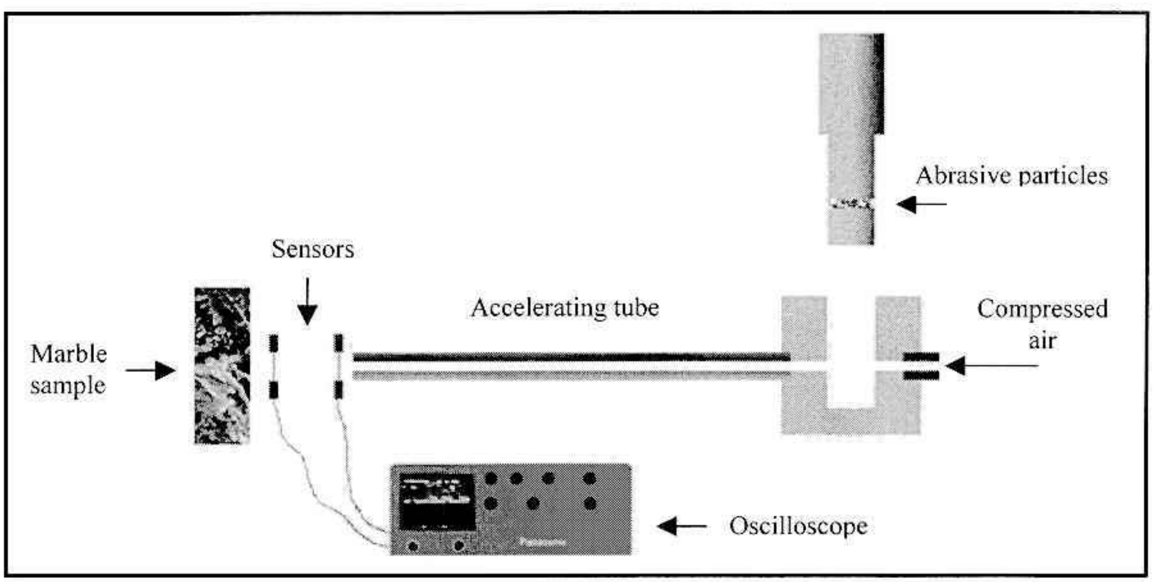

Figure 2. Operating principle of the testing system

Figure 3. The abrasive loading device

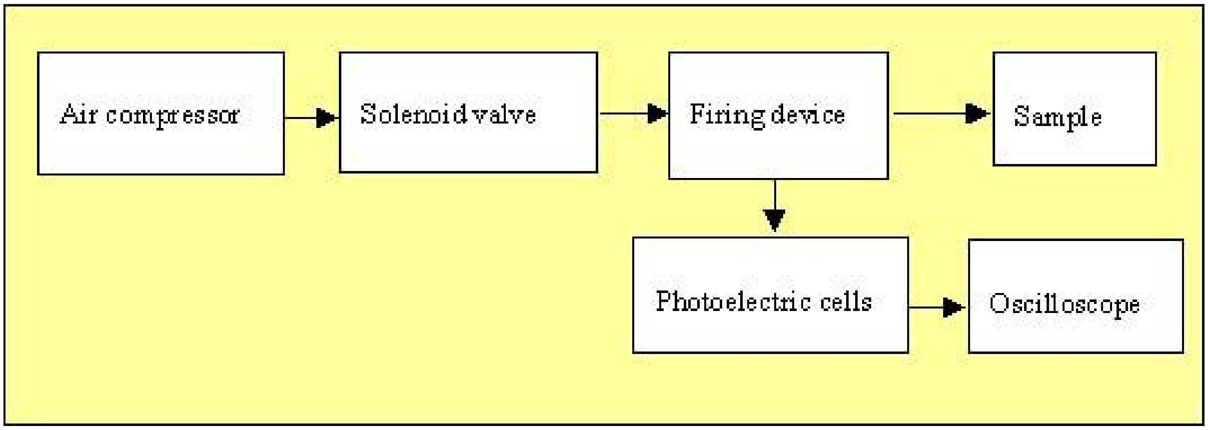

Figure 4. Block diagram of the components of the testing system

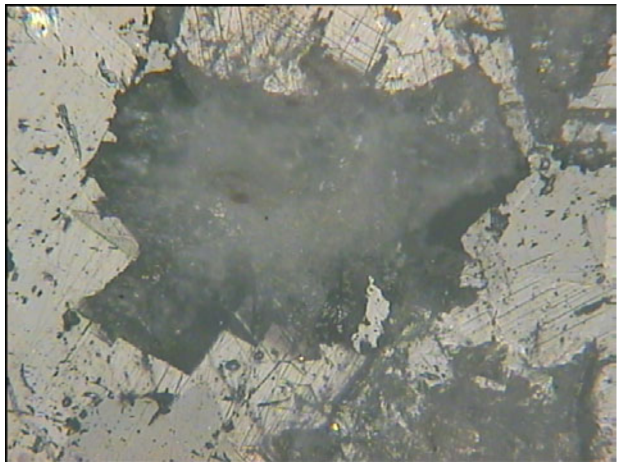

Figure 5. A crater on the sample surface observed through an optical microscope

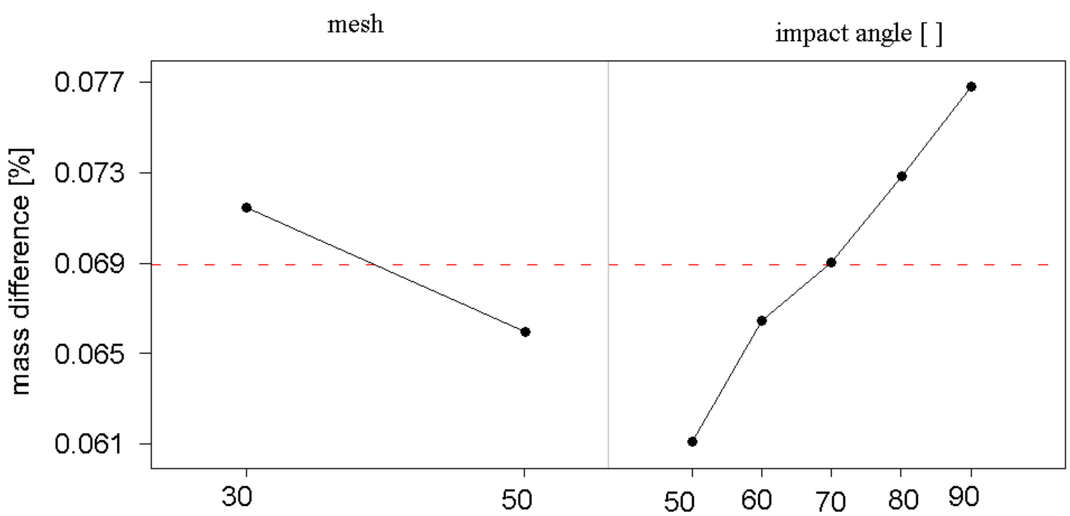

Figure 6. Main Effects Plot of mass reduction vs. mesh and impact angle

2003 WJTA American Waterjet Conference
August 17-19, 2003 ♦ Houston, Texas

Paper 3-C

MODELING JET CUTTING OF OIL SANDS

J. T. Bartley
Department of Mechanical and Industrial Engineering
University of Manitoba
Winnipeg, Manitoba, Canada

B. Singh
Department of Mechanical Engineering
Lakehead University
Thunder Bay, Ontario Canada

ABSTRACT

This paper presents a newly developed theoretical model for water jet cutting of oil sands, and the model is validated using existing experimental data from other researchers. Control volume analysis of jet penetration and jet cutting coupled with the rheological model of a Bingham plastic have been used to develop and solve the model equations in a closed form. Evaluations of coefficient parameters (coefficient of friction and coefficient of damping) contained in the model were done by trial and error application of the theoretical equations to each data set. Values of the coefficient parameters for water jet cutting of oil sands were found to be of similar magnitude for a variety of jet pressures and nozzle diameters. Unlike the theoretical models of other researchers, the models developed in this work distinguish between the separate cases of water jet penetration (where the nozzle remains fixed relative to the material) and water jet cutting (where the nozzle traverses relative to the material).

Organized and sponsored by the WaterJet Technology Association

1. INTRODUCTION

The oil sands deposits in Alberta contain reserves of crude bitumen estimated to be more than 180 billion cubic meters (Camp, F.W., 1976). Existing methods to recover bitumen from these deposits may be generally divided into those which depend on surface mining combined with some further processing, and those which operate on oil sands in situ. The surface mining techniques are applicable to shallow deposits (less than 40 meters of overburden), and in situ methods are suitable for deposits deeper than 200 meters. The surface mining based techniques result in recovery of over 90% of the bitumen in the mind oil sands, but require very large capital investments, and thus restrict the size of producing plants to be over 10,000 cubic meters of bitumen per day. A large part of the capital investment as well as operating costs is due to the use of heavy machinery and the associated power plant requirements for strip mining operations. The in situ methods require smaller capital investments and permit plants producing as little as 200 cubic meters of bitumen per day to be economically feasible, and unlike surface mining, in situ methods provide possibilities for gradual build-up of capacity as cash flows develop. However, in situ methods result in recovery of less than 30% of the available bitumen (for example, one of the most successful in situ method based project, the Imperial Oil Cold Lake Heavy Oil Project, recovers only about 21% of the bitumen available). Further, the lack of communication between wells due to low effective permeability of the deposit is a major problem in in situ recovery techniques. Finally, there is no suitable method available at present to recover bitumen from the zones of intermediate depths (40 to 200 meters). The amount of bitumen available in these zones is as much as 25% of the total resource (Camp, F.W., 1976). Thus there is a need for the development of a bitumen recovery method which: (1) reduces requirement for capital investments and makes smaller projects feasible for shallow deposits; (2) allows gradual build-up of capacity as cash flows develop; (3) permits high recovery of the resource; (4) can be used to develop and maintain controlled fractures; and (5) allows production of bitumen from the zones of intermediate depths. It is to meet these requirements that the use of high pressure water jets to cut oil sands is of some interest.

The use of water jets for cutting of oil sands has been investigated by several researchers(Gates, E.M. and R.R. Gilpin, 1981; Law, D.J., et al., 1987; Wagner, C.G., E.L. Hodges, 1985; McRoberts, E.C., and D.S. Cavers, 1988; and Singh, B., et al., 1989). All of these have been experimental studies. Past attempts to theoretically model water jet cutting have approached the problem of water jet/material interactions by incorporating experimental coefficients, or by including specific material properties such as porosity and permeability. Hashish and du Plessis (1978) included, in their theoretical model for water jet cutting, two parameters that presumably accounted for the frictional forces and damping effect on the water jet. Material failure and erosion due to an impinging water jet is random in nature at the microscopic level; and modeling such microscopic effects is difficult or impossible, as past attempts have been largely unsuccessful (Hood et al., 1990). Hashish and du Plessis (1978) demonstrated that by incorporating friction and damping effects into their theoretical model from a macroscopic point of view, which included a control volume analysis, general interactions between a water jet and material can be effectively accounted for.

Based on the macroscopic control volume analysis of water jet/material interactions, utilized by Hashish and du Plessis (1978), theoretical model for water jet cutting has been newly developed in this paper. Data from published experiments were grouped according to common jet parameters (jet pressure and nozzle diameter) and plotted with theory, mostly with exposure time as the independent variable. The various experimental parameters in the theoretical model were determined for each data set, and possible trends, similarities or discrepancies in the parameter values were identified. From application of the theoretical model, its predictive power was assessed and limitations elucidated.

2. DEVELOPMENT OF THE THEORETICAL MODEL

Due to the relative success of the theory of jet cutting developed by Hashish and du Plessis (1978), the theoretical model presented here incorporates many of their original assumptions about flow of the jet in the kerf (slot made by the jet). It has been observed that during jet cutting, small steps are produced in the material which are broken away under the hydrodynamic forces of the jet (Hashish and du Plessis, 1978; Hood et al., 1990). The jet penetrates through a series of steps before it is traversed to an uncut portion of the material, or the jet becomes too slow to penetrate farther. The rheological model for a Bingham plastic was used by Hashish and du Plessis (1978) to account for the time-dependent response of the material failing under the force of the jet. They observed that the material did not fail immediately on impact, but rather a small time delay was necessary for the stresses to develop in the material. The present work differs from that of Hashish and du Plessis (1978) however, in that a distinction is made between the processes of water jet penetration and cutting. It is assumed that the cutting process utilizes only the leading edge of the water jet, whereas penetration involves the entire circumferential surface area of the water jet in the hole.

Consider the pictorial representation in Fig. 1 of a typical water jet cutting scheme (Hashish and du Plessis, 1978; Hood et al., 1990). The water jet enters the top of the hole with velocity V_1 and cross sectional area A_1. At the bottom of the hole, the water jet strikes an area A_2, or area of penetration; here the jet has velocity V_2 and subsequently exits the control volume and penetrates the deepest portion of the hole wall with velocity V_3. The instantaneous depth of penetration is represented by Z, and rate of penetration by $\dot{Z}$. The jet is assumed to penetrate into the material at a faster rate than it is traversed at; and only the leading half of the jet is utilized due to the traversing action of the process.

2.1 Conservation of Mass

Water entering the top part of the control volume in Fig. 1 must be balanced by that leaving the control volume. Several simplifying assumptions can be made for the present case: steady flow; incompressible flow; isotropic fluid; and an expanding control volume; i.e., increasing Z. Due to the expanding control volume, relative velocities must be incorporated into the analysis. The relative magnitudes of velocities at point 2 are shown in Fig. 2. The jet exit velocity $\vec{V}_3$ is a vector composed of the radial exit velocity V_{3R} and its downward component $\dot{Z}$, as shown in Fig. 3. The conservation of mass for the control volume can be written as

$$\dot{m}_{exit} = \rho A_1 V_1 - \rho A_2 \dot{Z} \qquad (1)$$

2.2 Conservation of Momentum

We make simplifying assumptions to ignore the body forces of the control volume and pressure gradients on the control surface and state the integral momentum equation as

$$\int_{CS} \vec{\tau}_w \, dA + \vec{F}_{normal} = \frac{\partial}{\partial t} \int_{CV} \vec{V} \rho \, d\forall + \int_{CS} \vec{V} \rho \vec{V} \cdot d\vec{A} \, . \qquad (2)$$

The left hand side of equation 2 represents shear and normal forces respectively, and the right hand side represents rate of change of momentum and momentum flux respectively. Expressing each term appropriately, we can write the momentum balance as

$$F_{normal} = \rho \, A_1 V_1^{\,2} - \frac{\rho \, C_f \, V_1^{\,2}}{2} \sqrt{\pi \, A_2} \, Z \, . \qquad (3)$$

2.3 The Differential Equation and its Solution

For the theoretical model of water jet cutting, we employ the rheological model of a Bingham substance to account for the time-dependent processes of material deformation. Then we can derive the differential equation

$$\frac{dZ}{dt} + \frac{C_f \, \rho V_1^{\,2}}{\zeta \, D_n} Z = \frac{\rho V_1^{\,2} - \sigma_o}{\zeta} . \qquad (4)$$

The above equation is solved to arrive at the final form for prediction of dimensionless penetration during water jet cutting:

$$\frac{Z}{D_n} = \frac{1 - \sigma_o / (2P_d)}{C_f} \cdot \left[1 - \exp\left(- \frac{C_f \, 2P_d}{\zeta \, U} \right) \right] . \qquad (5)$$

Alternatively, the solution can be retained with time t. In this context the solution can be employed to predict depth of penetration during jet cutting based on time T_e that a particular section of the material, of length D_n, is exposed to the forces of the water jet. This exposure time is calculated as $T_e = D_n / U$, and the solution then becomes

$$\frac{Z}{D_n} = \frac{1 - \sigma_o / (2P_d)}{C_f} \cdot \left[1 - \exp\left(- \frac{C_f \, 2P_d}{\zeta \, D_n} T_e \right) \right] . \qquad (6)$$

2.4 Applicability of the Solutions for Jet Cutting

Whether Equation (5) is applied to the data for water jet cutting, or Equation (6) is applied, the coefficients of friction and damping, C_f and ζ, must be determined specifically from the data. If data are known from experiments using a constant traverse rate U then Equation (5) is more suited; whereas Equation (6) is more descriptive of the effects caused by varying the traverse rate. Although the solutions each contain the dimensionless ratio Z/D_n, the effects on penetration depth due to variations of the nozzle diameter are not definitive, and the solution may not account for such effects.

3. APPLYING THE THEORETICL MODEL

The theoretical model contains various parameters that required evaluation. Data from previously published experimental studies of jet cutting were collected and organized according to the variables of interest. Once the parameter values were obtained, the prediction capability of the model was assessed based on comparisons between calculated dimensionless depth of penetration Z/D_n and corresponding data.

Data for water jet cutting of oil sands were obtained from Gilpin and Gates (1980); the data were for the case of jet cutting in the laboratory environment and jet cutting in the field, or natural in-place environment. The major divisions among the data existed between traverse speeds U; as a result, data for the same U were plotted versus jet pressure. The model of jet cutting, given by Equation (5), was then applied to the data by obtaining the appropriate parameter values. Strength σ_o was set at 1.2 MPa; and for a specific traverse speed U and range of pressure P_d, the coefficient parameters C_f and ζ were obtained by trial and error to proivde a best fit of Equation (5) through the data. The laboratory data (for U = 0.14 m/s and U = 0.67 m/s) were plotted together and a single set of coefficient parameters obtained. Due to significant scatter of the field data even among the same nozzle diameters, data for each of the traverse speeds U = 0.2 m/s and U = 0.48 m/s were plotted separately for application of Equation (5). A single set of C_f and ζ values were obtained by trial and error that were applicable to both speeds. Data for the particular case of U = 0.2 m/s and D_n = 3.2 mm were found not to lie in the trend along with other data for this speed, and so they were plotted separately for application of Equation (5). In addition to the graphical comparisons, tabular comparisons of the theory and data were produced, indicating the correlation coefficient and average deviation.

4. RESULTS

Application of Equation (5) to the data for water jet cutting of oil sands resulted in obtaining coefficient parameters C_f and ζ to suit a range of nozzle diameters, jet pressures and traverse speeds (Table 1). Values of C_f were found to lie between 0.011 and 0.017; and values of ζ between 0.1 × 10^7 kg/m² s and 0.41 × 10^7 kg/m² s. One set of coefficient parameters were obtained for adequate prediction of the laboratory data; but two sets of parameters were required for the field data. The data for D_n = 3.2 mm, for cutting field oil sands, required a lower friction coefficient and higher damping coefficient than was obtained for larger nozzles (Table 1). The match between Equation (5) and the data for cutting in the laboratory gave a correlation of 0.95 and average deviation of 26.8% (Table 2). For the field data, a correlation of 0.87 and average deviation of 21.0% was obtained (Table 3).

The model for water jet cutting, given by Equations (5) and (6), was also applied to data from water jet cutting of various substances in order to estimate their coefficient parameters C_f and ζ, and predict Z/D_n versus either jet pressure P_d or exposure time T_e. In general, the theory was found to follow the trends of the data with good accuracy, depending on the continuity of the data and their degree of scatter (Figure 4). The model for water jet cutting supported previous findings (Cooley, 1974; Harris and Mellor, 1974) that depth of cut is a strong function of both jet pressure and traverse speed.

4.1 Discussion of Results

The data for water jet cutting of oil sands in the laboratory were accurately predicted with one set of coefficient parameters for the two traverse speeds used (Table 2). Equation (5) followed the more curvilinear trend of the lower speed results, while delineating a linear path through the data for the higher speed results. Gilpin and Gates (1980) developed a correlation equation to fit the laboratory data, which were said to represent the high and low traverse speed response out of six traverse speeds used in their experiments. They applied their laboratory correlation equation to the field data, but they found it underestimated the main trend of the data by about a factor of two. The data for jet cutting of oil sands in the field showed a significant degree of scatter (Table 3), and hence, the theoretical predictions given by Equation (5) can only at best be a mean prediction. One set of coefficient parameters was found suitable for both traverse speeds (U = 0.2 m/s and U = 0.48 m/s), except for the case of D_n = 3.2 mm. In order to follow the data for the smallest nozzle diameter, C_f dropped from 0.017 to 0.011 and ζ increased from 0.1×10^7 kg/m² s to 0.41×10^7 kg/m² s. The change in coefficient values, for the 3.2 mm nozzle, was most likely due to the inability of the jet to overcome the presence of water in the kerf and effectively penetrate the oil sand. This indicates that nozzles greater than 3.2 mm in diameter are more effective for cutting oil sands in the field.

5. CONCLUSIONS

The theory for water jet cutting was found to agree reasonably well with the extensive data covering a wide variety of materials, from oil sands to strong rocks such as granite and marble. The high correlations found between Equations (5) and (6) and the data (> 0.9), in addition to moderate average deviations (~ 25%), were evidence of a linear relationship between the theory and the data. In some instances it was shown that closer predictions (average deviations < 9%) of the data could be achieved if the coefficient parameters were varied for cases where the data appeared to be discontinuous. The cause for such discontinuities in the data trends may have been due to a transition of the cutting action from erosion or fracture to repeated impacts by water drops as traverse speed U increased, an explanation suggested by Hashish and Reichman (1980).

From the limited analysis of the data for oil sands, a particularly weak substance, a narrow range of values for C_f and ζ was obtained. For most of the oil sands data, including data for various nozzle sizes and two traverse speeds, a single set of coefficient parameters was found to be applicable, providing mean predictions of Z/D_n for all the data. Weaker rocks such as sandstone and oil sands tend to be more porous and contain smaller size grains than stronger rocks like marble and granite, which are dense and well cemented; consequently, strong rocks may possess greater sensitivity to variations in the jet parameters over softer rocks. The predictive power of the theory for water jet cutting depends on the type of substance one intends to investigate: strong rocks may require a range of coefficient parameters dependent on traverse speed, nozzle diameter and the jet pressure used; but weak rocks may be sufficiently characterized by just one set of parameters.

If water jet cutting data, obtained for two or more different nozzle diameters, appear continuous as a lumped data set in nondimensional form (Z/D_n), then the present theory, given by Equation (5), is sufficient for providing a mean prediction of Z/D_n and for accounting for jet power fluctuations due to changes in the nozzle diameter and pressure. The present theoretical model for predictions of Z/D_n against jetting time, given by Equation (6), in addition to being suited for predicting single pass cutting trends at various traverse rates, is also suitable for predicting multipass cutting trends due to the relative continuity of the data.

The present theoretical models for water jet cutting are essentially modifications of the model by Hashish and du Plessis (1978) with their constant $2/\sqrt{\pi}$ preceding C_f replaced with unity, as shown in Equations (5) and (6). Consequently, comparison of the coefficient values, for the same rocks and data source, with those of Hashish and du Plessis (1978) revealed negligible differences. The present theories and analysis contradict the findings of Hashish and du Plessis (1978) however in that they did not report observing a step-wise penetration trend in the data; and they assumed that continuous water jet penetration could be accounted for by their cutting equation by letting $U \to 0$. Moreover, methodologies in evaluating the coefficient parameters differed in that trial and error was employed in the present analysis to obtain suitable values of C_f and ζ for each data set, whereas Hashish and du Plessis (1978) based their coefficient values on low or zero traverse rate data (i.e., for continuous penetration). The theoretical model developed in the present work distinguished between the water jetting schemes of continuous jet penetration and jet cutting.

6. ACKNOWLEDGMENTS

This work has been supported by the Natural Sciences and Engineering Research Council of Canada, and the Imperial Oil University Research Grants Program.

7. REFERENCES

Camp, F.W., **The Tar Sands of Alberta, Canada,** Cameron Engineers Inc., Denver, Colorado, 1976.

Cooley, W.C., "Correlation of Data on Jet Cutting by Water Jets Using Dimensionless Parameters," 2nd Int. Symposium on Jet Cutting Technology, BHRA Fluid Engineering, Cambridge, England, 1974.

Gates, E.M., and R.R. Gilpin, "Jet Piercing of Oil Sands, "**Transactions of ASME, Journal of Energy Resources Technology,** Vol. 103, pp. 330-335, December 1981

Gilpin, R.R., and E.M. Gates, "Jet Cutting of Oil Sands," University of Alberta Departmental Report No. 22, 1980.

Harris, H.D., and M. Mellor, "Penetration of Rocks by Continuous Water Jets," 2nd Int. Symposium on Jet Cutting Technology, BHRA Fluid Engineering, Cambridge, England, 1974.

Hashish, M., and M.P. du Plessis, "Theoretical and Experimental Investigation of Continuous Jet Penetration of Solids," **ASME Journal of Engineering for Industry,** Vol. 100, pp. 88-94, 1978.

Hashish, M., and J.M. Reichman, "Analysis of Water Jet Cutting at High Traverse Rates," 5th Int. Symposium on Jet Cutting Technology, BHRA, Fluid Engineering, Hanover, FRG, 1980.

Hood, M., R. Nordlund, and E, Thimons, "A Study of Rock Erosion Using High Pressure Water Jets," **Int. Journal of Rock Mechanics,** Vol. 27, No.2, pp. 77-86, 1990.

Law, D.H., J.H. Masliyah, and K. Nandkumar, "Abrasion of Frozen Oil Sands Under the Influence of Turbulent Axisymmetric Jets," **AOSTRA Journal of Research,** Vol. 3, pp. 177-181, 1987.

McRoberts, E.C., and D.S. Cavers, "Geotechnical Considerations in Borehole Hydraulic Mining of Oil Sands," 4th UNITAR/UNDP Conference on Heavy Oil and Tar Sands, Edmonton, 1988.

Singh, B., K. Redford, and V.R. Puttagunta, "A Hydraulic Jet Mining Technique for Recovering Bitumen from Alberta Oil Sands," Paper 27, 5th American Water Jet Conference, Toronto, Canada, 1989.

Wagner, C.G., and E.L. Hodges, "Downhole Hydraulic Mining System," 3rd Int. Conference on Heavy Crudes and Tar Sands, Long Beach California, 1985.

8. NOMENCLATURE

A_1	Area of cross section of the water jet at the inlet to the hole
A_2	Area of cross section of the water jet at the hole bottom (area of penetration)
C_f	Coefficient of friction between the water jet and the hole or kerf wall
$\vec{F}_{normal}$	Normal force acting on the bottom control surface
$\dot{m}_{exit}$	Rate of fluid mass flow exiting the control volume
P_d	Dynamic pressure of the water jet exiting the nozzle
T_e	Exposure time of a traversing water jet on a substance
t	Time
U	Traverse or feed speed of the material relative to the nozzle
$\vec{V}_1$	Velocity of the water jet at the inlet to the control volume

$\vec{V}_2$ Velocity of the water jet at the hole or kerf bottom

$\vec{V}_3$ Total velocity of the waste water crossing the control surface

$\vec{V}$ Velocity of the fluid crossing the control surface

$\cancel{V}$ Volume within the control surface

Z Depth of penetration

$\dot{Z}$ Time rate of penetration

Greek Symbols

ρ Density of the jet fluid

σ Normal stress within the model

σ_o Material strength, or resistance to permanent deformation

$\vec{\tau}_w$ Shear stress acting on the side of the control volume

ζ Coefficient of damping between the water jet and the material

9. TABLES

Table 1. Parameter values for water jet cutting of oil sands.

Testing environment	U (m/s)	D_n (mm)	C_f	ζ $\times 10^7$ (kg/m^2 s)
Laboratory	0.14, 0.67	1.6, 2.4, 3.2	0.012	0.28
Field	0.2	3.2	0.011	0.41
	0.2, 0.48	6.4, 11.1, 15.9	0.017	0.10

Nozzle stand-off distance $S = 5D_n$ to $100D_n$; material strength $\sigma_o = 1.2$ MPa. Jetting pressures P_d ranged from 2.8 MPa to 33.2 MPa for the laboratory and from 2.0 MPa to 26.0 MPa for the field. Values of the coefficient of damping ζ require multiplication by 10^7.

Table 2 Experimental and theoretical dimensionless depth of cut of oil sands in the laboratory.[1]

U (m/s)	P_d (MPa)	$(Z/D_n)_{exp.}$	$(Z/D_n)_{theo.}$	% Deviation
0.14	2.8	15.7	10.31	34.3
	3.3	29.5	12.47	57.7
	6.7	23.2	25.52	10.0
	7.9	17.5	29.53	68.7
	8.5	33.5	31.42	6.2
	12.8	29.5	43.15	46.2
	20.5	54.1	57.83	6.8
	25.4	60.5	64.18	6.0
	33.0	71.5	70.96	0.7
0.67	3.2	1.5	2.71	80.6
	3.6	2.0	3.12	56.0
	6.7	8.5	6.23	26.7
	8.0	4.6	7.49	62.8
	8.5	8.5	7.98	6.1
	13.0	11.4	12.17	6.7
	20.5	20.5	18.66	8.9
	23.9	26.5	21.40	19.2
	25.5	24.3	22.65	6.7
	33.2	28.2	28.31	0.3

Correlation coefficient between $(Z/D_n)_{exp.}$ and $(Z/D_n)_{theo.}$ is 0.95; the average deviation is 26.8%. Theoretical results based on σ_o = 1.2 MPa, C_f = 0.012, $\zeta = 0.28 \times 10^7$ kg/m^2 s. Three nozzle diameters were used in the experiments: D_n = 1.6 mm, D_n = 2.4 mm and D_n = 3.2 mm.

[1]Experimental data from Gilpin and Gates (1980).

Table 3 Experimental and theoretical dimensionless depth of cut of oil sands in the field.[1]

U (m/s)	D_n (mm)	P_d (MPa)	$(Z/D_n)_{exp.}$	$(Z/D_n)_{theo.}$	% Deviation
0.2	3.2	12.2	24.0	24.12	0.5
		20.0	36.0	36.61	1.6
		26.0	44.5	44.60	0.2
	6.4	5.0	32.0	29.63	7.4
		9.8	44.5	44.78	0.6
		10.0	40.0	45.19	12.9
		11.3	24.0	47.54	98.0
		12.6	46.0	49.44	7.4
		12.8	53.5	49.70	7.1
		15.8	52.0	52.73	1.4
		16.8	44.0	53.46	21.5
	11.1	5.0	18.5	29.63	60.1
		5.4	21.0	31.40	49.5
		5.4	23.5	31.40	33.6
		8.8	29.0	42.53	46.6
	15.9	2.0	12.0	11.86	1.1
0.48	6.4	15.8	43.75	38.11	12.8
	11.1	8.8	21.5	25.42	18.2
	15.9	2.6	7.0	7.61	8.7
		2.6	11.0	7.61	30.8

Correlation coefficient between $(Z/D_n)_{exp.}$ and $(Z/D_n)_{theo.}$ is 0.87; the average deviation is 21.0%. Theoretical results based on σ_o = 1.2 MPa, C_f = 0.017, $\zeta = 0.10 \times 10^7$ kg/m² s, except data for D_n = 3.2 mm which were based on C_f = 0.011, $\zeta = 0.41 \times 10^7$ kg/m² s.

Note: Experimental Z/D_n values are means for each pressure due to the range of kerf depth Z measured during the experiments.

[1]Experimental data from Gilpin and Gates (1980).

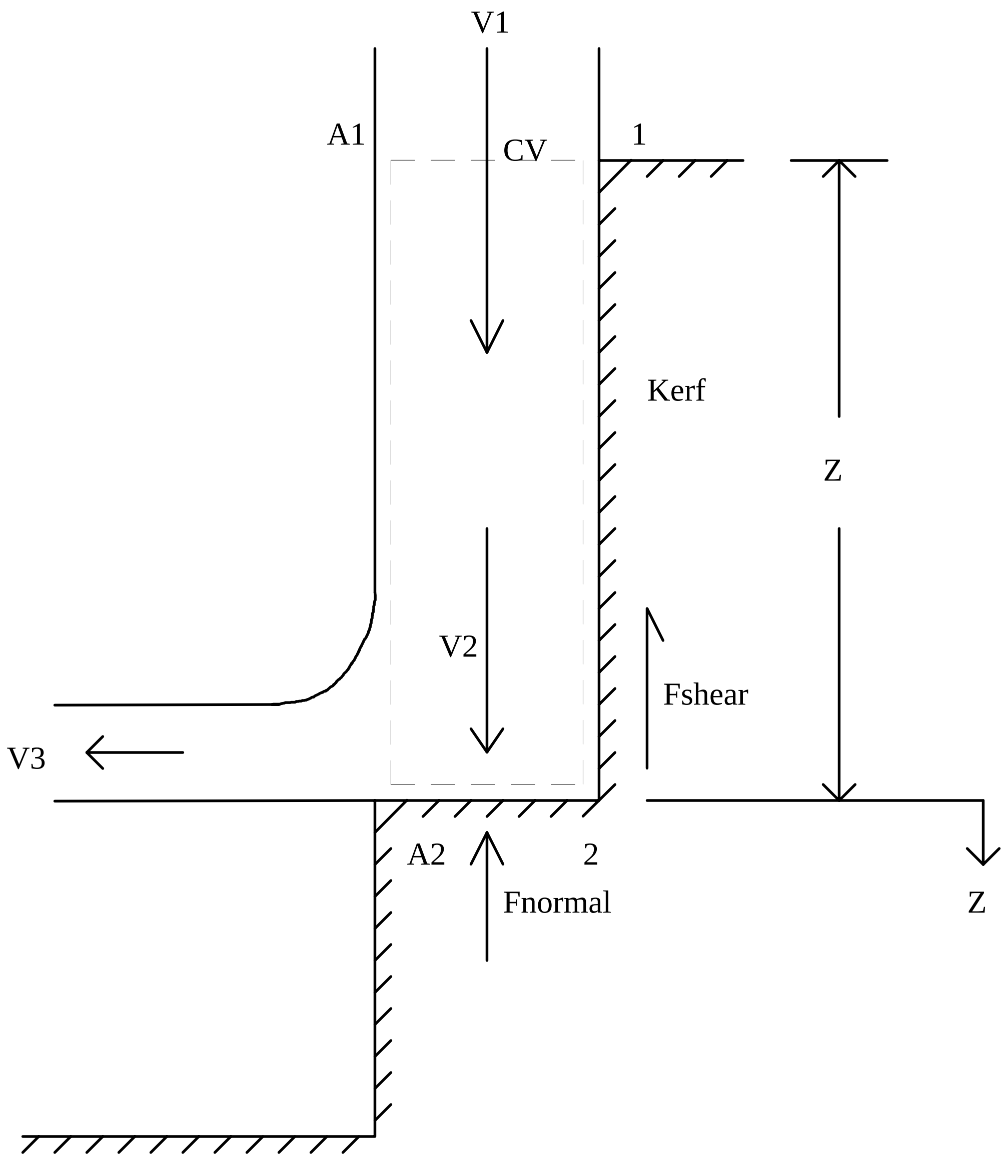

Figure 1. Pictorial representation of water jet cutting, and control volume.

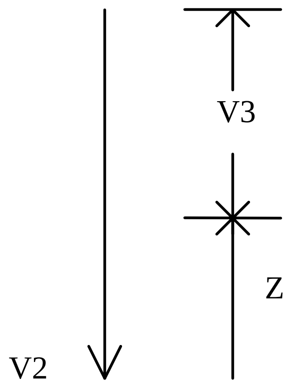

Figure 2. Relative velocity diagram for jet cutting.

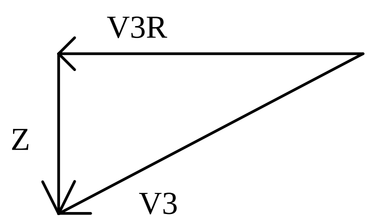

Figure 3 Components of velocity $\vec{V}_3$.

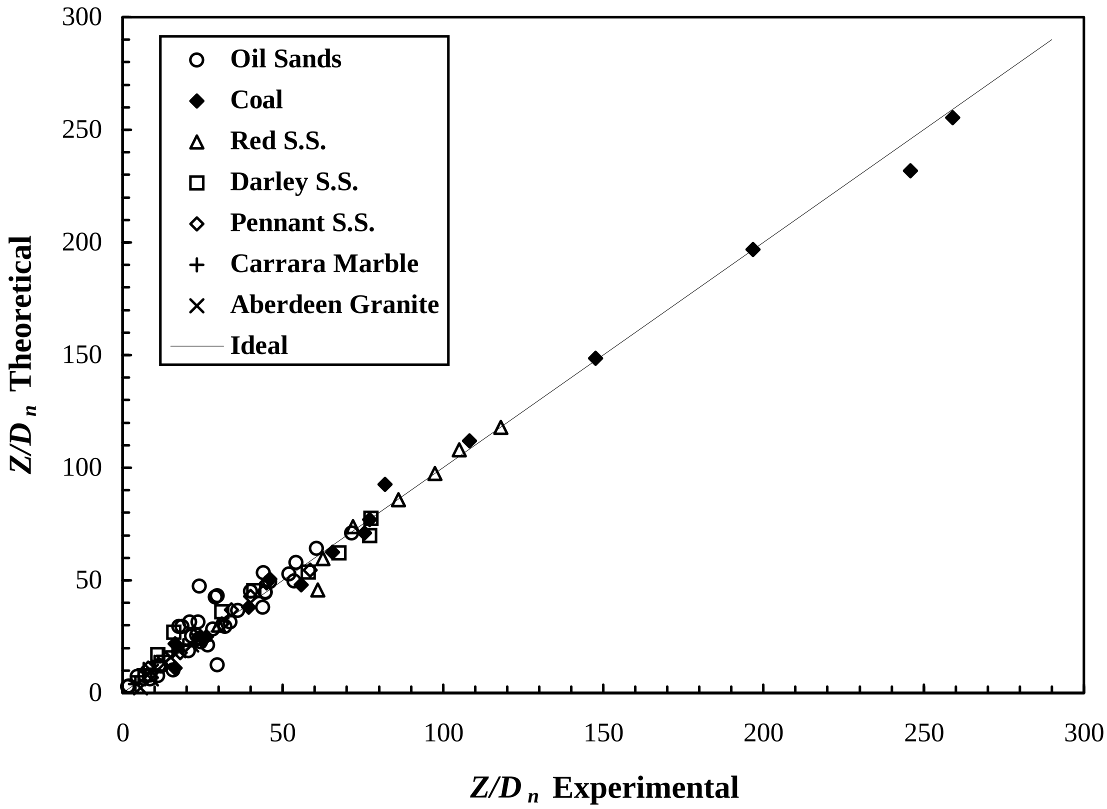

Figure.4. Composite comparison of theoretical (model) Z/D_n versus experimental Z/D_n for water jet cutting of various rocks.

2003 WJTA American Waterjet Conference
August 17-18, 2003 Houston, Texas
Paper 4-C

WATERJET RESEARCHES AT SÃO PAULO UNIVERSITY:

PART 3 WATERJET METHODS OF CUTTING DIMENSIONAL STONE

Guillermo Ruperto Martín Cortés, Carlos Tadeu Lauand, and Wildor Theodoro Hennies
Mining and Petroleum Engineering, Department of Polytechnic School, University of São Paulo, São Paulo, Brazil

ABSTRACT

Dimension stone or rocks in general can be cut with ultra-high Abrasive Water Jet. As water is a soft natural tool, there provide better environmental friendly procedures. Also the advanced technology produces less waste, as it is an automatic technique, more precise and provides reproducibility. To open deeper groove there is possible to substitute the one pass method by multiple pass technique. A systematic study of samples of dimension stone was programmed and realized in laboratory assays. The samples are from three granites and one marble of the São Paulo State. These samples were tested in acquired machinery bought from USA, model 2652A from the OMAX Corporation and with financial support of FAPESP, São Paulo State Agency for research support. The interpretation of the results permit to determine the performance of the equipment and also which kind of method (single pass or multiple pass) may by applied by economical reasons. Determinations of smooth cut and rough cut depths were made. Also was evaluated the taper of the kerf and the roughness on the generated surfaces by the water jet, to give a measure of its quality or surface finishing. This procedure is also a subject analyzed on this paper.

1. INTRODUCTION

In 1998 a research program was prepared with the aim to install and operate a modern water jet system. The use of abrasive waterjet systems to cut rocks was the main aim of the first researches at the Mining and Petroleum Engineering Department, Polytechnic School at the University of São Paulo, Brazil (Lauand et al, 2000a).

Some results of these researches deal not only with rock cutting but treat also with secure combustible pipe cutting using suspension abrasive, were presented in Greece, and were Master in Engineering and PhD programs under development (Lauand et al, 2000b, Mendes et al. 2000, Martín C. et al 2000).

The laboratory equipment used to cut the engineering materials is a 2652A model system of OMAX Corporation bought in Seattle, with financial support of FAPESP, the São Paulo State Agency for Research support.

The main results of the first phase laboratory assays using the single pass method were the work of Lauand Master in Engineering Program and there were presented in the 11th American Conference in 2001 (Lauand et al. 2001).

2. METHODS OR MODES OF WATER JET CUTTING

Dimension stone can be cut with advanced technique of ultra-high pressure (pressure above 2,041 bar) Abrasive Water Jet tools. As water is a natural fluid, it has the advantage to furnish better environmental friendly procedures. Another advantage of the process is to produce less waste because it is a high precision automatic technique with very thin slotting.

There are two different modes of open a slot or kerf with an abrasive water jet: 1) in a single pass or 2) by multiple pass of the nozzle over the target material. In the first phase of the researches the procedure of single pass was analyzed.

Using the same set of rock samples – three granites and one marble of São Paulo State – straight cuts were realized using both methods, the single pass cut, and multiple pass cut to make comparisons about the performance of the equipment and the cutting results.

In this second method a greater speed can be used to move the nozzle, and the groove is open in more than one pass. The main advantage is to have not to open first the total deep of the target sample and with these lesser time is needed to make the total cut. Other important aspects to the researches is to test the quality of the generated kerf surface to define which is the best combination of traverse speed and number of steps or passes to utilize for optimization the procedure. Additionally taper measures were also made.

As mentioned above there are to different modes to cut with an abrasive water jet nozzle in a single pass and in a multiple pass as shown in figure 1.

If the nozzle transverse speed is very slow, it is possible to cut the total thickness of the target material in only one pass. On the other hand, when the speed is increased the cut is only partial and there is necessarily more than one pass to cut the material.

Another important aspect is that in a single pass and also in the multiple pass methods, there can be distinguished two regions in the cut, an upper region in where the cut is even or smooth, and a under region in where the cut is rough or wavy (see Figure 1).

3. DATA OF SINGLE AND MULTIPLE PASS METHOD TESTS

In the first series of tests with single pass the tentative was to cut some fixed thickness of 50 mm of a rock, using the qualities from 1 to 5, with machinability number of 322 in granite and 535 in white marble (Zeng & Kim, 1998). The Machinability Number is an empirical equation that has

the following expression: $$h = \frac{N_m p_w^{1.25} m_w^{0.687} m^{0,343}}{CD^{0.618} u^{0.866}} \qquad (1)$$

Where C = constant 8,800 for metric system, N_m = Machinability Number, P_w = water pressure in MPa, m_w = water mass, m = abrasive mass, u = nozzle transverse speed.

The results of these tests are shown in Figure 2 and it is possible to see that the target of 50 mm of smooth cut was not attained and the data are from 36.7, 38.6 and 37.9 respectively for the red Capão Bonito Granite, silver Interlagos Granite and black Piracaia Granite. The transverse speed of the nozzle used in the quality 5 to a target of 50 mm of cut depth was 0.731 mm/s.

In the case of the white Marble of Campos do Jordão in cut with quality 5 use 1.311 mm/s and the attained depth was of 31.3 mm of smooth cut.

The used pump pressure of the system during the test was about 290 MPa (42 kpsi), water flow of 3.6 L/min and abrasive flow of 5.3 g/s. The used abrasive was garnet 80#.

In the PhD work multiple pass method were used to cut the same rocks and using the same data above only number of pass and traverse speed were varied.

4. MAIN RESULTS

Three main result observed in the research deal with depths of smooth and total cut in mm, surface finishing of kerf measured on perthometer, and finaly the taper measurements.

The assays to better preview the results were made in the Campos do Jordão white marble with thickness of about 130 mm. The results of the tests are given in Table 1. In this case no attempt was made to machinability numbers but there was commanded a constant traverse speed between 4 and 16 mm/s and also from 1 to 8 as the number of pass tested.

Using the software Surfer it was possible to construct level figures and 3D views of the results of Table 1 in where the Campos do Jordão white marble was assayed. Figure 3 shows a 3D diagram in which is shown the kerf depths, in where we can distinguish the smooth cut surface and the total cut surface in millimeters. In Figures 4 and 5 the same respectively for the smooth and total cut depths in millimeters but with level lines.

The same was made for the granites which results are given in Table 2. In this case constant traverse speed between 1 and 16 mm/s and also from 1 to 16 number of pass were used. The Figures 6, 7, 8, 9, 10 and 11 shows the surface level lines in mm of the smooth and total cut depth and Figures 11, 12 and 13 a 3D diagram view of the granites.

Surface finishing of kerfs were evaluated in the perthometer in Italy and were discussed partly in a paper presented at last year (Martín Cortés et al., 2002) in a Mine Planning Event.

Finally Table 3 shows some data about taper measurements that was also evaluated for the black Piracaia granite and in Table 4 the resulting taper for some assays of this same granite. Some assays were made using greater number of pass and greater traverse speed that can be attain about 64 mm/s.

5. CONCLUSIONS

As main conclusions of this extend researches of a PhD in engineering program we can summarize the following:

About the depths of smooth and rough-cut, they are inversely proportional to the traverse speed. As much as bigger is the speed minor they are the smooth cut and rough-cut depths as can be observed in the Figures.

On the contrary, the relationship between smooth cut and rough cut with the number of steps is directly proportional. When bigger number of pass is used, bigger they are the smooth cut and rough-cut depths obtained.

To the mono-mineral rocks as marble and for porphyritic granites as black Piracaia, the aspect of cut surface is similar to that of metals, but in case of granular textures of the other two granites the presence of bigger quartz crystals, determine the cut process, that is a very important mineralogical characteristic against the waterjet cut method. They was studied the behavior of the quartz crystals in the waterjet cutting system by binocular microscope combined by over dimensioned scanning pictures. The surface finishing or roughness is associated to this mineral properties behavior in the cut procedure depending in its region in the smooth cut area or rough area. In the last there are a fragile rupture.

About the taper, the evaluated data indicate convergence in the smooth cut region, however, in the regions of rough-cut this behavior in the irregular and many times it is divergent.

6. REFERENCES

Lauand, C.T.; Martín C., G.R.; Hennies, W. T.; Ciccu, R. 2000a The Brazilian Program of High Pressure Water Jet to Cut Ornamental Rocks. In: International Conference on Environmental Issues and Waste Management in Energy and Mineral Production, 6., Calgary, 2000. *Proceedings*. Calgary, 2000. p. 711-16.

Lauand, C.T.; Martín C., G.R.; Hennies, W. T.; Ciccu, R. 2000b Rock Technological Parameters Useful to Water Jet Cutting Systems. In: International Symposium on Mine Planning and Equipment Selection, 9^{th} Athens, Greece Rotterdam, Balkema, 2000, p.625-630.

Lauand, C.T.; Martín C. G. R.; Hennies, W.T.; Agus, M. 2001. Performance of Water Jet Cutting System in Dimension Stone 11^{th} Minneapolis WaterJet Technology Association St. Louis, MO, USA p. 58-77.

Martín C., G.R.; Lauand, C.T.; Hennies, W. T.; Ciccu, R. 2000 Abrasives in Water Jet Cutting Systems. In: International Symposium on Mine Planning and Equipment Selection, 9^{th} Athens, Greece Rotterdam, Balkema, 2000, p.641-645.

Martín Cortes; G. R.; Hennies, W. T.; Lauand C. T. 2002 Dimensional stone cutting with water jet: Surface Finishing In: International Symposium on Mine Planning and Equipment Selection, 11^{th} Bousov, Czech Republic 2002.,p.43-48.

Mendes, M.L.A.; Soares, L.; Hennies, W.T.; Ciccu, R.; Bortolussi, A. 2000 Application of Pre Mixed Abrasive Water Jet for Maintenance of Oil and Gas Ducts In: International Symposium on Mine Planning and Equipment Selection, 9^{th} Athens, Greece Rotterdam, Balkema, 2000, p. 653-656.

Zeng, J. & Kim, T. 1998 Application of a brittle erosion model for abrasive waterjet cutting of asphalt concrete. In Momber, A (ed.) Water Jet Application in Construction Engineering A.A. Balkema Roterdam p. 149-159.

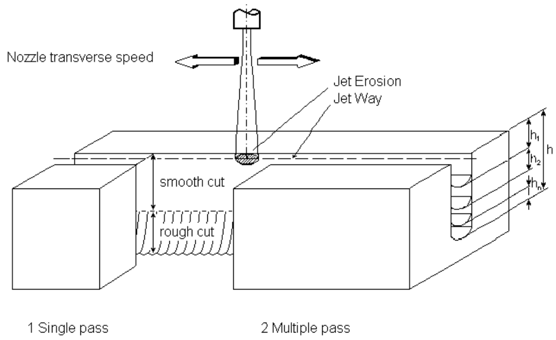

Figure 1 Single and Multiple pass procedure for waterjet cut

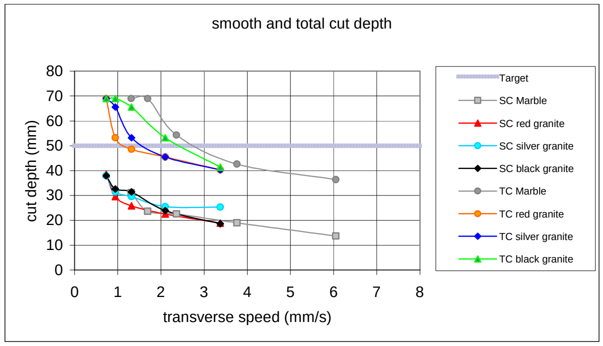

Figure 2 Tests of granites and marble with single cut.

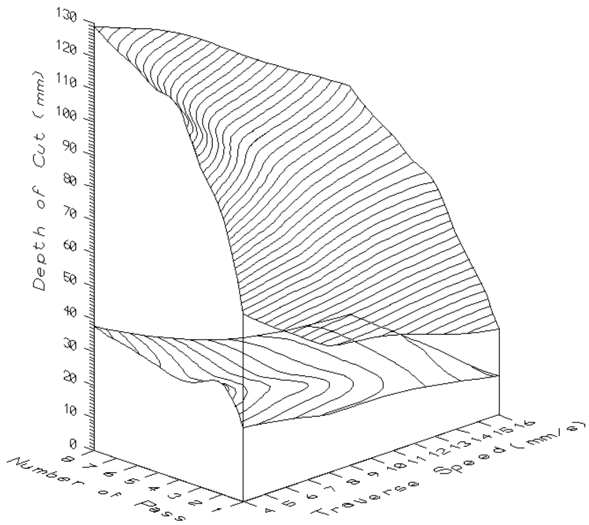

Figure 3 Resulting depths of smooth and total cuts at Campos do Jordão white marble.

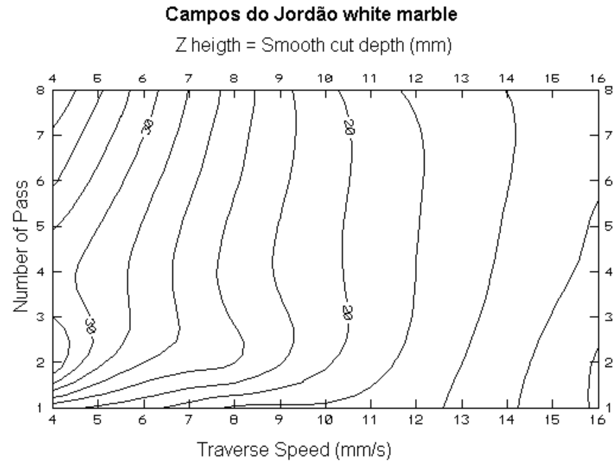

Figure 4 Smooth cut depth in mm for Campos do Jordão white marble.

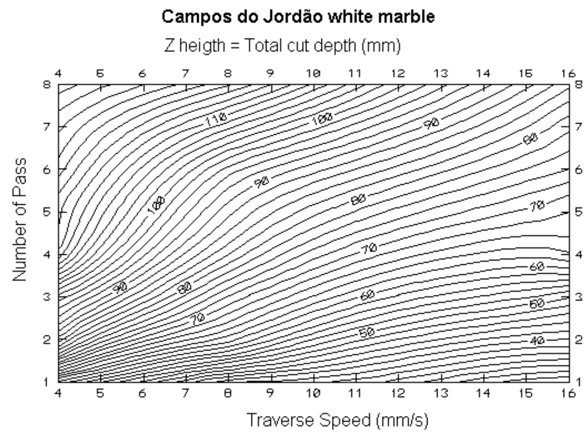

Figure 5 Total cut depth in mm for Campos do Jordão white marble.

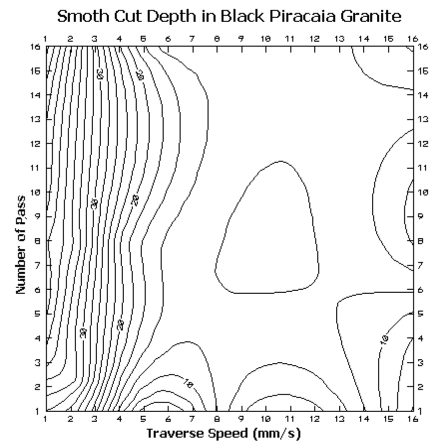

Figure 6 Smooth cut depth in mm for Piracaia black granite.

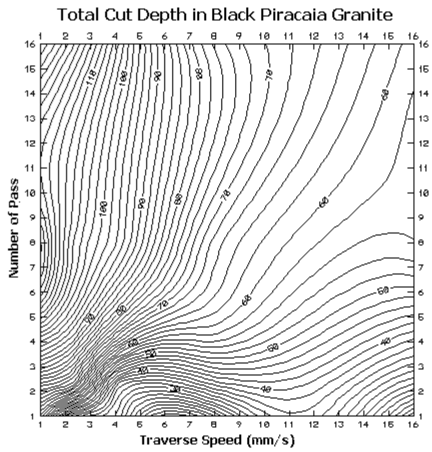

Figure 7 Total cut depth in mm in the black Piracaia granite.

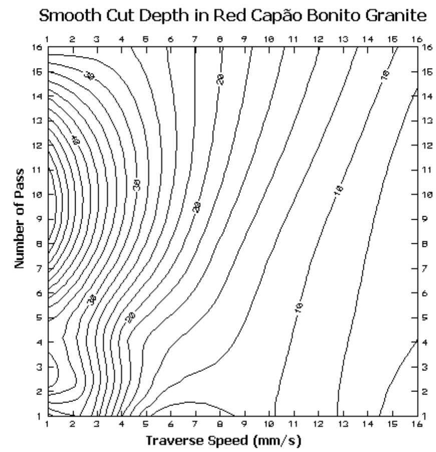

Figure 8 smoth cut depth in red Capão Bonito granite.

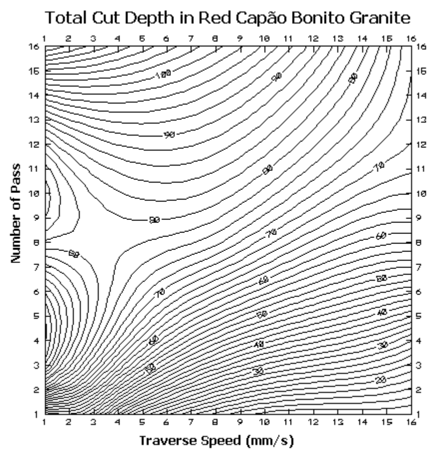

Figure 9 Total cut depth in mm in the red Capão Bonito granite.

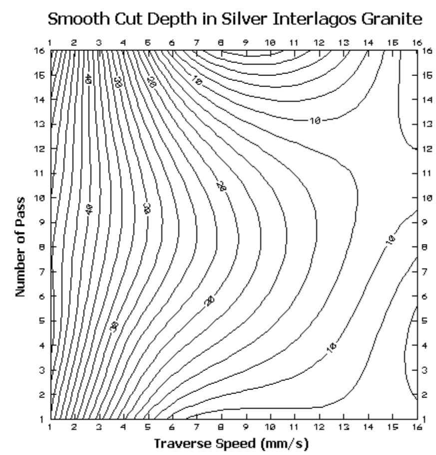

Figure 10 Smooth cut depth in the silver Interlagos granite.

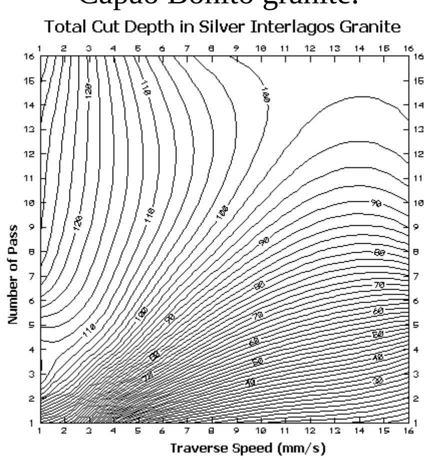

Figure 11 Total cut depth in the silver Interlagos granite.

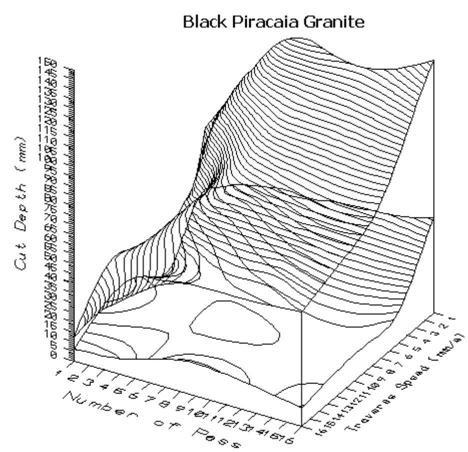

Figure 12 A 3D view of total and smooth cut depth in Piracaia granite.

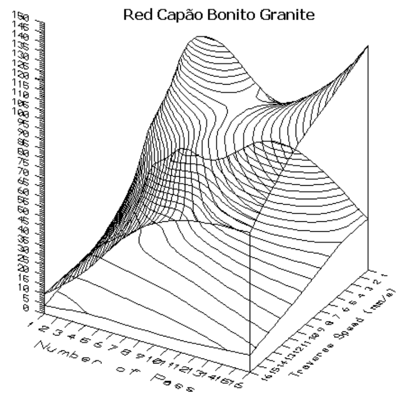

Figure 13 A 3D view of total and smooth cut depth in Capão Bonito granite.

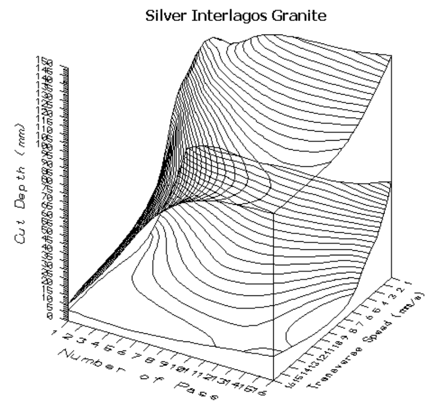

Figure 14 A 3D view of total and smooth cut depth in Interlagos granite.

Table 1 Campos do Jordão white marble assays results

Assay Number	Traverse speed (mm/s)	Time of Assay (s)	Abrasive Consume (kg)	Number of pass	Smooth cut (mm)	Total cut (mm)
1	4	50	0.265	1	22.60	56.99
2	4	100	0.530	2	33.16	82.90
3	4	200	1.060	4	30.61	112.38
4	4	400	2.120	8	37.74	129.16
5	8	25	0.133	1	17.61	38.58
6	8	50	0.265	2	24.32	61.22
7	8	100	0.530	4	23.21	82.07
8	8	200	1.060	8	25.16	118.25
9	16	13	0.066	1	11.74	26.00
10	16	25	0.133	2	11.74	38.58
11	16	50	0.265	4	13.42	62.90
12	16	100	0.530	8	14.92	84.56

Table 2 Granite assays results

Assay N°	Traverse speed (mm/s)	Assay Time (s)	Abrasive Consume (kg)	N° of pass	Piracaia black Granite		Red Capão Bonito Granite		Silver Inter-lagos Granite	
					Smooth cut (mm)	Total cut (mm)	Smooth cut (mm)	Total cut (mm)	Smooth cut (mm)	Total cut (mm)
1	1	200	1.060	1	29.94	61.46	24.93	49.86	41.69	84.84
2	1	400	2.100	2	33.88	76.44				
3	1	800	4.200	4	38.61	99.29	32.80	96.44	46.81	111.17
4	1	1600	8.400	8	40.19	122.14				
5	1	3200	16.800	16	48.86	130.00	26.24	116.00	57.10	132.00
6	2	100	0.525	1	26.00	38.61				
7	2	200	1.060	2	33.45	71.75	33.10	70.41	34.93	98.10

(continue)

Table 2 Granite assays results (continued)

Assay N°	Traverse speed (mm/s)	Assay Time (s)	Abrasive Consume (kg)	N° of pass	Piracaia black Granite		Red Capão Bonito Granite		Silver Inter-lagos Granite	
					Smooth cut (mm)	Total cut (mm)	Smooth cut (mm)	Total cut (mm)	Smooth cut (mm)	Total cut (mm)
8	2	400	2.100	4	33.10	92.99				
9	2	800	4.200	8	37.30	108.24	42.64	78.73	41.69	120.67
10	2	1600	8.400	16	38.03	120.67				
11	4	50	0.263	1	10.24	29.25	15.10	34.12	17.55	42.42
12	4	100	0.525	2	14.63	31.45				
13	4	200	1.060	4	19.39	67.87	18.66	69.81	26.01	99.58
14	4	400	2.100	8	19.75	96.54				
15	4	800	4.200	16	21.21	103.85	26.24	108.91	24.14	113.36
16	8	25	0.133	1	11.70	19.02				
17	8	50	0.263	2	12.43	35.11	11.00	27.00	10.24	36.57
18	8	100	0.525	4	12.43	56.31				
19	8	200	1.060	8	12.12	66.90	15.65	74.63	21.55	96.61
20	8	400	2.100	16	13.16	76.06				
21	16	13	0.066	1	5.85	12.43	4.00	10.00	6.58	10.24
22	16	25	0.133	2	6.58	25.60				
23	16	50	0.263	4	8.04	38.03	6.00	29.00	5.12	40.96
24	16	100	0.525	8	16.09	55.58				
25	16	200	1.060	16	9.70	59.15	9.03	72.22	14.12	98.84

Table 3 Piracaia black granite Kerf Width in mm.

Jet approach	Measure Local (mm)	Kerfs					
		1	2	3	4	5	6
Entrance (L_T)	(1) 0 – 49	1.60	1.50	1.70	1.50	1.50	1.90
	(2) 69 - 127	1.70	1.50	1.60	1.30	1.40	1.70
	(3)147 - 196	1.50	1.50	1.50	1.50	1.30	1.80
	(4) Mean	1.60	1.50	1.60	1.43	1.40	1.80
Exit (L_B)	(5) Smooth	0.95	1.00	1.00	1.10	1.00	1.20
	(6) Striated	1.30	1.30	1.50	1.40	1.20	1.30
	(7) Wavy	4.50	2.00	1.90	2.30	2.00	1.90
	(8) Mean	2.25	1.43	1.47	1.60	1.40	1.47
Traverse speed mm/s		2	4	8	16	32	64
Pass Number		2	2	4	8	16	32

Table 4 Relation between entrance/exit to taper determination in Piracaia granite

Relation(T_R)	2/2	4/4	8/8	16/16	32/32	64/64
1 - (1)/(5)	1.68	1.50	1.70	1.36	1.50	1.58
2 - (2)/(6)	1.31	1.15	1.07	0.93	1.17	1.31
3 - (3)/(7)	0.33	0.75	0.79	0.65	0.65	0.95
4 - (4)/(8)	0.36	1.05	1.09	0.89	1.00	1.22

$T_R > 1$ = Convergent, $T_R < 1$ = Divergent

WATERJET RESEARCHES AT SÃO PAULO UNIVERSITY:

PART 4 DIMENSION STONE EXPLOITATION

WITH HIGH-PRESSURE WATERJETS

Alexandre Sant'Anna, Guillermo Ruperto Martín Cortés, Carlos Tadeu Lauand, and Wildor Theodoro Hennies
Mining and Petroleum Engineering, Department of Polytechnic School, University of São Paulo, São Paulo, Brazil

ABSTRACT

The application of high-pressure water jets has evolved quickly in some fields of engineering and for the Department of Mining and Petroleum Engineering of the Polytechnic School of the University of São Paulo two applications have particular interest: First, cut of plates in the process of beneficiation of end products in the field of dimension stone and second, the exploitation executed to win rock blocks-from the deposit. For the cut of plates, the abrasive water jet module, installed in the Laboratory of Mechanics of Rocks already possess dependences and reasonable accumulated knowledge. This research proposal is also related with mining of dimension stone and intends to know a new technology that is being introduced in countries that compete with Brazil in this market. The study of rock block extraction in the deposit, using water jet action is its main target. This technology concurs with traditional methods as the use of helicoidally wires, diamond wires and explosive and apparently, presents some economic and environmental advantages. For knowing this technology, not only the detail of the cut process is necessary, but the evaluation of the real environmental benefits in the Brazilian situations of work, its economic viability, the qualification of workmanship, for its implantation and a preliminary evaluation of possible national suppliers of machines, components and spare parts for these equipment.

1. INTRODUCTION

In the system of cut of deep grooves by Ned-Jet 2000 (257 MPa, 23 l/min) vertical grooves of 1,8 m of depth are opened in granite. These grooves skirt the block whose deep is freed by dismounting by explosives and removed by one crane. This system is used in the States of the South Dakota and California. A more detailed description of systems similar is argued in articles of Ciccu & Bortolussi, 1998 and Hlavac & Sitek, 1988. Beyond the two quarries of the United States cited by Savanik (1997), others in France, Italy and Canada are related.

In the explotation of dimension stone in quarries, pure water jets have been used to open grooves in granites in a certain number of local tests. The excellent information is summarized in Table 1. The first field tests had been made in the United States in the granite of Elberton district (Georgia) using a spear with rotating double nipple and a unit of intensifier pump. The results had been promising but the development did not continue due to limited reality of the equipment. In Milbank (South Dakota), a similar concept was adopted using a lower pressure and one more raised water flow, since that it was evident that the granite could efficiently be disintegrated by moderate pressures.

At the same time, a new approach was followed in the red granite quarry in Colorado using a single generated oscillating jet of high pressure and very low flow rate. In this in case that, despite low the involved power, the cut ratio were satisfactory until the extension of that the water jet had become the dominant technology for the extraction of the individual blocks of horizontal and vertical the face by means of grooves.

In Quebec, (Canada), a machine integrated based in the use of a rotating jet with two angular sheaf was tested, trusting raised hydraulically power again the moderate pressure.

The field tests also had been devoted for the study of the removal of the residues of cut in the case of open cuts (in one or both extremities) and blind cuts.

Again, in Milbank, new equipment was constructed and tested using a single jet reaching the rock in a convenient angle while the spear crossed vertically.

In France, a sandstone formation this being cultivated using the water jet for opening of the vertical and horizontal grooves in the front of the quarry, while, the back face is detached by traction for low of each column of blocks by means of a hoisting machine. The cut head is constituted of three jets in angle (two round and a flat) balancing laterally with alternating movement while the jet is dislocated in the same direction. A pump of high power, low pressure used due low the resistance of the rock.

The excellent results reached with the sandstone had encouraged the manufacturers to also apply the system for granite cut, although with some substantial modification in the pump and the drawing of the spear. The pressure was raised for 200 MPa and the cut head consisting of nine imprisoned nipples small-diameter to a support of nipple in rocking movement.

In the last years, three Italian manufacturers have worried about the equipment development of water jets to open grooves in granite. One of these machines is substantially an improvement of the Colorado archetype and uses a high-intensifier pressure pump of a low ratio of flow to generate a single oscillating jet. The others use similar spear that one tested in Milbank, but they are basically different in the arrangement and features of the pump. The system is occult in a energy package with the pump on a side and the structure of the spear in another unit. This structure connects the pump by flexible tubing and it is moved, on tracks placed in the top or the base of a group of benches. It was projected to cut in any direction, making that the support of the spear can be placed horizontally or vertically.

2. OBJECTIVES & PROGRAM GOALS

The objectives of the research are to get information enough to evaluate the technical economical liability of the introduction of this new technology in the national mining area. For a correct evaluation it is needed to know, if this technology must be faced as a trend, or, only one liable application in special conditions, and, consequently to evaluate, if the use of this technology increase the competitiveness of the national mining sector.

Basically, the researchers intend to technical compare economically and different processes of cuts of rocks in the deposits.

As in the market of dimension stone the paid price for the finished product depends on some factors, some subjective ones, “two rocks in same conditions of explotation and improvement can have different remunerations in function, for example, of the colors”, the form to become competitive the extraction of the rock of lesser value is the reduction of costs with increase of the productivity.

To evaluate this new technology of cut of rock by water jet in the extraction of blocks in quarries is necessary to answer questions as: A) Which is the market conditions so that the costs of implantation and operation of a new technological process are absorbed and remunerated? B) The necessary investments are reasonable for small the e average producing? C) The eventual benefits would contemplate the exporters in such a way as the producers for the domestic market? D) Which the real benefits to the environment and the security in the work propitiated by the new technology? E) Which the possible impacts, which had to the substitution of the technologies, in the generation of job and income in the producing region? F) Which would be the necessities of qualification of the workmanship hand? G) Is opportune or premature to introduce the education of this technology in the graduation programs and after-graduation?

3. JUSTIFICATION

What justify the research are economic factors. To reach reasonable participation in the world-market of dimension stone Brazil is pressured by the increasing participation of new competitors as China and India and by the lack of investments in technological innovation.

This situation led to the creation of a new project of the Center of Mineral Technology (CETEM) financed by the Ministry of Science and Technology (MCT), called Net of Technology in Ornamental Rocks (RETEC Rocks) with the objective to increase the competitiveness of the sector and to diminish the technological imbalance. This net congregates amongst other institutions the Institute of Technology Research (IPT), Nucleus of Technology of the Ceará State (NUTEC), National Institute of Technology (INT) and the SENAI.

The researcher (Peiter et al, 2001), Coordinator of Studies and Development of the agency, concludes that to remain itself competitive and to increase its participation in this market Brazil would have to invest to USS 1,0 billion in ten years in the renewal of its industrial park therefore while our industrial park has average age of 10 years the Chinese industrial park, bigger world-wide producer, does not exceed 4 years.

The price of the processed rock reaches up to 10 times the value of the rude rock and the product half-finished up to 4 times the value of the rude rock. Brazil is currently the sixth worldwide greater exporter in physical volume and the biggest exporter of crude granite blocks and only the twelfth exporter of processed rocks.

Still according to Peiter, studies show that to each US$ 1,0 exported billion is generated enters 50 a thousand and 70 a thousand jobs. With the foreseen growth of 15% in the Brazilian exportations it has the expectation of the generation of the 17,5 a thousand 24,5 a thousand jobs up to 2006 in the sector. It is in this context that the knowledge of a technology that is introduced in competing countries and that still is not applied in Brazil assumes basic importance.

3.1 Worldwide scene

The notified worldwide production of ornamental rocks and covering is of approximately 55 million metric tons/year, having evolved of a level of only 1,5 million tons/year in the decade of 20. The estimation that the businesses of the sector put into motion at least USS 30 billions/year, placing itself 20,8 million tons in crude and processed rocks in the international market.

The worldwide projections of consume/production and exportations indicate the maintenance of the trend of growth of the international market. For example, for 2025, it is projected fivefold of the worldwide consumption and international transactions of 2,1 billion equivalent square meters/year.

3.2 Commercial characterization

Of the commercial point of view, the ornamental rocks and of covering, are basically classified in granites and marbles, what perform about 90% of the worldwide production. Natural slates, quartzite, rock soap, serpentines, basalts, conglomerates are also distinguished in the sector.

The average international prices for blocks of marbles and granites, is placed between US$ 400 and 1.200 per cubic meter, while that the average price of the benefited material varies of 30 US$ 60 per square meter. The chromatic standard is the main attribute considered for commercial qualification of a rock.

As dimension material, therefore, used to advantage in the ornamental volume, rocks of covering they have commercial value very significant front to other substances of mineral origin. The comparative picture of its value in weight relatively to ores of iron and gold, that constitute commodities minerals sufficiently known and important in the Brazilian guideline of production and exportation, are presented in Table 2:

Observing average prices of the ornamental rocks and covering rock plates in the domestic markets and external, one perceives that the index of aggregation of selling value of blocks is equivalent to three times its cost of production. Each cubical meter of rock unfolds of 32 to 35 square meters of plates, allowing to generate about R$ 3,200 in finished products in the domestic market, or USS 3,000 in the external market.

3.3 Sector picture

The Brazilian sector picture can be illustrated by the production of 500 commercial varieties of rocks, between granites, marbles, slates, quartzite, travertine, rock soap, basalts, serpentinite, conglomerates, rock talk and materials of the type Miracema rock, Cariri rock and Morisca rock, derivatives of almost 1,300 fronts of extraction. The granites arose about 60% of the Brazilian production, while 20% are relative travertine marbles and almost 8% the slates. Table 3 shows some data about year 2000.

The Brazilian sector of ornamental rocks puts into motion about USS 2.1 billions/year, including approximately commercialization in the domestic markets and exports and the transactions with machines, equipment, imput, materials of consumption and services, generating about 105 a thousand jobs right-handers in 10,000 companies. The domestic market is responsible for 80% of the commercial transactions and the marble shops represent 65% of the universe of the companies of the sector.

The separation of the blocks of ornamental rocks into plates gives mainly through the use of sawing loom. The improvement park operates almost with 1,600 sawing looms, and has capacity of 40 million square meters/year.

4. FUTURE PREVIEW

Projecting an annual growth of 15% in value for the Brazilian mining industry, compatible exportations to the average of the last 3 years and therefore feasible tax for next the 3 years, a US$ and US$ platform will be reached 355 million in 2002, 618 million in 2006. In year 2000, the Brazilian exportations had suffered an increment from 12% in weight and 5,9% in the percentile participation in weight of processed rocks in the total exported, translating the related growth of 16,8% in value on 1999.

On the basis of a compatible simulation with the performance of the sector in year 2000, that it admits increment of 10% to the year in weight of the exportations, beyond increment of 5% to the year of percentile participation in weight of processed rocks in the exported total, the Brazilian exportations would reach USS invoicing 750 million in the year of 2006; this would represent the duplication in weight and the threefold in value of the Brazilian exportations. If increment of 10% to the year of percentile participation in weight of processed rocks in the exported total will be admitted, would have the same duplication in weight however fourfold in value of the exportations, having reached itself USS 1 billion in the year of 2006.

Recent studies of the World Bank show that to each USS exported billion it is generated of the 50 a thousand 70 a thousand jobs. Considering it projection of 15% of annual increment of the exports of the sector of rocks, the generation of at least 17,5 a thousand 24,5 a thousand jobs can thus be esteem until year 2006. According to other simulations, that more foresee accented and possible growth of participation of processed rocks in the exportations, the sector will be able to generate up to 54,1 a thousand jobs in the same period.

From simulation of demand for the industrial park, elaborated through the projections of exportation and consumption in the domestic market, it is glimpsed necessity of aggregation of at the very least 560 new sewing presses, 190 new polishing machines and 50 new cut-blocks, until year 2006.

The attendance of the necessary demands for update of the industrial park, foresees investments of at the very least USS 1 billion up to 2015. The industry of industrial goods, installed in Brazil, does not have capacity of attendance of the projected demand.

The Block production is the object of the research proposal. Objectifying the attendance of the projected demand of sawing for 2015, it will be necessary to reach a primary production of blocks of the order of 14 million tons per year, what it represents an increment of 3.5 times the current production. Considering a stabilized universe of 1.000 active quarries in Brazil, they would be necessary investments of conversion of the current average primary production of 150 cubic meters by month for quarry, for about 500 cubic meters by month, what represents fixed capital investment of about US$ 350,000 for quarry up to 2015, totalizing US$ 350,000,000.

4.1 Goals of the PhD thesis

Considering that any that is the commercialization modality, blocks, half finished or finished, all the phases depend on the cut of blocks and the research objective is to know a new technology that applies in this phase of production.

A process that benefits to a productivity and the yield of the cut of the blocks in the deposit will equally benefit to all the too much phases of the improvement process the objective of the research is to evaluate technique and economically this process and to compare it with the processes currently in use in Brazil (Hennies et al.,1996; 1999, 2000; Stellin et al., 2001). To establish alternatives of its use with or without the conventional procedures already however in use is goal of the studies to carry through.

5. MATERIALS AND METHODS

It is intended to divide this research in 4 phases that are bellow described:

PHASE 1 is Field Research, through visits to the mining enterprises and laboratories tests that study or already is used of the process of cut by water jet under high pressure in the cut of blocks in the deposit for evaluation of the factors: a) Productivity in function of the dimensions of the blocks and the type of mined rock; b) Interferences and potentials damages to the environment; c) Professional Qualification of the involved workers in the processes of operation of the equipment in the cut, maintenance of the used equipment and management of the costs of the processes. In this phase one intends that the researcher carry through:

A short period of training in the Department of Geoengineering and environmental Technology of the Universitá degli Studi di Cagliari (Sardinia,-Italy) that possess accumulated knowledge on this technique and that for some times collaborated with the Department of Mining and Petroleum engineering of the Polytechnic School, of University of São Paulo.

It is also intended to visit also the Department of Mining Engineering of the University of Missouri - Rolla Minnessota- Minneapolis, with Prof. Summers, who possess knowledge accumulated on this technique and mining that already are used of this process of blocks mining with waterjets and that they are located in the Province of Quebec in Canada and some States in U.S.A.

PHASE 2 Research to be carried through in the laboratories of the Polytechnic School for evaluation of the performance of the national rocks with commercial importance in the process of cut for waterjet under high pressure evaluating: a) Speed of cut in function of the type of rock b) Production of tailing for unit of mass of cut rock c) Classification of its tailings and possibilities of its commercial exploitation

PHASE 3 Field Research, through visits to the selected granite, marble and sandstone mining enterprises for evaluation of factors as: a) Productivity in function of the technology of cut currently used b) Alteration of the environmental conditions and its managements in function of the technology of cut currently used; c) Qualification of the workmanship in function of the technology of cut currently used; d) Foreseen interest in the substitution of the technology in function of the costs and productivity and benefits; e) the possibilities of professional qualification of the current workmanship in function of the new basic, specific abilities and of management demanded by the new technology.

PHASE 4 Spreading of the results to the actors interested by means of the composition of the PhD thesis.

6. CONCLUSIONS

In this paper the main conclusion are that it is possible to define better rock block extraction alternatives using new production systems. Alternatives can be found, to optimize the application of advanced technical methods alone or conjugated with other traditional mining methods. These combining alternatives will conduce to future procedures that present more attractive economic results on one side, and also environmental friendly work conditions one the other.

7. REFERENCES

Ciccu, R. & A. Bortolussi 1998 Waterjet in dimensional stone quarrying. In Momber, A (ed.) Water Jet Application in Construction Engineering . Balkema Roterdam p.289-305.

Hennies, W. T. & Stellin Jr., A. 1996. Dimension stone industry and environmental preservation in Brazil. In: International Conference on Environmental issues and Waste Management in Energy and Mineral Production, 4., Cagliari, 1996, *Proceedings SWEMP'96* Cagliari DIGITA. Universitá di Cagliari, 1996, v.1, p 75-84.

Hennies, W. T.; Stellin Jr., A.; Cretelli, C.; 1999. Jet piercing application for red granite block mining in São Paulo, Brazil. In: Int. Symposium on Mine Planning and Equipment Selection, 8° *Proceedings* Dnipropetrovsk: National Mining University of Ukraine, 1999, p.21-26.

Hennies, W. T. & Stellin Jr., A. 2000. Contribution to the Study of cutting mechanism of Capão Bonito Granite, São Paulo State, Brazil. In: International Symposium on Mine Planning and Equipment Selection, 9th Athens, Greece Rotterdam, Balkema, 2000, p.573-576.

Hlavac, L. M. & L. Sitek 1998 Rock quarrying and related mining applications of liquid jets. In Momber, A (ed.) Water Jet Application in Construction Engineering A.A. Balkema Roterdam p. 277-288.

Peiter et al. 2001. Rochas ornamentais no século XXI: Bases para uma política de Desenvolvimento Sustentado das Exportações Brasileiras CETEM/ABIROCHAS 160p.- http://www.cetem.gov.br/reteqrochas/

Savanick, G. A. 1997 Hydraulic Mining Section 6.0 Fluid Jet Technology 5th Edition (ed. T.J. Labus & G.A. Savanick) Water Jet Tech. Association, Saint Louis, USA 12pp.

Stellin Jr., A.; Hennies, W. T.; Soares, L.; Fujimura, F.; 2001. Dimension Stone Block Extraction by Steel Wires MPES 2001, New Dehli, India, p. 215-222.

Table 1 – Industrial equipment significant features, tested in the field

Equipment, locality	Rock	Nozzle (mm) (n°)	Pressure (MPa)	Flow (l/min)	Power (kW)	Cut Ratio (m2/h)
C – Elberton, USA	Granite	0,50 (2R)	280 (I)	11	52	1,17
C – Milbank, USA	Granite	1,20 (2R)	165 (?)	76	209	n.a.
C – Colorado, USA	Granite	0,36 (1O)	310 (I)	5	26	0,6
C – Quebec, Canada	Granite	1,40 (2R)	140 (P)	76	175	1,15
D – Rothbach, France	Sandstone	1,20 (3S)	80 (P)	60	160	6,5
D – Lanhelin, France	Granite	0,60 (9S)	200 (P)	70	330	1,5
C – Milbank, USA	Granite	0,90 (1O)	260 (I)	29	87	n.a.
C – Valdossola, Italy	Gnaisse	0,50 (1O)	350 (I)	8	47	1,7
D – Sardinia, Italy	Granite	0,96 (1O)	200 (P)	18	60	2,4
D – Japan (Underg.)	Granite	0,96 (1O)	200 (P)	18	60	1,1

Equipment C = Compact system D = Unit system
Lance: R = Rotation, O = Oscillating, S = in balance
Pump: I = Intensifier, P = Piston. Source: Ciccu & Bortolussi, 1998.

Table 2 - Some data about ore and rock values.

Iron (1)	Gold (2)	Ornamental Rocks (3)
US$ 22/tonelada	US$ 93/tonelada	US$ 185/tonelada

(1) Ore base value US$ 22/metric tone
(2) Ore base value US$ 9,3/g, in ore with 10 g/metric tone.
(3) Mean Value US$ 500/cubic meter in international market, admitting density of 2,7 tons/cubic meter.

Table 3 – Estimated Value of Commercial Transations in Brazil on the Sector – Year 2000

	R$ millions	US$ millions
Exports	502.27	271.54
Imports	40.57	21.93
Domestic Market	3,285.00	1,775.67
Machines, Insumes e Services	100.00	54.05
Total	3,927.84	2,123.19

(Base US$ 1,00 = R$ 1,85)

2003 WJTA American Waterjet Conference
August 17-19, 2003 • Houston, Texas

Paper 5-C

COMPARATIVE PERFORMANCE STUDY OF POLYACRYLAMIDE AND XANTHUM POLYMER IN ABRASIVE SLURRY JET

S.V.Chacko, A.Gupta, D.A Summers
University of Missouri-Rolla
Rolla, Missouri, USA

ABSTRACT

It has been established that the abrasive slurry jet (ASJ) or DIAjet system can outperform a conventional abrasive water jet (AWJ). This is, in part, because the ASJ delivers comparable performance at a much lower pressure than the conventional abrasive water jet (AWJ). It has been shown that the introduction of a small amount of polymer into the ASJ process leads to a significant improvement in cutting performance. Various polymers impact the cutting performance of abrasive suspension jets differently due to differences in their rheological properties. The study compares the effectiveness of polyacrylamide and xanthan based polymers in an abrasive slurry jet system. The parameters studied include hydration time, the gel strength, ability to hold the abrasive in stable suspension, and, viscosity variations with shear-rate. Jet penetration distance in concrete blocks was used as a measure of the effectiveness of the different polymers and concentrations.

Organized and Sponsored by WaterJet Technology Association

1. INTRODUCTION

Initially the use of abrasives in waterjet applications was limited due to their detrimental effects on the lifetimes of nozzles and other component parts. Advances in nozzle materials have led to significant improvements in nozzle life and thus the viability of using abrasives. In the mid 70s to mid 80s the water-jet industry was focused primarily on the use of very high pressure, low flow rate systems. Such systems were built around intensifier type pumps and were largely only practical for use in premium industrial applications.

Beginning with a Master thesis at Cranfield [1] investigators at BHRA developed a system that later became known as the DIAjet (Direct Injection of Abrasives) [2]. In this system, the abrasive was metered into the flow of the pressurized water through a holding tank. In this system, which has since been given the more generic name of Abrasive Slurry Jetting (ASJ), the abrasive was mixed with water and pumped into a storage tank with the help of a jet pump or charging pump. Since the abrasive is introduced far behind the nozzle, it has sufficient time to reach the speed of the water and then to accelerate with it. As a result equivalent penetration is achieved compared with an AWJ of the same flow rates but at much lower jet pressure. The drawback to the more widespread use of the system has historically been because it has been used with an increased consumption of water and abrasives. However, more recently it has been shown that these higher flow rates are not necessary and that the improvement in performance can be achieved at equivalent abrasive and water flow rates. This development allowed the use of much lower pressure values to achieve cutting performance comparable to very-high-pressure intensifier systems. Subsequently, a number of designs have been proposed by different groups to improve the basic process of abrasive injection.

2. BACKGROUND

2.1 Polymers in Waterjets

A series of articles published in the mid-sixties indicated that the addition of a small concentration of certain long chain polymers to water significantly reduces the friction forces on water traveling through pipes and hoses. This concept was initially utilized for reducing friction losses in fire hoses and ultimately led to the introduction of polymers into a higher-pressure waterjet. Overall system efficiency was improved due to a reduction of friction forces.

The improvement in the performance of waterjets with the addition of polymers was subsequently found to go much beyond a simple reduction in friction losses. Franz reported an improvement in jet performance and depth of cut up to 300% with an addition of long chain polymers for cutting wood products [3]. Szymani identified the advantages of reduced wetting characteristics of polymer solutions when cutting corrugated boards [4]. This opened up the potential of using a waterjet in a wide range of cutting and cleaning applications (Polymerblasting) [5]. Some of such long chain polymers utilized in the industry are polyacrylamide (SUPER-WATER®), Polyox®, Separan-AP-273®, xanthan, guar (Jaguar®), etc.

Hollinger and Mannheiemer [6] showed that addition of the optimal concentration of polymer substantially increases the cutting ability of the jet in very precise cutting. This suggests that there is an optimum concentration of polymer to be mixed with abrasive and water in other circumstances. If the polymer concentration is too low the abrasive is not suspended in water satisfactorily, if it is too high, the suspension becomes too viscous to flow effectively.

Initial studies by Leach and Walker [7] showed that the range of a normal round jet is around 200 jet-diameters. Experience at UMR and the work of Barker and Selberg [8] shows that the two most important factors that contribute to increasing the range are the straightness of the flow into the nozzle and the internal surface finish of the nozzle. Tests at UMR have shown that a dramatic increase of range to about 2000 jet diameters is obtained by incorporating flow straighteners and improving the internal surface finish to 6 microns (which they achieved by nickel plating). Application of similar improvements is not practical in the presence of abrasives since the abrasive flowing through the nozzle rapidly wears out the surface finish. The addition of polymers offers an economical and readily available solution to reduce the friction and greatly increase the effective range of the abrasive jets.

An improvement over conventional ASJ performance by the addition of a small concentration of long-chain polymer to the mixture of abrasive and water is referred to as abrasive polymer-suspension jet (APSJ). As discussed above, the addition of polymer to the initial suspension of abrasive leads to a more stable suspension, reduced friction losses and increased jet cohesion that leads to improved range. Thus, polymer plays a very crucial role in an APSJ system and contributes significantly to the overall system efficiency and the jet penetration rate.

In transferring the energy from the pump to the jet, and then to the target, there is a considerable pressure loss due to fluid friction. The pressure loss depends upon the diameter and the length of the pipe from the pump to the nozzle. Labus [9] suggested the following equation for calculating the pressure loss in driving the water through the line:

$$\Delta p(bar/m) = \frac{\mathbf{0.597} \times Q^{\mathbf{2}}}{\mathbf{100} \times D^{\mathbf{5}} \times R_e^{\mathbf{0.25}}} \quad \ldots\ldots\ldots (1)$$

Where: D is the internal diameter of pipe, cm, and R_e is the Reynolds number for the flow.

In general, about half of the energy delivered to the fluid at the pump can be lost in overcoming various fluid friction losses by the time it reaches the nozzle, in a number of field applications [10]. The addition of a small concentration of polymer has been found to significantly reduce this friction loss.

With the addition of polymer in the APSJ, friction losses are greatly reduced. The polymer added to the slurry allows efficient transfer of energy from the high-pressure water to the abrasive and keeps the water and abrasive focused for a greater distance after exiting the nozzle. Polymer helps the abrasive particle to ‘glue’ and accelerate to speed of the pressurized water, thereby increasing the jet penetration or throw considerably.

Traditionally, a long-chain polymer, such as a polyacrylamide has been used to prepare slurry in the APSJ system at UMR. This polymer provides excellent jet cohesion and range but offers a limited ability to hold the abrasives in suspension [11]. The problem gets more severe in applications where there is a need to hold larger abrasive particles in stable suspension for an extended duration of time. This is of concern because the suspension must be constantly agitated for satisfactory performance. Incorporating an agitation unit in a pressurized transfer vessel is impractical. Further, polyacrylamide spills are very persistent and slippery and may lead to safety concerns.

3. EXPERIMENTAL SET UP AND METHODOLOGY

3.1 Abrasive Slurry Stability Tests

In order to understand and quantify the abrasive suspension characteristics of polyacrylamide, tests were conducted for varying grades of garnet mixed with a range of polymer concentrations. Garnet samples were screened to tight tolerance in the range of 80 mesh and 36 mesh was suspended in polyacrylamide solutions at concentration levels varying from 0.25 to 0.75 percent. Various slurries were prepared by the proper hydration of polymers in water to the desired concentration levels, followed by the addition of the desired concentration of the selected garnet abrasive particles. Initially, the slurries were well stirred to prepare stable suspensions that were then stored in transparent containers and left undisturbed for an extended time duration.

Suspensions of 80-mesh garnet were reasonably stable for a few hours when the concentration was greater than 0.5 % polyacrylamide. However, as illustrated in Figure 1, the 36 mesh garnet settled out in a matter of only a few hours at all levels of polyacrylamide concentration tested. Concentrations greater than 0.75% polyacrylamide are not practical since such solutions become too viscous to work with. These test results point to a problem that may hinder the vision of a widespread application of APSJ in simple-to-use mobile systems. In such systems, the stability of the abrasive slurry stored in an enclosed transfer vessel must be ensured for the success of intermittent operations. However, abrasive slurries prepared using the polyacrylamide polymer have been shown to destabilize after a few hours.

In order to address this problem, similar stability tests were carried out using a xanthan polymer. Xanthan is a biopolymer that is popular in many industrial applications and is an additive in many food-products such as ice cream and salad dressings. Preliminary studies with the xanthan polymer are promising. Experiments have shown that it has a far greater abrasive suspension capacity and can hold the abrasives in suspension for much longer duration than can the polyacrylamide. Slurries prepared with xanthan concentrations equal to or greater than 0.5% led to stable suspensions with 80 mesh and 36 mesh garnet for time periods extending over a number of days as shown in Figure 2. In addition, xanthan is biodegradable and the spills are less slippery and much easier to clean. Xanthan also exhibits unique shear thinning characteristics that are of great practical value. However, a biocide must be added to xanthan slurries stored for an extended time, in order to prevent fermentation.

3.2 Abrasive Slurry Jet Penetration Tests

As described in the previous section, xanthan solutions can provide an excellent stability for abrasive slurries. However, the cutting effectiveness of the abrasive slurry jets prepared with xanthan is not well understood. The goal of the penetration tests conducted in this study is to compare the cutting effectiveness of slurry jets prepared with polyacrylamide and xanthan.

In order to create an APSJ, a suspension of abrasive is prepared in polymer-thickened water and placed on the downstream side of the pump in a containment vessel. The containment vessel isolates the abrasive laden slurry from the pressurized water as shown in Figure 3. A conventional high-pressure positive displacement water pump is used to pressurize the water. Part of the water leaving the pump is diverted to the transfer vessel through a flow control valve. The water introduces the abrasive slurry, at a rate controlled by the flow control valve, into the primary stream of high-pressure water from the pump. The abrasive laden water is then carried to and accelerated through the nozzle. The polymer ensures that the water and abrasives stay focused within the delivery line and after exiting the nozzle.

This study was conducted using a high pressure APSJ pumping system powered by a small gasoline engine as shown in Figure 4. The unit has a designed delivery capacity of 19 liters/min (5 gallon/min) at about 35MPa (5075 psi). The gasoline engine and the high-pressure triplex water pump are readily available from a variety of high pressure cleaning system manufacturers. The complete system including the engine, pump, water tank, transfer vessels and the abrasive mixing unit was assembled on a single, relatively portable pallet for use in remote locations.

For this test program, the cutting nozzle was mounted on a linear translation table and a rectangular block of concrete was held steady under the nozzle path during the test. Figure 5 illustrates the set-up including the controller used for linear translation of the nozzle across the sample face. To ensure a constant offset of the nozzle throughout the cutting test, the top face of the concrete block must be held parallel to the traverse path of the nozzle. All the concrete blocks selected for the test came from the same batch to ensure consistency in the test results.

The concrete blocks were cut with 34.5 MPa (~5000 psig) and the traverse speed was kept constant at 12.7 mm/minute (0.5 inch/min) (Figures 5 and 6). Refer to Table 1 for the parameters used during the test. A minimum concentration of 0.5% (by weight) for Xanthan and 0.25% (by weight) for polyacrylamide was selected as an earlier test had shown that below these concentrations the abrasive begins to settle immediately after mixing. This is especially true for the polyacrylamide as even at a 0.25% concentration the abrasive does not stay in suspension for more than a few minutes.

The blocks were cut first with a varying concentration of xanthan in the slurry and the maximum depth of cut at each concentration was measured as reported in Table 2. Abrasive concentration was kept constant during all tests. Similar tests were then conducted with a varying concentration of polyacrylamide and the depths of cut are reported in Table 3.

3.3 Test Results and Analysis

The plot of Depth of cut versus polymer concentration is shown in Figure 7. A small improvement in the depth of cut is observed as the xanthan concentration is increased from 0.5 to 0.75%. However, on increasing the concentration from 0.87 to 1%, a marked increase in the depth of cut was observed. The maximum depth of cut, 132mm, was obtained at 1% concentration. At 1.25%, there is a small decrease in the depth of cut. Xanthan slurry at 1.5% was too viscous to be pumped into the transfer vessel.

The plot of the depth of cut with polyacrylamide concentration is also shown in Figure-7. Contrary to expectation, the maximum depth of cut, 179 mm, was obtained with a concentration of 0.25% polyacrylamide and thereafter, the cut depth decreased as polyacrylamide concentration was raised to 0.5 and 0.75%, respectively.

While it was observed that the polyacrylamide gives a better depth of cut at 0.25% concentration, this might lead to the conclusion that lower concentrations should be studied. However, as explained earlier, working with a solution of 0.25% polyacrylamide and below is not practical because the abrasives settled out of the suspension very rapidly. Historically, slurries prepared at a 0.5% concentration of polyacrylamide have been used with the UMR abrasive slurry jet system. It was observed that Xanthan at 1% concentration and Polyacrylamide at 0.5% provide very similar cutting performance.

3.4 Rheology of Polymers

The results of the suspension and penetration tests prompted an investigation into the rheological properties of the two polymers. The goal is to understand the relative performance of two polymers in the context of their rheological characteristics.

It is apparent that the time dependence of viscosity or the thixotropic nature of the two fluids is important in understanding the slurry stability. This refers to the weak interactions between the polymer molecules that allow the fluid to flow when agitated or when a shear strain is applied, but lead to formation of a pseudo-crystalline structure (gel strength) when the shear strain is removed. The measure of the amount of structure that has formed at any specific time is called the Gel strength. Gel strength can be measured using a Rotational Viscosimeter illustrated in Figure 8. Gel strength may be a better measure of the capacity of the polymers to hold the abrasive in a stable suspension.

The results of gel strength measured at zero sec, 10 sec and 10 minutes for both xanthan (0.5% concentration in the slurry) and polyacrylamide (0.25%) are tabulated in Table 4. The shear rate was varied by changing the RPM of the viscometer and the corresponding shear stress was noted in $lb/100ft^2$. All the readings are converted to S.I. units. As can be observed, the gel strength of xanthan increases within the measured time span while it reduces for the polyacrylamide. This provides a possible answer to the question: "why doesn't the polyacrylamide suspend the abrasives very well, especially at lower concentration even though the slurry is very viscous?"

Another key feature of interest is in the shear rate dependence of slurry viscosity. The slurry is essentially at zero shear rate in the transfer vessel and goes through a tremendous shear rate as it exits the nozzle. Such data could possibly explain the jet characteristics after exiting the nozzle. Shear stress readings ($lb/100ft^2$) measured at varying shear rates (RPM) using a rotational viscometer are listed in Table 6 for xanthan slurry and in Table 7 for the polyacrylamide slurry. For a Newtonian fluid such as water, a linear relationship is observed between shear stress and shear rate, as indicated by a dotted line passing through the origin. The slope of this line gives the viscosity of a Newtonian fluid. From the plot, it is observed that both polymer slurries deviate from the linear.

Both Xanthan and Polyacrylamide, and many other polymers, are know to exhibit non-Newtonian behavior, i.e., the shear rate versus shear stress exhibits a non-linear relationship. As the shear rate increases, the shear stress increases at a decreasing rate. Such fluids are called pseudoplastic or shear-thinning fluids. The apparent viscosity of such fluids decreases as the shear rate increases. Such fluids are often modeled using a power-law model [12] according to which shear stress is related to shear stress:

$$\tau = K\,\gamma^{n} \quad \ldots\ldots\ldots. (2)$$

Where, τ = Shear Stress, Pascal ($lb/100ft^2$ x 0.4788) [13]

K= Consistency index, $Pa\text{-}s^n$

γ = Shear rate, s^{-1}

n = Flow behavior index

Shear rate is related to the rotational speed of the viscometer [12]:

$$\gamma = 0.2094 N \frac{\frac{1}{r_1^{2/n}}}{n\left[\frac{1}{r_1^{2/n}} - \frac{1}{r_2^{2/n}}\right]} \quad \ldots\ldots\ldots (3)$$

Where γ = Shear rate, s^{-1}

N = Rotational speed of the viscometer, RPM

n = Flow behavior index

r_1 = Radius of the inner Bob in cm. (1.724 cm)

r_2 = Radius of the outer Rotor in cm. (1.84 cm)

The flow behavior index for all Newtonian fluids is 1.0. For power-law fluids, it has been observed that the flow behavior index must be known for an accurate calculation of the shear rate. However, the shear rate is proportional to RPM and a value for the flow behavior index, "n" is readily obtained by fitting a power-law curve through the measured shear stress vs. RPM plot of data listed in Table 6 and Table 7. With an established value of "n", the shear rate is calculated using equation 3. The shear stress reading obtained from the Viscometer ($lb/100ft^2$) is converted into Pa [13]. The shear stress and shear rate is then plotted as shown in Figure 9.

The rheological behavior of both polymer systems is well represented by a power-law model as shown in Figure-9. The Consistency index, K, and the flow behavior index, n, are obtained from the best-fit trend line. The power-law parameters for xanthan and polyacrylamide slurries are listed in Table 8.

At any shear rate, the apparent viscosity is a ratio of the shear stress to the shear rate given by

$$\mu_{app} = \frac{ShearStress}{ShearRate} \quad \ldots\ldots\ldots (4)$$

Based on equation (2),

$$\mu_{app} = K\gamma^{n-1} \quad \ldots\ldots\ldots. (4)$$

Where the units of apparent viscosity μ_{app} = Pa .s

It was noted from Table 9 and Figure 10 that the viscosity of Xanthan is about half that of Polyacrylamide at any shear rate. Both polymers exhibit a shear-thinning trend as the shear rate increases. As a point of comparison, a wall shear rate for the fluid emerging from the nozzle can be estimated as:

$$\gamma = \frac{\mathbf{32}Q}{\pi D_n^{\mathbf{3}}} \quad \text{.........} \ (5)$$

For the test parameters listed in Table 1, the shear rate through the nozzle is: $2.633 \times 10^6\ s^{-1}$. It is well known that at such high shear rates, the polymer solutions tend to behave as Newtonian fluids with a constant viscosity comparable to that of water, approximately 1.0 $\times 10^{-3}$ pa.s [14]. This suggests that at the point of contact with the nozzle wall, the slurry acts in a similar manner to water. However, for the slurry slightly removed from the walls, the shear rate drops rapidly to zero and the central portion of slurry acts as a thick viscous paste. The consequence of such shear dependent viscosity of the polymer slurries is that the core of slurry moves through the nozzle and beyond as a cohesive plug lubricated by low viscosity at the wall. Detailed studies of xanthan rheology [14] have shown that rotational viscometers tend to give too low a value for the power law n and too high a value for k. Such values are not supported at the lower shear rates prevalent in the slurry storage vessels. At such low shear rates, the reported viscosity for 0.5% xanthan slurry is approximately 1 kPa.! This is about a thousand times larger than the largest value measured in our studies. Such behavior may explain the remarkable abrasive suspension demonstrated by xanthan.

4. CONCLUSIONS

Based on this preliminary study, the results obtained by using xanthan as an abrasive suspension agent are quite promising.

1. With its unique property of gel strength increasing with time, the abrasive settling in an APSJ transfer or mixing tank can be greatly reduced. This also opens up the possibility of preparing the slurry ahead of time and having it taken to a remote location where a slurry-mixing facility may not be available. After the slurry is pumped into the transfer tank, if there is any unexpected delay in operating the unit, a xanthan slurry does not pose as great a problem since it can keep the abrasive suspended for long periods.
2. The penetration tests for xanthan at 1% concentration are comparable to the results obtained with an APSJ with a 0.5% concentration of Polyacrylamide.
3. The best depth of cut was achieved with a 0.25% concentration of polyacrylamide, but this can only be used in situations where the suspension is used almost immediately, because of the poor suspension ablility of this concentration.
4. The shear thinning property of the xanthan also helps in site cleanup as it is very easy to clean the mixing tank of any spilled material. The time saving is

considerable when compared to the cleaning of a spill of the polyacrylamide. This unique property of xanthan has significant implications.

5. ACKNOWLEDGEMENTS

Several students from UMR both at the graduate and undergraduate level have contributed in the design and development of the equipment and during the course of experimental study. The administrative and technical assistance provided by the staff of Rock Mechanics and Explosive and Research Center at UMR is much appreciated. The authors also gratefully acknowledge the Petroleum Engineering Department at UMR for the use of their Drilling Fluids Laboratory and providing us with all the technical assistance.

6. REFERENCES

1. Fairhurst, R.M., Abrasives Water Jet Cutting, Msc thesis, Cranfield Institute of Technology, January, 1982.

2. Fairhurst, R.M., Heron,R.A., and Saunders, D.H., "Diajet"-A New Abrasive Waterjet Cutting Technique," 8th International Symposium on Jet Cutting Technology, Durham, UK, September,1986, pp.395-402.

3. Franz, N.C., "Fluid additives for improving high velocity jet cutting," paper A7, 1st International Symposium on Jet Cutting Technology, Coventry, UK, April, 1972, pp. A7-93- A7-104.

4. Szymani, R., A study of corrugated board cutting by high velocity Liquid Jet, Msc thesis, University of British Columbia, September, 1970.

5. Howells, W.G., "Polymerblasting with super-Water from 1974-89: A review, "International Journal of Water Jet Technology, Vol.1, No. 1, March, 1990, pp. 1-16.

6. Hollinger, R.H., and Mannheiemer, R.J., "Rheological Investigation of the Abrasive Suspension Jet, "6th American Water Jet Conference, Houston, TX, August, 1991, pp. 515-528.

7. Leach, S.J., and Walker, G.L., "Some Aspects of Rock Cutting by High Speed Water Jets, "Phil. Trans. Royal society, London, Vol. 260A, 1996, pp.295-308.

8. Barker, C.R., and Selberg, B.P., "Water Jet Nozzle Performance Tests", paper A1, 4th International Symposium on jet cutting Technology, Canterbury, UK, April, 1978.

9. Labus, T.J., "Fluid Mechanics of Jet". Fluid Jet Technology, fundamentals and Applications", A Short Course, Toronto, Canada, August, 1989.

10. Summers, D. A. (1995), Waterjetting Technology, Book, E & FN SPON, ISBN #: 0 419 19660 9, First Edition 1995, pp.26.

11. "Drilling Fluids and Oil Well Cements," Petroleum Production Laboratory, UMR, 2000.

12. A.T.Bourgoyne Jr., Chenevert, M.E., Millheim, K.K., Young Jr., F.S., Applied Drilling Engineering, SPE Text Book Series 2, pp.131-139.

13. Koederitz, L.F., Introduction to Petroleum Reservoir Analysis, 1998, pp 6-17.

14. Rheology Technical Bulletin, Kelco Oilfield Group, Monsanto Company, 1996.

7. TABLES

Table 1. Parameters selected for the Experiments.

Parameters	**Units**
Pressure	34.5Mpa (5000 psi)
Flow	19 L /min (5 gpm)
Nozzle diameter	1.07 mm (0.042 inch)
Offset	5mm (0.2 inch)
Traverse speed	12.7mm/min (0.5 inch/min)
Sample blocks	Concrete
Volume of abrasive slurry used per cut	8 liters
Abrasive Type	80 mesh Garnet
Abrasive concentration	50% by weight

Table 2. Concentration of Xanthan versus Depth of Cut in the Concrete Block.

Xanthan concentration, %	**Depth of Cut mm**
0.5	76
0.75	79
0.87	105
1	132
1.25	130.3

Table 3. Concentration of Polyacrylamide versus Depth of Cut in the Concrete Block.

Polyacrymide concentration, %	**Depth of Cut mm**
0.25	179
0.5	134
0.75	116

Table 4. Gel Strength reading from Rotational Viscometer.

XANTHAN		
Measured At:	**Gel Strength lb/100ft^2**	**Gel Strength Pa**
0 sec	10	4.79
10 sec	13	6.22
10 min	16	7.66

POLYACRYLAMIDE		
Measured At:	**Gel Strength lb/100ft^2**	**Gel Strength Pa**
0 sec	17	8.14
10 sec	16	7.66
10 min	12	5.75

Table 5. Shear stress versus Shear rate for 0.5% Xanthan concentration.

XANTHAN			
Shear Rate, RPM	**Shear Rate (γ), sec^{-1}**	**Shear Stress, (lb/100ft^2)**	**Shear Stress, Pa**
3	6.10	9	4.31
10	20.35	16	7.66
20	40.69	18	8.62
40	81.38	20	9.58
70	142.42	23	11.01
100	203.46	24	11.49
200	406.91	30	14.36
300	610.37	35	16.76
450	915.55	39	18.67
600	1220.74	43	20.59

Table 6. Shear stress versus Shear rate for 0.25% Polyacrylamide concentration.

POLYACRYLAMIDE			
Shear Rate, RPM	**Shear Rate (γ), sec^{-1}**	**Shear Stress, (lb/100f2)**	**Shear Stress, Pa**
3	6.00	17	8.14
10	19.99	23	11.01
20	39.98	28	13.41
40	79.97	33	15.80
70	139.94	39	18.67
100	199.92	43	20.59
200	399.84	52	24.90
300	599.76	61	29.21
450	899.64	72	34.47
600	1199.52	83	39.74

Table 7. Rotor and Bob dimensions of the Rotational Viscometer.

Radius of	**c.m**
Bob (r_1)	1.724
Rotor (r_2)	1.84

Table 8. Power Law Rheological Model.

Power Law model		
	n	**K (Pa. s^n)**
Xanthan	0.2695	2.955
Polyacrylamide	0.2926	4.558

Table 9. Viscosity –Shear Rate relation of Xanthan and Polyacrylamide.

XANTHUM			POLYACRYLAMIDE	
Shear Rate (γ), sec^{-1}	**$\mu_{app.\ viscosity}$(Pa . s)**		**Shear Rate (γ), sec^{-1}**	**$\mu_{app.\ viscosity}$(Pa . s)**
6.10	0.706		6.00	1.36
20.35	0.377		19.99	0.55
40.69	0.212		39.98	0.34
81.38	0.118		79.97	0.20
142.42	0.077		139.94	0.13
203.46	0.056		199.92	0.10
406.91	0.035		399.84	0.06
610.37	0.027		599.76	0.05
915.55	0.020		899.64	0.04
1220.74	0.017		1199.52	0.03

8. FIGURES

Figure 1. Slurry Stability test for 36 mesh Garnet in polyacrylamide solutions of concentration: 0.25%, 0.5% and 0.75%. All garnet settled after 5 hours.

Figure 2. Slurry Stability test for 36 mesh Garnet in Xanthan solutions of concentration: 0.5%, 0.75% and 1.00%. Garnet still in stable slurry after 24 hours.

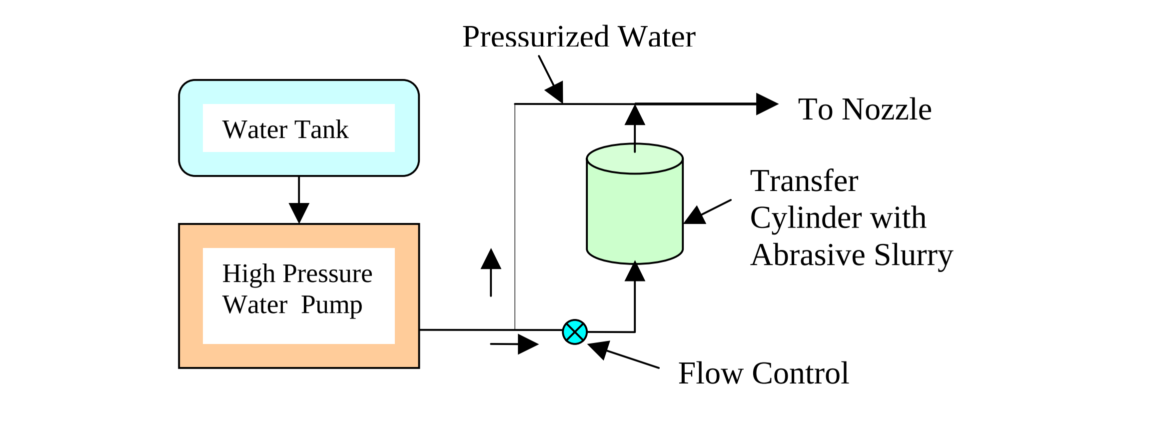

Figure 3. Schematic of an Abrasive Slurry Jet (ASJ) system.

Figure 4. Gasoline engine driven, portable High pressure ASJ system.

Figure 5. Top: Sample undergoing a cut.
Bottom: Controller for linear traverse across the sample.

Figure 6. Close up of a sample block after being cut.

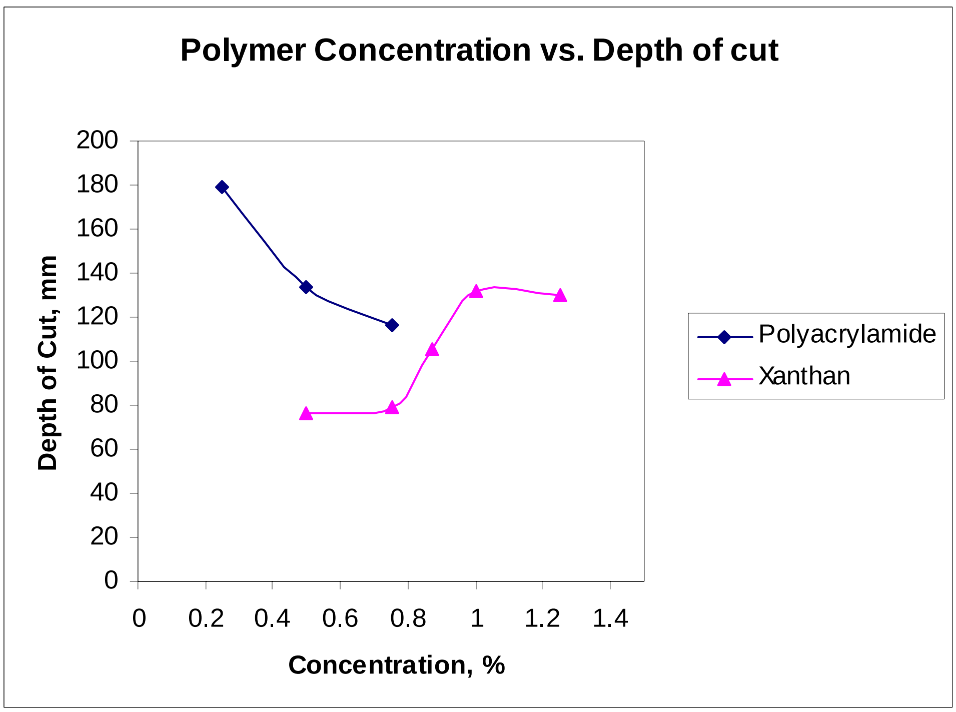

Figure 7. Variations in Depth of cut with concentration of polymer.

Figure 8. A typical Rotational Viscometer (Ref: Fann Instrument Company).

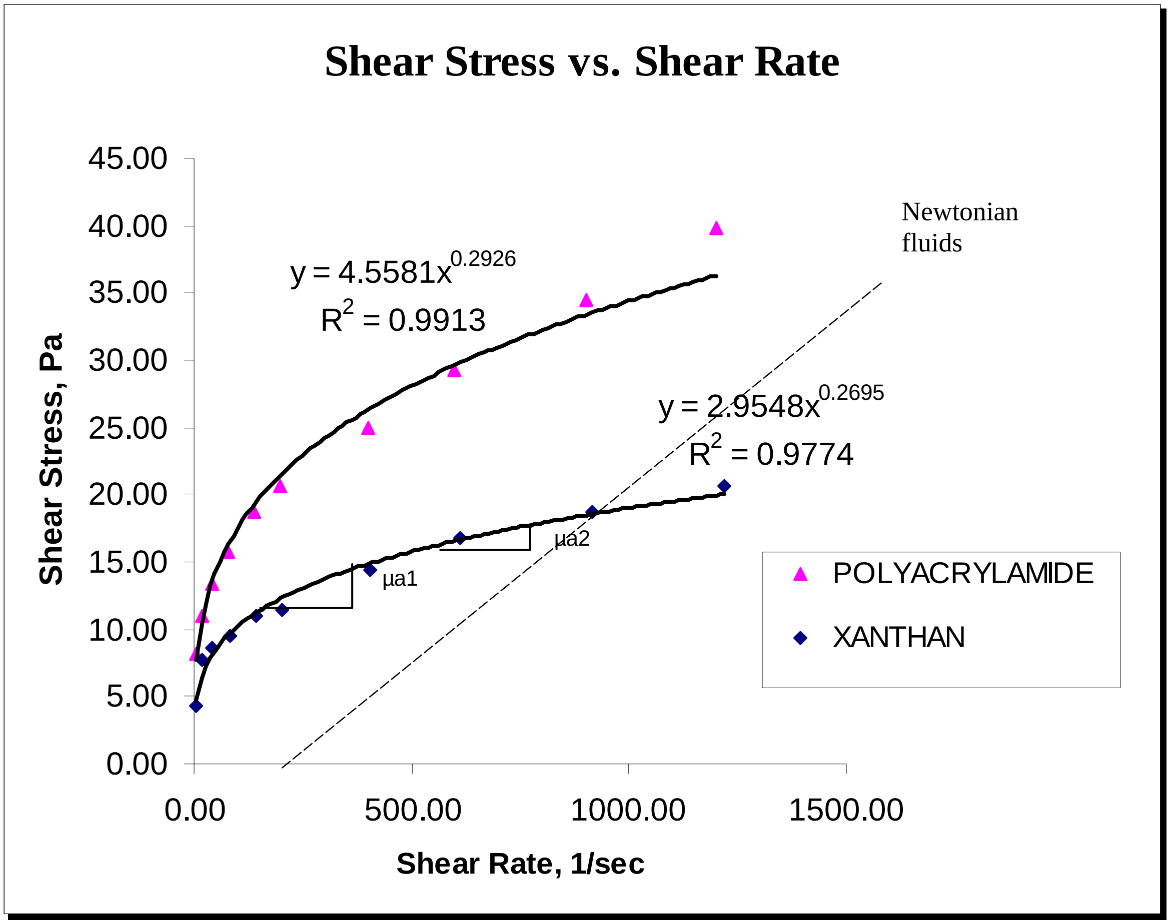

Figure 9. Shear stress measured at varying shear rate in a Rotational Viscometer.

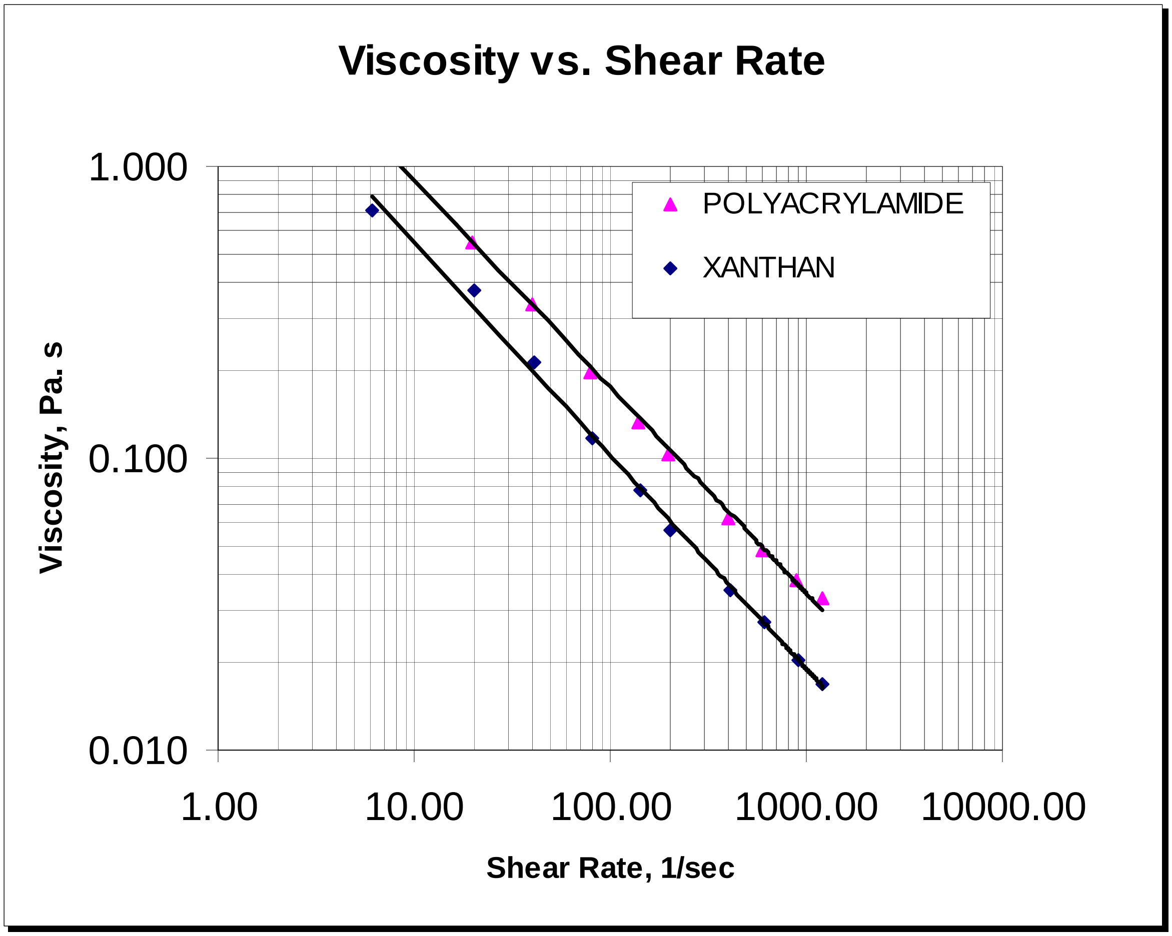

Figure 10. Variation of Viscosity with Shear Rate.

2003 WJTA American Waterjet Conference
August 17-19, 2003, ● Houston, Texas

Paper 6-C

INVESTIGATION OF THE HIGH-SPEED WATER SLUGS

O. Petrenko*, V. Samardzic*, E.S. Geskin*,
G.A. Atanov**, B. Goldenberg*, A. Semko ***

New Jersey Institute of Technology
Newark, NJ 07102-1982

ABSTRACT

The intrinsic shortcoming of the conventional waterjets is the use of expensive and heavy pumping facilities. What is more important, the peculiarities of the waterjet-substrate interaction impede energy exchange between the incoming jet and the workpiece. These shortcomings are eliminated if a continuous jet is replaced by an array of the water slugs. The slugs are generated by the direct energy injection into water and subsequent ejection of portion of the water via the nozzle. The speed of the generated slugs and subsequently effectiveness of the material removal is enhanced if the slug maintains a free surface in the course of the acceleration in the barrel. In this case the water velocity exceeding 1500 m/sec can be attained. A device for slug formation will constitute an effective and versatile manufacturing tool.

A laboratory scale prototype of a device forming super-high speed water slugs termed the water cannon was constructed and tested. The tests included the investigation of the external ballistics of the slugs as well as materials piercing and breakage. The capabilities of the technology in question were illustrated by the destruction of a non-dischargeable explosive device with no explosion and deformation of steel. It was shown, however, that the process is effective only at a narrow range of operational conditions.

* - New Jersey Institute of Technology, ** - Donetsk Open University, Donetsk, Ukraine, *** - University of Donetsk, Donetsk, Ukraine

1. INTRODUCTION

The presented work involved investigation of a device generating high speed water slugs and termed the water cannon. The slugs were accelerated by the direct injection of energy in water contained in a barrel. The energy can be delivered via the mechanical impact, gas expansion, electrical discharge, laser beam, etc. In the experiments, discussed in this paper the energy was injected into water via the powder explosion. Fast moving boundary of the cavity generated by the explosion products accelerated the water slug contained in the barrel. Main acceleration, however, was attained by the superposition of the pressure and rarefaction waves generated during the impact as well as during the water flow through the long tapering nozzle. This acceleration was due to the energy redistribution in the water. While the velocity of the bulk of water remaining in the barrel drops, water in the nozzle accelerates. Redistribution of the energy transferred from the powder to the water results in the energy accumulation in a small fraction of the water expelled from the nozzle. As the result, extremely high speed of the slugs, expelled from the nozzle was attained. Due to non-homogeneous pressure and the velocity distribution in the water during its acceleration the dynamic pressure of the slug substantially exceeds static pressure in the barrel that is pressure exerted on the walls of the barrel. Comparatively small pressure on the wall is one of the principal advantages of this process.

The high speed impulsive jets constitute a unique material processing tool. A water slug impacting the substrate surface acts as a powder charge deposited on this surface. The cumulative jets, utilizing this principle are the main armor piercing tool. There is a variety, of other possible applications of the impulsive jets (Atanov, 1987, Summers, 1995). It was shown (Leach and Walker (1966), Cooley and Lucke (1974), Atanov (1987), Petrenko (2002, 2002a) that the water cannon can be successfully used for material fracturing (rock breakage mining, structure demolition, etc.). Another potential application of water cannons is piercing of metal and other plastic materials. At the same time the current use of super high speed jets is practically limited to the armor piercing.

There are several barriers preventing the adoption of the water cannon by the industry. One of the obstacles impeding the use of the water cannon is instability of the generated slugs. The superposition of the compression and rarefaction waves which caused water acceleration at the same time brings about energy redistribution within the slug. While the head of the slug accelerates up to extremely high velocity the slug tail decelerates. Such velocity distribution generates instability within the slug and its fast decomposition. Thus an effective stand off distance of the slug is limited and does not exceed several centimeters. Low available stand off distance constitutes one of the major obstacles to the practical use of the water cannon.

In this study several experiments were carried out in order to examine slug decomposition. An imaging technique was used to monitor slug deformation between the barrel and the target. Then an anemometer for slug velocity measurement was designed. The interaction between the slug and target was also studied.. The performed experiments involved the destruction of explosive devices, demolition of concrete and piercing of steel. Some peculiarities of the slug-substrate interaction were investigated.

2. VELOCITY MEASUREMENT

A device for measuring velocity of the slug's head (Atanov, 1987). was constructed. The device operation involved measuring the time between intersecting two parallel light beams by the flying water slug. In order to generated two parallel rays with a precise distance the beam emitted by a semiconductor laser was split by a prism. Photodiodes were used as light detectors. The photodiodes outputs were fed to the DataLab's DL 2B08 multichannel recorder and stored on a magnetic medium. Then the acquired signals were fed to C1-73 oscilloscope for visual evaluation. The general view of the device is shown on the Fig. 1. The anemometer was used for several measurements, however backflow of the fluid destroyed the receiving part of the device. The measured velocity of the slug was approximately 1000 m/s.

In the second version of device the light beams were replaced by the metal cords (Fig. 2). The current running through the cords was interrupted as the slug sequentially broke the cords. The time interval between the current interruptions was measured by a timer. The measured values of the velocity were in the range of 1100 +/-200m/s.

The third version of the device integrated both techniques. As it is shown on Fig. 3 the infrared beams generated by IR LEDs light source replaced the laser beams and graphite rods replaced metal cords. This device will be used in the next series of experiments.

3. INVESTIGATION OF EXTERNAL BALLISTICS OF THE SLUG.

A set up for investigation of the slug's external ballistics was constructed. The set up (Fig.5) consisted of the Flowmaster system (double-pulsed laser generating the background light, high-speed camera and the data processing system), water extruder, extruder mounting and synchronization device. Stand off distance of the cross section of the velocity measurement varied between 21.5mm and 84mm. The slugs were generated by the water extruder (Petrenko et. al., 2002 and 2002a). The extruder constituted a modified power tool where the powder charge accelerated a metal piston which expelled water load via converging nozzle. The weight of the powder charge was 0.39g, the water load was 4.2 g, the weight of piston was 105 g, the barrel and nozzle diameters were correspondingly 9 mm and 2 mm. In the course of experiment 2-D PIV Flowmaster system of LaVision Inc. was used to capture the images of a flying slug and to measure the velocity field of the slug.

The principle of the 2-D PIV operation is shown on Fig. 4. The general view of the set up is depicted on Fig.5. Here a camera captures two consequent images of the flow. For this capture a flow is highlighted by short laser impulses. Seeding particles are added into the fluid if needed. In order to obtain the velocity distribution the captured images are analyzed for correlations in the data processing system. In the presented here experiments laser generated background rather than the light sheet was used.

At the stand of distance of 21.5 mm the measured average water slug's forefront velocity was 128.3 m/, while at the stand of distance of 36 mm it was 200 m/s and at the stand of distance of 84 mm the average velocity was 500 m/s. Maximum radial velocity of the jet observed in these experiments was 175 m/s. At each particular observed pulse images of the slug forefront were obtained. The measured velocity of the front of the slug (Fig. 6) changed from 123 m/s at 21.5mm stand off distance to 500 m/s at 84 mm. Such velocity variation was predicted by the numerical analysis of slug motion (Fig. 7). As it follows from this chart water exit velocity initially increases and then decreases. Due to redistribution of the kinetic energy within the slug maximum front velocity is attained at a certain time after the exit from the nozzle.

The images of the slug are depicted on Fig. 8. As follows from this figure two major deformation of the slug occurs in the course of its motion. Velocity redistribution brings about the redistribution of the water mass along slug axis. As the result, in the course of the motion the main part of water is accumulated in the front of the slug. In addition, the hydraulic resistance of the air causes the expansion of the surface of the slug's front. As the result, the slug obtains the shape of a mushroom.

4. NEUTRALIZATION OF THE EXPLOSIVE CHARGE.

In order to evaluate the interaction between the impacting slug and workpiece the neutralization of explosive devices were carried out. The attempt was made to neutralize three devices. In two cases impact resulted in the explosion. In the third case, however, the device was destroyed with no explosion. (Fig. 9)

The feasibility of explosion-free explosive destruction is due to speed of the propagation of the stress wave generated in the impact zone. The rate of this propagation enables us to turn content of the explosive device inside out before the detonator was able to explode device.

5. CONCRETE DEMOLITION

The previous experiments involving demolition of concrete and enforced concrete plates (Petrenko et. al. 2002, 2002a) were continued. In this case, however, the kind of powder was changed and the mass of the charge was reduced to 30 g from 40 g. As the result the effectiveness of demolition was dramatically reduced. While in the previous experiments a single shot decomposed a concrete block protected by a 6 mm steel plate in a several fragments in new experiments a similar block without protection was broken only into two parts. (Fig. 10)

6. INVESTIGATION OF METAL DEFORMATION BY WATER SLUGS

Two series of experiments involved impact of the steel substrate by the water slugs. The set up used in one of the series of the experiments is shown in Fig. 11. In this case a special holder supported a target while the heavy tires supported both, the water cannon and the target holders. Such design assured stability of the cannon and the target during experiment as well as simplicity of experiment performance.

The results of the first series of experiments are depicted on Fig. 12. These experiments involved impacting of steel plates having different thickness. The results of the impacts varied from the piecing (Fig. 12 c) to metal deformation (Fig. 12a). These experiments demonstrated sensitivity of the process results to the process conditions.

The second series of the experiments involved impacting single steel plates as well as two and three attached plates. Piercing of a single plate is shown in Fig. 13. As it is depicted on this picture, the impact generated the sharp edges at the slug entrance and the rupture at its exit. The result of the impact of two attached steel plates is depicted on Fig. 14. The smooth piercing of first plate is completely different from the rupture of the second plate. Figure 15 shows the deformation of three attached plates. As the results of the impact all three plates were heavily deformed, but no rupture occurred.

Figure 16 shows piercing of a steel pipe by the water slug. In this case despite to a comparatively large stand off distance as well as well as the change of conditions of the slug motion the slug ruptured the pipe walls at the entrance and the exit.

The experiments Figs 12-16 demonstrated the feasibility of the various deformation of a plastic media by the high-speed water slugs as well as feasibility to control this deformation.

7. CONCLUSION.

The performed experiments showed that the slug generated by the water undergoes a dramatic modification in the course of motion between the nozzle exit and a target. Fluid convection within the slug brings about accumulation of both, the mass and the momentum in the front of the slug. This properties redistribution improves impact conditions. At the same time, the aerodynamic résistance of the atmospheric air brings about the head losses. The breakage of the concrete and deformation of steel plates and a pipe show the strong effect of the impact conditions on the target behavior. Thus, the optimization of the process conditions in the course of the slug based material processing is a necessary stage of the process design.

8. ACKNOWLEDGEMENT.

This study was supported by NSF Grant " Development of Water based Machining Technology" and NJ Center for Micro Fluidic Control. The facilities for measurement of the slug velocity and capture the slug image were provided by the LaVision, Inc.

9. REFERENCES

Atanov, G.A. "Hydro-Impulsive Installations For Rocks Breaking." - Kiev, Vystcha shkola. 1987 (in Russian.).

Atanov G. "The Impulsive Water Jet Device: A New Machine For Breaking Rock" // "*International Journal of Water Jet Technology.*" Vol. 1, No 2, 1996. – PP. 85 – 91

Leach S.J., Walker G.L. "The application of high speed liquid jets to cutting." *// Phil. Trans. Roy Soc. of London*, 260-A, 295 (1966).

Cooley W.C. and Lucke W.N. "Development and Testing of a Water Cannon for Tunneling." In: *Proc. of the 2nd International Symposium on Jet Cutting Technology*. Cambridge, England, 1974, Paper J3

D. A. Summers "Waterjetting Technology", E. &F.N. Spon., London, 1995

O. Petrenko et. al. "Investigation Of The Material Fracturing By High Speed Water Slugs." In *Waterjetting Technology*, *Proceedings of BHRA 2002 Conference*, Aix Provance, 2002.

O. Petrenko. Et. al. "Investigation Of Material Deformation By The High-Speed Water Slugs", in proceedings of 2002 ASME International Congress, New Orleans, Nov 2002

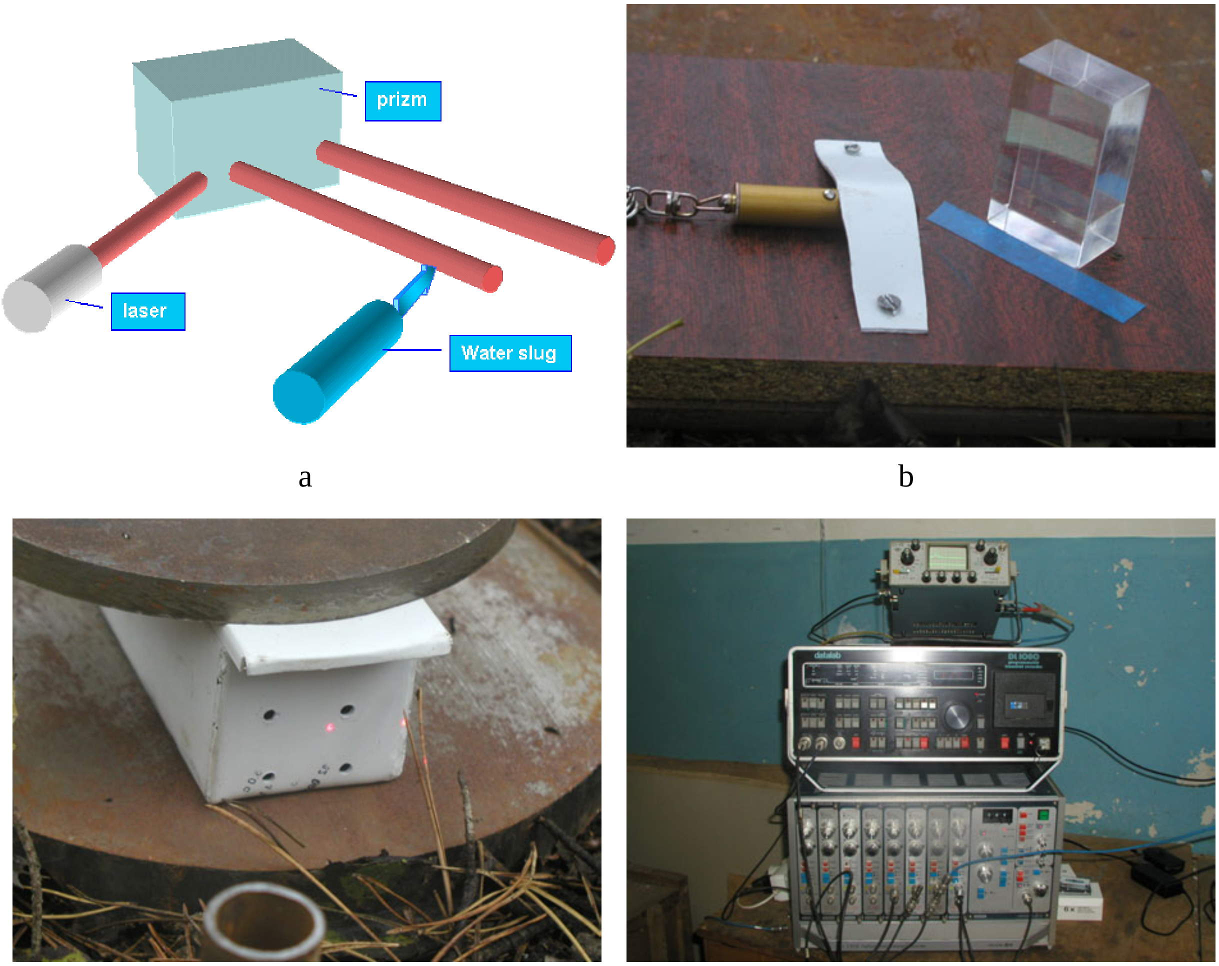

a b

c d

Figure 1. The Schematic of the device for measuring water slug's head velocity.
a) schematic of slug-beam interaction; b) general view of the device;
c) plastic box containing photodiodes; c) signal processing system

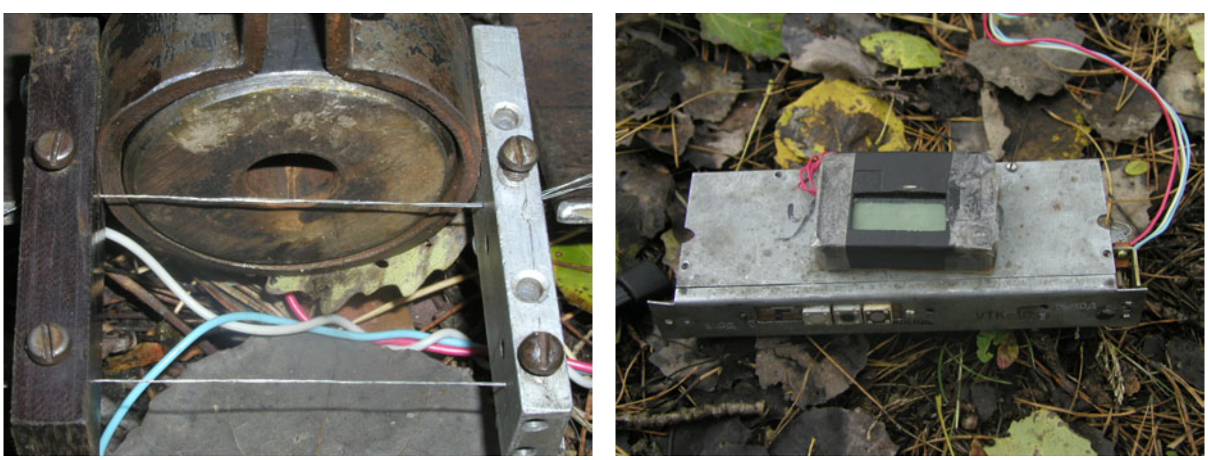

a b

Figure 2. Slug's head velocity measuring unit.
a) sensing cords; b) timer.

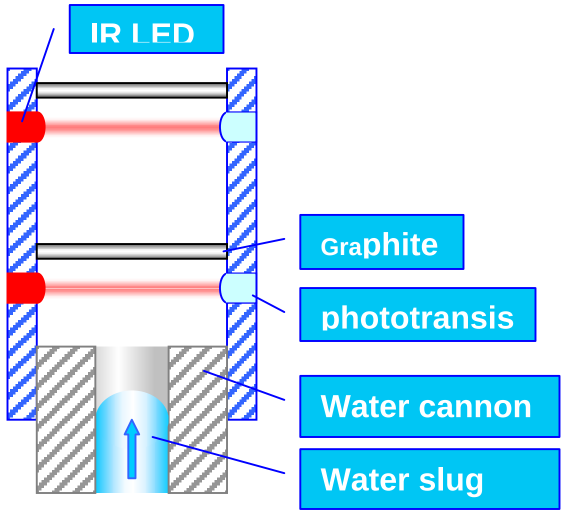

Figure 3. Schematic of integrated velocity measuring device.

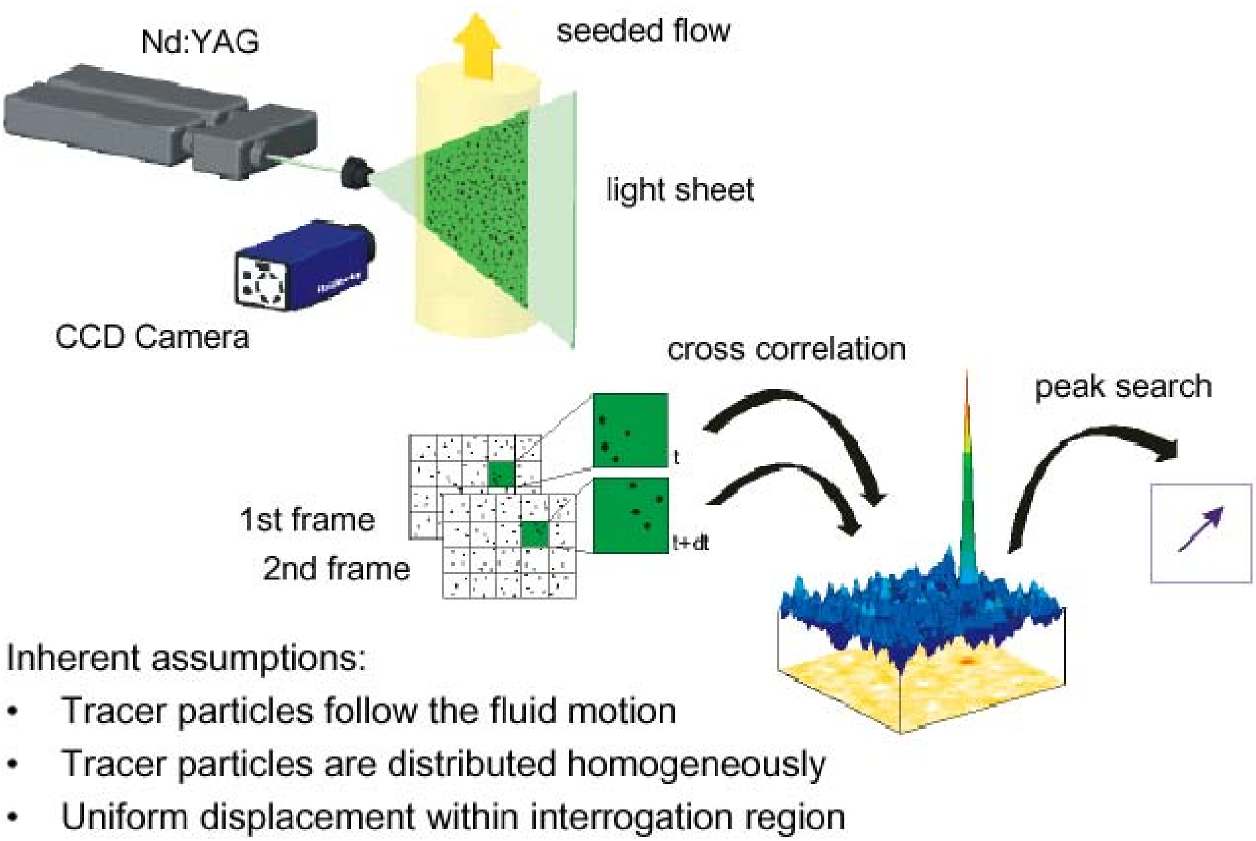

Figure 4.Conceptual schematic of PIV operation (courtesy of LaVision)

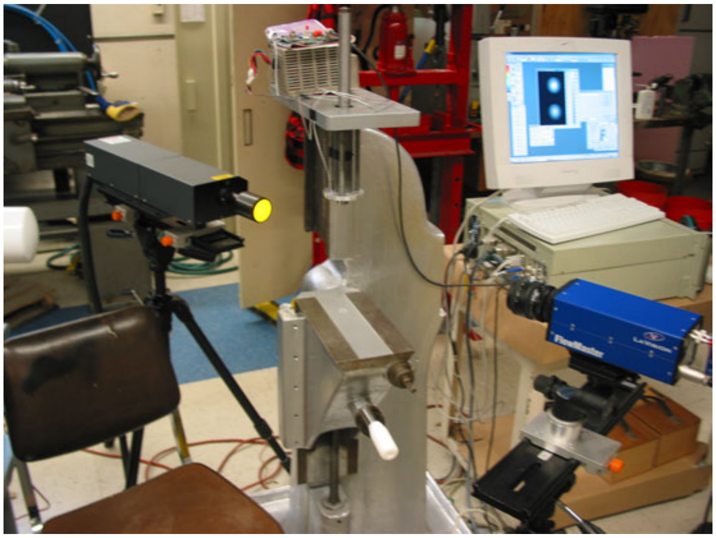

Figure 5.Experimental set up for measurements of high speed waterslug

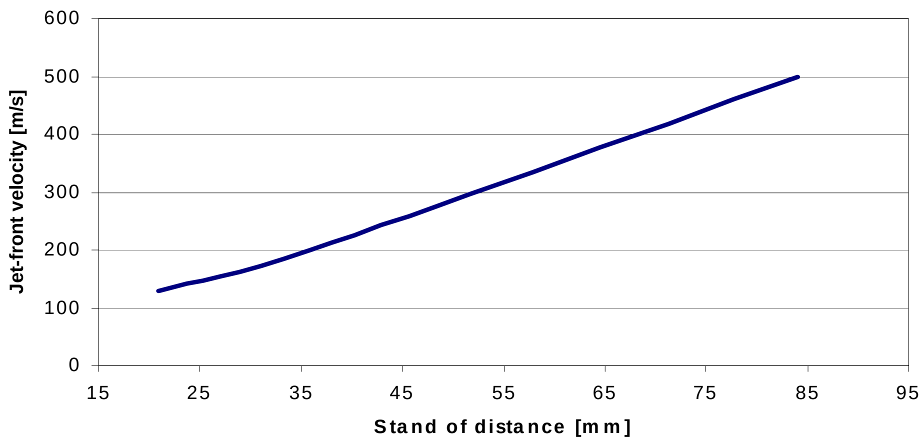

Figure 6. Stand of distance vs. jet-front velocity for extruder testing.

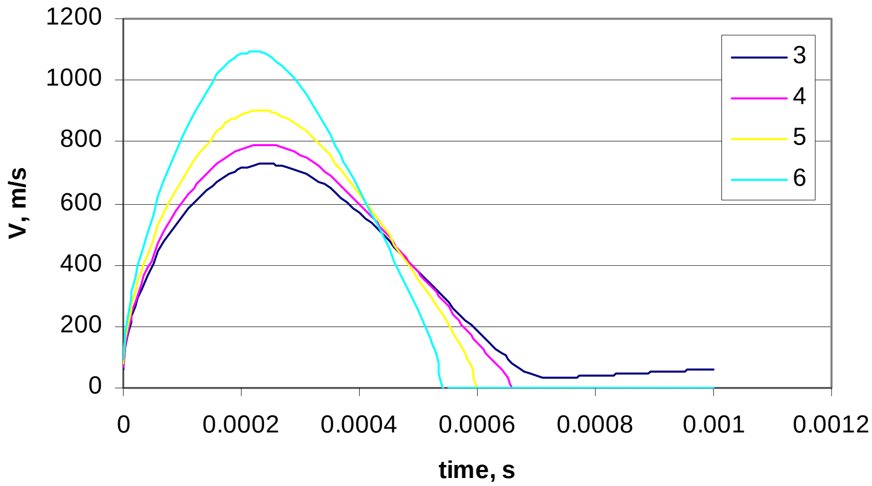

Figure 7. Outflow speed *V*, and pressure *P*, vs. time
at different piston KE levels. Water load is 4.1g.

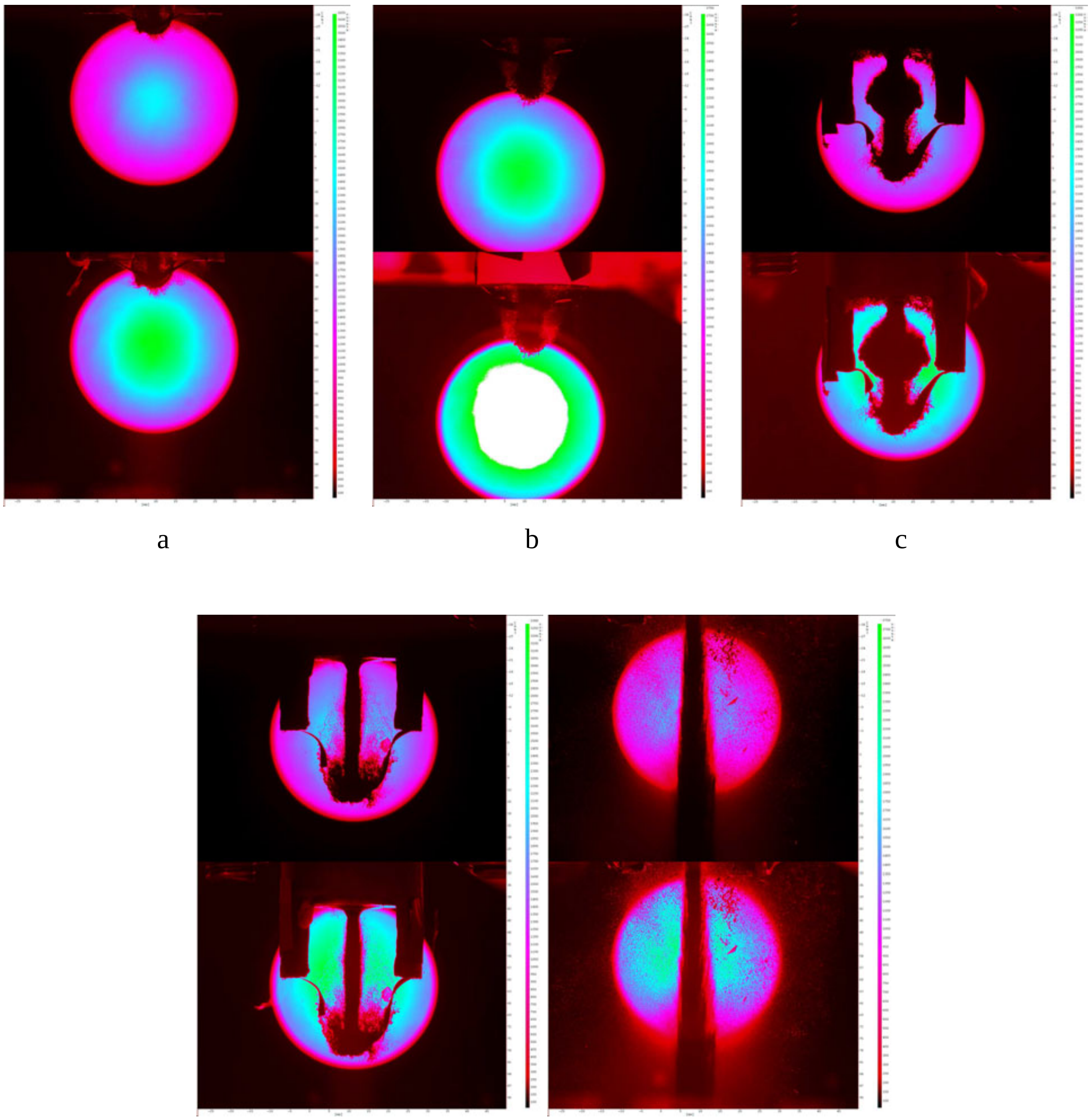

a b c d e

Figure 8. Images of sequential slug development in the air obtained by 2-D PIV: a) jet exiting the nozzle; b) SOD=21.5mm, average velocity=128.3m//s;c)and d) SOD=36mm, average velocity =200m/s;; e) SOD=84mm, average velocity=500m/s

a b c

Figure 9. Successful neutralization of a soft-case explosive setup.

a b

Figure 10. Demolition of a 20X29X120cm concrete block.
A cavern and the crack through the block as the result of a shot to the center of the block.

Figure 11. Experimental setup for steel plates penetration.

a b c

Figure 12. Steel piercing by water slug. Water load – 230g, powder charge – 30g

a) 8mm thickness, SOD – 5.5mm, b) 5mm thickness, SOD – 40mm,
c) 6mm thickness, SOD – 80mm

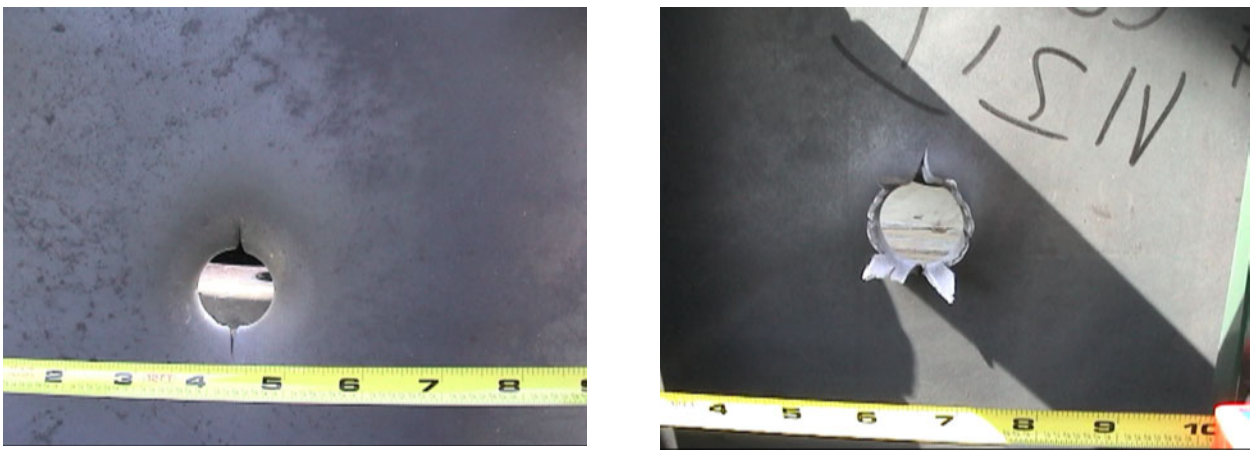

a b

Figure 13. Penetrated 4.8mm steel plate. Front (a) and back (b) views.

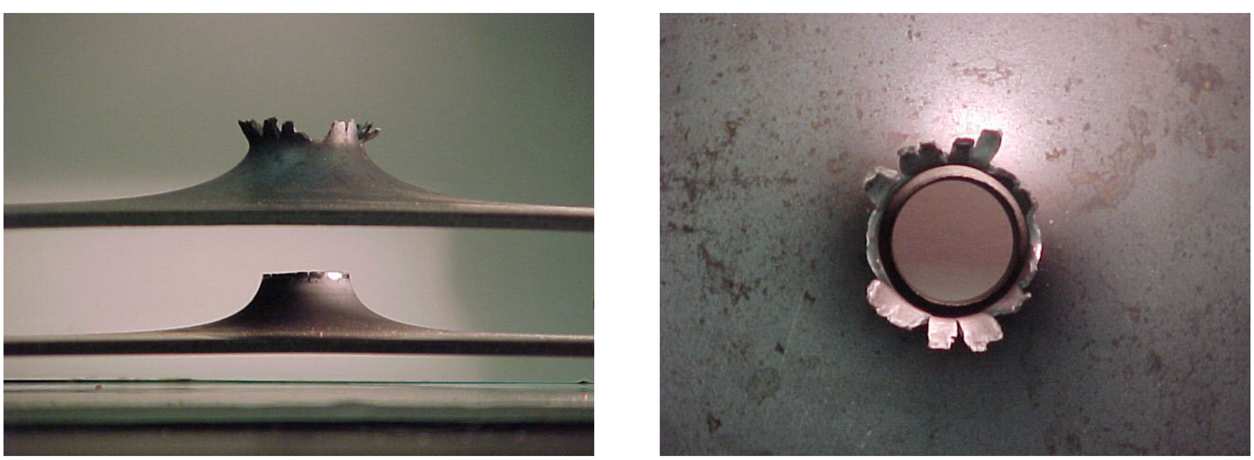

Figure 14. Two steel plates, each 4.8mm thick were ruptured by 250g water slug

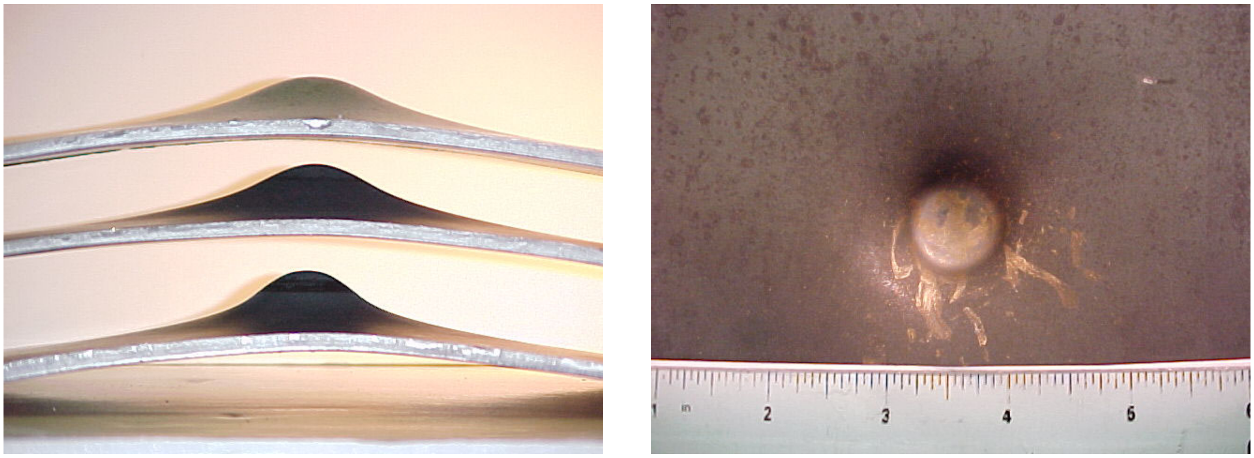

a b

Figure 15. a) Three steel plates (each 4.8mm thick) heavily distorted by 250 g water slug together.
b) front view of first plate indentation

a b

Figure 17. Penetration of a steel pipe.
a) Initial setup. b) Through penetration of the pipe resulting in two holes.

2003 WJTA American Waterjet Conference
August 17-19, 2003 • Houston, Texas

Paper 1-D

INSIDE AWJ NOZZLES

Mohamed Hashish
Flow International Corporation
Kent, WA, USA 98032
mhashish@flowcorp.com

ABSTRACT

This paper addresses several issues on water-air, and abrasive interaction inside abrasive-waterjet (AWJ) nozzles. It is aimed at providing quantitative and qualitative observations on selected AWJ-associated phenomena. The waterjet formation is addressed including its spreading characteristics and flow coefficients. Upstream flow Reynolds's number has been found to be a critical parameter for jet coherency. The air entrainment and the influence of nozzle conditions are addressed by presenting the AWJ and abrasive feed line characteristic curves. The axial mass and power distribution of the abrasives and their kinetic power inside AWJ mixing tubes are presented along with the kinetic power efficiency of AWJ. This shows that the AWJ kinetic power efficiency cannot exceed 25% and that the abrasives are very sparse inside AWJ nozzles. Abrasive particle fragmentation showed that this process in highly sensitive to jet alignment, especially when the ratio of waterjet diameter to mixing tube diameter is relatively large. The importance of AWJ vacuum assist for process and abrasive feed reliability has been discussed. Attributes to the mixing tube axial and radial wear pattern have been presented.

1. INTRODUCTION

Abrasive-waterjet nozzle systems consist of several components that influence their overall performance. These components serve different functions covering a multitude of issues such as fatigue, fluid flow behavior, erosion, and tribology. The proper design for each component is critically dependent on its geometry and material. Typically, the components that constitute an AWJ nozzle are:

- Ultra High Pressure (UHP) water tube: This UHP tube provides the high-pressure water to the orifice. It must be fatigue resistant and correctly sized to produce coherent jets with minimal pressure drop.
- Orifices: The orifice is the device that converts the potential energy to kinetic energy. An orifice is typically made out of diamond, sapphire, or ruby and mounted in metallic orifice mounts. The orifice must resist fluid flow erosion, chipping from the impact of small particulates, and should produce a qualitatively deterministic jet. In most cases, a coherent jet is needed.
- Orifice mounts: The orifice mount is a metallic part that holds the relatively small size orifice. The holder should be of sufficient strength not to adversely deform under the pressure loads. It should also insure that the water does not leak around the orifice or its mounting surfaces. It is also important that the orifice holder holds the orifice in an accurate location in the AWJ nozzle body.
- Abrasive receiving (mixing) chamber: The waterjet exits the orifice to the receiving (mixing) chamber where abrasives are also fed. The rush of the abrasives into this chamber subjects it to wear, and thus hard material liners may be used. Also, abrasives, especially fines, may settle and cake in areas of stagnant flows. Correct sizing of this chamber may eliminate abrasive caking and the need for protective liners.
- Nozzle body: The nozzle body contains all the ports and connection required for utilities (mainly water and abrasives) and mounting the other components. Abrasives are fed through a side port that may be perpendicular or inclined to the waterjet. This body may also contain a vacuum assist port, flushing, and venting ports (1-3). A machine collet may be used to hold the mixing tube accurately in the nozzle body and thus it must be accurately fabricated.
- Mixing tube: In the mixing tube, momentum transfer occurs from the waterjet to the abrasive particles. Also, the abrasives are axially directed to produce a collimated AWJ. The alignment of the waterjet stream inside the mixing tube is of critical importance to nozzle wear uniformity and the overall effectiveness of the AWJ. Alignment may be achieved by either precession fabrication of critical components (4,5) or by providing provisions for manual alignment (6). The mixing tube contains an upstream conical area to facilitate abrasive entry.
- Sensor ports: Advanced AWJ nozzle components may contain sensing ports for monitoring critical parameters. An example is monitoring the “health” of the waterjet orifice by measuring the vacuum pressure (7) just downstream of the orifice.

Figure 1 shows typical AWJ nozzle components and important issues associated with each of these components

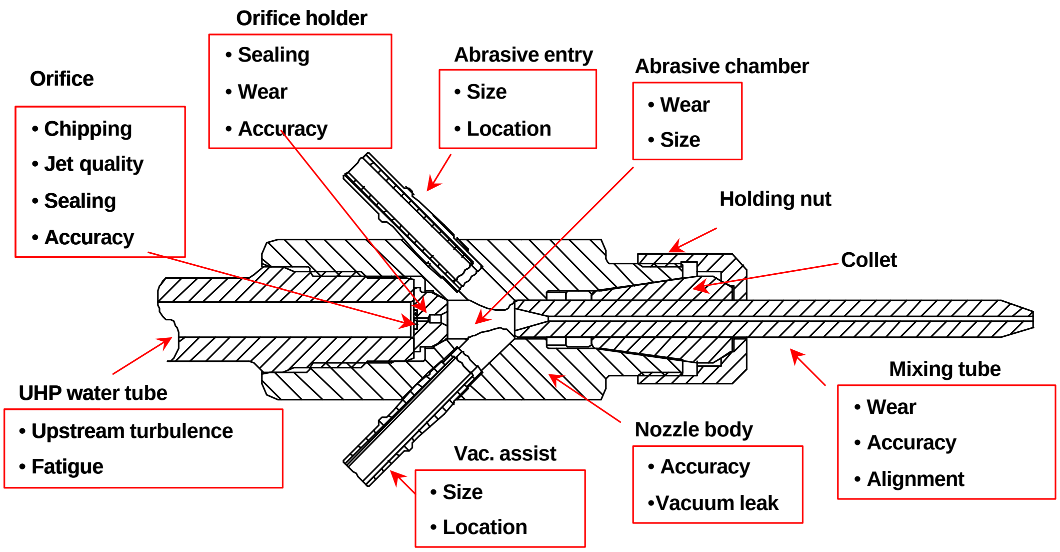

Figure 1. Typical AWJ Nozzle Components and Issues

In addition to the above components, an AWJ nozzle system may include a UHP on/off valve and the abrasive feed systems (7-9). These components will not be addressed in this paper but their effect on nozzle performance will be discussed. This paper starts upstream of the AWJ nozzle addressing waterjet formation, the suction process, mixing and acceleration of abrasives, wear, and other jet effects. Conclusions are then presented at the end of the paper.

2. OBSERVATIONS

2.1 Effect of UHP Water Tube

The inside diameter and length of the UHP water tube are important in controlling the coherency of the waterjet. Geller (10) performed experiments to determine the effects of tube diameter, *d*, and the level of turbulence upstream of the orifice. Figure 2 shows three photographs of jets with different tube sizes. As can be seen, the jet coherency improves when the tube size reaches about 6-mm in diameter. Any further increase in tube diameter does not further improve coherency for flow rates up to 8 liter/min. Geller hypothesized that the enlarged tube diameter may have acted as a pseudo reservoir, which decreased the turbulence. Turbulence generators such as rods and turbulence dampers such as screens do not affect jet quality.

Struve (11) used the area ratio d^2/d_n^2 to characterize the effect of the upstream tube size. He used a doubling length as a measure of jet coherency. This doubling length is the downstream jet length at which the jet diameter is twice the original jet diameter at the orifice exit. He observed that a maximum improvement in coherency occurs around an area ratio of 200 to 500. Struve (11) showed no correlations between the data on jet coherency and orifice size. Tan (12) correlated Struve's data to the upstream Reynolds number and found this correlation to be more appropriate than that using the area ratio. The Reynolds number is proportional to d_n^2/d. Figure 3 shows Struve's data (11) correlated by Tan (12); the improved correlation is seen between data using different orifices.

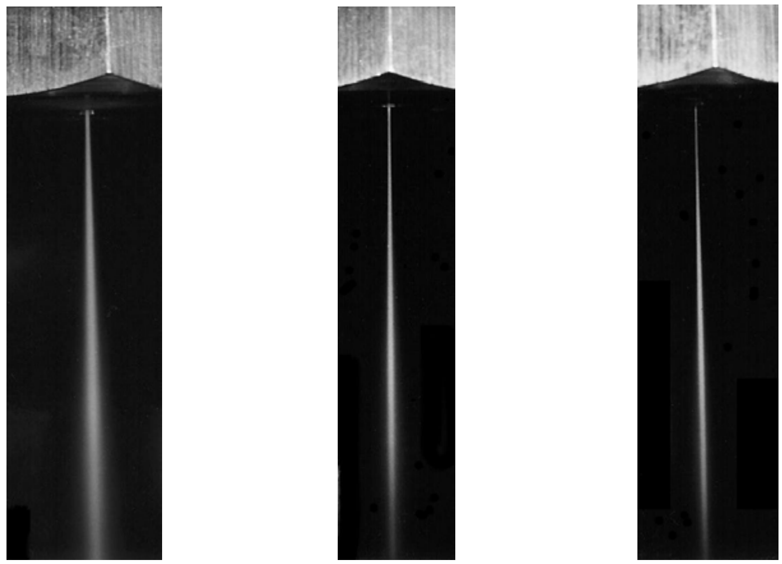

d = 3.1 mm d = 6.4 mm d = 9.5 mm

Figure 2. Jet Spreading Characteristics with Different Tube Diameters (d_n = 0.25 mm; P = 345 MPa)

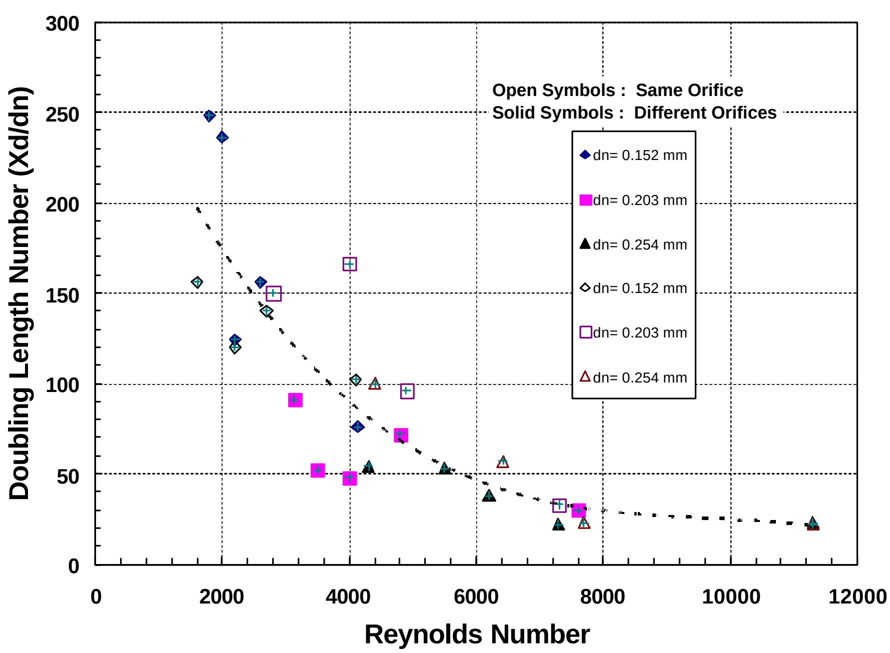

Figure 3. Dependency of Jet Coherency Length on Reynolds Number

Other factors that have been found to affect jet coherency include the following:

- Upstream tube length – An upstream length of at least 20 tube diameters was found to be important in producing coherent jets.
- Orifice edge geometry and condition – A chipped edge on an orifice is the most important factor that affects jet quality.
- Downstream geometry of orifice holder – The downstream geometry should minimize the interaction of air with the jet.

2.2 Waterjet Orifice

Waterjet orifice materials used in AWJ nozzles are either made out of diamond, sapphire, or ruby. The selection of the orifice material to be used is based on cost and performance. A typical lifetime of a sapphire orifice is about 100 hrs while the diamond orifice lasts 1000 hrs or more. The most critical factor that determines the orifice life is the upstream water condition. Unfiltered water will reduce orifice lifetime significantly. In AWJ, fine abrasives may travel upstream when the water shut-off valve is activated due to hydraulic transient phenomena. The introduction of abrasives particles via this mechanism to the UHP tube upstream of the orifice is a most critical factor that affects the orifice lifetime. Methods of preventing this migration of fine abrasives have been investigated. For example, Hashish and Craigen (1) used a venting port in the orifice holder. This venting port communicates, an otherwise low-pressure zone, to the atmosphere, thus preventing abrasives from flowing upstream to the low-pressure zone. When this port is placed underneath the orifice holder, wear of the bottom side of this orifice holder will be reduced. It must be understood here that this porting method slightly reduces the effectiveness of abrasive entrainment and thus accurate sizing of the venting port and the air suction through it is important. Another method is to sequence the on/off operations of the abrasive feed and UHP water on/off valves. The abrasive on/off valve must be shut off prior to the water on/off valve with sufficient time to allow the evacuation of most of the abrasives out of the receiving chamber. Similarly, keeping the vacuum assist on until after shutting the jet off will minimize abrasive upstream motion. To further increase the lifetime of waterjet orifices, a small edge rounding at the top surface may be used. This will reduce the coherency of the waterjet but may be acceptable in AWJ nozzles.

Orifice specifications and dimensional tolerances are significant factors in AWJ operation. For example, the perpendicularity of the orifice-mounting surface to the axis of the hole must be kept within a fraction of a degree; otherwise, the jet may not flow freely through the mixing tube. For example, an out-of-perpendicularity by 0.1 degree will cause this to happen for most AWJ orifice/mixing tube combinations. The tolerance specification of the diameter of the orifice affects the jet power. For example, using the English system, an orifice of 0.0054-inch diameter and another of 0.00046-inch diameter can both be referred to as an 0.005-inch orifice. However, the larger orifice will deliver 37% more power than the smaller one. Accordingly, the fourth digit of nozzle diameter specification in inches must be considered.

A UHP seal must be used to seal the orifice in the orifice holder to prevent UHP water from leaking around and below the orifice, which in turn, dramatically affects the jet quality and the orifice holder lifetime.

The orifice overall coefficient of discharge, C_d, includes the coefficient of velocity, C_v, the contraction coefficient, C_c, and the compressibility factor, y. It also depends on other qualitative factors such as the orifice edge condition and the inlet radius. The typical method used for measuring the coefficient of discharge is to measure the jet flow rate over a certain period of time, to calculate the average flow rate, and then to compare this value to the theoretical one. Care must be taken in conducting the experiments and measurements. For example, if the actual diameter of a nominal 0.25-mm-diameter orifice is 0.26 mm, an error of 8% will occur just due to measurement error. This error may be larger than the effect of compressibility.

Several experimental investigations have been performed to measure the overall coefficient of the orifice. Hashish (13) showed the dependency of the coefficient of discharge on pressure up to 345 MPa. This work was later extended to 690 MPa. The following simple first-order linear equation was derived based on experimental observations for sapphire orifices with a sharp edge entry:

$$C_d = 0.785 - 0.00014\,P - 0.197\,d_n. \tag{1}$$

This equation is accurate to within 8% and slightly underestimates the coefficient of discharge as pressure increases. It shows that increasing the jet size and pressure reduces the overall coefficient with more sensitivity to orifice diameter. This suggests that, for a given jet power, it is more efficient (higher C_d) to increase the pressure than to increase the orifice diameter to convert the pressure's potential energy to kinetic energy. A more comprehensive study is needed on this topic to develop a more accurate model for C_d in terms of pressure, orifice size, and shape.

2.3 Abrasive Waterjet Velocity

The abrasive particle velocity in an AWJ depends on the waterjet velocity. The waterjet velocity can be calculated from Bernoulli's equation for momentum balance and the water compressibility equation. The resulting equation is (14):

$$V_j = \sqrt{\frac{2L}{(1-n)\,r_o}\left[\left(1+\frac{P}{L}\right)^{1-n} - 1\right]} \ . \tag{2}$$

Where L = 300 MPa and $n = 0.1368$ at 25°C. These constants have been deduced from Bridgman's data (15) and the water compressibility equation:

$$\frac{r}{r_o} = \left(1+\frac{P}{L}\right)^{n} . \tag{3}$$

We now define V_{th} as the theoretical waterjet velocity for incompressible flow:

$$V_{th} = \sqrt{\frac{2P}{r_o}} \ . \tag{4}$$

From Equations (2) and (4), we can define the compressibility coefficient, ψ, as:

$$\psi = \frac{V_j}{V_{th}} = \sqrt{\frac{L}{P(1-n)}\left[\left(1+\frac{P}{L}\right)^{1-n} - 1\right]} \quad . \tag{5}$$

The above compressibility factor and the coefficient of discharge, C_d, can be used to express the waterjet velocity:

$$V_j = C_d \, \psi \sqrt{\frac{2P}{\rho_o}} \quad . \tag{6}$$

A simple formula for the abrasive axial velocity distribution has been derived (16) based on the momentum and continuity equations of the liquid and solid flow. The force acting on a particle moving at a velocity V in the mixing tube is:

$$F_p = \frac{1}{2} \rho_o A_p (U - V)^2 \quad . \tag{7}$$

Newton's equation for particle motion can be written as:

$$F_p = m_p V \frac{\partial V}{\partial x} \quad . \tag{8}$$

The overall momentum balance equation at a location x from the entry of the mixing tube is:

$$\dot{m}_w V_j = \dot{m}_w U + \dot{m}_a V \quad . \tag{9}$$

The above equations can be solved to yield the following equation for the particle velocity V at a distance x:

$$x = \frac{1}{K}\left[\frac{\lambda}{\lambda - 1} - \ln\left(\frac{1}{1-\lambda}\right)\right] \quad , \tag{10}$$

Where

$$K = \frac{3 C_D (1+r)^2}{4 S_a \, d_p} \tag{11}$$

When the jet breaks up into droplets and mixes with air, the virtual specific gravity of the mixture can be assumed to be equal to (d_n^2/d_m^2) instead of 1. This will mathematically alter S_a in the above equation by the same ratio. λ in the above equation is defined as:

$$\lambda = \frac{V}{V_{\max}} = \frac{V}{V_j/(1+r)} \tag{12}$$

where $r = \dot{m}_a/\dot{m}_w$ is the abrasive loading ratio, and $V_{max} = V_j/(1+r)$ is the maximum possible abrasive particle velocity. In the above equation, λ can be considered a mixing tube length factor that approaches unity as the mixing tube length approaches infinity. This is different from the momentum transfer efficiency, which expresses the ratio of the actual particle velocity V_a to the theoretical abrasive particle velocity *V*. Accordingly, if ζ is defined as the momentum transfer efficiency, then:

$$\zeta = \frac{V_a}{V} \tag{13}$$

Relating the actual abrasive particle velocity to the maximum theoretical particle velocity V_{max} defines an overall momentum transfer efficiency ζ_o, which can be expressed as:

$$\zeta_0 = \zeta\lambda = \frac{V_a}{V_{\max}} = \frac{V_a}{V_j/(1+r)} \tag{14}$$

Table 1 shows the mixing tube length for different cases for a mixing tube length factor of 90%, i.e., λ = 0.9.

Table 1. Mixing Tube Length for λ = 0.9

Mesh No.	$\boldsymbol{r} = \dot{m}_a/\dot{m}_w$	0.1	0.12	0.15	0.2	0.25
	$\boldsymbol{d_p}$ **(mm)**	**Mixing tube length, $\boldsymbol{l_m}$ (mm)**				
16	1.65	439	423	401	369	340
36	0.76	202	195	185	170	157
60	0.38	101	98	93	85	78
80	0.25	67	65	62	57	52
100	0.13	34	33	31	28	26

Observe that larger particles require longer mixing tubes; note also that as the abrasive flow rate increases, shorter tubes can be used to attain the maximum velocity. For the commonly used 100 mesh abrasives, for example, a mixing tube length of only 33 mm is required for an abrasive loading ratio of 0.12. The typical mixing tube length used in industry for this case, however, is about 76 mm. The additional length is used to collimate the jet and to raise the value of λ to about 0.95, as can be calculated from the above equations. Note that the additional 43 mm of mixing tube length contributes only 5% to the maximum possible velocity.

One of the early methods of measuring abrasive particle velocity inside AWJ mixing tubes was performed by Hashish (17) and Swanson, et al (18). Hashish (17) used a ceramic (alumina) mixing tube with a coil wrapped around its outside diameter and connected to a direct-current power supply to create a magnetic field. A moving particle in this field will generate current in a secondary coil. Two secondary coils were used to pick up the signals of a moving conductive particle. The average particle velocity was calculated by dividing the distance between the two secondary coils by the time difference of the recorded signals. More details on this setup can be found in (14). Table 2 shows selected results of velocities near the exit of the mixing tube.

Table 2. Abrasive Particle Velocity Data

d_m (mm)	l_m (mm)	P (MPa)	d_n (mm)	Abrasive material	Mesh size	$\dot{m}_a$ (g/s)	V_a (m/s)	V_j (m/s)	$V_{\max}$ (m/s)	Efficiency z_o
1.57	76	173	0.457	Steel shot	170	11.3	285	490	420	0.680
1.57	76	173	0.457	Steel grit	50	11.3	320	490	420	0.763
1.19	76	138	0.356	Steel grit	50	7.5	311	439	334	0.931
1.19	76	207	0.356	Steel grit	50	7.5	369	537	428	0.861
1.19	76	276	0.356	Steel grit	50	7.5	474	620	509	0.932
1.19	76	207	0.356	Steel shot	170	7.5	333	537	428	0.777

The maximum possible abrasive particle velocity is calculated from the simple momentum balance equation given in the above table as $V_{a_{max}}$. The ratio of the actual abrasive particle velocity to the theoretical one is listed in the last column and is defined as the overall momentum transfer efficiency ζ_o as mentioned above. For a relatively larger ratio of mixing tube diameter to waterjet orifice, this efficiency will be relatively low as shown in the table.

2.4 AWJ Power Efficiency

The power transmission efficiency is defined as the ratio of the kinetic power of the abrasive particles to that of the waterjet stream. The maximum possible power transmission efficiency is obtained when the momentum transfer efficiency is 100%.

The waterjet stream hydraulic power, E, is:

$$E = \frac{1}{2}\dot{m}_w V_j^2 \quad , \tag{15}$$

The abrasive kinetic power E_a can be calculated from:

$$E_a = \frac{1}{2} \dot{m}_a V_a^{\ 2} \quad , \tag{16}$$

Dividing question (16) by equation (1), and using $r = \dot{m}_a / \dot{m}_w$, and $V_a = z_o V_j / (1+r)$ from equation (14), the maximum possible power efficiency can be expressed as:

$$\boldsymbol{h} = r\boldsymbol{z}_o^2 / (1+r)^2 \quad , \tag{17}$$

From this equation, it can be determined that the maximum possible power efficiency of AWJ is 25% which occurs when x_o= 1 and the loading ration r =1, i.e. when the mixing tube is very long and the abrasive flow rate equals the water flow rate. This is not a practical condition for cutting with AWJ but may be for cleaning operations. The abrasive particle velocity at this theoretically maximum efficiency condition is 50% of the waterjet velocity. At a practical loading ratio of 0.125, the maximum power efficiency is 9.88% and the maximum abrasive particle velocity is 89% of the waterjet velocity. Using a momentum transfer efficiency x_o of 90%, the AWJ power transmission efficiency is only 8%. Figure 4 shows the range of AWJ power efficiency for different loading ratios, r, and momentum transfer efficiencies z_o.

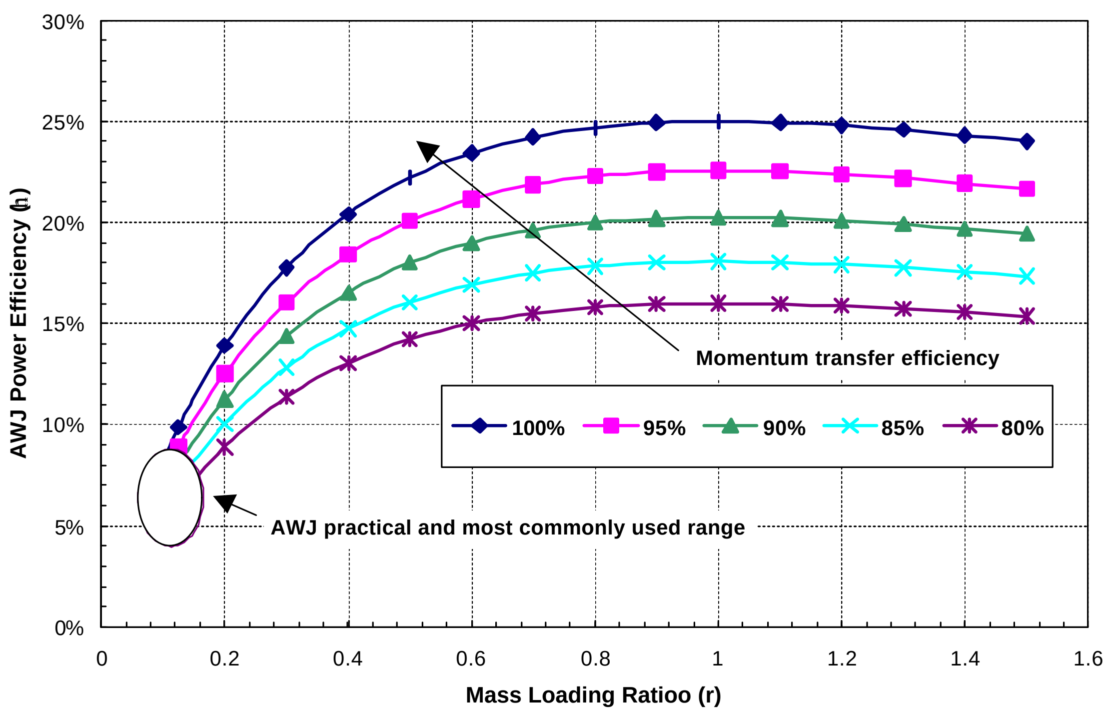

Figure 4. AWJ Power Efficiency

2.5 Mixing Visualization

To visualize the entrainment process in AWJ nozzles, a special nozzle was made using Plexiglas to show the area between the waterjet orifice exit and the entry plane of the mixing tube (19). Figure 5 shows a picture of this nozzle. The design allowed us to change the distance between the orifice and the mixing tube quite easily, as well as the rest of the abrasive and hydraulic parameters.

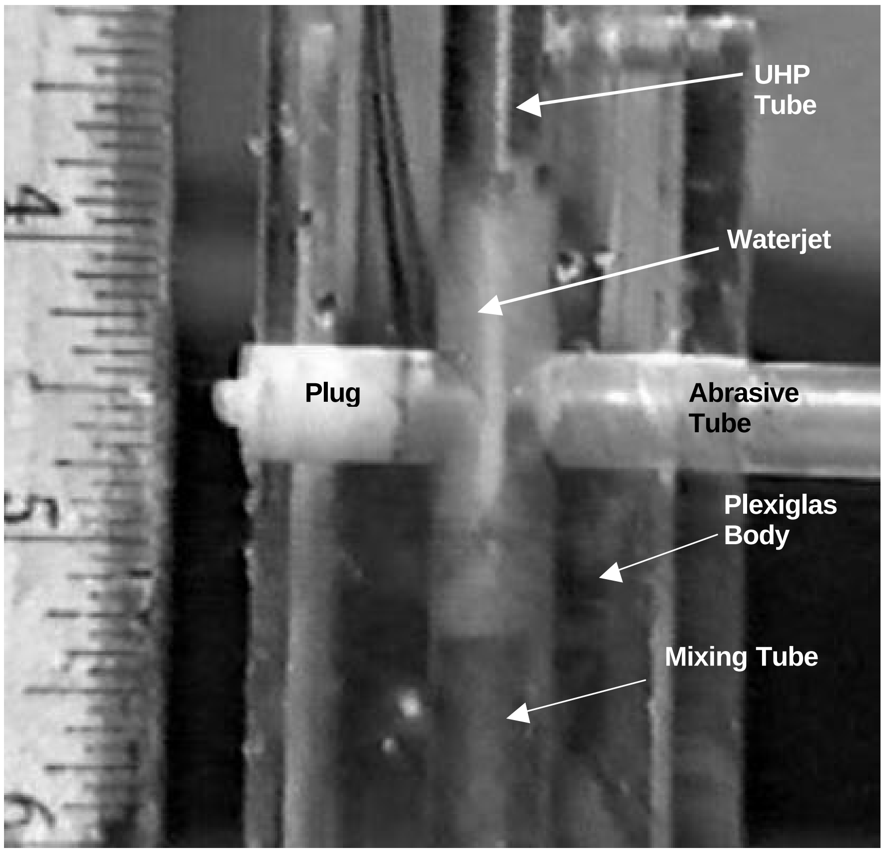

Figure 5. Plexiglas AWJ Nozzle for Visualization

Using the Plexiglas nozzle shown in Figure 5, the location of the abrasive entry port was studied. Tests were also performed without a mixing tube but with small-diameter holes in the Plexiglas instead. This allowed us to visualize the spreading of the AWJ and the extent of the wear pattern within the mixing tube. It was observed that, when the distance between the orifice and the abrasive entry port increases, the abrasive will first travel towards the orifice and impact on the bottom of the waterjet orifice holder, causing severe wear. Increasing the distance between the abrasive entry port and the mixing tube entrance caused abrasives to cake on the wall, preventing visualization. It was observed that the entrainment of relatively large particles plugs the abrasive flow. Tests clearly illustrated the need for particle sizes less than the distance of $\frac{1}{2}(d_m - d_n)$ to prevent plugging. It was observed that a vortex-type flow dominates the flow pattern in the suction zone. Osman et al. (20) performed an extensive visualization study on the interactions among air, water, and abrasives in AWJ nozzles. They emphasized that the vortex phenomenon provides the initial mechanism of abrasive entrainment.

2.6 AWJ Suction Process

The entrainment of air in AWJ nozzles is a key process for cutting performance. The air is used as a carrier of the abrasives and, thus, must be of adequate momentum and velocity to perform this transport process effectively. Studies have been performed to characterize the jet pump performance of AWJ nozzles (21). An experimental setup used to measure the air flow rate as a function of the pressure inside the mixing chamber was presented by Hashish (14). Plugging the abrasive (air) port will result in the maximum vacuum pressure inside the mixing chamber but zero airflow rates. Figure 6 shows AWJ nozzle suction characteristics at different pressures; the curves are typical of jet pump performance.

The air entrainment characteristics in feed lines (hoses) can be obtained experimentally by measuring the air flow rate at different pressure differences between the ambient pressure and the suction pressure. Data were generated for several types of feed line materials, lengths, and diameters. Figure 6 shows a sample plot of hose characteristics that can be used with AWJ nozzle characteristic lines to determine the air flow rate. Selecting conditions with adequate air flow rate is of importance for achieving a reliable abrasive feed process. However, it is important to realize here that the air velocity in the feed line is a parameter of equal importance. This velocity should exceed a certain threshold for stable flow.

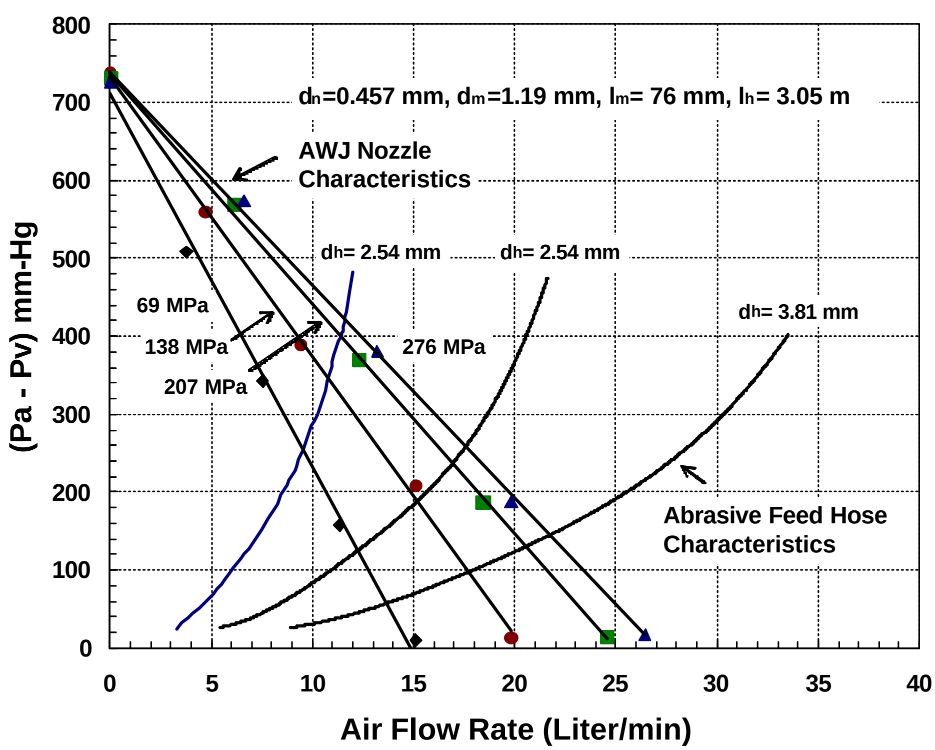

Figure 6. AWJ Nozzle and Suction Hose Characteristics

The use of vacuum assist was introduced to allow jets with weak air entrainment performance to draw more air and, thus, provide a more effective abrasive-carrying capacity.

2.7 Vacuum Assist

Vacuum assist is accomplished by adding a port to the abrasive receiving chamber in an AWJ nozzle and connecting this port to a vacuum (suction) source. Hashish, et al (2) developed AWJ nozzle vacuum assist concepts while addressing precision drilling of small diameter holes in fragile materials. Examples of these materials are ceramic-coated jet engine parts, composites, laminated materials, and glass. The sudden impact of waterjet on these materials may cause chipping, delamination, or fracture. This was either attributed to the level of high pressure or the lack of abrasives at the initial periods of jet impact. The lag time between the start of the waterjet and the arrival of abrasives to the mixing chamber may be long enough to cause the above damage. Starting the vacuum assist and establishing an abrasive flow into the AWJ nozzle prior to starting the waterjet will eliminate this lag time. The use of lower waterjet pressures to reduce the impact pressure on the material result in weak air entrainment capability and less reliable abrasive transport process to the nozzle. The vacuum assist will enhance the suction capability of the relatively low pressure or small-diameter waterjets and thus improving the reliability of the low-pressure operation.

It was observed that the size of the vacuum assist port is not a critical parameter as long as the suction air flow is sufficient for abrasives transport. Accordingly, a relatively small diameter port will be required. No studies were performed to determine the sensitivity of the vacuum assist performance to its location. However, nozzles with vacuum assist ports at 30 to 180 degrees from the abrasive inlet port have been successfully used.

It is important that the parameters of the vacuum assist be selected such that abrasives do not escape to the vacuum source when the waterjet is fully developed.

2.8 Particle Fragmentation

Abrasive fragmentation in AWJ mixing tubes has been observed (22,23). The abrasives encounter three zones in which fragmentation occurs. The first zone is on the top of the mixing tube where abrasives enter the receiving chamber and collide with the waterjet and the nozzle walls at different angles. The second zone is in the entry section of the mixing tube where the abrasives are accelerated by the waterjet and may bounce several times on the wall of the mixing tube until their velocity vector coincide with the main axial flow. In the third zone, downstream of the mixing tube entry zone until its exit, the abrasives accelerate to relatively high velocities and collide with the wall of the mixing tube at shallow angles. This may result in particle fragmentation or edge rounding.

The fracturing of abrasives inside the mixing tube is a function of several factors, such as jet pressure, orifice and mixing tube diameters, and mixing tube length. Waterjet alignment inside the mixing tube is a key factor that affects abrasive particle fragmentation. Tests were performed to study the effect of the above parameters (22). The effect of jet/mixing tube alignment is shown in Figure 7. As expected, misalignment contributes to increased particle fragmentation. This results in reduced cutting effectiveness and premature mixing tube wear. The shapes of the collected garnet, aluminum oxide, and silicon carbide particles were very similar to their original shapes, i.e., fragmented particles had the same sharpness and roundness as the original material but at a reduced size distribution.

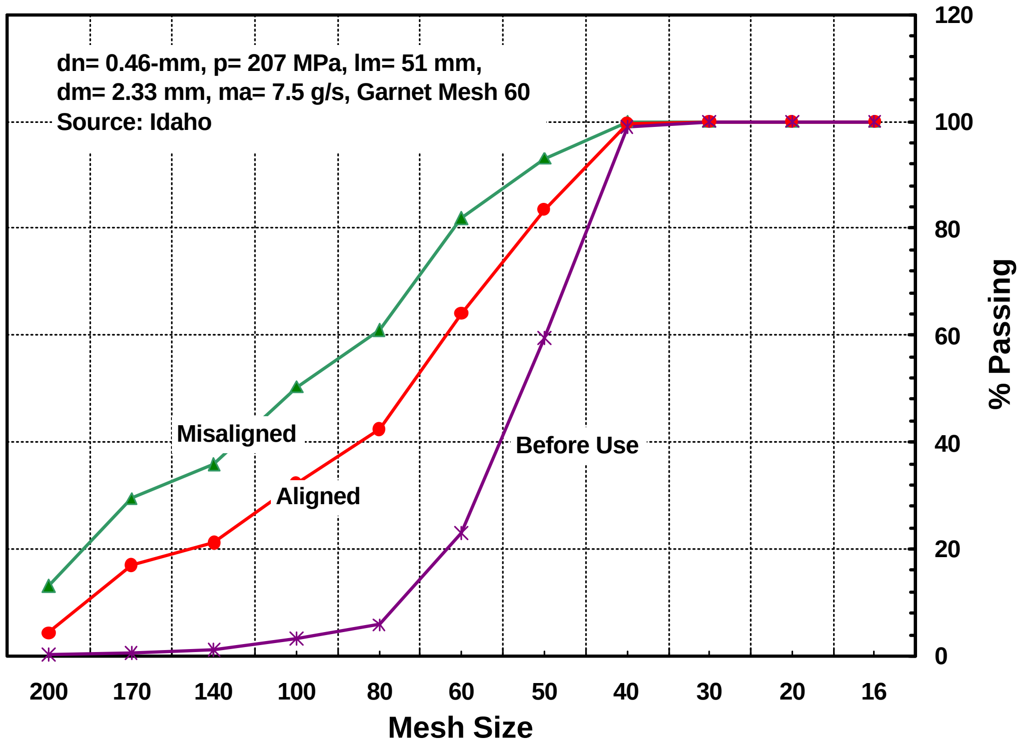

Figure 7. Effect of Jet/Mixing Tube Alignment on Garnet Fragmentation

2.9 Mixing Tube Wear

There are several axial and cross sectional mixing tube wear patterns (24). Axial wear patterns can be classified into divergent wear, convergent wear, wavy wear, and blowout wear. The following is a quick description of these patterns:

- Divergent Wear: Divergent wear will occur if the abrasives are significantly harder than the nozzle material, for example, when silicon carbide with WC, ceramic, or Roctec® nozzle material. After a period of time, the shape of the nozzle will begin to resemble the shape of the spreading jet.
- Convergent Wear: In convergent wear, the nozzle wears faster at the upper sections than at the lower sections. This indicates that the nozzle material threshold for toughness is less than its threshold for hardness. This is the most commonly observed wear mode when garnet (or softer abrasives) is used with WC and Roctec® nozzles.
- Wavy Wear: It was observed when inspecting axially split or X-rayed mixing tubes that a wavy pattern of wear may exist. This pattern is more pronounced when the ratio of waterjet diameter to mixing tube diameter is relatively low. This may be attributed to strong jet oscillations (resonance) resulting in lateral impacts. More understanding is needed for this phenomenon.

- Blowout wear: It is occasionally observed that the mixing tube fails with the jet exiting from its sidewall. This is mainly attributed to either severe misalignment or a flaw on the mixing tube material.

Cross sectional wear patterns can either be uniform or irregular. Irregularity in cross sectional wear patterns is attributed to three factors. These are eccentricity, angular misalignment, and abrasive distribution. Eccentricity results in a noncircular wear pattern but is consistent from top to bottom. Angular misalignment results in somewhat random radial wear patterns. Waterjet misalignment in the nozzle, however, is the most critical parameter that affects this type of wear pattern. Uniformly round wear patterns is observed with good jet alignment.

Table 3 shows the relationship of mixing tube wear to other AWJ parameters.

Table 3. Observed Trends of AWJ Mixing Tube Wear

Parameter	Trend
Pressure (*p*)	Weight loss varies linearly with pressure. Exit diameter initial wear rate varies linearly with pressure.
Waterjet Size (d_n)	Wear rate increases rapidly with waterjet diameter increase, approximately in proportion to d_n^{2}.
Abrasive Particle Size (d_p)	There is a size at which maximum wear rate occurs. For soft abrasives, larger abrasives result in increased wear rate.
Abrasive Flow Rate (m_a)	There is an optimum abrasive flow rate for maximum wear rate.
Abrasive Material	Most critical if certain threshold hardness is exceeded (25).
Mixing Tube Diameter (l_m)	Exit diameter wear rate is reduced as mixing tube length increases (25).
Mixing Tube Length (d_m)	The smaller the diameter the faster the initial wear rate.
ecentricity (*e*)	Significantly affect radial uniformity of wear. However, a 0.2 mm offset was found harmless by Nanduri et al (26).
Angular Misalignment (a)	Has a significant effect on wear pattern and cutting performance.
Abrasive Entry Angle (b)	Was found not to affect wear rate or pattern unless d_n/d_m is relatively small (<0.2).
Distance from Orifice to Mixing Tube (d)	Linearly affects mixing tube wear at entrance.
Nozzle Cooling	No effect was observed.

3. CONCLUSIONS

In this paper, different phenomena occurring inside AWJ nozzles have been discussed. This covered a wide range of disciplines, such as fluid flow, design, and tribology. The following is a list of factors that affect AWJ nozzle operation:

- The Reynolds number is an important parameter that affects the coherency of a waterjet. The overall orifice coefficient of discharge is a function of the pressure and orifice size.

- The AWJ suction characteristic should be combined with abrasive hose characteristic to determine air flow rates and abrasive carrying capability.
- Visualization of the mixing process showed that abrasives swirl and travel upstream in AWJ receiving chambers and accordingly they must be minimized.
- A simple abrasive acceleration model was presented to help in selecting nozzle length. Also, a simple AWJ power efficiency analysis was performed.
- Abrasive particle fragmentation is sensitive to several AWJ parameters. Jet alignment is most critical among these parameters.
- Several patterns of mixing tube wear have been presented along with reasons for these patterns to occur.

4. REFERENCES

1. Hashish, M., and Craigen, S., (1990) "Abrasive-Waterjet Nozzle Assembly for Small Hole Drilling and Thin Kerf Cutting" US Patent Number 4,951,429, August.

2. Hashish, M., Craigen, S., and Tacheron, P., (1990), "Apparatus for Piercing Brittle Materials with High Velocity Abrasive-Laden Waterjets" US Patent Number 4,934,111. February.

3. Hashish, M., and Craigen, S., (1990), "Method and Apparatus for Drilling Small Diameter Holes in Fragile Materials with High Velocity Liquid Jets" US Patent Number 4,955,164. September.

4. Hashish, M, et al., (1992) "Liquid Abrasive Cutting Jet Cartridge and Method" US Patent Number 5,092,085. March.

5. Hashish, M, et al, (1992) "Liquid Abrasive Cutting Jet Cartridge and Method" US Patent Number 5144,766, September.

6. Jarzebowicz, R., (1989), "Nozzle Attachment For Abrasive Fluid-Jet Cutting System," US Patent number 4,817,874, April.

7. Hashish, M., et al, (1994), Abrasive Waterjet Nozzle for Intelligent Control," US Patent number 5,320,289, June.

8. Hashish, M., Monserud, D., Bondurant, P., Coleman, W., Hake, J., Craigen, S., and White, G. (1993) "A New Abrasive-Waterjet Nozzle for Automated and Intelligent Machining," Proceedings of the 7th American Water Jet Conference, Seattle, WA, pp. 829-843, August.

9. Hashish, M. (1994) "Agile Machining with an Intelligent Abrasive-Waterjet System," Manufacturing Science and Engineering, ASME, PED- Vol. 68.1, pp. 887-894.

10. Geller, E. W. (1974) “The Effect of Upstream Channel Size and Turbulence on a High Speed Waterjet,” Flow Equipment Note No. 20, Flow Research Company, September.

11. Struve, R. G. (1984) “The Effect of Upstream Channel Size on the Coherent Length of High Speed Waterjets,” Flow Technical Report No. 317, Flow Research Company, Kent, WA, December.

12. Tan, D. K. M. (1985) “Reynolds Number Dependency of the Spreading Rate of High Speed Waterjets,” Flow Technical Communication No. 198, Flow Research Company, Kent, WA, December.

13. Hashish, M. (1989) "Pressure Effects in Abrasive-Waterjet Machining," ASME Transactions, Journal of Engineering Materials and Technology, Vol. 111, No. 3, pp. 221-28.

14. Hashish, M., (2002), “AWJ Studies,” 16th International Conference on WaterJetting, BHR, Aix en Provence, October, 16-18.

15. Bridgman, P. W. (1970) The Physics of High Pressure, Dover Publications, Inc., New York, First edition.

16. Hashish, M. (1981) “Simplified Analysis for Abrasive Particle Acceleration in Abrasive-Waterjet Mixing Tubes,” Flow Research Technical Note, Flow Research Company, Kent, WA, March.

17. Hashish, M. (1985) “Measurement of Abrasive-Waterjet Particle Velocities,” Flow Technical Report No. 320, Flow Research Company, Kent, WA, March.

18. Swanson, R. K., Kilman, M., Cerwin, S., Traver, W., and Wellman, R. (1987) “Study of Particle Velocities in Water Driven Abrasive Jet Cutting,” Proceedings of the Fourth American Waterjet Conference, Berkeley, CA, June.

19. Hashish, M., and, Craigen, S. C. (1984) “Video on Abrasive Waterjet Mixing Visualization,” Flow Research Company, Kent, WA, May.

20. Osman, A. H., et al. (1997) “Visual Information of the Mixing Process Inside the AWJ Cutting Head,” Proceedings of the 9th American Waterjet Conference, WJTA, Dearborn, MI, pp. 189-209.

21. Hashish, M. (1984) “Suction Characteristics of Abrasive-Waterjet Nozzle Experimental Data,” Flow Technical Report No. 319, Flow Research Company, Kent, WA, November.

22. Hashish, M. (1985) “Fragmentation of Abrasive Particles in Abrasive-Waterjet Mixing Tubes,” Flow Industries Technical Communication CTL-35, Analysis report by Altany and Associates, Inc, Seattle, WA, September 4.

23. Galecki, G., and Mazurkiewicz, M. (1987) ”Hydroabrasive Cutting Head, Energy Transfer Efficiency,” Proceedings of the Fourth American Waterjet Cutting Conference, Dornfeld, D., and Hood, M., eds., WJTA, pp. 109-11.

24. Hashish, M., (1997) “Mixing Tube Material Effects and Wear Patterns,” Proceedings of the 9th American Water Jet Conference, Dearborn, MI, August, pp. 211-222.

25. Hashish, M., (1994) “Observation of Wear of Abrasive-Waterjet Nozzle Materials,” ASME Transactions, Journal of Tribology, Vol. 116, pp. 439-444.

26. Nanduri, M., Taggart, D., and Kim, T., (1995) “Effect of Offset Bores on the Performance and Life of Abrasive Waterjet Mixing Tubes,” 8th American Waterjet Technology Conference, Houston, TX, August 26-29, pp. 459-472.

5. NOMENCLATURE

A_p	Cross-sectional area of particle
C_c	Contraction coefficient
C_d	Coefficient of discharge
C_D	Drag coefficient
C_v	Coefficient of velocity
d	Diameter of high-pressure tube
d_m	Mixing tube diameter
d_p	Particle diameter
d_n	Nozzle diameter
E	Jet hydraulic power
F_p	Force on abrasive particle
K	Water stiffness
l_m	Mixing tube length
L	Water constant
m_p	Particle mass
$\dot{m}_a$	Abrasive flow rate
$\dot{m}_w$	Water flow rate
n	Constant
P	Pressure
r	Abrasive loading ratio
R	Radius of curvature
Re	Reynolds number
S_a	Abrasive particle specific gravity
U	Water velocity
V	Volume
V_a	Abrasive particle velocity
V_j	Waterjet velocity
$V_{\max}$	Maximum abrasive velocity
V_{th}	Velocity for incompressible flow
x	Distance along mixing tube length
l	Particle velocity ratio
r	Water density at pressure P
r_o	Water density at $P = 0$
y	Compressibility coefficient of velocity
ζ	Momentum transfer efficiency
h	Power efficiency

2003 WJTA American Waterjet Conference
August 17-19, 2003 • Houston, Texas

Paper 2-D

QUANTITATIVE STUDY OF ABRASIVE CONTAMINATION IN A DUCTILE MATERIAL DURING ABRASIVE AQUA JET MACHINING (AAJM)

K. PATEL
University of Ballarat, Ballarat, Victoria, Australia

F. CHEN
Swinburne University of Technology, Hawthorn, Victoria, Australia

ABSTRACT

In the area of grit blasting it is well known that microscopically small abrasive debris get trapped on the surface and due to impact grit might cause surface fracture and fraction of it embeds. The same problem is appearing in Abrasive Aqua Jet Machining (AAJM), especially in the so-called deformation wear zone or striation zone. The experiment study undertaken here for commonly used ductile material, aluminium. The result is significant and indicating that as the depth of cut increases the grit contamination increases for ductile material. Al-Mg4, 5Mn is used as a base material for manufacturing most of the aircraft/aerospace components. The comparison study was carried out between straight cutting and oscillation cutting and it was observed that the oscillation cuts are 10 times better than straight cut for ductile material with respect to particle contamination. Alternate Technology is suggested to overcome this problem.

Organized and Sponsored by the WaterJet Technology Association

1. INTRODUCTION

Abrasive Aqua Jet Machining (AAJM) is a non-traditional machining method. Commonly know as abrasive water jet machining (AWJM) that offers a productive alternative to conventional techniques. Material removal occurs through erosion and results from the interaction between an abrasive water jet and the work-piece materials. The basics of AAJM are in detail reviewed by Momber and Kovacevic [1]. The AAJM is considered to be a very promising machining tool for difficult-to-machine materials. However, there are certain drawbacks in that technology one of which may be the contamination of the surfaces generated during the machining process by fractured abrasives. This contamination may generate serious problems with the further treatment of these surfaces, such as grinding, welding and/or coating. In aerospace materials like fibre-reinforced plastics (FRP), particles trapped between individual fibres will cause delamination. Other service properties, namely fatigue resistance, will be influenced negatively due to surface contaminants.

Although particle embedment is a short-come of this technology systematic quantitative investigation about the microscopic contamination and work about how to reduce this contamination was conducted by Chen et al. [4] on a brittle material like mild steel. Some investigations have been performed for the blasting of steel surfaces by air-driven solid particles. Griffith et al. [7] found that, the higher the blasting angle, the higher the contamination; the maximum of 9% occurred at a 90° blasting angle. Depending on the impact angle, up to 10% of a steel surface is covered by embedded grit which causes serious adhesion problems to subsequent coatings.

In this study, a quantitative microstructure analysis using scanning electron microscopy (SEM) and advanced image processing were performed to investigate abrasive embedment at the cut surfaces during abrasive water jet (AWJ) cutting for ductile material. A nozzle oscillation technique was applied to the AWJ cutting process to reduce the particles embedment and to improve the surface quality.

2. EXPERIMENTAL STRATEGY

In this study, a commonly applied industrial metal, namely aluminium was selected as a sample material. The physical properties and chemical compositions of the aluminium and unused abrasive particle materials are listed in Table 1 and 2.

Table 1. Mechanical properties of the specimen material

Property	**Material** Al 5083 (ISO R209 – Al-Mg4, 5Mn)
Density	2710 kg/m^3
Elongation	11%
Tensile strength	268 MPa
Yield strength	144 MPa

The AWJ equipment used was a Flow® waterjet cutting system consisting of a hydraulic pressure intensifier, an abrasive storage and metering device, an abrasive mixing-and-acceleration head, and a robotic traverse system.

Table 2. Elemental composition

Aluminium	Abrasive Garnet
Al = 92.74%	Fe = 50.55 %
Mg = 4.32%	Si = 22.37%
Mn = 1.87%	Mg = 9.14%
Fe = 1.07 %	Ca = 9.14%
	Ti = 2.13%
	Mn = 1.63%

The machining parameters were varied as follows: pump pressure p = 345 MPa (50,000 psi) and 380 MPa (55,000 psi); traverse rate ν_T = 2.0 m/s and 3.0 mm/s for cutting the aluminium samples. The fixed parameters were:

Abrasive mass flow rate m_a = 6 g/s;
Stand-off distance S_D = 2 mm,
Focussing nozzle diameter d_f = 1.33 mm;
Impact angle Ψ = 90° (for straight cutting)
The type of abrasive used was a commercial garnet Mesh #80.
The length of any generated cut was L = 50 mm.

Two types of cutting tests were performed. The first type involves the straight cutting of the specimen; it is called "straight cut" throughout the paper. The second type involves the use of a oscillation technique for the cutting head, oscillating the head in the X – Z plane with certain frequencies and angles. The oscillation frequency levels tested are f_0 = 3 and f_0 = 4 Hz, and the oscillation angles are Ψ_0 = 2.5° and 3.5°. This type of test is called "oscillating cut" throughout the paper. The nozzle oscillation technique and its performance were described in detail by [4] and [5].

3. ANALYSIS STRATEGY

The primary aim of this experiment is to study the effect of abrasive particle embedment at different cutting depths using straight cut and oscillation cut. This can be carried out using two distinctive different but very similar methods. Firstly, using SEM the pictures can be taken at different predefined cutting depths using same parameters like contrast, brightness, electron bombarding (excitation/ acceleration voltage), probe current and magnification. Then pictures are scanned or read with the help of image processing software. The percentage of particle embedment for a particular area can be found out for different cutting depths using the area acquired by abrasive particles and Al particles in case of aluminium.

The analysis of the surfaces was carried out as illustrated in Figure 1; it was conducted on the five depth levels shown in this figure. Two different methods were utilised to measure the abrasive contamination. However, the basic step of both methods was the microscopic inspection of selected areas from the machined surface at defined cutting depths by SEM at different modes with a magnification of 80X with back scattered and secondary electron mode.

In the first analysis method, the chemical composition was estimated from the SEM-images using image processing software. This software gives the percentage concentration of any element for a particular imaged section. The size of any scanned cross-section is 1.68 mm² (see Figure 1 below).

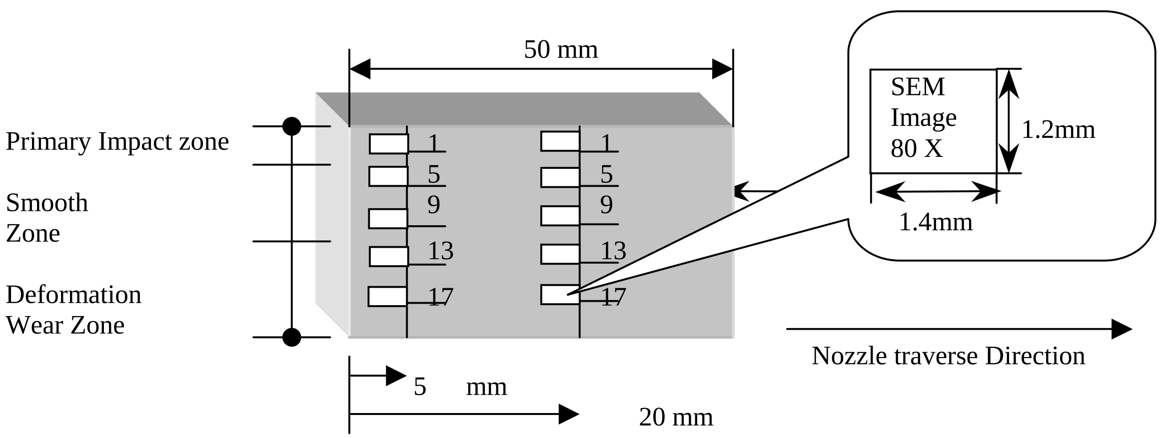

Figure 1. Analysis method for the cut surface.

This analysis method involves the estimation of the element composition of the plain sample materials as well as of the unused abrasives. The results of this part of the study are presented in Table 2.

In the second analysis method, using the SEM pictures, the chemical composition from the image can be taken out again using advanced image processing software, which can give the composition of all elemental concentration associated for a particular image area in percentage. To differ the percentage of impurity using this software was one of the challenges it was eliminating to prove that how much accurate it was? Since for all the analysis the same software was used. It is necessary to find the surface composition of materials and the unused abrasives, which can help to find out on which particular element we need to concentrate. The analysis here carried out is using second method because first was not readily available or was expensive.

It should be noted that only quantitative estimation study have been carried out. There may be difference in the value but was not any percentile difference since the same software was used. Because this method can only count the number of embedded particles, but can not differentiate the embedded particles’ sizes or the exact area occupied by the embedded particles, the results from this method were used to crosscheck the results obtained from the first method. The criterion for the contamination is the number of detected particles, N_P. After cutting sufficient care was taken for the surface which were suppose to examine, not touch ant thing which may cause loss or misleading information. We found that the elemental composition as stated in table 2.

Now, Mn and Mg are present in both materials in some to some quantity showing in-homogeneity, which may count in error so are not taken into consideration for contamination. If we take Fe and Si as major elements in percentage that can define degree of contamination then it present in particularly, in abrasive in form of FeO and Fe_2O_3, therefore it may help us in getting result for aluminium contamination. From this primary analysis, it can be said that the percentage of Si and Fe can be defined as a “Degree of Contamination (DC)” in AWJ machining. According to this analysis, the percentage of silicon (A_{SI}) and iron (A_{FE}) detected at any target surface (A_{TS}) after the AWJ cutting is defined as “Degree of Contamination” (DC) at AWJ-machined surfaces:

$$DC = (A_{SI} * A_{FE}/ A_{TS}) * 100\% \qquad (1)$$

4. Results and Discussion

In total, 120 SEM images, 120 EDX diagram (Count vs. KeV) and 120 quantitative analysis results were carried out during this research study.

In Aluminium following observations were made:

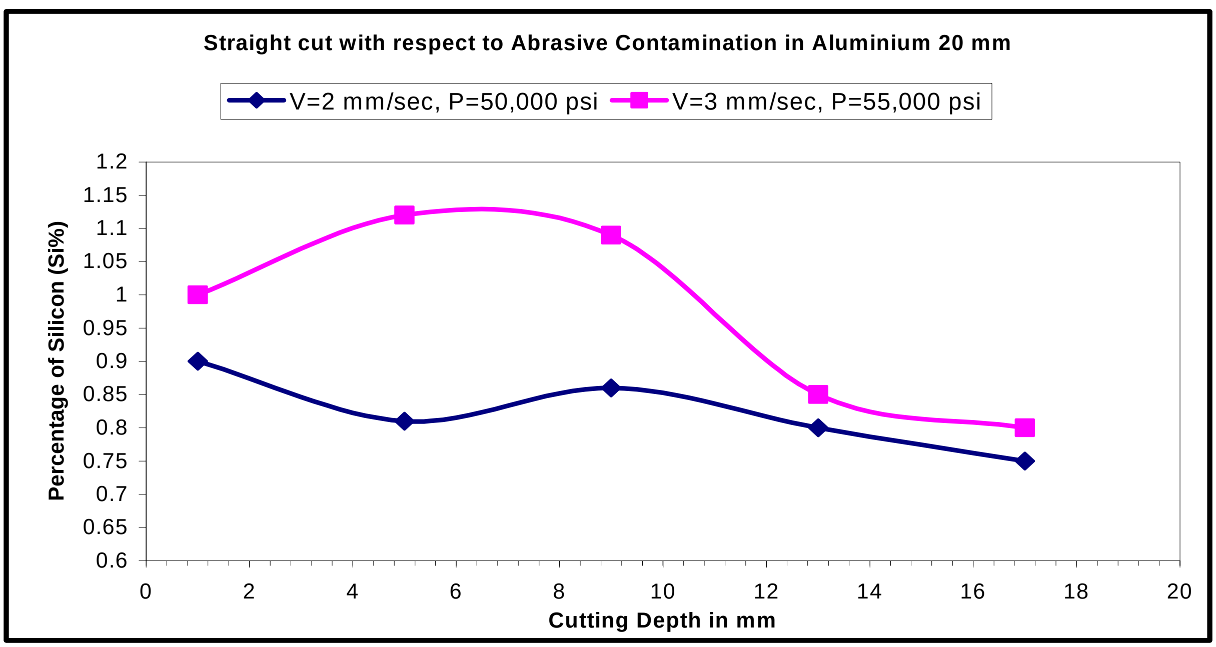

Figure 2. Variation of abrasive particle contamination in straight cutting of aluminium samples.

For straight cut,

- As pressure and traverse speed increases DC decreases by 20% (Figure 2)

- As the depth of cut increases DC decreases by 20% (Figure 2)

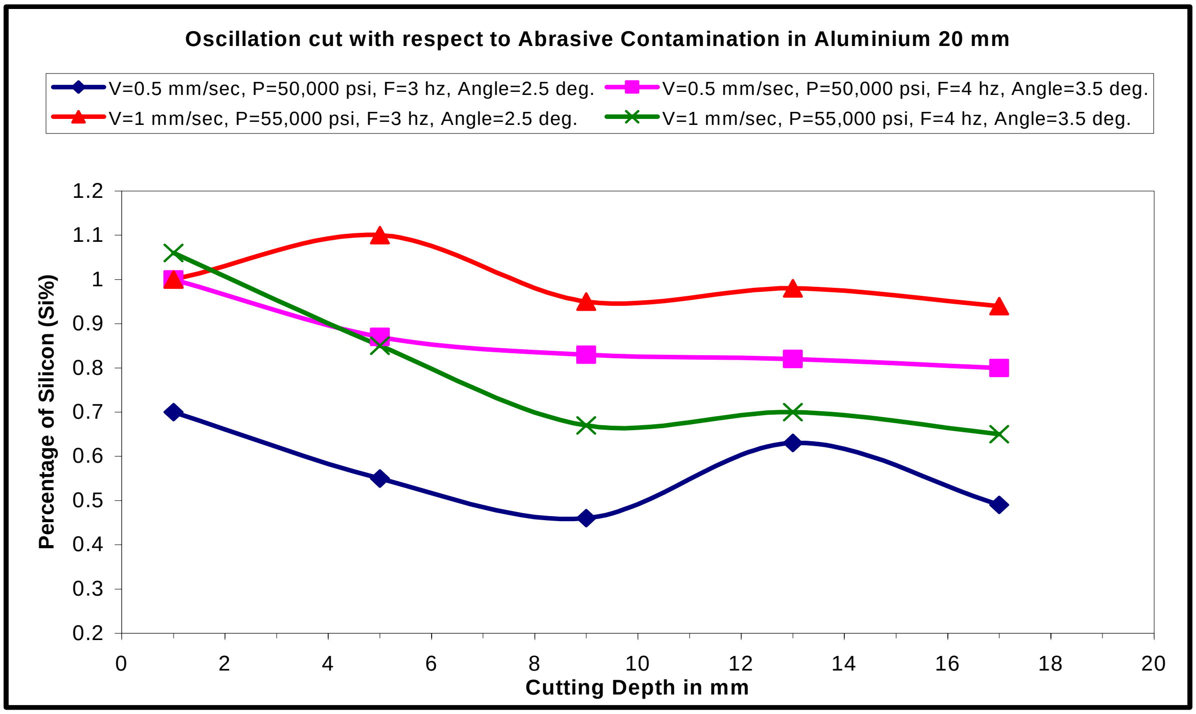

Figure 3. Variation of abrasive particle contamination in oscillation cutting of aluminium samples.

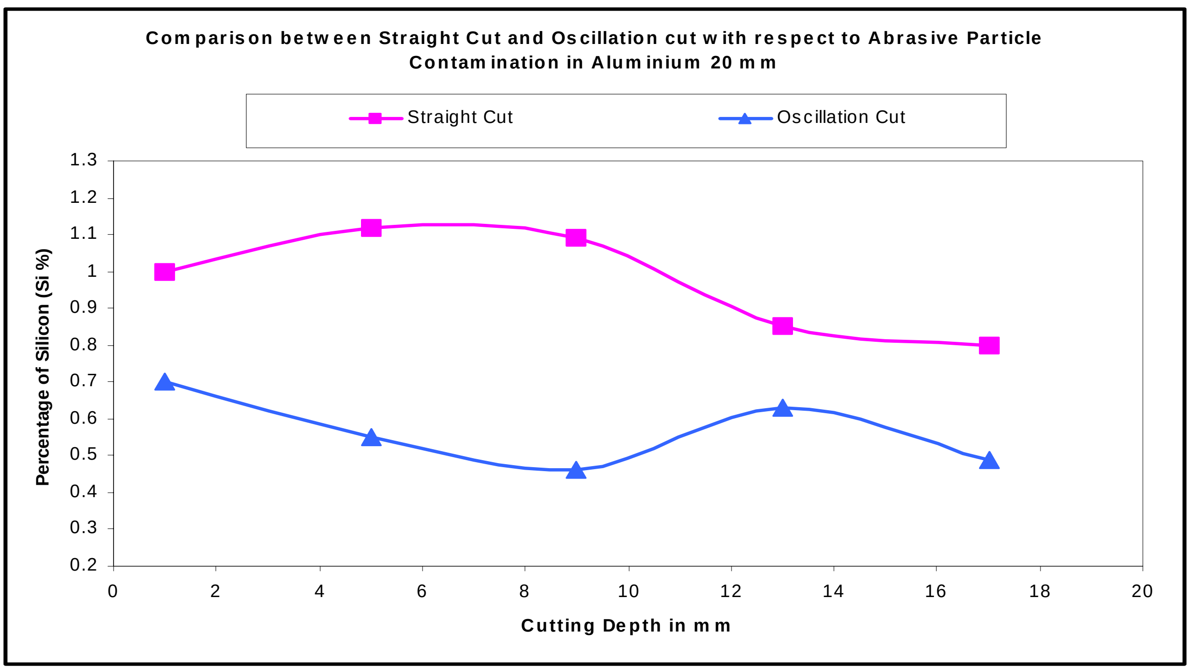

Figure 4. Comparison of abrasive particle contamination between oscillation and straight cutting of aluminium.

For oscillation cut,

- As the oscillation frequency, oscillation angle, pressure and traverse speed increases DC decreases by more than 20% (Figure 3)
- As the depth of cut increases DC decreases by more than 20% (Figure 3)
- In the smooth zone DC is nearly 0.45% compare to 1.15% of straight cut (Figure 4)

The same work was done using different technique with the help of professional image processing software. The alternative aim behind this work was to cross check the results produced by SEM elemental concentration software. While taking SEM pictures, care was taken to have same amount of illumination with respect to brightness and contrast for each picture. Any picture of material will give illumination intensity between 0 (dark) and 255 (white). The technique was adapted in this software to count the same amount of intensity of particles. It was found that embedded abrasive particles were glowing a lot. Therefore, In the case of aluminium since the whole material itself is illuminating the intensity 255 was selected and only 100% white illuminating objects was able to count. The images obtained by this software are shown in Fig. 5 & 6 for aluminium at same cutting depth. The error from this software is approximated between 1% and 5%. The following observations were made from the results obtained using particle count software:In Aluminium following observations were made:

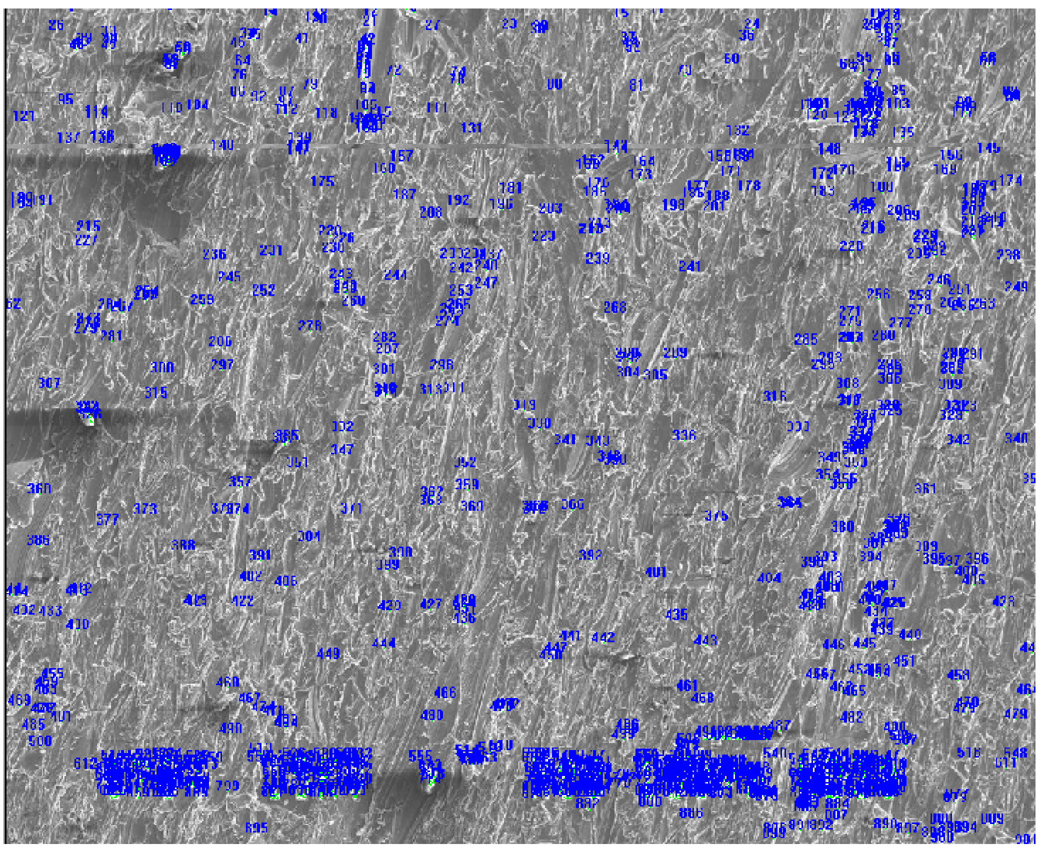

Figure 5. Particle count for straight cutting in aluminium.

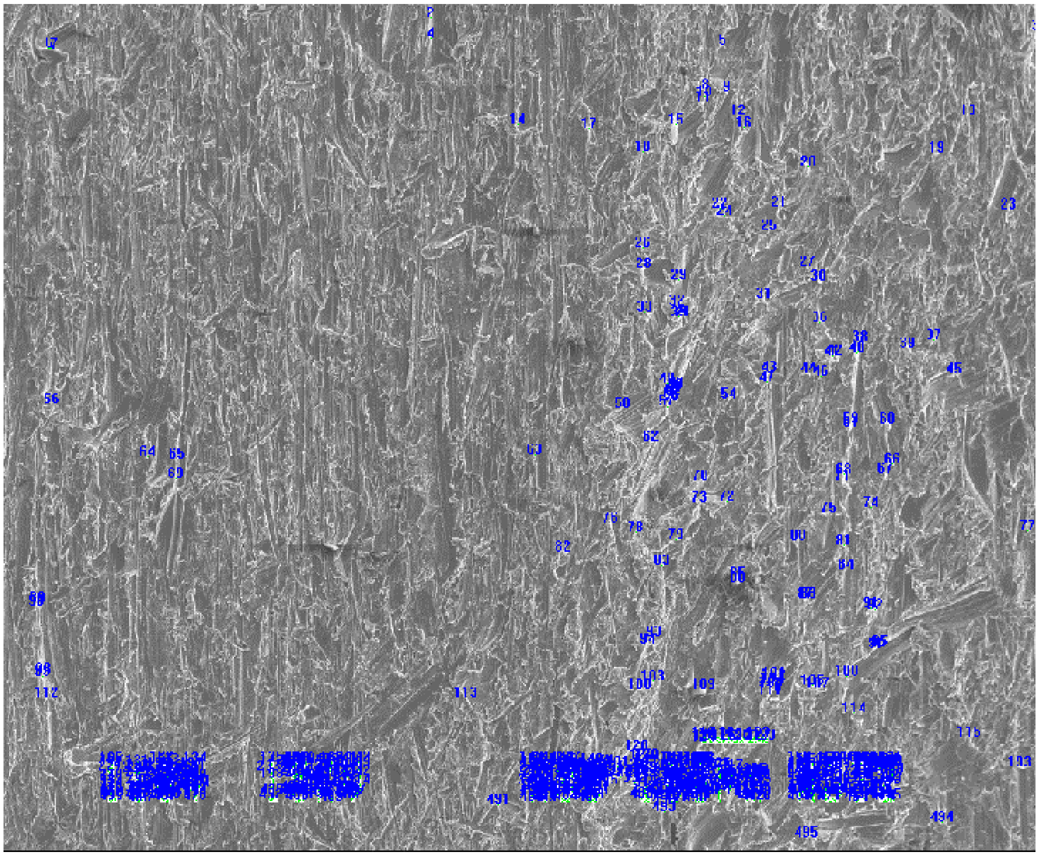

Figure 6. Particle count for oscillation cutting in aluminium.

For straight cut,

- As pressure and traverse speed increases number of particles decreases by more then 20% (Figure 7).
- As the depth of cut increases number of particles decreases by more than 20% exceptional case at v = 1 mm/sec (Figure 7).

For oscillation cut,

- As the oscillation frequency, oscillation angle, pressure and traverse speed increases number of particles decreases by more than 80%, exceptional case at v = 0.5 mm/sec (Figure 8).
- As the depth of cut increases number of particles decreases by more than 50% (Figure 8).
- Overall, considering the extreme values oscillation cut is nearly ten times better than the straight cut for aluminium (Figure 9)

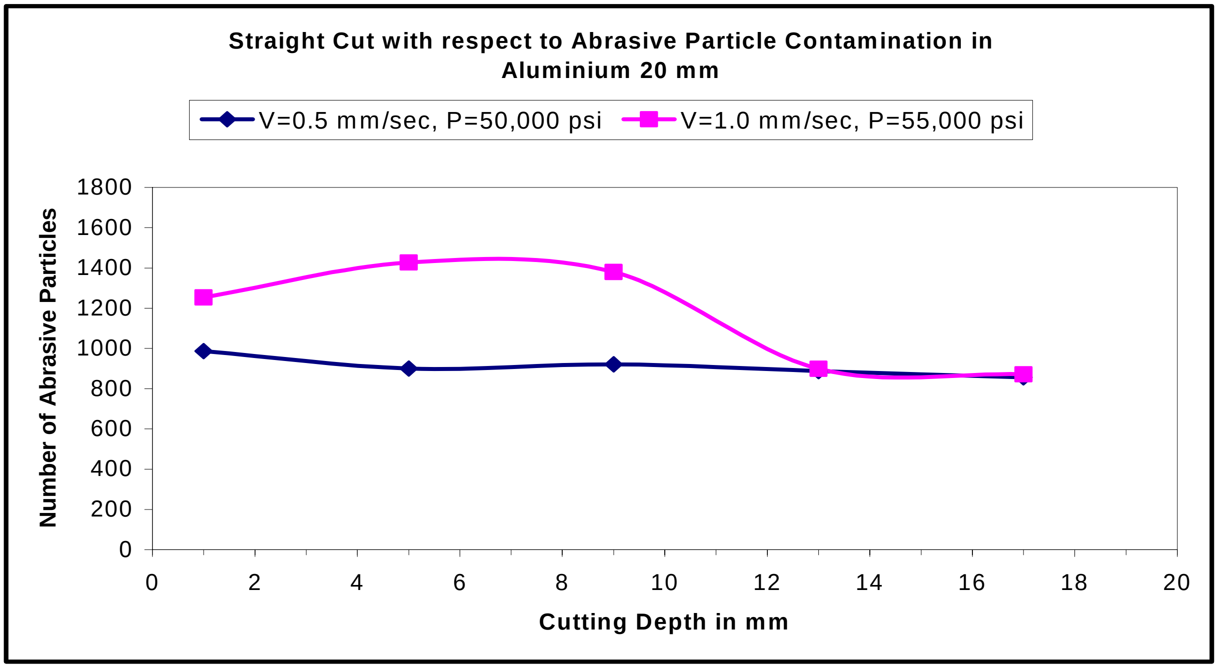

Figure 7. Straight cut with respect to abrasive particle contamination in aluminium.

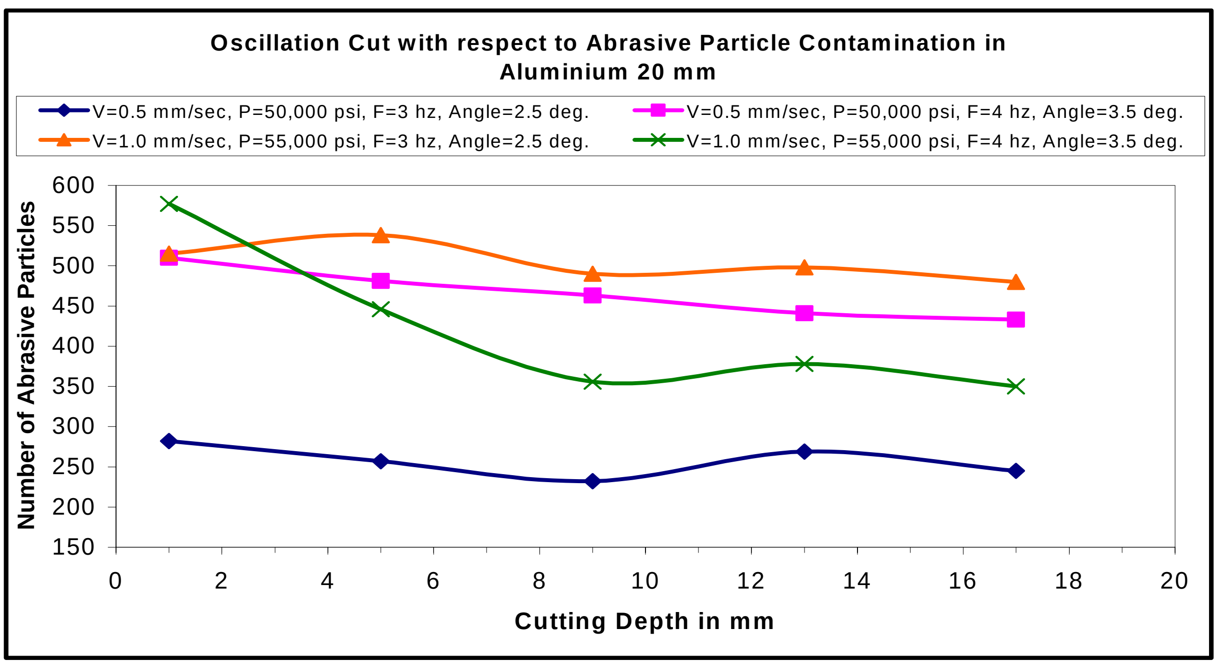

Figure 8. Oscillation cut with respect to abrasive particle contamination in aluminium

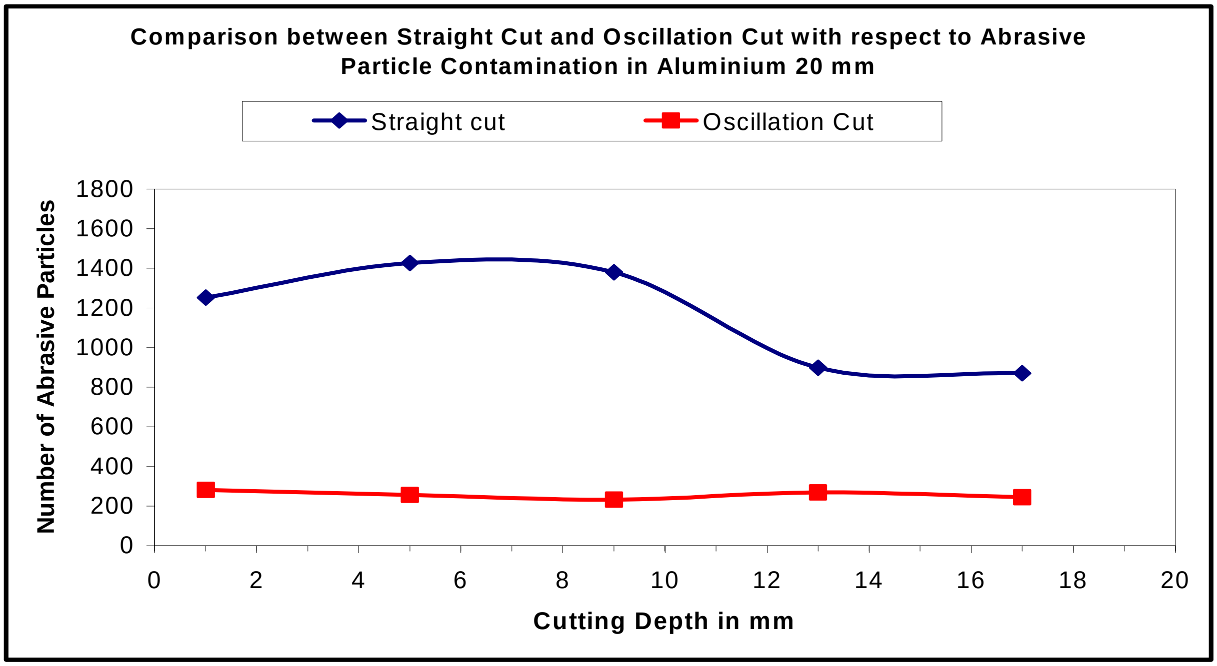

Figure 9. Comparison between straight cut and oscillation cut with respect to particle contamination in aluminium.

4. CONCLUSIONS

It is obvious from the above results that oscillation cutting reduces grit contamination ten times with compare to straight cut for ductile materials. But fails to eliminate the problem of abrasive contamination, which is critical for manufacturing aerospace/ aircraft components. The oscillation technique is limited to type of machine used for AAJM In particular, machine with a more than 3 degree of freedom.This can finally be machined easily with conventional machining operations but it is not possible in all cases where material is to be used directly after AWJ cutting because the properties of material do not allow to machine with conventional machining for example aerospace-aircraft composite material, FRP, rubber, foam, sandwich materials etc. The result of the investigation is most probably delivering further evidence for the development of the ice jetting systems since this system won't generate any grit contamination. In all samples quite amount of chlorine was also found. This leads to one step further in development of ice jet system to make sure of total elimination of chlorine if using for medical, food and aerospace industries

5. FURTHER STUDY

1. **[2]**
2. **[3]**
3. **[4]**

6. REFERENCES

[1] Momber A.W., Kovacevic R., Principles of Abrasive Water Jet Machining. Springer Verlag Ltd., (1998)London.

[2] F. Chen, E. Siores, K. Patel and A. Momber, Minimising particle contamination at abrasive waterjet machined surfaces by a nozzle oscillation technique, International J. Mach. Tools Manuf., Vol. 42 (2002) 1385-1390.

[3] F. Chen, E. Siores and K. Patel, Improving the cut surface qualities using different controlled nozzle oscillation techniques, International Journal of Machine Tools and Manufacture, Vol. 42 (2002) 717-722.

[4] K. Patel, F. Chen and E. Siores, Effect of various cutting nozzle oscillations on the abrasive waterjet cutting quality, Proc. 6th Pacific Rim International Conference on Water Jetting Technol., Sydney (2000).

[5] Siores, E., Wong, W.C.K., Chen, L., Wagner, J.G., Enhancing abrasive waterjet cutting of ceramics by head oscillation techniques. Annals of the CIRP, Vol. 54 (1996) 327-330.

[6] Siores, E., Chen, F.L., Momber, A.W., 2000, Introduction of a new precision cryogenic icejet system for processing materials. Proc. 6th Pacific Rim International Conference on Water Jetting Technol., Sydney (2000) 136-139.

[7] Griffith, B.J., Gawne, D.T., Dong, G., A definition of the topography of grit-blasted surfaces for plasma sprayed alumina coatings, ASME J. Manuf. Sci. Engng., Vol. 121 (1999) 49-53.

[8] Chen, L., Siores, E., Wong, W.C.K., 1998, Optimising abrasive waterjet cutting of ceramic materials, J. Mater. Proc. Technol., Vol. 74, pp 251-254.

2003 WJTA American Waterjet Conference
August 17-19, 2003 • Houston, Texas

Paper 3-D

POTENTIAL OF POLYMERIC ADDITIVES

FOR THE CUTTING EFFICIENCY OF ABRASIVE WATERJETS

H. Louis, F. Pude, Ch. von Rad
Institute of Materials Science
University of Hannover, Germany

ABSTRACT

Abrasive Waterjets are a multifunctional cutting tool in two senses. On one hand they can serve for different machining processes like contour cutting, turning, milling and drilling. On the other hand practically all technical materials can be processed.

However this high potential is reduced by the limited efficiency of the jet. One promising approach to increase the efficiency of this tool is the addition of polymers to the water. This changes the rheologic properties of the fluid and has influence on the jet in several aspects. The pipe friction in the tubing system can be reduced and the jet stability can be increased. These effects improve the particle acceleration process for both abrasive water injection jets and abrasive suspension jets. This leads to a shift of the optimal cutting head dimensions as well as the suspension nozzle geometry.

The influence of the polymers on the jet disintegration process and the following optimisation potential has been studied and are presented in the following paper.

1. INTRODUCTION

Abrasive waterjets are a very flexible tool in various aspects. Not only has the machining of practically all technical materials allowed their application in numerous fields. Also the large variety of process parameters allows the adaption of the jet properties to several machining tasks. This leads to the possibility of using abrasive waterjets not only as a tool for the generation of straight cuts but also for 3-dimensional contours. The variation of standoff distance and traverse rate allows the milling and engraving of contours. However due to their punctual contact with the work piece abrasive waterjets also can serve as a tool for drilling and even turning (Brandt et al., 2001).

Unfortunately the efficiency of abrasive waterjet technology as a tool in the specific machining methods is far below the competing thermal or conventional mechanical technologies. One approach to reduce this disadvantage in efficiency is to implement polymeric additives into abrasive waterjet technology and to take advantage of the positive effect known from pure waterjets.

2. POLYMER APPLICATIONS IN WATERJET TECHNOLOGY

In 1970 Franz discovered the jet stabilising effect of additives in high pressure waterjets (Franz, 1970). As additives he used substances of different type and chemical structure like glycerine, gelatine and polyethylene oxide. The strongest effect was achieved with a linear, long chained polymer, Polyox WSR-301, which lead to a tripling of the cutting efficiency and almost to the prevention of jet divergence. These findings lead to manifold research activities investigating this phenomenon. Although the effect was also studied with further polymers and the effects were quantified, the phenomena only were partly understood.

In the late 80's polymeric additives were first used for the generation of abrasive suspension jets. This type of jet is generated by a premixed suspension in a high pressure storage vessel separated by a disk piston. The suspension is indirectly pressurised by water from the pump, which drives the suspension out of the storage vessel and forms an abrasive suspension jet in the nozzle. The major task of the polymer in this process is to stabilise the suspension. High polymer concentrations, enhancing the fluid viscosity to more than 4 magnitudes allow the reduction of the sedimentation rate to a minimum. However also discovered was the fact, that the jet stability was significantly improved by the use of polymers (Hollinger et al., 1989). But due to the limited volume of the suspension and abrasive wear in valves and nozzles this method never reached technological relevance.

Recently polymers also have been applied to abrasive water injection jets. Water was replaced by a polymer solution of Super-Water, a partitially hydrolysed polyacrylamide. The cutting system however was only adapted in the way of polymer addition. The high pressure system including pump tubing, valves and cutting head remained unchanged. Although using a cutting system – not optimised for the use of polymer solutions, a positive influence of the polymer could be observed. The cutting efficiency could be increased by 20%, which also could be taken advantage of by a reduction of abrasive consumption between 25% and 30% (Holmquist et al., 2000). Therefore in this field a further efficiency potential can be expected.

3. DRAG REDUCTION

The potential of polymeric additives for the reduction of pipe friction has been investigated since the 50’s. This effect has been used not only in waterjet technology but mainly in applications of lower pressure levels, where long lengths of hoses and tubes have to be used. Typical application fields are fire-fighting, deep drilling and the improvement of the flow in sewers.

The polymer concentrations used for these applications are in the range below 100 ppm, where the fluid viscosity practically remains unaffected. Therefore the effect of drag reduction is not directly related with viscosity and Reynolds number, but the presence of the long chained molecules in aqueous solution leads to an interaction with the eddies of the turbulence. In a turbulent pipe flow there is a laminar sub-layer at the wall. Above this layer in Newtonian fluids like water the logarithmic flow profile with a relatively low velocity gradient follows. In drag reducing fluids however the molecule-eddie-interaction leads to the formation of an elastic layer between these two layers. This is characterised by a high velocity gradient so that the velocity level of the logarithmic layer, which covers the main area, is lifted (McCormick et al., 1990).

The effect of polymers on the pipe friction in waterjet cutting system has been investigated by measuring the pressure loss between the pump and the nozzle for a given pump pressure. The resulting flow rate has also been measured by collecting the fluid in an energy dissipating catcher. The polymer was a partially hydrolysed polyacrylamide, Praestol 2540. The parameters are typical for waterjet and abrasive waterjet cutting systems.

pressure:	$p = 0 \dots 300$ MPa
nozzle:	$d_D = 0{,}4$ mm
tube diameter:	$d_R = 3{,}2$ mm
tube length:	$l_R = 20$ m
polymer concentration:	0 … 0,2%

The relation between the pressure loss and the flow rate (proportional to the average flow velocity) is plotted against the polymer concentrations in figure 1.

The results confirm the perception on drag reduction behaviour from other fields. The effect is significant, but only at very low concentrations. At higher polymer concentrations the positive effect of polymers on pipe friction is lost by the increase of viscosity and consequently viscous friction. The overlay of the drag reduction effect with the viscous friction causes a minimum at very low concentrations, possibly even below 0,025%.

4. JET STABILITY

The positive effect of polymers on jet stability is well known since Franz presented his results (Franz, 1970) on the positive influence to the public. The scope of the effect ranges from the increased power density over an improved independence of the cutting result from the standoff distance to the reduced wetting of the work piece close to the cutting process (Franz, 1976). Several approaches have been followed to explain the increased jet stability of polymer supported waterjets by the increased viscosity. However the polymer solutions not only behave viscous, they behave viscoelastic.

Without outer influence the long chained molecules are coiled together leading to a strong interaction with each other, which physically causes a significant increase of viscosity. Under shear stress the molecules are stretched and aligned orthogonally towards the velocity gradient in line with the flow velocity. Therefore depending on the shear rate in the fluid the viscosity in flow direction drops whilst the damping efficiency of movements orthogonal to the main flow direction (i.e. turbulent movements) is enhanced.

After leaving the nozzle the fluid only is subjected to the surrounding air, so that the shear stresses, which it is exposed to almost disappear. Then the molecules coil up again and the viscosity increases again leading to a stronger fluid coherence. This effect refers to the elastic component of viscoelastic fluid behaviour.

The polymer influence on the jet structure has been evaluated by photography (figure 2) as well as by laser optical Particle-Dynamic-Analysis and by experiments on material damage. All methods showed the same influence of polymers on the jet stability.

This effect macroscopically the effect appears by a significant reduction of jet divergence, which can be observed in the left and middle part of figure 2 at cutting parameters. Microscopically it can be observed, that the jet structure is different. The fluid is kept together by increased cohesion forces, so that the disintegration process is delayed to larger standoff distances and is shifted to larger fluid packagess.

5. ABRASIVE WATER SUSPENSION JETS

Abrasive water suspension jets are formed in a suspension nozzle, which consists of an inlet part and a cylindrical part. The jet formation can be regarded as a pipe flow of a two-phase suspension. In this flow the mechanisms of drag reduction also become operative, so that the nozzle coefficient can be increased up to 12% by the effect of polymers. This increased fluid velocity has positive effect on the particle velocity and finally on the efficiency of the abrasive suspension jets.

However another effect is even more significant. In the nozzle the velocity distribution among the cross section correlates with the logarithmic flow profile of turbulent pipe flow characterised by high shear rates close to the wall and low shear rates in the biggest part of the section. Polymer solutions show a shear thinning behaviour, so that their viscosity is reduced by an increase of shear rate. This leads to a distribution of viscosity in the pipe flow, which is characterised by high viscosities in the main part of the flow section and viscosities in the range of water close to the wall. The high level of viscosity reduces the turbulence in the fluid, which again has an impact on the interaction between the fluid and solid particles. Figure 3 shows the figure of drag resistance between a fluid and a spherical particle.

The increase of viscosity due to the polymer solutions shifts the Reynolds Number to a range, where the force of resistance between the fluid and the particles is significantly higher than it is using water as for conventional abrasive suspension jets.

The amount of this effect naturally depends on the working parameters of the abrasive suspension jet cutting system and the type of polymer as well as its concentration. The effect shown in figure 3 refers to an abrasive suspension jet at the following parameters.

pressure:	65 MPa
abrasive flow rate:	2 kg/min
nozzle diameter:	1 mm
fluid:	Polyox Coagulant, 0,5%

These theoretical considerations have been verified by experimental investigations. The results of the cutting tests performed are presented in figure 4.

For both nozzles a significant efficiency increase can be observed by the evaluation of the depth of kerf. As to expect because of the long acceleration length and better alignment of abrasive particles the efficiency of the jet generated with the long nozzle (D9) is higher than the efficiency of the jet generated by the short nozzle (D1) for all fluids. However the increase of efficiency of the jet by the short nozzle is higher than the increase of the jet by the long nozzle. This can be explained by the fact, that the abrasive particles in the long nozzle reach a higher percentage of the fluid velocity than in the short nozzle (Brandt et al., 1998). However the improved acceleration process due to the polymer reduces this difference significantly. This underlines the theoretical considerations on the polymer influence on the acceleration process.

6. POLYMER SUPPORTED ABRASIVE WATER INJECTION JET CUTTING

Abrasive water injection jets are formed in a cutting head. A waterjet is generated by a water nozzle, passes through a mixing chamber, where it disintegrates into droplets and re-enters a secondary focussing tube. This creates a low pressure in the mixing chamber, which allows the pneumatic transport of abrasive material into the waterjet. The addition of polymers to the water reduces the jet divergence and the disintegration into droplets (figure 2). In comparison to conventional abrasive waterjets this reduces the air suction of the jet pump to a level of 70% for a polymer solution of 0,2% Praestol 2540, a long chained co-polymer on the basis of polyacrylamide. On the other hand the reduced jet divergence opens the possibility of changing the nozzle ratio to higher values (e.g. shifting the ratio between water orifice and focussing nozzle from 1:3 to 1:2). This increases the power density of the jet by the factor of 2,25.

The second major effect of polymers on AWIJs is a changed acceleration process of the abrasive particles. Independent of the type impact (elastic or inelastic) the optimal energy transfer is at equal mass of impacting droplet and impacted particle. Assuming particles of mesh 80 with an average particle diameter of 264 μm and considering the density of garnet, the optimal droplet size would be at 410 μm. Since the droplets of waterjets are significantly smaller, the fluid cohesion improving effect of polymeric additives improves the efficiency of the particle acceleration process.

The effect of polymers on the efficiency and stability of abrasive waterjets has been experimentally investigated by experiments of material removal.

The experiments have been carried out at the following set of parameters:

pressure:	300 MPa
orifice diameter:	0,4 mm
focussing nozzle:	0,8 mm x 75 mm
fluid:	Praestol 2540 solution
polymer concentration:	0% … 0,2%
tarverse rate:	1000 mm/min
standoff distance:	50 mm
abrasive:	Barton Garnet 125 μm – 180 μm
material:	AlMgSi0,5

The removal profiles are given in figure 5.

The addition of polymeric additives increases the removal depth by a factor up to 2,9. A further increase of polymer concentration does not seem to be effective, since the gain of depth from a concentration of 0,1% to 0,2% is small. On the other hand the removal width almost stays constant. The reason for this is the consistence of abrasive water injection jets containing a high percentage of air. Therefore abrasive injection jets always are disintegrated into droplets, so that the stabilising effect of the polymers on the waterjet does not significantly benefit the divergence of the abrasive water injection jets. The experiments show, that polymeric additives improve the efficiency of the generation process of abrasive water injection jets, however do not significantly increase the jet stability.

The application of polymeric additives on abrasive injection jets for cutting therefore only show effects significantly smaller. Experimental investigations on kerfing showed that the efficiency increase to be achieved not only depends on the polymer and its concentration but also on the cutting depth. (figure 6). Whereas at a depth of kerf, achieved without polymer, of 35 mm in Aluminium the polymer could lead to an increase of 32%, at a kerf depth of 16 mm (conv. AWIJ) an increase of 52% could be observed.

7. SUMMARY AND CONCLUSIONS

Polymer molecules in aqueous solution form clews; however when exposed to shear stress their chains are elongated and aligned to the current. This behaviour is reversible and macroscopically is described by shear thinning and viscoelastic behaviour.

This behaviour can be taken advantage of in various aspects of waterjet technology:

- In tubing systems an elastic layer of a high velocity gradient is formed by the polymers. This leads to an increased velocity level in the main part of the flow and finally to a loss of pipe friction. In tubing systems this appears at very low concentrations in suspension nozzles at higher concentrations.
- After leaving the nozzle the shear stress, which the fluid is exposed to, drops significantly. This causes an increase of the viscosity of the polymer solution and therefore an improved fluid cohesion, so that the jet divergence and the disintegration into droplets are reduced.
- During the formation of abrasive suspension jets the velocity profile in the nozzle forms leads to a polymer increase in the main part of the current keeping a low viscosity at the zones of high shear stress in close to the wall. The viscosity increase enhances the drag resistance between the fluid and solid particles so that the abrasive particle acceleration process is improved, which leads to an increase in cutting efficiency up to 160%.
- The increased fluid cohesion due to the viscoelasticity leading to the disintegration into larger fluid packages improves the energy transfer from the droplets to the abrasive particles. Additionally the reduced jet divergence allows changing the ratio between the water orifice and the focussing nozzle to a higher energy density of the jet. Due to the composition of abrasive waterjets the efficiency increase by polymer addition depends on the cutting depth. At low cutting depths an efficiency increase of more than 50% can be achieved.

Polymers open a large variety of possibilities of improving the efficiency of waterjets and abrasive waterjets. However they affect the jet generation processes in a multiple way, so that it is necessary to carefully examine, how the viscoleastic properties of the fluid can be taken advantage of.

8. ACKNOLEDGEMENTS

The authors are part of the Waterjet Laboratory Hannover WLH at the University of Hannover and members of the German Waterjet Society AWT.

9. REFERENCES

Brandt, S.; Louis, H.; Milchers, W.; Mohamed, M.; Pude, F.; von Rad, Ch., “Abrasive waterjets – a multifunctional tool for advanced materials”, *Proceedings of the 7th European Conference on Advanced Materials and Processes*, The Federation of European Materials Societies, 2001.

Franz, N. C., “High velocity liquid jet”, *United States Patent, 3,524,367,* 18th August 1970.

Hollinger, R. H.; Perry, W. D.; Swanson, R. K., “Precision cutting with low pressure abrasive suspension jet”, *Proceedings of the 5th American Waterjet Conference*, pp. 245-252, WJTA, St. Louis, 1989.

Holmquist, G.; Howells, W. G., “The effectiveness of Super-Water® in venturi abrasivejet cutting – a preliminary examination”, *Report No. 5*, Göteborg, Sweden: Chalmers Lindholmen University College, 2000.

McCormick, C. L.; Hester, R. D.; Morgan, S. E. Safeddine, A. M., “Effects of molecular parameters, salvation and polymer associations on drag reduction performance”, *Macromolecules*, Vol. 23 (1990), pp. 2132-2139.

Franz, N. C., “The interaction of fluid additives and standoff distance in fluid jet cutting”, *Proceedings of the 3rd international symposium on jet cutting technology*, pp. A5/67-A5/75, BHRA, Cranfield, 1976.

Brandt, C; Brandt, S.; Louis, H.; von Rad, Ch.; von Berlepsch, T., “Modelling of the particle acceleration in suspension jet nozzles”, *Proceedings of the 14th Conference on Jet Cutting Technology*, pp. 119-129, Professional Engineering Publishing Ltd., London, 1998.

10. FIGURES

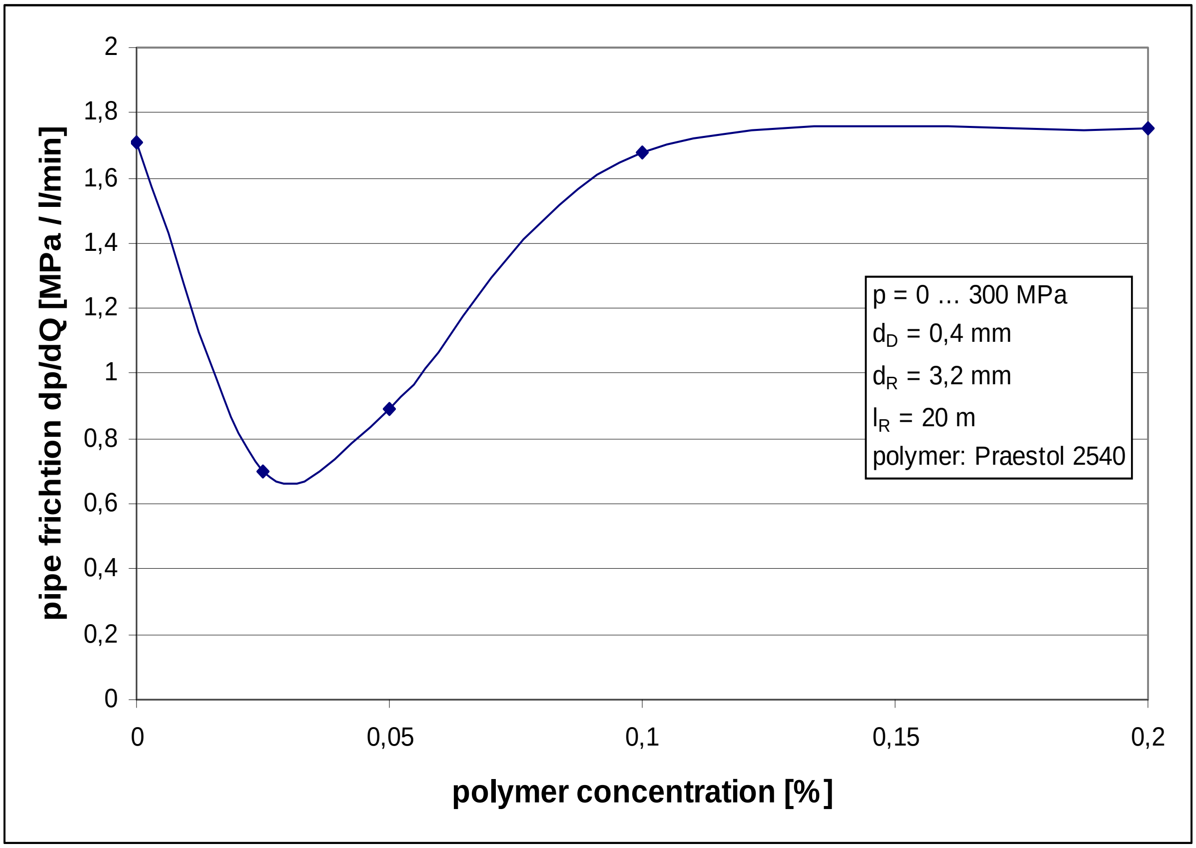

Figure 1: Pipe friction as a function of polymer concentration

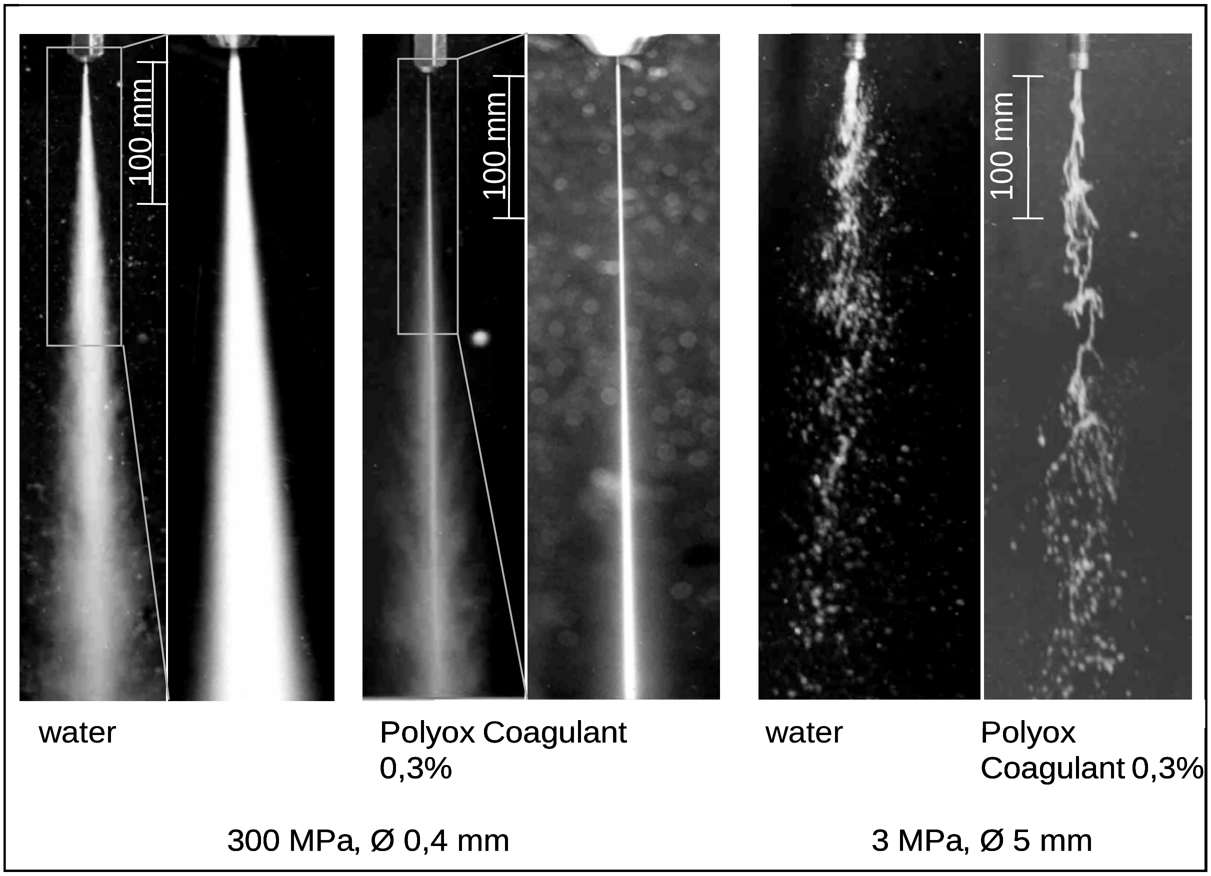

Figure 2: Jet stability of waterjets and polymer supported waterjets

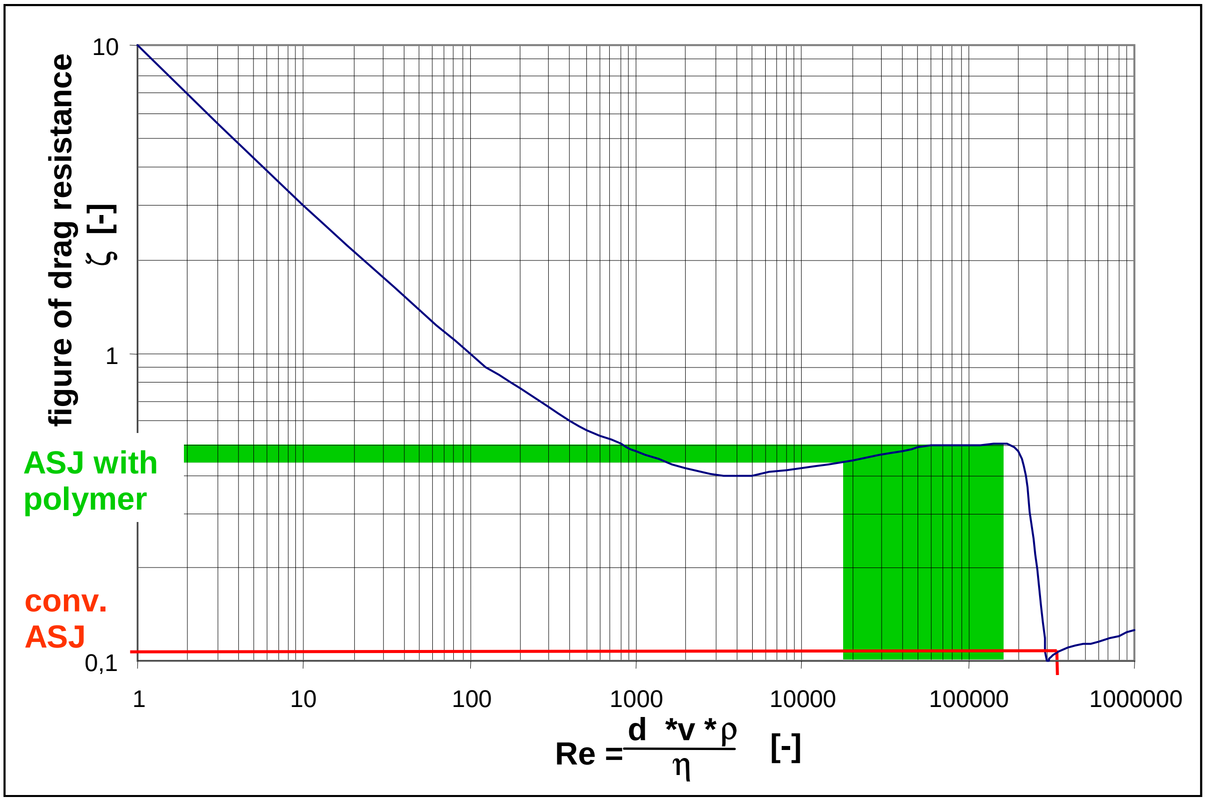

Figure 3: Drag resistance of spherical particles in flowing fluids

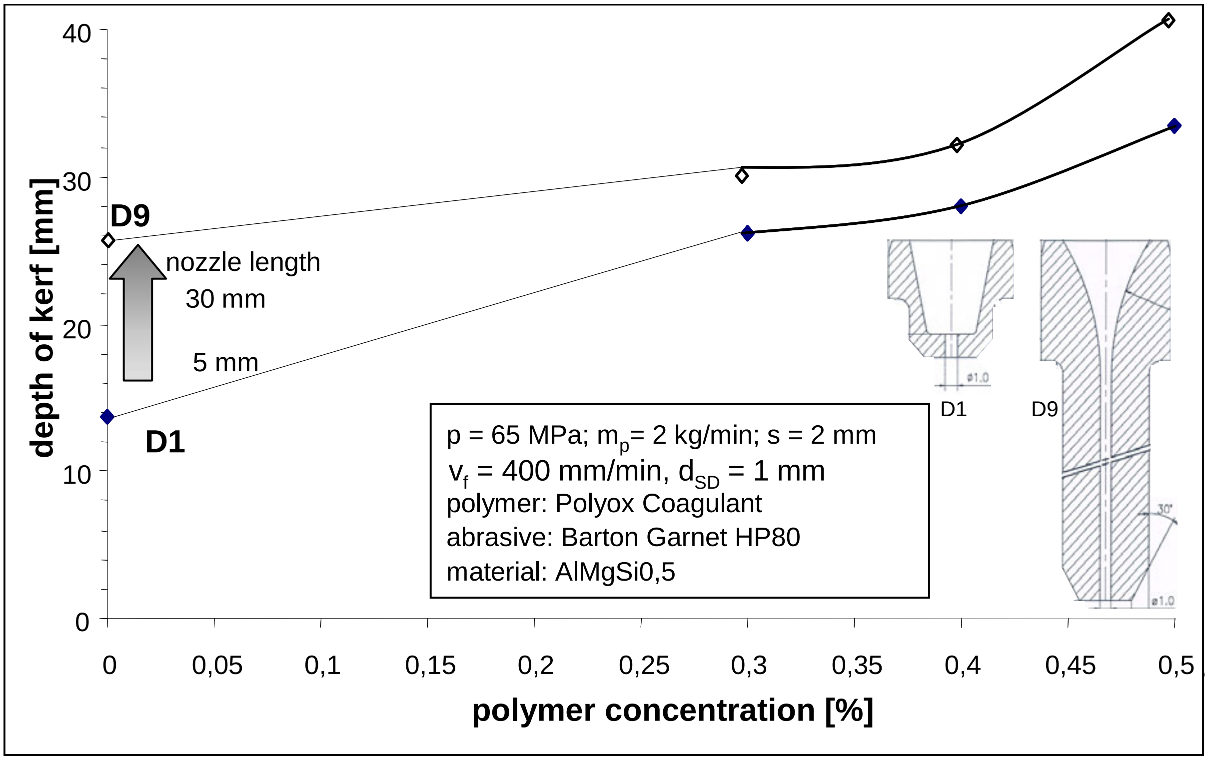

Figure 4: Polymer influence on cutting efficiency of abrasive water suspension jets

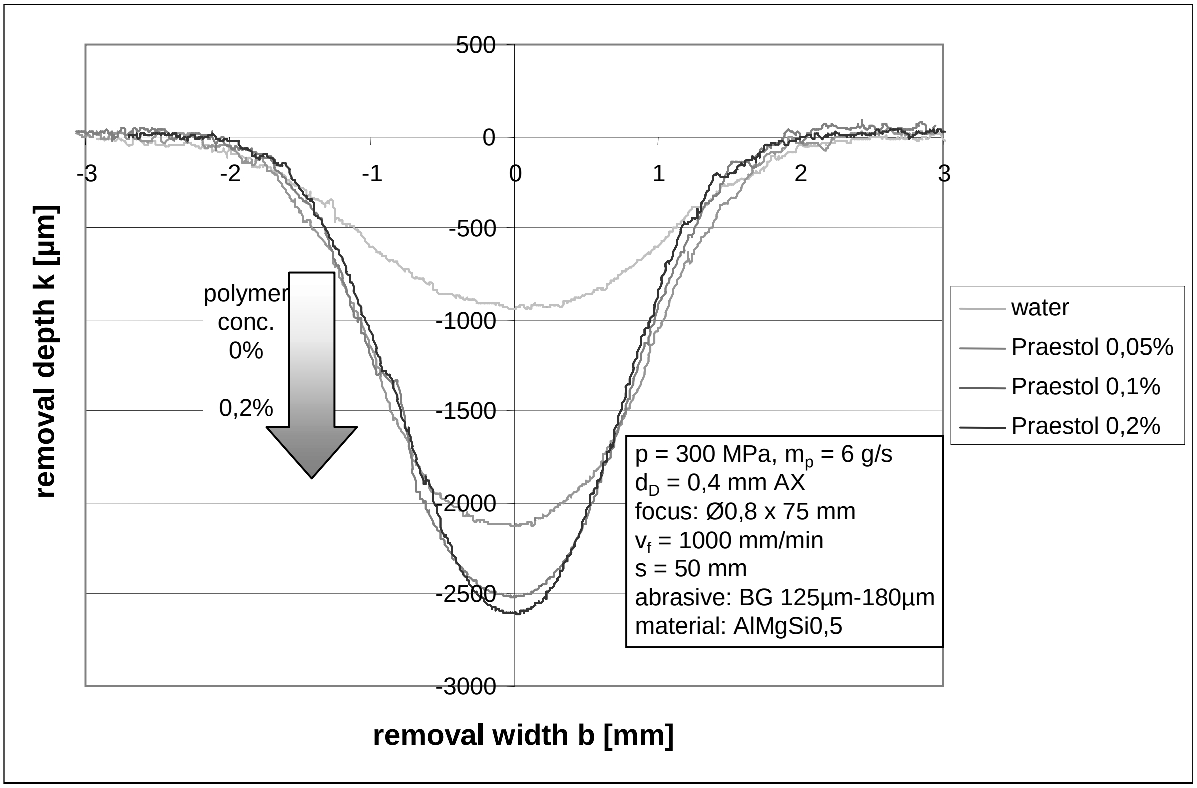

Figure 5: Polymer influence of removal profile of abrasive injection water jets

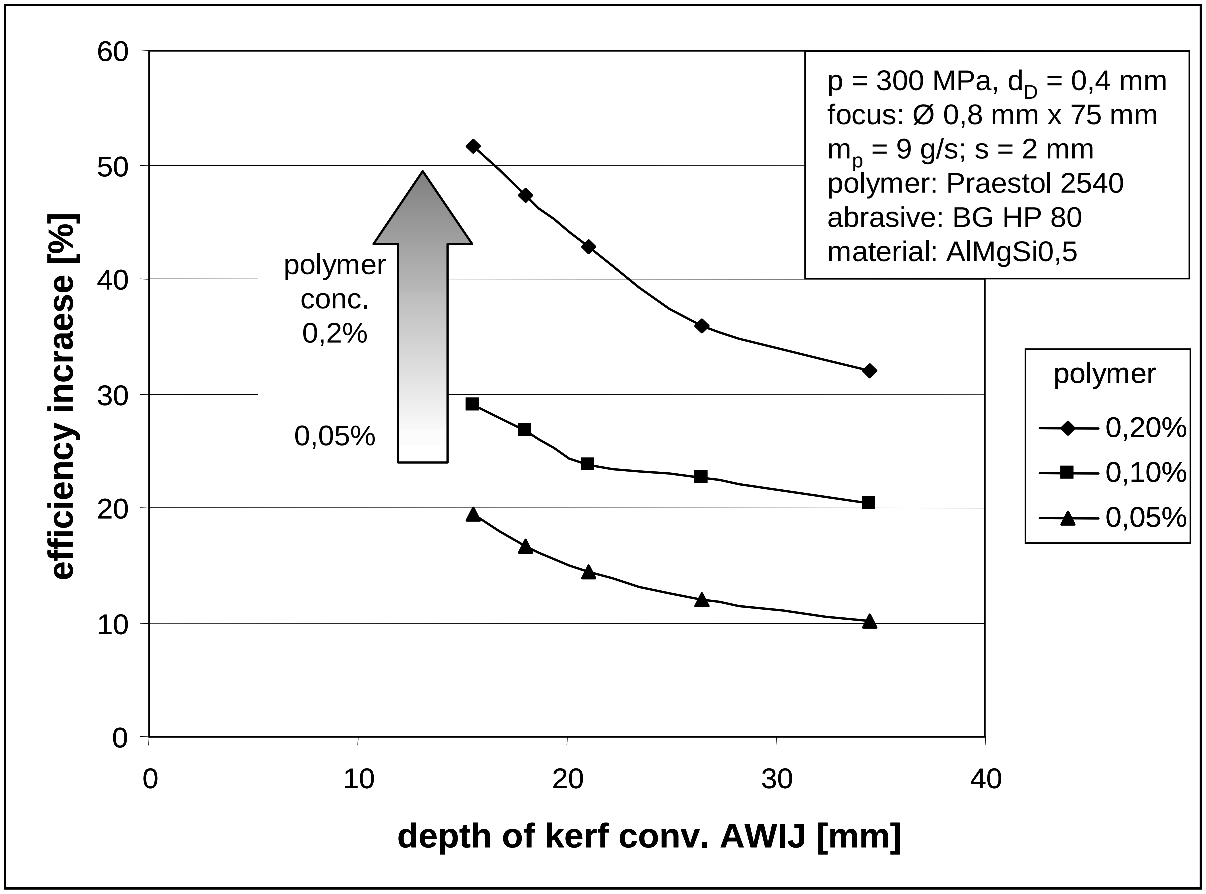

Figure 6: Relative efficiency increase at abrasive water injection jets by polymers

2003 WJTA American Waterjet Conference
August 17-19, 2003 • Houston, Texas

Paper 4-D

BENDING RADIUS DEPENDENCE IN AWJ MACHINING OF STONE FREE-FORM PROFILES

M. Monno
Dipartimento di Meccanica, Politecnico di Milano
Milano, Italy

Carrino L., W. Polini, S. Turchetta
Dipartimento di Ingegneria Industriale, Università degli Studi di Cassino
Cassino (FR), Italy

ABSTRACT

Artistic works represent a wide field of application in natural stone. The traditional process uses a diamond mill, which rotates on its own axis, cutting a marble marquetry characterised by a free form profile. The abrasive water jet cutting of marble has demonstrated to be an effective alternative to the traditional process.

The present work reports an experimental study on the ability of the AWJ technology to cut profiles of different bending radii through different values of the AWJ cutting parameters. The deviations of the machined profile from the designed one has been assumed to estimate the ability of AWJ technology to machine marble free-form profiles. A 2D shape that is industrially used for decorative applications has been used as sample. It has a complex geometry that may be schematically represented by a sequence of circles that are characterised by many different radii. A set of experimental free-form cuts has been performed on Perlato Royal Coreno marble and the generated profiles have been measured in order to identify their geometric deviations from the designed one. The geometrical deviations have been put into relationship with both the process parameters and the profile bending radius. The obtained results have been compared to those achieved by the traditional diamond mill technology. The efficacy of the two alternative processes have been investigated and compared. Technical and economical aspects have been discussed.

Organized and Sponsored by the WaterJet Technology Association

1. INTRODUCTION

Artistic works represent a wide field of application in natural stone. Free-form profiles are involved in internal and external paving of civil house and monument. Once realised manually, the mosaic paving are now mass-produced by means of traditional or innovative machining technologies.

The traditional process uses a diamond mill, which rotates on its own axis, cutting a marble marquetry characterised by a free form profile. This is an old technology that involves both process and tool parameters whose values are defined on the base of the experience of builders and end-users.

The abrasive water jet cutting of marble has demonstrated to be an effective alternative to the traditional process. A limit of AWJ technology is the quality of the cutting surfaces: the morphological characteristics of AWJ generated surfaces present a great scattering as the process variables are changed or as the distance from the impinging surface is increased (Miranda et al., 1993). A critical aspect in the stone field is the aesthetic appearance. This means that the quality of the manufactured products is a fundamental variable, but it seems not to be influenced by the morphological parameters, such as roughness or waveness, of the cutting groove surface. The functionality of the stone products is preserved whatever the value of the morphological parameters.

Different approaches exist in literature studying the relationship among process parameters and cutting efficiency. Cheung et al. (1976) compares a submerged water jet with a free jet operating in air for concrete and red granite cutting in terms of cut depth. Matsuki et al. (1988) deepen the comparison considering the influence of the impinging angle and stand off distance on the depth of cut in rock machining. Koyohashi et al. (1990) introduce further parameters, such as rock temperature, physical properties of the rock, water jet pressure, nozzle diameter, traverse speed rate and stand off distance whose influence on cut depth is analysed. Bortolussi and Ciccu (1993 and 1996) studied the relationship between the cutting specific energy or the specific erosion and the jet parameters on one side, and the rock-related properties on the other. Miranda et al. (1996) analysed the fractured surfaces machined with different values of the water pressure, the abrasive flow rate and the feed rate on Rosa de Borba marble and Moca Creme calcareous stone. All these works consider only the penetration capability of jet inside the stone material involving the minimum cutting energy without taking into consideration the further important factor that is the machined quality.

The present work reports an experimental study on the influence of the AWJ cutting variables on the quality of marble free-form cuts, that is on the deviations of the machined profile from the designed one. The cutting of free-form profile, generally called contouring, represents the main application of AWJ together with the quarry excavation. It is commonly used to produce decorations or ornamental products, such as flooring, covering and so on.

The present work reports an experimental study on the ability of the AWJ technology to cut profiles of different bending radii through different values of the AWJ cutting parameters. The deviations of the machined profile from the designed one has been assumed to estimate the ability of AWJ technology to machine marble free-form profiles. A 2D shape that is industrially used for decorative applications has been used as sample. It has a complex geometry that may be schematically represented by a sequence of circles that are characterised by many different radii. A set of experimental free-form cuts has been performed on Perlato Royal Coreno marble and the generated profiles have been measured in order to identify their geometric deviations from the designed one. The geometrical deviations have been put into relationship with both the process parameters and the profile bending radius. The obtained results have been compared to those achieved by the traditional diamond mill technology. The efficacy of the two alternative processes have been investigated and compared. This work deepens the consideration of Carrino et al. (2001).

2. MARBLE USE FOR FLOORING

The use of natural stone is very important for the carrying out of flooring, as regards the functional and perceptive aspects, they guarantee an excellent reaction when put into practice. It is in the perceptive field that their performance and expressive capacities are compared to those of many other materials susceptible to analogous destination and gain a characteristic quality thanks to the possibility of original decorative creations, particularly sought after for delegation places and for personalized environmental solutions.

The superficial aspect of the flooring determines important consequences on the spatial perception of the internal environment and takes on formal implications which the designers very often consider in an inadequate way.

It is enough to think of the effects that design and colour of the flooring produce on the perception of a three-dimensional space: floors and ceilings are at par, even if they only define horizontal surfaces that outline the environment, they are able to influence the entire internal space.

It is not enough to plan the building as a functionally integrated whole of inhabited spaces, carried out by closing and carrying structural elements, and an operative device of technological systems etc. However, a specific plan of each single internal flooring is necessary. In fact the flooring can constitute the characterizing element of certain premises or the starting point to plan the alterations of an internal environment.

The generating elements of the design of flooring, which in architectural terms can create the aesthetic and perceptive values, are the type of material, the colour, the surface finishing and the geometry-laying. The material used for the flooring can be of both type: natural and artificial. Naturalness and artificiality have different properties, but most of all they have different ways of perception, which although subjective, meet with the cultural reference and the collective memory of the consumers.

The sensation of the colour not only depends on the type of material, but also on the conditions of the surface which can be more or less smooth or rough, shiny or opaque, bright or dull, which the material shows at the moment of the extraction or is given by subsequent surface processing.

The geometry-laying of a flooring is influenced by the used type of elements. It is possible to take these elements back to two fundamental typologies: it turns out that one is based on the use of trimmed slabs, while the other on the use of tiles.

Trimmed slabs carry out flooring where the choice and the processing of the material take place only on the basis of a precise work order. On the other hand the dimension and the conformation of each slab are fixed on the basis of a plan especially elaborated in relation to the architectonic characteristics of the environment and of the designer's constituent aim.

Therefore, it is a very personal solution able to guarantee the utilisation of the decorative valence of natural stone material, moreover it allows to insert specific ornamental motifs able to satisfy all the needs of prestigious environments. The other typology of implementation, based on the use of mass-produced tiles with standard dimensions according to the producers' choice, are widely differentiated from the solution of trimmed slabs. This is due to the fact that as the design of the flooring is bound to the prefixed shapes and dimensions for tiles, but also to the possibility of matching them.

Polished tiles allow to simplify and quicken the lay down, as they can be put in practice through gluing and do not need further finishing.

Geometry-laying is linked to the decision of producing stone elements in conformity with standard size, from which the name laying derives. It is carried out by mass-produced elements or it can be prepared in accordance with planned measures, from which the name lay down derives, carried out by elements which are not part of a mass-production.

The flooring made from elements which are not taken mass-produced is obtained by using slabs with given dimensions, shapes and veins which are selected in the planning stage. These slabs are selected based on the plan of the environment. In this range of solutions there are various types of lay down geometry. They include: lay down geometry with polygonal elements and lay down geometry for elements with curved sides. The first can be made up of designs which are complex, unique or repetitive. They require a specific planning of details for the reproduction of geometrical and chromatic schemes and have a remarkable decorative effect. The second one is analogous to the first, however, it is more difficult to implement due to the adoption of elements from various curve shapes. Marquetry coverings also belong to this category of flooring – flooring which displays particular designs such as rosettes, décor and centres of premises. They are achieved with marquetry techniques or gluing with shapes and combinations of suitable material in order to obtain their aesthetic characteristics. The marquetry technique is achieved by inserting thin elements into the predisposed area in the bigger and thicker slabs. The gluing technique makes provisions for element assembling, having complementary shapes. This is done on a base which is made up of a slab with a thickness which is lower than the final one. At the same time it bears a shape which is the same as the final one. Using these solutions helps obtain designs which are located in defined areas or developed all over the flooring. They may have remarkable chromatic and decorative properties which are due to the ability of geometric compositions bearing more complex shapes and curved lines.

The production process of flooring that is constituted by curved elements consists of the following stages:

1. the cutting of the components which make up the flooring
2. the assembling of the components
3. gluing and puttying
4. surface finishing
5. packaging (if necessary)

The critical stage of the process is the cutting of the components. The final quality of the product strongly depends on the quality of the cut of every single component. At the moment regulations regarding the rules and measurement procedures for the quality standards of products being tested do not exist. The required standards can be divided into two categories: medium and high standard of quality. Medium standard of quality makes provisions for the manufacturing of components which, upon assembling, allow for the presence of a space between a piece and another with a 1 mm length. It is only under one condition that the problems tied to the quality details of the cut surface do not exist. This is when the cut simply runs through the material such as the coinciding of the cut grooves, the wave on the wall of the groove and the roughness, which are evaluated on a width of 10 mm, do not obstruct the assembling of the components. For the processing which requires a high standard of quality, in other words, or for products assembled with minimum leak lines of 0.5 mm, more accurate cut operations are required compared to the first type. This is so in order to obtain coinciding parameters and form error which are contained. A relevant aspect for the quality of the product is related to the dimensional control of the cut profile. This kind of error determines both the size and the constancy of the leak along the profile once various elements have been assembled. This is important especially when cutting natural stone using water-jet because even by using the correct radius of water jet, the obtained real profile may at times manifest evident distortions in comparison with the plan.

Distortions of this type are due to the nature of the material and to the acceleration and deceleration transitor of the machine’s axle. Natural stone materials can display strong structural characteristics that are characterised by a strong anisotropy, with different areas in the part that offer resistance to variable removal. Depending on the trajectory taken from the top of the cut compared to the weaving of the material, cuts with variable lengths can be obtained and are hard to control. Another characteristic is the porosity of the material which, in a way, can help the cutting process however it may also cause problems as far as the prediction of cut length is concerned. The complexity of the trajectory that has to be taken in some parts of the profile causes an acceleration (the speed of advancement) which is different from the one established. This is due to the fact that the lengths of the spaces for acceleration and deceleration which are necessary to reach the established cut speed, can be greater than the pieces of profile which are present between two discontinuities. Consequently, there will be areas with nominal cut speeds alternating in areas in which speed cut is inferior, with a greater erosion on the jet’s behalf. Therefore giving a groove length of greater cut. These elements do not usually obstruct the composition of the final product, however, they might provoke a defect such as the presence of stucco in various lengths among the single components. This has a negative effect on the appearance of the assembled product. Furthermore, the quality of the product depends on the used process parameters. Currently, companies that work natural stone do so based on the empirical indications received from the tool supplier. This usually becomes a solution, however, none of the work is done to optimise the tools, the labour, the reduction of waste to lessen its impact on the environment, or to improve the working conditions for the labourers involved.

3. EXPERIMENTAL PROCEDURE

3.1 Test material

A stone material exhibits a hardness, which renders it difficult to machine, and a very low thermal expansion coefficient, which makes it suitable for external applications.

The experimental material was Coreno Perlato Royal marble. It is mainly constituted by $CaCO_3$ with inclusions of seaweed and fossils that produce light and dark spots appreciated from an aesthetic point of view. Its mechanical properties are higher than those of White Carrara marble, as shown in Table 1, indicating that this material could play an important role in many civil applications.

3.2 Experimental phase

There are a lot of possible 2D shapes of a marquetry constituting a flooring that may not be classified on the base of standard feature, such as circle, square and so on. In general they are very complex, because of their irregular profiles, making the machining very hard. This means that the cutting shape deeply influences the resulting quality when it is related with the process parameters. Therefore, it is needed to accurately analyse the cutting shape before starting the machining in order to optimise the choice of the process parameters. It is not possible to define general considerations, which result independent by the shape to cut, in order to ease the machining. The attention has been focus on a 2D shape that is industrially used for decorative applications (see Figure 1). It has a complex geometry that may be schematically represented by a sequence of arcs of circles that are characterised by many different radii, as shown in Figure 2. This shape has been used as experimental geometry in the following and it has been cut by slabs of 10 mm thickness. In fact 10 mm is the value of the flooring thickness commonly used for decorative applications.

The traditional technology uses two diamond mills to cut the experimental shape. A mill of 15 mm diameter that produce a rough geometry and divide it from the slab, as shown in Figure 3. Finally a finishing cut produces the marquetry shape by a mill of 3 mm diameter (see Figure 3). The tool characteristics are the result of a specification particularly suitable for machining Coreno Perlato Royal material, as recommended by diamond tool producers. The value of the tool rotation speed industrially used is about 5000 rpm, while the feed rate is a function of the tool diameter. Its value is higher for 15 mm mill than for 3 mm mill. This is due to the reduced tool resistant section. An equivalent feed rate may be calculated by considering the ratio between the cutting length and the whole cutting time: it is equal to about 112 mm/min. A sample of six shapes has been produced by means of traditional technology with the previously defined parameters.

The machining of stone or marble represents the main field of AWJ application together with gasket cutting. However, the choice of process parameters needs to be optimised. Therefore, the first step is represented by the analysis of the influence of the process parameters on cutting efficiency and quality. A set of experimental cuts has been designed and machined. The three process parameters deeply influencing the material removal mechanism, as discussed in the previous work (Carrino et al. 2000), have been considered as factors of the experimental plan. The levels of the process variables have been selected in order to maximise cutting efficiency.

The remaining process parameters have been considered fixed during the experimental phase. The values of all the process parameters are shown in Table 2. In particular the abrasive is barton garnet, which is widely used for AWJ machining; also the two mesh values of the abrasive are extremely diffused. As can be derived from Table 2, each cut has been replicated three times, yielding a total of 54 cuts. The experimental cuts have been perfomed in a random sequence, in order to reduce the effect of any possible systematic error.

3.3 Measurement procedure

The quality of a decoration is generally measured in terms of reduced deviation from the designed shape. The designed shape is the 2D profile developed by means of a CAD software. This profile was used to define the part program of the CNC machining centre or of the AWJ equipment: it means to translate it into a set of coordinate of points that define the tool path related to the machine reference frame. During this step the mill diameters have been measured and their values have been used to define the trajectory of the tool axis. The focuser diameter has been used for the trajectory of the abrasive water jet.

Once machined, the 2D profile has been measured by a coordinate measuring machine (see Figure 4). The actual contour of each cut shape has been obtained by probing the profile at 338 discrete measuring points. The distance between two following points is equal to 2 mm. In particular the actual profile has been measured at a distance of 2 mm and 7 mm from the upper cut edge. In this way it has been possible to evaluate the decrease of the jet efficiency with depth along the cutting groove. In fact the lower profile is covered during application and is, therefore, not critical from an esthetical point of view. The used probe has a 3 mm diameter in order to minimise the effect of the mechanical filtering.

The deviations of the measured points from the 2D CAD model have been calculated for each cut shape. These deviations represent the errors of the actual profile from the nominal one due to the machining process: they include form, orientation and location errors (see Figure 5). They are a function of the geometry of the profile: in this case they depend by the radii of the arcs of circles constituting the shape of the flooring marquetry. They are caused by the chippings between tool, jet or mill, and the material being cut.

The result of the measuring procedure has been the distributions of the geometric deviations: 108 distributions for AWJ technology and 12 distributions for the traditional milling technology. Each distribution has been characterised by the first four statistical moments: mean, variance, skewness and kurtosis. The mean is a commonly used measure of the centre of a batch of data. The variance is a measure of how far the data are spread about the mean. The skewness is a measure of asymmetry, while the kurtosis is a measure of how different the deviations distribution is from the gaussian distribution. Moreover, the median value has been calculated too because of the non-normality of the distribution data. It is used to indicate where the centre of the data is. The median is in the middle of the data: half the observations are less than or equal to it, and half are greater than or equal to it.

Finally, the suitability of the produced profiles implies that the taper of the cutting grooves is not so elevated to compromise the profiles joint. In a previous work it has been verified that the taper obtained on a thickness of 19 mm is very small (Carrino et al., 2000). Therefore, it is possible to assume that the taper on a thickness of 10 mm is further reduced and it does not compromise the flooring setting.

4. AWJ RESULTS AND DISCUSSION

In this work the analysis of variance model was employed to determine the influence of the AWJ cutting parameters and profile bending radius on the distributions of the geometric deviations. This means to define the influence of the process parameters on the average of the deviations between actual and nominal profiles. The fundamental hypotheses of the ANOVA applicability to the experimental data (that are the normality and the homogeneity of the variance of the residuals) have been verified. Moreover, the response trend (increase or decrease) as a function of the process parameters has been evaluated by means of the Main Effects Plots.

The results of these analyses show that, apart from abrasive mesh, all the process parameters that are involved in the material erosion process influence the variables of deviations, as summarised in Figures 6-7.

The abrasive mass flow rate and the feed rate are the main cause of variation of the average deviation: an increase in the abrasive mass flow rate or a decrease in the feed rate produce a lower geometric deviation from the nominal profile. These results are independent by the measurement position along the cutting grooves: they are the same for 2 mm and 7 mm positions. Moreover, the mean values of deviations seems not to significantly increase along the cutting depth. This is probably due to the shape of the jet that has a very reduced diameter and remains better focused for high values of abrasive mass flow rate and low values of feed rate. Moreover, a decrease of the feed rate gives to the high number of abrasive particles included in the water-jet the time needed to accurately erode the cut volume.

The average values increase along the cutting depth, even if the general behaviour remains the same. A high abrasive mass flow rate implies a high number of abrasive particles included in the water-jet; each particle contributes eroding an elementary volume and all the eroded volumes gives the last shape of the contour profile. Therefore, increasing the abrasive mass flow rate means to increase the probability to change the shape of profile.

At last, the abrasive mesh does not significantly affect the geometric deviations of the obtained profile, while its effect on morphological characteristics of the cutting surface seems to be very strong. This is confirmed by many analysis on metal material where the roughness of the cutting surface is a very important morphological parameter by a functional point of view (Capello et al., 1996).

Moreover, the mean deviation of the machined profile from the nominal one strongly depends by the bending radius of the profile. It decreases with the increase of the bending radius of the profile; even if it is strongly connected to the length of the curvilinear path and to the changes in cutting direction between two consecutive curvilinear outlines. This means that, once the jet has changed the cut direction by passing from a curvilinear outline to the following one, the length of the following curvilinear outline, that is characterized by a value of the bending radius, may be not enough for jet to achieve a stable cutting condition (i.e. the jet decelerates in order to change the cut direction and, therefore, it has to accelerate in order to achieve the planned cutting parameters, but the length of the curvilinear path may be not enough to achieve the planned values along the curvilinear path). An example are the short curvilinear outlines along the lower part of the profile in Figure 2. This implies that it is hard for jet to follow a path characterized by short curvilinear outlines with very different bending radii.

It can be stated that the profile of the flooring marquetry depends on the interaction between the material and the jet shape, that is, by the abrasive mass flow rate and the feed rate. The average value of the deviations ranges between 0.22 mm and 0.64 mm at 2 mm depth and between 0.23 mm and 0.73 mm at 7 mm depth.

Therefore, in operative conditions the values of these two process variables must be fixed and controlled in order to decrease the geometric deviation from the CAD designed profile.

5 COMPARISON BETWEEN AWJ AND DIAMOND MILLING

A visual inspection of the cuts underlines that those machined by diamond mill present a wider chipping spreading on the upper cut edges than those obtained by AWJ technology. The situation is inverted for the lower cut edges.

A deep analysis was carried out on the average deviations of the actual profile from the nominal one. The distribution obtained merging the six samples machined by diamond mill was compared with the distributions of minimum and maximum errors due to AWJ technology. The first is formed by the samples that were cut with the highest value of abrasive mass flow rate (500 g/min) and with the lowest value of feed rate (350 mm/min) as previously described. The second distribution is constituted by the samples cut with the lowest value of abrasive mass flow rate (300 g/min) and with the highest value of feed rate (750 mm/min).

AWJ allows to obtain average deviations ranging from about 0.07 mm to 0.16 mm at a depth of 2 mm, if we cut the profile with the highest value of abrasive mass flow rate and the lowest value of feed rate. In fact, the diamond mill allows to achieve an average value of deviations included between 0.06 mm and 0.31 mm. The standard deviations are very similar for the two cases. However, a wrong choice of AWJ process parameters may move the machine profile away from the nominal one, such as adopting 300 g/min as abrasive mass flow rate and 750 mm/min as feed rate involves an average deviation ranges between 0.23 mm and 1.23 mm with a value of the related standard deviation higher than that due to the two previous cases.

The same considerations are valid for a depth of 7 mm where we can obtain an average deviation ranging between 0.11 mm and 0.21 mm when we choice rightly AWJ parameters, while diamond mill achieves only an average deviation ranging from 0.10 mm to 0.31 mm.

Therefore, an important technological result is that AWJ technology allows to reproduce the designed profile of the flooring marquetry more accurately than milling technology permits if its process parameters are opportunely choosen. This result together with the possibility to cut profiles whose bending radius is one tenth of that for milling makes AWJ technology the most promising process to cut the free-form profiles of decorative applications, such as flooring, civil covering and so on, by a technological point of view.

6. CONCLUSIONS

The AWJ technology results to be very competitive in the field of decorative applications. It allows to reproduce the designed profile more accurately than traditional technology does, once chosen the process parameters. The geometric deviations from the designed 2D shape may be strongly decreased by increasing the abrasive mass flow rate or decreasing the feed rate. This result together with the possibility to cut profiles whose bending radius is one tenth of that for milling makes AWJ technology the most promising process to cut the free-form profiles of decorative applications, such as flooring, civil covering and so on, by a technological point of view.

However, it is needed to take into account that the average deviation of the machined profile from the nominal one strongly depends by the value of the bending radius characterizing the profile. Once known the average value of deviations for each radius characterizing the profile, it is possible to correct the jet path in order to reduce the distance between machined and nominal profile. This theme is matter of further study.

7. ACKNOWLEDGMENTS

This work has been carried out with the funds received by the Italian M.I.U.R. (Ministry of Instruction, University and Research) within the project entitled “Stone manufacturing technologies” (COFIN01).

8. REFERENCES

Agus, M., Bortolussi, A., Ciccu, R., Kim, W.M., Manca, P.P., “The influence of rock properties on waterjet performance”, *Proceedings of the 7th American Water Jet Conference*, pp. 427-442, Water Jet Technology Association, St. Louis, Missouri, 1993.

Agus, M., Bortolussi, A., Ciccu, R., Vargiu, A., “Abrasive-rock interaction in AWJ cutting”, *Proceedings of the 13th International Symposium on Jet Cutting Technology*, pp. 509-519, BHRA Fluid Engineering, Cranfield, Bedford, England, 1996.

Capello, E., Monno, M., Polini, W., Semeraro, Q., “AWJ Machining: Surface quality as a constraint”, Proceedings of the *13th International Symposium on Jet Cutting Technology*, BHRA Fluid Engineering, Cranfield, Bedford, England, 1996.

Carrino L., Monno M., Polini W., Turchetta S., “Study of cutting quality and efficiency in stone production”, *Proceedings 15th International Symposium on Jetting Technology*, pp. 133-146, BHRA Fluid Engineering, Cranfield, Bedford, England, 2000.

Carrino L., Monno M., Polini W., Turchetta S., “AWJ to machine free-form profiles in natural stone”, Proceedings of the 2001 WJTA “American Waterjet Conference” volume I, pagg. 305-323, Minneapolis, Minnesota, 18-21 agosto 2001.

Cheung, J.B., Hurlburt, G.H., “Submerged water-jet cutting of concrete and granite”, *Proceedings of the 3rd International Symposium on Jet Cutting Technology*, pp. 49-62, BHRA Fluid Engineering, Cranfield, Bedford, England, 1976.

Deshpande, J.V., Gore, A.P., Shanubhogue, A., “Statistical analysis of nonnormal data”, *John Wiley & Sons*, 1995.

Koyohashi, H., Kyo, M., Rekiguchi, R., Matushita, Y., Tokioka, M., “Experiments and multivariate analysis of hot dry rock cutting with high pressure water jet”, *Proceedings of the 10th International Symposium on Jet Cutting Technology*, pp. 27-43, BHRA Fluid Engineering, Cranfield, Bedford, England, 1990.

Matsuki, A., Okumura, K., Nakadate, H., “Some aspects of slot cutting of rocks with high speed water jets both in air and in water”, *Proceedings of the 9th International Symposium on Jet Cutting Technology*, pp. 495-511, BHRA Fluid Engineering, Cranfield, Bedford, England, 1988.

Miranda, R.M., Lousa, P., Mouraz Miranda, A.J., Kim, T., “Abrasive water jet cutting of portuguese marbles”, *Proceedings of the 7th American Water Jet Conference*, pp. 443-457, Water Jet Technology Association, St. Louis, Missouri, 1993.

Miranda, R.M., Kim, T.J., “Abrasive waterjet cutting of marble and calcareous stones: a phenomenological study”, *Proceedings of the 13th International Symposium on Jet Cutting Technology*, pp. 415-424, BHRA Fluid Engineering, Cranfield, Bedford, England, 1996.

Monno M., “Selection of Process Parameters for AWJ cutting”, *International Conference on Cutting Technologies (ICCT ’97)*, Hannover, March 5-6, 1997.

9. TABLES

Table 1. Mechanical properties of Coreno Perlato Royal and White Carrara

Material properties	**Coreno Perlato Royal**	**White Carrara**
Density [kg/m^3]	2740	2705
Water absorption [%]	4.0	0.06
Compressive strength [MPa]	163	131
Compressive strength to ageing by frost [MPa]	162	126
Young modulus [MPa]	72000	75000
Flexural strength [MPa]	12,8	16.9
Abrasion resistence	0.95	0.52
Impact resistance [cm]	32	61
Knoop hardness [MPa]	2001	1463

Table 2. AWJ experimental plan

FIXED FACTORS	**Levels**	**Variable factors**	**# LEVELS**	**Levels**
water pressure [MPa]	350	abrasive mass flow rate [g/min]	3	300-400-500
orifice diameter [mm]	0.30	feed rate [mm/min]	3	300-500-750
nozzle diameter [mm]	1	abrasive mesh	2	80 - 120
abrasive kind	garnet			
standoff distance [mm]	2			
# passes	1			

Replications	3
Total cuts	54

10. GRAPHICS

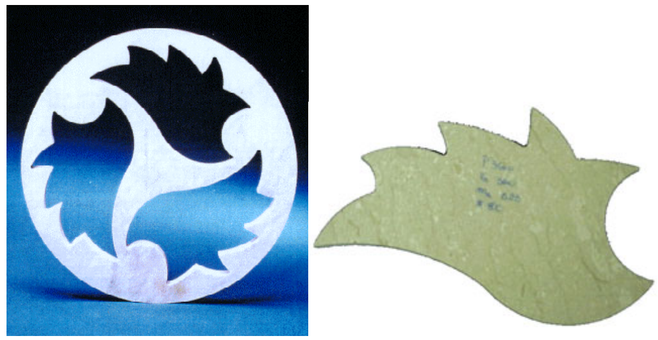

Figure 1. Decorative application (Courtesy Brembana Macchine)

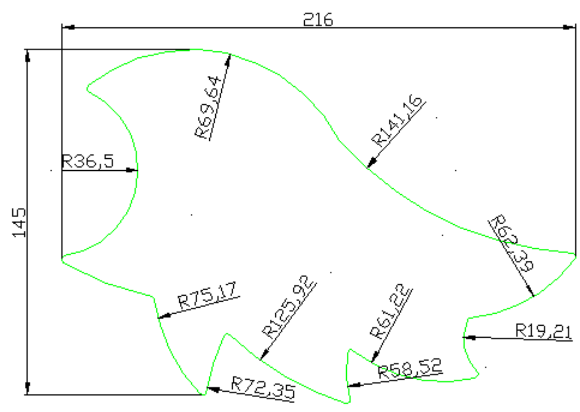

Figure 2. Experimental 2D shape

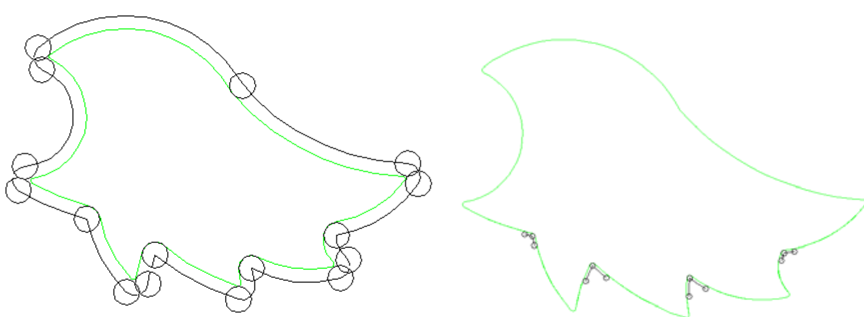

Figure 3. Milling trajectory

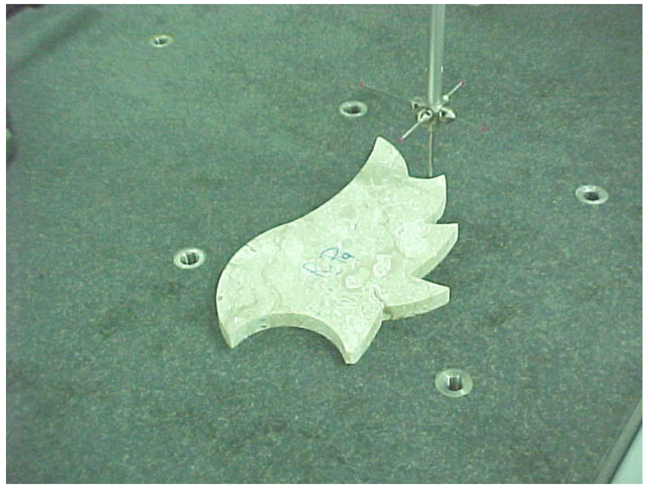

Figure 4. Measurement of machined profile by CMM

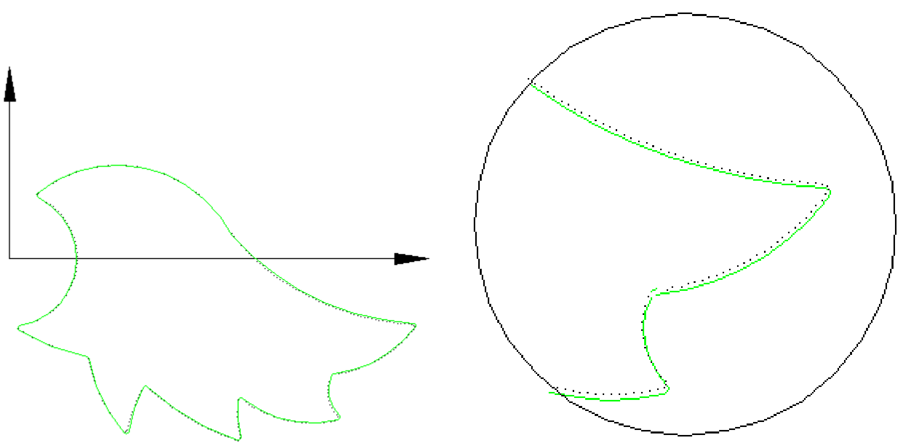

Figure 5. Measurement procedure

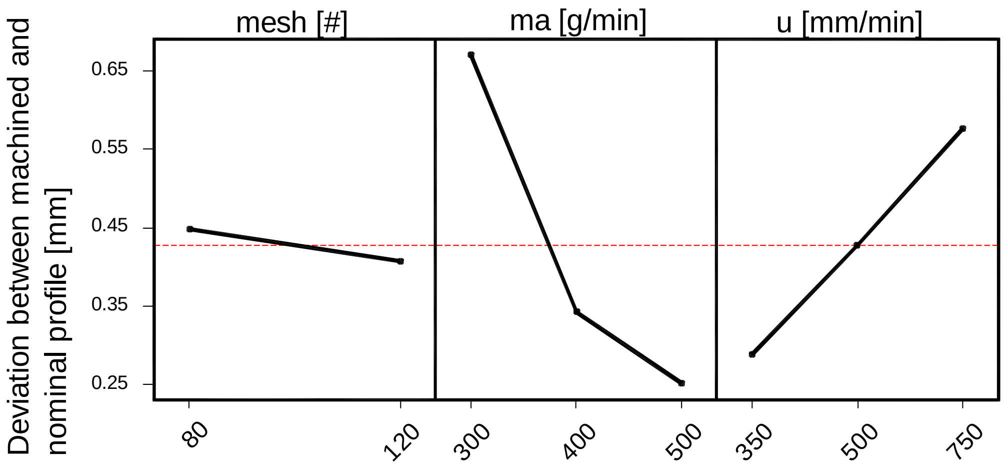

Figure 6. Main Effect Plot of average deviation vs. AWJ process parameters at 2 mm depth

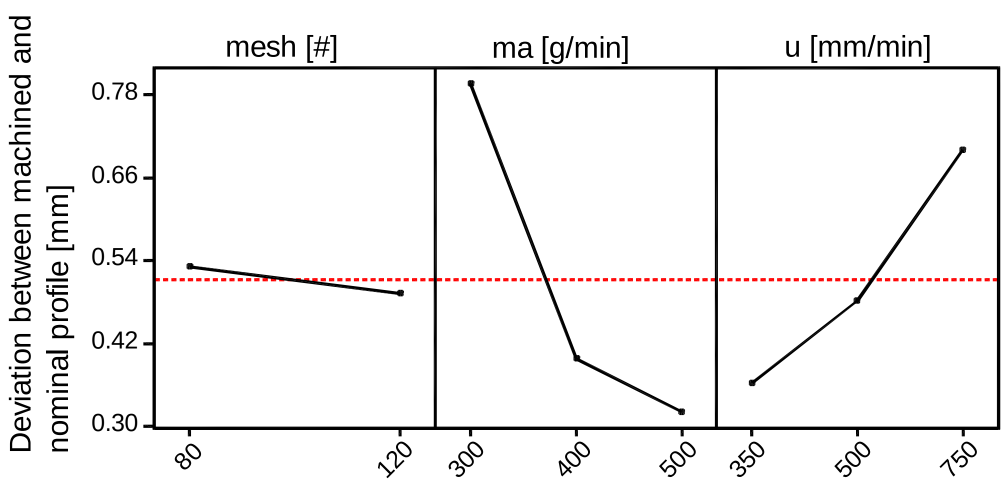

Figure 7. Main Effect Plot of average deviation vs. AWJ process parameters at 7 mm depth

2003 WJTA American Waterjet Conference
August 17-19, 2003 ● Houston, Texas

Paper 5-D

ADVANCED ERROR CORRECTION METHODOLOGY APPLIED TO ABRASIVE WATERJET CUTTING

J. Olsen, J. Zeng, C. Olsen, and B. Guglielmetti
OMAX Corporation
Kent, Washington, U.S.A.

ABSTRACT

First introduced in the last decade, the concept of “compute first, move later” for motion control optimized the abrasive waterjet cutting process. Using a cutting model that varied cutting speed around corners and along arcs provided a greater degree of accuracy. Recent innovations in corner-cutting strategy allow the cutting of external corners without sacrificing speed or surface quality. The latest development in machine-control hardware and software advances the error correction methodology in abrasivejet machining to the next generation. The nozzle automatically tilts along the cutting path, compensating for taper error as well as lag error at corners. A tool tip tilt mechanism lets the nozzle tilt quickly about the material entry point without large accelerations and vibrations. This paper provides insight into the development of these advanced error correction technologies as applied to abrasivejet cutting.

Organized and Sponsored by the WaterJet Technology Association

1 INTRODUCTION

After two decades of development, abrasive waterjets have become a mainstream technology that works hand-in-hand with other machining technologies in modern machine shops. Abrasivejets cut five to ten times faster than EDM. While lasers are limited to non-reflective materials, abrasivejets are not. Abrasivejets can cut thicker materials than lasers, and the production cost is two-thirds less. Fixturing is less complicated on an abrasivejet than on a traditional machining center, and setup time is reduced. As the abrasivejet becomes accepted in more and varied applications, however, the challenges increase. Greater productivity (faster machining times) and higher accuracy are two constant and often contradictory challenges.

Consider the challenge of higher accuracy. These errors and defects can be found on parts machined by abrasivejets:

- Striation marks along the bottom half of the cut surface
- Jet lag errors at corners of the path and on small arcs
- Taper and barrel errors
- Geometrical error from kerf width change
- Lead-in and lead-out defects
- Frosting and rounding on top of the kerf
- Burrs at the bottom of the kerf

Previous work by Zeng et al. (1999) addressed striation marks and jet lag errors at corners of path and on small arcs. A jet shape modeling concept has been described by Henning and Anders, which shed light on real-time taper error compensation. The feasibility of such compensation was also proven later by Knaupp et al. A work by Groppetti et al. investigated edge rounding on top and burrs at bottom of the kerf. A study by Anderson and Johansson was devoted to lead-in and lead-out defects.

This paper presents a systematic approach for error correction starting from a new concept of motion control.

2 THE CONCEPT OF “COMPUTE FIRST, MOVE LATER”

A machine tool controller essentially does three things: it accepts a tool path as input, which is defined by a relatively small number of parameters; it provides a user interface; and it generates the physical position of a tool along multiple axes as a function of time.

Most machine tool controllers accept their input in the form of “G Code,” consisting of sequential movement commands interlaced with On/Off commands for various machine functions. A three line sample of G Code is shown below:

```
000 G00 X1 Y2
010 M73
020 G01 X2 Y3 F120
```

In this example, the lines are sequentially numbered in steps of 10. The first line indicates that the nozzle should move to coordinates X1, Y2 at a preset rapid traverse speed. The next line turns on something, such as a cutting jet. The third line moves the nozzle to coordinates X2, Y3 at a speed of 120. The controller executes these commands one at a time, and performs any calculations necessary to coordinate the multiple axes as the motion proceeds. Some controllers process a few lines ahead, helping to manage accelerations at sharp turns of the path.

This code can be written by hand or generated automatically with a CAD/CAM program. Note that this type of controller requires the exact motion path and the desired speed of motion as input. The part shape and the tool path shape usually have a one-to-one relationship independent of the speed and accelerations along the path in machining applications. But this assumption is not true for abrasivejet cutting.

In 1996 a patent was issued on a different control mechanism called "compute first, move later." This control mechanism was developed specifically for abrasivejet cutting. The same functions are performed, but by using the large memory and computing power of modern personal computers, they may be performed in a different order. In this type of controller, the part shape is first described by a series of lines and arcs, much like the G Code representation, but without any data regarding speeds of motion. The entire tool path is then interpolated with speeds set according to a model of the abrasivejet cutting process. At this point, the path is stored digitally in a large data array with about five kilobytes per centimeter of the tool path. Here it can be iteratively manipulated to correct for various abrasivejet behaviors, producing a part of the desired shape and tolerance.

The ability to process the entire path iteratively is a major advantage in abrasivejet machining. First, there is the ability to look ahead for the entire length of the path. In a thick material, a sharp corner near the end of the path may require the abrasivejet to slow at the start of the path. In a thin material, high speed on a straight portion of a path may require tilting of the nozzle to avoid taper on the edge of the part.

The error correction phases described below manipulate the large data array that represents the path by changing the speeds as a function of path geometry, and by inserting tilting motions to compensate for the natural taper produced by the abrasivejet. This results in more accurate parts.

3 ERROR CORRECTION PHASE 1: REDUCING GEOMETRICAL AND COSMETIC ERROR

On parts cut with an abrasivejet, the most profound errors are the striation marks and jet lag errors at corners and arcs. These errors often make the parts either cosmetically unacceptable or outside of tolerance requirements.

An abrasivejet cutting model was published by Zeng et al. in 1992. The model predicted the cutting speed for a given quality index, combined with other process parameters. By selecting a proper quality index in the range of one to five, the striation marks along the cut surface are partially or completely eliminated. Choosing a quality index of "one" creates a separation cut, a very rough cut without any concern for surface finish. Choosing a quality index of “five” creates a smooth and striation-free surface.

Employing a similar idea, the amount of permissible jet lag errors at corners and arcs is used to calculate an effective quality index. This effective quality index depends on the angle of corners, and the radius of arcs. The result of using the effective quality index at corners and arcs is a reduced cutting speed at these locations.

By using the “compute first, move later” concept and the PC-based software infrastructure built on this concept, the transition of cutting speed at corners and arcs can be conveniently handled at increments of one motor step. In practical terms, this means the cutting speed can be varied every 12 microns or so along the path. Varying the speed one motor step at a time is a vast improvement over the traditional CNC controller—it allows higher cut quality at corners.

4 ERROR CORRECTION PHASE 2: BALANCE OF SPEED AND QUALITY

These advances to abrasivejet machining technology have been available since 1993. Since then, the technology has been improved even further—the cutting process is faster, and cuts are more precise. Some of the more recent enhancements include:

- Automatic setting of lead-in length and speed based on a pierce model, providing the fastest possible dynamic piercing
- A new cornering strategy that treats every possible corner geometry uniquely
- Automatic addition of “corner passing” based on a cutting model built into the software, speeding up outside corners where there is room to do so

4.1 Stage 1: Piercing

There are many ways to pierce a material. A material can be pre-drilled mechanically, pierced by a stationary abrasivejet, pierced by moving the jet back and forth over a fixed distance (“wiggle” piercing), or dynamically pierced by turning on the abrasivejet and then slowly moving across the material. Each of these has its advantages, and each is appropriate for different situations. The two most popular methods are dynamic piercing and wiggle piercing, because they generally offer the fastest piercing with the most convenience for a wide variety of applications.

Wiggle piercing has been a good balance between fast piercing, short pierce distance, and ease of programming. It is generally faster than most implementations of dynamic piercing, and is especially good for piercing thick material in small spaces, such as piercing a 6 mm hole in 5 cm thick steel.

Dynamic piercing is limited by the difficulty in determining and setting the ideal lead-in length and speed for each pierce point in the path. This is solved with the use of a dynamic piercing model that looks at the machining conditions and automatically sets the pierce length and speed based on the geometry of the part and the pump and nozzle setup.

Using this model, it is possible to greatly speed up piercing performance without any user intervention or knowledge of the process. If a tiny hole is being pierced, then the lead-in will shrink, and the piercing speed will be reduced to make up for the loss of room. If the hole is larger, the pierce length will increase to the optimal length, and the speed will be increased appropriately. This makes dynamic piercing ideal for most applications, with the exception of small holes in thick materials, where wiggle piercing may still be the preferred choice.

4.2 Stage 2: Corner Corrections

The main drawback of earlier controller technologies was that the controller treated outside corners with the same cutting model parameters as inside corners. The controller slowed more than necessary for outside corners.

By applying separate cutting models to inside and outside corners, both speed and precision are improved. Outside corners can be machined much faster, and inside corners can be machined at precise speeds and accelerations that minimize blowout and kickback more than previously possible.

4.3 Stage 3: Corner Passing

Corner passing refers to the concept of overshooting a corner, reversing the abrasivejet, and then continuing along the tool path. The advantages of corner passing are that software can program the corner passes automatically and determine the best geometry to use, adding corner passes only when and where needed

To use corner passing, software first computes how much jet lag there will be at each outside corner by using the built-in cutting model. If there is room to do so, the software automatically adds a short element slightly longer than the length of one jet lag past the corner.

This allows the controller to move the abrasivejet at full speed past the corner. The controller then accelerates back to the corner, and continues cutting. All this motion occurs at virtually full cutting speed, allowing for dramatically faster machining of outside corners.

Figures 1 and 2 show the same tool path calculated for 2.5 cm thick mild steel. Lighter areas show fastest abrasivejet motion while darker areas are slower. In Figure 2, the lead-in length has been increased for dynamic piercing, outside corners are treated differently than inside corners, and corner passing allows for even faster jet motion.

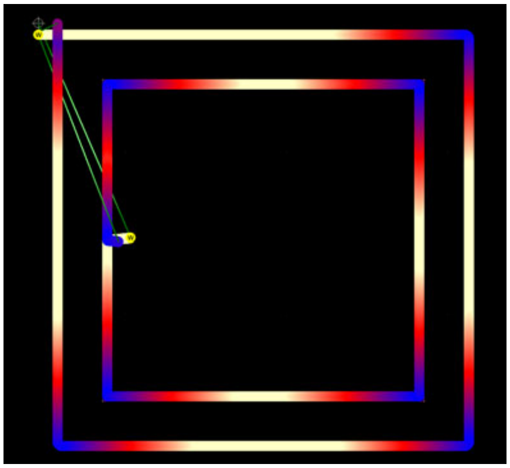

Figure 1. With no optimizations other than basic corner compensation, the part takes 17.1 minutes to machine.

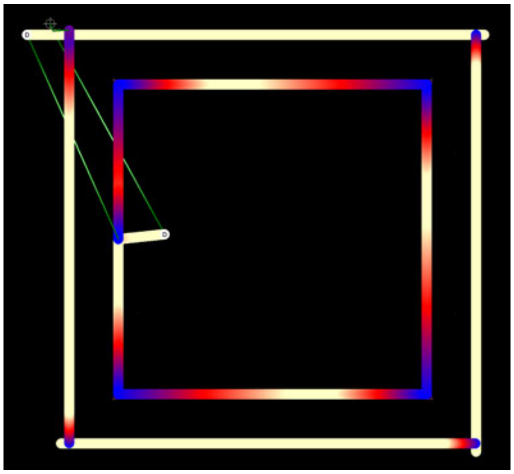

Figure 2. With the addition of optimized dynamic piercing, corner strategy, and corner passing, machining the part speeds up to 13.7 minutes.

Tests showed that for 150 different parts ranging from mechanically simple parts to complex artworks, an average speed increase of 128.4% was achieved. One part machined slightly slower (98% of previous speed), 14 parts machined in excess of 150% faster, and one part had a machining speed increase exceeding 200%. Tests were done with several material and thickness settings.

The parts also come out to slightly higher tolerance. By slowing down less on outside corners, there is less opportunity for the kerf width to grow. Figure 3 shows a 20 cm thick aluminum rectangle machined using corner passing.

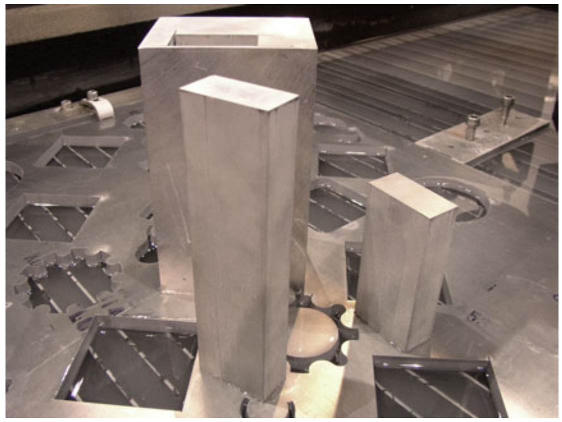

Figure 3. A 20 cm (eight inch) thick aluminum rectangle machined using corner passing to improve the quality of the outside corner, while simultaneously speeding up part cutting significantly

Figure 4. A high tolerance part machined from 1 cm (0.4") stainless steel.

In Figure 4, notice the high quality inside corners. While the corners are not perfect, the amount of washout has been reduced to almost nothing. The sharpness of the inside corner, therefore, becomes primarily a function of the nozzle diameter. Corner passing increases the tolerance of this part by preventing excess kerf width growth from slowing down around outside corners.

5 ERROR CORRECTION PHASE 3: ELIMINATING TAPER

5.1 Adaptive Cutting with a Tilting Nozzle

The third phase of error correction is the easiest to understand, but the most difficult to implement. The nozzle needs to be tilted by an amount sufficient to remove the natural taper of the jet stream. Implementation of this concept requires three things:

- Predicting the amount of taper caused by the jet stream

- A mechanism for mechanically tilting the jet
- A five-axis control system capable of producing the required coordinated motion

As discussed previously, the nozzle speed must be varied along the path to achieve sharp corners and precise radii. As shown in Figure 5, the shape of the taper produced by the jet is a function of speed. Thus, the nozzle must tilt to different angles along the path according to the speed of motion.

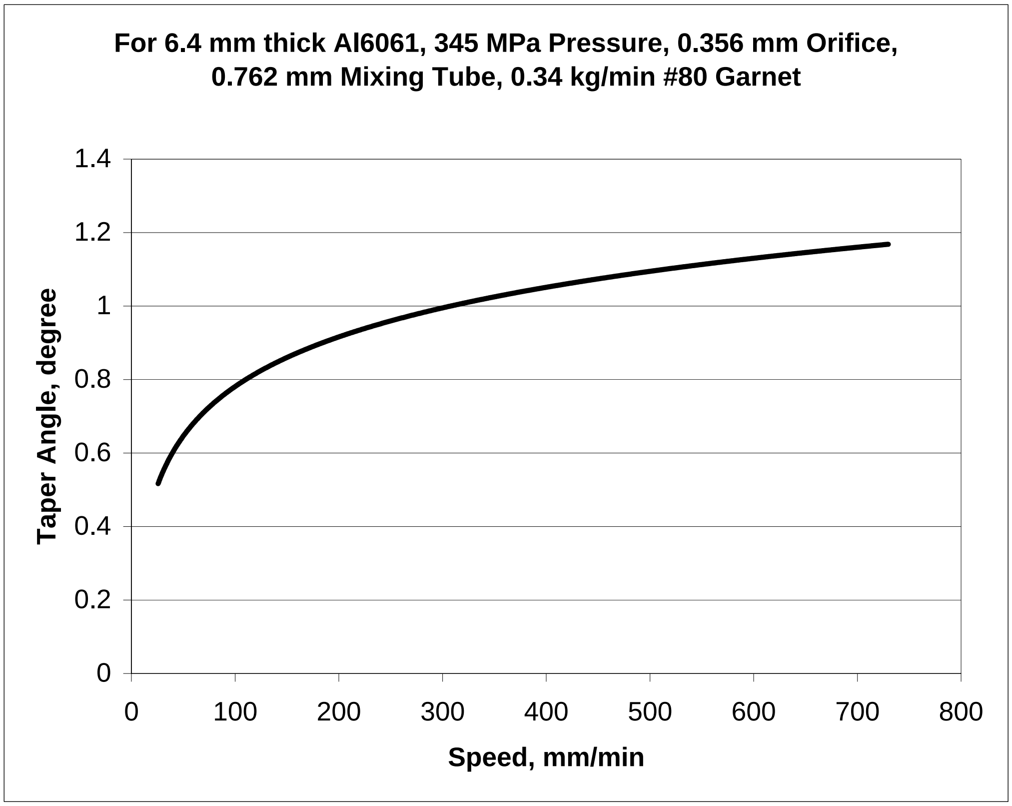

Figure 5. Taper angle as a function of speed

5.2 Tool Tip Tilting Mechanism

The mechanism for tilting the nozzle must provide quick response to follow the angle required by the X-Y path motion. Typically, the tilting mechanism will be carried on a large X-Y table used for cutting parts from plates of material. Quick motions of the tilt head imply high accelerations of the X-Y mechanism, unless the tilting mechanism pivots about the nozzle tip.

A patent application has been recently filed for a mechanism closely approximating a nozzle tip pivot and reducing the accelerations required by the X-Y mechanism. The mechanism is easiest to understand by first considering a two-dimensional simplified version (see Figure 6).

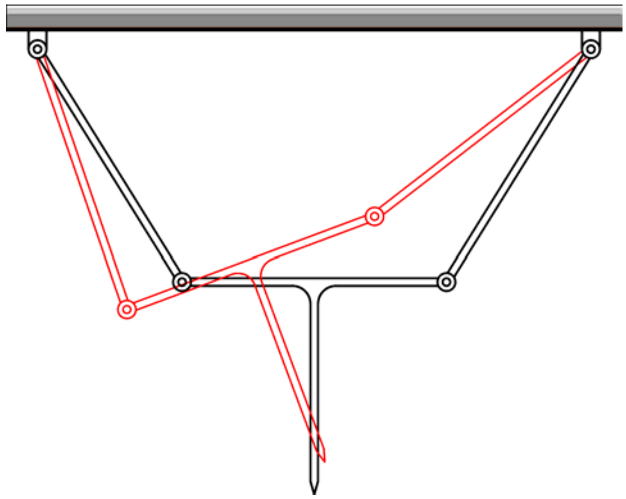

Figure 6. Two-dimensional simplified version of nozzle tip pivot, showing two positions

A nozzle is mounted on a plate, supported by two links connected to a stationary top plate. When the plate moves sideways, the nozzle tilts while the tip remains almost stationary. For the small angles needed to remove taper produced by the jet, the X-Y axes need to move only a few tens of microns to compensate for the tip motion.

This idea was then extended to a three-dimensional mechanism where a third link is added and the lines defined by the three-link spherical pivots join at the nozzle tip. The three-link mechanism has one more degree of freedom than the two-dimensional example in Figure 6. Adding this degree of freedom also means the movable plate can twist about a vertical axis. For the device to be useful, this motion must be controlled. The motion is restrained by replacing one of the links with a drive shaft that has a universal joint at each end. A photograph of a prototype of this mechanism is shown in Figure 7 where a ball has been placed at the tool tip location for testing.

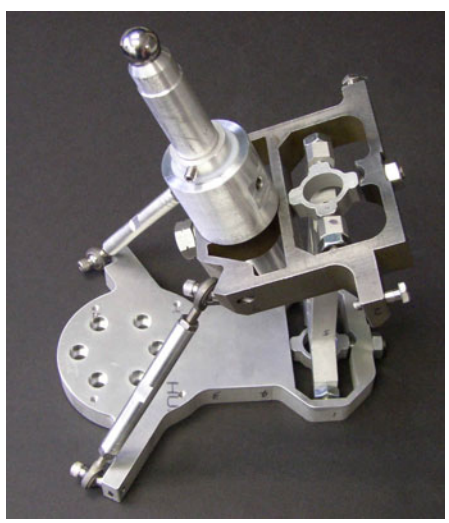

Figure 7. Early prototype of tool tip tilting mechanism

The prototype shown in Figure 7 was driven with two linear actuators that moved the tilting plate attached to the nozzle. After some experimentation with the model, it became obvious that a simpler and more compact mechanism could be built by actuating the yokes of the universal joints with rotary actuators. Figure 8 shows a solid model of the final design now in production.

Figure 8. Solid model of final design for tool tip tilting mechanism

The software for implementing the tilt begins with the tool path corrected for the other jet errors. The speed at each point in the path is known, so the taper angle normal to the path motion can be calculated. A calculation is then performed to find the required positions for the two rotary actuators that drive the universal joint yokes. For all but the smallest angles, the tilt requires a slight correction to the positions of the X, Y, and Z actuators. This correction is added, and the software performs the same operations at the next point on the path. At present, this calculation is performed at 790 points per centimeter of the tool path.

5.3 Taper Modeling

Experience shows that taper is affected by process parameters such as material thickness, type of material, size of nozzle, and size of abrasive particles. An experimental pilot study on quantifying taper was done a few years ago. This screening experiment evaluated 11 variables: material machinability, thickness, water pressure, orifice diameter, mixing tube diameter, mixing tube wear condition, abrasive material, abrasive mesh size, abrasive flow rate, stand-off distance, and quality index.

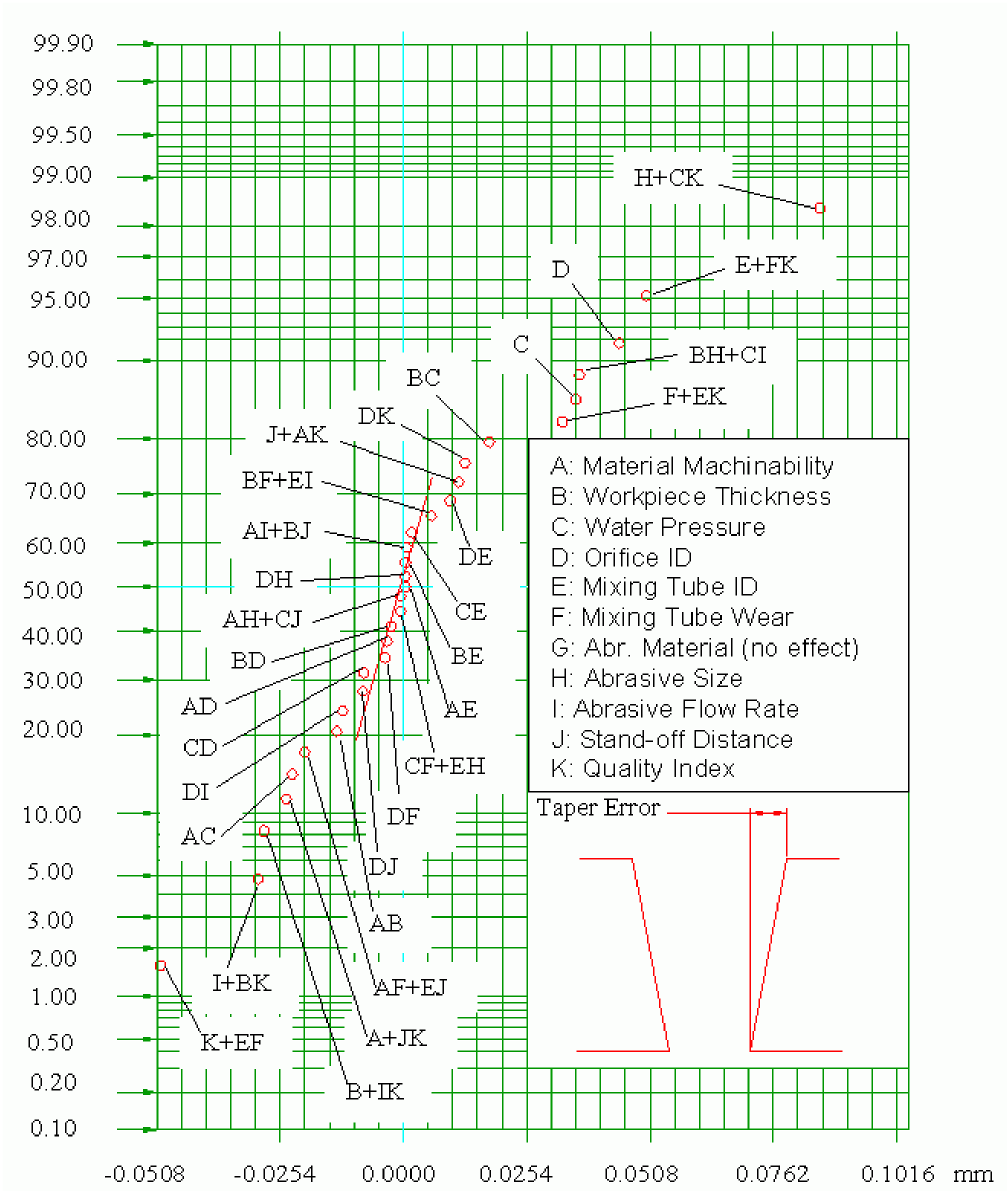

Figure 9. Effects of process parameters on taper error

The results are illustrated in Figure 9. The main effect of each variable is showed as a single letter, e.g., letter "D" stands for the main effect of the orifice inside diameter (ID). The interaction effect of two variables is showed as a two-letter word, e.g., "AB" stands for the interaction effect of machinability and thickness. In some cases, a main effect may be confounded with an interaction effect such as "H+CK." Since interaction effects are usually small compared to main effects, this graph is still useful as a tool to sort out the main effects. Those effects on or close to the straight line that passes through "0.0000, 50.00" are considered noises and are ignored. Those far away from the straight line are important effects.

The pilot study showed that seven of the variables were most important in determining taper and therefore, an experiment with seven variables could be implemented to develop the taper model.

The seven variables were abrasive size, orifice inside diameter, water pressure, quality index, abrasive flow rate, workpiece thickness, and machinability. Even though the mixing tube inside diameter has a strong effect on taper, it was not considered as a variable in this experiment because of the fixed ratio between the inside diameter of the mixing tube and the orifice.

The resulting model is a quadratic function of main effects and interactions with a total of 28 terms. Figure 10 shows the correlation between the model and the observed taper errors, which shows the model predictions agree quite well with the observed values.

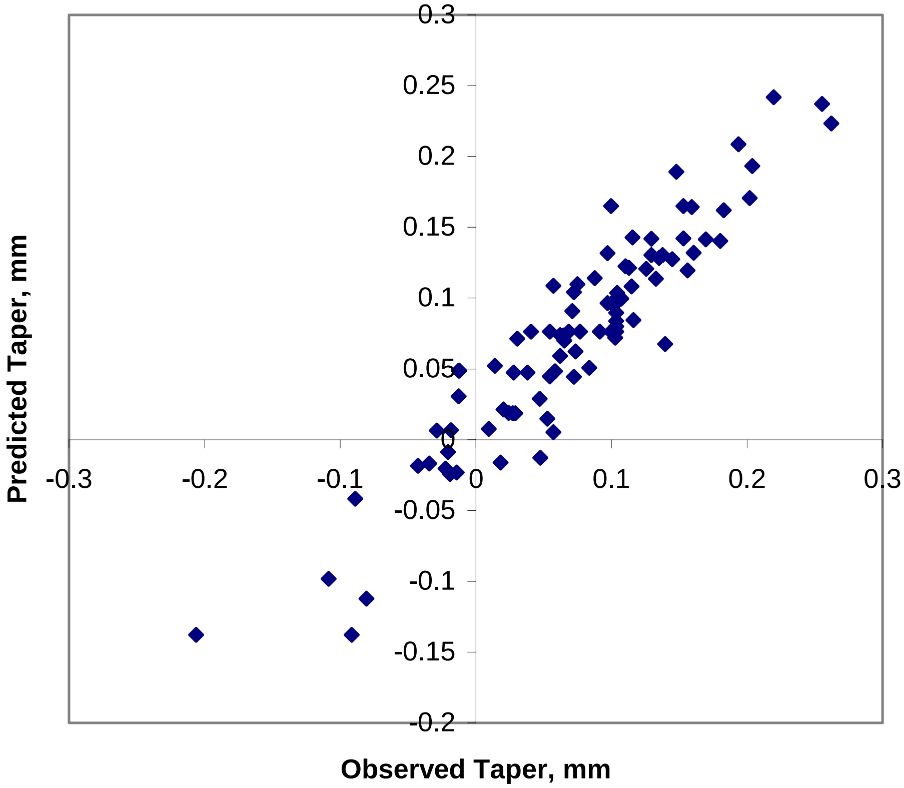

Figure 10. Predicted vs. observed taper error

5.4 Experimental Results

Figure 11 shows two 50 by 50 mm squares (6.4 mm thick aluminum) machined with and without the tool tip tilting mechanism. Taper measurements were done using a dial indicator accurate to 2.5 microns, on seven spots evenly spaced across the 50 mm length of two opposite sides. The results are shown in Table 1.

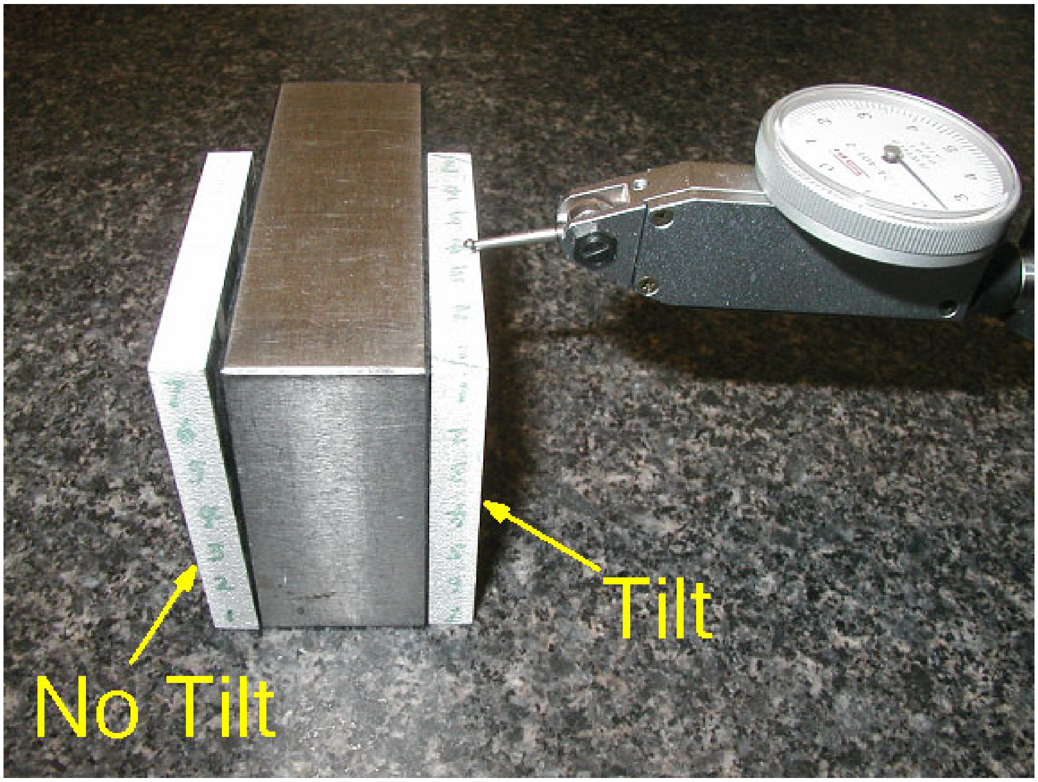

Figure 11. Samples cut with and without the tool tip tilting mechanism

Table 1. Taper Measurements (mm)

Spot No.			1	2	3	4	5	6	7	Average
No Tilt	Side A	Top	0.000	-0.013	-0.018	-0.010	-0.023	-0.013	-0.025	
		Bottom	0.183	0.183	0.183	0.183	0.183	0.180	0.183	
		Taper	**0.183**	**0.196**	**0.201**	**0.193**	**0.206**	**0.193**	**0.208**	**0.197**
	Side B	Top	0.000	-0.003	-0.010	-0.010	-0.013	-0.005	0.005	
		Bottom	-0.008	0.005	-0.015	-0.033	-0.020	-0.020	-0.025	
		Taper	**-0.008**	**0.008**	**-0.005**	**-0.023**	**-0.008**	**-0.015**	**-0.031**	**-0.012**
Tilt	Side A	Top	0.000	0.005	0.010	0.003	0.003	0.003	0.008	
		Bottom	-0.010	-0.013	0.028	0.025	0.010	0.023	0.013	
		Taper	**-0.010**	**-0.018**	**0.018**	**0.023**	**0.008**	**0.020**	**0.005**	**0.007**
	Side B	Top	0.000	-0.015	0.000	-0.018	-0.020	-0.008	-0.005	
		Bottom	-0.015	0.005	-0.008	0.008	-0.008	0.015	0.018	
		Taper	**-0.015**	**0.020**	**-0.008**	**0.025**	**0.013**	**0.023**	**0.023**	**0.012**

Without tilting, the sample shows a taper error of 0.197 mm on one side and –0.012 mm on the other. The difference in taper error on these two sides indicates a perpendicularity error between the nozzle and the sample surface. The average taper for both sides is 0.092 mm (0.0036 inch).

Using the tool tip tilting mechanism, the taper errors on the sample are 0.007 and 0.012 mm on the two opposite sides. The average is 0.009 mm (0.0004 inch) and the difference between the two sides is 0.005 mm (0.0002 inch). Both the taper error and the perpendicularity error were corrected.

To demonstrate that the tool tip tilting mechanism is able to handle more sophisticated patterns, two parts of a gear pattern were cut as shown in Figure 12.

Figure 12. Gears cut with tool tip tilting mechanism

6 CONCLUSIONS

The method of “compute first, move later” allows sophisticated calculations and adjustments for error correction at every motor step. The use of a cutting speed model combined with the ability to vary the tool path speed one step at a time provides a convenient way to minimize the striation marks and most jet lag errors at corners and arcs. Innovative techniques such as corner passing and multiple-acceleration schemes enhance productivity and quality at the same time. Finally, the development of a patent-pending tool tip tilt mechanism and a taper model improves the quality of abrasivejet machining by eliminating taper.

7 REFERENCES

Anderson, U. and Johansson, B., "Cutting Quality Improvement by Start and Stop Procedures for Closed-Contour Cutting," *Proceedings of the 16th International Conference on Water Jetting*, October 16-18, 2002: Aix-en-Provence, France, pp 259-266.

Groppetti, R., Gutema, T., and Lucchio, A. D., "A Contribution to the Analysis of Some Kerf Quality Attributes for Precision Abrasive Waterjet Cutting," *Proceedings of the 14th International Conference on Jetting Technology*, September 21-23, 1998: Brugge, Belgium, pp 253-269.

Henning, A. and Anders, S., "Cutting-Edge Quality Improvements through Geometrical Modeling," *Proceedings of the 14th International Conference on Jetting Technology*, September 21-23, 1998: Brugge, Belgium, pp 321-328.

Knaupp, M., Meyer, A., Erichsen, G., Sahney, M., and Burnham, C., "Dynamic Compensation of Abrasive Water Jet Properties through 3-Dimensional Jet Control," *Proceedings of the 16th International Conference on Water Jetting*, October 16-18, 2002: Aix-en-Provence, France, pp 75-90.

Olsen, J. "A Bend in the Stream," *Cutting Tool Engineering.* Volume 48, Number 1, February 1996.

Zeng, J., Kim, T.J., and Wallace, R.J., "Quantitative Evaluation of Machinability in Abrasive Waterjet Machining," *Proceedings of the 1992 Winter Annual Meeting of ASME*, "Precision Machining: Technology and Machine Development and Improvement," PED-Vol.58, Anaheim, 1992, pp 169-179.

Zeng, J., Olsen, J., and Olsen, C., "The Abrasive Waterjet as a Precision Metal Cutting Tool," *Proceedings of the 10th American Waterjet Conference*, August 14-17, 1999: Houston, Texas, pp 829 – 843.

2003 WJTA American Waterjet Conference
August 17-19, 2003 • Houston, Texas

Paper 1-E

WJ DECOATING

M. Annoni, M. Monno
Politecnico di Milano - Dipartimento di Meccanica
Milano, Italy

ABSTRACT

The development of material removal processes able to strip the surface of coated components, used in the aeronautical engines' field in order to improve their performances against thermal and mechanical actions, is one of the research focusing points in this field.
The removal processes suitable for this application have to decoat complex geometry components without damaging the metallic base material: chemical treatments are currently used for these purposes but they imply a strong environmental impact. Among the mechanical processes, waterjet shows many interesting characteristics able to satisfy the requirements in terms of productivity, flexibility, precision and environmental sustainability.
In the frame of this work, two different kinds of coating have been considered (a thermal barrier and an abradable coating) and an analysis on the waterjet process parameters' effects on the removal capability has been carried out leading to a performance evaluation.

Organized and Sponsored by the WaterJet Technology Association

1. INTRODUCTION TO THE THERMAL SPRAYING TECHNOLOGY

Thermal spraying is a generic term to describe a collection of coating processes involving material transport at high speeds and temperatures. Particles or droplets of coating materials are accelerated at high speeds, heated and then thrown towards an object (i.e. the substrate) where they deform creating a mechanical bond with the underlying surface. The rapid solidification rate of 1 million °C/sec provides a fine microstructure and metastable phases that provide properties not attainable with other material production processes. Bonding of the particles or droplets depends upon both the material being deposited and the process used for deposition. The surface to be covered commonly needs to be roughened, for example by sand blasting, to provide a basis for mechanical bonding. It can be immediately noticed that waterjet treated surfaces, after the decoating of the exhausted layers, naturally present the roughness characteristics needed to bond the new layers without using other processes. Surfaces that can be coated include plastics, glass, ceramics, metals, paper and composites. Coating strength is dictated by the strength between the coating structural elements, known as cohesive strength, and the strength of the coating to the underlying base material, termed adhesion strength. The cohesive strength depends upon the material properties and also on the porosity within the coating. The material delivery in thermal spray is provided by a torch/gun or, more simply, a nozzle that establishes a thermo kinetic condition for heating and transporting the feedstock. The list of thermal spraying processes incorporates flame spraying, two wire arc spraying, plasma spraying, detonation gun, high velocity flame spraying (HVOF) and cold spraying. The sprayed materials can be metals, ceramics or polymers. [1].

2. APPLICATIONS OF THE THERMAL SPRAY TECHNOLOGY

2.1 Mechanical wear control

The mechanical wear control is the most common application of the Thermal Spray processes; it implies a deep knowledge about the physical properties of the surfaces in contact. Among the controlled wear mechanisms, it is possible to mention: abrasion, erosion and fretting corrosion. This last phenomenon takes place whenever small amplitude alternating sliding between two surfaces happen for many cycles. For example, interference couplings sometimes allow relative movements of some nanometers when loaded with alternating forces. This leads to two kind of damaging: surface wear and fatigue wear. Fretting corrosion usually takes place on turbine blades and on the compressors' seals [2].

2.2 Dimensional control

The use of seals coated with abradable material by means of Plasma Spray is common: this way it is possible to control and reduce the gap between rotor and stator through which the gas passes in turbines, obtaining an increase of the efficiency and a fuel cutback. The abradable coatings also reduce the risk of collision between rotating and static components inside the machines. In order to be competitive, the plasma spray coating technology applied to the gap control has to satisfy some requirements: easy application; easy removal in case of overhaul; no damage to the downstream components because of the particles removed by wear. For enhanced abradability, the energy for particle detachment must be reduced so it is made use of small matrix particles, a polymer, to generate porosity, and solid lubricants or release agents to act as dislocators within the coating. During thermal spray deposition, the polymer phase lowers the coating stresses, thereby allowing the deposition of thick coatings. When burnt-out in a subsequent heat treatment, the abradability of the coatings is further improved. These coatings are used in the original manufacture to provide the best possible seals in the first instance. They are also used during overhaul to repair any excessive clearance produced during service. Substantial improvements in engine performance and efficiency can be obtained by operating with clearances smaller than those achieved in the original manufacture where abradable coatings were not used [3].

2.3 Thermal barriers

In order to protect the metallic parts exposed to high temperatures, such as the combustion chambers of gas turbines, in which even 1000 °C can be reached, thermal spray coatings can be usefully applied allowing to reach higher temperatures and higher efficiencies. The protection is extended also to chemical phenomena which take place at high temperatures, like sulfidation and oxidation. Zirconium oxides are a valid protection for oxidation, while Nickel-Aluminum alloys (95% - 5%), can be applied against corrosion.

2.4 Dimensional recovery

Thermal spray technology is also used to restore the initial dimensions of worn surfaces by applying coatings of controlled thickness.

3. STATE-OF-THE-ART DECOATING PROCESSES

In the aeronautic industry, in order to maintain high safety standards, every single mechanical component is subject to a program of preventive maintenance: after a defined number of working hours, the engines are stripped and overhauled. The base materials of many components are high resistance alloys, iron, nickel or titanium based; their surface is often coated by layers of recovery, anti wear or anti friction materials: this coatings are usually produced by Plasma Spray techniques, as the ones considered in this study. In order to carry out the maintenance of the components, all the coating material has to be removed (bond- and top-coat). After the removal, the base material surface is treated by sand blasting in order to increase its roughness and improve the adhesion of the bond coat. The following recoating process requires that the base material surface is completely clean and not damaged by the removal operation. In the Table 1, the characteristics of the most diffused decoating treatments are evidenced. A particular attention goes to the chemical decoating: the removal of the coating layers is obtained by means of substances which chemically react with the material they are made of; the components are placed in heated tanks containing solutions suitable for the coating to be removed. The chemical agents have to be periodically replaced because of their saturation. The main disadvantages of the chemical removal have been indicated in Table 1, but the most important is clearly the environmental impact, which is sufficient for requiring an alternative decoating method. This work aims to study the applicability of the waterjet technology to decoating treatments avoiding the drawbacks mentioned for the other techniques [5].

4. FIRST EXPERIMENTAL STAGE: PRELIMINARY TESTS ON DIFFERENT MATERIALS

The first approach to the decoating process applied to aeronautical interest materials has been focused on the typologies indicated in the Table 2, which have been provided by FiatAvio, a leading Italian company operating in the field of aeronautical engines. The application of waterjet technology to the decoating process comes from the need to reach the complete removal of the coating layers preserving the base material: the waterjet operates with different mechanisms on the target materials according to their ductility, thus it is possible to set the process parameters in order to remove the surface layers without producing undesirable effects on the base material [6], [7], [8].

For some industrial applications, as the ones studied in this work, the base surface is coated by at least two layers of different materials: the bond coat and the top coat. The bond coat is usually a ductile, very dense and not much porous material and its more common functions are to fix the top coat to the base material and to prevent oxidation. The top coat can have different functions: in a gas turbine it can be used as recovery or abradable material or as a thermal barrier. According to its application, the top coat can be ductile or very brittle. Starting from this considerations, the preliminary phase of the experimental work has analyzed the process parameters' effects on the available coatings in order to determine the best materials on which the work should have to focalize. The object has been to find out a representative material for the easy-to-work coatings for the hard-to-work ones, under the point of view of the removal rate. It has been decided to make use of a pure waterjet, situation in which the difference in the behavior of ductile and brittle materials is more evident. The Table 3 reports the monitored process parameter during the preliminary experimentation [9].

The first set of experiments has been focused on the determination of the parameters' ranges able to satisfy the requirement on the absolute lack of base material damaging on naked specimens (without coatings) (Table 4 (a)); the removal has been considered null if less than 1 mg. The second set of experiments has tested the machinability of the studied coatings (Table 2) at two different levels of energy (Table 4 (a), (b)). The evaluation parameter has been the volume removal, calculated from the weight removal by means of the coatings' densities. A suitable fixturing system has been carried out for the plane rectangular workpieces and a controlled drying procedure has been applied after the treatment in order to avoid the humidity effects on the measurements. The tests have carried out the following results:

- Easy-to-work coatings (in both the energy conditions): METCO450NS (base material: AISI410) and METCO450NS+ZRO154 (base material: Ti230).
- Hard-to-work coatings (in both the energy conditions): METCO443NS.

5. SECOND STAGE: TESTS ON THE MATERIALS OF INTEREST

The results of the first preliminary phase have been discussed with the industrial partner in order to define the set of coatings on which the analysis had to be focalized. The Table 5 reports the selected combinations.

The specimens provided for this part of the work have been rectangular (150x25 mm) and plane, but the thickness of the coatings has been higher compared to the specimens of the first phase (about 1 mm against 0.1 mm). For this reason, the parameters' ranges have been modified and optimized under the point of view of the removal capability of the jet (Table 6).
The results of the ranges' optimizing experimentation have been evaluated by means of:

- Kerf width.
- Presence of the top- and bond-coat (qualitatively based on the different colors of the materials after a suitable chemical treatment).
- Base material removal.

The preliminary work carried out by means of the described experimental runs has allowed to notice a trend in the behavior of the kerf width: when the feed rate starts increasing, at a fixed value of water pressure, the kerf width is initially low and the base material is removed (Figure 2, (a)). Going on with the feed rate increasing, the kerf width gets larger and the base material is not affected (the jet operates horizontally, lifting top- and bond-coat and removing them as brittle materials; Figure 2 (b)). Then the kerf gets narrow again showing oscillating widths because of the low amount of energy (Figure 2 (c), (d)). The mentioned phenomenon takes place at different energy contents in function of the material to be removed. In the Figure 2, the results coming from the second preliminary phase on METCO450+ZRO154 (base material: Ni C263) have been presented. The work carried out up to this point has allowed to fix the ranges of the process parameters for the following factorial plan (Table 6).

6. THE MAIN EXPERIMENTATION

Once determined the ranges for the factorial plan, the experiment have been carried out according to the procedure of Table 7. The number of the carried out experiments has been 48 per each kind of coating.

6.1 Weight removal results

The ZRO154 is evidently more dense than the METCO601 (Table 5); this produces, together with a different minimum pressure value for the two kinds of coating, very different mean values in the removal performance on the analyzed materials (Figure 3). It can be noticed that the effect of the water pressure is opposite on the two coatings.

6.2 Kerf width results

A study based on the removal capability in terms of volume (calculated by means of the materials' densities) is not allowed by the layered composition of the coatings. The only way, alternative to weighting, to compare the jet performance on the studied coatings has been to consider the width of the created kerf. The specimens coming from the weight analysis have been treated in order to acquire information about the kerf widths. The applied procedure has been:

- Grinding and polishing of the lateral surface.
- Acid attack to evidence the different layers.
- Verification of the removal completeness.
- Measurement of the kerf transversal width by means of an optical microscope (144 measures per kind of coating).

The differences between the kerf widths obtained on the two kinds of coating can be related only to the properties of the top coats: the lower values of the METCO450+ZRO154 mean that this coating needs a higher level of energy to be removed on the bottom of the kerf (Figure 4 (bottom)), while it needs less energy for the removal in weight (Figure 3). The information coming from the weight, volume and kerf width analyses could be considered together in order to draw some considerations also on the removal mechanism (ductile or brittle) of the two coatings: for example, the ratio between the mean weight removal (ZRO154/METCO601) (Figure 3) is: 0.85/0.22=3.86, but the ratio between the densities is: 5.4/1.7=3.18; thus, if the presence of the bond coat is neglected, it can be drawn that the weight removal, favorable for the ZRO154, cannot be explained only by the different densities, but some other phenomena take place, such as a higher volume removal for the ZRO154 due to a brittle mechanism based on cracks formation and expansion. Moreover, if the width of the cleaned zone is considered, it can be noticed that the ZRO154 shows the lowest mean value, which means that the higher removed volume has a smaller base, i.e. the ZRO154 kerf has more inclined walls (V shape for ZRO154 and U shape for METCO601). These considerations, having a limited reliability due to the different low pressure values for the two coatings and to some simplifying hypotheses, can be useful for further analysis and can indicate some guidelines: the METCO601, used as abradable material, has a more regular behavior, similar to a ductile material behavior, whereas the ZRO154, used as thermal barrier, shows a typical brittle removal mechanism.

The ANOVA analysis shows similar trends for the effects of the process parameters on the kerf widths for the two coatings: this could allow a common modeling explanation having their mechanical properties as parameters. All the process parameters are influential for METCO601, starting from the most significant: pressure, angle, stand off distance and feed rate. On the ZRO154, the angle is not statistically significant; the other parameters can be listed, in order of importance, as follows: pressure, feed rate and stand off distance (Figure 4). The best removal conditions can be obtained for high values of pressure and stand off distance, low values of feed rate and a perpendicular jet inclination. This last indication points out that, generally speaking, the behavior of the two coatings can be considered as brittle, even if some distinctions can be made. Further studies could be carried out on the modeling of the represented trends basing on a comprehensive energy parameter [11].

7. BEST REMOVAL CONDITIONS

7.1 Technological best

The object of this section has been to determine the best removal conditions related only to the top performance of the jet, without considering economical aspects. Looking at the graph of the Figure 4 (top), the best removal conditions in terms of kerf width are the conditions *ps*, *pvs* and *pas*, but the impact angle has not been statistically significant for the ZRO154, thus the condition *ps* can be taken as reference for the further work; the impact angle can be kept constant at 90°. The graphs of Figure 4 (bottom) suggest to select high values of pressure, but the available plant has been already set at its limit with 350 MPa.

Also the feed rate has been kept constant for the further experimentation: its increasing would have produced a removal decrease, while its decreasing would have been dangerous for the base material. The only modifiable parameter has been the stand off distance: increasing its value has been possible and its effects could have been reasonably positive for the kerf width (Figure 4 (bottom)). The stand off distance range for the factorial plan has been selected basing on the mean values of the other parameters inside their ranges, but, in this last analysis, focused on the best removal conditions, the amount of available energy is higher, thus it can be foreseen an increase in the maximum usable value of stand off distance. The process parameters for the technological best has been set as indicated in Table 8.

7.1.1 Metco601

The Figure 5 (top) shows an increase of the kerf width up to a 90 mm stand off distance: an increase of this process parameters causes a break-up of the jet into small particles [12], which is not sensible at the beginning, where only the positive effect of the increase of the jet cross section plays a significant role; going on, the decrease of the specific energy on the jet cross section gets stronger than the mentioned positive effect and a peak is reached; higher values of stand off distance become not convenient. The standard deviation of the kerf width results has been considered, taking into account only the conditions under the threshold value of 5%. The technological best removal value corresponds to a stand off distance of 110 mm, with a kerf width of 1.84 mm.

7.1.2 Zro154

Considering the ZRO154, the trend of the kerf width is less steep (Figure 5 (bottom)). As it has been already outlined, this coating requires a higher amount of energy in order to obtain larger kerf width at the bottom: the same increase of sod causes less positive results in the first part of the curve. Taking into account the standard deviation of the results, the best condition has been obtained for a stand off value of 80 mm, with a kerf width of 1.58 mm.

7.2 Industrial best

In this section of the work, the best removal condition has been determined considering the constraint of the highest level of productivity. In this situation, the possibility to make use of a multiple nozzle cutting head has been taken into account; for this reason, the further experimentation has been divided in two parts, considering a cutting head configuration with one and with two nozzles.

7.2.1 Single nozzle

Basing on the graph of Figure 4 (top) it is evident that the best condition in this case is *pvs*: its absolute result is slightly lower than the *ps* result but it is obtained with the maximum feed rate (it has to be reminded that the angle effect can be neglected for the ZRO154 and its value has to be fixed at 90° to obtain the best quality on the METCO601). As for the technological best condition, only the stand off distance can be better investigated. The parameters of the experimentation have been presented in Table 9.

7.2.1.1 Metco601

Comparing to the technological best removal condition, the mean kerf width reduces of about 15% in the present case (Figure 6 (top left)). The trend is positive up to sod = 120 mm, but, reasonably due to the high values of feed rates, the curve is not so regular and the standard deviations have been higher. The condition which respects also the threshold on the deviation is sod = 90 mm and kerf width = 1.53 mm.

7.2.1.2 Zro154

In these conditions of high pressure and high feed rates, it seems that the ZRO154 is more stable considering the kerf widths (Figure 6 (bottom left)). In any case, the trend is very similar to the one registered for the technological best condition, even if the kerf width mean value is lower. The optimal condition is: sod = 70 mm and kerf width = 1.50 mm.

7.2.2 Double nozzle

When treating configurations with multiple nozzles, the intensifier power has to be considered in order to guarantee to be able to carry out the work without requiring too large size plants and investments. In this case, the value for the water pressure has been fixed at 250 MPa, the minimum tested value in the main experimentation, and it has been decided for a double nozzle configuration. The parallel jets have been supposed not to interfere; this hypothesis allows to carry out the experiments with a single nozzle, doubling the effect on the kerf width at the end. The parameters' values for this set of experiments have been indicated in the Table 9. The following results refer to the performance of a single nozzle operating in the condition selected for a double nozzle configuration. The combined effect of the parallel nozzles has been considered in the following.

7.2.2.1 Metco601

As it could be foreseen, the mean kerf width has reduced due to the lower value of pressure and the trend has been still positive with the stand off distance increasing (Figure 6 (top right)). The best condition has been obtained at the stand off distance value of 80 mm, where the kerf width has been 1.35 mm, 2.70 mm if the double nozzle configuration is considered.

7.2.2.2 Zro154

At low values of pressure, ZRO154 does not behave well, because the kerf width shows high deviations from the mean value. Comparing to the single nozzle configuration tests, it can be drawn that the parameter which plays the most important role on the kerf width standard deviation is the water pressure. Since this last condition is not applicable because of its instability (Figure 6 (middle right)), it has decided to test also a different combination of process parameters (feed rate = 4000 mm/min instead of 6000 mm/min) to be used in case of double nozzle configuration on ZRO154 (Table 9). Also in this case, the standard deviation on the kerf width is high (Figure 6 (bottom right)), but it has been possible to find out a condition in which the deviation threshold has been satisfied: sod = 80 mm and kerf width = 1.35 mm (2.70 mm for double nozzle configuration).

7.3 Comparison between the optimal conditions

Once the best conditions have been determined for the different analyzed situations, a comparison between them can be carried out.

7.3.1 Metco601

The trends for the mean kerf widths are always positive (Figure 7 (top left)). The difference between the technological best and the industrial best with 1 nozzle is due to the different value of feed rate (2000 mm/min vs. 6000 mm/min). The difference between the industrial best with 1 nozzle and with 2 nozzles is due to the difference in pressure (350 MPa vs. 250 MPa). Starting from the lowest curve, the amount of available energy increases; the maximum difference between the lowest curve and the highest reaches 25% of the kerf width. It has to be reminded that the mean kerf width value for the curve of the technological best with two nozzles has to be doubled in order to determine what the width can be in case of a single pass made with the double nozzle configuration: it is clearly the most productive condition.

7.3.2 Zro154

For this kind of coating, it has been already pointed out how the technological best with two nozzles and feed rate of 6000 mm/min has not guaranteed the required standard deviation (the lowest curve in the graph of Figure 7 (top right). The curve of the industrial best with two nozzles compared to the curve of industrial best with one nozzle evidences how, at high stand off distances, the effect of the pressure is more important comparing to the effect of the feed rate: the reduction of feed rate (4000 mm/min vs. 6000 mm/min) has not been able to compensate the reduction of the pressure (250 MPa vs. 350 MPa). The pressure seems to be the most important factor for the removal steadiness.

7.4 Comparison between coatings

The graph of the Figure 7 (bottom) represents the different behaviors of the two kinds of coating studied in this work; the reported condition is the industrial best with two nozzles (P = 250 MPa; v_{ZRO154} = 4000 mm/min; $v_{METCO601}$ = 6000 mm/min). Up to a value of stand off distance where the amount of specific energy on the workpiece has been still able to remove material by brittle mechanism on the ZRO154, the mean kerf widths are quite the same for the two coatings, even if the parameters' set for the ZRO154 determines a higher value of energy (lower feed rate). After a value of 80 mm of stand off distance, the specific energy has been not sufficient to remove by brittle mechanism and the mean kerf width has decreased. The removal on the METCO601 is more regular, confirming a ductile kind of removal mechanism.

8. LARGE SURFACE REMOVAL

The last part of the experimentation focuses on the determination of the distance between the axes of two jet passes in order to optimize the removal on large surfaces. At first, four values of overlapping between kerfs have been tested (-25%, 0%, +25% e +50%), then a more specific analysis has been carried out in the ranges of interest. The process parameters for METCO450+METCO601 have been the industrial best ones (2 nozzles) and, for METCO450+ZRO154, the industrial best ones (1 and 2 nozzles) (Table 10). Refining the analysis, it has been evidenced how the best overlapping between kerfs for the double nozzle configuration is 6.25% for both the kinds of coating. Instead, the single nozzle industrial best condition for the ZRO154 requires an overlapping of 12.5%.

9. RESIDUAL STRESSES AND PROCESSING TIMES

A first qualitative analysis has been carried out to compare the residual stresses produced by the waterjet treatment comparing to the other current removal methods. Both the coatings reveal an homogeneous compression condition after the jet treatment, the best situation for the fatigue resistance, while the METCO601 specimens, treated by chemical substances, show a variability of the stress conditions passing from compression to traction zones and the ZRO154 grinded specimens show a traction stress condition, dangerous for the fatigue resistance of the components. Also a preliminary analysis of the processing times has been carried out. It has to be reminded that the mechanical processes require sensible fixturing times due to the need to guarantee that a minimum amount of base material is removed during operations. Waterjet is less sensible to the variations of the workpiece position, as it has been confirmed by the trends of the mean kerf width varying the stand off distance. This makes the waterjet treatment faster than the other traditional mechanical processes. The comparison between waterjet and chemical treatment has to be carried out basing on the amount of specimens which can be contained in a tank. Basing on the indications coming from the industrial partner, the chemical treatment times for a tank containing 800 specimens like the ones object of this work, is about 8 hours. In order to cover the same total surface, waterjet processing takes about a quarter of time using the double nozzle configuration (fixturing times have not been considered). This analysis has not the object to be comprehensive but to give a first impression about the performance of the waterjet technology in decoating applications: this promising results have to be further investigated and validated.

10. CONCLUSIONS

This work has the aim to present the first experimental results regarding the waterjet decoating process carried out on specimen of aeronautical interest. The steps followed during the work can be summarized as follows:

- Different coatings’ behavior testing (specimens provided by FiatAvio): determination of the process conditions able to remove coatings without damaging the base material and selection of the most interesting materials on which the analysis had to be improved.

- Determination of the process parameters' ranges on the selected kinds of coating: METCO450+ZRO154 (thermal barrier) and METCO450+METCO601 (low temperature abradable material). At the end of this step, the optimal ranges, in terms of preservation of the base material and in terms of productivity and quality of the process, have been selected for both the studied coatings.
- The ranges coming from the step before have been used to carry out a factorial experimental plan on the performance of the process (weight removal and kerf width); the effects of the process parameters on the observed variables have been determined.
- Basing on the results of the factorial plan, the best working conditions have been determined under the point of view of the absolute removal capability (condition called *technological best*) and under the point of view of the productivity (condition called *industrial best*); for the industrial best condition, the analysis has been extended to a double nozzle cutting head configuration.
- A comparison between the behavior of the two studied coatings has been carried out determining a brittle like removal mechanism for the METCO450+ZRO154 and a ductile like one for the METCO450+METCO601.
- The industrial best conditions have been applied to remove large surfaces of coating material; the value for the passes' overlapping has been determined in order to obtain the maximum cleaning effectiveness.
- The favorable stress conditions after the waterjet treatment (compression) have been preliminarily pointed out and compared to the performances of grinding (traction) and chemical treatments (variable).
- Also the advantages of the waterjet treatment in terms of processing time have been indicated.

The main advantages of using waterjet as a decoating process are:

- Negligible environmental impact.
- High productivity performance.
- Versatility on complex geometry components and on different coatings.
- Scalability of the plants (multiple nozzle cutting head configurations).
- High level of automation.

At least three future lines of research can be foreseen starting from the present work:

- Formulation of a model based on the jet energy content, able to represent its effect and, consequently, the effect of the process parameters on the removal performance in the ranges of interest.
- Investigation on the possibility to directly reapply the plasma spray coatings after the waterjet treatment without sand blasting.
- Study on the fatigue resistance of the waterjet treated components.

11. ACKNOWLEDGEMENTS

Special thanks go to Stefano Bertola and Luca Colombini for the important work carried out.

12. REFERENCES

[1] http://www.azom.com/default.asp
[2] A. W. Batchelor, G. W. Stachowiak: Engineering Tribology, Elsevier, Tribology Series Volume 24, 1993.
[3] http://www.gordonengland.co.uk
[4] http://www.sermatech.com
[5] J. D. Watson: Thermal Spray Removal with Ultrahigh-Velocity WJ, 7th American Waterjet Conference, 1993.
[6] H. Louis, W. Schikorr : Fundamental aspects in cleaning with high speed water jets, 6th International Symposium on Jet Cutting Technology, UK, 1982.
[7] S. Wu, T. Kim: An application study of plain waterjet process for coating removal, 8th American Waterjet Conference, 1995.
[8] C. Öjmertz: A study on Abrasive Waterjet Milling, PhD Dissertation, Chalmers University of Technology, Göteborg, 1997.
[9] A. Cornier, T. Mabrouki, K. Raissi: The study of HP pure waterjet impact as the primary mechanism of paint decoating process, 14th International Conference on Jetting Technology, 1998.
[10] http://www.sulzermetco.com
[11] B. M. Colosimo, M. Monno, Q. Semeraro: Process Parameters Control in Water Jet Peening, Int. Journal of Materials and Product Technology, vol. 15, No. 1-2, 2000.
[12] R. Houlston, G. W. Vickers: Surface cleaning using water-jet cavitation and droplet erosion, 4th International Symposium on Jet Cutting Technology, England, 1978.

13. TABLES

Table 1. Current industrial decoating processes (drawbacks have white background)

Sand blasting	**Grinding**	**Chemical treatment**
An air flow accelerates particles, usually metallic, towards the component to be treated inside a suitable chamber. Brittle materials, such as zirconium oxides, can be successfully cleaned	This method is applied on ceramic materials making use of diamond grinding wheels	The process does not need the workpiece fixturing, it is able to completely remove the coatings without damaging the base material and it is applicable also to complex geometry parts
Masking is required to protect parts not to be treated	Very long times, due to the process itself, the workpiece fixturing and the machine configuration	High environmental impact
Imperfect coating removal	Necessity to remove some base material in order to guarantee the complete coating removal (reducing the number of the component reconditioning treatments and, thus, its life)	Long removal times (never less than 24 hours)
Impossibility to be applied to ductile material coatings	Applicability only to simple geometry components	Treating components covered by multiple layers requires to make the piece pass through various chemical tanks with a dramatic increase of the process time
If the bond coat is ductile, a following chemical decoating is needed		Necessity to apply masks when some parts of the component do not have to be treated
		Impossibility to treat some kinds of material such as zirconium and magnesium oxides and ceramics in general

3D Milling			
This process reaches important removal rates also treating complex geometry components	Necessity to remove some base material in order to guarantee the complete coating removal	A very precise workpiece fixturing is needed	The tool wear has to be taken into account

Table 2. Coatings and base materials analyzed in the first preliminary experimental stage

Coatings				
Commercial Name	**Function**			
METCO450NS (95Ni5Al)	Recovery material or antifretting material at high temperatures. It provides superior oxidation, heat, and sulfidation resistance (source: Sulzer Metco [10])			
METCO601NS (Al12 Si40 Polyester Blend)	Abradable material at low temperatures (<350 °C)			
ZRO154 ($ZrO_2Y_2O_3$)	Thermal barrier. Characteristics: ceramic material, thermal shock resistance, used for turbine combustors, airfoils, diesel engine pistons, valves, cylinder heads (source: Sulzer Metco [10])			
METCO443NS (Ni18Cr6Al)	Recovery or high temperature anti fretting material			
METCO450NS (Bond coat) + **METCO601NS** (Top coat)	Low temperature abradable material			
71VF-NS (WC 11Co)	Impact and rub wear resistant material; medium temperature fretting resistance			
72F-NS (WC 12Co)	Impact and rub wear resistant material; medium temperature fretting resistance			
81NS (CrC 25 NiCr)	Impact and rub wear resistant material; high temperature fretting resistance			
METCO450NS (Bond coat) **+** **ZRO154** (Top coat)	Thermal barrier			
Base materials				
Ni alloy C263	Steel AISI410	Ti alloy Ti230	Al alloy 6061T4	Steel Jethete M152

Table 3. Process parameters of the preliminary experimentation

Parameters		Short name	Notes
Water pressure	[MPa]	**P**	
Cutting head feed rate	[mm/min]	**v**	
Stand off distance	[mm]	**sod**	kept constant at 20 mm
Impact angle	[degree]	**ang**	kept constant at 0° (measured from the vertical)

Table 4. Condition of maximum allowed energy (a) and condition of lower energy (b)

Parameters		Condition of maximum energy allowed (a)	Lower energy condition (b)
Water pressure	[MPa]	200	100
Cutting head feed rate	[mm/min]	2000	4000
Stand off distance	[mm]	20	20
Impact angle	[degree]	0	0

Table 5. Coatings and base materials selected for the further experimentation

Name	Base Material	Bond Coat	Top Coat	Function
METCO450+METCO601 (also called METCO601)	Ni alloy C263	**METCO450NS** (95Ni5Al)	**METCO601NS** (density: 1.7 g/cm^3) (Al12 Si40 Polyester)	Low temperature abradable material
METCO450+ZRO154 (also called ZRO154)	Ni alloy C263	**METCO450NS** (95Ni5Al)	**ZRO154** (density: 5.4 g/cm^3) ($ZrO_2Y_2O_3$)	Thermal barrier

Table 6. Factorial plan parameters' ranges

Parameters		METCO450 +METCO601	METCO450 +ZRO154	Notes
P	[MPa]	150-350	250-350	the upper value depends on the plant capability; the lower value is higher for METCO450+ZRO154 because, at 150 MPa, it is in the final phase of the removal trend in function of the feed rate (in the studied range of v), so the kerf width becomes irregular and not acceptable
v	[mm/min]	2000-6000		the upper value exceeds the tested range, but the results at 5000 mm/min have been promising, so it has been decided to test the process at higher productivity
sod	[mm]	20-60		range in which the trend of the kerf width in function of the stand off distance is monotone and positive
ang	[degree]	0-20		first attempt range

Table 7. Experimental procedure for the factorial plan

1	preliminary specimen drying	**5**	defixturing
2	preliminary weighting	**6**	compress air drying (water removing)
3	specimen fixturing	**7**	removing of the humidity by dryer
4	waterjet treatment (single crosswise pass)	**8**	weighting

Table 8. Technological best condition's process parameters

Parameters		Values	Notes
P	[MPa]	350	
v	[mm/min]	2000	
sod	[mm]	20-120	step = 10 mm
ang	[degree]	0	
			number of experiments = 33 per coating

Table 9. Industrial best condition's process parameters

		Industrial best (1 nozzle)		Industrial best (2 nozzles)	
Parameters		**Values**	**Notes**	**Values**	**Notes**
P	[MPa]	350		250	
v	[mm/min]	6000		6000	
sod	[mm]	20-120	step = 10 mm	20-120	step = 10 mm
ang	[degree]	0		0	
		number of experiments = 33 per coating		number of experiments = 33 per coating	

Table 10. Large surface removal process parameters. Picture: removal performance on ZRO154 (double nozzle) varying the overlapping; from the left: -25%, 0%, 25%, 50%

Parameters		METCO450 +METCO601	METCO450 +ZRO154	
		Double Nozzle	**Double Nozzle**	**Single Nozzle**
P	[MPa]	250	250	350
v	[mm/min]	6000	4000	6000
sod	[mm]	80	80	70
ang	[degree]	0	0	0

14. GRAPHICS

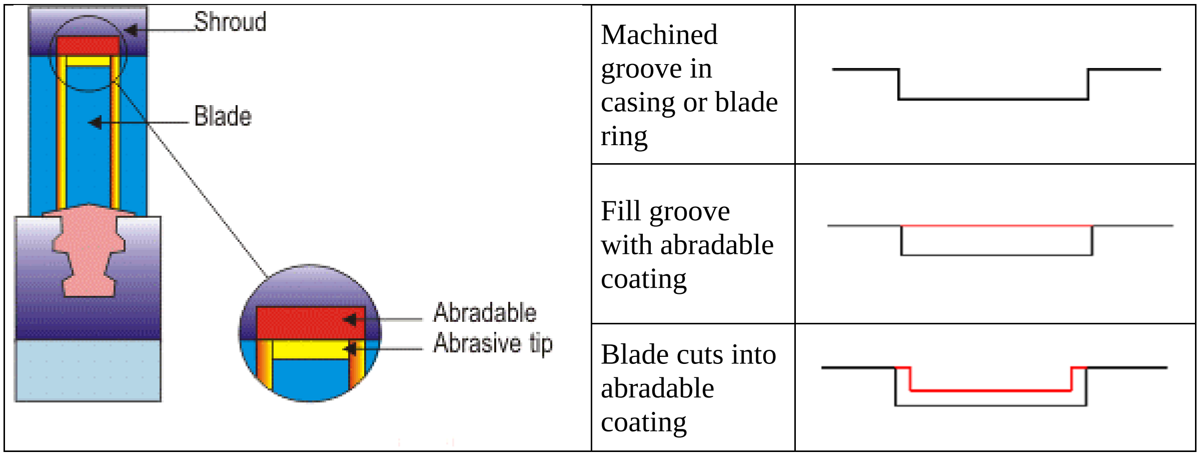

Figure 1. Function of an abradable seal [1], [4].

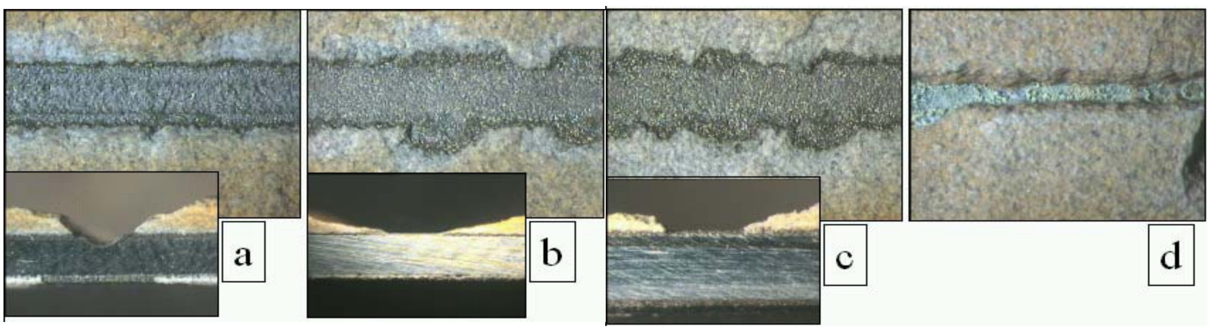

a) P = 350 MPa, v = 30 mm/min: base material removal.

b) P = 250 MPa, v = 1000 mm/min: complete coating removal; base material not affected; more inclined kerf walls.

c) P = 150 MPa, v = 2000 mm/min: uncompleted removal of METCO450 (low energy): in the lateral view, METCO450 still appears.

d) P = 150 MPa, v = 5000 mm/min: uncompleted removal of the top coat too; very narrow kerf.

Figure 2. Optical microscope observations (16x) after a chemical treatment able to give the three present materials different colors.

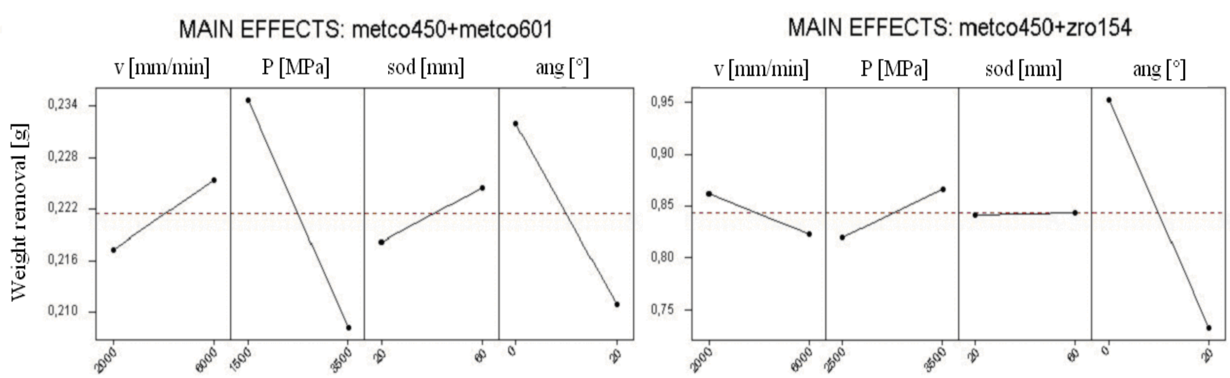

Figure 3. Effects of the process parameters on the weight removal.

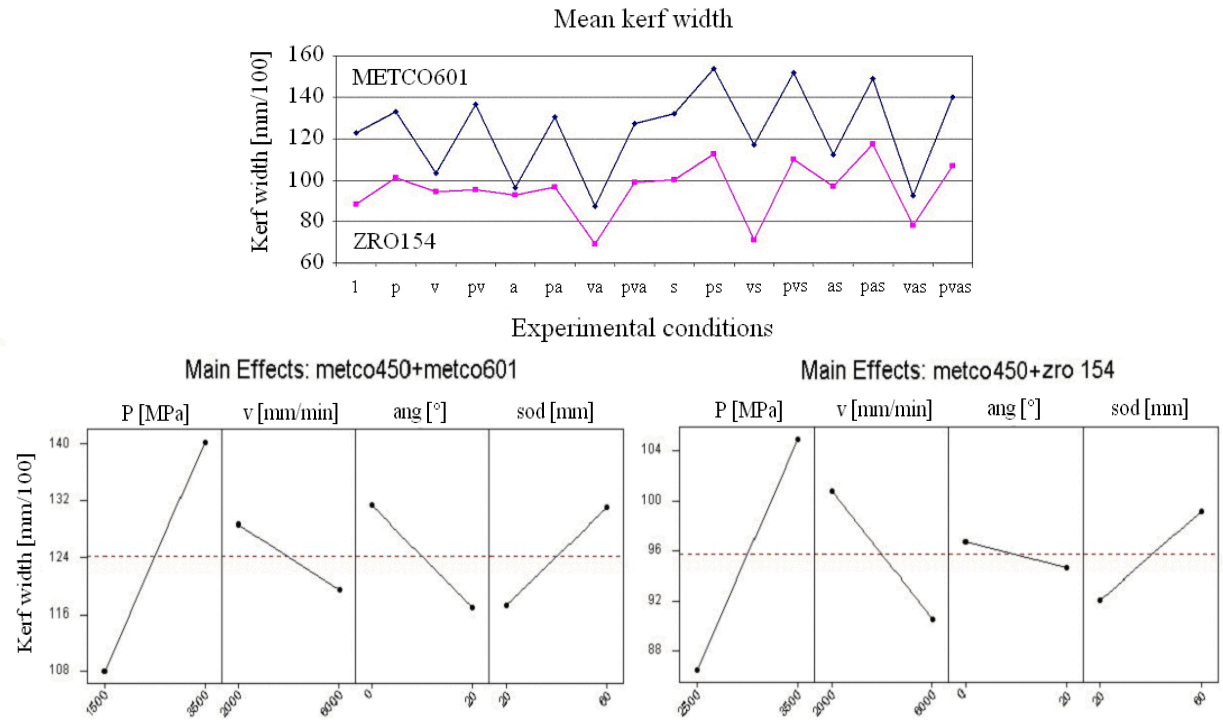

Figure 4. Top: kerf width values in function of the experimental conditions of the factorial plan. Experimental conditions' labels: the presence of the letter representing a parameter means that it is at its high value (*p*=pressure, *v*=feed rate, *a*=angle, *s*= stand off distance; *1*=all the parameters at their low value). The results of the *ps* and *pvs* conditions have been very similar, as if the feed rate had lower effects for high values of pressure. Bottom: process parameters' effects on the kerf width.

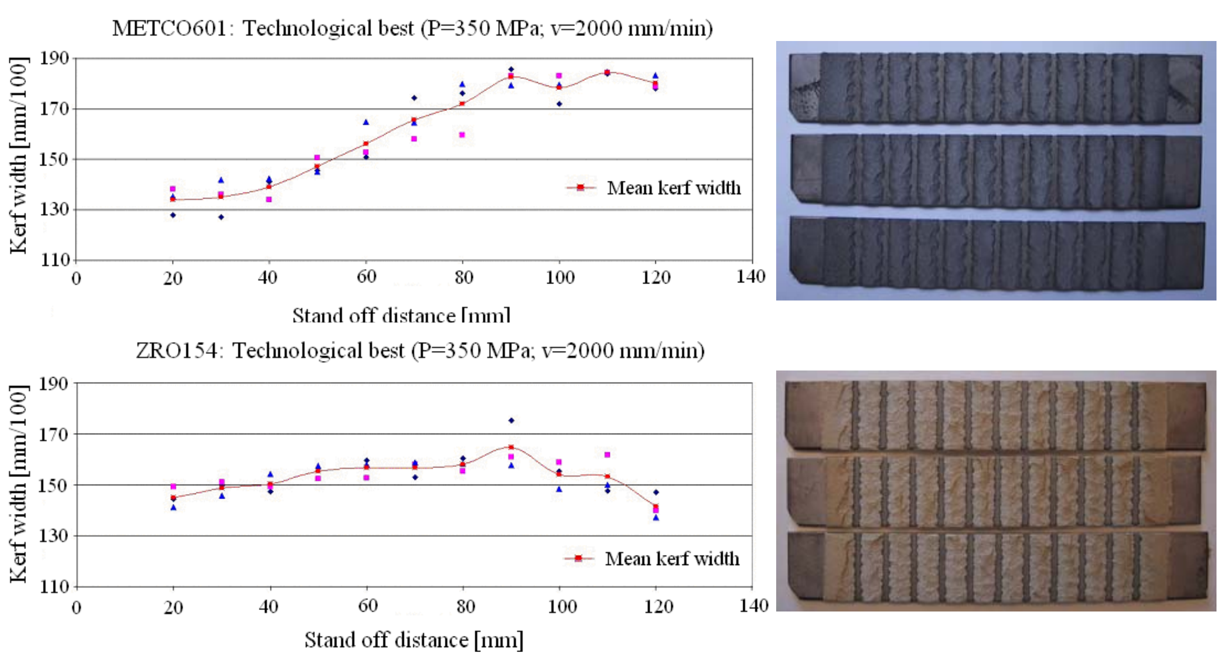

Figure 5. Technological best condition's experimental runs in function of sod. METCO601 (top), ZRO154 (bottom). Lines in the graphs join the kerf width mean values at each condition. Pictures: treated specimens.

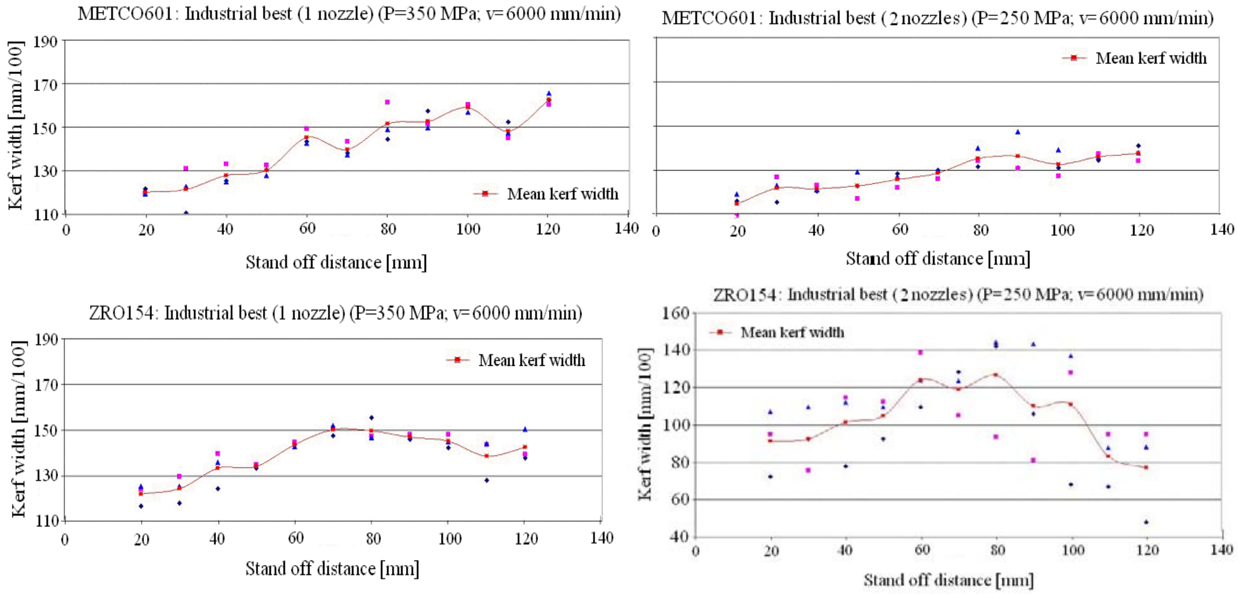

Figure 6. Kerf width in function of the stand off distance. First column: industrial best (1 nozzle). Second column: industrial best (2 nozzles). Lines in the graphs join the kerf width mean values at each condition.

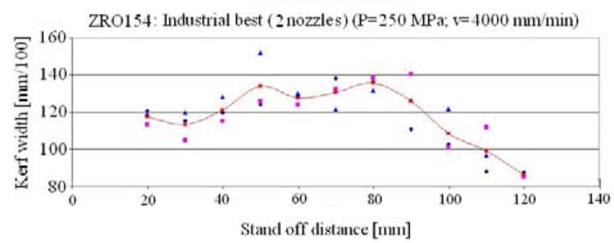

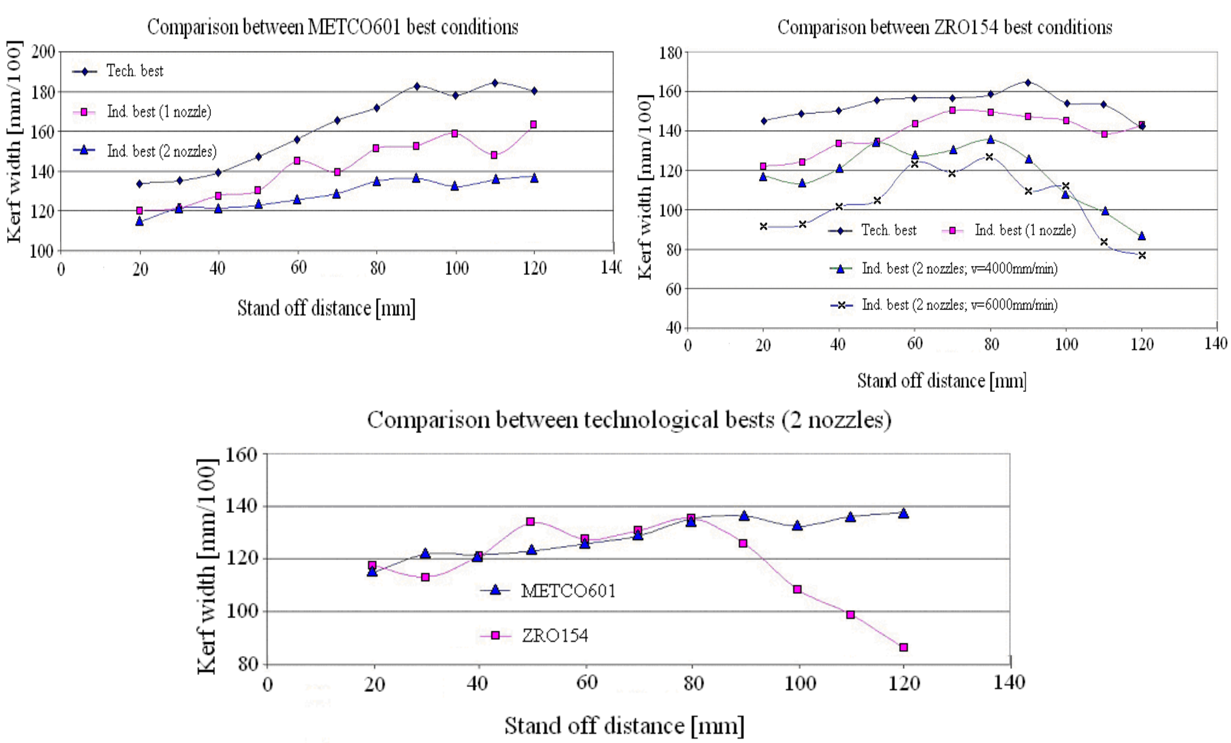

Figure 7. Comparison between best conditions in function of sod. METCO450 (top left), ZRO154 (top right). Bottom: comparison between industrial best conditions (double nozzle) of METCO601 and ZRO154 in function of sod.

2003 WJTA American Waterjet Conference
August 17-19, 2003 • Houston, Texas

Paper 2-E

RADIOLOGICAL DECONTAMINATION OF ARMORED PERSONNEL CARRIERS WITH CONTINUOUS AND PULSED WATERJETS AT UMEA, SWEDEN

W. Yan, A. Tieu, B.Ren and M. Vijay
VLN Advanced Technologies Inc.
Ottawa, Ontario, Canada

D.S. Haslip, T. Cousins, D. Estan and T. Jones
Defence R&D – Ottawa
Ottawa, Ontario, Canada

E.J. Waller
SAIC, Canada

B.E. Sandström, K. Lidström, T. Ulvsand and G. Ågren
FOI NBC-Defence
Umeå, Sweden

ABSTRACT

Radiological decontamination experiments were carried out at the National NBC Defence Centre in Umeå, Sweden, under the Swedish-Canadian accord. A Swedish light armoured vehicle was contaminated by driving it on a track upon which Sodium-24 in particulate form had been spread. The contamination pattern on the vehicle was characterized by a series of measurements with a Geiger-Mueller contamination probe and with Liquid Scintillation Counter measurements of swipes. A conventional high-pressure hot water (200-psi, 130^0) spray, similar to that used by the Canadian Forces, was then used to decontaminate the vehicle. The contamination pattern on the vehicle was then re-measured. This procedure was then repeated using forced pulsed *(FP)* waterjet. The results of the two trials are compared herein. Contamination remained in some areas of the vehicle, particularly the wheel wells. This was due to large standoff distances where the jet was continuous. Nonetheless, overall the performance of forced pulsed waterjet was observed to be better than the hot water blasting. As the trials were conducted on an *ad hoc* basis, and only for short period of time (< ½ hour), the results indicate that further systematic investigation would be required to totally decontaminate the vehicles in the future.

Organized and Sponsored by the WaterJet Technology Association

1. INTRODUCTION

Nuclear and radiological hazards are a continuing problem for military forces in Canada and around the world. Although the probability of use of nuclear weapons has waned somewhat from its peak during the cold war, there still remains the possibility that armed forces could be involved in a conflict in which nuclear weapons are used. Recent events also highlight the possibility that terrorists could use nuclear or radiological weapons against civilian populations Eggen (2002). Thus, nuclear and radiological defences remain a high priority for militaries and governments.

Perhaps the most devastating aspect of a nuclear or radiological attack is the resulting radioactive contamination. Radioactive contamination is (in peace time) strictly regulated worldwide, and acceptable levels of contamination are extremely low Anon (2000a). In addition, radiological decontamination is generally very difficult because the contaminant must be physically removed (as opposed to biological or chemical contaminants, which need only be de-activated or destroyed *in situ*). This tenacity of radiological contamination means that demolition or disposal of contaminated buildings and equipment may be the best (or even the only) option following an attack. It thus behooves researchers to push forward the investigation of new and potentially more effective decontamination techniques.

This paper looks at the decontamination of a SISU XA-180 Light Armoured Vehicle after it was driven on a wet and icy road upon which radioactive particulates was spread (Umeå, Sweden). These data are considered useful for identifying the parts of the vehicle that become most contaminated when a vehicle is forced to drive through contaminated areas. Decontamination trials with the forced pulsed waterjets were attempted based on the earlier promising results reported by Tieu, et. al (2002b). For comparison, conventional high-pressure hot water (200-psi, 130^0) spray was also included, similar to the procedure followed by Tieu, et. al (2002b). The capabilities of the two methods are evaluated and compared.

It must be stated in passing no technical details on the forced pulsed waterjet technique is given here. The details are given by Tieu, et.al (2002b).

2. EXPERIMENTS

These experiments took place in the NBC test facility (NBC-Bana) of the Swedish NBC Defence Centre (Totalförsvarets Skyddscentrum) in Umeå, Sweden. Sodium-24 in the form of powdered sodium silicate was mixed with sand and loaded into the seven containers in the trailer depicted in Figure 1. The driver of the van pulling the trailer can activate a switch that empties these containers slowly through the vertical tubes shown below the plastic containers. The tubes are oscillated left and right to produce a more uniform deposition pattern on the ground. The radioactive material was set down on a 4.2-metre wide, 500-metre circumference track. The material was released at a constant rate, so variations in road contamination were achieved by driving the van at different speeds over different segments of the track. Road conditions were wet and icy, and the surface was roughed up by a snowplow prior to spreading of the material. Weather conditions during the trials consisted of light freezing rain.

Figure 2 shows two maps of the road. The first (on the left) is a sketch; the second is a "bubble plot" showing the dose rates at 1-m above the ground around the track, as measured by a BTI Microspec-3 mapping gamma-ray spectrometer Anon (1999). The areas of the bubbles are proportional to the dose rates. The dose rates in turn are proportional to the contamination level on the road. Based on the microshield calculations, Anon (1998), the total Sodium (Na-24) contamination level on the road was estimated to be about 0.56 MBq/m2, or 1.2 GBq on the track.

The test vehicle for the trials was a SISU XA-180 Light Armoured Vehicle, pictured in Figure 3. The XA-180 drove around the contaminated track 10 times, and then returned to the measurement area. The contamination pattern was then characterized with the ABP-100 alpha-beta probe, Anon (2002c), and with swipes. A Swedish team without previous experience of decontaminating the XA-180 then decontaminated the vehicle with the high-pressure hot water spray. This is the same system developed by DRDC Suffield, but without the CASCAD decontaminant foam, Anon (2001a). Following this procedure, the remaining contamination on the vehicle was re-measured. The XA-180 was then driven out onto the track again for 10 laps, before returning to the measurement area. As before, the contamination pattern was characterized. Decontamination trials were then attempted using the ***FP*** waterjet system. The remaining contamination on the vehicle was again re-measured. The operating parameters of the ***FP*** machine were:

Pressure: 55.2-MPa (8,000-psi)
Diameter of each orifice in the dual-orifice rotating nozzle body: 1.016-mm (0.040-in)
Total water flow: 27.4-litre/min (7.26-usgpm)
Total hydraulic power: 31.6-kW (42-hp)

The operating pressure was constrained so that the paint on the XA-180 would not be removed. Nonetheless, at some locations, loosely adhered paint was removed. It is indeed a pity the duration of the trials lasted only for about ½ hour. This is especially so in view of the fact that considerable efforts were made to get machine ready and in shipping it to Umeå.

3. CONTAMINATION OF THE VEHICLE

The most complete characterization of the vehicle contamination was performed with an ABP-100 alpha-beta probe. These measurements are given in Table 1 for both contamination trials (after each 10-lap circuit). The two sets of measurements bear some resemblance to one another, especially in the general trends described below. However, a comparison also reveals that individual contamination measurements at a given position on the vehicle are not reproducible for the two experimental trials. These pairs of measurements varied by up to a factor of five. The average values over the two trials are also shown superposed on the vehicle in Figure 4. The numbers in the circles correspond to the location numbers in Table 1 (those "below detectable levels (BDL)" are not listed.

The detectable limits varied with position due to the presence of a large radioactive source near the decontamination area. Measurements on the rear and driver's side had a detectable limit of 2.9 cps; measurements on the other two sides had a detectable limit of 4.7 cps. Measurements above the detectable limits are assigned an uncertainty of 10%. This is likely an underestimate at low count rates and an over-estimate at higher rates, but it is a reasonable approximation for this work.

The contamination levels on the vehicle followed a relatively predictable pattern. Namely, very little contamination was observed on the front or rear of the vehicle, or anywhere on the upper half of the vehicle. On the other hand, significant contamination was noticed on the lower halves of the vehicle sides, especially in the wheel wells. It is worth noting that positions 26, 27, 31, and 32 (Fig. 4) are on or around the two propellers at the rear of this amphibious vehicle. However, because of the vehicle design, this part of the vehicle is essentially part of the wheel wells for the rearmost wheels. These were the most highly contaminated surfaces on the XA-180. It is quite reasonable that the wheel wells were contaminated to the highest level, since the tires are responsible for “kicking up” the contamination. However, it is also worth noting how little contamination accumulated in some of the other areas under the wet conditions prevailing during these trials.

No calibration of ABP-100 response to a Na-24 area source was performed. However, based on measurements of Sr-90 and Cl-36 beta sources, Haslip & Cousins (2000b), a reasonable calibration factor was approximately 30 cps/(Bq/cm^2). Thus, the measured contamination levels on the vehicle ranged between 0 and 13 Bq/cm^2 (0.13 M Bq/m^2). Since the average contamination level of the track was estimated at a few MBq/m^2, the maximum contamination level of the vehicle was 1-10% of the average road contamination. This is considered to be a non-negligible quantity for a drive of only 5 km. That does not imply that the contamination level would continue to increase. Previous work has shown that contamination of the vehicle would eventually reach equilibrium with self-decontamination processes, Ulvsand, Ågren, and Lidström (2000c). Indeed, the choice of 10 laps was based on the equilibrium point observed in previous trials in Umeå.

Contamination levels on the XA-180 were also assessed by swipe tests on vehicle surfaces. Swipes were measured in a Liquid Scintillation Counter (LSC). Such techniques are generally very sensitive assays of removable contamination, although obviously they are not effective for the level of fixed contamination. These locations were primarily in the wheel wells of the vehicle, where probe measurements are more difficult, due to the possibility of probe contamination. The two sets of measurements are shown in Table 2. As was noted above, general trends in contamination levels are consistent in the two data sets (e.g. location ‘**I**’ is always less contaminated than any other surfaces), although the contamination levels at a given location were far from reproducible. In fact, these data were less reproducible than the probe measurements. The average measurements for each location are superposed on the vehicle as shown in Figure 5, where the letters in the circles correspond to the letters in Table 2. Values in the table are shown as “BDL” if they are consistent with zero given their uncertainties. These uncertainty estimates are felt to be conservative.

Because swipes were taken largely in similar areas, there are few general conclusions that can be drawn about vehicular contamination. However, one can easily see that the swipe data support the earlier observation that contamination did not collect on the upper half of this vehicle. No differentiation can be made, however, between the data collected from the other nine locations.

It is worth noting that both the probe data and the swipe data show that the contamination levels in the second trial were generally smaller than those in the first trial. One possible explanation is that the vehicle initially had dirt that is effective at trapping contamination. Once this material is removed in the first decontamination, the vehicle as a whole is not as easy to contaminate. In addition to reducing contamination levels on subsequent trials, this process may also inflate the decontamination efficacy in the first trial (when this material is present and easy to wash off). This must be kept in mind in trials involving multiple decontaminations of a single vehicle. In this trial, however, both vehicles were washed before the trials so other explanations must be sought. One possibility is that each circuit of the track redistributes the activity in such a way that contamination on subsequent circuits is less pronounced.

For a few locations, both swipe and probe measurements were made. Namely, probe locations 7, 8, 23, 24, and 25 correspond to swipe locations I, J, B, E, and H, respectively. It is tempting to compare these two sets of measurements so as to derive an exact calibration factor for the probe measurements. The situation was not that simple. Using a probe calibration factor of 30 cps/(Bq/cm2), it was found that the probe contamination values always exceeded those of the swipes. This implies that the calibration factor is underestimated. However, the discrepancy between the two sets of contamination values varied from a factor of 2 to a factor of 30, indicating that no reliable calibration factor could be derived from these data. This does not mean that the data are invalid. Rather, it emphasizes that the probe measures total contamination, while the swipe measures removable contamination. These considerations imply that the probe measurement should always equal or exceed the swipe measurement (as observed). Furthermore, the ratio between the two measurements should vary as the ratio of fixed to removable contamination varies (and a distribution of these ratios is observed). Indeed, as described in the next **Section**, that not all of this contamination was easily removable.

4. DECONTAMINATION

As described in **Section 2**, the experimental protocol consisted of contaminating the vehicle, measuring the contamination levels, decontaminating the vehicle, and re-measuring the contamination levels. This sequence of events was performed twice, once with conventional high-pressure hot spray, and once with the ***FP*** waterjet. This section presents the post-decontamination measurements.

Post-decontamination was characterized as before, with the ABP-100 alpha-beta probe and with LSC measurements of swipes. The ABP-100 measurements are presented in Table 3. As in the previous **Section**, many of the measurements fell below the detectable limits of 2.9 cps on the driver's side and rear, and 4.7 cps on the other sides. Measurements above the detectable limits are once again assigned an uncertainty of 10%.

The vast majority of these measurements were below detectable limits (BDL). In fact, the only measurements showing significant levels of contamination are at positions 23 through 30, the wheel wells and the driver's side propeller housing. Decontamination in these areas was hampered by two key factors. First, these surfaces are more difficult to access than vehicle sides. Second, there are spots of corrosion in the wheel wells that might be expected to accumulate contamination and be difficult to flush. This appears to have held true for both the conventional and ***FP*** waterjet, although in the case of the latter, the standoff distance was too large to aim precisely at the spot (discussed later).

It is difficult to use this Table alone to evaluate the efficacy of the decontamination efforts. In general, the measurements have to be put into context, such as by relating them to initial contamination values. This is done in Table 4. This Table presents results only for locations at which there was initially some measurable contamination. Columns 2 and 3 show the ratio of the contamination level following decontamination to that before, for the two decontamination methods. Where the contamination level following decontamination was below detectable limits (BDL), the ratio is expressed as a 1 confidence limit. The rightmost column is a comparison of the two methods for that position. These comments are discussed in the following paragraph.

Approximately two-thirds of the locations were decontaminated below detectable limits by both systems. Three more locations had small but measurable residual levels of contamination after decontamination, although no measurable levels had been present before. This is presumably the result of contamination splashing from one location to another during the decontamination process. In these cases, however, the activities involved were small. This left five vehicle locations with significant non-null results. These are locations 23, 24, 25, 28, and 30, all of which are in the wheel wells. The results for each of these are summarized below:

Location 23: The conventional system left contamination producing 19 cps, while the ***FP*** system left contamination producing 5.7 cps. Ratios cannot be compared for this case because no initial measurement was taken for the conventional system, but the conventional ratio would likely have been somewhat larger than the ***FP***'s 5%.

Location 24: Both systems fared poorly. The ***FP*** system left about 75% more contamination (6.6 cps vs. 3.7 cps), but as a ratio of initial levels this is much larger (75% vs. 14%).

Location 25: The conventional system produced a sizable splashing effect, turning a 39 cps contamination level into an 81 cps contamination level. The ***FP*** system had almost no impact on the contamination, leaving 93% of the original contamination.

Location 28: The conventional system produced a small splashing effect, turning a 115 cps contamination level into a 159 cps level. The ***FP*** system left 55% of a 230 cps contamination area.

Location 30: The conventional method left no measurable contamination. The ***FP*** system left a 68 cps contamination level where no measurable contamination had been before, indicating spreading by significant splashing.

This analysis was also performed with the data from the swipes. Table 5 shows the contamination levels as determined by LSC measurements of swipes following the two decontamination attempts. Most of the results are below detectable limits, although a few spots still had measurable levels. The ratios of contamination levels before and after the decontamination attempt are found in Table 6, along with a comparison of the two methods.

Seven of the ten locations have essentially null results. Although the conventional method left measurable levels more often, its decontamination ratios are in accord with those of the ***FP*** system. Location '**I**' experienced some splashing following the conventional decontamination. The two exceptional cases are locations B and H. These are described below:

- **Location B**: Both methods left 10-20% of the initial contamination. This location correlates with probe position 23 (driver's side front wheel well), where residual contamination was also observed with the probe.

- **Location H**: Both methods left 30-50% of the initial contamination. This location corresponds to probe position 25 (driver's side rear wheel well), where decontamination was also observed to be poor according to the probe. It should be noted that the residual percentages are lower for the swipes than for the probes, implying a component of "non-removable" contamination.

Thus, there is evidence to support the theory that some contamination infiltrated into the corroded areas, making decontamination difficult. It should be noted, however, that the swipe measurements indicate the presence of removable contamination remaining on the vehicle. Based on the swipe results, the conventional and ***FP*** systems performed equally well.

5. DISCUSSION

The results from this investigation appear to indicate that the overall performance of the ***FP*** system was only slightly better than the conventional hot waterblast system. This is rather surprising in view of the earlier work done in Canada, Tieu, et. Al (2002b), where the results were far superior compared to the conventional system. This, in fact, was the reason for the project in Sweden. There are several reasons for the unexpected poor results, the most important being the duration of only 20 minutes allowed for testing with the ***FP*** machine. Therefore, the tests could be conducted only on an ***ad hoc*** basis. This was indeed unfortunate considering all the efforts that went into pre- and post preparations of shipping the machine to Sweden. The observations listed below clearly indicate the shortcomings in the project.

- The most important requirement was that the paint from the vehicle must not be removed. This requirement, combined with the fact that the engineer of VLN was not a trained operator, made it very difficult to test at appropriate operating conditions.

- The short duration made it virtually impossible to set up appropriate scaffolding etc., to ensure comfort and safety of the operator. Since he did not have the firm foothold, and due to large reaction forces, he could not possibly operate the gun steadily and effectively.

- In order to meet the condition listed above, and in order to decontaminate the entire vehicle, very large standoff distances were used (see Figs. 7 and 8). As discussed in the earlier work, at these standoff distances, the pulse disintegrates into droplets and the coherency is lost, Tieu, et. al (2002b). From this standpoint, there was no difference between the ***FP*** and the conventional systems. The slight advantage, or the disadvantage of migrating (spreading) by splashing the radioactivity into other areas, stems from the fact the speeds of the ***FP*** droplets are significantly higher than the conventional system because of the higher pressure employed.

- Uncertainty in the measurement techniques employed to measure the levels of activity before and after decontamination trials, suggesting more precise instruments must be employed.

- These observations clearly indicate that, if the ***FP*** technique is to be accepted as a standard for decontamination of armored vehicles, more controlled procedure must be adopted. For instance, since the time is not a factor in decontaminating the entire vehicle, lower pressures ($\cong$ 4,000-psi) can be employed without removing the paint, and employing multi-pass procedure to remove the activity spread by splashing. Furthermore, trained operators must be employed, or the operation can be semi-automated to control the standoff distances, etc.

6. CONCLUSIONS

A Swedish SISU XA-180 LAV was driven around a wet and icy contaminated track so as to become contaminated. Decontamination of the vehicle was attempted with two methods, a conventional high-pressure water spray and a ***FP*** waterjet. Neither method was able to achieve thorough decontamination of the vehicle. In comparing the methods, the ***FP*** method produced a slight advantage. However, the lessons learnt from this highly challenging, but unrealistically short duration project, indicate:

- ***FP*** technology has significant potential for radioactive decontamination of armored vehicles and would meet the NATO standards, if appropriate steps are taken (see Tieu, et. al).

- ***FP*** technology also shows promise for chemical decontamination of armored vehicles, despite the scatter in the data and the uncertainty of the measuring technique (see Tieu, et. al).

- International collaboration was indeed a very rewarding experience, and suggests effective team response to deal with critical situations (attack by terrorists) is possible.

7. ACKNOWLEDGMENTS

VLN Advanced Technologies Inc., gratefully acknowledges DREO (Defence Research Establishment Ottawa), Department of National Defence Canada (DND) for the contract. Thanks are also due to Mr. J. Halling and his associates at ISS at Stockholm, who were quite helpful in receiving, setting up and testing the VLN's machine before the trials at Umea.

8. REFERENCES

Eggen, D., "U.S. Detains Alleged Dirty Bomb Terrorist," *Washingtonpost.com*. (Washington, D.C.: The Washington Post Company), June 10, 2002a.

Anon, "Nuclear Safety Orders and Directives," *Director General Nuclear Safety*, Defence R&D Canada, 2000a.

Tieu, A., Yan, W., Vijay, M.M., Cousins, D., Haslip, D.S., Sparkes, S.E., Jones, T.A., and Estan, D., "Chemical and Radioactive Decontamination of Armored Vehicles Using the High-Frequency Forced Pulsed Waterjet Machine," *Proceedings of the 16th International Conference on Water Jetting*, BHR Group Limited, Cranfield, Bedfordshire, MK43 0AJ, England, 2002b, pp. 609-626.

Anon, "BTI Spectroscopic Survey System Microspec-3 Operating Manual," *Bubble Technology Industries Inc.*, Chalk River, ON, Canada, 1999.

Anon, "Microshield Version 5 User's Manual," *Grove Engineering*, Rockville, MD, USA, 1998.

Anon, "ADM-300 Multi-Probe Universal Survey Monitor," *Canberra Eurisys S.A.*, St. Quentin, France, 2002c, (http://www.eurisysmesures.com/produits).

Anon, "CASCAD Decontamination Foam," *NBC Team Ltd.*, Fort Erie, ON, Canada, 2001a, (http://www.nbcteam.com/decon.shtml).

Haslip, D.S., and Cousins, T., "Comparison of Performance of the Automess 6150 and the NRC ADM-300C," *Report DREO TM 2000-091*, Defence R&D Canada – Ottawa, ON, Canada, 2000b.

Ulvsand, T., Ågren, G., and Lidström, K, "Contamination and Decontamination of All Terrain Carrier 206 during Winter Conditions," *Report FOA-R—00-01661-861—SE*, FOI Umea, Sweden, 2000c.

9. GLOSSARY

This paper contains several definitions and units on radiological activity. For the convenience of the readers not familiar with Nuclear Radiation Physics, the following explanations are included.

Alpha, Beta & Gamma rays: These are the products of radioactive decay of an unstable atom, for example, decay of Uranium ($_{92}U^{235}$) atom.
Activity: The unit of radioactivity is the **bacquerel** (Bq) or the **curie** (Ci).
Background: This is the radiation from the outer space, usually called cosmic radiation.
Bacquerel = 1 decay/s, that is, one atom decays in one second.
Curie = 3.7 X 10^{10} decays/s (a very large unit). Therefore, 1 Ci = 3.7 X 10^{10} Bq. Millicurie (mCi) = 10^{-3} Ci; Microcurie (μCi) = 10^{-6}Ci; Nanocurie (nCi) = 10^{-9}Ci and Picocurie (**p**Ci) = 10^{-12}Ci.
Half-life ($T_{½}$): This is the duration after which only 50% of the original atoms remain.
Dosage: This is the term used to describe exposure (personnel or equipment) to a radioactive source. The unit of measurement = Rem/hr (R/hr); 1 millieR/hr = mR/hr = 10^{-3}R/hr). The allowed dosage ranges from 0.5 R to 5 R/year.

Table 1. Count rates on the ABP-100 alpha-beta probe for various locations on the XA-180. A contamination level of 1 Bq/cm2 would produce a count rate of approximately 30 cps. “BDL” stands for “Below Detectable Limits (locations not listed below)”. Locations are identified in **Figure 4**.

LOCATION	FIRST ROUND CONTAMINATION (CPS)	SECOND ROUND CONTAMINATION (CPS)
5	4.0 ± 0.4	BDL
10	10.3 ± 1.0	28.5 ± 2.8
11	9.3 ± 0.9	BDL
12	52.5 ± 5.2	25.0 ± 2.5
16	45.2 ± 4.5	24.2 ± 2.4
17	BDL	7.8 ± 0.8
18	106.2 ± 10.6	26.4 ± 2.6
19	7.2 ± 0.7	6.2 ± 0.6
20	8.4 ± 0.8	7.2 ± 0.7
21	BDL	6.1 ± 0.6
22	BDL	6.3 ± 0.6
23	No measurement	110.8 ± 11.1
24	26.6 ± 2.7	8.9 ± 0.9
25	38.9 ± 3.9	165.4 ± 16.5
26	284.6 ± 28.5	165.4 ± 16.5
27	268.7 ± 26.9	144.5 ± 14.4
28	115.3 ± 11.5	229.8 ± 23.0
29	96.0 ± 9.6	30.0 ± 3.0
31	383.9 ± 38.4	190.2 ± 19.0
32	No measurement	126.3 ± 12.6

Table 2. Contamination levels on the XA-180 as determined by LSC measurements on vehicle swipes.

LOCATION	FIRST ROUND CONTAMINATION (Bq/cm2)	SECOND ROUND CONTAMINATION (Bq/cm2)
A	0.297 ± 0.031	2.347 ± 0.185
B	0.300 ± 0.031	0.304 ± 0.031
C	0.234 ± 0.026	0.139 ± 0.019
D	0.583 ± 0.052	0.224 ± 0.025
E	0.506 ± 0.046	0.052 ± 0.014
F	0.528 ± 0.048	0.024 ± 0.013
G	0.644 ± 0.057	0.091 ± 0.016
H	0.282 ± 0.030	0.132 ± 0.019
J	0.353 ± 0.035	0.093 ± 0.016

Table 3. Count rates on the ABP-100 alpha-beta probe for various locations on the XA-180 following decontamination. A contamination level of 1 Bq/cm2 would produce a count rate of approximately 30 cps. "BDL" stands for "Below Detectable Limits (locations not listed below)".		
LOCATION	**CONVENTIONAL DECONTAMINATION RESIDUALS (CPS)**	**VLN DECONTAMINATION RESIDUALS (CPS)**
5	BDL	4.5 ± 0.4
6	BDL	3.4 ± 0.3
13	3.8 ± 0.4	BDL
23	19.2 ± 1.9	5.7 ± 0.6
24	3.7 ± 0.4	6.6 ± 0.7
25	81.4 ± 8.1	153.4 ± 15.3
26	4.5 ± 0.4	BDL
27	3.6 ± 0.4	BDL
28	159.0 ± 15.9	126.8 ± 12.7
30	BDL	68.0 ± 6.8

Table. 4. Percentage of initial contamination remaining on the vehicle following decontamination by the conventional and forced pulsed jet method.			
LOCATION	**DECON RATIO (CONVENTIONAL)**	**DECON RATIO (PULSED)**	**COMPARISON OF METHODS**
5	< 72%	Splashing	Forced pulsed (***FP***) slight splashing
6	No initial	Splashing	***FP*** slight splashing
10	< 28%	< 10%	Both OK
11	< 31%	No initial	Both OK
12	< 5.5%	< 11%	Both OK
13	Splashing	No initial	Conventional slight splashing
16	< 10%	< 20%	Both OK
17	No initial	< 60%	Both OK
18	< 4.4%	< 18%	Both OK
19	< 65%	< 76%	Both OK
20	< 56%	< 65%	Both OK
21	No initial	< 78%	Both OK
22	No initial	< 75%	Both OK
23	Lots remains	5.1 ± 0.7%	***FP*** better
24	13.9 ± 2.0%	75 ± 10%	Both poor
25	210 ± 29%	93 ± 13%	Conventional splashing, ***FP*** poor
26	1.6 ± 0.2%	< 1.7%	Both OK
27	1.3 ± 0.2%	< 2%	Both OK
28	138 ± 19%	55.2 ± 7.7%	Both poor

Table 5. Contamination levels on the XA-180 as determined by LSC measurements on vehicle swipes. Measurements are made following decontamination.		
LOCATION	**FIRST ROUND DECONTAMINATION RESIDUALS (Bq/cm2)**	**SECOND ROUND DECONTAMINATION RESIDUALS (Bq/cm2)**
A	BDL	BDL
B	0.032 ± 0.013	0.052 ± 0.009
C	BDL	BDL
D	BDL	BDL
E	0.021 ± 0.013	BDL
F	BDL	BDL
G	0.015 ± 0.012	BDL
H	0.127 ±0.019	0.039 ±0.008
I	0.028 ±0.013	BDL
J	0.013 ± 0.012	BDL

Table 6. Percentage of initial contamination remaining on the XA-180 following decontamination by two methods, as determined by swipe measurements.			
LOCATION	**DECON RATIO (CONVENTIONAL)**	**DECON RATIO (*FP*)**	**COMPARISON OF METHODS**
A	< 3.7%	< 0.2%	Both OK
B	10.7 ± 4.6%	17.2 ± 3.3%	Both poor
C	< 5%	< 4%	Both OK
D	< 1.9%	< 2.4%	Both OK
E	4.2 ± 2.5%	< 10.6%	Both OK
F	< 2.3%	< 25.4%	Both OK
G	2.3 ± 1.9%	< 6%	Both OK
H	44.9 ± 8.1%	30.0 ± 7.3%	Both poor
I	Splashing	No initial	Conventional splashing
J	3.7 ± 3.5%	< 6.2%	Both OK

Figure 1. The vehicle used for spreading the radioactive sodium (Na-24) on the track. The seven plastic containers are each filled with an equal amount of sand and sodium.

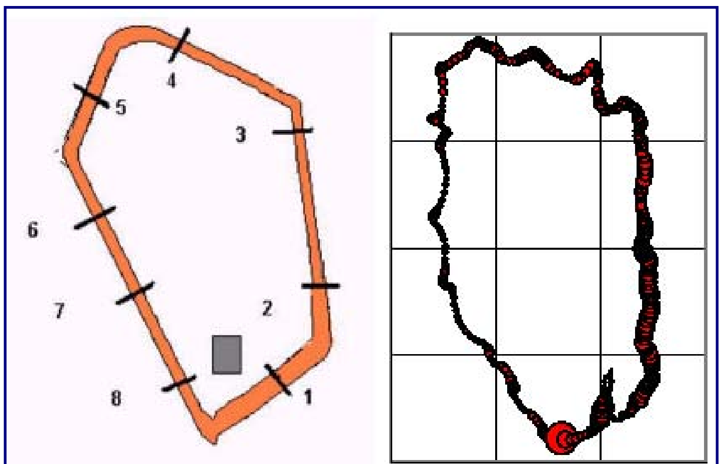

Figure 2. A sketch-map of the contaminated road at the test facility of the National NBC Defence Centre at Umeå.

Figure 3. A general view of the SISU XA-180 light armored vehicle.

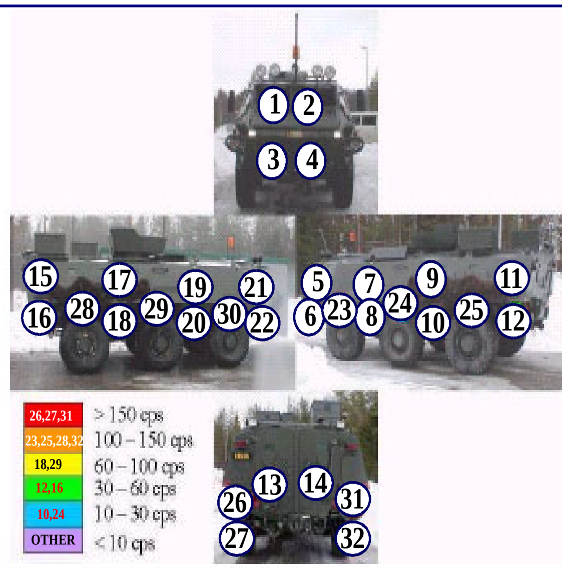

Figure 4. Contamination levels on the vehicle, as measured with the ABP-100 alpha-beta probe (see Table 1).

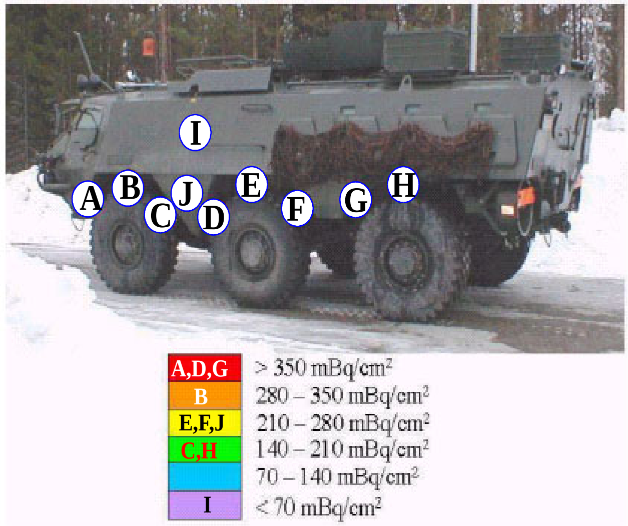

Figure 5. Contamination levels on the XA-180, based on swipe measurements. Locations A-H are on the wheel wells of the vehicle. The letters denoting the positions are used throughout the text.

Figure 6. General view showing decontamination on the backside of the vehicle.

Figure 7. General view showing decontamination in the wheel wells of the vehicle.

Figure 8. General view showing decontamination on the sides (& front) of the vehicle.

2003 WJTA American Waterjet Conference
August 17-19, 2003 ● Houston, Texas

Paper 3-E

FORMATION AND APPLICATION OF A RECTANGULAR JET

E.S.Geskin* and B.Goldenberg
Department of Mechanical Engineering
New Jersey Institute of Technology
University Heights
Newark, New Jersey, USA

ABSTRACT

Depending on the kind of application, a water stream should operate either as a knife or saw (cutting) or as a scraper or brush (milling, cleaning, decoating, etc.). The use of a rectangular jet with a precisely controlled aspect ratio enables us to attain both these goals. Several versions of the slot nozzle used in generating a rectangular jet were constructed and tested at the NJIT's Waterjet laboratory. The experiments performed showed the effectiveness of this nozzle even at an early stage of its engineering. In particular, the specific water consumption by the slot nozzle was significantly reduced and the productivity greater than that of the commercial round nozzles under comparable operational conditions. It was demonstrated that rectangular jets constitute an effective machining and cleaning tool.

Organized and Sponsored by the WaterJet Technology Association

1. INTRODUCTION

A high speed fluid stream has a potential of becoming a major tool for material removal. This potential, however, is still yet to be utilized. One of impediments to the expansion of the jet in applications for material separation is the low energy efficiency of the process. An improvement in jet geometry will increase this efficiency.

Practically speaking, all existing nozzles have a round orifice, as it is much easier to generate a round opening than an opening of any other geometry. Further, a round jet has a minimal surface-to–volume ratio that gives the minimal head loss per a unit of mass. The cost of the nozzle fabrication and the stability of the streams generated assure the competitiveness of the round nozzles. The round jet geometry has, however, significant shortcomings. The principal shortcoming is a limited energy delivery to the substrate and a poor energy efficiency. Several avenues have been adopted by industry in order to address these shortcomings. The energy delivery to the impingement zone might be dramatically increased by high speed nozzle rotation (Summers, 1995). This technique is widely used in jet based surface processing. A rotating nozzle increases the productivity and energy efficiency of jet cleaning; however, it involves the use of rather complicated facilities. More important, in this case the impact zone is still circular, although the diameter of the circle by far exceeds the nozzle diameter. Nevertheless, the rotational nozzle has been adopted by industry. Another approach to the improvement of the jet-substrate interaction is the use of a fan jet (Summers, 1995). This nozzle changes the geometry of the impact zone and thus enhances process productivity. However it negatively affects the momentum of the stream. Finally, non-round nozzle geometries have been designed and commercialized by nozzle manufacturers (Aqua-Dyne, 2003).

Practice had found the optimal shape of a conduit for energy transfer during material processing. A typical surface processing (cleaning, decoating, etc.) tool is a brush or its modifications, such as a scraper or rake. The typical material separation (cutting, sawing, drilling, etc.) tool is a knife or its modification, such as found in machining tools. The principal geometric feature of all these tools is a rectangular tool-workpiece interface with the maximum possible aspect ratio. While the geometry of the high energy beams (laser, waterjet, plasma, etc.) is determined by the physics of the beam formation, the geometry of the solid tool is mostly determined by the conditions of the energy exchange between the source and the workpiece. Thus, it is reasonable to suggest that a rectangle with a large aspect ration is an optimal geometry for the water nozzle.

A rectangular nozzle with a variable aspect ratio was developed at the NJITA Waterjet Laboratory. The nozzle forms a high-speed jet with a controllable geometry by expelling a fluid from the high-pressure chamber through a specially designed rectangular port [Geskin and Goldenberg, 2002)].These nozzles were successfully used for metal depainting, derusting and graffiti removal. Special experiments were carried out in order to compare the performance of this invented nozzle and a commercial nozzle. The tests showed the effectiveness of the NJIT nozzle even at an early stage of its engineering. Particularly, the specific water consumption of the newly developed nozzle was significantly below that using a comparable commercial nozzle.

This paper presents the results of the preliminary testing of a rectangular nozzle with a high aspect ratio (a slot nozzle) designed by the Waterjet Laboratory of NJIT. Firstly, a simplified analysis of the energy utilization by the round and rectangular impact zones is given. Then the results of the experiments demonstrating stability and relative effectiveness of the slot jet are given and a possible direction for an improvement in the nozzle design is suggested.

2. DEFFICIENCY OF ROUND JETS

Figure 1 illustrates the interaction between a round jet and the substrate. Although this figure as well as the analysis below is concerned with a traversing jet , it is equally applicable to rotational jets. As it is shown in Figure 1, the substrate A is subject to treatment (cleaning, decoating, etc.) by jet B. moving with speed V in the direction of the arrow. The treatment is due to the energy delivered to the substrate A by the jet B. The section “a” is a part of substrate A, while the section “b” is a part of jet B. Because the widths w of the sections “a” and “b” are equal, the section “a” of the substrate is treated by section “b” of the jet only. The length of the sector “b”, λ determines the duration of the interaction between the jet B and the section “a”. Here $\lambda = \frac{F_b}{w}$ is the average length of the chord of the section "b" and F_b is the area of the section “b”. The energy which the section “a” receives from jet B, while the jet is impacting the substrate A, is delivered only by section “b”. The energy of the rest of the jet does not affect section “a”. The amount of energy delivered to section “a” by jet B is proportional to the duration of the ‘a”-“b” interaction (residence time) i.e., the length λ of the section “b”

Let us assume that the kinetic energy is evenly distributed across jet B and that the kinetic energy of the water is completely transferred to the substrate A in the course of the water impact on the substrate surface. Thus the energy E absorbed by section “a” in the course of the jet-surface interaction is (Geskin et.al, 1998, Leu et al, 1998, Meng et al,1998)

$$E = \frac{\lambda F_a e}{V} \tag{1}$$

where F_a is the area of section “a”, e is the kinetic energy of the jet per unit of the jet cross sectional area and per unit of time, V is the traverse rate of the nozzle. Because, for a given set of operational conditions, the values of F_a, e and V can be assumed constant, the amount of energy delivered to the substrate is

$$E = k\lambda \tag{2}$$

where k is a constant. Thus, for given jet characteristics and traverse rates the amount of energy delivered to a substrate is a function of λ. The energy required for the surface treatment E_0 is given by the equation:

$$E_0 = k\lambda_0 \tag{3}$$

Here λ_0 is the length of the section that delivers the required amount of energy to section “a” under given process conditions.

In treating substrate A by moving jet B (Figure 2) sections a', a_0 and a" are subjected to the impacts of sections b', b_0 and b" characterized by lengths λ', λ_0 and λ'' where $\lambda' < \lambda_0 < \lambda''$. Thus section b_0 delivers the required amount of energy to section a_0. On the other hand, section a' does not acquire sufficient energy and should be treated again, while section a" gains an excessive amount of energy. The insufficient and excessive energy supplies not only result in energy loss but also reduce the resulting surface quality. Section a'' might be damaged by the extra energy delivered in the course of treatment. Section a' also might gain extra energy and be damaged during additional treatment.

Let us now discuss total energy use during surface treatment by a moving jet. Let us assume that under a given set of operational conditions the length of chord AB is equal to l_0. Then the part of the substrate impacted by the segment ABCDEF (Figure 3) will receive excessive energy, while areas treated by the segments AGB and EHD will receive insufficient amounts of energy. The amount of excessive energy delivered to the surface of the substrate is proportional to the areas of segments BCD and AFE and this energy is lost. The energy delivered to the substrate by the AGB and EHD segments is also lost, because the substrate surface subjected to treatment by these parts of the jet must be treated a second time. The useful energy, i.e., the energy necessary and sufficient for the surface treatment is proportional to the area of the rectangle ABDE. An optimal energy utilization is attained if the ratio of the area ABDE to the cross-sectional area of the jet is maximal. This is attained if $\lambda = \frac{d}{\sqrt{2}}$ where λ is the length of the chords AB and BD and d is the jet diameter. With this condition, the area of the square ABDE occupies 64% of the cross-sectional area of the jet. Because the energy delivered by the jet's segments AGB, BCD, EHD and EFA is lost, the minimum energy loss experienced during this use of a round jet will make up 36% of the energy supplied.

Let us assume now that a section "a" is treated by a rectangular jet ABCD (Figure 4). Let us also assume that the length of the edge AB assures the delivery of energy to the substrate A required for surface treatment. The width of the jet that is equal to segment BC determines the width of the strip swept i.e. the rate of surface treatment. If the same rate of treatment is attained by a round jet,then the energy delivered by the shaded areas of the jet cross section is lost. Thus the use of a round nozzle for surface treatment necessarily results in energy losses which might constitute a significant part of the available jet energy.

3. INVESTIGATION OF THE STABILITY OF A RECTANGULAR JET

Several versions of the slot nozzle were constructed and tested in NJIT's Waterjet Laboratory. The first series of tests involved an evaluation of jet stability. A general view of the jet developed is shown in Figure 5. The figure shows that the slot nozzle generates a stable, coherent jet, which maintains its stability at L/b>2500, where L and b are the sizes of the rectangular stream. The stable, coherent jets can also be developed at large (Figure 6) and low (Figure 7) water flow rates. Figure 7 demonstrates he feasibility of generating micron sized streams using a slot nozzle. The stability of the rectangular jet is demonstrated by the behavior of the rebounding jet (Figure 8). Figure 9 demonstrates the peculiarities of the rectangular jet-substrate interaction. The nozzle shown on this picture is supported by the rebounding stream only. This stream, however, in addition to exerting a force compensating for the weight of the nozzle creates a vacuum that strongly attaches the nozzle to the substrate surface. As is shown in Figure 10 the streams generated by both round and rectangular nozzles are rather similar. Thus, the experiment performed shows that a slot nozzle generates a stable, coherent jet having an adequate stand off distance.

4. INVESTIGATION OF THE EFFICIENCY OF A RECTANGULAR JET

In order to determine the effectiveness of material removal by a slot nozzle, this nozzle was used for several surface processing operations. During this test the nozzle was guided manually (Figure 11). One of the experiments involved the removal of graffiti from a marble wall. (Figure 12). No damage to the substrate was observed in this operation. Figure 13 shows the removal of hard paint from a steel surface. Depainting a highly porous surface is depicted in Figure 14. Here the paint was completely removed from part of a brick subjected to cleaning. Figure 15 shows the removal of oxides from an aluminum shield used for substrate protection during vapor deposition. The jet practically completely removed these oxides. Removal of heavy rust from a steel surface is shown in Figure 16. Restoration of heavily rusted kitchen pan is depicted in Figure 17. The experiments described above show the feasibility of using slot nozzles for various surface processing operations. The effectiveness of the slot nozzle is demonstrated by Figure 18. As shown in this figure and Table 1, the productivity of a slot nozzle exceeds that of the conventional one by an order of magnitude.

In the experiments performed, the thickness of the jet was determined by the conditions set during nozzle fabrication and, in principle, can be reduced even further. The width of the stream was maximal and was determined by the available pump flow rate. The nozzle traverse rate was selected so that a desired level of surface cleanliness could be obtained.

5. CONCLUSION

The experiments performed in this work show that a rectangular jet has potential for improving surface processing techniques. The most realistic immediate application of the nozzle developed is in the maintenance of civil infrastructure, for example in graffiti removal. The nozzle can also be used to improve cutting capabilities. Finally, two novel avenues for nozzle application might emerge. One might involve processing of large (roads, airports, beaches) surfaces and large volumes (waste management). Another one might bring about the development of such technologies as the fabrication of thin films, composites, etc.

6. ACKNOWLEDGEMENT

This study was partially supported by the NJ Center for Micro Fluidic Control and by NSF grant "Development of the Water Based Machining Technology", DMI 9900247.

7. REFERENCES

D.Summers. Waterjetting Technology, E&FN Spon, London (1995)

Aqua-Dyne, Inc, Houston, TX, Company Catalog 2003

E.S. Geskin and B. Goldenberg, US Patent (pending) "Method of the Jet Formation and Apparatus for the Same", Application 10-119/777 (April 11, 2002)

E.S. Geskin, in Waterjet in Civil Engineering, A. Momber, A.A. Balakema, Rotterdam (1988)

M.C Leu, P. Meng, E.S.Geskin and L. Tismenetskiy, ASME Trans. J. Manuf. Sci. Eng., 120, 571-577 (1998)

P. Meng, M.C.Leu and E.S.Geskin, ASME Trans.Manuf. Sci. and Eng., 120, 578-589, (1998)

8. NOMENCLATURE

A- substrate
a-section of the substrate
B-jet
b-section of the jet
d-nozzle diameter
E- energy absorbed by the substrate
e-specific kinetic energy of the jet
F_b -area of the section b
k-constant
L-stand off distance]
λ - the length of the sector
V-traverse rarate
w-jet width

9. TABLE

Table 1. Comparison of the cleaning efficiency of different nozzles

Kind of nozzle	Kind of deposit	S, mm^2	P, MPa	F, L/min	D, mm	Rate of cleaning cm^2/min
Commercial nozzle (Figure6a)	Hard paint from a car body	0.34	86	1.0	10.0	3.2
NJIT nozzle (Figure6b)	Hard paint from a car body	0.48	93	0.8	10.0	58.0

Here

S –cross- sectional area of the nozzle opening, mm^2

P – water pressure, MPa

F –water flow rate, L/min

D – standoff distance, mm

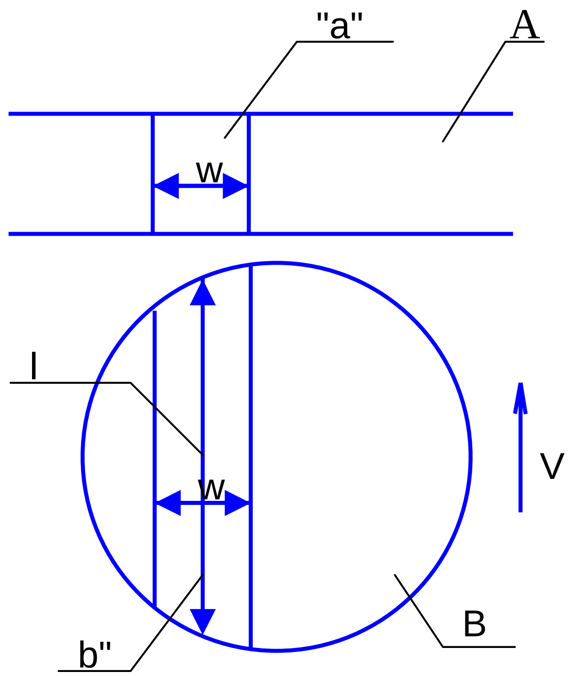

Figure 1. Schematic of cleaning substrate *"A"* by jet *"B"* moving with a speed *V*. section "b" is a part of jet B impacting section "a" of substrate A.

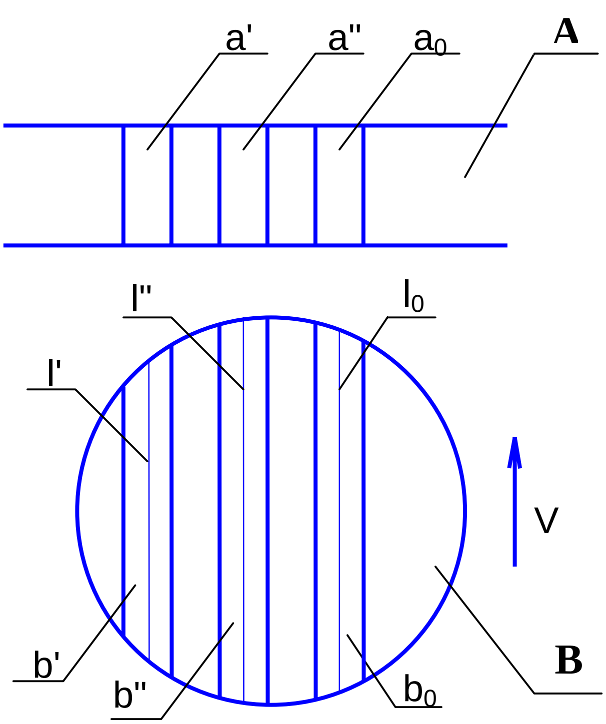

Figure 2. Schematic of cleaning section **a'**, **a"** and $\mathbf{a_o}$ of substrate **A** by moving jet B. Notice different durations of cleaning section **a'**, **a"** and $\mathbf{a_o}$

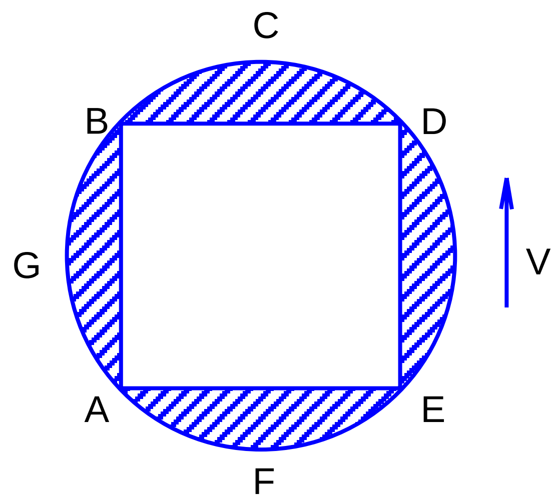

Figure 3. Schematic of water utilization in the course of cleaning by a round jet moving with a speed V. A part of the stream energy proportional to the area ABDE (AB=l_0) is utilized. The part of the stream energy proportional to the shaded area is lost.

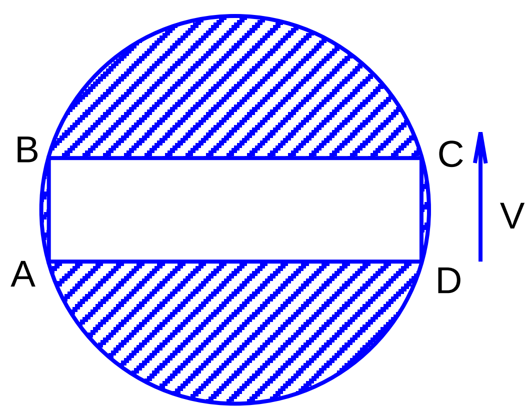

Figure 4. Utilization of the energy of the rectangular and round jets
Notice $AB=l_0$ the part of the energy of the round jet proportional sheded area is lost

Figure. 5.A rectangular jet. Water pressure 68 MPa, water flow rate6.5 l/min, slot 12.5x0.0375 mm, scale 1:1, The jet maintained its coherence at L/b>2500

Figure .6. A rectangular jet generated by NJIT nozzle at a pressure of 140 MPa and a flow rate of 17.0 l/min., scale 1:1

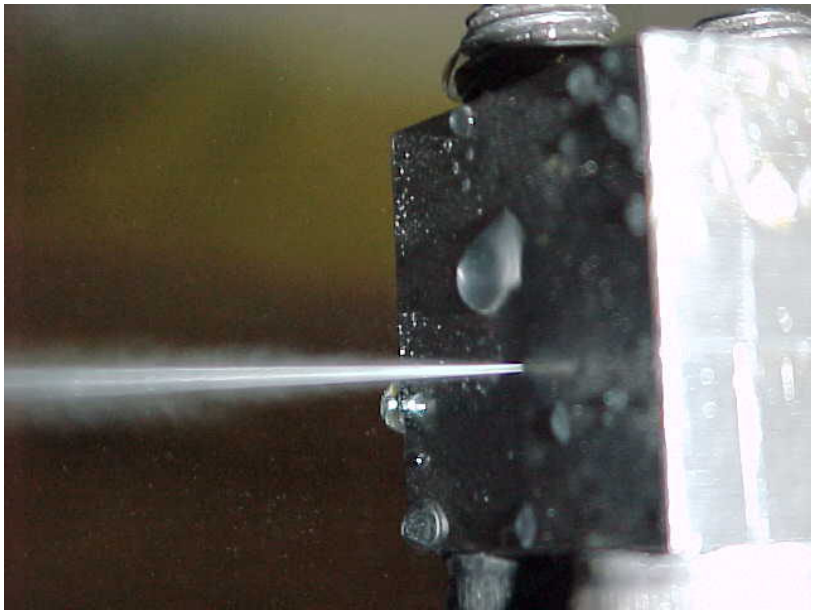

Figure 7. A rectangular jet generated at a water pressure of 270 MPa, 0.1 l/min,and a flow rate of 0.1 l/min. Slot: 0.065x 0.0025 mm, scale 2:1, , A jet core is maintained at L/b=40,000

Figure8 A rectangular jet generated at a water pressure of 238 MPa, flow rate 9 l/min , slot 10 x0.0315 mm , scale 1:2, The rebounding jet maintains its coherence at L/b=800

Figure.9. A view of the rectangular stream normal to the nozzle axis and developed between the nozzle body and the substrate (brick) Water pressure -68 MPa, water flow rate -6.5 l/min. The slot: 12.5 x 0.0375 mm. Scale 1:4. Notice The stream normal to the nozzle exit, maintained coherence at the distance of 15,000 L/b. brick.

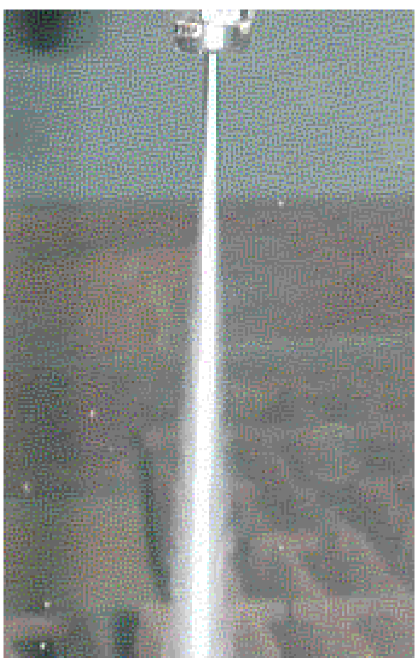

a)

b)

Figure 10. Water stream generated by a commercial and a NJIT nozzles

a) Commercial round nozzle, ID=0.7 mm, pressure P= 86 MPa, flow rate=1l/min
b) NJIT nozzle, pressure P= 93 MPa, flow rate =2.9 l/min, scale 1:2

Figure 11. Using the slot nozzle with manual guiding.

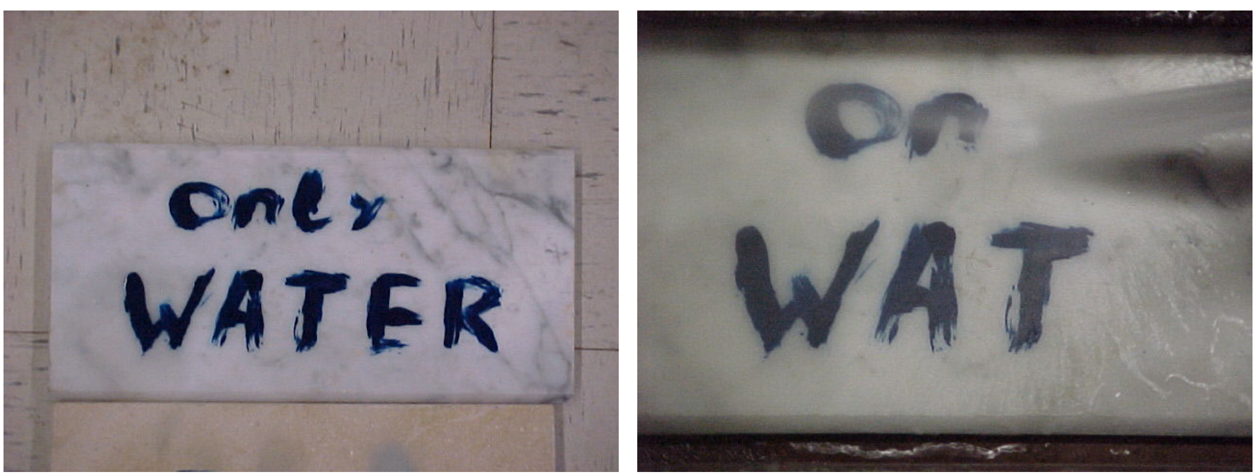

a) b)

Figure12. Removal of graffiti using NJIT nozzle at a water pressure 68 MPa and a flow rate 6.5 l/min. a) - prior to cleaning, b) - in process., scale 1:4

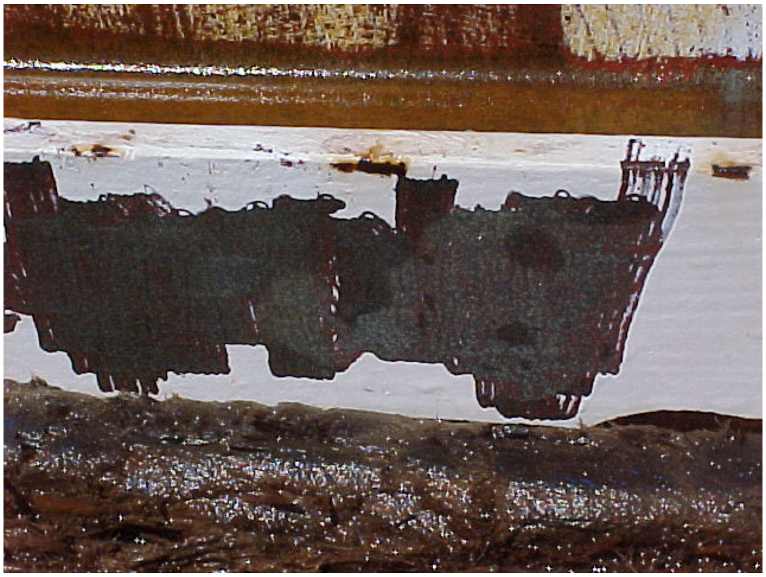

Figure13 Removal of a hard paint. Water pressure240 MPa, 9 l/min, slot 0.4x0.0015"Scale 1:3, Rate of depainting 55 cm^2/min

Figure 14.   Depainting of a porous brick. Water pressure -68 MPa, water flow rate -6.5 l/min. The slot: 12.5 x 0.0375 mm. Scale 1:4. Notice: The jet was used to remove a paint(rustoleum , inc light marine grade, hard hat fast drive, industrial coating finish) from the left part of the upper edge of the brick. The area of 400 cm^2 was depainted in 50 sec.

Figure 15. The surface of an aluminum screen before and after removal of high temperature oxide deposit. Water pressure-68 MPa, water flow rate 6.5 l/min

Figure16   Removal of heavy rust presence. Pressure 240 MPa, water flow rate 9 l/min slot 0.4x0.0015", scale 1:4

Figure 17 . Derusting of a heavily rusted pan. Water pressure 65 MPa , water flow rate 6.5 l/min. Slot 12.5x0.0375.

a) Commercial nozzle, cleaning rate 3.2 cm^2/min

b) NJIT nozzle, cleaning rate 58.0 cm^2/min

Figure18 Compare speed and quality cleaning a surface of the car body using commercial nozzle 0.1 mm (a) and a NJIT nozzle 0.4x0.0015 (b)., scale 2:1

2003 WJTA American Waterjet Conference
August 17-19, 2003 ● Houston, Texas

Paper 4-E

MANUFACTURING CASE STUDY

INVOLVING MAJOR OIL COMPANY

Michael T. Gracey, P.E.
Weatherford ALS
Houston, Texas

R.O. Berry, Jr.
Acme Cleaning Equipment, Inc.
Houston, Texas

ABSTRACT

A high-pressure Hot Water Washdown unit for an offshore platform was manufactured to specifications written by an international engineering group and managed by an engineering procurement contractor (EPC). The documents, drawings, electronic submittals, approval cycle, inspection and final acceptance testing required for the project, doubled the scope of work for the equipment, when compared to the historical methods of procuring this type of equipment. With other companies demanding similar specifications for their equipment, the trend cannot be ignored if a pump supplier is to participate effectively in this type of project.

1.0 INTRODUCTION TO THE CASE STUDY

The procurement process is becoming more rigorous for the supply of offshore equipment to Major Oil Companies. It may have developed because of regulatory bodies, high cost of insurance or it may have come from financial or safety concerns. Whatever the reason, engineering to be done by the vendor and the increased documentation requirements must be considered during the bidding process. When a request for a bid was received in July 2001 from an engineering procurement contractor (EPC), it seemed straightforward when compared to past and present job specifications even though it was noted that the list of technical information and submittals was greater than normal. In late October 2001, an award was received for a High Pressure Hot Water Washdown Unit from the EPC to be supplied to a major oil company for the first phase of their project. The unit was to provide wash water at 1800 PSI, 40 GPM, 150 degree F to four work stations on an offshore platform being built for Angola with a job name "Part A". Figure 1 shows the high pressure, positive displacement pump with force feed packing lubricator that was selected to meet the specification.

The project was anything but straightforward:

- The purchase order was let before the work was fully defined
- A large number of submittals were due 2-4 weeks after the order date
- The system was not defined fully and questions could not be answered
- The kick-off meeting took two months to schedule
- Changes were requested that took additional time to submit
- The prime contractor, main subcontractor and component vendors were overwhelmed by the unexpected demands of the job.

2.0 HISTORY – THE OLD WAY AND THE NEW WAY

Hot water is being used in areas such as oil and rubber removal as discussed in Reference 8.1 and has long been used in the pressure washer industry. Both the prime contractor and the subcontractor have had experience in manufacturing pumping units, hot water wash units and high-pressure water jetting equipment. The main subcontractor, Acme Cleaning, has manufactured wash down equipment for the oilfield since 1971 and has been involved in numerous EPC projects. Weatherford, the prime contractor, builds high-pressure pumps and packages for a variety of pumping requirements including water jetting and has also worked with an EPC in many projects. In Reference 8.2 Ultra-High water jetting is used to remove existing coating from an offshore rig while lower pressure water jets described in Reference 8.3 are used in unusual ways. Some of the pumps ordered by oil companies are for methanol injection, re-start pumping, and petrochemical products or for handling special pumping requirements. The specifications are followed and documentation is provided at the end of the job as required by the purchase order. It takes approval drawings, material certifications and operational instruction manuals to complete the job. Welding procedures, welder qualification, and inspections are a normal part of the process also. The common practice used prior to this project was to review the high points of the request for quote and then quote equipment to meet the performance specification. The customer would note changes and the re-quote would usually become part of the purchase order. This project started with the verbal announcement that “you have the job” and the purchase order would be sent later. The proposal sent to the customer had exceptions and requests for clarification, but there was no reference to the quotation in the written purchase order, only that the equipment was to be built in compliance with the specifications. The acknowledgement to the purchase order stated that is was accepted on the condition that the price was based on the proposed equipment and that any changes would change the price accordingly. When questions were asked of the EPC, the standard answer was “Build it according to the specifications”.

3.0 OBSTACLES TO THIS JOB

There are the normal reasons for delay of progress on a job. These include vacations, holidays, other projects, lack of personnel, and becoming familiar with the requirements of the job. There is time needed for engineering, system drawings and approvals by the customer, but usually in a few weeks, that part of the process is over. The subject of this paper had some unusual aspects and like the infamous “Catch 22”, the long specification documents had some parts were not clear and some parts that were in direct conflict with other parts. The required clarification from the customer took days, weeks and months. The subcontractors were in a no-win situation because they were being pushed to keep the schedule while they waited on answers to their questions about the specification. Each submittal had to be sent to the international engineering company electronically and accompanied by certain forms. It took about four weeks to get a return on the document and when it was returned, there was a “status” assigned. A1, A2, N1, N2, ….. Each of the codes have an associated meaning such as N2 which means “ Comments as noted, Proceed with Fabrication in Accordance with Comments, Resubmit Corrected Drawings as ‘Final Certified’ within two weeks or sooner. The obstacle in this approval method is that the next submittal of the document comes back with additional comments, so it is not really approved after all. When you order the component or build the item, it is subject to change. When the job started, a call came from the customer’s first expeditor saying that we need to have a list of documents submitted now. The process was started and documents / drawings were submitted for approval. Weeks later when the document was returned, it may have had an N2 status and we were told by the second expeditor to order or build the item because it has N2 status. Next time through the document may come back with more notes or it might be rejected, so the wrong thing was on order or fabrication had to be halted. When you go through the process 95 times, serious problems arise. Extra costs are incurred and delays accumulate. The expeditors were calling the subcontractors and vendors to push for delivery and meanwhile, answers could not be obtained about the specification requirements. Meetings were scheduled that seemed to raise more questions and bring more personnel into the loop. Now it was time for the procession of inspectors, which gave directions to get the job moving, but later is countermanded by the next inspector. If 95 documents could be submitted once or maybe twice, the paperwork would be more reasonable, but a document (set of drawings, engineering calculations or forms) might go through the system multiple times (up to 5-6 times) even after the equipment has been shipped.

4.0 OVERCOMING THE OBSTACLES

In more than one meeting, the project was offered back to the EPC because the obstacles appeared insurmountable, but each time there were promises that the EPC would help with the hurdles. There was an attempt on their part to help with the requirements, but the specifications were just as confusing to the EPC as they were to us. The obstacles were overcome by trying the following:

- A " Divide and conquer" approach to spread the workload to vendors and subcontractors.
- A person was hired for document control to help with the large amount of electronic submittals.
- The project manager took over communication with the expeditors and inspectors.
- The project engineer and the main subcontractor negotiated the first change order and helped with the subsequent change orders, while defining the customer's requirements until the project manager could take over the financial negotiations.
- Vendors were contacted on a regular basis for updates on documents and drawings until the information was received for submittal or resubmitted.
- The project manager should be involved during order acceptance and start of the project, but in this case, was not available at the first part of the project.

The fact that there was no penalty cause for late delivery in the purchase order was one of the only redeeming factors about the job. It was also made clear in the quotation and in the acceptance letter that items such as PMI (positive material identification) and full system test were not included and even a statement was received that the full test was not required. These were unknown cost and would have to be quoted, if needed. The obstacles were gradually overcome and Figure 2 shows the skid mounted offshore package with heater, tanks and stainless steel piping in the final stage of completion. Figure 3 shows the heater control panel with marine cable to the water heater. The air actuated control valves are shown in Figure 4 along with the pressure and temperature transmitters. Figure 5 includes the fiberglass reinforced plastic (FRP) detergent holding tank and the chemical injection installation.

5.0 FINAL ACCEPTANCE TEST

Quality Control Plans, Test procedures and numerous inspections were part of the project. The Final Acceptance Test (FAT) was planned from the beginning, but exception was taken to parts of the test as additional costs. The reasons for not quoting the full test, was the 390KW heater on the unit would require the renting of 500 KW generator and the customer instructed us not to quote it. The pressure and bypass temperature control valves were controlled by equipment supplied by others so it was agreed that the pump, piping, hose and guns would be shop tested to satisfy the final acceptance test. Later in the program, it was decided that a full functional test was required after all and there was more negotiation about the manpower and electrical needs. A large generator was rented and the necessary manpower was provided to run the pump, heater, controls and four pressure washer guns. That included water tank, supply hoses and charge pump but the most difficult item was to provide a simulation of the customer's control of the discharge pressure. Figure 6 shows the 500 KW portable generator required to power the water heater and run the system.

6.0 CONCLUSIONS

The new way of doing business increases the scope of engineering and documentation. The product such as a High Pressure Hot Water Washdown Unit may be fairly simple, but the purchase order may include specifications that must be fully understood before acceptance of the project. The lessons learned on this project include:

- Take no shortcuts when it comes to studying every word of the specifications. Take exceptions so that it can be clarified or negotiated.
- Get document approval before starting the delivery schedule because of the delays caused by the document approval process.
- To avoid one of the greatest delays, request that all notes and changes should be done on the first submittal on a document.
- Extra time should be allowed for vendors to furnish documents to be submitted for approval. Time will also be needed for rework / resubmittal.
- Progress payments should be required if the approval cycle is going to delay the progress on the job.
- All commercial issues should be negotiated before the equipment is shipped because it is a position of strength.
- Take exceptions to requirements that are beyond the scope of supply such as full operational test when others are to supply controls.

Figure 7 & Figure 8 shows the High Pressure Hot Water Washdown Unit after the final acceptance of the equipment including testing, customer inspection and documentation.

7.0 ACKNOWLEDGMENTS

The authors want to thank Mr. Gary McCann, Mr. Emil Levek and Mr. Weimin Dai of Weatherford and Mr. Calder Gibson of Acme Cleaning for their valuable input during this project. We also acknowledge Mr. Randy Mulvaney of Chromalox and Mr. Rick Noppe of R&N Manufacturing for their important contributions.

8.0 REFERENCES

Michael T. Gracey, WHERE THE RUBBER MEETS THE RUNWAY, Cleaner Times, December 2001.

Michael T. Gracey, USING 40,000 PSI WATER JETTING FOR FIELD WORK, 10th American Waterjet Conference, August 14, 1999.

Mike Gracey, UNUSUAL USES FOR HIGH PRESSURE JETTING, Cleaner Times, December 1997.

9.0 GRAPHICS

Figure 1 -Triplex plunger pump, designed for 40 gpm at 1800 psi with 150^{o}F water, fitted with an oiler which is belt driven off of the pump shaft, 316SST dampeners on both inlet and outlets and a redundant pressure relief valve.

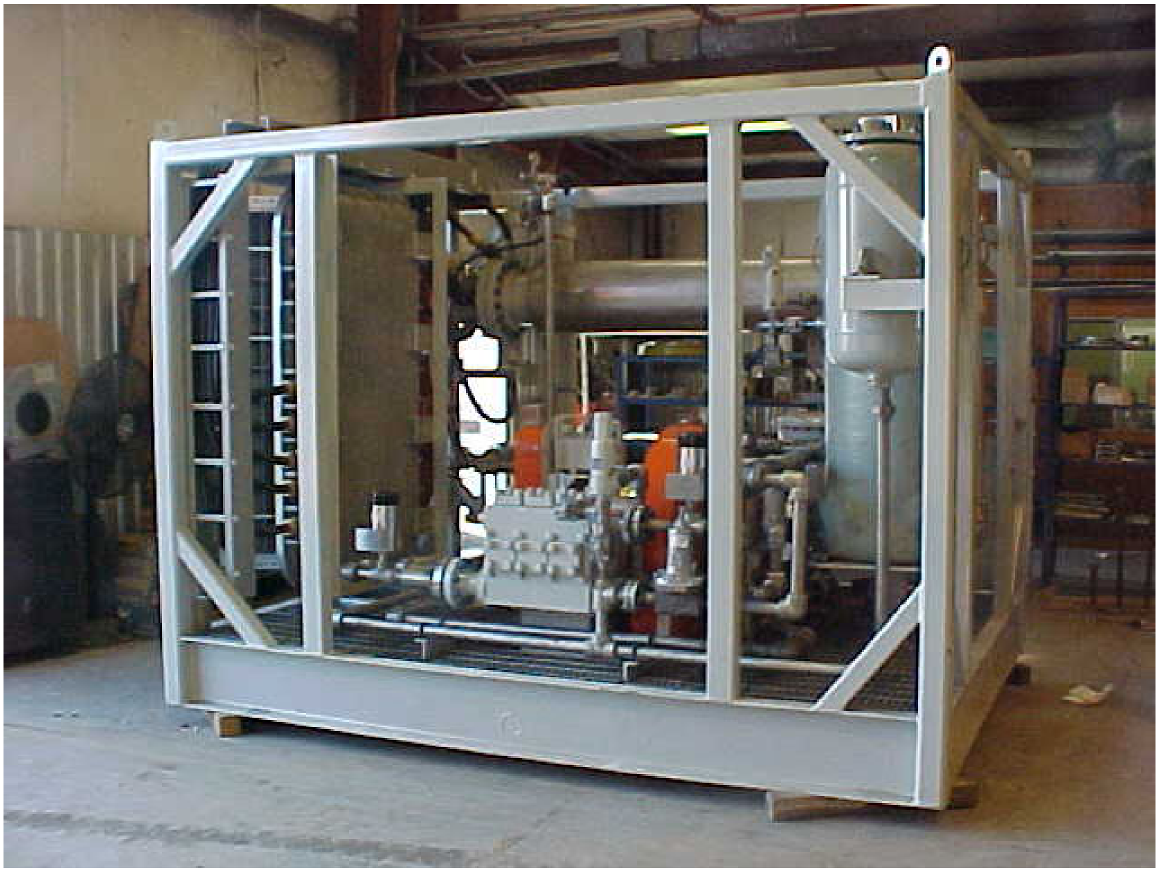

Figure 2 -The heater panel is at the far left end, heater is at upper rear, pump is in the center, surge tank is at the top right and detergent tank is behind the surge tank.

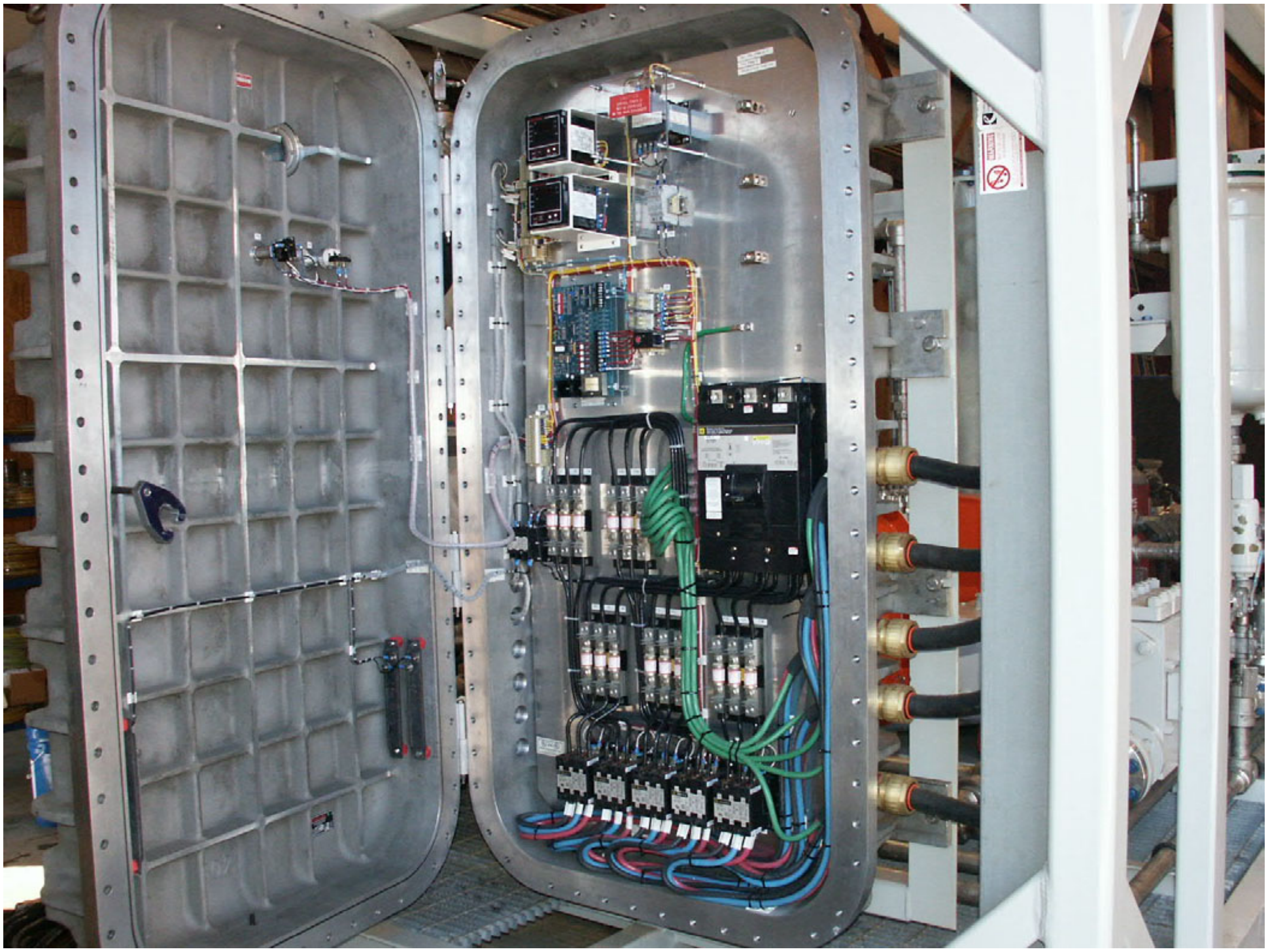

Figure 3 – The NEMA 7 and 4X enclosure are shown with staged power to the heater along with the controllers for high temperature shutdown and outlet temperature regulating. The remote emergency shutdown is also mounted inside the enclosure. Cable glands are rated for Class I, Division I, Groups A, B, C and D hazardous areas as well as being rated for marine applications.

Marine cable is certified Type P, IEEE 45, flame retardant, mud resistant and suitable for use in Class I, Division I marine environments. Cable tray is fiberglass with 316SST hardware.

Figure 4 - Pressure and temperature transmitters are designed for hazardous area operation and are constructed of materials suitable for offshore environments. Tubing for pressure transmitter and compressed instrument airlines is 317L stainless steel material with 316SST fittings. Control valves are 316SST, Class 600 construction with air-operated actuators which have 316SST materials or offshore coating system. Pipe supports have non-metallic wear pads with U-bolts that are Fluorokoted and have a non-metallic jacket.

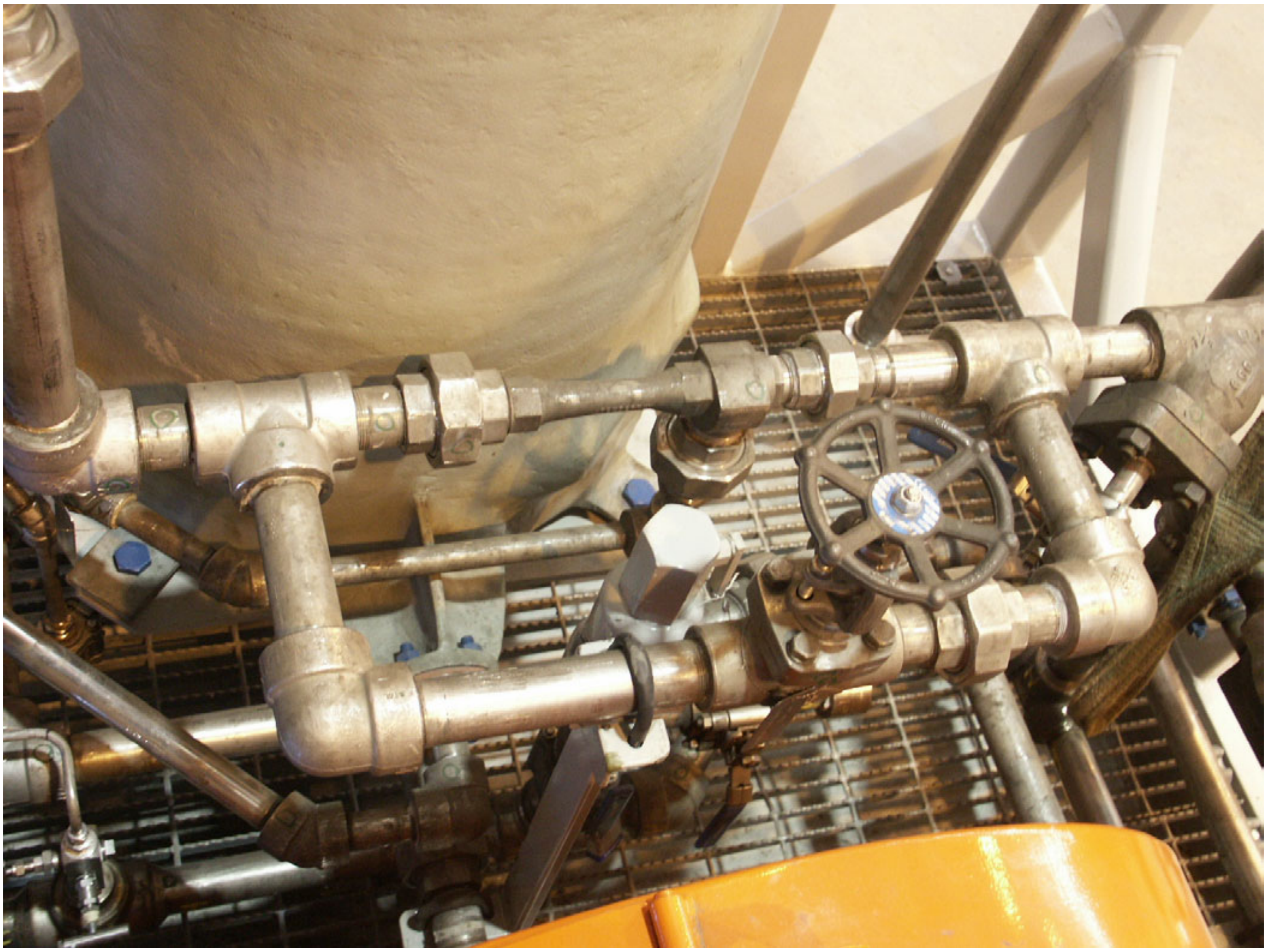

Figure 5 - Custom built chemical holding tank (upper left) is constructed of fiberglass reinforced plastic with UV protection, 115 gallon capacity, fitted with armored sight glass and mounted with Xylan coated hardware. Piping is ASTM A312 GR. TP316/TP316L (dual stamped) material.

Figure 6 – The 500 KW generator was needed to run the 390 KW heater and 40 HP motor on the High Pressure Washdown Unit.

Figure 7

Figure 8

2003 WJTA American Waterjet Conference
August 17-19, 2003 • Houston, Texas

Paper 5-E

DEVELOPMENT OF AIRPORT

RUNWAY RUBBER GLUE REMOVING VEHICLE IN CHINA

Xue Shengxiong, Zuo Xu*, Chen Zhengwen, Peng Haojun, Wang Yongqiang, Fan Yibin
General Machinery Research Institute
Hefei, Anhui Province, P. R. China

* Beijing Capital International Airport, Beijing, P. R. China

ABSTRACT

Safety requirements make the airport runway rubber glue removing vehicle has become one of the most concerned things by Chinese airports. We have been researching in design and applications in this area for 5 years and developed trailer glue removing unit (70MPa, 110kW), single-function truck carried glue removing unit (70MPa, 2×110kW) and multi-function truck carried glue removing unit (110 ~ 170MPa, 46 ~ 122L/min, 350hp). In this paper, we introduce mainly the functions and key technologies of our latest product, which are: 1) combine three functions of glue removing, mark lines removing and oil stain cleaning in a single unit; 2) produce different working conditions to fit the varied requirements for three functions and 3) install the three executing mechanisms on a single surface cleaner. Our design has been patented by Chinese Patent Bureau and put into application in the integrated cleaning vehicle made for Beijing Capital International Airport, China.

1. INTRODUCTION

The requirement that friction factor of the runway surface must not be less than 0.5 has been stated in operating regulations for more than 140 civil airports including about 40 international airports. So, it is essential to clean the adhered rubber glue layer generated by the friction between runway surface and tyre during landing in time and regularly to ensure an adequate and safe length of the clean runway surface for airplanes' landing and takeoff. Recent years, high pressure waterjet technology has been successfully used in removing the glue layer on runway surface and gained wide recognition. Normally, the cleaning frequency is once every month for large airports, once or twice every year for medium-sized airports and once every two years for small airports.

Along with the application of waterjet technology in cleaning glue layer, there are still needs for cleaning oil stain on parking apron and removing mark lines on runway surface. Can we combine the three functions into a single unit to simplify the cleaning process for airport? This may be difficult because of their different working conditions and parameters. Our tests show that pressure of 30~40MPa is adequate to clean oil stain while the required pressure for glue layer cleaning is 70~100MPa, but for mark line removing, the pressure must be 150~170MPa. And more, the much more large working areas of oil stain and glue cleaning than those of mark line removing require that the flow rate needed for efficiently cleaning oil stain and glue layer is much more large than that needed for removing mark line. Based on experiences gained from our development of trailer unit and single-function truck carried unit and users' demand for integrated unit, we develop the third generation unit - the multi-function truck carried cleaning total set.

2. CLEANING MECHANISMS FOR DIFFERENT RUNWAY SURFACES

Now, there are both concrete and bitumen runways existing at the same time in China, especially for some large civil airports. The reason for this situation is that the bitumen runways are mainly constructed by overlaying the concrete runways that are broken and cannot be repaired with a layer of bitumen sands to extend their service lives.

There are large and obvious differences in removing glue layer on concrete runway compared with working on bitumen runway, which are determined by their structural characteristics. From the eye of structure analysis, concrete runway is compact and has a relatively smooth surface while the bitumen runway is loose and has a relatively rough surface. This difference leads to different glue adhering mechanisms during high speed friction process between runway and airplane's tires when landing and taking off. As shown in Figure 1, Glue adherence on concrete runway appears to be a flat style, all glue adheres to surface of runway and can not penetrate into the base, so there is a distinct dividing line between the places with and without glue adherence. But for bitumen runway, glue not only adheres on its surface, but also penetrates and fills in the holes and gaps below surface because of its loose structure. So it is hard to distinguish the adhering glue from bitumen.

The basic requirement for cleaning glue layer on runway surface is to remove the glue completely while having no injury to runway; that is to say, the raw materials of runway should not be removed. As we know, striking force is the main factor of high pressure waterjet operation, which is governed by following equation:

$$F = k\pi d^2 P \cos\alpha$$

Where F is the striking force, N;
d is the nozzle diameter, mm;
P is working pressure of jet, MPa;
α is the striking angle of jet;
and k is the influencing factor considering the rotating speed of jet, to fixed waterjet, k=1.

As shown in above equation, striking force is in direct proportion to nozzle diameter, which influences the jet diameter. If all water flows through two or four bigger nozzles, the powerful cylindrical jet streams will cut annular paths on runway surface if rotation speed is below a threshold value because of the concentrated striking force. And damage to runway surface is generated. Tests show that application of cylindrical jet on bitumen runway tends to harm runway surface severely. During these tests on bitumen runway, the cylindrical jet stream with larger diameter erodes runway surface easily and damage the raw roughness severely. But, considering that the large striking force it has is better for removing rubber glue on surface efficiently, cylindrical jet and nozzles are normally used during cleaning process on concrete runway. To cleaning process on bitumen runway, we develop atomizing rotary nozzle head. It divides a single cylindrical nozzle into several atomizing micro-hole nozzles. The atomizing jet generated by reduction of nozzle diameter and increase of working pressure combined with the effect of rotation has the characteristics of evenly distributed jet streams and much more less or no damage to runway surface. Usually, working pressure for cylindrical rotating jet head is 70MPa, while that for atomizing rotating nozzle head is 100MPa and rotation speed is within the range of 600~700rpm.

Figure 2a shows the cylindrical rotary nozzle head and its adopted nozzles, Figure 2b shows the atomizing rotary nozzle head and its adopted nozzles. Figure 3 shows the contrast of cleaning effect before and after cleaning process on different runway surfaces. Figure 3a is result on concrete runway and Figure 3b is that on bitumen runway.

3. THREE STEPS IN DEVELOPING AIRPORT RUNWAY CLEANING VEHICLE

Figure 4 shows the trailer glue removing unit we produced in 2001. In this unit, a high pressure reciprocating pump set driven by diesel engine with working pressure of 70MPa, flow rate of 70L/min and power of 110kW is installed on a trailer. During cleaning process, the trailer is drawn by truck or tractor, while the rotary surface cleaner is separated from trailer and driven to rotate and run by hydraulic system to ensure a stable rotation speed and automatic running under preset constant speed which are crucial to cleaning successfully with no harm to runway surface. This design costs less and is very suitable for cleaning in Chinese small airports. But it also has the disadvantage of complication. It needs auxiliary vehicles such as water tank vehicle and lighting vehicle to cooperate during cleaning so that the cleaning process has to be separated at intervals every 20 to 30m limited by the length of connected two hydraulic oil hose and a high pressure water hose. This makes the cleaning very inconvenient.

The important achievement we gained from above development is the successful use of atomizing rotary nozzle head. In year of 2002, we adopted this technology in improving and repairing the rubber glue removing vehicle produced by Harben Company, U.K. and imported by Beijing Capital International Airport. The crank shafts in this radial piston pump are mainly damaged, and more, the original cylindrical rotary nozzle head is not suitable for working on bitumen runway surface. So it has to be improved. The parameters of this unit are 70MPa pressure, 2×70L/min flow rate and 2×110kW power. The renovated unit has been putting into normal and regular operation successfully for about 4 months. Figure 5 shows this technically renovated glue removing vehicle. This renovation proves the success and advantages of our developed atomizing rotary nozzle head and gives us a chance to promote the commercialization of waterjet technology in airport runway glue removal area in China.

This year, the international bidding for a new airport runway glue removing vehicle issued by Beijing Capital International Airport gives us a new chance to develop waterjet technology in this area. After thoroughly judging the maintenance requirements for Chinese airports from our customers and carefully analyzing the feasibility of removing oil stain, rubber glue layer and mark line by using high pressure and ultra high pressure waterjet, we put forward the design of combining these three functions in a single unit. In this design, we choose the runway surface glue removal as the main function, while the whole unit can be changed to work under pressure of 30 to 40MPa to clean oil stain and work under ultra high pressure to remove painted mark line. The total price is nearly the same as that of single function glue removing vehicle. This careful and thorough design that is accordant with Chinese present situation and has a reasonable price won the bid finally after defeating two American companies and three German companies. Our totally new multi-function design has the advantages possessed by separated designs for these three functions in developed countries nowadays and can fulfill the customers' demands of doing more things while cost less. Figure 6 shows the multi-function airport runway glue removing unit. It is now being under applying for Chinese patent.

4. TECHNICAL CHARACTERISTICS OF MULTI-FUNCTION AIRPORT RUNWAY SURFACE GLUE REMOVING VEHICLE

The overall assembly drawing of multi-function airport runway surface glue removing vehicle is shown in Figure 7. This unit is consisted of main pump set, water tank, hydraulic system, surface cleaner, control table and modified chassis. It has several technical characteristics listed as following:

4.1 Application of Multi-speed Pump Set

We choose the multi-speed pump set to fulfill the three required cleaning purposes in a single unit. In order to reach the required up to $2000m^2/h$ cleaning speed, two ∅1000mm atomizing rotary nozzle heads are installed abreast and work simultaneously under working pressure from 70 to 100MPa, which is determined by different kinds of runway surfaces and different thickness of adhering rubber glue layer. So the flow rate of supplied water is set to up to 120L/min in this relatively lower pressure. Based on above working flow rate, we switch flow to supply water to the lined nozzle head through a high pressure switching valve and use several nozzles with larger diameter to lower working pressure to about 30 to 40MPa, then the oil stain can be also cleaned. But for the difficult mark line removing process, the strong adhesive force caused by the high strength cold dissolving paint and coarse runway surface make it necessary to use ultra high pressure waterjet with pressure up to 150 to 170MPa to clean these mark lines thoroughly. During this cleaning process, the needed flow rate is relatively small because the narrower width of mark line makes the diameter of surface cleaner be much more small and number and diameter of nozzles be smaller.

Considering the above three kinds of requirement for cleaning purpose, the parameters of adopted multi-speed pump set are selected as shown in Table 1.

The designing method of this multi-speed pump set is to change the running speed of main pump through mechanical mechanism to supply maximum flow rate within every pressure stage range. It breaks through the general reciprocating pump's limit of constant flow rate with changing working pressure, makes full utilization of diesel engine's power, creates four stable working conditions and achieve the required multi-function in a single unit. In Figure 8, the performance curves of general reciprocating pump and chosen multi-speed reciprocating pump are listed respectively. Figure 8a shows that of general pump and Figure 8b shows that of multi-speed pump.

4.2 Multi-Function Surface Cleaner

It is an innovation to install three nozzle heads with separated function on a single surface cleaner. This surface cleaner can be lifted and laid down by hydraulic cylinders. All of its working parameters can be monitored through instruments installed on control table in driving cab of chassis.

In this combined cleaner, lined nozzle head with fan nozzles installed on it is used to clean oil stain on parking apron. It works under pressure of about 35MPa and has a cleaning width of 2.5m. At the meantime, the two atomizing rotary nozzle heads are used to remove rubber glue layer on runway surface. There are 28 atomizing nozzles on each head with 7 on each rod. They are mounted at the outer 2/3 part of the spraying rod to make full use of covering width and diameter. The rotary seal is aramid fiber combined seal and can resists pressure up to 120MPa. These two rotary nozzle heads are driven by two hydraulic motors, whose speed can be adjusted by regulating supplied hydraulic oil's flow rate. Besides, an ultra high pressure cylindrical solid jet nozzle head with 4 nozzles is introduced to clean mark lines. Driving force for this head comes from the reaction torque generated by the 4 inclined nozzles. The ultra high pressure rotary seal is of precise metallic clearance seal type, it can withstand a maximum rotation speed of 1000rpm and allow a maximum flow rate of 76L/min to pass through. Considering that width of most mark line is about 250mm, the cleaning diameter of ultra high pressure head is designed to be 300mm.

4.3 Modification of Super Low Speed Chassis

All equipment is loaded on an ISUZU CXZ81Q heavy-duty chassis whose load capacity is 147000N (15tons). According to requirements of normal cleaning process, speed for rubber glue removing is about 12 to 20m/min, speed for mark line cleaning is about 8 to 12m/min or even lower. Since the surface cleaner is fixed on the chassis and moves along with the chassis, the chassis must be specially modified to have the ability to run at very low speed of minimum 500m/h. Keys to this modification lie in adding another three super low speed gear positions in transmission system while keeping the raw transmission system of chassis unchanged.

The true and feasible modification way is to add an additional big ratio reducer and a clutch between transmission shaft and rear bridge of chassis to fulfill a two-stage speed reduction for existing gear position. The clutch can be clutched and released to suit needs of running speed changing from running on road to cleaning process.

5. EXISTING PROBLEMS

After the three stages in developing airport runway glue removing vehicle have been experienced, high power ultra high pressure waterjet technology has been successfully and maturely put into commercialization. But there are still some problems existing.

First, our efforts these years are still inducting or piloting the market. Although there are many airports in China, few of them are oversize airports with strong economy power. Most sized international airports are still hold the wait-and-see attitudes toward waterjet glue removing equipment and relying on professional cleaning companies to do the cleaning works. So, though we have succeeded in this project for Beijing Capital International Airport, which is No. 1 in China, there still needs hard working in promoting the market.

Second, the airport runway glue removing vehicle is a non-standard product. The varied aims and functions required by every airport and the differences in their economic strength make the cost and amount of after sale service for this product are higher than other general waterjet products. And more, the multi-function it has also puts forward higher requirements for operation and maintenance.

And last, customers in airports demand their purchased large-scale equipment has higher operation reliability, faster maneuverability and higher degree operation comfort. So, besides carefully designing and assembling main pump set, modified chassis and surface cleaner to ensure them meeting designed performance, special emphases should be put on the selection and installation of small parts in hydraulic system such as connectors and static seals, etc. to prevent oil leakage when cleaning on runway, because the leaked oil will reduce the runway surface friction factor sharply and is very hard to clean thoroughly.

6. CONCLUSIONS

The multi-function truck loaded glue removing vehicle which is aimed at Chinese large-scale airports as shown in Figure 6 and trailer glue removing vehicle which is aimed at Chinese middle or small size airports as shown in Figure 4 can fully satisfy the maintenance needs for Chinese runway surfaces. The successful application of airport runway glue removing vehicle in China marks the success of international cooperation in high pressure waterjet technology between G. D.

Company, U. S. A., Bosch-Rexroth Company, Germany and us. It will be sure to promote technology of high power waterjet equipment set in China

REFERENCES

1. Thomas J. Lahss, “Fluid Jet Technology - Fundamentals and Applications, WJTA, 1999.

2. John E. Wolgamott and Gerald P. Zink, “Self-Rotating Nozzle Heads”, Proceedings of the 6th American Water Jet Conference, Houston, Aug 24-27, 1991.

3. David A. Summers, “Waterjetting Technology and Application”, WJTA, 1995.

4. Xue Shengxiong etc. “High Pressure Waterjet Technology and Application”, China Machinery Industry Press, Beijing, 1998.

5. Xue Shengxiong, etc. “Test Research of Super High Pressure Reciprocating Seal under 300MPa”, Proceedings of the 8th American Waterjet Conference, Houston, Texas, Aug 26-29, 1995, pp547-556.

6. Zhou Dan, “Runway Cleaning at Shanghai New Airport”, Jet News, Nov 2000.

7. Xue Shengxiong, etc. “Difference and Similarity of The Glue Removal for Airport Concrete Runway and Bitumen Runway”, Proceedings of the 2001 WJTA American Waterjet Conference, Minneapolis, Minnesota, Aug 18-21, 2001, pp589-599.

8. J. Van Dan, T. Kupscznk, “Removal of Non-Skid Coatings from Aircraft Carrier Decks”, Proceedings of the 2001 WJTA American Waterjet Conference, Minneapolis, Minnesota, Aug.18-21, 2001, pp579-588.

9. Richard F. Schmid, “Ultra High Pressure Waterjet for Coating Removal”, Proceedings of the 10th WJTA American Waterjet Conference, Houston, Texas, Aug 14-17, 1999, pp895-902.

10. D. Wright, J. Wolgamott, G. Zink, “Nozzle Performance in Rotary Applications”, Proceedings of the 10th WJTA American Waterjet Conference, Houston, Texas, Aug 14-17, 1999, pp905-919.

Table 1 Parameters of Multi-speed Pump

Speed	Working Pressure (MPa)	Flow Rate (L/min)	Power (HP)
1	108	122	350
2	149	89	
3	170	64	
4	170	46	

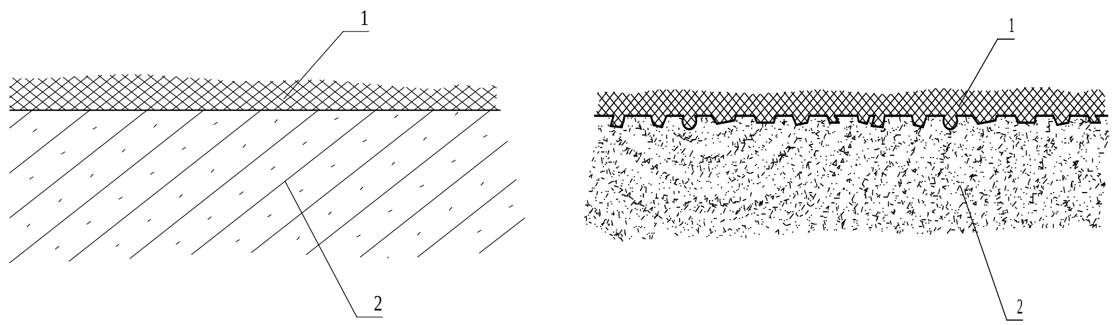

Concrete Runway Bitumen Runway

Figure 1 Glue Adhering Mechanisms on Different Runways

1. Adhering Glue Layer 2. Runway Base

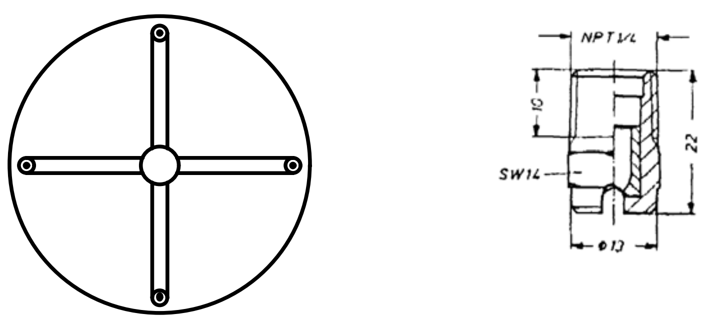

Figure 2a Cylindrical Rotary Nozzle Head and Nozzles

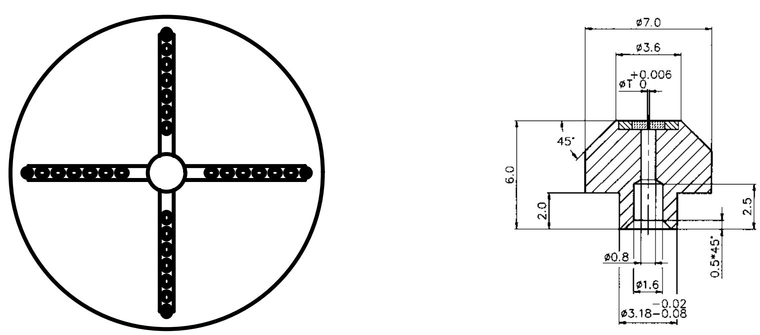

Figure 2b Atomizing Rotary Nozzle Head and Nozzles.

Figure 2 Rotary Nozzle Head and Nozzles

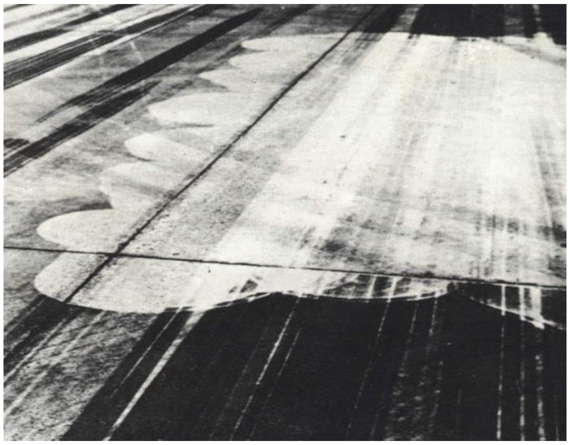

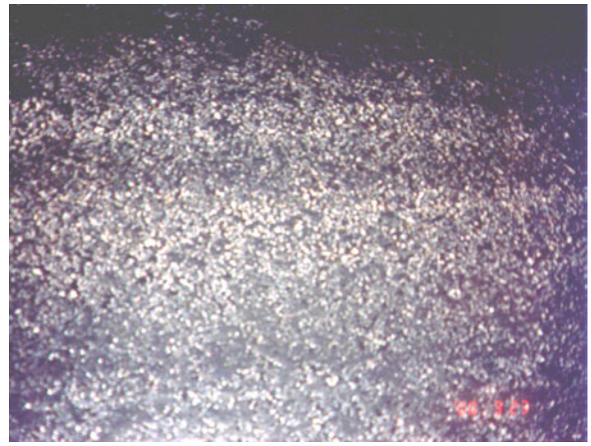

3a Concrete Runway **3b** Bitumen Runway

Figure 3 Cleaning Effect Pre- and Post- Cleaning Process on Different Runway

Figure 4 Trailer Glue Removing Unit

Figure 5 Technically Renovated Glue Removing Vehicle

Figure 6 Multi-Function Airport Runway Glue Removing Unit

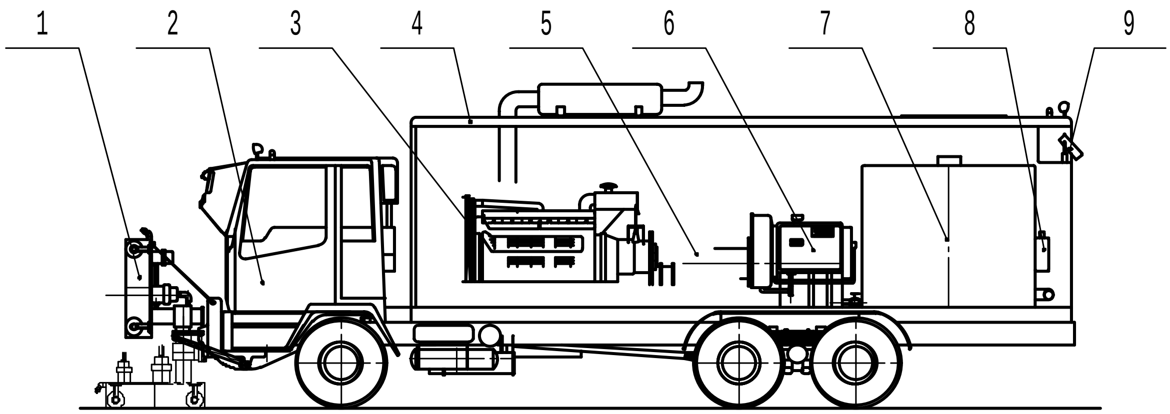

Figure 7 Overall Assembly Arrangement of Multi-Function Airport Runway Surface Glue Removing Vehicle

1. Surface Cleaner 2. Chassis 3. Diesel Engine 4. Cuboid Compartment
5. Speed Regulation Mechanism 6. High Pressure Pump 7. Water Tank
8. Fire Extinguisher 9. Camera Head

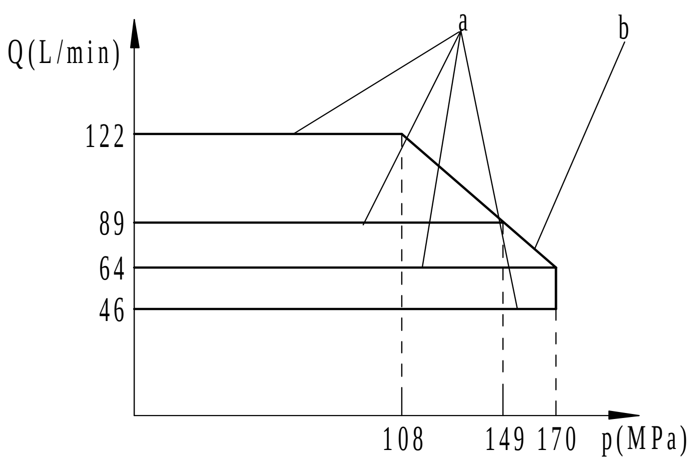

a General Reciprocating Pump **b** Multi-Speed Reciprocating Pump

Figure 8 Performance Curves of Reciprocating Pump

2003 WJTA American Waterjet Conference
August 17-19, 2003 • Houston, Texas

Paper 3-A

DEVELOPMENT OF A PRODUCTION LINE FOR PACKAGING WITH WATERJETS

Axel Henning, Bernd Biesinger, Peter Willems, Wolfgang Rauh
Fraunhofer Institute for Manufacturing Engineering and Automation
Nobelstr. 12, 70569 Stuttgart, Germany

Horst Ranke
Lasercomb GmbH
Siemensstr. 2, 73274 Notzingen, Germany

ABSTRACT

Packaging is gaining more and more importance for the marketing of products. Already in the early stage of development marketing-relevant considerations are taken into account, which decide over target groups and marketing strategies. For design analysis and the essential sampling of the packaging hitherto manufacturing possibilities were of insufficient quality (manual manufacturing, sample plotter) or very cost-intensive (punching units). Both manufacturing options are no satisfying alternative from the user's point of view. At the stage of sampling and prototype production, as well as the individual production of small series, flexible systems are needed, which are capable of quick, cheap and most of all high quality manufacturing of even small series.

In the context of this project concepts for manufacturing solutions with the water jet, which consider these requirements, are developed. Therefore, in a first step existing systems and techniques are evaluated. Based on these results, industry-specific hard and software concepts for the overall system are provided. This includes the concatenation of the system and the technical integration of further necessary manufacturing processes (grooving, cutting and milling).

With such a system new markets for small series production and sample production of cardboard packaging can be opened for the usually small and middle sized companies of equipment manufacturers. The users of the technology thus could increase their geometrical and logistic flexibility and improve the economy of small series especially.

1 INTRODUCTION

Subject of this paper is the development of a system for the processing of cardboard boxes for the packaging industry (PoP - Production of Packaging). The production of packing and folding boxes is characterised by very high numbers of items. Therefore, also mass production procedures, such as offset printing and punching, are used in conventional manufacturing. The high preparation expenditure for the production of models and tools is economically justifiable due to the very high numbers of pieces. Also very high qualities are obtained here because of the matured techniques.

While producing the models or at the design and acquisition phase, small and middle numbers of items of the folding boxes are needed. Here, at present, one resorts to sample plotters, which are able to provide rough prototypes. This kind of production is however characterized by a very high expenditure of time. Further more the systems at present available on the market can only provide unsatisfactory quality of samples, so that for sampling series tools are often prepared also for smallest numbers of items, despite very high costs.

Within the range between the complex series tools and the so far qualitatively unsatisfactory plotters appropriate systems are missing at present. With the project requested here solutions are compiled, which are able to supply both economically and qualitatively satisfying results for small to middle numbers of items.

In a first step, existing systems available at the market were analysed on their suitability. All necessary process steps for the cutting and grooving of the folding boxes were taken into account, thus also the production of the plate cavity. After the evaluation of particular procedures and the assessment, concepts for small standard equipment were compiled. Here not only the actual manufacturing steps (grooving, cutting) were considered, but also the concatenation of the system in the production process, as well as handling mechanisms. Especially by approaching automation and flexibility large advantages could be achieved here. Moreover, using alternative cutting procedures, as e.g. water jet technology, flexibility could be increased, since no dies must be provided.

A special emphasis of the efforts was thereby on the creation of standardized and consistent concepts. These accompany the manufacturing process from the production planning, up to controlling of the system and manufacturing logistics. With intelligent control concepts the production procedures can be optimised thereby.

The work in the project was therefore aiming on developing concepts for a production system as well as the appropriate software, which is the foundation for a new generation of systems for production of small series of folding boxes and cardboard packaging. With this compared with the conventional manufacturing systems an significant increase in flexibility, shorter preparation time were obtained which result in large substantial advantages for the manufacturing of ready-made cardboard boxes.

With this kind of machining mainly small and middle companies processing cardboard packaging (service) can open up new markets. This way high quality ready-made cardboard boxes and packing can be manufactured economically in small series also. With higher flexibility existing customers can be served a broader pallet (from small series to mass products) and new customers can be won. Thus, also the manufacturers of the working systems profit by extending existing markets in the field of small series and by developing new markets in sampling and in building of packaging prototypes.

2 TECHNICAL STANDARD

For series production of folding boxes, with a quantity of 10.000 and more, costly punching units and printing machines are used today. These use specially manufactured tools to blank the two-dimensional pre-form out of box board or corrugated cardboard before printing it. Furthermore the plate cavity has to be designed and manufactured.

The typical course of manufacture is as follows: special punching machines are equipped with stamping tools in order to punch the cardboard packaging shapes out of the raw material with a number of strokes up to 5000 pieces per hour. For this, multiplex instruments are used, thus up to 10 punching procedures can take place simultaneously. This means that a number of 10.000 cardboard boxes are punched in about 10 minutes. For smaller production numbers the manufacturing and scaffolding of the according tools, explained further down, is totally unprofitable. Basically, for quantities between 1.000 and 2.000 pieces, there is the possibility to work with a manual punching die and the corresponding matrix. With these every single raw piece is placed inside separately and punched by hand. Here indeed, the great effort of tool manufacturing has to be taken into account just the same, additional to personal cost for the manual work. For even smaller numbers there is no possibility for industrial manufacturing of cardboard packaging. In this case it is necessary to fall back to handmade plywood boxes or standard dimensioned cardboard boxes. As a consequence non optimised packaging, for example in size, is often used, and accomplished by a product-specific sticker instead of an imprinted label. Principally a high quality cardboard box of the size of a shoe box with an edition of several millions costs ca. $0.25 – $0.40. For a number of 10.000 pieces the costs increase to ca. $0.75 - $1.00, due to the costs for the matrix, ca. $500 – $1000, as well as the tooling time. For even smaller editions, which are principally feasible, the tooling costs etc. outweigh the material costs. Therefore an edition of 1.000 items, of the example above, would cost about $7.50 – $10.00. This is, of course, absolutely unprofitable from the economic point of view.

2.1 Conventional Manufacturing with Punching Tools

For the production of a conventional matrix lines (thin grinded steel strips) are clamped in highly precise slotted plywood panels. Figure 1 shows an adequate sample of a finished matrix. To eject the cardboard out of the matrix after the punching process, a spring-loaded bedding, in shape of a foamed inset etc, often must be fixed. Figure 2 shows an adequate inset, inserted in a matrix.

Simultaneously to the punching process a groove is made, where later the seam will be. This is done by a blunt line with less head room, so as not to slice the cardboard. The groove is made against a corresponding Pertinax-counter punch.Here after, the finished cardboard box is assembled, like shown in figure 4, for example. Plug connections and glued joints are used for assembly.

2.2 Manufacturing Prototypes with Sample Plotters

On the other hand there are sample plotters, which are able to cut parts out of box board or corrugated cardboard by using simple all-round tools. Due to the lack of precision and the high temporal expense it is not possible to produce numbers larger than 10 units with these sample plotters. The quality is not suitable for manufacturing marketable cardboard boxes.
In order to manufacture the Pertinax bedding for the groove a milling module is fixed on the sample plotter.
This cardboard box, imprinted with the sample plotter shown in figure 3, requires 20 minutes execution time. Furthermore, the imprinting is sufficient for a sample survey, yet not so for a marketable product. Plotters, allowing better printing quality and, above all, a considerably higher process speed, are not available on the market worldwide.

3 DEVELOPMENT WORK

The development of the PoP System was carried out in different steps from the definition of requirements to the testing with real prototypes.

3.1 Definition of Requirements

Here the definition of demands (speed, accuracy etc.) on the system and on its boundary conditions are made. Therefore relevant companies (users and manufacturers) are contacted and the respective experts are interviewed. On basis of the obtained knowledge, a requirement profile for the planned production system was elaborated..

3.2 Analysis of Existing Systems

At this operating point systems available on the market available systems were analyzed. On the one hand this concerns mass production systems and on the other hand function plotters. In each case, the systems are evaluated and graded regarding the acquired requirement profile. Special attention is given thereby to concatenation of the systems and integration into the productions process.
Beside the existing systems, also the procedures used so far are evaluated. These are examined especially on their flexibility and the expected product quality.Both, systems and procedures, are graded in the context of an efficiency analysis regarding valued criteria.

3.3 Compiling System Concepts

On basis of the results of the evaluation of procedures and systems, the overall system wassubdivided into different subsystems. For each subsystem solution types are worked out and shown in a morphologic box. The subsystems do not only include process steps, as for example carriage, control system, cutting and grooving apparatus or material transport mechanism, but also the specification of the development environment or the control platform.

This way different possibilities were collected for each subsystem. From the arising multitude combination options sensible “paths” were selected. These possible concepts were compared and evaluated with the help of an efficiency analysis. From this one of the many possibilities is selected for realisation.

At this operating point the selected concept is substantiated. For this detailed concepts for the individual subsystems are worked out. Beyond that, the interfaces between the subsystems are defined. Particularly on the control level this step is of importance. Components available on the market are selected for each subsystem.

3.4 Qualification of the Manufacturing Methods

For processing of cardboard packaging different procedures (milling, grooving, cutting) are needed. In particular for the cutting procedures, the alternative of conventional treatment are blade and water jet cutting. For a selection of the suitable procedure, in this phase comparing studies are accomplished. Here, cutting quality and capacity and also flexibility are especially taken into regard. Beyond that, when cutting with water jets, possible water absorption is examined. The selected procedure is optimized according to the requirements of a high avialablity and feasibility of the overall system.

3.5 Process Specific Adjustment of Components

At this operating point the cutting concept was developed and components were selected. Therefore, in a first step, it is necessary to examine to which extent components that are available on the market (e.g. cutter head, cutting table) can be used for this application. The single components were thereby examined on there suitability for this case of application, regarding the special requirements (minimum humidity of the cut parts, demanded cutting capacity etc.). Based on the investigations, suitable components were selected. On basis of the selected components, usually used on the market, the cutting system was designedand optimized. Components for the special tasks had to be be constructionally adjusted here. The realization of the cutting system and the selection of the components (e.g. guiding system, control unit) were closely coordinated with the software conception.

3.6 Conception of the Control Software

For running the system, concepts for the control software weredeveloped. These concepts allow generating the control code as well as monitoring the process, based on the given working task.

The foundation for such programming is set by the development environment and the hardware platform. Therefore, in a first step, appropriate systems were selected according to the requirements and the manufacturing system. Corresponding concepts were compiled for all necessary software modules. These had to consider the special requirements, particularly in user's interfaces and guidance. For example, the expected expertise of system operators and the ergonomics had to be adapted to industrial environments.
In detail the following modules were needed:

- User Interface
- manual system control
- process definition (defining mode of handling and task)
- process conditioning and preparation (CAD/CAM, generation of cutting path, calibration, process specific adaptations)
- Process regulation and monitoring (time-synchronized data communication, system controlling and system regulation, monitoring machine condition)

3.7 Realization and Testing

After realization of the system the provided concepts and selected or modified components and modules were tested at the institute's water jet system. Beyond that, already in the conception phase project partners, with whom the compiled concepts and modules could be realized and converted, were found. Apart from the technical realization with the selected procedures also the software modules were integrated.

4 APPLICATION

A concatenated complete processing system for the grooving and cutting out of a two-dimensional pre-form, by using water jet technology, was developed in cooperation between LaserComb GmbH and the Fraunhofer Institute for Manufacturing Engineering and Automation (IPA). The institute itself can look back on an experience of many years in the field of water jet technology. Numerous research contracts with national and international research institutions as well as the industry, have established rich experience and good machine equipment in this field. LaserComb has long term experience in manufacture and distribution of sample plotters.

The system consists of two working stations, which are connected over a chain conveyor. The automatic supply and removal of box board makes a fully automated system operation possible. Both working stations have two X-Y - linear motion units each, on which a die head each is set. The die heads of the first station are equipped with a grooving skid or grooving wheel as well as with a cutting blade. Here, as the first processing step, grooves are worked into the box board and possible perforations are made with the cutting blade. Tool meshing and orientation are controlled via one linear and one rotatinal axis. Additionally a milling tool can be attached to the die heads, which produces a plate cavity for grooving solid fiber board. The die heads of the second station are equipped with water jet devices. Here the two-dimensional outline of the packaging is cut out. With the help of a high-pressure water jet pump, pressures up to 400MPa can be achieved. By using high pressure, combined with very small nozzle diameters, unwanted humidity intake of the box board is minimized. The control of all together 13 axes is taken over by a NC – control unit. The software, needed for this, was developed at the IPA. With its assistance a layout, developed with a CAD system, can directly be transferred to the system and manufactured in the requested number of items.

5 CONCLUSIONS

With this kind of fabrication both sampling prototypes, and cardboard boxes and packing, ready for sale, can be manufactured economically and with high-quality in small series to approx. 10,000 pieces. The high system flexibility allows especially small and middle companies that are manufacturing cardboard boxes to provide a broader product range to their customers and may help to win new customers.

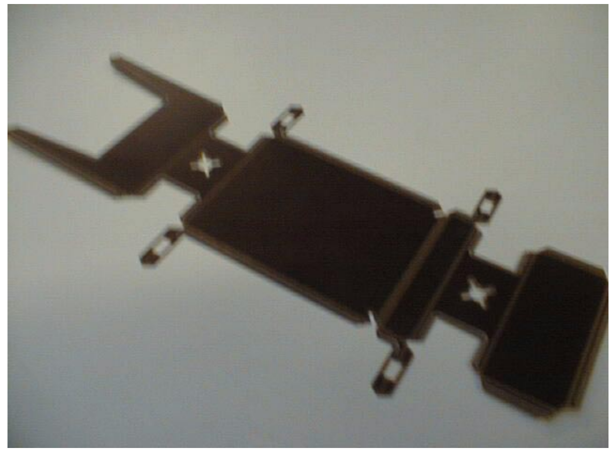

Figure 1: Conventional cutting tool

Figure 2: Pertinax-counter plate with grooves

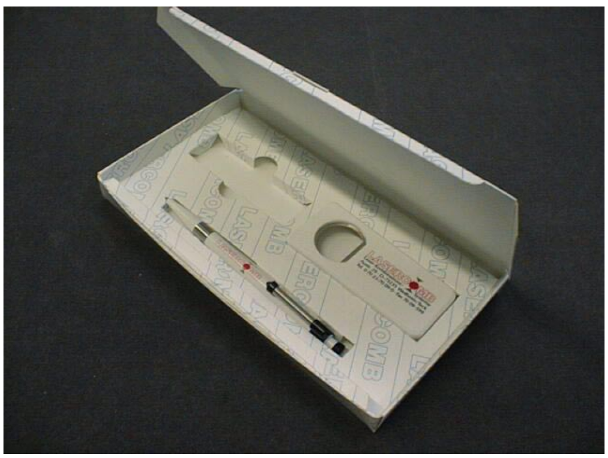

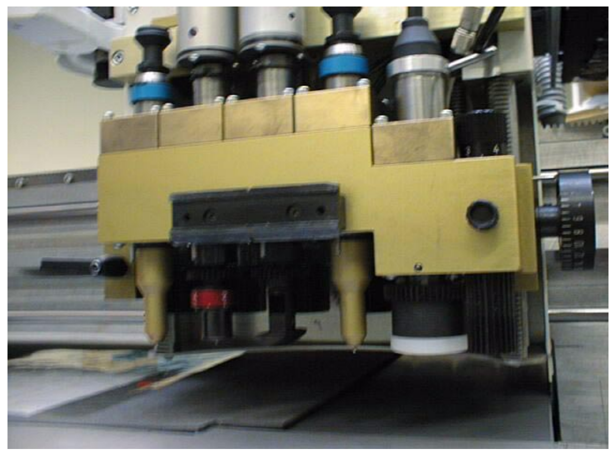

Figure 3: Product example

Figure 4: Conventional tool

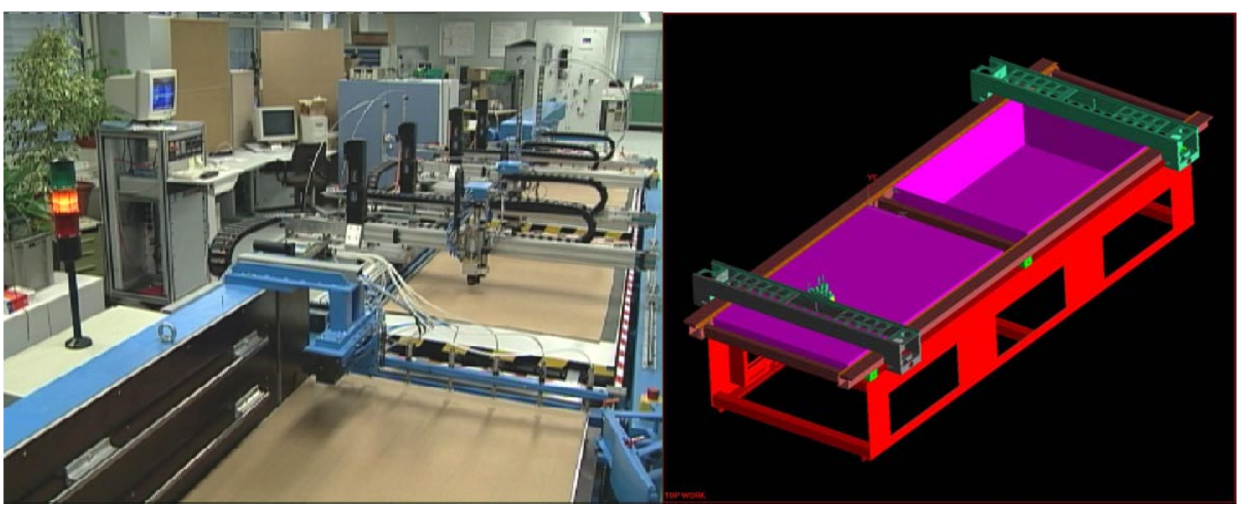

Figure 5: Design and realisation of system for Production of Packaging (PoP)

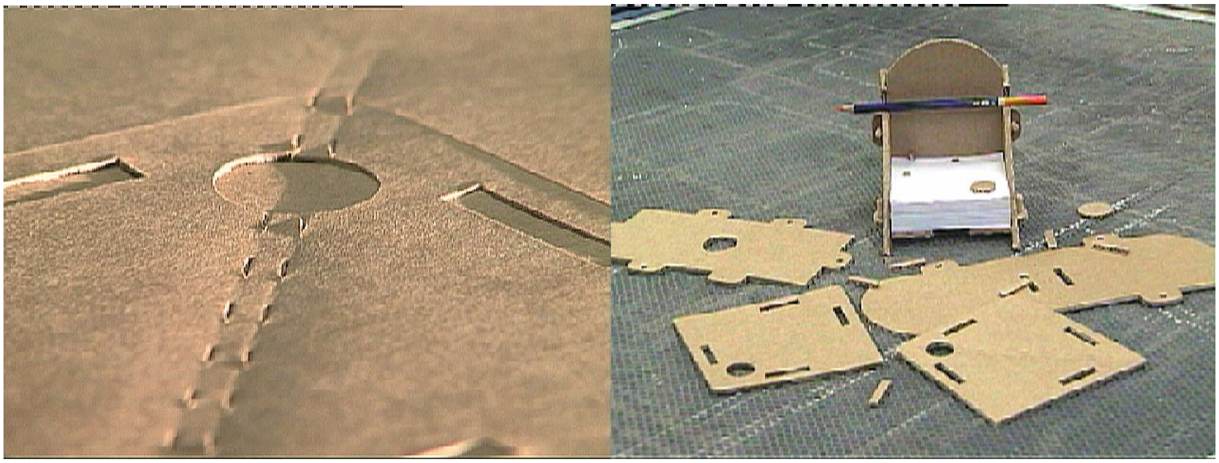

Figure 6: Waterjet cutting and product example

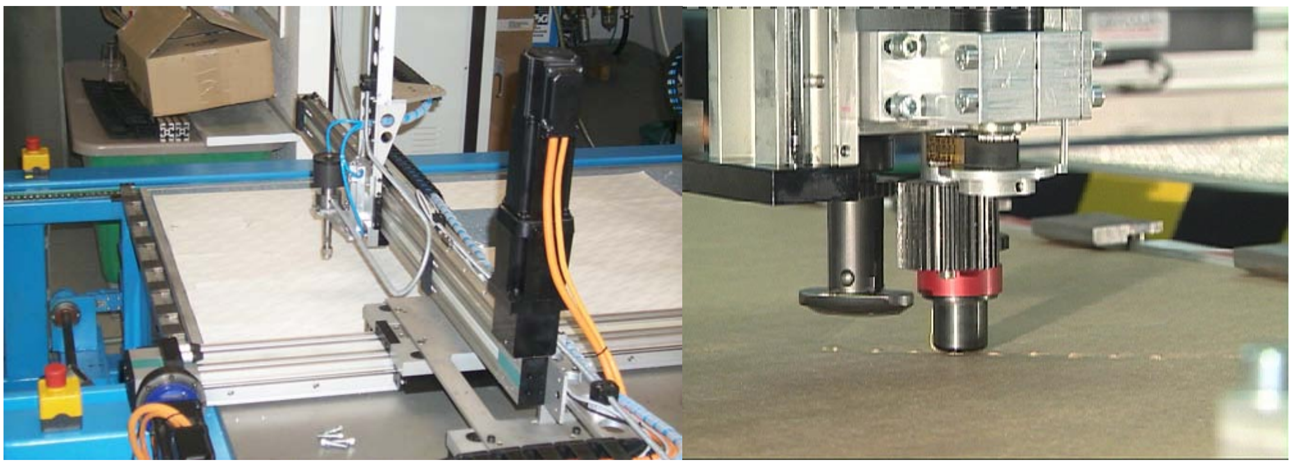

Figure 7: Tools of the PoP system (Waterjet cutting and perforation/grooving blades)

Figure 8: PoP system with cardboard feeder

2003 WJTA American Waterjet Conference
August 17-19, 2003 ● Houston, Texas

Paper 2-F

PURE WATERJET FOR SANDWICHES - THE SECOND STEP

Franz H. Trieb
Bohler Hochdrucktechnik GmbH
Kapfenberg, Austria

ABSTRACT

Waterjet cutting has a long tradition as an appropriate cutting method for the food industry. Frozen fish, meat and vegetables, chocolate bars and ice cream are already cut by waterjet. To cut sandwiches the conventional method are oscillating blades. The result and quality of the cutting surface is strongly depending on the food which is between the two slices of bread. For the waterjet it is not really important whether there is ham, tomato or egg inside. How efficient the cutting technology works is depending mainly on the pump system and the installed high pressure components. A multi cutting head unit is in use simultaneously. Flow rate and working pressure as well as the reliability of the high pressure pump influences velocity, flexibility and of course the costs of each cutting procedure. The first industrial production line is already installed. The paper gives an overview of the application of waterjets to cut sandwiches. From the incoming bread to the end product, packed and ready for selling. It presents an comparison between the conventional blade cutting method and the new application with pure waterjets and gives an outlook on the advanced second unit.

Organized and Sponsored by the WaterJet Technology Association

1. INTRODUCTION

For many years waterjet cutting has been a proven and reliable method in several ranges of material processing and is also used in many fields of the food industry. Fish, meat, vegetables, pastries, chocolate and ice cream products are cut by pure waterjet. The thermal stress is low and deformations rarely appear even on soft materials due to the low cutting forces. This technology is especially interesting because of the continuously renewing and thus bacteriologically uncomplicated cutting tool.

Meanwhile, due to the development of standard components, this technology has become reliable and economically attractive and also in the range of food cutting has turned into a significant alternative to conventional cutting methods.

2. CUTTING OF FOODSTUFF

The cutting process has a crucial function in foodstuff industry. Unlike cutting up, cutting is a technical process which separates an object according to the cutting tool geometry towards its forward feed direction creating two adequate interfaces. Cutting processes are used in purifying, cleaning, portioning and separating procedures. Currently the majority of cutting processes is carried out by mechanical tools.

For an assessment of cutting technology, more factors than the mere cutting capacity have to be considered. The utilization of blades entails the risk of contamination of the blade by the object to be cut. If the operator does not notice that risk in time, large quantities of rejects can be produced. The jet tool avoids this problem by producing constantly a new "blade" in the shape of liquid. This liquid is processed before the beginning of the cutting process. The waterjet thus represents a steadily sharp tool that does not require any additional set-up time for sharpening (1).

2.1 Requirements on Cutting Process

The requirements on the cutting process are various. They differ in accordance with each case of application and with the demands made on the product. The type of product as well as the product state play an essential part. Cutting of sandwiches, for example, requires that the cutting tool is able to divide simultaneously various products. There are different kinds of sandwiches with various kinds of fillings. No matter if the filling is salad, tomatoes, sausage, ham, cheese or filling masses with egg and seafood - in any case the cutting tool has to produce an "appetizing" profile over the whole cutting surface. Dents and fissures make the product unsightly converting it into a "shelf warmer". In any case, the demands applying to all cutting processes regarding hygiene and waste minimizing, better utilization of raw material are very high. Availability of the production plant and economical efficiency of the process must be ensured as well.

2.2 Mechanical Cutting of Sandwiches

Currently sandwiches are conventionally cut by means of oscillating saw blades. The product is being cut by a method similar to the cutting with a compass saw. During the cutting procedure two slices of bread and the respective filling, must be pressed together and held.

The sandwich is moved past the saw and diagonally cut. The friction between the blade and the goods produce forces which may also cause deformations on the objects to be cut. If mechanical cutting were carried out without fastening, the acting cutting forces would displace the sandwiches and the filling. The appropriate sharpness of the applied blades has to be ensured. Edgeless tools lead to an increase of the cutting forces and consequently to a diminution of the cutting quality.

2.3 Waterjet Cutting of Sandwiches

In comparison with mechanical cutting the waterjet cutting procedure presents a lot of essential advantages. The most important is that the material to be cut is not deformed. Due to the low orifice diameter which ranges between 0.10 and 0.15 mm, the cutting slot is very small, which consequently leads to a minimization of the waste material or the rejects. The jet of liquid is constantly sharp and, above all, constantly new.

The waterjet avoids all the problems concerning the contamination of cutting blades and the expensive cleaning involved. There is no set-up time for changing edgeless blades. The fact that the waterjet evades solid obstacles cutting along them has no negative effect on cutting of sandwiches, since it is not allowed that the filling contains solid materials such as cartilages and pieces of bones.

A summary and a comparison of advantages and disadvantages of mechanical cutting and pure waterjet cutting is presented in Table 1. As the table shows, one of the disadvantages of the waterjet method is the high noise level of the free jet. Considering that the sandwich material differs in height, it is necessary to keep an adequate minimum distance between the lower edge of the orifice holder and the upper edge of the sandwich. This fact causes a considerable noise level. The accessibility which must be ensured for daily cleaning to be carried out after the end of production, makes it also nearly impossible to take significant measures for sound insulation around the jet catcher device.

2.4 Basic Examinations

Empirically, a waterjet of high stability and jet coherency has positive effects on the cutting result. The interaction between waterjet and sandwich is considerably reduced and diminishes smears on the cutting edges. The cutting result has been satisfactory as well in the orifice diameter ranging between 0.10 and 0.15 mm as in the tested pressure ranging between 200 MPa und 300 MPa. A tendency of improved cutting quality at reduced orifice diameters and low working pressures was detected (2).

Figure 1 and 2 show a reference cut of sandwiches filled with egg and cress and seafood. Data were detected at a working pressure of 300 MPa, an orifice diameter of 0.10 mm and a distance of 45 mm between the lower edge of the orifice holder and the sandwich support. Comparison measurements and test cuts revealed a great divergence in noise level and cutting result of orifices provided by different manufacturers. Depending on the manufacturer and the type of orifice the noise level is ranging between 88 and 97 dB(A). The detailed results are shown in Figure 3.

3. APPLIED HIGH PRESSURE TECHNOLOGY

In the field of high pressure technology, pressure is generated by means of conventional high pressure pumps with intensifier. Tubes, fittings and valves are used similar to other waterjet cutting applications.

3.1 High Pressure Pumps

Like in other fields of application, also in food processing technology only stainless steel is employed for the medium-contact components. If there is no mechanical separation on the intensifier inside the high pressure pump between oil hydraulic actuator and high pressure cylinder, food grade oil has to be applied as hydraulic fluid. In this connection, special attention has to be paid to the fact that the oil tank of the hydraulic drive unit is fabricated of stainless steel or plastics, otherwise the applied hydraulic oil might be affected.

In case of installing spacers between the actuator and the high pressure cylinders, the application of commercial hydraulic oil is possible. The advantage that offers the utilization of low-priced standard oil has to be compared with the expensive design with spacers.

Since in most cases the system works at 300 MPa with orifices diameters ranging between 0.10 and 0.15 mm, the water consumption with 0.3 to 0.7 l/min is very low. Due to the simultaneous application of four orifices the flow rates are between 1.2 and 2.8 l/min. Depending on the available high pressure pumps (Figure 4), the installed power supply ranges from 18.5 to 30 kW per cutting unit (3).

3.2 Waterjet Cutting Unit

The cutting unit consists of four waterjet valves which are installed on the same bar and moved synchronously. For the first plant a single high pressure line has been installed. The distribution of high pressure water takes place directly in front of the cutting heads. For the second and new production plant each cutting valve has its own high pressure supply (Figure 5). Three tube coils for each valve are installed to compensate the cutting movement The total required cutting length is 175 mm.

The entire cutting cycle takes 3 seconds. In that time four sandwiches are cut simultaneously. After each cut the valves are closed and the conveying belt with the sandwiches moves up for the next cycle. For reasons of plant engineering a longitudinal cut with constantly active waterjets is not possible.

As mentioned above the applied orifices have a diameter of 0.10 to 0.15 mm. Sapphire orifices are in use. According to the filling material of the sandwiches, the working pressure is around 300 MPa.

The first cutting unit was equipped with a line catcher. All four waterjets sprayed into one vessel which caused a rather high noise level. For the second unit four single catcher units have been installed. Each catcher is synchronized with the corresponding cutting head and moves with it. This improvement reduced the noise level for more than 6 dB(A).

4. PRODUCTION LINE

The whole production plant (Figure 6) is divided in twelve sectors. The bread magazine is located in the front of the production line. The bread is filled and sorted manually. In the second station a pick-and-place robot (Figure 7) puts simultaneously eight slices of bread on the conveying belt. This station is followed by a control section for manual correction in case of misplacement of bread slices (Figure 8).

Now the slices of bread are automatically spread with butter (Figure 9). Respectively four of the eight slices are coated with the mass by an automatic filling machine (Figure 10). This unit is used in case of pasty fillings only. Other fillings such as ham, cheese or salad are applied manually in the manual filling area (Figure 11). Now sandwiches are closed with the second slice coated with butter and transported to the cutting station.

Respectively four sandwiches are cut diagonally (Figure 12 and 13) at the same time. Then the second half of the sandwich is placed on the first half and put into the furnished packing by a pick-and-place robot (Figure 14), hermetically sealed and manually sorted into shipping boxes (Figure 15). On each single production line every minute 60 sandwiches are produced. At the moment 28,000 sandwiches cut by waterjet leave the two production plants per day. The sandwiches are not frozen, they are put on the market as fresh food. Best-before time: Two days!

5. CONCLUSION

Today waterjet cutting technology is already widely spread in foodstuff industry. Still it is necessary to find out in each individual case if its application is organizationally efficient and, of course, economical. In case the cutting result should meet with the requirements, the saw blade might be preferred as competitive method for economical reasons. Precisely in the case of long cutting edges the higher cutting capacity of the blade is inclined to exclude alternative procedures.

The advantages of mechanical cutting mainly lie in the field of mass production. The first two sandwich production plants in which the high pressure waterjet cutting technology has been installed, impresses by its flexibility, high availability and process reliability as well as by its uncomplicated and dynamic handling. Further plants are planned for installation within begin of next year.

6. REFERENCES

(1) Henning, A., 1995, "Potentials of Application in High Pressure Waterjet Technology", IPA-Meeting, Automation in Food Industry, Stuttgart, Germany.

(2) Von Rad, C., 2002, "Cutting of Sandwiches by Pure Waterjet, Study of Institute of Material Science", University of Hanover, Hanover, Germany.

(3) Trieb, F., 2002, "Sandwiches - A New Application for Pure Waterjet Cutting", Proceedings of the 16th International Conference on Water Jetting, BHR Group, Aix-en-Provence, France, pp. 193-200.

7. TABLES

Table 1. Advantages and disadvantages, comparison between mechanical cutting and pure waterjet cutting of sandwiches

Mechanical cutting		**Waterjet cutting**	
Advantages	Disadvantages	Advantages	Disadvantages
No moistening of the cutting edge	Deformation	No deformation	Moistening of the cutting edge
Higher cutting capacity	Larger cutting slot	Small cutting slot	Lower cutting capacity
Low priced equipment	Longer set-up times	Short set-up times	Costly equipment
Low noise level	The tool turns sticky	No cleaning of the tool	High noise level
	Problems with solids	Suitable for all fillings	

8. GRAPHICS

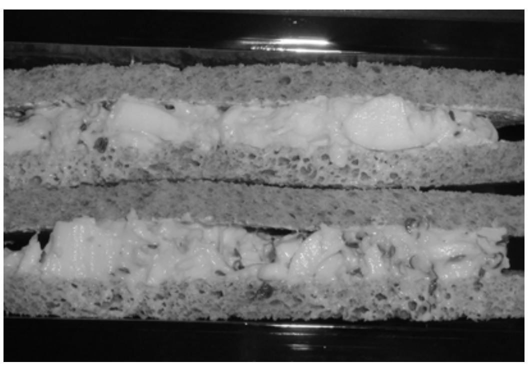

Figure 1. Reference cut "Egg and Cress"

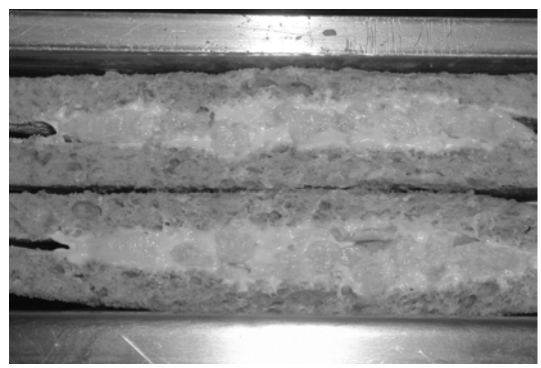

Figure 2. Reference cut "Seafood"

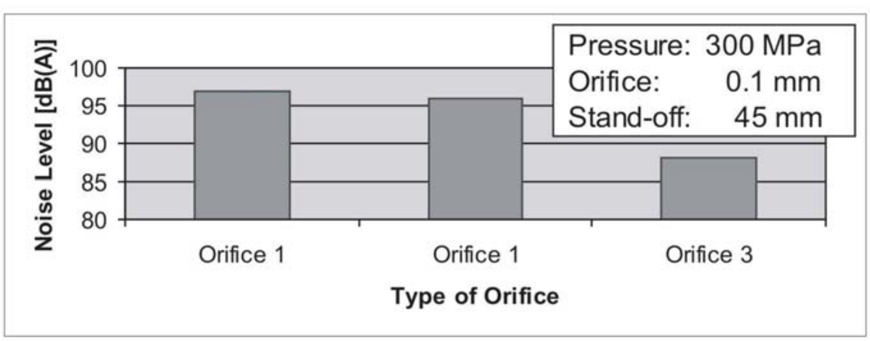

Figure 3. Noise level of different orifice type
(source: Institute of Material Science, University of Hanover)

Figure 4. High pressure pump (source: Bohler Hochdrucktechnik)

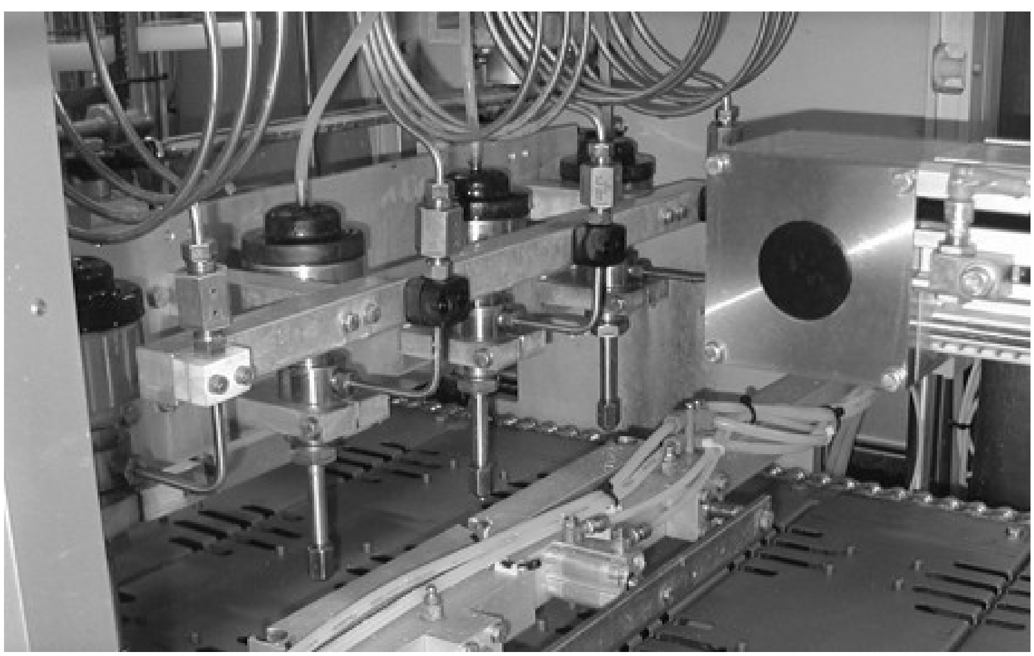

Figure 5. Cutting unit with four waterjet valves (source: Bohler Hochdrucktechnik)

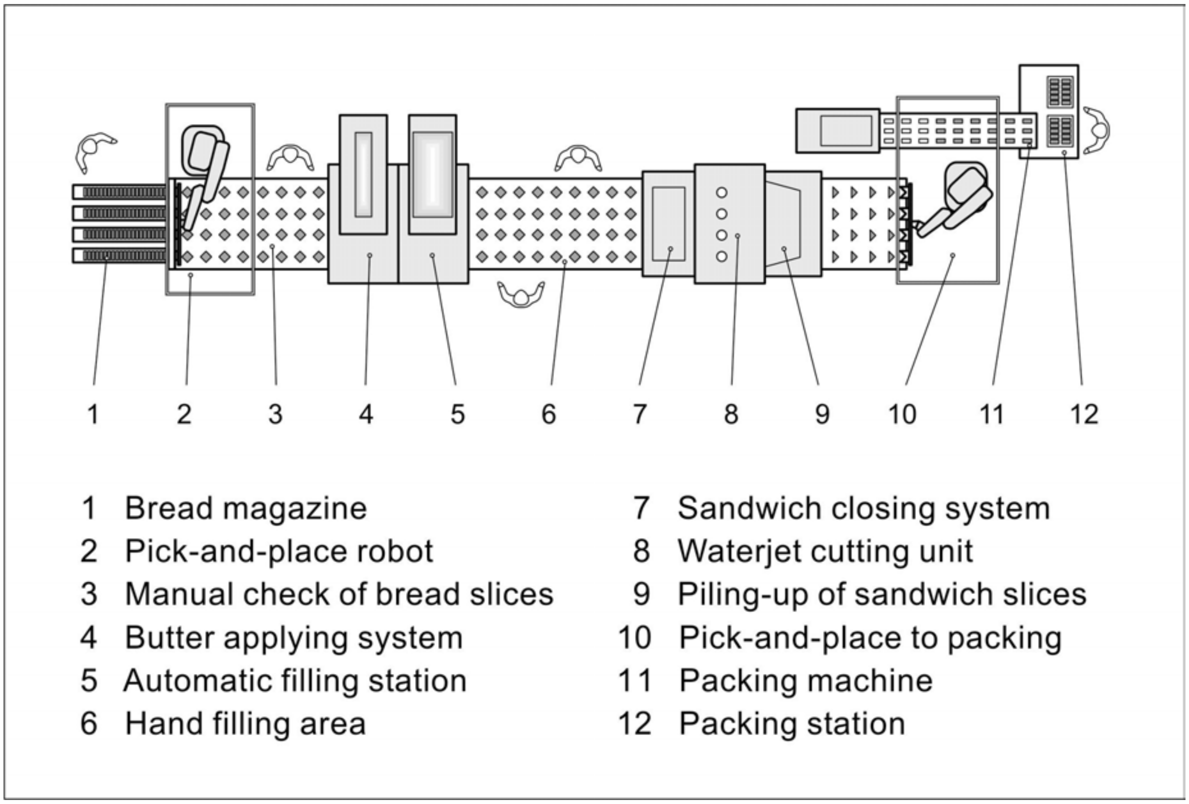

Figure 6. Overview of the complete production line for sandwiches (source: Lieder Maschinenbau)

Figure 7. Pick-and-place of bread

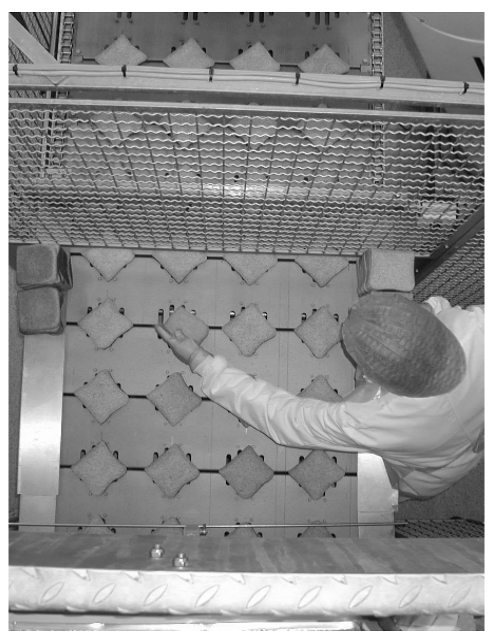

Figure 8. Manual bread correction

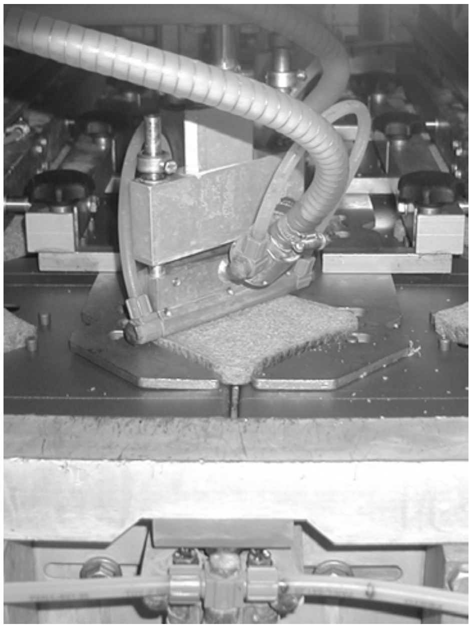

Figure 9. Butter on the bread

Figure 10. Bread with egg and cress

Figure 11. Single bread slices with butter as well as egg and cress

Figure 12. Cut unit in operation

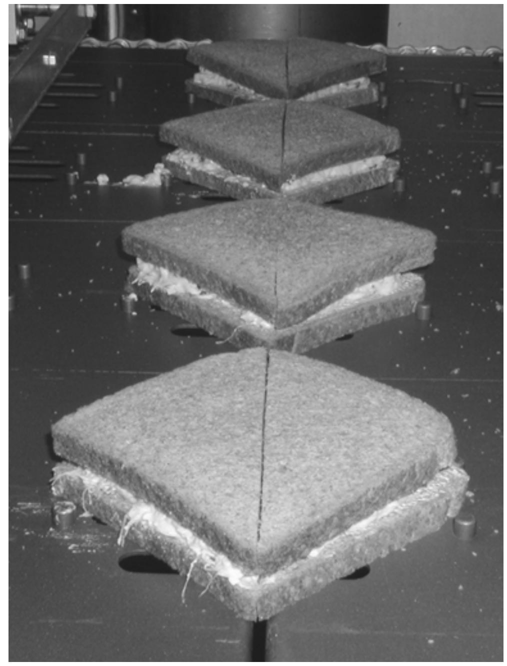

Figure 13. Cut sandwiches

Figure 14. Pick and place to packing

Figure 15. Packed sandwiches

2003 WJTA American Waterjet Conference
August 17-19, 2003 ● Houston, Texas

Paper 3-A

ABRASIVE WATERJET USED AS A TOOL FOR PRODUCING MATERIALS TEST SPECIMENS

U. Andersson, G. Holmqvist, K.M.C. Öjmertz,
Chalmers Lindholmen University College
Department of Mechanical Engineering
Göteborg, Sweden

ABSTRACT

This paper is high-lighting the potential for abrasive waterjet machining in the field of producing test specimens, pointing out advantages such as high machining efficiency, low material waste and flexibility in the sense that the method can be used for any material. Further, specimens can readily be cut from complex or difficult-to-handle work pieces as tubes or large sheets of material. Also, the benefit of being able to easily cut combinations of materials, as can be found in welded, soldered or adhesive joints are shown. Two different applications are presented in this paper.

The first case deals with cutting of weld metal test specimens from plates and tubes. The benefits over conventional methods as sawing and milling are discussed from a geometrical point of view, as well as from a material properties point of view considering for instance work hardening in several of the machined material types. Further, the number of machining operations needed is significantly reduced.

In the second case, test specimens in an intermetallic compound (molybdenum silicide, MoSi2) were produced using abrasive waterjet turning. It was found that the cost of manufacturing the test specimen with AWJ turning could be considerably lower than the cost using conventional manufacturing methods. An additional potential benefit from using AWJ in this context is the fact that the work piece for the specimen could be cut out from the bulk material of the product to be manufactured.

1. INTRODUCTION

Abrasive waterjets (AWJ) have due to its versatility become widely accepted as a tool for manufacturing parts out of virtually any material for various applications. The method is used in small job shops as well as in advanced manufacturing facilities in aerospace industry.

In modern industry high demands on product quality and safety, require standardized work procedures and accreditations. Due to this fact, test engineering has become a growing market. A significant field is the testing of materials and materials joints. Here, AWJ cutting has proved to be an efficient alternative to conventional machining in the manufacturing of the test specimens. Since the method causes minimal thermal and mechanical surface integrity deterioration it is becoming increasingly used in material testing laboratories for test specimen preparation. In Sweden, several laboratories have found the versatility of AWJ cutting so useful that they have invested in a system of their own. This paper presents two Swedish applications where AWJ have proved useful for manufacturing of test specimens.

Testing and analysis of material samples is made on a regular basis at the different steps of a product's life cycle. For example, test specimens need to be produced for:

- Materials testing (e.g. tensile strength, impact toughness, fatigue strength and metallographic studies).
- Verification of manufacturing processes (e.g. local strength of material in components, welds, solderings and metallographic studies).
- Damage analyses of failed components (predominantly metallographic studies).

For the *first two applications*, metal test specimens can be directly turned to shape from solid bars. The circular shape is often preferred as edge effects can be minimized. In case of plate or tube material, or a full component, they are generally sawed out and then machined to specified shape, related to the type of testing. For hard materials, e.g. engineering ceramics, this procedure becomes more demanding, usually requiring diamond grinding for material removal. In general, also AWJ machining can be an efficient alternative method for machining this type of materials, sometimes enhanced by the use of alumina abrasives which significantly increase material removal rates for several engineering ceramics (Kahlman et al).

In the case of a *damage analysis*, the analysed object is a failed component. In general, only the location of actual material failure is of interest, whereas in such cases, the need is to extract only such a small portion of the component as to be able to accommodate it in the analysis equipment (e.g. SEM, microscope etc.).

Surface finish requirements of test specimen differ depending on choice of test method and material of the specimen. In general, tensile test specimens for material testing that are not high strength or that are ductile are usually rather insensitive to surface finish effects. The reduced sections of machined test specimens must, however, be free of detrimental characteristics such as cold work, chatter marks, grooves, burrs, etc. For fatigue testing surface irregularities become more critical (ASM Handbook, 2000).

Testing laboratories find the AWJ process producing surfaces of satisfactory quality for tension tests of metals. The effect of surface irregularities of AWJ cut surfaces on fatigue properties is an area that still needs further investigation. A study on AWJ cutting of extra high-strength steel was performed in order to investigate however AWJ cut surfaces produced fatigue lives comparable to conventional cutting methods of structural steels (Holmqvist et al., 1999). These tests indicated that the AWJ produced surfaces on fatigue test specimens yielded fatigue strength levels comparable to test specimens produced by machine flame cutting or shearing, as specified by the International Institute of Welding (Hobbacher, A., 1996). It was, however, noticed that on those individual test samples yielding the shortest fatigue life, the crack was initiated on the surface rather than at a corner, which was the case of most of the specimens. This indicates that on some specimens the AWJ process might have produced relatively rare irregularities or imperfections, possibly related to individual abrasive grains embedded in the surface, that act as initiation sites and thereby reducing the fatigue life.

2. EXTRACTING WELD AND SOLDERING SAMPLES OUT OF PLATES AND TUBES WITH ABRASIVE WATERJET CUTTING (APPLICATION 1)

2.1. Background

At present Sweden is adapting to European and international welding regulations. This means that a great number of welders need a certificate according to the Swedish standard SS-EN 287 (SIS, 1997) from an independent third party research laboratory to prove their welding skills. The standard SS-EN 288 (SIS, 1995) provides conditions under which tests are to be carried out i.e. welding process, welding position, material, dimensions, type of Welding Procedure Specification (WPS) etc. Every welder has to perform a number of procedure tests which will be subject to an evaluation proving the quality of the welds.

The evaluation consists of both destructive and non-destructive testing. To the non-destructive tests counts fracture tests in the surface as well as underbedded cracking. The destructive testing includes metallography as well as tension, bend and impact tests.

2.2. Extracting test specimen

The destructive testing requires test specimens with a certain geometry and surface integrity depending on type of test that is to be carried out. The conventional method to extract test specimen includes:

1. *Sawing* – To extract a rectangular section out of the plate or tube. To access the inner of the material, i.e. the welded area, sawing is needed. (See figure 2.)
2. *Milling* – Milling is used to produce the correct tension test specimen shape.
3. *Grinding* – If the material is sensitive to work hardening (e.g. copper, titanium), the strain hardened surface of the test specimen resulting from the milling operation needs to be removed by grinding.

As an alternative to using these three operations, abrasive waterjet cutting has shown to be an interesting alternative method for extracting test specimens. This applies especially for the commonly used testing of butt welds of plates and tubes, see figure 1 and 2. For tubes, generally several test specimens are extracted consecutively along the perimeter. Det Norske Veritas Sweden AB (DNV) have used abrasive waterjet cutting for extraction of test specimens since 1997, and the test specimen preparation has furthermore been studied at Chalmers Waterjet Lab. The results finally convinced DNV last year (2002) to make an investment in a 2½-axis machine intended solely for this purpose.

DNV uses AWJ cutting for plates and tubes in all types of materials like steel, high-alloyed steel, stainless steel, titanium, copper etc. The most important advantages and drawbacks for this AWJ application are:

Advantages with AWJ:

- No heat affected zones.
- Negligible strain hardening of outer layer (does consequently not require subsequent material removal).
- Cuts various materials and shapes (contours) with the same tool.
- Can easily be used for both plates and tubes.
- Time and cost savings are made by reducing sawing, milling and grinding to a single AWJ cutting operation.
- The test specimen can be extracted directly from an arbitrary location within the plate or tube, without any excessive material removal, see figures 1 and 2.

Drawbacks with AWJ:

- A blasting effect occurs inside the tube which is hard to avoid, even when a catcher is inserted in the tube. This damages the surfaces of the non-cut specimens.
- Small diameters combined with greater wall thickness lead to geometrical errors of the test specimen.
- Cut surfaces are not suitable for all types of tests without subsequent surface finishing treatment (e.g. fatigue testing of hard materials).

3. ROUND CROSS-SECTIONED TENSILE TEST AND FATIGUE TEST SPECIMENS IN INTER-METALLIC COMPOUND (APPLICATION 2)

3.1. Test Material and Conventional Manufacturing Methods

In this industrial case test specimens from an inter-metallic compound were produced using abrasive waterjet turning. The material was predominantly a molybdenum silicide (MoSi2), which is used as a refractory material for industrial furnaces and heating applications. The standard process for the manufacturing of parts in the material, usually rods or tubes, is by extrusion of a prepared paste, followed by drying and sintering. Among the material characteristics can be pointed out a Vickers hardness of 9-11 GPa and a fracture toughness of 3-4 MPa√m. The material can thus be characterized as relatively hard and very brittle, and the characteristics correspond to that of engineering ceramic materials. These features render the material very difficult to machine, why previously possible machining methods for producing more intricate shapes have been limited to electro-discharge machining and/or diamond grinding and polishing. The method of choice until today for producing round cross-sectioned test samples in the material has been to use diamond wheel grinding to the final shape from a rod. Technically, forming (pressing) of a green body to a more near-net-shape would be possible. However, this has not been used for this material and would therefore require extensive testing and development. Furthermore, it would only be economical for large production series.

When testing the material properties of inter-metallic materials as well as engineering ceramic materials, there is generally a quite large scatter in test results. The reason for this is according to Carlström (1989) that these materials are very sensitive for defects, as well as the fact that the defect-density can vary considerably. The defects can be in the form of pores, impurities or accumulations of material components due to poor mixing. The sensitivity for defects is generally higher for materials with low fracture toughness, which is typical to these materials.

3.2. Test Specimen

Figure 3 shows the geometry of the test specimen. Generally, round cross-sections of a test specimen is favorable since edge effects are avoided, making results more reliable and generally more consistent. The geometry in this case can be used for either tensile or fatigue testing. A fatigue test requires a surface roughness in the middle part of the specimen to be 0.2 µm or better. A threading of the ends can be a necessity for some types of equipment. In the present case, a testing device equipped with a hydraulic gripping mechanism is to be used, why a plain cylindrical shape is sufficient.

3.3. Machining of Test Specimens using AWJ Turning

The work piece for the AWJ turning operation was a rod of 25 mm in diameter. Figure 4 displays a rod and an AWJ machined specimen. The glossy surface of the rod is a glass phase of the material occurring from the material processing. This phase is slightly more brittle than the base material. Figure 5 shows a specimen being turned. The rod was fixed in a chuck. No tail-stock was used. It was shown that the specimen could be turned in a series of 5 cuts using a parameter setting for typical abrasive waterjet cutting applications. Both ends were cut-off using AWJ turning. The geometry and surfaces produced were adequate for a tensile test. The surface roughness (Ra) produced was in the range of 2 μm. Consequently, for a fatigue test, the specimen would have to be polished.

3.4. Advantages and Possibilities using AWJ Turning

The cost of manufacturing the test specimen using AWJ turning should in this case be compared to using diamond wheel grinding. As no optimization effort was made yet for the selection of the AWJ turning process parameters, the exact savings can not be quantified. However, considerable economical savings from using AWJ turning can be foreseen in this early stage for this application.

In a similar industrial case for which a new material is being developed, larger pieces will be cast and sintered, and the final shape will be produced using a combination of AWJ machining, EDM and grinding operations. Due to an inherent variation of defect-density it would be advantageous to be able to extract the specimen from the same material batch as the actual part. This yields representative measurements of material properties. In this context an important feature of the abrasive waterjet is that it can be applied to cut out work pieces from a larger bulk material. As it is possible to use AWJ turning for producing cylindrical shapes also for irregularly shaped cross sections, a test specimen can easily be turned from, for instance, a square work piece. Figure 6 shows schematically an extraction of a square-sectioned work piece. The cut-out can be made using slotting (milling) or cutting, depending on the thickness of the bulk material. For the part in question a feasibility study is under way looking into the possibility of extracting a specimen work piece. This must be made in an appropriate stage of the manufacturing taking into account the whole manufacturing of the part.

4. CONCLUSIONS

- AWJ has shown to be a viable method for extracting weld test specimens out of plates and tubes.
- The most important advantages in cutting weld test samples are reduced costs and a negligible influence on the cut surface properties.
- Abrasive waterjet turning has a potential for economical savings in manufacturing of round cross-sectioned test specimens in difficult-to-machine materials such as ceramics and inter-metallic compounds.
- Tolerances and surfaces produced using AWJ turning are adequate for round cross-sectioned tensile test specimens.
- It is possible to use AWJ turning also for irregularly shaped cross sections. Therefore, work pieces for a test specimen can easily be extracted from the bulk material of a part, giving a better representation of the materials characteristics.

5. REFERENCES

ASM Handbook, “Volume 8: Mechanical Testing and Evaluation”, *Publ. ASM International, Materials Park*, Ohio, USA, 2000.

Carlström, E. et al: “Keramguiden”, Swedish Ceramic Institute, 1989.

Hobbacher, A.: “IIW Fatigue design of welded joints and components” *Abington Publishing*, 1996.

Holmqvist G., Öjmertz, K.M.C., Bergengren, Y. and Fronzaroli, M.: ”Influence of Abrasive Waterjet Cutting on the Fatigue Properties of Extra High-Strength Steel ”, *proc. 10th American Water Jet Conference*, Houston, TX, USA, 1999.

Kahlman, L.; Öjmertz, C. and Falk, L.: ”Abrasive-waterjet testing of ceramic thermal wear”, *Wear*, n.248, 2001, p.16-28.

SIS – Metalliska material (Swedish Standards Institute – Metallic Materials): “SS-EN 287-(1-2), Approval testing of welders – Fusion welding - Part 1 to Part 2”, 1997.

SIS – Metalliska material (Swedish Standards Institute – Metallic Materials): “SS-EN 288-(1-9), “Specification and approval of welding procedures for metallic materials - Part 1 to Part 9”, 1995.

6. FIGURES

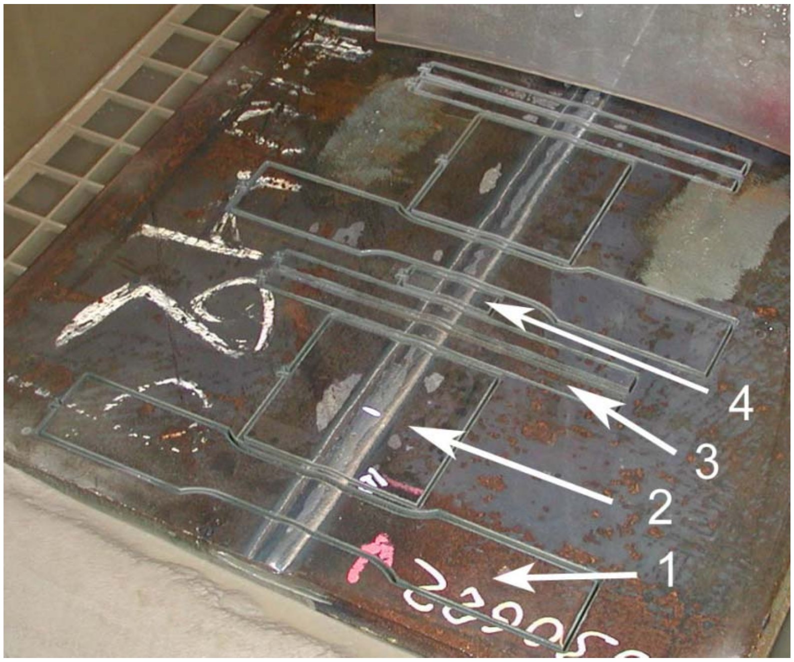

Figure 1. Different types of weld test specimens taken out of one procedure test:

1. Tensile test
2. Impact test (to be split up into smaller test pieces)
3. Bend test
4. Metallography

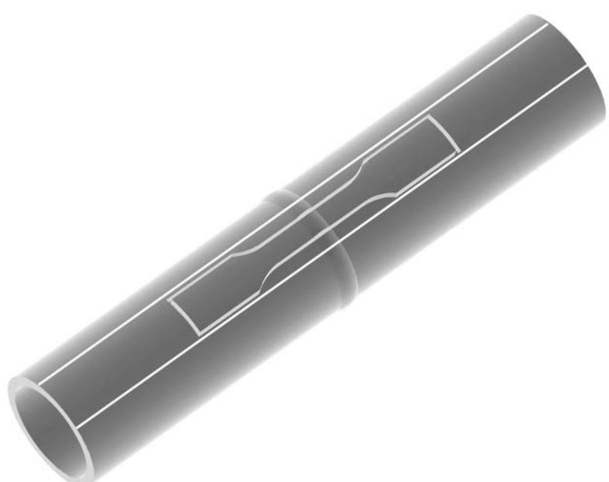

Figure 2. Schematic picture of one weld tensile test specimen taken in a tube. The lines show how the test specimen is to be extracted using sawing.

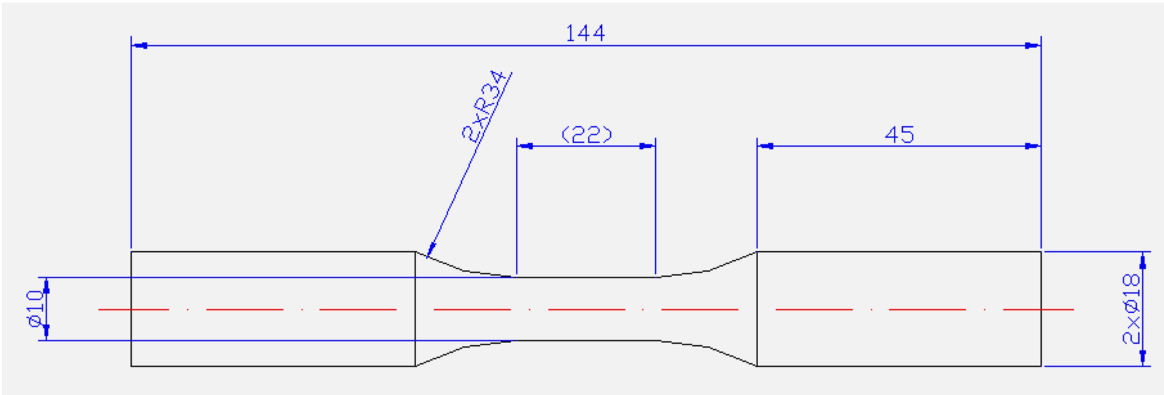

Figure 3. Test specimen geometry for testing of inter-metallic compound.

Figure 4. Work piece (top) and turned final test specimen (bottom).

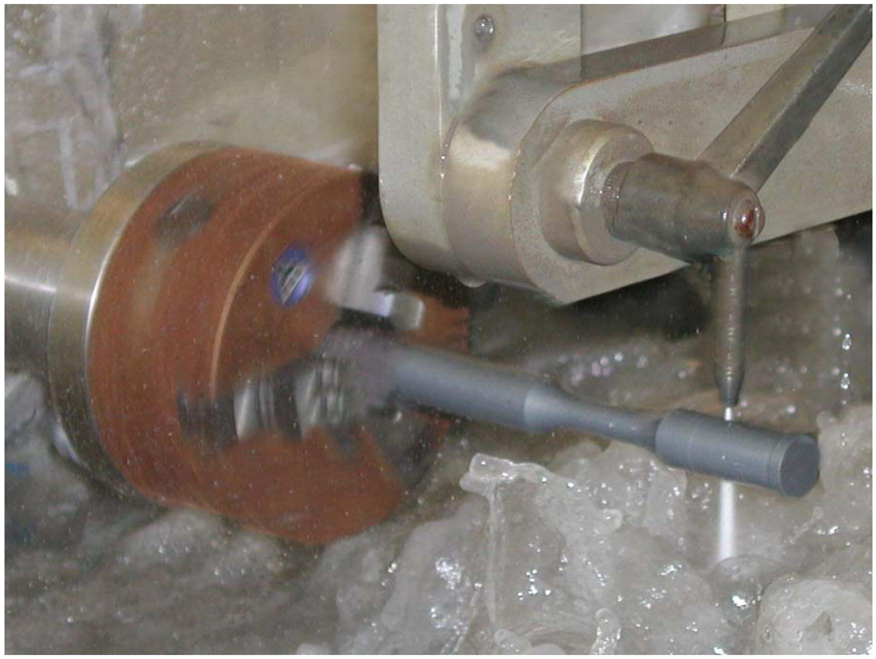

Figure 5. AWJ turning of fatigue test specimen.

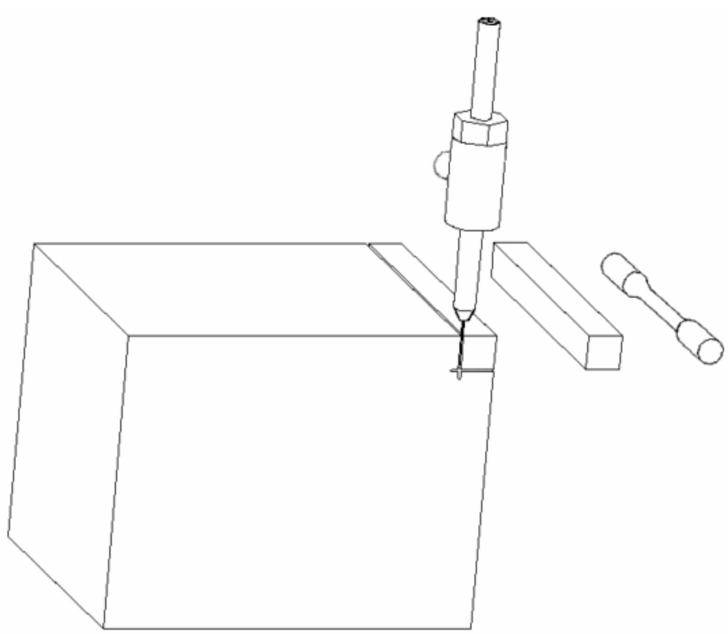

Figure 6. AWJ extraction of workpiece from a larger piece of material.

2003 WJTA American Waterjet Conference
August 17-19, 2003 • Houston, Texas

Paper 3-A

A STUDY OF ABRASIVE WATERJET MACHINING OF KEVLAR COMPOSITE

Rahmah Bte Abdullah*, Ahsan Ali Khan
Mechanical Engineering Department,
International Islamic University Malaysia,
Jalan Gombak , 53100, Kuala Lumpur, Malaysia

M. Ramulu
University of Washington
Seattle, Washington, USA

ABSTRACT

Recently, there has been a development of modern ballistic armor due to the creation of high performance composite materials based on aramid fibers with better weight reduction, higher strength and toughness. However, aramid fibers (Kevlar) are very difficult to machine by conventional machining techniques. In this paper, an experimental study was conducted using abrasive waterjets (AWJ) in cutting Kevlar reinforced phenolic composite. Experimental design was used to measure systematically the influence of cutting parameters on the surface roughness and kerf taper ratio of Kevlar composite specimens. Stylus profilometry was used to measure the surface roughness and a visual inspection including Scanning Electron Microscopy was conducted. ANOVA technique was utilized to evaluate the influence of cutting parameters on the kerf taper and surface roughness changes as a function of cutting depth. Mathematical models were developed to predict the surface roughness and kerf taper in terms of the cutting parameters of a Kevlar composite to cutting depths of 9 mm.

1. INTRODUCTION

Composite materials offer not only high strength-to-weight ratios and stiffness-to-weight ratios but also possess increased toughness and greater reliability along with good corrosive resistance properties [1] . As the use of composite structures becomes ever more demanding and widespread, the use of fibers other than fiberglass and carbon fibers is likely to increase. The creation of aramid fibers called “ Kevlar “is a manmade organic fiber, with a combination of properties allowing for high strength with low weight, high chemical resistance, and high cut resistance. The material is also flame resistant; does not melt, soften, or flow; and the fiber is unaffected by immersion in water [2]. This unique properties has lead to the big breakthrough in the development of modern ballistic armor because Kevlar is known to be five times stronger than steels and ten times than aluminum [3]. This type of composite has its applications in ballistic helmets and lightweight armored vehicle as well as bank counters, safe rooms, and guard stations. Being an armor material, Kevlar protects against ballistic attacks which could be an assault with conventional handguns, shotguns and rifles with variable destructive potentials and concentrations of impacts. In contrast to the metallic materials, the use of a composite material such as Kevlar has its most potential benefit to meet most of the important design criteria such as minimal extra weight and thickness as well as high flexibility of fitting and forming. However, as with other composite materials, Kevlar poses a lot of problems for its manufacturing process especially in machining.

Aramid materials, while excellent in their ballistic protection capabilities, are difficult to process and fabricate. The toughness of aramid fibers causes the composites of these kinds to be extremely difficult to cut and always require special cutting bits, drills, and mills that can both stretch and cut the fibers [4-11]. Even though a majority of composite components can be produced by near-net-shape manufacturing methods, composite parts often require post-mould machining and drilling to meet dimensional tolerance, surface quality and other functional requirements [12-18]. It is also still difficult to mould holes and slots without disturbing the fibers around them [1, 19-21]. It is only through machining that can produce intricate shapes and desired tolerances. However, the material behavior of fiber reinforced composites is inhomogeneous due to the diverse fiber and matrix properties, fiber orientation, and relative volume of matrix and composites which limit the potential use of traditional methods for net shape trimming. Therefore, the machining of fiber-reinforced composite materials (FRCM) differs significantly compared to conventional metallic materials and always poses problems not frequently seen for metals due to the non-homogeneity, anisotropy and their abrasive characteristics. In addition, fiber reinforced composites due to lack of plastic deformation, fine, powdery chips and fiber particles together with a high proportion of dust will be released into the air during the machining of the materials [11, 18]. Thus, industrial safety regulations require that particular attention be paid to the dust generated during the machining process, since some of them is very fine and therefore dangerous to health [11]. Furthermore, some of the chemicals released due to heat and thermal damage during the machining of polymer based composites, can be harmful. Both inorganic fibers and organic compounds released during machining of polymer based composites can cause respiratory and other medical problems. Even though fibers used in composites have diameter ranges from 9-24μm are not respirable, the split fibers during machining could be very hazardous. Furthermore, the quality of cut surface when machining fiber reinforced thermoplastics depends largely on the angle between the fiber orientation and the machining direction [11]. This produces different levels of surface quality in accordance to the orientation of the fibers in relation to the tool feed direction. Due to the high tool wear and high costs of tooling experienced with conventional machining, abrasive water jet cutting technology has been envisaged to offer an attractive alternative as non-contact material removal process in the manufacturing of composite materials [7]. Indeed, waterjet (WJ) and abrasive waterjet (AWJ) are receiving considerable attention and have been introduced at the industrial level because of the beneficial characteristics of material removal. The high velocity jet of water transfers momentum to the abrasive particles, accelerating them to their impingement on the workpiece [19-23]. Specific advantages of these machining methods in relation to their ability to machine difficult-to-cut materials without thermal stresses and their omni directional cutting capability has given the most promising technique to be applied in machining composites [14]. By having its remarkable potential, AWJ system have been suggested for the machining of fiber-reinforced composites (FRP) which have made significant contributions in the aerospace applications where graphite/epoxy composite has been widely used [15-18].

The purpose of this paper is to present the influence of AWJ cutting parameters on the surface roughness and kerf taper of an abrasive water jet machined Kevlar dominated ballistic material namely as Kevlar-reinforced phenolic. Surface roughness and kerf taper were designated as criteria for assessing the quality of the machined surface. Examination of the machined surface was conducted with the aid of an optical microscope, scanning electron microscope (SEM), and surface profilometer. Empirical models are developed for the prediction of surface roughness and kerf taper in terms of the selected cutting parameters.

2. EXPERIMENTAL SETUP AND PROCEDURES

2.1 Material

Two test panels of a composite ballistic type namely as Kevlar – reinforced phenolic with the thicknesses of 9.2 mm thick were used for machining throughout the study. Both of the test panels have the same sizes of 300 mm x 300 mm each. The Kevlar laminates were used and hand laminated in the prepreg form, namely as Kevlar 129, modified phenolic resin, manufacture's style 258 (2x2 basket weave) and having its areal weight of $410 g/m^2$. The plies had a 12 microns of fiber diameters and the laminate consisted of 22 plies with a ply thickness of approximately 418 microns and arranged in (0, 90) configurations. The composite panel is multi-directional since the fabric of the aramid fiber is already a multi-directional product and was layered ply by ply to the desired thickness. Typical Kevlar 129 mechanical properties are: tensile strength of 3.4 GPa, 3.3% elongation with a modulus of 99 GPa

2.2 Experimental Set-up

All experiments were conducted with an Ingersold Rand model water jet with the designed pressure of 50,000 and driven by a single- intensifier, Model 25 Hp water jet pump. The controller used in abrasive waterjet machine is Acramatic 2100 CNC control and supplied by Vickers Electronic System. Gravity feed hopper and a workpiece table are other important features provided with this unit. The primary components of the nozzle assembly for this study consist of a 0.254 mm diameter sapphire jewel that transforms the high pressure water into a collimated jet, an abrasive mixing chamber, an abrasive inlet tube, and a 0.762 mm internal diameter carbide water jet nozzle insert. All experiments were conducted using garnet as the abrasive with the mesh size of # 80. This size was selected due to its most applications in industrial operations of abrasive water jet machining. Abrasive was delivered to the waterjet head from a hopper with a micrometer- adjusted orifice which regulated the rate of abrasive delivery.

2.3 **Experimental Design and Analysis**

A designed of experiment (DOE) is the simultaneous evaluation of two or more factors (parameters) for their ability to affect the resultant average or variability of particular product or process characteristics [24, 25]. Since AWJ machining involves with a lot of parameters a factorial design was chosen to conduct the experiments. The main objectives in the machining process are to determine the set of cutting conditions which can produce a high degree of surface smoothness and kerf quality which are considered as the response variables. It is also important to obtain information about the effect of the main experimental parameters on the response or yield of the experiment. Experimental design was used in outlining the course of this investigation by choosing the three level design 3^k factorial design as the approach for the statistical analysis. The three level are referred to as low, intermediate and high levels. The full factorial 3-level 4-factors with a total of 81 treatment combination of runs with no replication were selected as the design of experiment.

In this particular research, four independent variables associated with the AWJ cutting process were selected and varied including jet pressure, standoff distance, traverse rate and abrasive flow rate. Parametric cutting conditions for the experiments are shown in table 1 which indicates the levels of each variable used. Water pressure and abrasive flow rate were selected according to the common range of applications, shop floor practice and equipment limitation. The levels of parameters were determined primarily based on the literature review of a few studies that were documented and successfully conducted on AWJ machining of Graphite/Epoxy laminates up to 19 mm thickness [16]. The values of the water pressure were determined to be high enough in order to supply sufficient energy in machining thick laminate of the composites and it was important that the traverse speeds to be applied in low values when machining thick laminate specimens.

A slot was machined approximately 10mm into the Kevlar laminate with full penetration as shown in Figure 1. The traverse length of the slots was not extended to obtain separate pieces in order to allow the kerf profile to be examined from an end view and enabling accurate kerf width measurements. The test samples were machined 20 mm x 20 mm to separate the test specimens and to expose the kerf face view of machining features for the total of 81 pieces in accordance to the DOE. The tapers of the machined surfaces were measured by using Motic Digital Microscope together with the application of Motic Images 2000. The microscope was used to measure the kerf geometry which was the top and the bottom kerf width. The values were used for the calculation of kerf taper (top kerf width / bottom kerf width). Surface finish measurements were taken with surface profilometer. The surface roughness measuring system device

(SURFPAK) SV-514 and it is a stylus-typed surface roughness measuring machine. The measurement of surface roughness of each machined specimen was obtained at four measurement depths cut : 1.0mm, 2.0mm, 4.6 and 7.2 mm. Due to the variability of surface finish data, multiple measurements were taken of each surface evaluated so that averages could be calculated. All surface roughness measurements were acquired using 0.8 mm (0.03 in) cutoff length. Machine surfaces were inspected using universal optical microscope . Whereas PHILLIP SL40 scanning electron microscope was used to examine the cutting mechanism for the visualization and scanning electron microscopy study for some of the cutting samples in its corresponding cutting conditions.

These data were subsequently used in assessing the main effects and interactions using analysis of variance (ANOVA). Multiple regression was used to find the coefficients of those main effects and interactions in order to develop the models.

3. MATHEMATICAL MODEL

The functional relationship of dependent variables and independent variables of the AWJ cutting process can be represented by the following second order polynomial

$$y(x) = \beta_0 + \sum_i \beta_i x_i + \sum_i \beta_{ii} x_i^2 + \sum_{j>i} \sum \beta_{ij} x_i x_j \qquad (1)$$

where β coefficients represents: β_0 = constant, β_i = first order or linear effect, β_{ii} = second order or quadratic effect and β_{ij} = interaction effects and x_is represents the AWJ cutting parameters : x_1= Supply pressure (psi), x_2= Abrasive flow rate (g/s), x_3= Standoff distance (mm), x_4= Traverse rate (mm/s) and x_5= The depth at which the surface roughness was measured (mm).

Based on a design of experiments approach, the surface roughness (R_a) and kerf taper ratio (T_R) can be represented in the form similar to the above equation which is also called multiple linear regression models as below :-

1. Surface Roughness :-

$$R_a(x) = \beta_0 + \sum_{i=1}^{5} \beta_i x_i + \sum_{i=1}^{5} \beta_{ii} x_i^2 + \sum_{i=1}^{4} \sum_{j=i+1}^{5} \beta_{ij} x_i x_j \qquad (2)$$

2. Kerf Taper Ratio :-

$$T_R(x) = \beta_0 + \sum_{i=1}^{4} \beta_i x_i + \sum_{i=1}^{4} \beta_{ii} x_i^2 + \sum_{i=1}^{3} \sum_{j=i+1}^{4} \beta_{ij} x_i x_j \qquad (3)$$

Data sets obtained from the full factorial, 3 level 4 factor design of experiment were used to determine the coefficients of equations (2) and (3) by using SPSS software version 11.0 regression analysis. Since there is a strong interplay between design of experiments and regression analysis, the results of the experiments are expressed quantitatively in terms of empirical models for taper ratio (T_R) and surface roughness (R_a) obtained from the multiple linear regressions .

4. RESULTS AND DISCUSSION

Figure 2 shows a typical photomicrograph of the AWJ cut slot view of kerf top width and end view which represents the kerf taper in Kevlar Composite. An optical evaluation of the machined surfaces as expected indicated the presence of three distinct regions along the cutting depth, each exhibiting unique surface features. These three regions are the initial impact zone, smooth cutting zone, and rough cutting zones in the order in which they occur along the penetration depth (not shown here). It has been documented in similar studies that cutting with an AWJ often produces a striated surface [12,13] as was observed on a number of the machined Kevlar composite specimens of this study. It was noted that the waviness on the machined surface increases with depth of cut and the highest degree of waviness appears within the deformation zone, nearest to the jet exit.

Another macro-characteristic feature associated with AWJ cutting in Kevlar composite is the kerf width at the jet entry and at jet exit for varying AWJ cutting conditions as shown in Figure 3. This view of top kerf width profile clearly illustrates the varying initial impact zone size and is evident of curvature (not a square cut) found to depend on the fiber orientation and jet cutting conditions. When cutting in the 90 degree plies, many of the surface fibers along the cut were broken some distance from the line of the cut causing a very rough appearance of the edge. While cutting zero degree plies, the matrix local to the cut failed where as the surface fibers dislodged. Similar observations were made with jagged and un-symmetric kerf width profile at the jet exit. Opposing grooves caused by the deflecting jet appear to increase the kerf width when viewing the kerf taper from the profile view at this magnification. Because of the variation of top and bottom kerf width as marked in the Figure 3 along the cutting slot due to the basket weave pattern of fiber orientation, kerf width measurements were averaged. Variation in the macro-features between the four specimens clearly indicates an influence of cutting parameters on removal characteristics.

Traverse rate or speed and standoff distance are the two major parameters of cutting process for a given supply pressure, the abrasive grit size and its abrasive flow rate. Figures 4 shows the effect of standoff distance on the kerf taper ratio and surface finish respectively for varying pressure of 25-45ksi, and abrasive flow rates of 5-10g/s. Abrasive flow rate had almost no effect on the taper ratio and the surface finish within our experimental conditions. This result makes choosing an abrasive flow rate as a less important problem for a selected garnet abrasive size of #80. However this does not mean any abrasive flow rate may be chosen. Therefore, as shown in Figure 4a the relationship between standoff distance and taper ratio is nearly proportional. Choosing a suitable standoff distance is important because a low standoff distance can cause serious abrasive rebounding effect. Surface roughness is found to be greatly influenced by the jet penetration depth or cutting depth regardless of other AWJ parameters (Figure 4b). The surface roughness is initially high, decreased at intermediate depth and increased as the jet exit approached. This is due to initially rough region that was observed near the jet entrance distinguished by the rounded kerf edge and have relatively rough surface texture. This region of the kerf consists of initial damage zone and found to have an average R_a of 8μm. The entrance region was followed by a region of notably smooth surface texture with limited damage phenomenon, typically referred to as the smooth cutting zone with an average R_a of 6 μm. The third region of surface topography exists from the end of the smooth cutting zone to the jet exit edge and is characterized by a rough cutting surface texture and waviness patterns that outline the path of jet deflection. This zone is commonly referred to as the rough cutting zone or striated surface zone which has an average R_a of 13μm. Qualitatively, AWJ machined surface average surface roughness values obtained in Kevlar/Phenolic composite were found to be greater than Graphite/Epoxy composite [15] and about two times higher than the R_a of conventionally machined surface roughness [4-7]. However, R_a and the size of these three regions on the machined surface are dependent on the level of the AWJ parameters.

After the experiment had been properly designed and done, data were analyzed by using ANOVA analysis method and details can be found in Reference [27]. Based on the analysis, for a selected abrasive size #80, the abrasive flow rate effect on taper ratio and surface roughness was found to be insignificant and it was consistent with others [15]. Therefore, all of the main effects and interactions had an influence on the kerf taper ratio, while in the surface roughness result, significant effect was the jet penetration depth and its interactions with supply pressure, standoff distance, and traverse speed. The response surface methodology is designed to develop a mathematical relationship to link the factors to the experimental response. Since the mathematical relationship for describing the experimental response in terms of the factors being considered was not known, the first step was to find a suitable approximation for this relationship. Using the ANOVA tables, suitable mathematical equations with unknown constants were developed. The next step was to determine the appropriate constant. Through the outputs of the stepwise method regression analyses, the models are represented for Taper ratio and surface roughness as Equation 4 and 5 respectively.

<u>Taper ratio</u>:-

$$LnT_R = 0.274x_3 + 0.552x_4 - 0.112x_4^2 - 0.000005248x_1x_3 + 0.00000834x_1$$

or

$$LnT_R = 0.274(\text{ Standoff distance }) + 0.552(\text{Traverse rate }) - 0.112(\text{Traverse rate})^2 - 5.248 \times 10^{-6}(\text{ Pressure })(\text{ Standoff distance }) - 8.34 \times 10^{-6}(\text{ Pressure})$$

or

$$T_R = e^{0.274x_3 + 0.552x_4 - 0.112x_4^2 - 0.000005248x_1x_3 + 0.00000834x_1} \qquad (4)$$

$R^2 = 0.971$

<u>Surface roughness</u>:

$$\frac{1}{R_a} = 6.136 \times 10^{-6}(\text{ Pressure }) - 4.870 \times 10^{-11}(\text{Pressure})^2 - 1.793 \times 10^{-3}(\text{ Traverse rate })$$

(Depth) – 1.271 x 10^{-3} (Depth)^{2} -2.494 x 10^{-7} (Pressure)(Traverse rate) + 6.784 x 10^{-3} (Depth) - 4.722 x 10^{-7} (Pressure)(Standoff distance) + 1.461 x 10^{-2} (Standoff distance) .
or

$$R_a = [1/(0.000006136 x_1 - 0.00000000004.870 x_1^2 - 0.001793 x_4 x_5 - 0.001271 x_5^2$$

$$- 0.0000002494 x_1 x_4 + 0.006784 x_5 - 0.0000004722 x_1 x_3 + 0.01461 x_3) \qquad (5)$$

$R^2 = 0.976$

Since the values of adjusted R^2 of the final empirical models obtained are 0.976 and 0.97 for the surface roughness and kerf taper respectively , they are considered very high . Thus, three tests, namely were conducted to diagnose the goodness- of- fit data as follows[24, 25, 27] :

i) Multicollinearity.

Multicollinearity is when there is a high correlation between variables in a regression equation. It is a case where two or more independent variables have a linear relationship between or among them. Multicollinearity is identified by the high value of R^2 and low values for t-statistics. Ignoring it can cause standard errors to be higher , thus making t-statistics lower , and possibly insignificant. However, results are still unbiased, forecasts are consistent , and confidence intervals are still valid.

ii) Normality

Normality for both of model results was tested by using the normal probability plot (NPP plot) to see how well the residual error is normally distributed . Under perfect normality, the plot will be a 45-degree line. By referring to Figure 5, both of NPP plots for the obtained models of the surface roughness and kerf taper show that the lines are very close to the 45-degree line.

iii) Heteroscedasity (Untrended error)

Durbin- Watson statistic was used in the regression analysis to test for the presence of first-order autocorrelation (both of positive and negative correlation) in the residuals of a regression equation . Small values of the Durbin-Watson statistic indicate the presence of autocorrelation. By referring to the significance tables at 5%, the statistic has a range from 0 to 4 with a midpoint of 2. In order to accept the Null Hypothesis (Ho:) stated as there is no significant correlation , the value of the Durbin Watson statistic must fall between 1.77 to 2.23 for both of models obtained above. For the kerf taper the value of Durbin Watson is 1.795 and thus, the null hypothesis is accepted. However for the surface roughness model , the Durbin Watson value is 1.76 which is a bit below of 1.78 to accept the null hypothesis.

The kerf taper ratio and surface roughness equations were plotted as surface plots (Figure 6 and Figure 7) to visualize the effects AWJ parameters. Although the pressure and standoff distance nearly have a linear effect but traverse speed has a nonlinear effect on kerf taper as shown in Figure 5. Surface roughness clearly was influenced significantly by pressure, traverse speed and standoff distance as presented in Figure 6. These results were similar to other fiber reinforced composite materials [13, 15-16]. The surface plots are useful in finding optimum combinations between two sets of factors.

Scanning Electron Microscope analysis was performed to observe micro phenomena of the machined surfaces at selected cutting depths of 2, 5, and 7mm. Figure 8 shows SEM micrographs taken within the smooth cutting, and rough cutting domains of Specimen M9 at low (250X) and high (1000X) magnifications at different cutting depths. As can be seen from Figure 8(a-c), the surface of the plies suggests that abrasive induced shearing and abrasive micro-machining, are the dominate modes of material removal. The fibers were spilt fractured and surrounding matrix appear to be machined, contrary to regions of macro-fracture induced by cantilever bending which are the effects of sustained loading forces. The cut surface is random in nature due to the host of abrasive attack angles at the face of the penetrating jet. Features of the post-machined fibers and interstitial matrix indicate that independent shear fracture of the constituents occurs during material removal. Nearly all matrix adjacent to the fibers was washed out after machining at the jet exit. This also caused the fiber pullout and greater disruption in plies.

Micro-cutting mechanisms was evaluated by examining the features of the 90° and 0° plies of Specimen M25 machined using the AWJ cutting conditions of P= 35ksi, SOD= 2mm, Feed rate = 0.5 mm/s, and Abrasive Flow rate = 10g/s at an observation depth of 2mm. Figure 8 and 9 shows the SEM micrographs of the machined surface 90° and 0° plies. Inspection the 90 degree plies on the machined surface suggests the exposed uncut fiber ends with disbanding of fiber/matrix interface and matrix cracking as shown in Figure 8a. Note also the trapped abrasives in between the disrupted fibers as the matrix was washed out during the machining. Fibers were not fractured as in Graphite/Epoxy composite but were failed in compression and shear mode. Micromachining and shearing fracture account for the dominant portions of material removal mechanisms in Kevlar and can be seen in Figure 8(b-c). Contrary to 90° plies, 0° plies have the some dislodged and exposed uncut fibers, but the matrix was remains intact on the machined surface with minor local failure as shown in Figure 9a. AWJ produced nearly a smooth surface and is evident in SEM micrographs of Figure 9(b-c). This phenomenon is most predominant near smooth cutting region as seen in Figure 7(b). However, the severity of matrix washout and fiber deflection and delamination increased at the jet exit.

5. CONCLUSION

The primary objective of this study was to obtain a measure of the influence of the AWJ machine parameters on the machined quality of a Kevlar laminate. Through experimental design, ANOVA, multiple regression analysis of surface roughness and kerf taper measurements, and an optical evaluation of machined specimens, the following conclusions were made:

1. AWJ is a viable cutting tool in machining Kevlar composite materials. Although small amount of ply delamination was observed on the jet entry and exit side, this could be minimized with selection of proper AWJ cutting conditions.

2. AWJ parametric influences on kerf taper and surface roughness were found to vary as a function of the cutting depth. Traverse speed and standoff distance are the most influential parameters affecting surface finish at shallow depths of cut. Traverse speed, and pressure effect on surface finish was found to be significant with increasing depths of cut. AWJ machined surface roughness in Kevlar composite was found to be twice that of the conventional machining produced surface roughness.

3. Mathematical models for surface roughness and kerf taper were developed based on regression techniques. The models successfully predicted the surface roughness and kerf taper of an AWJ machined Kevlar laminate to cutting depths of 9.0mm and can be used for determining cutting parameters for tailored surface quality.

6. REFERENCES

1. Ramulu, M. and Kraja, S.E., Abrasive Waterjet Piercing of Holes in Carbon Fiber Reinforced Plastic Laminate" in *33rd International SAMPE proceedings*, Vol. **33**, 2002, pp.1327-1339.
2. Brent Strong , A. Polymeric Reinforcing Fibers Kevlar , Spectra , and Others . Brigham Young University .http://www.cfa-hq.org/documents/PolymericReinforc…
3. http://blackarmor.com/Car_Material_Specs.htm
4. Bhattacharyya, D., Allen, M.N. and Mander , S.J., "Cryogenic Machining of Kevlar Composites" in *Processing and Manufacturing of Composite Material*, ASME PED-Vol. 49 / MD – Vol.27, T.S. Srivatsan and S. Chandra eds., ASME (1991) , pp. 133-147.
5. Bhattacharyya,D and Hollingan,D.P., "A Study of Hole Drilling in Kevlar Composites", *Composite Science and Technology*, 58, 1998, pp.267-283
6. Won, M.S., and Dharan, C. K. H., "Drilling of Aramid and Carbon Fiber Polymer Composites" *Journal of Manufacturing Science and Engineering*, Vol.124, No.4, 2002, pp. 778-783
7. Konig, W. and Grass, P., and Wilerscheid, H., "Machining of Fiber Reinforced Plastics", *Annals of the CIRP*, Vol. 38, No. 1, 1989, pp. 119-124.
8. Konig, W., Grass, P., Heintze, A., Okcu, F., and Schmitz-Justin, C., "Developments in Drilling and Contouring Composites Containing Kevlar" *Production Engineering*, Vol.63, No. 8, 1984, pp. 56-61
9. Konig, W., Wulf, Ch., Grass, P., and Wilerscheid, H., " Quality Definition and Assessment in Drilling for Fiber Reinforced Thermosets", *Annals of the CIRP*, Vol. 34, No. 2, 1985, pp. 537-547.
10. Doerr, R., Green, E., Lyon, B., and Taha, S., " Development of Effective Machining and Tooling Techniques for Kevlar Composites" Technical Report # AD-A117853, Dupont, 1982.
11. Konig, W. and Rummenholler, S., "Technological and Industrial Safety Aspects In Milling FRPs " in *Machining of Advanced Composites* .ASME MD-Vol.45/PED-Vol.66 , M. Ramulu and R. Komanduri eds ., ASME (1993) pp. 1-14.
12. Hamatani, G. and Ramulu, M., "Machinability of High Temperature Composites by Abrasive Waterjet", ASME *Journal of Engineering Materials and Technology*, Vol. 112, No. 4, 1990, pp. 381-386.
13. Hashish, M., "Machining of Advanced Composites with Abrasive-Waterjets", *Manufacturing Review*, Vol. 2, No. 2, 1989, pp. 142-150.
14. Ramulu, M. and Arola, D., Water Jet and Abrasive Water Jet Cutting of Unidirectional Graphite/Epoxy composite . *Composites* , Vol.24, No. 4 ,1993, pp. 299-308.
15. Ramulu, M.and Arola, D., "The Influence of Abrasive Water Jet Cutting Conditions on the Surface Quality of Graphite/Epoxy Laminates", *International Journal of Machine Tools and Manufacture,* Vol.34, No. 3, 1994 ,pp. 295-313.

16. Arola , D. and Ramulu , M., "A study of Kerf Characteristics in Abrasive Water jet Machining of Graphite/ Epoxy Composite", *Journal of Engineering Materials and Technology*, Vol.118**,** 1996, pp. 256 – 265.
17. Colligan, K., Ramulu, M. and Arola , D., "Investigation of Edge Quality and Ply Delamination in Abrasive Water Jet Machining of Graphite/Epoxy", *Machining of Advanced Composites* . ASME MD Vol .45- PED Vol.66, M. Ramulu and R. Komanduri eds ., ASME (1993) pp. 167-185.
18. Colligan, K. and Ramulu, M., "Edge Trimming Of Graphite/ Epoxy With Diamond Abrasive Cutters", *Machining of Advanced Composites* . ASME MD.Vol.45/PED.Vol 66, M. Ramulu and R. Komanduri eds ., ASME (1993) pp. 97-115.
19. Hashish, M., "Precision Drilling of Composites With Abrasive Water Jets" ,*Machining of Advanced Composites* . ASME MD Vol .45- PED Vol.66, M. Ramulu and R. Komanduri eds ., ASME (1993) pp. 217-225.
20. Hashish, M., Ramulu, M., Kunaporn, S., and Posinasetti, P., "Abrasive Waterjet Machining of Aerospace Materials" , in *33rd International SAMPE Proceedings*, Vol.33, 2001, pp.1340-1354.
21. Shanmugam, D.K., Chen, F.L., Siores, E, and Brandt, M., "Comparative Study of Jetting Machining Technologies over Laser Machining Technology for Cutting Composite Materials". *Composite Structures*. Vol.**57**, 2002, pp.289-296.
22. Lemma, E., Chen, L., Siores, E, and Wong, J., "Study of Cutting Fiber Reinforced Composites by Using Abrasive Waterjet with Cutting Head Oscillation", *Composite Structures*. Vol.**57**, 2002, pp.297-303.
23. Momber, A.W. and Kovacevic, R. 1988 . *Principles of Abrasive Waterjet Machining* . Springer-Verlag London Limited.
24. Montgomery , D.C. 2001. *Design and Analysis of Experiments* . 5th Edition . John Wiley and Sons, Inc.
25. Ross, J. P . 1996. *Taguchi Techniques for Quality Engineering* . 2nd Ed. Mc Graw- Hill , New York.
26. Shobert , B. A. *Seminars* . *Material Selection For Armored Vehicles* . http ://www.iacsp.com/body_seminars.html . Accessed on 4th October 2002.
27. Abdullah, R, B., *An Experimental Study of Abrasive Waterjet Machining of Composite Ballistic Materials* a MSME thesis submitted to International Islamic University of Malaysia, Malaysia, 2003

Table 1: Design of AWJ cutting Experiments
Material: Kevlar – reinforced phenolic
Abrasive Material: Garnet, Mesh#80

Variable (Factors/ Parameters)	Experiment Set For *KEVLAR – REINFORCED PHENOLIC*		
	Level 1 (low)	Level 2 (medium)	Level 3 (high)
Pressure (Psi)	25,000	35,000	45,000
Standoff (mm)	4	3	2
Traverse Speed (mm/s)	0.5	1.5	3.0
Abrasive flow rate(g/s)	5	7.5	10

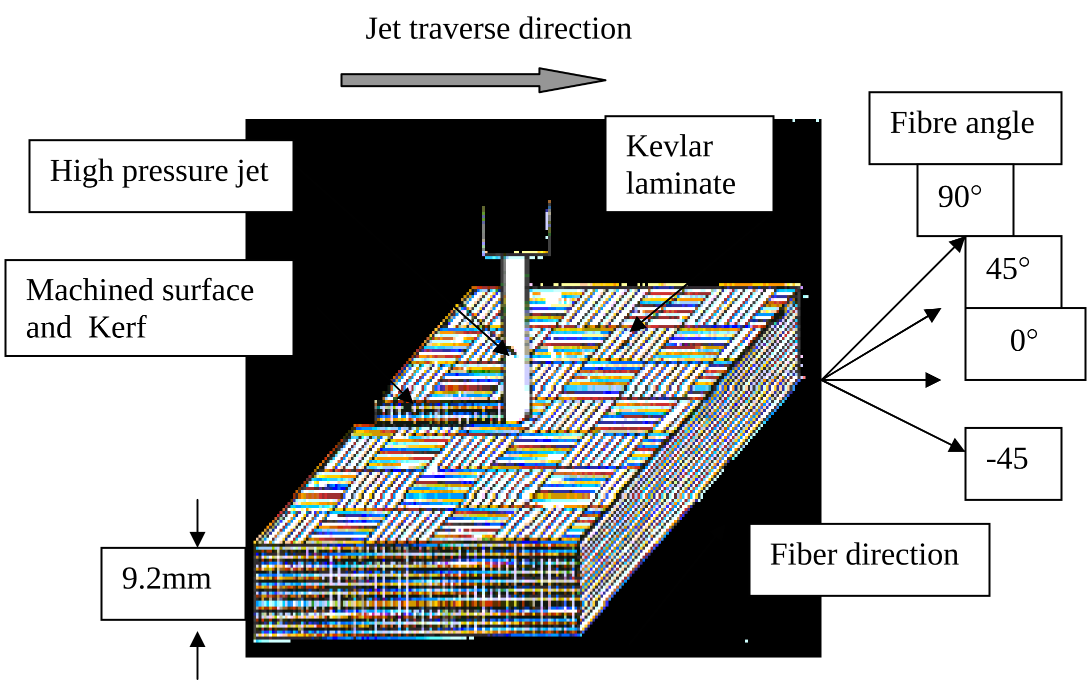

Figure 1:: Illustration of AWJ cutting on Kevlar laminate

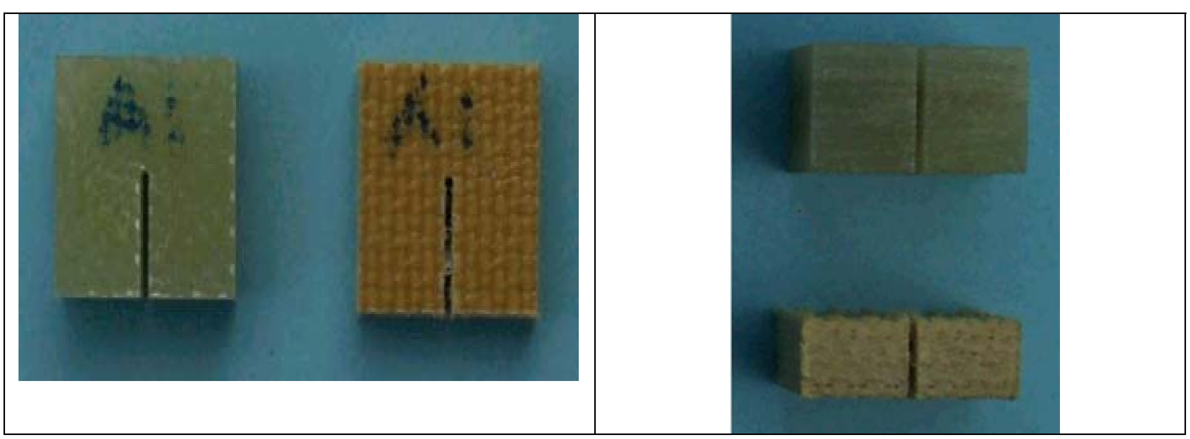

Figure 2: Typical AWJ Cut Slot View of Top and End View in Kevlar Composite

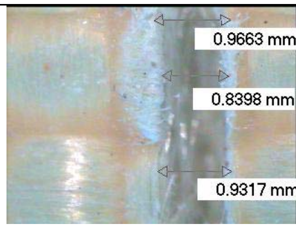 H27 Top a) Cutting condition : P= 45ksi , SOD= 2mm,	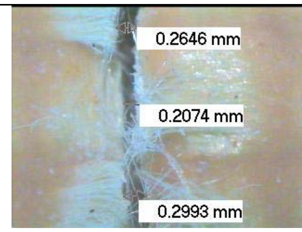 H27 bottom Traverse rate = 3 mm/s , Abrasive Flow rate = 10g/s
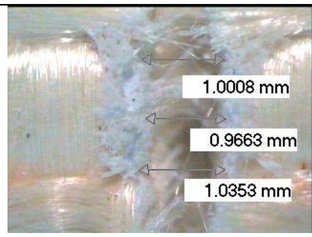 L23 TOP b) Cutting condition : P= 25ksi , SOD= 3mm,	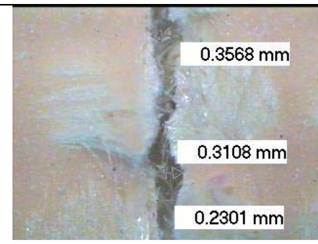 L23 Bottom Traverse rate = 3 mm/s , Abrasive Flow rate = 10g/s
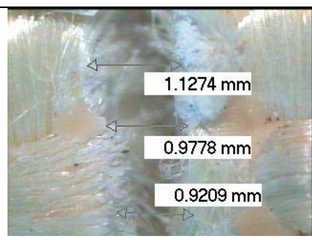 M12 TOP c) Cutting condition : P= 35ksi , SOD= 4mm,	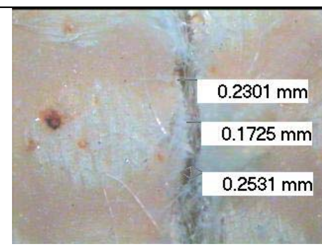 M12 bottom Traverse rate = 1.5 mm/s , Abrasive Flow rate = 7.5g/s
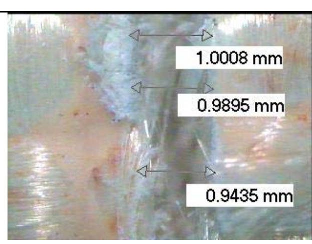 M16 TOP d) Cutting condition : P= 35ksi , SOD= 2mm,	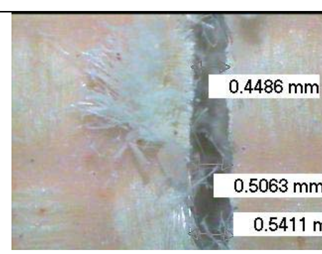 M16 bottom Traverse rate = 0.5 mm/s , Abrasive Flow rate = 7.5g/s

Figure 3: Characteristic Features of Jet Entry and Exit Surface of the Cut Slot

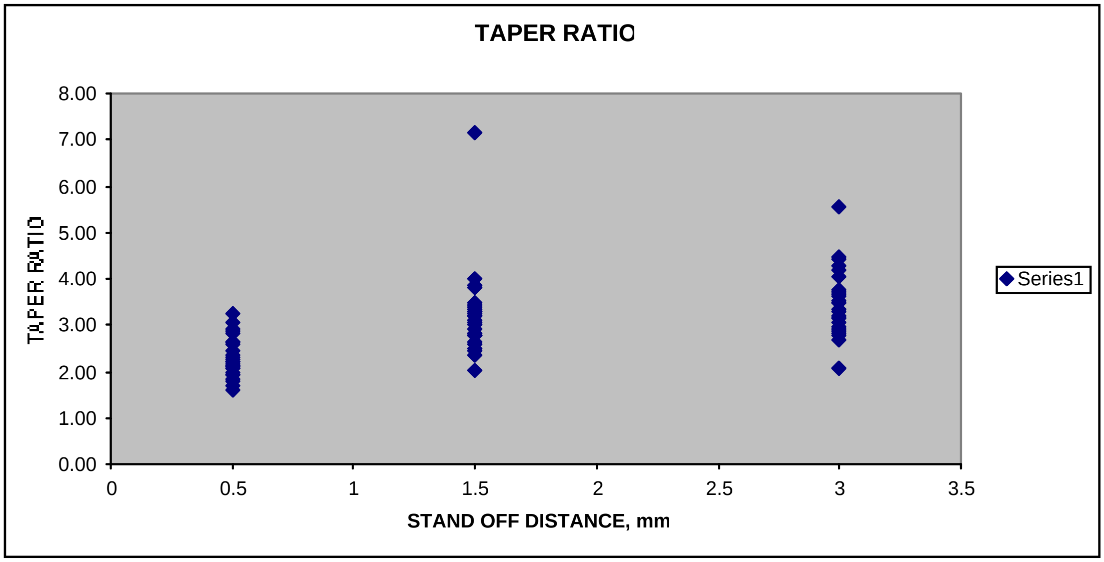

(a)

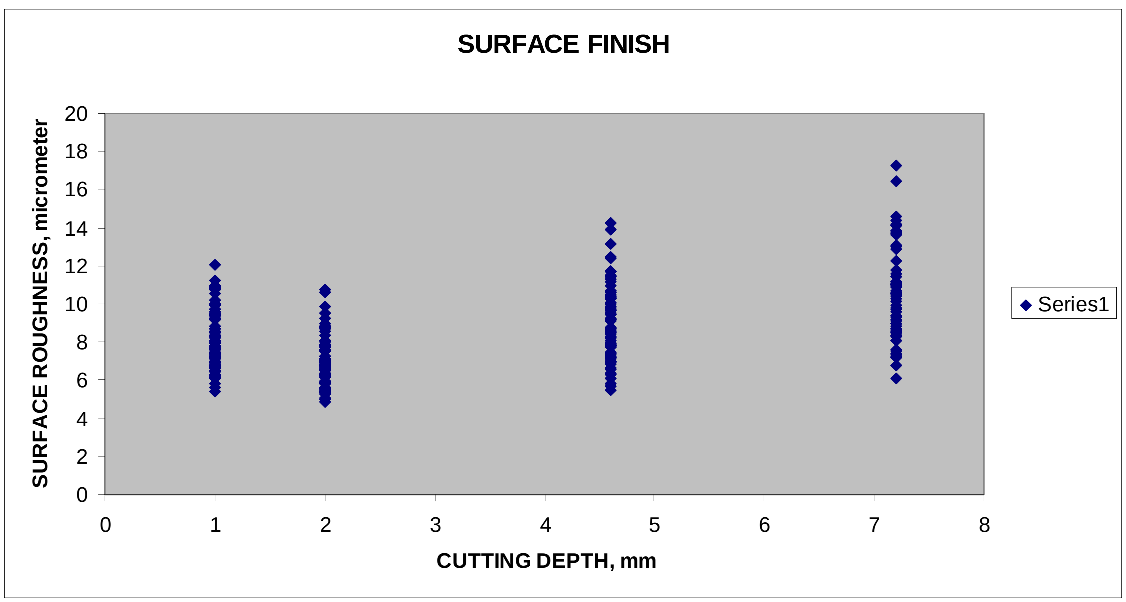

(b)

Figure 4: Effect of Cutting conditions on Taper Ratio and Surface Roughness.

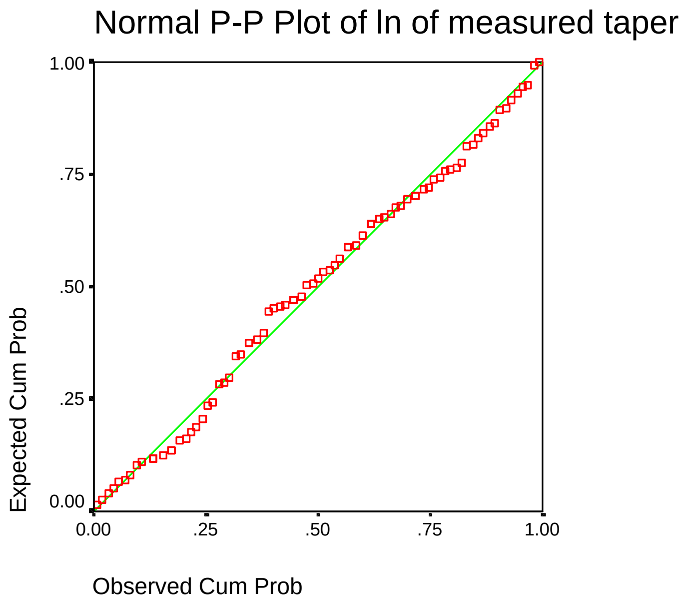

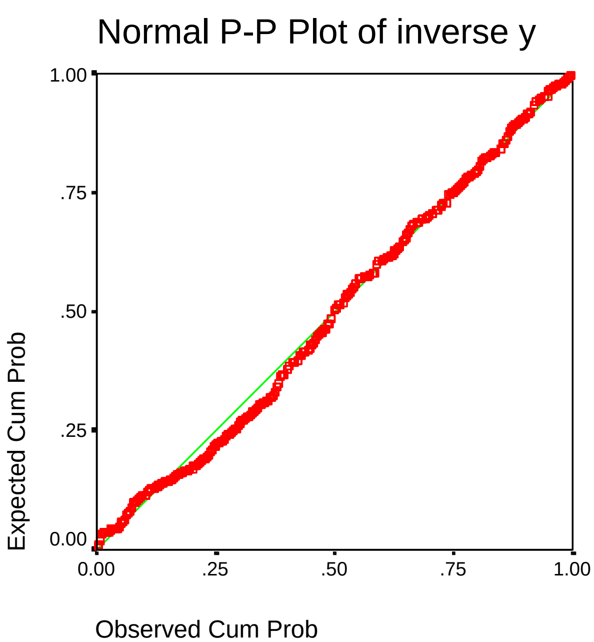

Inverse y = Surface Roughness

Figure 5: Normal P-plot for Taper ratio and Surface Roughness

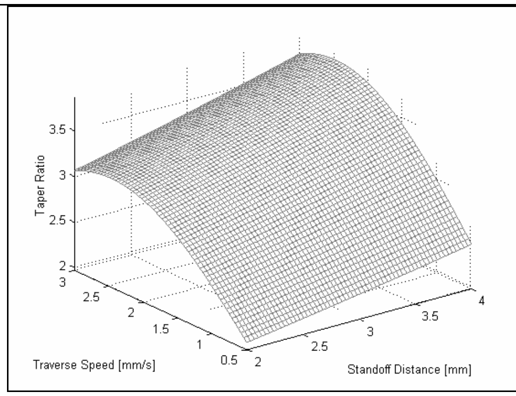

a) Pressure is 35000 psi, Standoff Distance Varies and Traverse Speed Varies

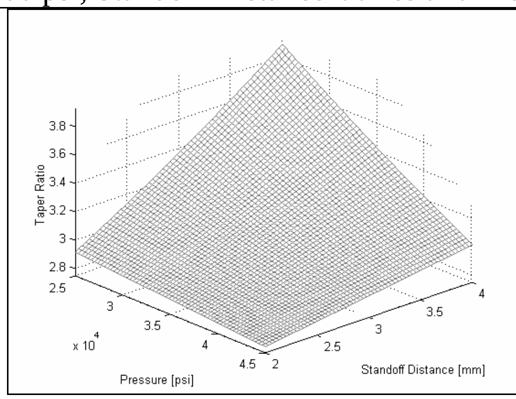

b) Traverse Speed is 1.5 mm/s , Pressure Varies and Standoff Distance Varies

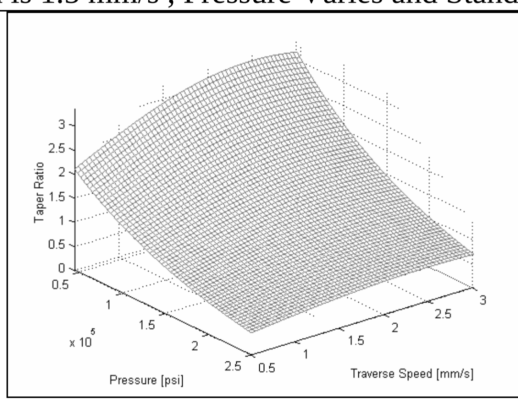

c) Standoff Distance is 3mm, Pressure Varies and Traverse Speed Varies

Figure 5: Surface Plot of Cutting Parameters Effect on Kerf Taper Ratio.

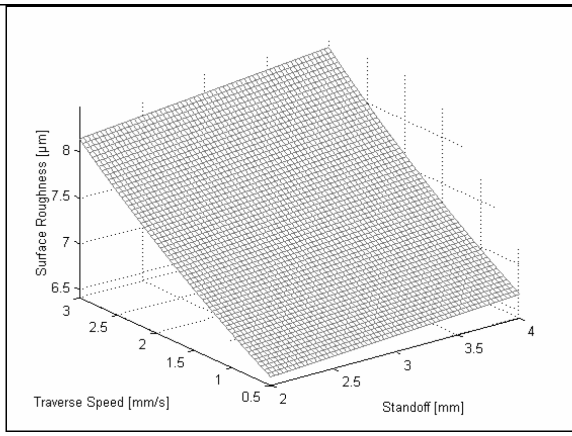

Pressure is 35000 Psi
Penetration Depth is 2 mm

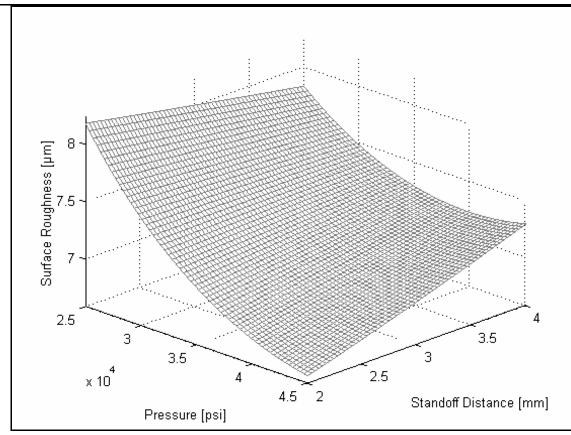

Penetration Depth is 2 mm
Traverse Speed is 1.5 mm/s

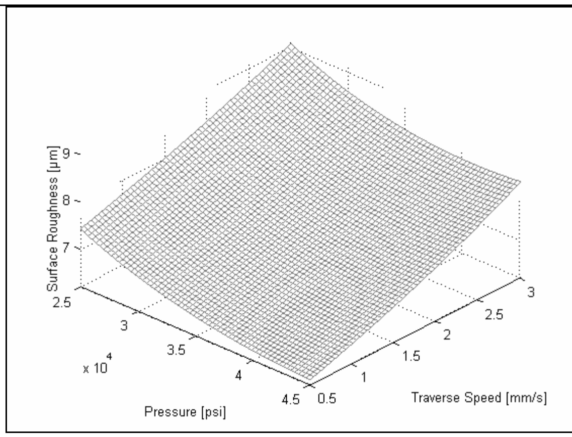

Penetration Depth is 2 mm
Standoff Distance is 3 mm

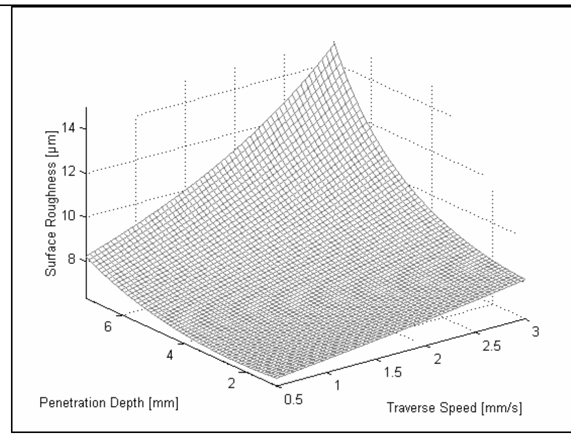

Pressure is 35000 Psi
Standoff Distance is 3 mm

Figure 6: Surface Plot of Cutting Parameters Effect on Surface Roughness.

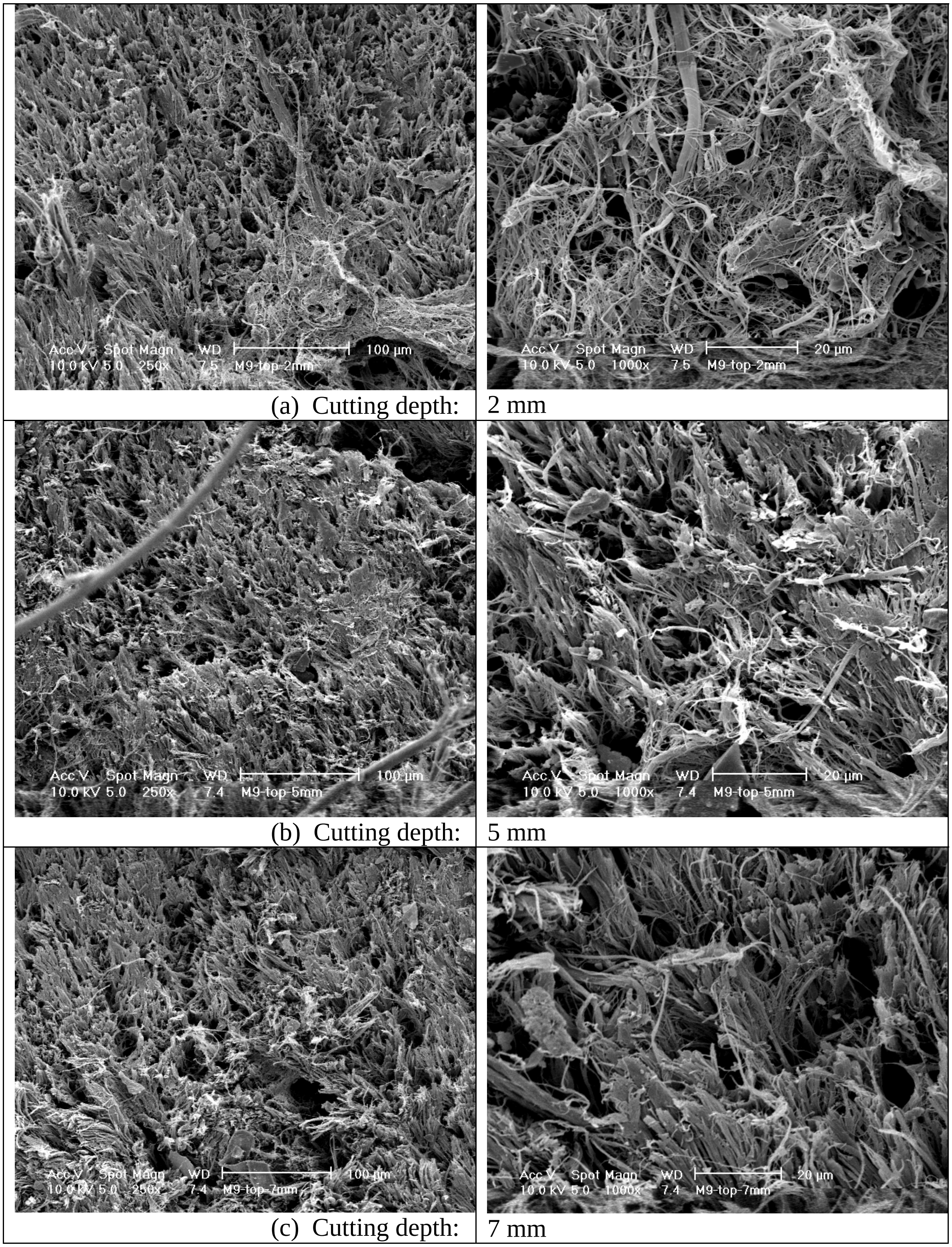

(a) Cutting depth: 2 mm

(b) Cutting depth: 5 mm

(c) Cutting depth: 7 mm

Figure 7: Typical SEM Micrograph of Machined Surface at Different Depth of Cut (Test M9)
Cutting Condition: P= 35ksi, SOD = 2mm, Traverse rate = 3 mm/s, Abrasive Flow rate = 5g/s

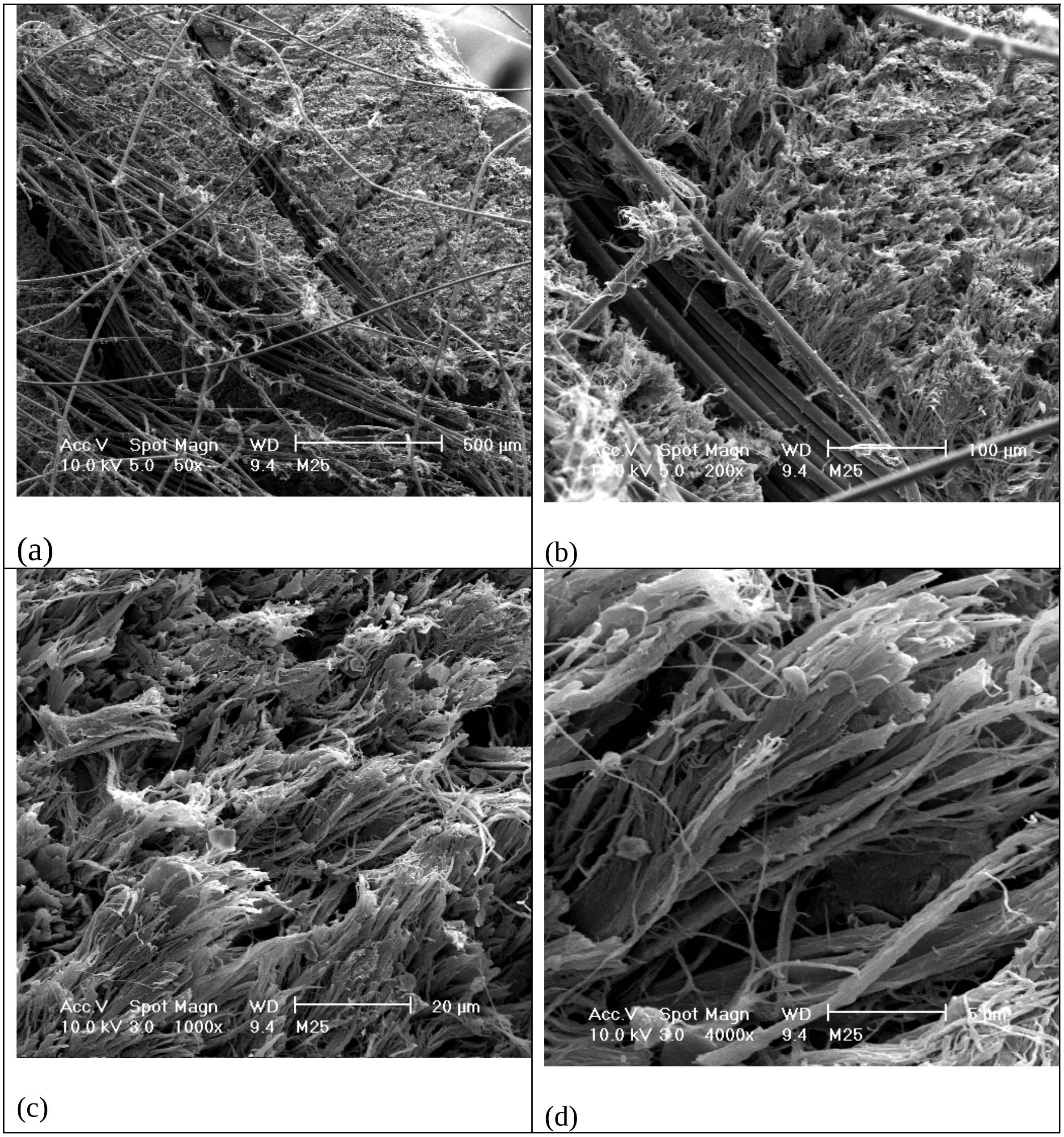

Figure 8: Typical SEM micrographs **(90deg fiber orientation)** taken at the depth of cut = 2 mm from jet entrance (test M25). Cutting condition: P= 35ksi, SOD= 2mm, Traverse rate = 0.5 mm/s, Abrasive Flow rate = 10g/s

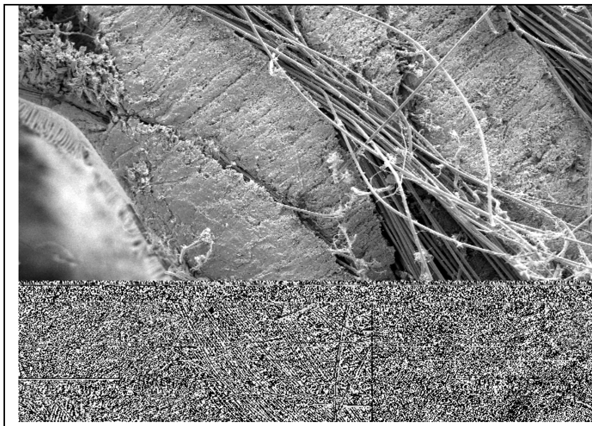

(a)

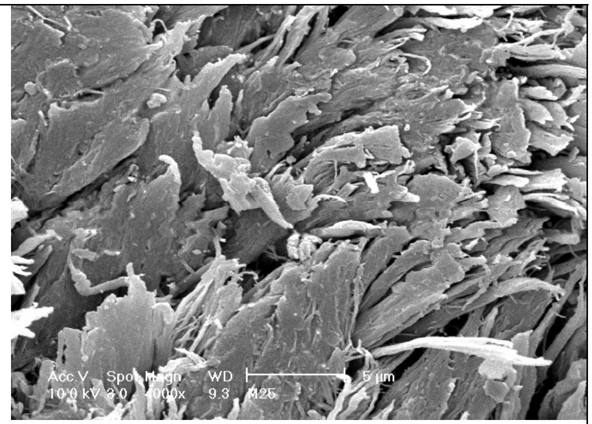

(b)

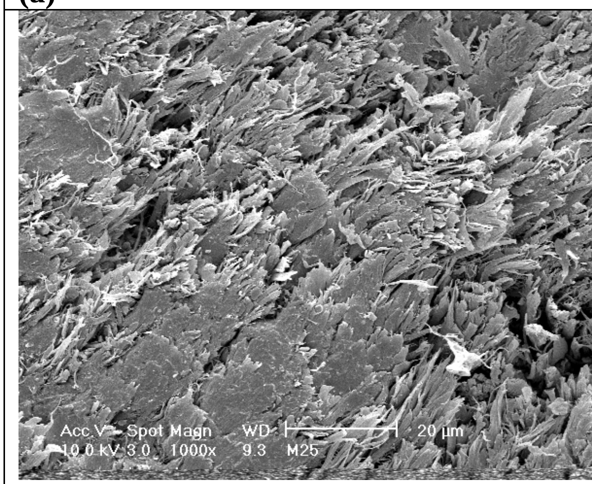

(c)

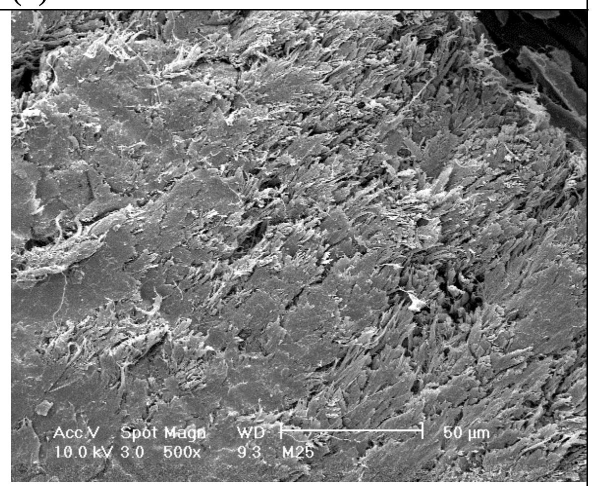

(d)

Figure 9: Typical SEM micrographs taken **(0 deg fiber orientation** at the depth of cut = 2 mm from jet entrance (test M25). Cutting Condition: P= 35ksi, SOD= 2mm, Traverse rate = 0.5 mm/s, Abrasive Flow rate = 10g/s

2003 WJTA American Waterjet Conference
August 17-19, 2003 • Houston, Texas

Paper 5-F

DEVELOPMENTS IN ABRASIVE WATERJETS FOR MICROMACHINING

D. S. Miller
Miller Innovations
Harrold, Bedford UK

ABSTRACT

Abrasive waterjets for micromachining can be generated by the entrainment method and by the abrasive suspension method. The development of an abrasive suspension valve allows suspension systems to micromachine multiple features per second, making them the preferred option for machining miniature components. Improvements to entrainment processes, to allow micromachining with entrainment abrasive waterjets, can be exploited for general machining. The paper postulates that it should be possible to more than double the cutting performance of abrasive entrainment cutting heads for general machining.

It is predicted that the exploitation of micromachining systems, based on the abrasive suspension method, will be carried out by companies not currently involved with abrasive waterjets. Exploitation of micromachining systems, based on entrainment processes, is expected to be by companies who already manufacture abrasive waterjets for the general machining market.

Organised and Sponsored by the WaterJet Technology Association

1. INTRODUCTION

Exploiting the entrainment of abrasive particles carried in air into high velocity waterjets, to form abrasive waterjets (AWJs), has given rise to a new and dynamic sector of the machine tool industry. At present all AWJ system manufacturers provide entrainment cutting heads that are similar in design. These cutting heads cannot generate jets under about 400microns in diameter, whereas jet diameters less than100microns are needed for micromachining. The paper discusses how improving entrainment processes enable entrainment cutting heads to operate with jet diameters less than 100microns.

From consideration of the fundamental fluid dynamic processes that could be used to generate abrasive waterjets, the author has concluded that entraining abrasive in the manner adopted in current cutting heads is one of the least effective of a number of methods of generating abrasive waterjets. This is an important conclusion since it provides the stimulus to look at alternative cutting head designs to see if they can be exploited commercially. The AWJ method of entraining abrasive will always be the simplest method of producing abrasive waterjets. The question is whether improvements in cutting performance and the range of operation of other methods of generating abrasive waterjets outweigh the increased complexities of these methods. The AWJ method cannot operate at the micromachining level so any method that is capable of micromachining is worthy of detailed investigation.

The most efficient method of generating abrasive waterjets is to pass a suspension of abrasive particles in pressurised water through a nozzle, known as the abrasive suspension jet (ASJ) method. The ASJ method has been shown experimentally to be up to 5 times more effective than the AWJ method, (Kovacevic et. al 1997). ASJ technology has what is known as great "charm" (Gosling 1994) because it seems to have a 'rightness' about it as being the best and most eloquent way of generating abrasive waterjets. In reality, developing ASJs to operate commercially at AWJ water pressures of 3000 to 4000bar is not possible because the materials and technologies do not exist to handle abrasive suspensions at ultra high pressures.

Although ASJs cannot be manufactured commercially to outperform AWJs, they are eminently suited for micromachining, provided they operate at less than twenty five percent of AWJs' water pressures. ASJs for micromachining are referred to as MASJs. Profiling and drilling studies reported in Miller (2001b, 2002), and in this paper, were carried out using MASJs operating at 700bar and with nozzle bore diameters between 40 and 60microns.

Recently, the author has begun investigating new designs of cutting heads that have the potential to more than double cutting speeds and cut surface area generation per kilogram of abrasive relative to AWJs. The cutting heads use entrainment processes so they do not suffer from the problems that bedevil ASJs of having abrasive/water mixtures at ultra high pressures. Early cutting results indicate that improving entrainment processes should allow cutting with jet diameters down to 40microns or so, which is ten times smaller than can be achieved with AWJs.

Improved entrainment jets are referred to as IAWJs. As the technologies under development for IAWJs are the subject of a number of patent applications the information given in the paper relating to IAWJs is of a general nature, however, this does not affect the main aims of the paper which are to:

- Present the author’s understanding of the range of jet diameters over which particular methods of generating abrasive waterjets are most suited (Section 2)
- Provide a comparative performance scale of IAWJs against AWJs (Section 3)
- Explain why ASJs are suitable for micromachining but not general machining (Section 4)
- Explain why micromachining requires valves that can open and close on abrasive suspension flows many times per second and why MASJs are likely to be preferred over IAWJs for micromachining systems that produce many small features (Section 5)
- Describe the background to the development of abrasive suspension valves (Section 6)
- Provide an update on micromachining with abrasive waterjets, including trials with abrasive suspension on/off valves (Section 7)
- Describe experimental tests that indicate that abrasive waterjets should be able to operate down to micron jet diameters (Section 8)
- Draw together inter-linking parts of the paper and consider exploitation routes for micromachining abrasive waterjets (Section 9)
- Draw conclusions on the application of MASJ and IAWJ machining systems (Section 10).

The paper caries the optimistic message that abrasive waterjets can repeat the success of laser machining systems through:

- Extending cutting, profiling, drilling and slotting to micron sized features to meet widespread industrial needs
- Experiencing a sustained period of cutting performance increase as improvements are made in the generation of cutting beams/jets
- Providing customised cutting beam/jet solutions to users’ needs rather than just having one method of cutting beam/jet generation.

2. JET DIAMETER RANGES OF ABRASIVE WATERJETS

Figure 1 shows the cutting jet diameters over which the author believes particular methods of generating abrasive waterjets will be used for precision machining. Also shown on Figure 1 is the cutting beam diameter range of lasers. Laser cutting beam diameters are typically several times the operating wavelength whilst abrasive waterjet diameters are several times the mean abrasive diameter. The shortest wavelengths for lasers are around 350nm which can be halved by frequency doubling. The smallest readily available abrasive is aluminium oxide with a mean diameter of 50nm although it is manufactured as small as 11nm.

It can be seen from Figure 1 that the diameter range of AWJs is quite restricted. The diameter ranges for IAWJs, shown on Figure 1 are intended to indicate that, as with AWJs, physical phenomena restrict the range over which a particular mode of entrainment works. As abrasive diameters are reduced additional forces can begin to affect abrasive flow, such as electrostatic forces between particles and between particles and passage walls, causing a particular IAWJ method to begin breaking down. It is likely to be some time before all IAWJ operating modes and their useful operating ranges are established.

The author is not aware of any fluid dynamic phenomena that could prevent MASJs operating down to the micron jet diameters indicated on Figure 1. The critical factors in determining minimum jet diameters are likely to be the ability to manufacture cutting nozzles, to control abrasive quality and system cleanliness. Diamond nozzles with bore diameters down to 10microns can be laser drilled and polished. Developments in the manufacture of components in diamond for micro electronic mechanical systems (MEMS) are likely to produce nozzles with micron and sub micron bore diameters. Good housekeeping and abrasive preparation is sufficient to minimise nozzle blockages down to nozzle diameters of 50microns or so. For nozzle diameters below 50microns the level of cleanliness and abrasive preparation becomes increasingly stringent. Below nozzle diameters of 10microns it will probably be necessary to use cartridge assemblies that include the abrasive suspension storage vessel and cutting head. Cartridges would need to be prepared in clean room environments. The flow through a 10micron diameter nozzle would be about 100ml of abrasive suspension per hour so that reusable cartridges of abrasive mixture could readily be installed onto machining systems.

3. PERFORMANCE SCALE

A scale based on 5 levels of performance is suggested to compare the effectiveness of different methods of generating abrasive waterjets by the entrainment method. Level 1 represents the cut surface area generation per minute of an AWJ of good performance, at the water pressure, water and abrasive flow rate at which the comparison is being made. Levels 2 to 5 correspond to 2 to 5 times the cut surface area generation per minute by an IAWJ for the same cutting head feed conditions as an AWJ.

A scale with 5 levels is adopted because the highest cutting performance that has been achieved so far is with experimental ASJs, at 5 times the performance of AWJs. For reasons described in Section 4, it is not practical to build commercial ASJs to operate at AWJ operating pressures, however, level 5 can be taken as a target to aim for in the development of IAWJs.

4. ASJ OPERATING RANGES

The reliability of high pressure fluid systems decreases exponentially with the number of valves and the difficulty of trouble shooting flow systems increases exponentially with the number of valves. Three or four valves in an abrasive waterjet circuit are sufficient to pose serious reliability and trouble shooting problems. An ASJ for general machining needs two pressure vessels to be able to supply a continuous flow of abrasive suspension to a cutting nozzle. Each vessel requires an inlet and outlet valve, a de-pressurisation and a re-pressurisation valve and there are usually one or two other valves in an ASJ circuit. With up to 10 valves and with severe safety and control problems caused by over ten percent water compressibility, there is no conceivable circumstance under which ASJs could operate reliably at the 3000 to 4000 bar water pressures used for AWJs.

Twin vessel ASJs operating at pressures up to 700 bar are used for on-site work where reliability levels that would be unacceptable in production environments can be tolerated. Utilisation of on-site systems can be as low as a few hundred hours per year but when they are used the added value on a project can be of the order of the cost of the abrasive waterjet equipment.

The abrasive required to run a MASJ for an hour can be contained in a single pressure vessel. For instance, a half litre vessel containing an abrasive bed can feed abrasive to a 50micron diameter nozzle for an hour. Vessels of this size can be recharged by hand with abrasive filled cartridges. Only two valves are required in MASJ flow circuits and the valves can be located in the clean water side of the circuit. By operating MASJ systems with water pressures of 700 bar or so, systems can be engineered to be reliable and easy to operate and trouble shoot. For reasons discussed in Section 5, it has been found necessary to develop quick acting on/off valves for installation just up-stream of cutting nozzles to allow multiple features to be cut per second. Such valves can be made reliable at the sizes required for micromachining.

The jet energy density per square millimetre of MASJs operating at 700bar is equivalent to that of an AWJ operating at 3000bar. However, MASJs operate with abrasive particle diameters that are only a tenth or so of AWJ particle diameters. Cutting performance deteriorates with reduction in particle diameters. Based on jet energy densities, MASJs operating at 700bar have performance levels of 0.5 or so of AWJs operating at 3000bar. Although cutting performance may seem rather low, MASJs can carry out many machining operations that are very difficult or impractical to carry out using any other machining method. It should also be noted that a characteristic of micromachining lasers is that they use pulsed beams and have low rates of cut surface area generation per minute.

5. CHARACTERISTICS OF MICROMACHINING ABRASIVE WATERJETS

5.1 Frequency of Jet On/Off Cycles

Micromachining abrasive waterjets can operate at similar cutting speeds to AWJs but they machine components that are typically a tenth the size of those machined by AWJs. This means micromachining abrasive waterjets need to be started and stopped ten times more often than AWJs. The extreme case is drilling holes in metal foils when theoretically a micromachining jet could drill tens or even hundreds of holes per second.

If the water flow has to be stopped when moving a cutting head to a new position, and there is no valve before a cutting nozzle, a MASJ system has to be de-pressurised and after moving the cutting head to the new position the system has to be re-pressurised. When reproducing small features that take fractions of a second to cut, up to 99 percent of the machining time and the pumping energy could be wasted in de-pressurising and re-pressurising MASJ systems. Valves that can start and stop abrasive suspensions are, therefore, essential to minimise cutting cycle times and energy waste. The valves should:

- Be able to open and close several times per second, with valves for system feeding nozzles under 50microns being capable of future developments to cycle ten or more times per second
- Open and close reliably on abrasive suspensions for tens of millions of cycles. Ten million cycles represents machining 1000 components with 10,000 holes, a not unrealistic requirement for components requiring many features such as screens.

Valves being developed to meet these requirements are described in Section 6.

5.2 IAWJs and MASJs Operating Ranges

IAWJ cutting heads work on the entrainment principle and have separate water and abrasive feeds. To stop and restart cutting in a new position involves stopping the abrasive flow and after a delay turning off the water, moving the cutting head, turning on the water and after a delay starting abrasive flow. Although steps can be taken to minimise time delays when cutting with IAWJs, much shorter time cycles could be achieved by MASJs fitted with abrasive suspension valves. As jet diameters are reduced below 100microns it becomes increasingly attractive, when producing many small features, to use MASJ systems rather than IAWJ systems.

6. ON/OFF VALVES FOR ABRASIVE SUSPENSIONS

Abrasive suspension valves are required to open and close against the system pressure. Valve seats have, therefore, to survive highly erosive conditions that are equivalent to those in abrasive waterjet mixing tubes and nozzles. Only valve seats made of diamond can withstand such erosive conditions.

A serious problem with conventional valves for high pressure applications is the need for an actuating mechanism that penetrates the pressure containment. Actuating mechanisms have to be robust to accommodate fluid pressure loads and they require high performance seals. Loads on actuating mechanisms increase and high rates of seal wear occur when abrasive particles are present in the fluid flowing through a valve. A valve design has been developed with an actuating mechanism that does not penetrate the pressure containment or need high pressure seals.

There are two basic types of valves. In one type a sealing element moves along the axis of a seat and is forced onto the seat to achieve a seal, and in the other a sealing element moves at right angles to a seat to align or mis-align flow passages. Valves that involve elements that move along the axis of a seat are not suitable for abrasive flows. If abrasive particles are present when seats are forced together point contacts occur that create local high contact forces and spoiling of brittle seat materials, such as diamond. Areas of spoiling grow with repeated valve closures until sealing capability is lost.

Valves for highly erosive conditions need mechanisms involving a valve element moving at right angles to a seat in such a way that abrasive particles cannot get between contacting surfaces. The valves developed for starting and stopping abrasive suspensions have two lapped diamond seats, one of which slides relative to the other to cover or uncover a flow passage. A pneumatically operated version of the valve is illustrated on Figure 2. When a flow circuit is pressurised fluid forces act through a tube feeding abrasive suspension to the moving seat to force the seats together. In effect the tube acts as a strut under buckling loads to transmit fluid pressure loads on the end of the tube to the valve seat. Because of the low coefficient of friction of diamond on diamond, actuating forces for the valve are modest. Further information on various versions of the valve is given in (Miller 2001a).

7. PROFILING AND DRILLING TRIALS

The trials described were carried out with MASJs and are a continuation of work reported in Miller (2001b and 2002). Diamond nozzles, with diameters between 40 to 60microns, were used with water pressures of 700bar. The abrasive was garnet powder with a mean particle diameter of 8microns.

An illustrative circuit for a MASJ is shown in Figure 3 and a photograph of a machining system in Figure 4. Note that the abrasive storage vessel is located directly above the cutting nozzle to limit the extent of the flow circuit subject to abrasive flows. Systems can operate with abrasive suspensions or with abrasive beds in the storage vessel; in the latter case the abrasive mixture is diluted before it reaches the nozzle.

Figure 5 is a photograph of test pieces cut from a variety of materials including metals, polymers, glass and composites. From the range of materials that have been profiled it can be concluded that MASJs cut the same materials as AWJs, albeit at a smaller scale. The test pieces range in thickness from 50microns to 4mm. Cutting speeds varied from up to 400mm/min for 50micron thick materials to 15mm/min for 3mm thick titanium.

Figure 6 shows part of a butterfly motif that illustrates the fine nature of features that can be reproduced. Web widths can be less the material thickness. Maximum metal thickness profiled with a 50micron diameter jet is 9mm but only at 1 to 2mm per minute. The cut depth to width ratio possible with MASJs is much greater than can be achieved with micromachining lasers.

Figure 7 shows a 33 x 33 array of holes, with mean diameters of 85microns, drilled on a 250micron pitch, in 50micron thick stainless steel using a 58micron diameter nozzle. Figure 8 is a larger scale view of part of Figure 7. The drilling rate was 2.5 holes per second, which was limited by the valve actuator response rather than the abrasive jet drilling capability. For a range of materials and material thickness hole diameters were about 1.5 times the jet diameter. Hole cross sectional areas are about twice the jet area as a consequence of jets turning back on themselves to escape from holes as they were drilled.

The effect of cutting with jet dwell at the start and end of slots can be seen from the poor quality of the slots in 150micron stainless steel shown in Figure 9. By optimising the movement of cutting heads, with the opening and closing of abrasive suspension valves, it is practical to virtually eliminate widening of slots, as shown by Figures 10.

8. TRIALS WITH NANO METRE DIAMETER ABRASIVE

Nano metre diameter abrasive is extensively used in the electronics, optics and other industries for material removal and polishing, and could be expected to cut materials if suspended in high velocity fluid jets. Trials were carried out to get an indication of whether nano metre diameter abrasive could be used for abrasive waterjets.

The smallest diameter nozzles available for the trial had 40micron diameter bores. There is a nozzle bore to particle diameter ratio above which cutting performance deteriorates with decreasing particle size. When the nozzle bore to particle diameter ratio is too high it is probable that particles entering the cutting zone interfere with each other and high drag forces cause particles to begin to follow water flow streamlines before impacting on the material being cut. Deterioration in cutting performance is observed with nozzle bore to abrasive diameter ratios above 10 to 1. Abrasive mean diameters of 3micron, 300nm and 50nm were used giving nozzle bore to abrasive diameter ratios of 13, 130 and 800.

The abrasive was aluminium oxide, with the 300nm and 50nm abrasive classed as de-agglomerated. The author could only sieve the abrasive through a 20micron screen, so it is highly likely that the abrasive contained a significant percentage of agglomerated particles.

Profiling with 3micron mean diameter aluminium oxide gave similar result to profiling with 8nicron mean diameter garnet. Low traverse rates were needed when profiling with 300nm mean diameter aluminium oxide, compared to 8micron garnet, but as Figure 11 shows cut edge definition was very good. Cutting rates with 50micron abrasive were extremely low and the cutting mode very different from any previously observed mode. When cutting 50micron thick stainless steel it was observed that on the jet entry side the surface was worn and highly polished over a width equivalent to the jet diameter. Once the jet broke through, at a particular location, it appeared that cutting virtually stopped to leave polished shelves on either side of the breakthrough. The breakthrough wandered across the jet impact area, leaving a very jagged outline to profiles. The cutting behaviour was consistent with the abrasive diameter being much too small for the jet diameter.

The trials indicated that, as expected, sub-micron abrasive particles cut materials such as stainless steel. There is a need for trials with smaller diameter nozzles and with better control over abrasive agglomeration and size distribution to determine the likely minimum diameter at which abrasive waterjets could operate

11. DISCUSSION

The trigger for the author to look at the possibility that entrainment cutting heads could be used for micromachining was a number of presentations and discussions at the International Conference on Water Jetting in October 2002. Inputs included:

- Information on the background to the development of AWJs in a Keynote Address (Hashish)
- Attention being drawn to only about two percent or so of the energy input to waterjets being transferred to abrasive particles in AWJ cutting heads (Hoogstrate et.al.)
- A presentation on the development of 4000 to 7000bar intensifiers to power AWJs and the deterioration in reliability of increasing pressures (Koerner et.al.)
- Experimental work that demonstrated that the performance of different manufacturers AWJ cutting heads is roughly the same (Srinon et.al.)
- No papers on improving the effectiveness of AWJ cutting heads.

A review of recent literature failed to find published work aimed at substantially improving the effectiveness of cutting heads. There was also a question of why AWJs have not being scaled down to operate at the micromachining level, it being normal in hydrodynamic research to build scale models of systems and components. The perceived wisdom is that scale models of AWJ cutting heads will not work, which is tantamount to saying that AWJ cutting heads were developed at the smallest size possible for the physical phenomena involved. From a knowledge of fluid dynamics, a more likely explanation is scaling down cutting heads in the past required components to be manufactured to dimensions, tolerances and finishes that could not be achieved with the available technologies. In addition it is likely there is insufficient understanding of the complex flow phenomena in cutting heads and their abrasive feed systems to be able to vary parameters so as to compensate for scale effects.

Having concluded that scaling down entrainment processes was a possibility, the question the author needed to answer was: would micromachining abrasive waterjets that worked on the entrainment method be a better commercial option than the MASJs the author had spent the previous five years developing? The answer was, if the author had not already developed the abrasive suspension valve for MASJs, the work on MASJs would most likely have been abandoned in favour of entrainment jets for micromachining. As it is, the ability to rapidly start and stop MASJs with a valve makes them the preferred option for micromachining components that have many small features.

11.1 Technology

Improving the performance of abrasive waterjets means increasing the kinetic energy of the abrasive particles before they leave cutting heads and/or increasing the energy density of particles impacting on work pieces. Achieving higher particle energies by increasing water pressures much above 4000bar is not an attractive option because it carries technical risks, involves substantial costs and has challenging safety implications. The transfer of energy from water to abrasive particles is reasonably efficient in the best AWJ cutting heads. This only leaves increasing the energy density of cutting beams/jets as the route to achieving commercially attractive improvements in performance. In physical terms, entrainment cutting heads need to operate with lower ratios of mixing tube diameters to waterjet diameters than is possible with current AWJs cutting heads.

Achieving lower ratios of mixing tube diameters to waterjet diameters improves cutting performance but it results in abrasive particle diameters being reduced in line with reductions in mixing tube diameters. The maximum reduction in particle size, relative to AWJs, is for ASJs. The reduction in particle diameters may account in part for why the performance of AWJs has been observed to be only five times better than AWJs, whereas, based on higher energy densities and narrower cutting widths, a tenfold increase might be expected.

In engineering it is unusual to find quantum jumps in performance, rather there are graduations, so it is reasonable to assume that IAWJs can be developed that operate with jet energy densities that span the performance scale range from 1 for AWJs up towards 5 for ASJs. The performance scale proposed in Section 3 is simplistic but if it stimulates the search for more effective ways of generating abrasive waterjets it will have served its purpose. In the longer term, performance scales need to be related to particle energies, particle energy densities and particle diameters.

11.2 Markets

After twenty years of commercial exploitation the lead companies in the abrasive waterjet industry are producing sophisticated CNC machining products that compare favourably with any sector of the machine tool market. Although there is considerable growth potential for abrasive waterjets systems at the lower cost end of the market, sophisticated abrasive waterjet systems are in direct competition with other machining methods. Competing technologies, such as lasers, are undergoing rapid improvements in performance and capabilities which abrasive waterjets need to match if they are to maintain and grow market share. The development of IAWJs will make an important contribution to the growth of the market for abrasive waterjets for general machining.

Abrasive waterjets have the potential to operate over the same range of cutting beam diameters as lasers. As yet abrasive waterjets are not used commercially for micromachining but the market for micromachining abrasive waterjets could develop rapidly, as happened with micromachining lasers in the early1990s. Starting from a small market presence in 1990 the worldwide revenues for micromachining laser systems are predicted by 2010 to equal the revenues from the sale of laser systems for general machining (Market Report 2003).

The development and exploitation of micromachining lasers has mainly been by companies who were not involved in manufacturing laser systems for the general machining market. Applications for micromachining laser systems are in areas such as electronics, medical and similar industries and are very different from the sheet metal and engineering applications for general laser machining systems. As micromachining abrasive waterjets applications will mainly be in the areas addressed by micromachining lasers, the exploitation of MASJs can be expected to follow a similar route to micromachining lasers.

Because of limitations in achieving sub second jet off/on cycle times, IAWJs are not likely to be developed for pure micromaching applications. Instead micromachining with IAWJs will be a facility that is available on small precision abrasive waterjet machining systems that can operate over the 400micron to sub 100micron jet diameter range.

Increasing the effectiveness of abrasive waterjets will allow greater diversity in the market. For instance allowing lower pressure, more reliable and lower cost pumping systems to be used for applications where the unique machining capabilities of abrasive waterjets are important rather than cutting speed.

12. CONCLUSIONS

Dedicated micromachining abrasive waterjets, MASJs, will use the abrasive suspension method. MASJs are likely to be exploited through companies new to abrasive waterjet manufacture and/or small existing abrasive waterjet manufacturers who concentrate on micromachining systems.

Improved entrainment abrasive waterjets, IAWJs, will be able to operate down to micromachining jet diameters. Exploitation of IAWJs for micromachining will probably initially be by one or more existing abrasive waterjet manufacturers integrating them on to small precision cutting systems.

For the waterjet industry in general the advent of higher performance cutting heads will have major effects on the products that can be provided to meet customer needs. These will range from systems that have higher cutting speeds and lower operating costs compared to current systems to systems running with cheaper, lower pressure pumps, where reliability and ease of use are more important than cutting speed.

13. REFERENCES

Gosling, W. *Helmsmen and Heroes*. Weidenfeld and Nicolson, London, 1994.

Hashish, M. "Abrasive-Waterjet (AWJ) Studies" *Proceedings of the 16th International Conference on Water Jetting*. BHR Group Ltd., Cranfield, 2002.

Hoogstrate, A.M., Karpuschewski, H. B. "Modelling of the Abrasive Waterjet Cutting Process in a Modular Way." *Proceedings of the 16th International Conference on Water Jetting*. BHR Group Ltd., Cranfield, 2002.

Koerner, P., Hiller, W., Werth, H. "Design of Reliable Pressure Intensifiers for Water-jet Cutting at 4 to 7 kbar." *Proceedings of the 16th International Conference on Water Jetting*. BHR Group Ltd., Cranfield, 2002

Kovacevic, R., et al "State of the Art Research and Development in Abrasive Waterjet Machining." Journal of Manufacturing Science and Engineering, Transaction. of the ASME, November 1997.

Market Report, "Laser Material Processing – 2003 Edition." Optech Consulting AG, 2003

Miller, D. S. "Abrasive Fluid Jet Machining Apparatus." International Patent Application No. PTC/GB02/01835, 2001a.

Miller, D. S. "Micro Abrasive Waterjet Cutting." *Proceedings of the 2001 WJTA American Waterjet Conference*, Minneapolis, 2001b.

Miller, D. S. "Micromachining with Abrasive Waterjets." *Proceedings of the 16th International Conference on Water Jetting*. BHR GroupLtd., Cranfield, 2002.

Srinon, R., Summers, D. A., Fossey, R.D., Tyler, L.J., Johnson, M. "Relative Performance of Commercially Available Abrasive Waterjet Nozzles." *Proceedings of the 16th International Conference on Water Jetting*. BHR GroupLtd.,Cranfield, 2002.

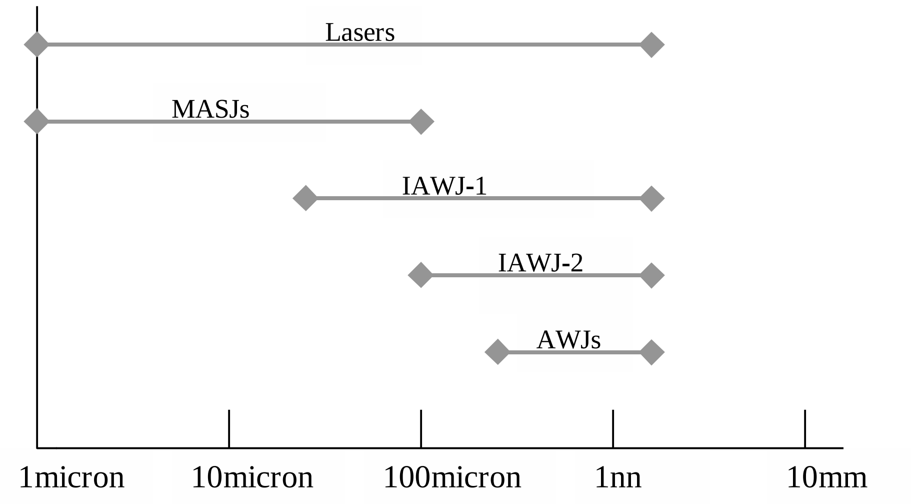

Figure 1. Jet Diameter Range of Abrasive Waterjets

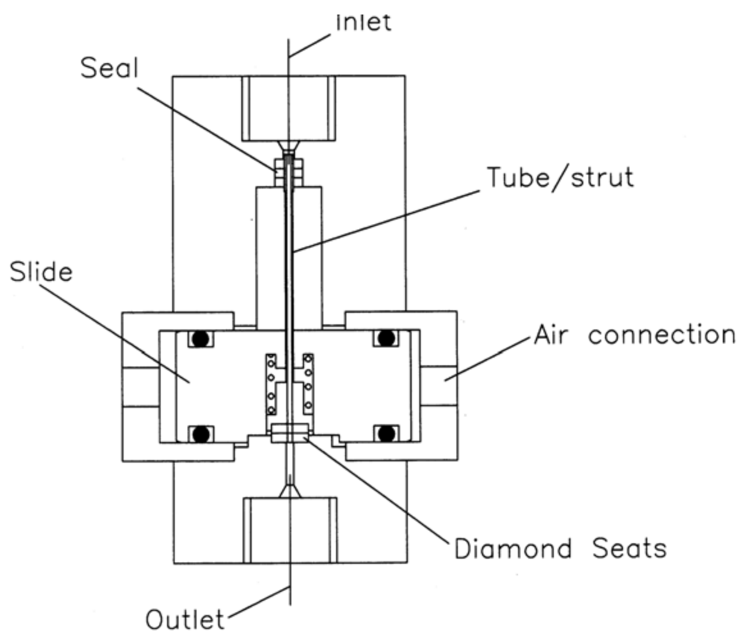

Figure 2. Abrasive Suspension Valve

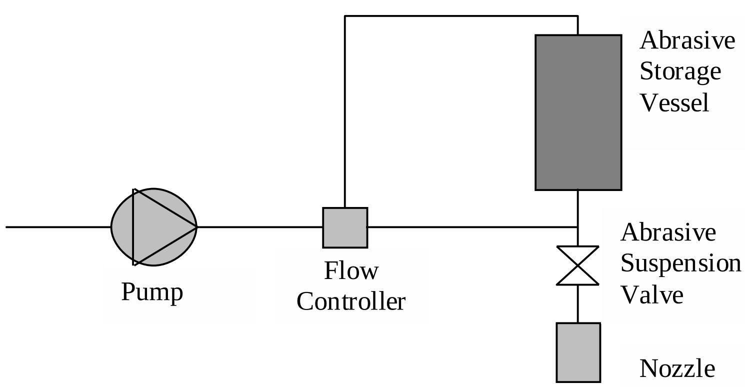

Figure 3. MASJ Flow Circuit

Figure 4. MASJ Development System

Figure 5 Examples of Materials Profiled with MASJs

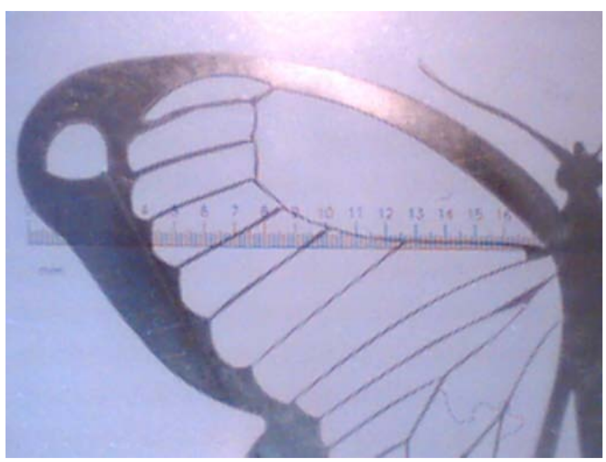

Figure 6. Example of Reproducing Thin Sections (Scale 100micron for smallest division)

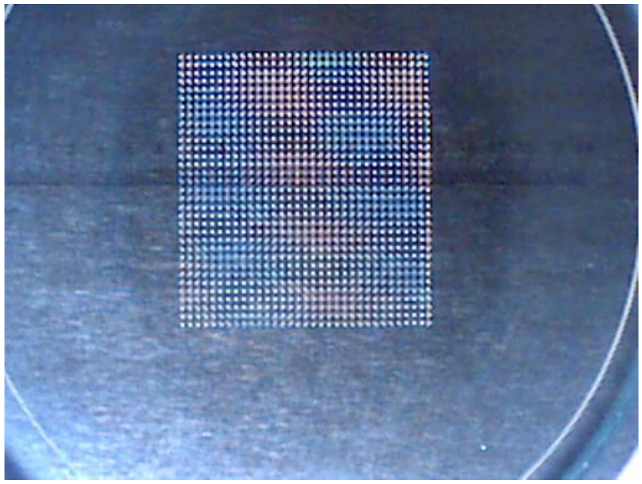

Figure. 7 33X33 Array of 85micron diameter holes drilled at 2.5 holes per second with 250micron spacing, nozzle diameter 58microns

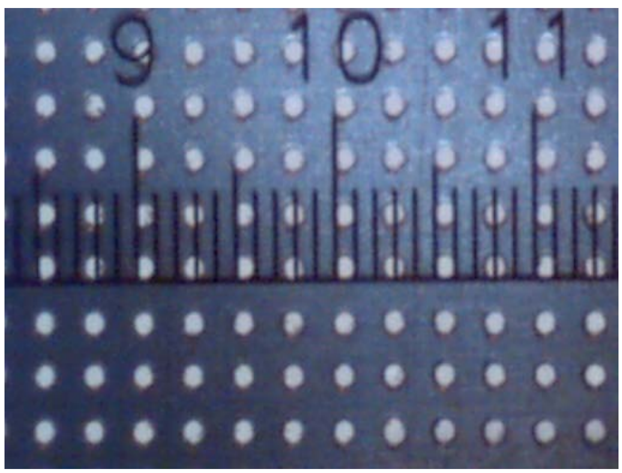

Figure 8. Holes as Figure 7 to larger scale, 50micron thick stainless steel

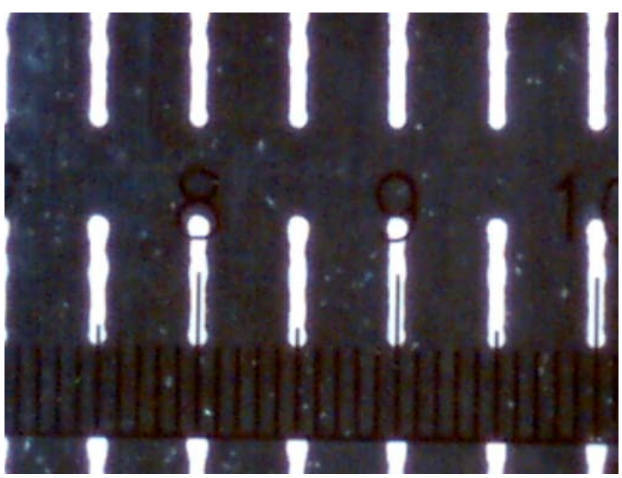

Figure 9. Slots cut with dwell at start and finish, 150micron thick stainless steel

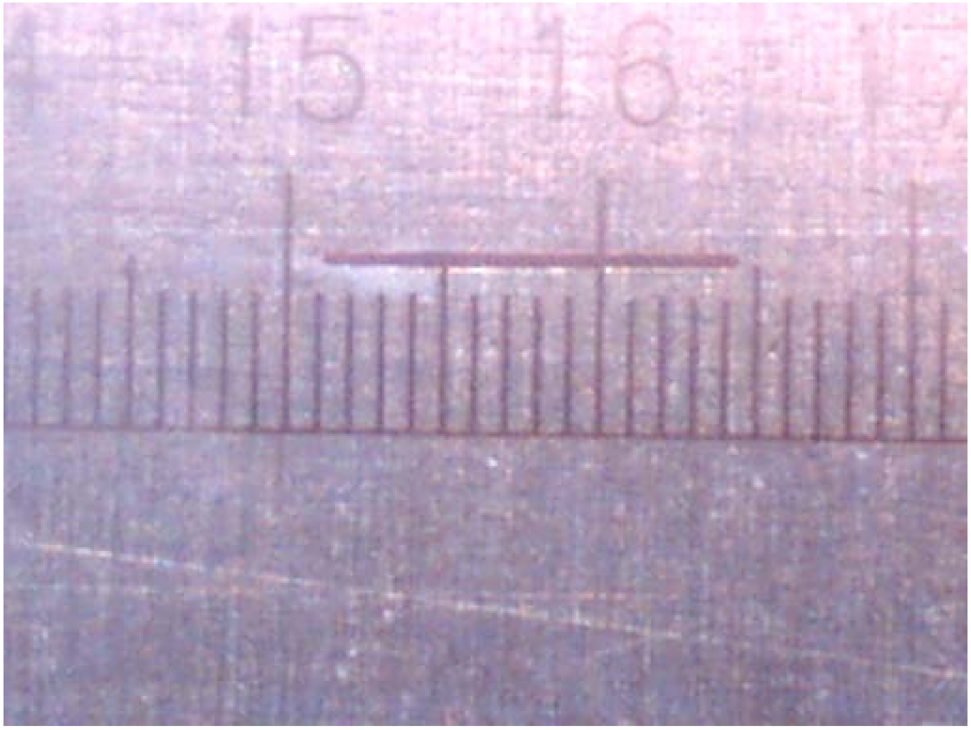

Figure 10 Outlet of Slot Cut in 50micron Thick Stainless Steel with a 40micron Diameter Jet Moving at 400mm/min.

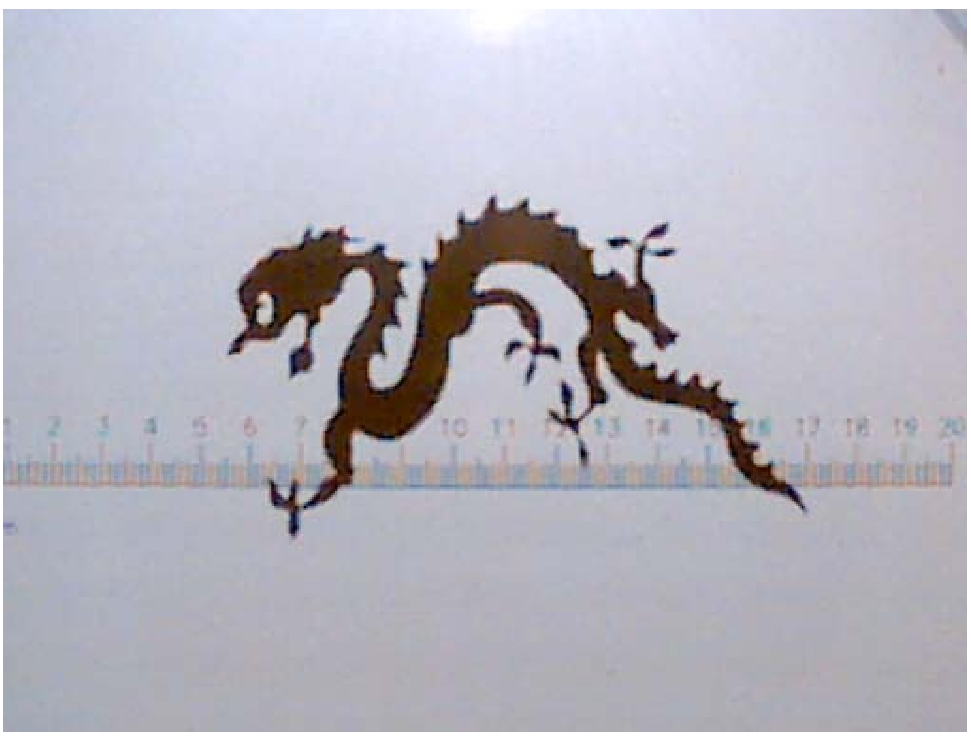

Figure 11 Profile from 50micron thick Stainless Steel, Cut with 300nanometre Abrasive Using a 40micron Diameter Nozzle

2003 WJTA American Waterjet Conference
August 17-19, 2003 • Houston, Texas

Paper 6-F

APPLICATION OF ABRASIVE WATERJET MACHINING IN UNDERGRADUATE ENGINEERING COURSES

D.G. Taggart, D. Chelidze, W.J. Palm and T.J. Kim
University of Rhode Island
Kingston, Rhode Island, U.S.A

B.E. Stucker
Utah State University
Logan, Utah, U.S.A

ABSTRACT

Modern abrasive waterjet machining systems provide an excellent means for quickly machining two-dimensional prototype components. The use of AWJ machining in undergraduate education courses has proven to be an excellent means for producing physical models that can be tested. The ability to validate student design analyses provides an effective pedagogical tool. AWJ has been implemented in several undergraduate courses at the University of Rhode Island. In one implementation, teams of students from three courses collaborated to develop a cost effective design of a 2-D mechanical component. The design activities included computer aided design of potential design configurations, finite element stress analysis, material selection and cost analysis. Each team's design was manufactured using AWJ and tested to validate design analysis predictions. AWJ has also been utilized extensively for individual and team senior projects. Examples of student research projects include the machining and analysis of minimum weight structures and development of controlled depth milling procedures. Most recently, the AWJ system has been used to manufacture components for URI's entry in the Society of Automotive Engineer's Mini-Baja competition.

1. INTRODUCTION

As part of a project funded by an education grant from the National Science Foundation, concepts of engineering graphics, mechanical design, numerical simulation, rapid prototyping and product testing were applied in project experiences performed by groups of vertically integrated teams of sophomores, juniors, seniors and graduate students. Students were asked to design components using a commercial computer-aided design software package, perform analytical and finite element stress analyses, manufacture components using rapid manufacturing methods, and test components to verify their mechanical performance [1]. Abrasive waterjet machining proved to be an effective method for manufacturing prototype components.

2. UNDERGRADUATE COURSE PROJECT ACTIVITIES

Abrasive waterjet machining has been implemented in different ways for various undergraduate engineering course activities. These activities include design and manufacture of mechanical components, experimental stress analysis and use of AWJ as a general machining tool in support of student project activities

2.1 Mechanical Design Activities

One example of waterjet machining in undergraduate courses took place during the Fall 2002 semester. This project was performed by teams of students from a sophomore level engineering graphics course, "Graphics for Mechanical Engineers" (MCE 201) and a junior level mechanical design course, "Applications of Mechanics in Design" (MCE301). In this project, a planar structural component was designed, machined using an abrasive waterjet (AWJ) cutting system and tested to evaluate its mechanical performance. AWJ's ability to machine a wide variety of materials allowed students to select from materials with widely varying mechanical properties. AWJ machining also provides the flexibility to machine any shape desired by the students. In addition to satisfying loading requirements, each team was required to consider material costs, machining costs and recycling costs. The design objective was to develop a design which satisfies the load and dimensional requirements shown in Figure 1. In addition to safely supporting the design load using a factor of safety of 2, the design objective was to minimize the cost function given by the formula:

$$\text{Cost per part} = \text{material cost} + \text{machining cost} - (\$\ .15 / g) * (40\ g - \text{part mass}) - \text{recycled material cost savings} \quad (1)$$

The material cost is that for the original 230 mm x 130 mm sheet. Using a hypothetical machining cost of \$ 30 / hr for a five head cutting machine (\$30 / hr÷5 = \$ 6 / hr = \$0.10/min), the machining cost per part was taken to be:

$$\text{Machining cost} = \$\ 0.10 * \text{total length of cut (mm)}/\text{AWJ cutting speed (mm/min)} \quad (2)$$

Note that the AWJ cutting speed is inversely related to the machining cost, leading to a dramatically lower machining cost for polycarbonate. The third term in equation 1,

($.15/g)*(40g–part mass), represents a cost savings/penalty associated with reducing the weight of the final component. This cost is realized over the life of the component due to improved performance. For example, if this were an aircraft or automotive component, the cost savings would be associated with reduced fuel consumption. The recycled material cost is computed by multiplying the mass of material removed times the material cost times the recycled material savings percentage given for each material. Selecting from candidate materials including mild steel, aluminum or polycarbonate, students were asked to minimize the cost per part by changing the shape of the part by removing material. Properties and costs of candidate materials are shown in Table 1. Note that the cost data shown in Table 1 is not realistic and cost data was adjusted in order to make the candidate materials more competitive. In an actual design optimization, accurate cost data would be required.

To simulate an actual industrial experience, multi-functional teams consisting of engineering and drafting personnel were formed. Drafting duties were performed by students in MCE 201. These students were responsible for creating CAD files using Solidworks for the various configurations to be evaluated. Students in MCE 301 were responsible for stress analysis activities including plane stress finite element analysis using ANSYS and imported CAD files created by the MCE 201 students. Each team performed several design iterations before selecting their final design for manufacture and testing. Typical student designs are shown in Figure 2. As shown in Table 2, student teams developed a variety of designs of varying cost effectiveness. The tradeoff between the varying cost parameters (materials cost, machining cost, weight savings premium and recycled material cost) is clearly seen. It is of interest to note that the most cost effective designs were those machined from polycarbonate. Although several of the polycarbonate designs carried the required load, the structural response was nonlinear due to out of plane buckling. More costly aluminum designs carried the required load without any such instability.

2.2 Experimental Stress Analysis Activities

In another course project, performed during the Spring 2002 semester, teams of students from "Manufacturing Processes" (IME 240), "Mechanical Engineering Experimentation" (MCE 314) and "Introduction to Finite Element Methods" (MCE 466) were required to design, manufacture, analyze and test a mechanical component. In this project, each team was required to develop their own experiment making use of available manufacturing, experimental and computational facilities. Several teams designed experiments in which components were machined from birefringent plates using AWJ. The experimental technique of photoelasticity was then used to evaluate the stress fields induced during loading. These stress fields were correlated with finite element stress analysis results. A typical correlation is shown in Figure 3 which shows the stress concentration associated with adjacent circular and elliptical holes.

3. AWJ IN SENIOR PROJECTS

The versatility and ease of use of modern AWJ machining systems allows students to easily machine complex 2-D components and to perform research studies examining the effects of various AWJ parameters on machining performance. As a result, AWJ machining has been implemented in several undergraduate senior projects. At URI, students may elect to do a senior project as one of the four professional electives required for graduation. Depending of the scope of the project activities, these projects can be either individual or team projects.

3.1 Design Optimization Studies

An active research topic in URI's Departments of Industrial and Manufacturing Engineeering and Mechanical Engineering is the design and manufacture of minimum weight structures. Optimization methods based on classical theory by Michell [2] have been developed and implemented in recent years [3,4]. These truss-like structures are designed such that all of the members are subjected to uniform uniaxial stress. An individual senior project was performed to validate this concept. In this project, an aluminum cantilever beam structure was machined using AWJ machining (Figure 4a). This component was then analyzed using finite element stress analysis (Figure 4b). The results of the finite element analysis demonstrated that the idealized states of uniform tension and compression were achieved except at the member intersection points, where a biaxial stress state is induced.

3.2 AWJ Milling Studies

Another individual senior project explored concepts of AWJ milling. In this process, single or multiple high speed passes of the AWJ provided removal of a controlled depth of material. Control of the depth and width was achieved by varying AWJ parameters such as standoff distance, pressure and traverse speed. To quantify the contour of the machined profile, an image of the profile was digitized and analyzed using a Matlab routine developed by the undergraduate student. It was found that the machined profile could be quantified using a Gaussian distribution.

Typical machined profiles are shown in Figure 5 along with the Gaussian fit to the digitized profiles. Examples are shown for the cases of wide, shallow grooves; grooves of moderate depth and width and deep, narrow grooves. It is evident that the Gaussian fit matches the observed profile rather well and provides an effective means of quantifying the experimental results. Note that for the deep, narrow grooves, flow of the deflected jet along the base of the groove resulted in a profile that was not detected by the Gaussian fit. Attempts to model multiple passes using mathematical superposition of single passes proved to give reasonable results for cases where the single pass machined grooves were wide and shallow. For cases where the single pass grooves were narrow and deep, subsequent passes exhibited asymmetric profiles due to deflection of the AWJ jet. Similar results have been previously reported in the literature [5]

3.3 Mini-Baja Component Machining

Recently, during the 2002-03 academic year, a team of students from URI competed in the "Mini-Baja" competition sponsored by the Society of Automotive Engineers. In this competition, collegiate teams from the USA and Canada design and construct an off-road vehicle and then compete in a variety of events. Since each school is provided with identical engines, a critical design component is to minimize the weight of the vehicle. Also, since the Mini-Baja

East competition includes a water event, the vehicles must float and be able to propel themselves through the water.

URI's Mini-Baja team made extensive use of the AWJ cutting facilities. In addition to providing a quick turnaround that allowed for design changes, AWJ also provided the ability to machine virtually any material and any 2-D contour. Examples of components (see Figure 6) include the carbon-epoxy composite vehicle number, drivetrain components and sections of foam for the floatation system. URI's entry in the 2003 Mini-Baja East competition held in Florida performed very well, placing 5th out of 49 schools [6].

4. CONCLUSIONS

This project has demonstrated that AWJ machining provides a flexible tool that can be utilized in a variety of educational contexts. The ability for students to easily manufacture and test physical prototype models provides valuable reinforcement of theoretical and analytical predictions. Just as the availability of computer simulation methods in the past 20 years has impacted the education of engineers, it is believed that the ability to easily produce physical models as part of the design process will have a similar impact. Due to the ability to machine nearly any material and complex shapes, AWJ machining provides an excellent tool for machining prototype components. Similarly, AWJ machining has proven to be a versatile technique for students performing individual or small group projects.

5. REFERENCES

1. Taggart, D. G., Stucker, B. E., Kegler, T., Chelidze, D. and Palm, W. J., "Integration of Mechanical Design and Prototyping Activities" *American Society for Engineering Education Annual Conference and Exposition*, 2002.

2. Michell, A. G. M., "The limit of economy of material in frame structures," *Philosophical Magazine*, 1904, Vol. 8, No. 47, pp. 589-597.

3. Dewhurst, P., "Analytical solutions and numerical procedures for minimum-weight Michell structures," *Journal of the Mechanics and Physics of Solids*, 2001, Vol. 49, p. 445.

4. Dewhurst, P., Taggart, D. G., Demircubuk, M., Nair, A. and Srithongchai, S., "The design of minimum-weight product structures: a preliminary case study combining theoretical optimum layour analysis with FEM studies," *ABAQUS Users' Conference*, Munich, Germany, June, 2003.

5. Laurinat, A., Louis, H., Meier-Wiechert, "A Model for Milling with Abrasive Water Jets, 7th *American Water Jet Conference*, August 1993, pp. 119-139.

6. Plaziak, D., "URI Students take race course," *Narragansett Times*, April 17, 2003, p. 1-C, 4-C.

6. ACKNOWLEDGEMENTS

This work was supported by the National Science Foundation (NSF), Directorate for Education and Human Resources (EHR), Division of Undergraduate Education (DUE), Course, Curriculum and Laboratory Improvement (CCLI) Award No. 0088315. The authors would also like to acknowledge the contributions of the following undergraduate engineering faculty and students who contributed to various aspects of the project: Dr. Peter Dewhurst, Dr. Jason Gomez, Justin Eighme, Susan Rhodes, Judy Groccia, and Greg Panebianco.

Table 1. Cost and Property Data

	Steel	Aluminum	Polycarbonate
Sheet thickness, mm (in)	6.22 (0.245)	6.10 (0.240)	5.46 (0.215)
Young's modulus, GPa (Msi)	200 (30)	69 (10)	2.4 (0.34)
Poisson's Ratio	0.29	0.33	0.39
Yield strength, MPa (ksi)	230 (34)	190 (28)	30 (4.3)
Density, kg/m^3 (lb/in^3)	7,800 (.283)	2,800 (0.1)	1,200 (.043)
Material cost, $/kg ($/lb)	1.30 ($.56)	14.68 ($6.67)	6.16 (2.80)
AWJ cutting speed, mm/min (in/min)	67 (2.65)	164 (6.45)	338 (13.3)
Recycled material savings (%)	1	25	5

Table 2. Comparison of Student Designs

Team #	Mat'l	Area (mm^2)	Length (mm)	Mass (g)	Buckling Load (N)	Max. Load (N)	Material Cost	Machining Cost	Cost Savings	Recycling Cost	Overall Cost
1	Poly	9053	1375	59.3	2100	3000	$1.21	$0.41	$2.90	$0.04	$4.47
8	Poly	9579	1393	62.8	1700	3000	$1.21	$0.41	$3.41	$0.04	$4.99
26	Poly	9531	1659	62.4	1000	3000	$1.21	$0.49	$3.37	$0.04	$5.02
18	Poly	9842	1205	64.5	1700	3000	$1.21	$0.36	$3.67	$0.04	$5.20
13	Poly	10700	1070	70.1	2150	3000	$1.21	$0.32	$4.52	$0.04	$6.00
15	Poly	10860	1331	71.2	2300	3000	$1.21	$0.39	$4.67	$0.04	$6.24
3	Poly	12155	1256	79.6	2400	3000	$1.21	$0.37	$5.95	$0.04	$7.49
21	Poly	12364	1045	81.0	2799	3000	$1.21	$0.31	$6.15	$0.04	$7.63
24	Poly	12330	1343	80.8	2300	3000	$1.21	$0.40	$6.12	$0.04	$7.69
19	Aluminum	2916	1114	49.8		3000	$7.50	$0.68	$1.47	$1.69	$7.96
12	Aluminum	2972	1573	50.8	710	710	$7.50	$0.96	$1.61	$1.69	$8.38
22	Aluminum	3080	1136	52.6	2200	2200	$7.50	$0.69	$1.89	$1.68	$8.40
23	Aluminum	3109	1129	53.1	2100	2570	$7.50	$0.69	$1.97	$1.68	$8.47
14	Aluminum	3244	1129	55.4		3000	$7.50	$0.69	$2.31	$1.67	$8.83
10	Aluminum	3394	1187	58.0		3000	$7.50	$0.72	$2.70	$1.66	$9.25
17	Aluminum	3500	1246	59.8		3000	$7.50	$0.76	$2.97	$1.65	$9.57
2	Aluminum	3617	1126	61.8		3000	$7.50	$0.69	$3.27	$1.65	$9.80
20	Aluminum	3884	1122	66.3		3000	$7.50	$0.68	$3.95	$1.63	$10.50
9	Aluminum	3894	1128	66.5		No	$7.50	$0.69	$3.98	$1.63	$10.53
5	Poly	15329	1189	100.4		No	$1.21	$0.35	$9.07	$0.03	$10.59
11	Aluminum	4030	1231	68.8	2600	2600	$7.50	$0.75	$4.32	$1.62	$10.95
25	Aluminum	5065	1567	86.5		3000	$7.50	$0.96	$6.98	$1.56	$13.87
7	Aluminum	5185	1089	88.6		3000	$7.50	$0.66	$7.28	$1.55	$13.90
6	Aluminum	5200	1574	88.8		3000	$7.50	$0.96	$7.32	$1.55	$14.23
4	Aluminum	5786	1318	98.8		3000	$7.50	$0.80	$8.82	$1.51	$15.61

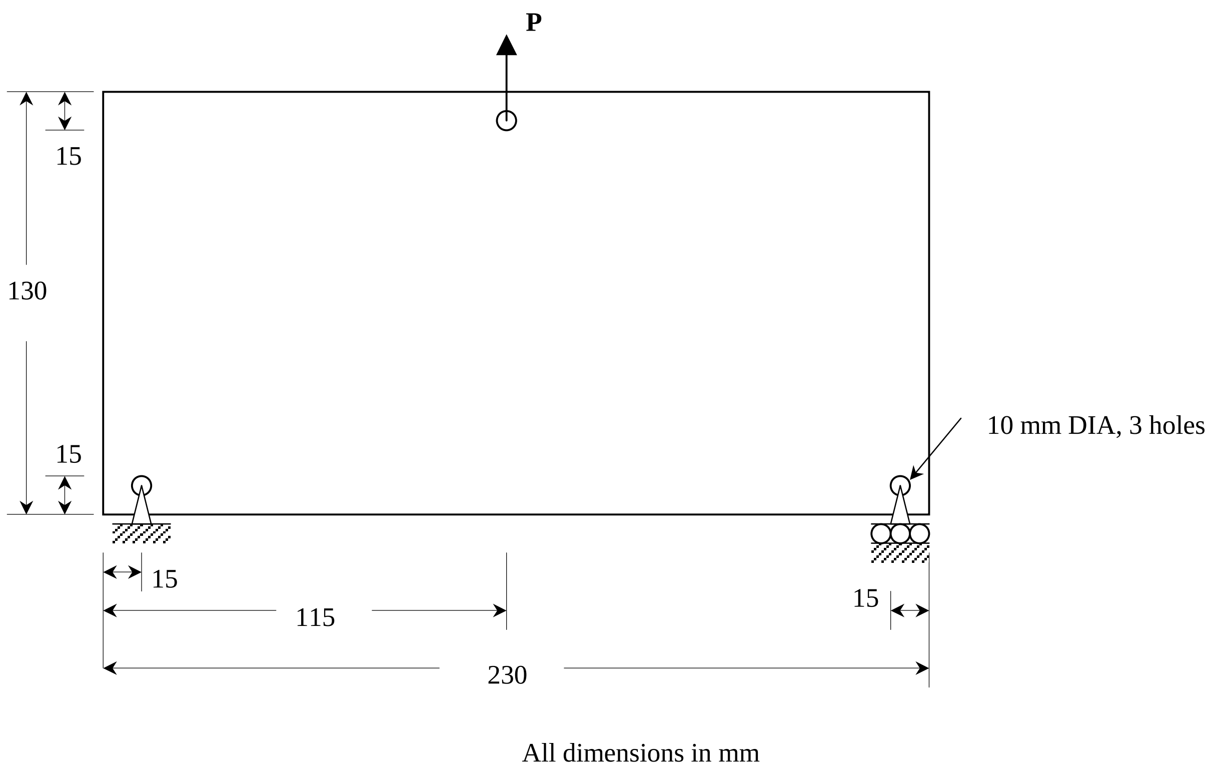

Figure 1. Geometry and configuration of loads for optimum design assignment

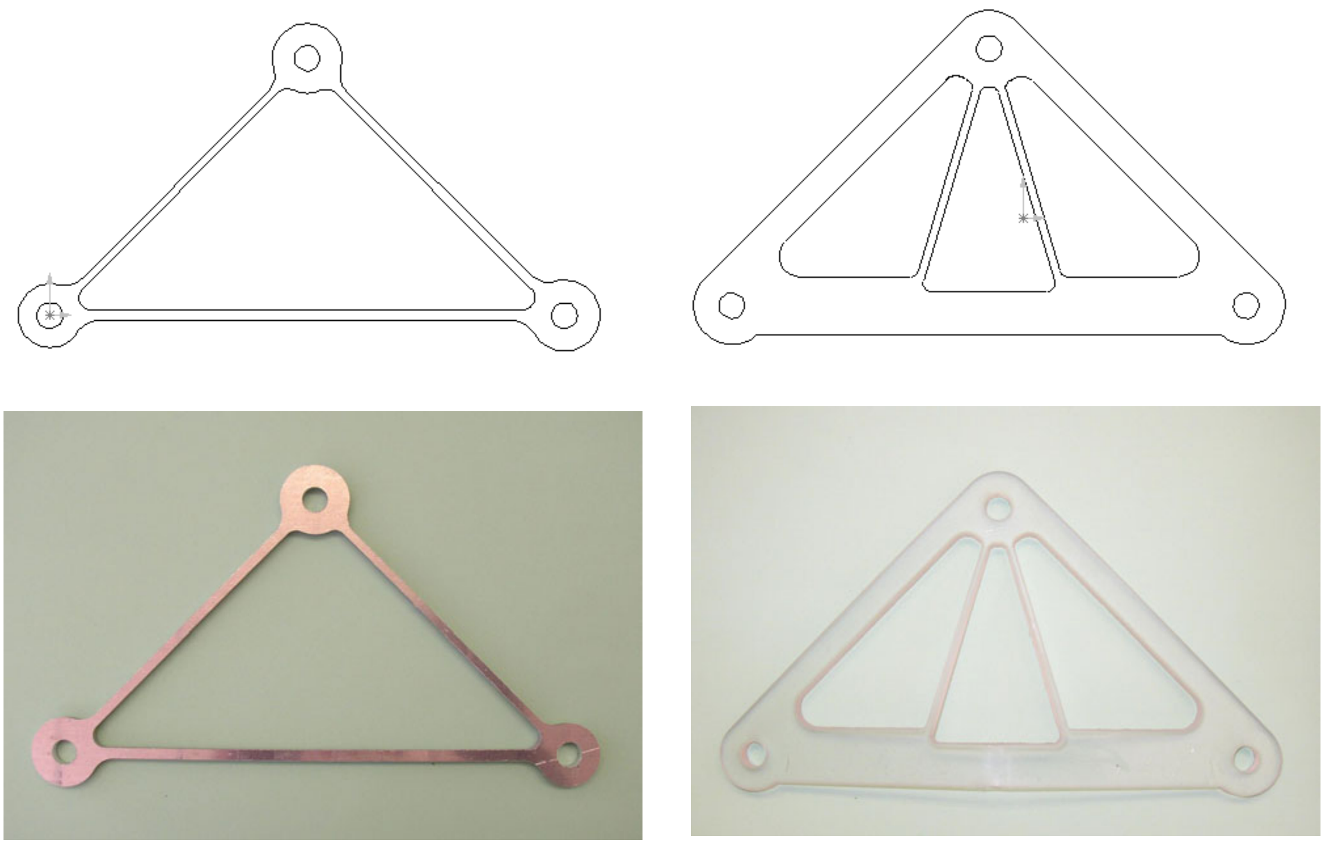

Team 19 Team 1

Figure 2. Student designs manufactured from aluminum (left) and polycarbonate (right), CAD models (top) and machined parts (bottom).

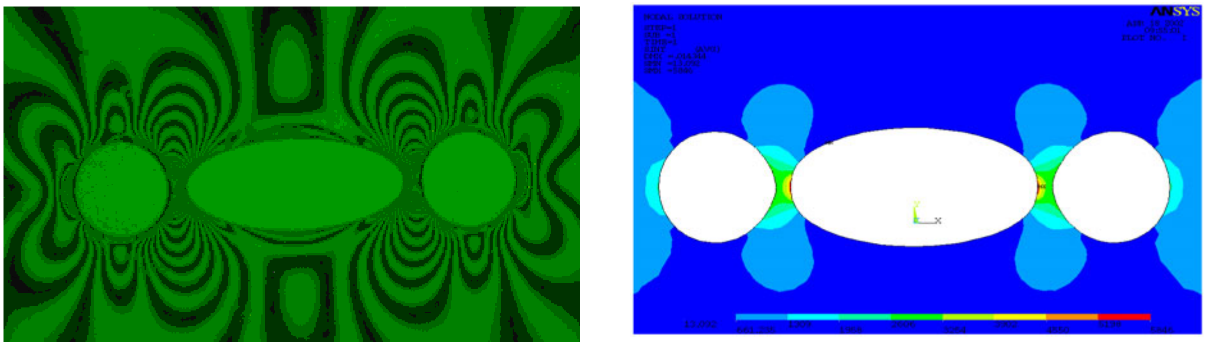

Figure 3. Correlation of results of experimental photoelasticity (left) and finite element stress analysis (right).

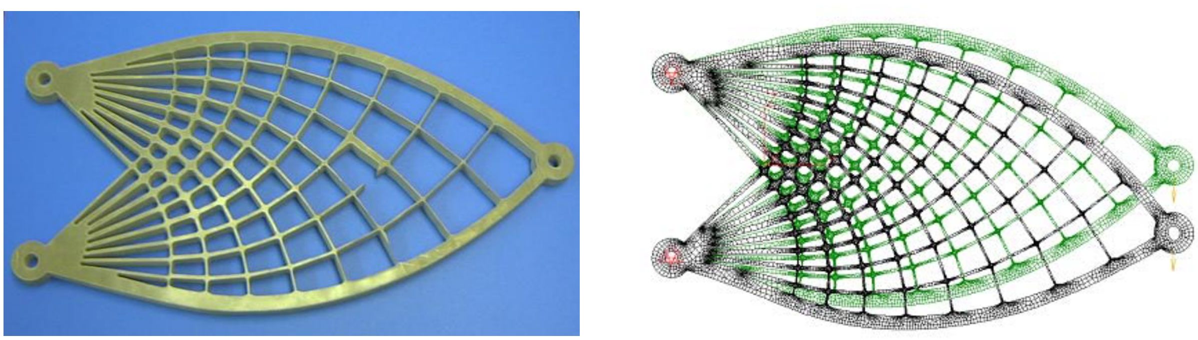

Figure 4. Minimum weight cantilever beam showing a) machined component (left) and b) finite element stress analysis (right)

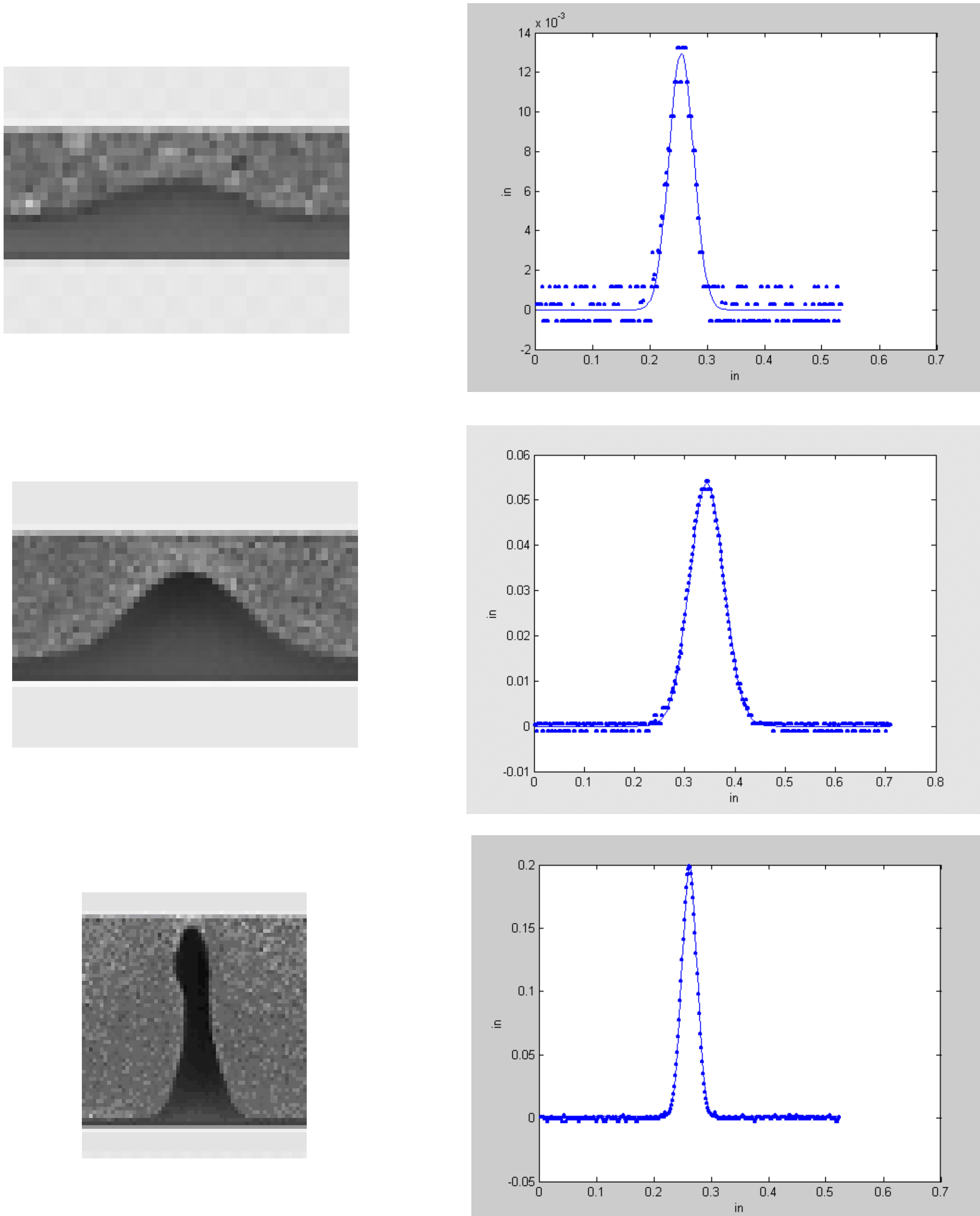

Figure 5. Typical result showing AWJ machined grooves (left) and digitized depth profiles (right).

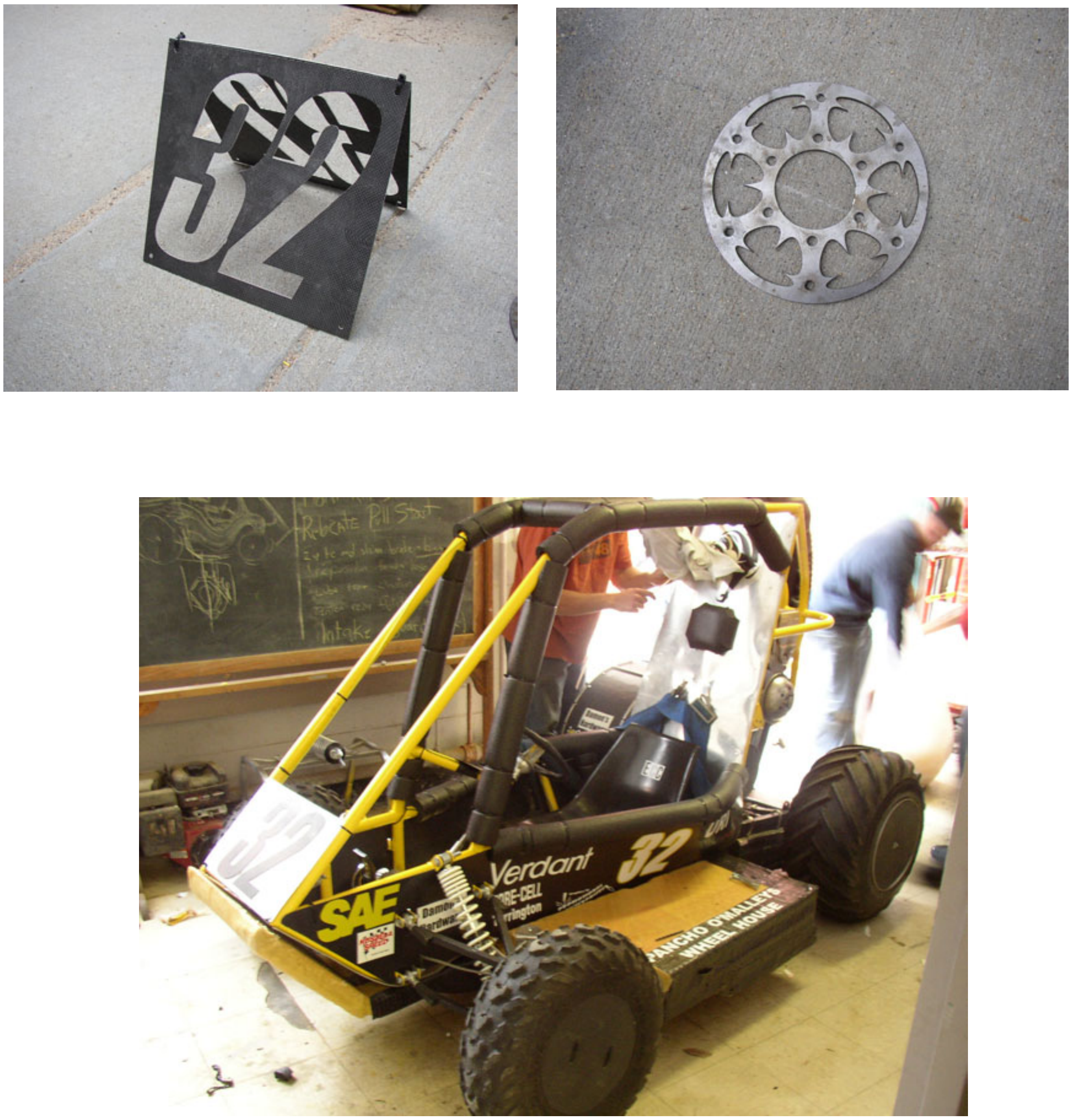

Figure 6. AWJ machined components for URI's entry into the Mini-Baja competition sponsored by the Society of Automotive Engineers: Carbon-epoxy composite vehicle number (top left), drivetrain component (top right), full vehicle (bottom).

2003 WJTA American Waterjet Conference
August 17-19, 2003 ● Houston, Texas

Paper 7-F

PURE WATER-JET CUTTING OF FRESH MEAT REDUCES THE RISK OF CONTAMINATION

M. Alitavoli
University of Guilan
Guilan, Islamic Republic of Iran

ABSTRACT

Ultra High Pressure Water-Jet (UHPW) has been widely used in the various industries for processing wide ranges of products from soft to hard-to-cut ones. As a clean and non-contaminated cutting process, the water-jet cutting technique is gaining popularity in food processing plants.

Despite the reports on the application of water-jet cutting technique in the food industry, no systematic parametric study has been reported on this topic yet. The main objective of this study was to investigate the hygienic aspects of pure water-jet cutting technique in contrast to the conventional meat cutting methods. Several cutting experiments was conducted both by pure water-jet and manual techniques such as knife and band-saw on the lamb meat samples. Biological experiments revealed that cutting meat by pure water-jet beam reduces the risk of contamination.

1. INTRODUCTION

The increasing demand of consumers for better quality and lower cost food products, and the public request for higher standards of life and health (Pierson, 1995), has prompted firms to take new approaches in further automating the food processing techniques.

By virtue of their cleanliness and avoidance of tool-food contact, water-jets can minimize the risk of bacterial contamination and eliminate downtime resulting from blade cleaning and blade sharpening requirement as they apply to manual and mechanised cutting systems (Ng W., 1994).

As the materials vary from one type to another, their related processes, handling, storage, etc. vary as well. For instance, when processing food products such as meat, microbiological and hygienic issues must be taken into consideration. Except few studies which focused on the application of water-jet to food products such as fish (Malone et al, 1994), corn (Gunaseekaran, 1987), and meat (Alitavoli, 1999) and (Jacobs, 1996), the majority of research efforts have been concentrated in the application of this technique to non-food related areas such as hard materials.

Based on the experiments and results on cutting the composite sample i.e., meat and bone samples from lamb, microbiological tests were carried out to establish the non-contamination/hygienic aspects of the water-jet cutting process.

2. PROCEDURE, EQUIPMENT, MATERIALS

To determine the reliability and cleanliness of the water-jet cutting procedure of meat, a micro-biological examination of the cut samples was required. In order to demonstrate microbial contamination on the surface of the cut specimen, a straight forward micro-biological 'swab test' was performed. The objective of this study was to examine various meat samples which were cut by:

- Pure water-jet stream
- Knife (normal condition i. e., samples were cut in a butcher shop)
- Knife (samples were cut by a deliberately contaminated knife with E-coli in the lab)

The purpose of the above was to check for any possible cross contamination between the cut slices which might transfer by the cutting device. A normal microbial comparison between a sample which was cut in the butcher shop and a sample which was cut by water-jet technique was pursued as well. Due to possible contamination of the tap water, samples of water exiting the nozzle were also to be examined. Several meat samples were extracted from the loin (back) section of lamb and carefully placed in sterilised plastic bags. The samples were fresh and approximately of the same size.

Apparatus for performing the experiments included the water-jet machine, a knife, and common micro-biological test devices such as a flame, egger plates, alcohol, forceps, and incubators, for maintaining the egger plates at a prescribed temperature for the detection of defective plates.

The samples were carried in sterilised bags in a cold condition in order to lower the risk of contamination. Within maximum 2 hours of the preparation period, samples were cut by the proposed cutting methods. Each sample was cut into 4 slices. Within 2 hours after cut, the slices were transferred to the lab for performing the swab test. To avoid any risk of contamination, following precautions were taken:

- Ensured the working area was clean and draught-free,
- Cleaned the work surface with a suitable disinfectant such as an alcohol mixture both before and after testing,
- Sterilised containers, apparatus forceps, etc., and instrument for handling the samples.

For the swab test, each slice was put inside an egger plate and left for 30 seconds. Then the slice was discarded. After placing all samples in the plates, they were then placed inside an incubator for nearly two days. Meat samples required a temperature of 25 degrees Celsius for developing bacteria. After two days the samples were removed from the incubator and transferred to a fridge. These tests were carried out according to British Standards for meat micro-biological testing (BS, 1989).

3. RESULTS

To obtain the results, egger plates were chequed for the number of colonies of microbes which were developed during the two days period on the plate surface. The purpose was to determine the number of colonies per centimetre square (expressed as Colony Forming Units per centimetre Square or CFUS) which were developed in the infected area. The more colonies in a unit of surface area, the more presence of contamination. The areas which contained far too many colonies for counting were labelled as TNTC (Too Numerous To Count). The colony formation for different samples i.e., knife cut (normal condition), water-jet cut, knife cut (contaminated condition) are shown in Figure 1. The two water samples are also shown in this figure.

Results for knife cut with deliberate contamination and normal condition showed a high concentration of small and large microbial colonies, which looked as one colony and were too difficult to count. The comparison of cut slices in these two samples showed a clear cross contamination between each cut.

In the case of samples cut by water-jet technique, some microbial colonies were observed but not as many as the other two tests. Table 1 shows these results.

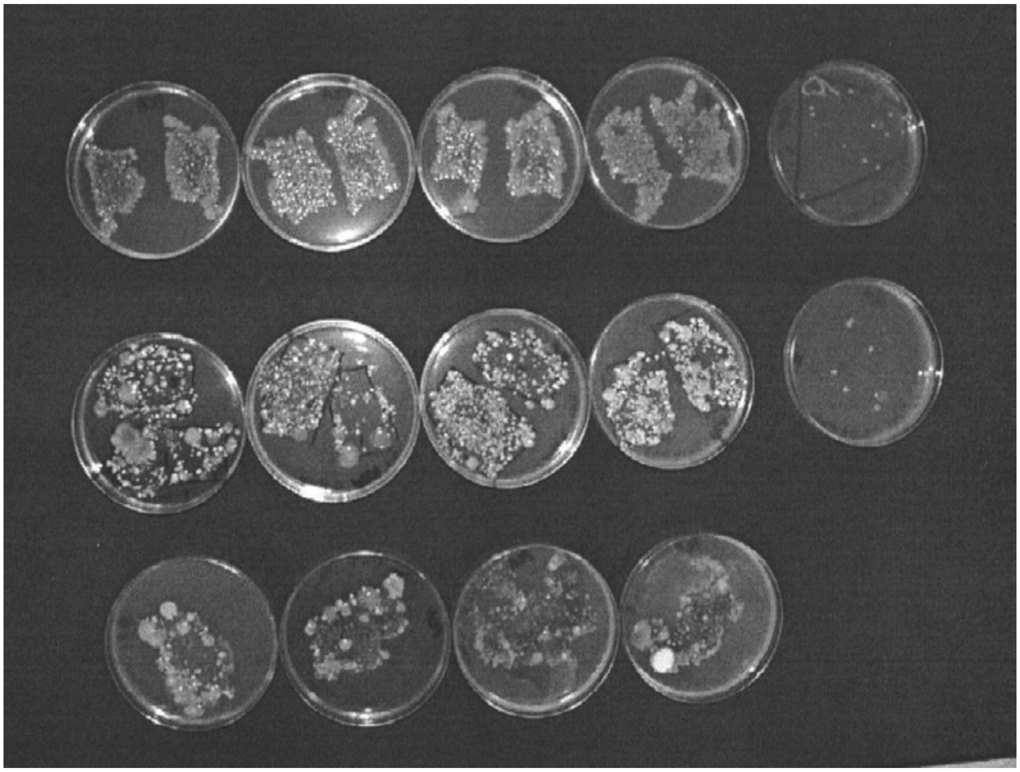

Figure 1. Microbiological samples of meat produced by water-jet, knife (normal and contaminated), and the water samples

Table 1. Microbial colony counts for meat samples cut by water-jet method

	Side	Area of each colony(cm^2)	Total no. colonies	Colonies per cm^2
Slice 1	1	15	196	13
	2	15	270	18
Slice 2	1	13	86	6
	2	13	274	21
Slice 3	1	15	164	12
	2	15	350	21
Slice 4	1	15	250	16
	2	15	280	19

In order to detect the possible source of contamination, two samples of water from the water-jet nozzle outlet was prepared. After a swab test for each sample, they were placed in incubator and kept for two days. One sample was kept at 25 and the other one at 37 degrees Celsius. To measure the contamination level of the water, a ratio of the colony counts at the two different temperatures were taken as follows:

$$Ratio = \frac{colonycountat\,25\deg reesCelcius}{colonycountat\,37\deg reesCelcius} = \frac{40}{23} = 1.7$$

In a normal condition, the ratio must be 10 to 1. Any ratio less than the normal ratio is not valid which means the water is contaminated. Table 2 illustrates the results for water examination.

Table 2. Microbial test results for water samples from WJ machine

	Area of colonies(cm^2)	**No. of colonies**	**Temperature (C)**
Sample 1	50	40	25
Sample 2	50	23	37
Ratio		40/23	

As seen in Table 2, the ratio is far less than the normal condition. In other words, the water used in these experiments was contaminated with some type of microbes.

4. CONCLUSION

In this section some experiments for determining the cross contamination between different meat samples, which were cut by water-jet technique, and knife (normal and contaminated) were performed. The results concluded that fresh meat slices produced by water-jet method showed:

- Lower contamination level as compared to the other cutting methods,
- Lower level of cross contamination amongst all.

In further tests of the water itself, it was revealed that the water at the nozzle outlet was also contaminated. Other sources of contamination such as the internal routes of the low and high-pressure lines might have caused the contamination. The meat samples might have been contaminated by the improper handling, water, splash from the water in the tank as the high-pressure jet hits the surface of water below the sample during cutting, and the environment. The results can be optimised by controlling the aforementioned limitations.

5. REFERENCES

Alitavoli M., Water-Jet cutting and process planning of meat products. PhD Thesis, 1999.

Gunasekaran S., Cooper M. T., Berlage G. A., and Krishan P., Image processing for stress cracks in corn kernels. Transactions of the ASAE, Vol. 30, No. 1, p.266, 1987.

Jacobs J., Machine vision for meat processing. Advanced Imaging. Vol. 11, PT 11, pp.21-24, 1996.

Malone D.E., Friedrich W.E., Spoonser N.R., and Lim P.P.K., Knowledge based control in the processing of highly varying products. Proceedings of IEEE International Conference on Robotics + Automation, PT. 4, pp.2903-2908, 1994.

Ng W., Lamb shoulder fleecer and rack frenching machines. 28th Meat Industry Research Conference, pp.201-208, 1994.

Pierson M., An overview of hazard analysis critical control points (HACCP) and its application to animal production for safety, The 75th Annual Meeting of the Conference of research Workers in Animal diseases, pp.1-10, 1995.

2003 WJTA American Waterjet Conference
August 17-19, 2003 • Houston, Texas

Paper 3-A

ABRASIVE WATERJET MACHINING OF AEROSPACE STRUCTURAL SHEET AND THIN PLATE MATERIALS

I. Conner
University of Washington
Seattle, Washington, U.S.A.

M. Hashish
Flow International Corporation
Kent, Washington, U.S.A.

M. Ramulu
University of Washington
Seattle, Washington, U.S.A.

ABSTRACT

Abrasive Waterjet (AWJ) machining is of particular interest for the cutting of structural metal alloys and composite materials of widespread use in the automotive and aerospace industries. An attempt is made in this paper to present the results of industry and university collaborative work on the machining of aerospace sheet and thin plate materials by AWJ, investigating surface quality, kerf features, the effects of varying certain process parameters. Cutting speed or traverse rate was found to have a significant effect on kerf quality in sheets and thin plates.

Organized and Sponsored by the Waterjet Technology Association

1. INTRODUCTION

The use of high-energy waterjets, produced by the expansion of pressurized water through a small orifice to produce a high-velocity collimated stream, has gained wide acceptance as an alternative method of machining for a wide variety of materials. The introduction of abrasive particles into the high-velocity water stream expands the domain of waterjet cutting applications to include an unlimited array of hard materials such as metals, ceramics, glass, stone, and polymer composites [1-6]. The ability of the abrasive waterjet (AWJ) to cut such materials economically and with minimal need for secondary processing has driven its continued growth as an alternative manufacturing process. This is particularly true in the aerospace industry, where applications continue to expand for titanium alloys, composite laminates, and other materials that present certain difficulties when traditional machining methods are applied.

2. BRIEF REVIEW ON MACHINING OF AEROSPACE MATERIALS

The use of advanced materials, particularly titanium and aluminum alloys, inconel, and polymer composite materials such as graphite/epoxy laminate, has been an important factor in the development of aerospace vehicles, with applications expanding in the fabrication of both aircraft structural elements and aero-engine components [7-9]. These advanced materials have many advantageous mechanical and physical properties, such as high strength-to-weight ratio, strength retention at high temperatures, and exceptional corrosion resistance, which make them materials of choice for a variety of aerospace engineering applications. Figure 1 illustrates the usage of these materials in a B-2 bomber, a military application. Machining and edge trimming are important processes in the manufacture of these components,

Though the conventional machining of inconel and titanium alloys has been the subject of extensive study, they are still generally classified as extremely hard-to-machine materials using conventional methods, exhibiting high temperature rises and rapid tool wear for most tool materials [9, 10]. The large temperature rise during machining is due to the high material strength, which induces large localized cutting stresses at the tool-workpiece interface. In the case of titanium, high chemical reactivity with almost all tool materials at elevated temperatures in turn accelerates tool wear. Also, inhomogeneous shear localization due to serrated, unstable chip formation gives rise to cutting force fluctuations which, combined with the relatively low elastic modulus of titanium, cause chatter and excessive deflection of the machined parts [10]. These and other difficulties associated with traditional machining methods have led to the increasing importance of AWJ machining as alternative process for these materials.

The use of composite materials in the aerospace industry continues to expand, and as with metals, traditional cutting and edge trimming methods have been developed using advanced cutting tool materials. In traditional machining of unidirectional graphite-epoxy composites by polycrystalline diamond (PCD) tools, chip formation, cutting forces, and machined surface characteristics are highly dependent on fiber orientation [11]. For positive fiber orientation angles up to 45°, chip size has been found to generally decrease with increasing fiber angle, with highly fragmented, powder-like chips produced at angles greater than 45°. Three distinct mechanisms of chip formation and material removal have also been identified, based on fiber orientation angle [11, 12]. In addition, fluctuations in tool reaction force also show a strong fiber orientation dependence, with large fluctuations at 0° (attributed to initiation/propagation mechanisms of chip formation), decreasing fluctuations for increasing angles up to 75°, and large fluctuations again appearing at angles of 90° and greater. The roughness of the machined surface is affected by the degree of matrix material smearing, which in turn was found to depend on fiber orientation angle. For orientations between 15° and 60°, the average surface roughness has been noted to remain nearly constant in both the longitudinal and transverse directions. While variations in the machining methods used can affect the resulting surface texture, measurements of the flexural properties of machined graphite/epoxy laminate suggest that there is little influence on the bulk material strength under bending loads [13, 14, 15].

Among the early motivations for the development of abrasive waterjet technology were the problems of fracturing and delamination encountered when applying conventional machining methods to many newly emerging polymer composite materials. Though still thought of as a non-traditional machining method, abrasive waterjet cutting has gained acceptance rapidly since its introduction in the early 1980s, particularly for use with the variety of difficult-to-machine materials used widely in the aerospace industry. The potential for reduced process costs, lower operational complexity compared with many traditional methods, and the absence of heat-affected zones in the working material resulting in a reduced need for secondary machining processes are among the factors which have made AWJ machining an increasingly attractive alternative for many of these applications.

In this study, common ductile and quasi-brittle aerospace sheet and thin plate materials were machined with an AWJ. Inconel 718, titanium and aluminum 7075-T6 alloys, and graphite/epoxy composite sheets of both tape and fabric composition were machined under numerous parametric combinations. A thorough analysis of kerf quality was conducted by profilometry and scanning electron microscopy. Influences of cutting parameters on kerf geometry (in terms of exit kerf width) and the quality of the machined surface (in terms of surface roughness) are presented.

3. EXPERIMENTAL WORK

3.1. Materials

Sample materials chosen for cutting experiments in this study included 1.6mm thick Inconel-718, Titanium (Ti6Al4V) alloy, 4mm thick 7075-T6 aluminum stock, and 4 to 5 mm thick Graphite/Epoxy sheets (tape and fabric) composed of 3501-6 resin and IM-6 fibers. For the composite samples, the average diameter of the graphite fibers was 6μm and the volume fraction of the material was near 0.65. Material selection was based on utilization within the aerospace industry and relatively ductile mechanical properties. Table 1 lists some representative properties of the materials studied.

3.2. Abrasive Waterjet Machining

All experiments were performed with a waterjet using pump pressures of 25-55 ksi, orifice diameters (d_n) of 0.228-0.457 mm, and focusing tube diameters (d_m) of 0.79-1.6 mm. All machining was conducted with garnet abrasives of mesh sizes #60, #80, #100, #150 and #250; abrasive flow rate (m_a) varied from 0.76 to 10 g/s [16]. Graphite/Epoxy specimens were machined from laminate stock parallel to one of the primary fiber directions, resulting in fiber orientations of 0°, 90°, 45° and -45° realized through the cut depth. All specimens were machined through a traverse distance of at least 25 mm to achieve steady cutting conditions. Design of experiments (DOE) of Taguchi was used in obtaining a total of 27 Gr/Ep specimens involving various parametric combinations of pressure, standoff distance, traverse speed, and grit size. Surface roughness and kerf taper models for AWJ machining of Gr/Ep composites were formulated and previously reported for these experiments [17]. A visual analysis indicated varying degrees of waviness on the kerf surface between specimens machined with different parametric combinations. Two specimens which exhibited different degrees of waviness were chosen to conduct further analysis regarding mechanisms of material removal in this study. Aluminum and composite specimens were machined with an AWJ nozzle assembly having d_n/d_m = 0.3 mm / 1.0 mm. Parametric values used in obtaining the aluminum and composite material results are listed in Table 2. Scanning Electron Microscope (SEM) analysis was conducted to inspect micro-features of the machined specimens with a Jeoul JSM-T330A Scanning Electron Microscope.

4. RESULTS AND DISCUSSION

4.1 Typical Surface Features

The precise characteristics of the surfaces produced by through-cutting of different materials by abrasive waterjets depend strongly on process parameters (e.g. water pressure, abrasive particle size and mass flow rate, and traverse rate of the cutting nozzle) as well as on various mechanical properties of the materials being cut. However, certain macro-scale surface features can be identified which are typical of AWJ-machined surfaces in general, for both metals and composite materials [5, 6]. Figure 2 shows representative photomicrographs of AWJ-produced cut surfaces in both (a) metal, and (b) composite samples. As seen in the figure, three separate zones can be distinguished on each surface, representing three distinct phases of cutting behavior along the penetration track, thought to arise from changes in abrasive attack angle and total jet energy at increasing cut depth. Following the terminology of Arola and Ramulu [1, 16], the region along the top edge of the kerf, at and just below the jet entry point, is known as the *initial damage region* (IDR). Below the IDR is the *smooth cutting region* (SCR), a band of uniform roughness containing little or no low-frequency waviness or other large-amplitude irregularity. Abrasive impact angles are much smaller here than in the IDR above, and the R_a surface roughness in the SCR has been found to depend chiefly on abrasive particle size. Still further down, the smooth cutting region fades gradually into the *rough cutting region* (RCR), where curved, low-frequency striations of increasing trough-to-peak height begin to appear, tracing the rearward deflection of the jet path as the cutting nozzle advances through the material. These striation patterns are a manifestation of increasing instability of the jet and erosion process as the penetration depth increases, and lead to irregularities in the width and straightness of the exit kerf. The relative extents of the three regions on a particular cut surface are highly dependent on process parameters, and optimization of the cutting process for a particular material often amounts to selecting a combination of jet pressure, abrasive mesh and feedrate, and jet traverse rate which will extend the SCR sufficiently near the jet exit to yield an acceptable kerf taper and surface finish throughout the thickness.

Material removal in AWJ cutting occurs primarily through shear deformation induced by solid abrasive particle impact, and secondarily by the hydrodynamic action of the high-velocity water stream. The energy of the jet dissipates with increasing depth of penetration, and its principal direction is altered by deflection off of the erosion front as it advances along the cut path. This rearward deflection of the stream is evident in the curved striation patterns visible near the jet exit or in the RCR as can be seen in Figure 2. The curved shape of the material erosion front causes the impingement angle of the jet to become increasingly obtuse with increasing cut depth, resulting in top-to-bottom variations in abrasive particle impact angle which are thought to contribute to the depth dependence of the kerf surface morphology [4, 18]. Hence the precise physical mechanisms involved in the formation of these features, particularly the striation patterns characterizing the RCR, have been a subject of considerable investigation, with efforts focused on understanding the observed macro-scale surface morphology in terms of the underlying micro-mechanisms of material removal [19]. Burr formation at the kerf exit is another effect dependent on material properties and the removal mechanisms, with burr sizes ranging from 2.5 to 12.5 μm observed in thin metal samples. Burr size generally increases with increasing traverse rate and decreasing material yield strength.

Figure 3 shows SEM micrographs of AWJ-cut surfaces of aluminum (a) and titanium (b) alloy samples. In the aluminum sample, considerable deformation has occurred due to the repeated impacts of abrasive particles against the surface of the ductile material. Moreover, with increasing cutting depth the overall jet deflection angle and randomness in the angle of abrasive particle attack can be seen to increase. Similarly, the micrographs of the AWJ-machined surfaces of the titanium specimens exhibit significant degrees of plastic deformation near the jet entrance (IDR). Within this region the machined surface comprises an irregular structure, which appears to have been formed through repeated bombardment by abrasive particles, plastic embrittlement, and subsequent erosion. The distance through which this zone extends from the jet entrance, which is primarily governed by the standoff distance and degree of jet expansion prior to impact, did not vary significantly between the AWJ machined specimens. The extent of the IDR from the point of jet entrance was limited to approximately 125 μm along the kerf depth. However, the characteristics of the machined surface from the end of the IDR to the point of jet exit were extremely different from those within the jet entrance region. The two views in Figure 3 (a) and (b) are representative of features typically noted in AWJ-machined metal samples, despite variations in operating parameters. Throughout the penetration depth, no distinct differences are noted except for the gradual increase in abrasive deflection with depth of jet penetration. The features visible in these thin sample micrographs are also representative of those noted on inspection of thicker samples exhibiting the pronounced waviness patterns of a fully-developed rough cutting region (RCR). Within the RCR of the titanium samples, no difference in material removal mechanism suggested by these microscopic features was noted, although in general a decrease in abrasive path length and increase in path randomness was noted with increasing depth of cut due to the loss of jet energy with increasing penetration depth. Surface examination by scanning electron microscopy revealed the predominance of the shear deformation mechanism of material removal for all metal alloy samples, consistent with our previous results.

The SEM micrographs of Gr/Ep laminates are shown in Figure 3 (c) and (d). As can be seen, the surface of the 90°-ply Gr/Ep laminate (c) suggests that abrasive-induced brittle removal, including shearing and abrasive micro-machining, is the dominant mode of material removal. Figure 3 (d) shows the features of the 0° plies, which suggest that abrasive shearing and brittle fracture account for most of the material removal, similar to the 90° plies. The matrix remains intact on the machined surface, even though the surfaces of some exposed fibers are fractured. Stray abrasive particles at the exterior of the penetrating jet cause shallow abrasive wear tracks, which can be distinguished perpendicular to the fiber axis. This phenomenon is most pronounced near the jet entrance region under a combination of high supply pressure and large abrasive particles (small garnet mesh size). Examination of the +45˚ and -45˚ fiber oriented plies shows that, similar to the 90˚ and 0˚ plies, nearly all the supporting matrix remains intact on the machined surface. Figure 3.e shows the typical delamination and abrasive particle embedment occurring at the jet exit under sub-optimal cutting conditions.

EDX-ray analysis of AWJ-machined titanium surfaces has also shown significant embedding of fragmented abrasive particles. Silicon, a component of commonly-used abrasives, is known to be detrimental for crack initiation and long-term fatigue properties of metals, so further study is warranted on how the presence of embedded particle fragments may affect the fracture toughness and fatigue life of AWJ-machined components.

4.2 Effects of Material Properties and Process Parameters on Kerf Quality

Surface roughness and kerf taper are affected both by the properties of the target material and by a set of independently-variable process parameters, including jet pressure, orifice and mixing tube size, abrasive material, abrasive particle size and flow rate, and traverse rate of the jet nozzle across the material. Data compiled for thin (1.575 mm) sheets of Inconel 718, titanium and aluminum alloy using garnet abrasive exhibit trends typical for other metals. Increasing the traverse rate for a fixed pressure, particle size, and abrasive flow rate generally increases the surface roughness (Figure 4), as higher cutting speeds lead to more sparsely-distributed particle impacts as well as greater jet deflection which promotes transition from the SCR to the RCR. The sensitivity of surface roughness to traverse rate is substantially greater for smaller abrasive flow rates (Figure 4.c), reflecting the tendency toward more rapid jet energy loss and earlier development of the RCR associated with lower abrasive flows. The exit kerf width decreases with increasing traverse rate (Figure 5), with the rate of decrease becoming less rapid with increasing abrasive flow rate (Figure 5.c); however, for a given mass flow rate of abrasive, the average particle size has relatively little effect on the exit kerf width (Figure 5.d).

Comparison of the surface roughness vs. traverse rate curves for different particle sizes at a fixed abrasive flow rate (Figure 4.d) shows that roughness generally increases with increasing particle size. This trend holds throughout the IDR and SCR, where roughness is determined largely by erosion channel size, but may reverse in the RCR as striation formation induced by jet deflection and loss of particle energy begins to predominate. Varying the jet pressure for a fixed abrasive flow rate and particle size reveals some pressure dependence of the roughness vs. traverse rate relationship; in general, higher pressures yield smoother cut surfaces at a particular traverse rate, regardless of abrasive particle size. Kerf width and surface roughness variations are presented empirically in Table 4; these equations hold for thicknesses from 2 to 16 mm.

Although the surface texture resulting from AWJ machining of FRP made of tape material was extensively studied, only limited studies were done on fabric material. 5mm thick samples of tape and fabric composites were cut under the same conditions (Table 3), and evaluated for surface characterizing parameters. Figure 4.e shows the functional relation between surface finish and depth of cut. Surface roughness in fabric material was found to be a bit greater than in tape material. In addition, the abrasive grit size has a significant effect on the quality of the surface. As expected, higher grit size numbers (smaller grain diameters) produced better surface finishes in these materials. However, the surface roughness increased with the cutting depth regardless of the material composition.

5. SUMMARY AND CONCLUSIONS

Thin plate samples of inconel, aluminum and titanium alloys, and graphite/epoxy laminates of various fiber orientations were machined by abrasive waterjet to investigate the effects of process parameters on cutting performance for these materials. Distributions of average surface roughness R_a were obtained by surface profilometry, with different pressure settings, abrasive mesh sizes, and abrasive flow rates used to investigate the influences of process parameters on the resulting surface texture. The results confirmed that smaller traverse rates and finer abrasive mesh sizes generally yield smoother cut surfaces in all the materials tested. Larger abrasive particles (up to 300 μm diameter) generally yield less pronounced increases in R_a with increasing cut depth, reflecting a more gradual decline in jet energy associated with the larger particles. Smaller particles (150 μm diameter) produce smaller wear tracks and a smoother surface initially, but because the jet energy dissipates more rapidly on increasing penetration depth, the development of large-wavelength striations in the RCR is more severe, raising the overall R_a value toward the lower edge. The Ti6A14V samples showed the sharpest rise in R_a under the smaller particle operating condition. Exit kerf width and the resulting kerf taper were found to be largely controllable through the choice of pressure, traverse rate, abrasive size and abrasive flow rate for each material

Considerable efforts have been focused on the development of mathematical models of the AWJ material removal process, involving both theoretical analysis and the correlation of large amounts of cutting test data to establish empirical relationships between process parameters and cutting performance [5, 17, 18, 20]. The primary goals are accurate prediction of edge quality for any given material and set of process conditions, and the systematic determination of optimal process conditions for a particular cutting application. Of particular interest recently has been the application of process modeling to the control of kerf taper, by incorporating taper predictions into the motion controls of 2-dimensional AWJ shape cutting systems to produce compensating tilting motions of the jet nozzle.

ACKNOWLEDGEMENTS

The authors (MR) sincerely acknowledge the financial support of The Boeing Company.

REFERENCES

[1] Hamatani, G., and Ramulu,M., " Machinability of High Temperature Composites by Abrasive Waterjet" *Symposium on Machining Composites*, ASME Bound Volume, PED, Vol. 35, 1988, pp. 49-60

[2] Hashish, M., "Machining Advanced Composites with Abrasive Waterjets", Manufacturing Review, Vol.2, No.2, 1989, pp. 281-287

[3] Hashish, M., "Controlled depth of Milling of Isogrid Structures with AWJs", Journal of Manufacturing Science and Engineering, Vol.120, 1998, pp. 21-27

[4] Hashish, M., “Waterjet Machining of Composites and Ceramics”, Chapter 13, in Machining of Ceramics and Composites, edited by S. Jahanmir, M. Ramulu, and P.Koshy, Marcel Dekkar,Inc., NY 2000

[5] Momber, A. W. and Kovacevic, R., Principles of Abrasive Water Jet Machining, Springer, 1998.

[6] Arola, D. and Ramulu, M., "Material Removal in Abrasive Waterjet Machining of Metals, Surface Integrity and Texture," *Wear*, Vol. 210, No.2, 1997, pp. 50 – 58

[7] Edwards, M.R.,“Materials for Military Helicopters”, Proceedings of the Institution of Mechanical Engineers, Part G; Journal of Aerospace Engineering , Vol. 216, 2002, pp 77-88.

[8] Winston, M.R., Partridge, A., and Brooks, J.W., “ The Contribution of Advanced High Temperature Materials to Future Aero- engines” , Proceedings of the Institution of Mechanical Engineers, Part L; Journal of Materials Science and Design , Vol. 215, 2002, pp 63-73

[9] Metals Handbook, Machining, 1999, Vol. 16, Ninth Edition, ASM International, Metals Park, OH.

[10] Machado, A.R. and Wallbank, J., 1990, Machining of Titanium and Its Alloys – a Review, Proceedings of the Institution of Mechanical Engineers, Part B; Journal of Engineering Manufacture, Vol. 204, pp 53-60.

[11] Wang, D.H., Ramulu, M., and Arola, D., Orthogonal Cutting Mechanisms in Graphite/Epoxy, Part l: Unidirectional Laminate, *International Journal of Machine Tool & Manufacture*, Vol. 35, No.12, 1995, pp.1623-1638.

[12] Wang, D.H., Ramulu, M., and Arola, D., Orthogonal Cutting Mechanisms in Graphite/Epoxy, Part ll: Multi-directional Laminate, *International Journal of Machine Tool & Manufacture*. Vol. 35, No.12, 1995, pp.1639-1648.

[13] Ramulu, M., Wern, C.W., and Garbini, J.L., "Effect of Fiber Direction on Surface Roughness Measurements of Machined Graphite/Epoxy Composite," *Composite Manufacturing*, Vol. 4, No. 1, 1993, pp. 39-51.

[14] Arola, D. and Ramulu, M., Machining Induced Surface Texture Effects on the Flexural Properties of a Graphite/Epoxy Laminate, *Composites*, Vol. 25, No. 8, 1994, pp. 822- 834.

[15] Wern, C.W., Ramulu, M., and Colligan, K., A Study of the Surface Texture of Composite Drilled Holes, *J. of Materials Processing Technology*, Vol. 37, No. 1-4, February 1993, pp. 373-389.

[16] Hashish, M., Kirby, M.J., and Craigen, S.J., Abrasive Waterjet Cutting Data for Thin Sheet

Metal and Wear of Mixing Tubes, Flow International Corporation Technical Report No. 404, April 1987.

[17] Ramulu, M. and Arola, D., The Influence of Abrasive Waterjet Cutting Conditions on the Surface Quality of Graphite/Epoxy Laminates, *International Journal of Machine Tools and Manufacture*, Vol. 34, No. 3, 1994, pp. 295-313.

[18] Hashish, M., On the Modeling of Abrasive Waterjet Cutting, 7th Int Symp. Of Jet Cutting Technology, Ottowa Canada, June 26-28, 1984, pp. 249-265.

[19] Arola, D. and Ramulu, M., Micro-mechanisms of Material Removal in Abrasive Waterjet Machining, *Processing of Advanced Materials,* Vol. 4, No. 1, 1994, pp. 37-47.

[20] Blickwedel, H. and Guo, N. S., 1991, Prediction of Abrasive Jet Cutting Performance and Quality, 10th International Symposium on Jet Cutting Technology, pp. 163-179.

Table 1. Typical Aerospace Material Properties

Material	Specific Gravity	E (GPa)	σ_u (MPa)	σ_y (MPa)
Graphite/Epoxy	1.85	39	965	N/A
Al7075-T6 aluminum alloy	2.70	72	579	505
Ti-6Al-4V titanium alloy	4.43	110	1171	1068
Inconel 718	8.19	213.	1241	1,103

Table 2. Typical AWJ Cutting Conditions

Table 2. AWJ cutting conditions for Aluminum and Graphite/Epoxy
Traverse rate varied: 0.7 – 2.5g/s

Test	Jet Pressure (MPa)	Standoff (mm)	Garnet #/size #/ (µm)	Abrasive Flow Rate (grams/s)
A	207	2.5	50/350	10
B	138	2.5	50/350	10
C	207	2.5	100/135	10

Table 3. Typical Traverse Rates in AWJ Cutting of Aerospace Materials

Material	Thickness, mm	Traverse rate, mm/s
Graphite/Epoxy	6 16 25	18 5 2.8
Al7075-T6 aluminum alloy	1.6 4 6 10 25 100	22 18 8 3 2 0.5
Ti-6Al-4V titanium alloy	1 2 3 6 12 25	25 16 8 7 2 0.9
Inconel 718	6 25	5 0.8

Table 4. Empirical Equations developed in AWJ Cutting of Composites

Material: Fiber Reinforced Plastc Composites

AWJ Parameters: x_1 = Supply pressure (MPa), x_2 = Standoff distance (mm),
x_3 = Traverse rate (mm/s), x_4 = Grit size (Mesh#)
x_5 = The depth of cut (mm), x_6 = Abrasive flow rate (g/s)

Arola and Ramulu [17]	**Kerf width Profile** W_{kerf}: $$W_{kerf} = 1.305 - 0.146x_3 - 0.019x_4 + 0.056x_5 - 0.000006x_1^2 + 0.015x_3^2 + 0.000076x_4^2 - 0.002x_2^3 - 0.000025x_5^3 - 0.0002x_1x_2 + 0.0006x_1x_3 + 0.000026x_1x_4 + 0.000077x_1x_5 + 0.0123x_2x_3 + 0.0003x_2x_4 - 0.0079x_2x_5 - 0.0117x_3x_5 - 0.0005x_4x_5 + 0.0001x_1x_2x_3 - 0.000007x_1x_3x_4 + 0.00005x_2x_4x_5 + 0.000066x_3x_4x_5 + 0.508x_5^{-0.10}$$ $x_5 > 0$, $R^2 = 0.97$ **Surface finish**: $$R_a = 1 - 0.008x_1 + 1476x_4 - 3.0241x_3 - 1.0704x_2 - 0.9781x_5 \; 0.0001x_1^2 - 0.0015x_4^2 - 0.28x_3^2 + 0.8398x_2^2 0.0626x_5^2 - 0.0002x_1x_4 + 0.0002x_1x_3 - 0.001x_1x_2 - 0.004x_1x_5 + 0.0664x_3x_4 + 0.0074x_2x_4 + 0.0119x_5x_4 - 1.055x_3x_2 + 0.119x_3x_5 - 0.0818x_2x_5$$ $R^2 = 0.96$

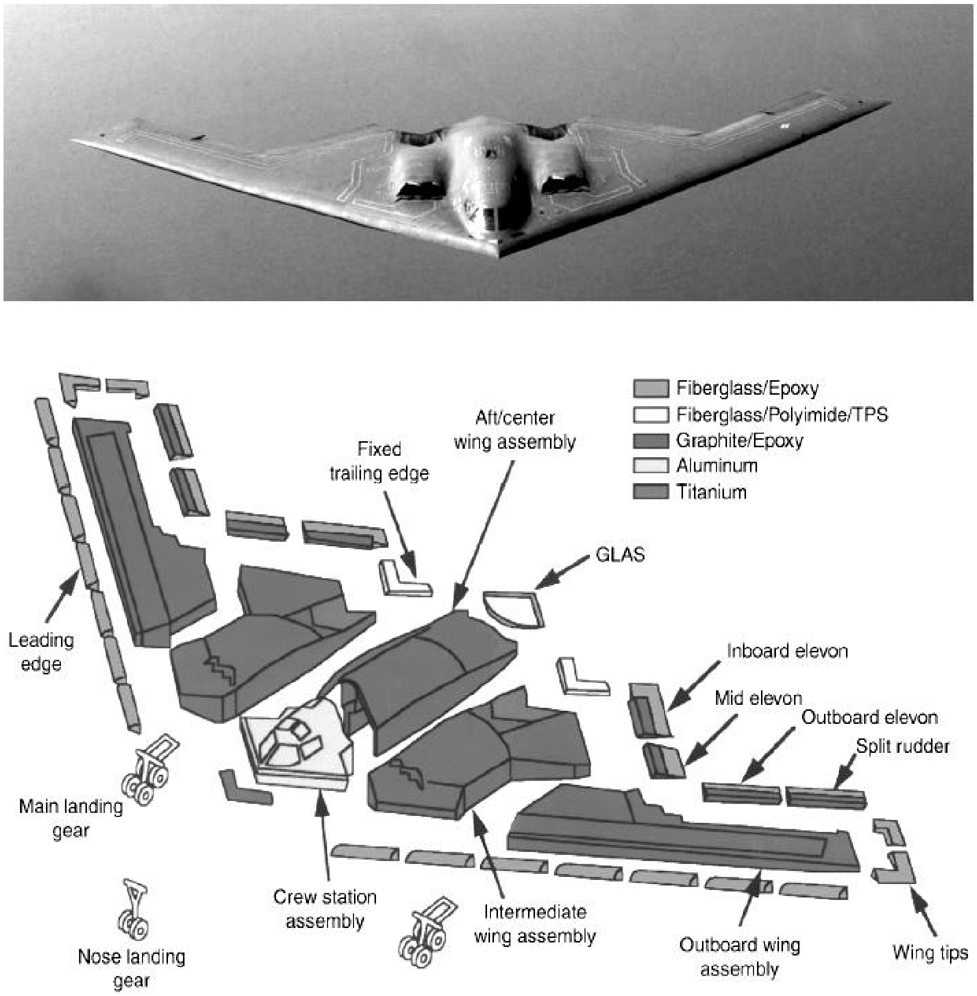

Figure 1: Materials used in the US Air Force B-2 Advanced "Stealth" Bomber [9]

(a) Kerf Surface of Sheet Metal Sample

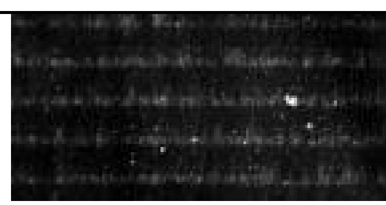

(b) Kerf Surface of Graphite/Epoxy Sample

Figure 2 : Typical Kerf Surface of Metal and Composite Sample

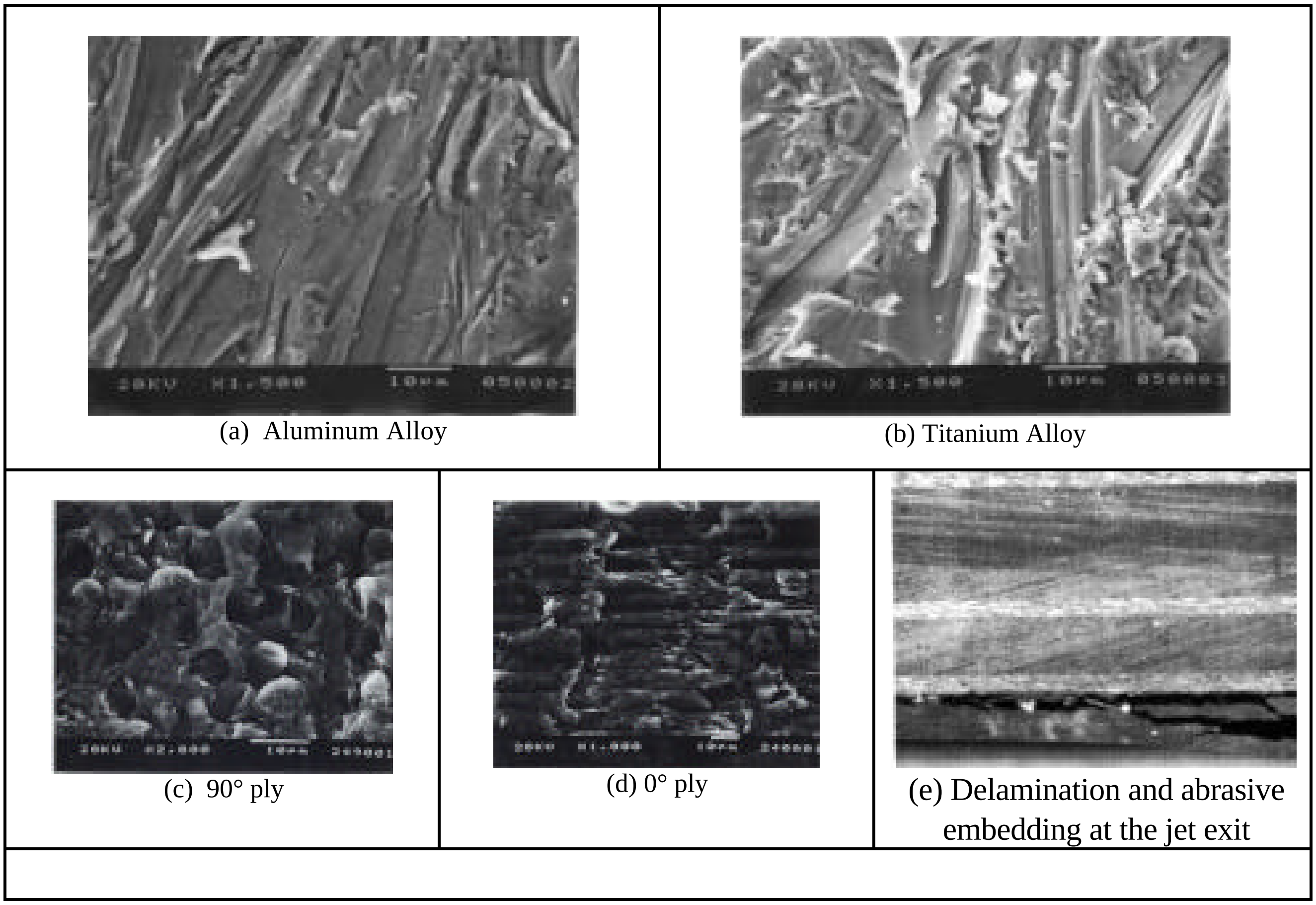

Figure 3. SEM Micrographs of AWJ-Machined (a) Aluminum alloy, (b) Titanium Alloy and (c) Gr/Ep Laminates

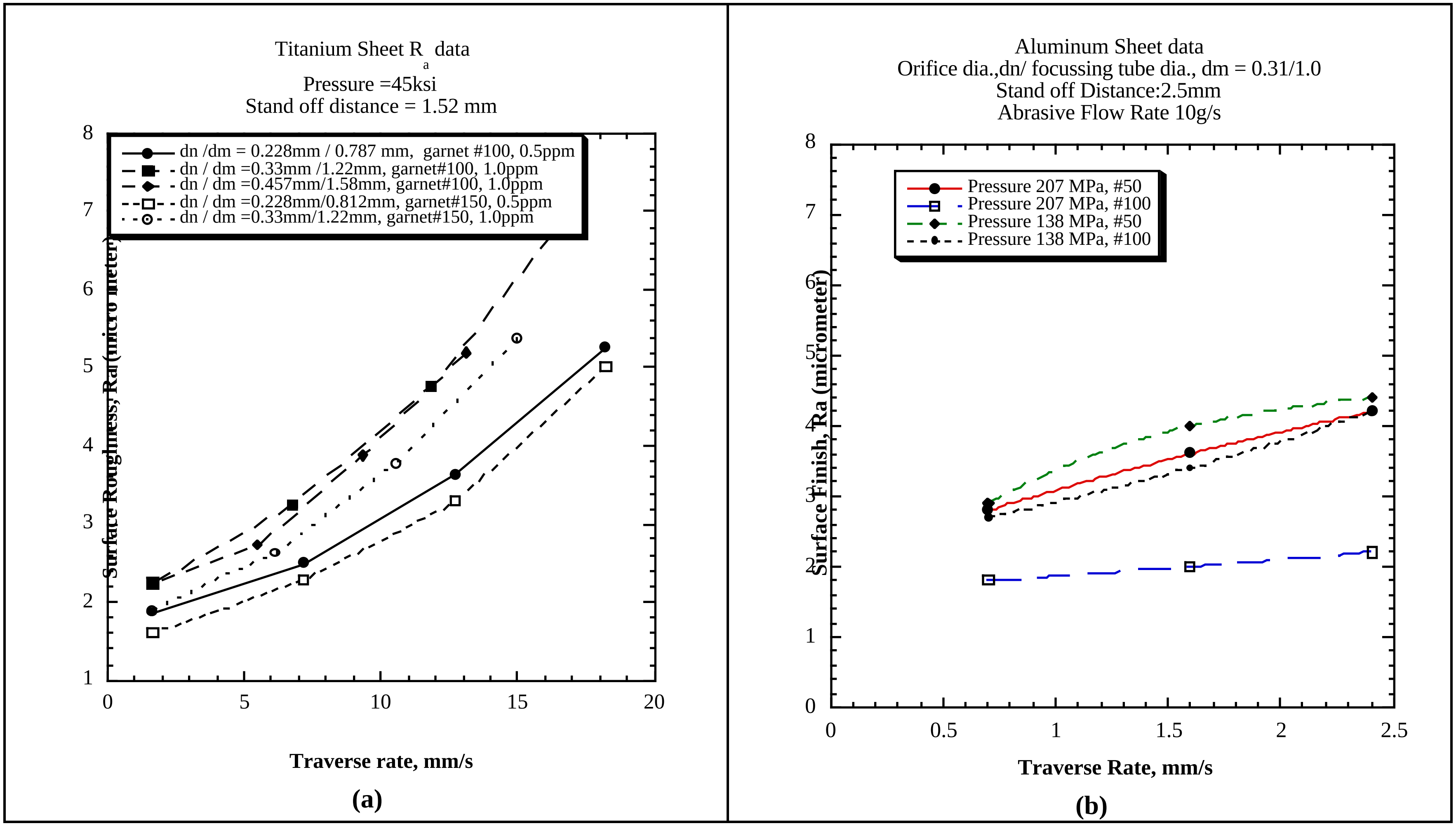

Figure 4. Surface Roughness Variations with Process Parameters for Titanium, Aluminum, Inconel 718, and Graphite/Epoxy (contd)

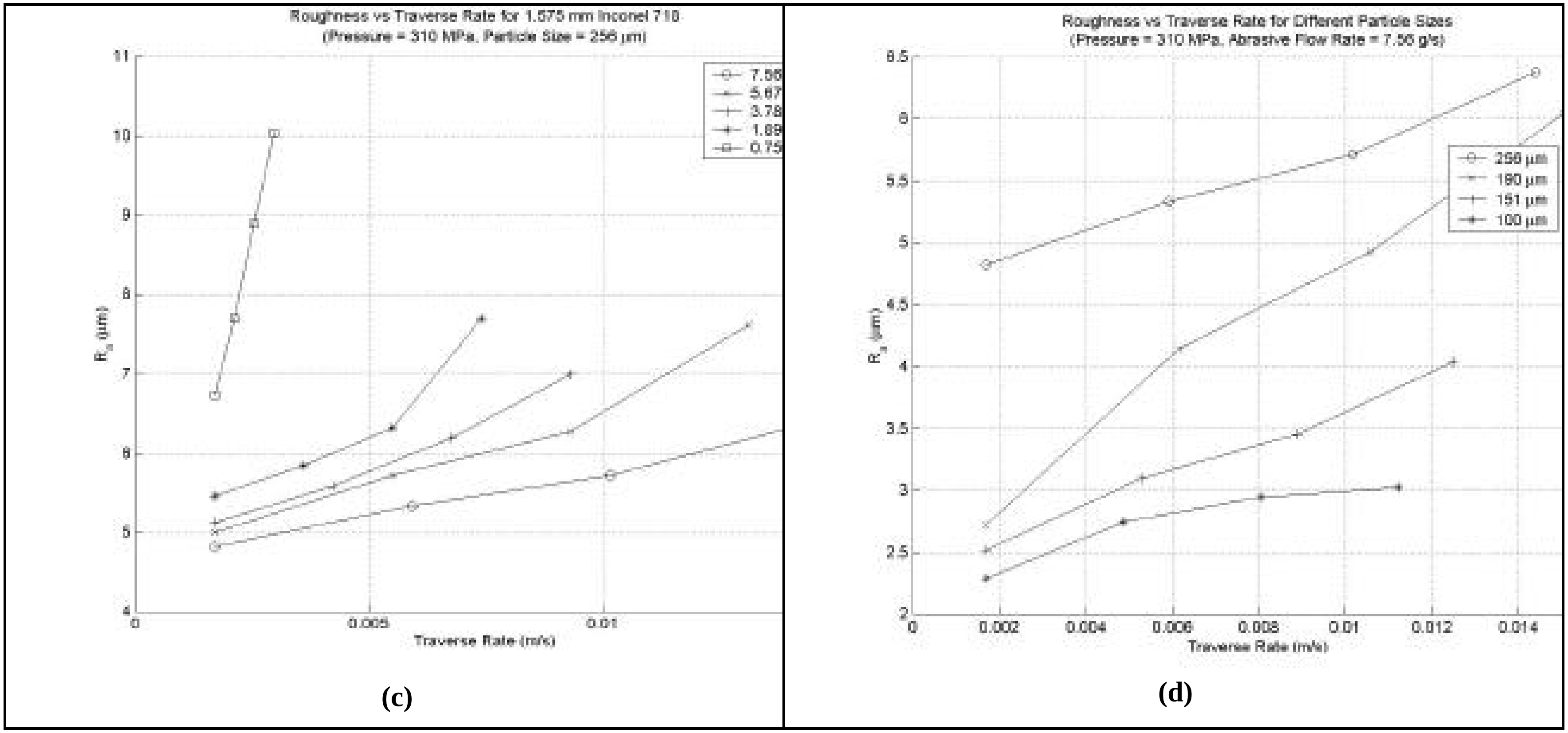

Figure 4. Surface Roughness Variations with Process Parameters for Titanium, Aluminum, Inconel 718, and Graphite/Epoxy (contd)

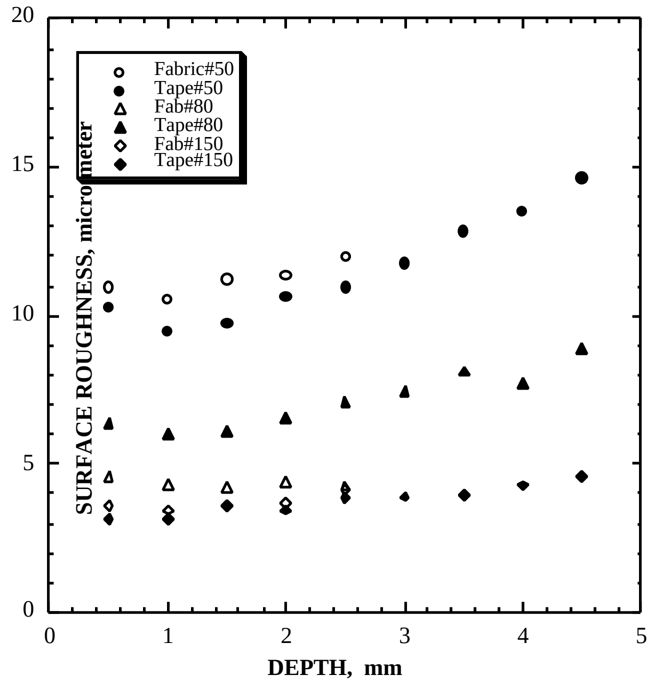

(e)

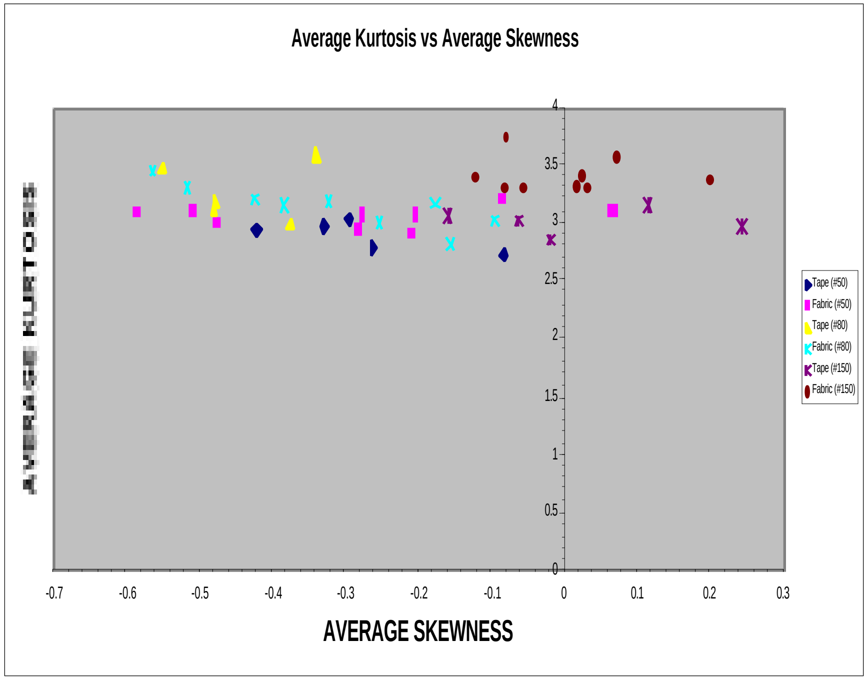

(f)

Figure 4. Surface Roughness Variations with Process Parameters for Titanium, Aluminum, Inconel 718, and Graphite/Epoxy

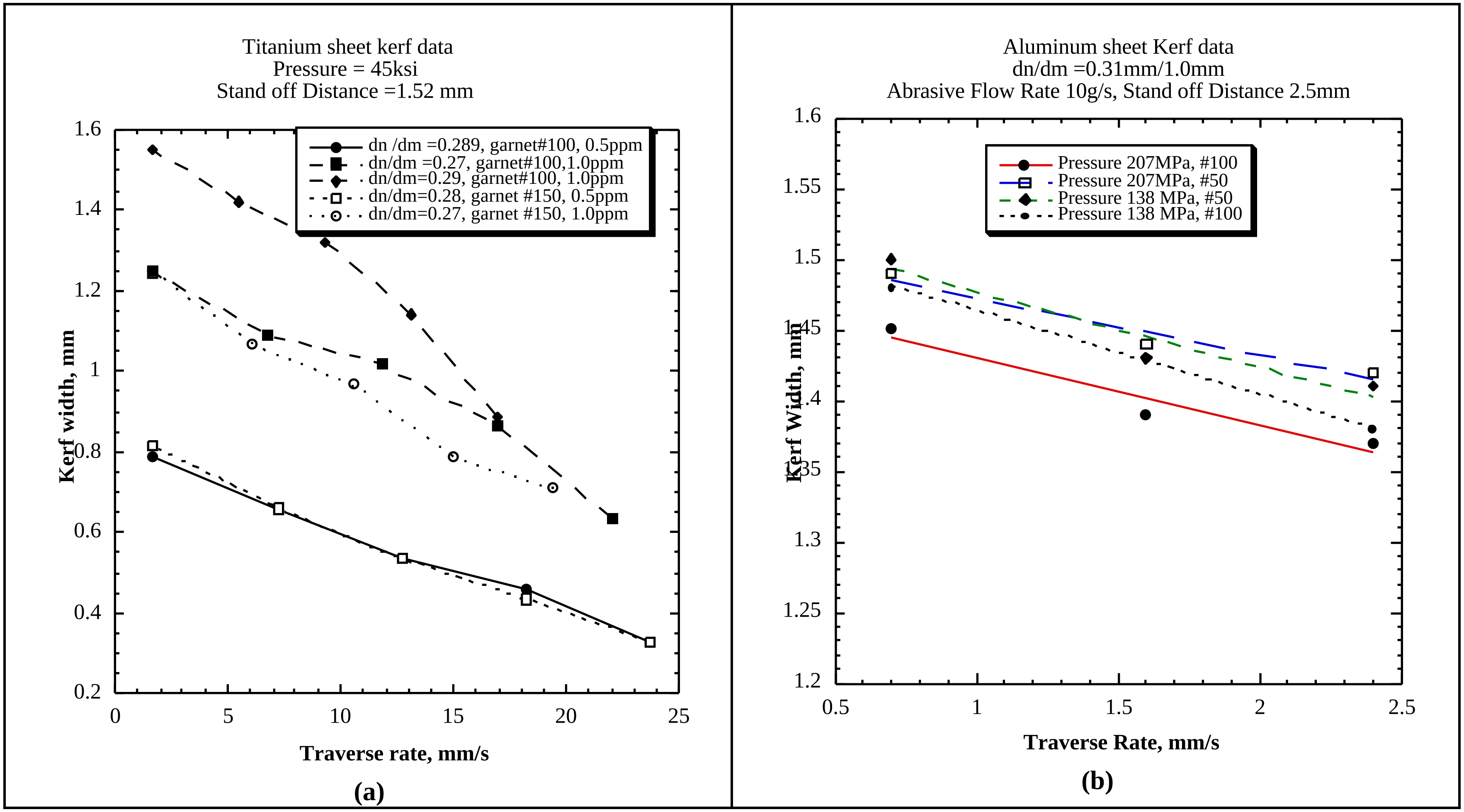

Figure 5. Kerf Width Variations with Process Parameters for Titanium, Aluminum and Inconel 718 (contd)

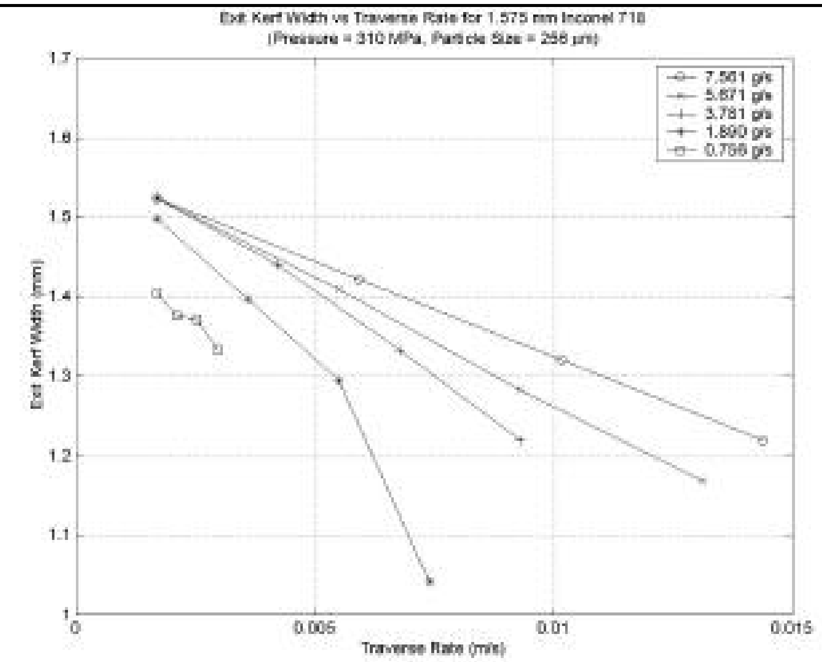

(c)

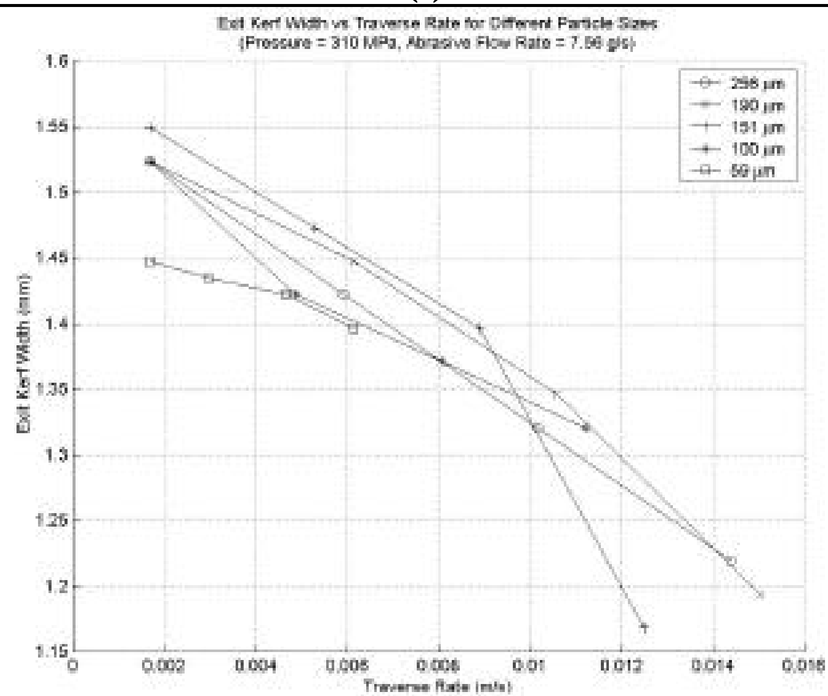

(d)

Figure 5. Kerf Width Variations with Process Parameters for Titanium, Aluminum and Inconel 718

2003 WJTA American Waterjet Conference
August 17-19, 2003 ● Houston, Texas

Paper 3-A

MEASUREMENT OF PARTICLE VELOCITIES IN HIGH SPEED WATERJET TECHNOLOGY

Anuja Dorle, L. John Tyler, David A. Summers
University of Missouri – Rolla
Rolla, Missouri, USA

ABSTRACT

The aim of this project is to measure the velocity of abrasive particles injected into high-velocity fluid flows and to study ways of improving the energy transfer that accelerates these particles. In water/abrasive jet cutting, the combination of abrasive particles and a high pressure waterjet produce an effective cutting stream, for a wide range of products. This research describes an investigation into abrasive particle behavior based on experimental determination of particle velocity.

In these experiments, small steel shot acts as a suite of magnetic particles and are mixed with the conventional garnet abrasive in the same size range. This mixture is injected into both conventional abrasive waterjet (AWJ) systems as well as into abrasive slurryjet (ASJ) systems to compare the two. In each case, the resulting cutting stream is directed through a pair of current-carrying coils spaced a fixed distance apart. The magnetic particles induce a signal in each of the coils in turn, which is recorded on a digital storage oscilloscope. Knowing the fixed distance between the coils and determining the time between the signal responses from each of the coils one can find the particle velocity.

Typical AWJ results show that, the general waterjet velocity ranges from 1000 to 2000 feet/second as a function of driving pressure. Within this waterjet stream velocity range, injected abrasive particles achieve average velocities of only about 400 feet-per-second indicating an inefficient energy transfer. The relatively low overall efficiency of the waterjet as an accelerating medium is explained by the failure of the particles to be effectively embedded into the jet stream and by the presence of air. The ASJ system gives a better acceleration over the AWJ system producing particle velocities close to that of the carrying waterjet.

1. INTRODUCTION

Conventional abrasive waterjet (AWJ) cutting is a technique in which abrasive particles are accelerated by a small diameter, high velocity waterjet and directed at the material to be cut [4]. High-pressure abrasive waterjet cutting technology makes use of water pressures above 250 MPa (equivalent to 35 Kpsi) to generate an abrasive laden water beam with a typical diameter below 1 mm.

While the more conventional AWJ process accelerates the particles in the waterjet stream after the water has accelerated, a more advanced process called the abrasive slurry jetting (ASJ) system in which the abrasive is premixed with the water before it is accelerated has recently become more popular and potentially more effective. In this technology the water and abrasive are mixed in the feed line from the pump and thus both accelerate together [8]. As a result this system is able to cut at one-quarter of the pressure of the AWJ system, at equivalent flow rates. It is one purpose of this work to explain this difference. Although there have been previous studies of abrasive velocity measurement from AWJ systems, this is the first that studies the two with a similar technique and then utilizes the results to explain the performance differences.

1.1 The Major Objectives

The purpose of this paper is to measure the abrasive particle velocity issuing from a high pressure AWJ nozzle as well as that coming from a nozzle fed by the ASJ system. The current method of mixing abrasive particles in AWJ technology with a very high velocity waterjet stream has limited the effectiveness of the system. The general water jet velocity is from 300 to 600 m/second or more. The abrasive particles enter the mixing chamber at essentially zero velocity, so the majority of particles have no chance of penetrating the jet until it disrupts with distance and instead bounce off into the nozzle walls and with each other [2]. They are further fragmented by impact with the jet itself. The present mixing and acceleration of the abrasive by means of the waterjet is relatively inefficient. To improve performance in water/abrasive jet cuttings, it would appear necessary to increase the abrasive particle velocity by some technique.

The abrasive particle velocity measurement is not only aimed at improving the AWJ or ASJ system cutting performance but also deals with several other parameters. The major goal of this paper is to design the system that gives the velocity and acceleration measurements on two different systems, conventional AWJ as well as ASJ. For each system the unit has been tested with different types of commercially available nozzles to compare the performance of the existing nozzle designs and examine ways of improving it. At the same time different sizes of steel shot and abrasives have been used in the testing and the trials were carried out from a minimum pressure of about 9 MPa (120psi) up to a maximum of 350 MPa (50000psi) (Table 1).

2. COMPARISON OF CONVENTIONAL AWJ & ASJ CUTTING SYSTEMS

AWJ cutting is a promising technology today, since it offers distinct benefits over conventional cutting tools, particularly in the cutting of very hard materials. In a conventional abrasive waterjet system abrasive particles are mixed with and accelerated by a stream of high velocity water produced through a nozzle onto the target [3]. In this method of abrasive injection the energy contained in the accelerated high pressure jet stream is used to create a suction which draws abrasive into the jet valve within a special mixing chamber (Figure 1). This system requires a mixing chamber where dry abrasives are mixed with high-pressure water.

The ASJ method feeds abrasive into the water from a containment vessel, which has been pressurized to the same pressure as the water stream. This system is also known as the Direct Injection of Abrasive jet or DIAjet (Figure 2). Research at UMR has shown that, at equivalent water flow rates, the ASJ system will cut as deeply as the AWJ system, but at a quarter of the pressure (Figure 3). Since the power of the jet is the product of the flow and pressure this might suggest that the AWJ system is cutting at only quarter of its potential [1]. Using the ASJ system one can currently gain higher efficiency as long as an excellent mixture can be obtained. Also, operating pressure can be reduced to a less expensive and more readily available level. In addition the AWJ system requires nozzles rigidly attached to the feed tube with the abrasive added near the cutting head, which is not possible in every case, such as cutting in remote areas or when cutting in some hazardous conditions [13].

3. WHAT IS PARTICLE VELOCITY

The use of the abrasive waterjet for machining or finishing purposes is based on the principle of erosion of the material upon which the jet hits [5]. Erosion is a word used today to describe a broad range of similar mechanisms relating to material removal by a series of independent, but similar impact events. Two common mechanisms of particle erosion are abrasion and fracture. Abrasive erosion is typically associated with shallow angles of impact, while fracturing and crack propagation is usually associated with perpendicular angles of particle impact although the failure mechanism is also controlled by the target material. Brittle materials generally fail by fracture, while ductile ones are removed by more of a plowing action of the particle. For significant material removal, in either case, one of the critical parameters is particle velocity. This topic presents the results of an experimental program of particle velocity measurement in abrasive cutting streams.

Most conventional abrasive injection systems entrain the abrasive at the cutting head and employ a small diameter waterjet to accelerate the abrasives. The water is pressurized and then expelled through a sapphire nozzle of diameter d [10]. The waterjet and the entrained stream of abrasives are then recollimated into an abrasive jet stream of diameter D by passing through a second colliminating nozzle of length L. Analysis of the momentum transfer between the waterjet and the abrasives is very complicated. To simplify the analysis, consider a single abrasive particle as it is picked up by the waterjets.

Abrasive particles induced in a steady jet of fluid do not reach the maximum jet velocity immediately, rather the particle velocity increases steadily until its velocity matches that of the surrounding fluid. This final fluid velocity will be somewhat less than that at which the waterjet stream entered the mixing chamber. Assuming that the abrasive particle was originally spherical in shape, then, according to the rules of fluid mechanics, the equation of motion of the spherical particle can be expressed as follows:

$$\frac{4}{3} \pi r^3 \rho_p \frac{dv}{dt} = \frac{1}{2} C_0 \rho_j \pi r^2 (u - v)^2 \qquad (1)$$

where:

r = sphere radius
ρp = particle density
v = particle velocity
Co = resistance coefficient dependent on Reynold's number; which may be taken as a constant to simplify the calculation.
ρj = jet density
u = jet velocity

If a property K is defined such that

$$K = \frac{8}{3} \frac{r}{C_0} \frac{\rho_p}{\rho_j} \qquad (2)$$

Then it is possible to derive from equation (1)

$$\frac{du}{dt} = \frac{(u - v)^2}{K} \qquad (3)$$

If equation (3) is now integrated with regard to time, assuming that at t = 0, v = 0, one can derive the approximate equation for particle velocity at time t as

$$v \cong u \frac{ut}{ut + \frac{8}{3} \frac{r}{C_0} \frac{\rho_p}{\rho_j}} = u \frac{ut}{ut + K} \qquad (4)$$

This equation can be rewritten in order to determine the time at which a certain relative velocity ratio (v/u) is achieved as follows:

$$t = \frac{v}{u} \frac{K}{u - v} \qquad (5)$$

One can also, by a double integration with regard to time, translate this into a distance which the particle will have to travel to achieve this velocity in the form

$$l_p = K\left[\frac{v}{u - v} - \ln\left(1 + \frac{v}{u - v}\right)\right] \qquad (6)$$

Conversely, this equation can be rewritten, substituting for K, in the form:

$$l_p = \frac{8}{3}\frac{r}{C_0}\frac{\rho_p}{\rho_j}\left[\frac{v}{u - v} - \ln\left(1 + \frac{u}{v}\right)\right] \quad (7)$$

Alternatively, equation (6) can be rewritten to determine the time t required for the particle to travel the distance of lp

$$l_p = K\left[\frac{ut}{K} - \ln\left(1 + \frac{ut}{K}\right)\right] \quad (8)$$

The above relatively simple calculation allows one to predict the relative acceleration and final velocity of the particles as a function of the distance from the point at which the abrasive is first entrained. Thus, one might for example, find that it would be necessary for the abrasive particle to travel a distance of almost 200 mm before it would achieve 95% of the jet velocity. In reality, the distance required may significantly differ from this value since the abrasive particle is not suspended in a pure water stream because the originally entrained air is also present in this three-phase flow. The presence of the air may reduce or increase the efficiency of the mixing process, extending or reducing the distance and time required to achieve maximum particle velocity.

4. PARTICLE SIZE

It is important to consider data from the measurement of abrasive crushing during abrasive passage through the nozzle assemblies [7]. Testing has shown that the abrasive cutting performance drops considerably below an abrasive size of 100 µm (140 mesh). The data on the product size distribution generated from the different nozzles was therefore re-evaluated measuring only the amount of abrasive that survived passage at a size of 100 µm and more (Table 2). This suggests that if a way could be found to feed the abrasive into the mixing chamber with a smaller number of collisions between particles then more of the particles at higher feed rates might survive and improve the cutting under those conditions [11].

The unit to measure the garnet abrasive particles is called Grit or Mesh. The particle size in mesh/grit and its equivalent size in micron are shown (Table 3). The steel shot that are mixed with the abrasive as magnetic particles have the opposite measuring terminology to that of abrasive measurement unit. If the mesh/grit number is large the abrasive is smaller (Table 3). In steel shot sizes, if the number is large the size is also large (Table 4).

Not only has the size of particle affected the velocity performance. The reduced particle speed is equivalent to that of a jet traveling at a lower pressure (roughly equivalent for example at 280 MPa to a jet traveling at 70 MPa) but then also it leaves the question as to where the energy has gone that was originally available.

5. EFFECT OF THE AIR CONTENT ON PARTICLE VELOCITY

Although similar experiments are not carried out to validate their conclusions, it is probable that the answer lies in work that was carried out at the School of Mines at Douai in France [6] where an investigation showed that the AWJ jet was made up of up to 95% air and that it was this air, and the need to accelerate it, that was absorbing the energy (Figure 4). Given that the air is using up to 75% of the energy available to accelerate the particles, it appears to be a fruitful line of investigation to investigate ways of introducing the particles into the water stream without the use of such large volumes of carrier fluid. While the ASJ system is one way of doing this, other designs built around existing AWJ nozzle designs are being looked at.

Two small additional observations are worthy of note. Firstly the smaller abrasive size seems to be accelerated to a higher initial velocity than the larger particles and secondly that the larger particles are not being accelerated much above the velocity given at 280 MPa. This might suggest that generally the collimating tube for the nozzle design is not long enough to allow the larger particles to be accelerated to full velocity at higher pressures, while it is long enough for the smaller particle sizes and lower pressures.

While there is much work that remains to be done on developing better nozzle designs, a more immediate concern, however, has been to examine the failure patterns that have been found in existing nozzle designs and to examine ways of improving that performance.

6. EXPERIMENTAL VELOCITY MEASUREMENTS

To make actual measurements of the particle velocities, a method illustrated in Figure 5 was developed. Initially the cutting stream immediately below the director nozzle is encircled by five small coils of wire connected to sensing electronics and timing circuitry. Magnetic particles of steel shot of the same general size as the abrasive particles are mixed with the abrasive and accelerated in the same stream [9]. When one of the magnetic particles passes through the second coil, the transit time between the fixed coil spacing distances can be measured accurately and this value is used to calculate the individual particle velocity. In this approach the important parameters to consider are the distance between the two coils, the diameter of the brass tube on which the coils are going to be wound, the amplifier IC, the noise filtering components, the choice of high strength magnets, etc [12]. Initial experiments were carried out using the distance of 3.7 cm between two adjacent coils and this distance was approximately estimated by the formula needed for the particle velocity V = distance between two coils/time or distance between two coils = velocity * time.

The factors related to the amplifier selection were gain bandwidth product, noise factor and cost. The AD524 is a precision monolithic instrumentation amplifier (Figure 6). It has guaranteed low offset voltage, offset voltage drift and low noise for precision high gain applications. The AD524 is functionally complete with pin programmable gains of 1, 10, 100 and 1000, and single resistor programmable for any gain. The use of a strong magnet mounted near each coil was intended to make the signal more visible. When coils cut an emf after sensing the movement of steel shot inside it, the strong magnet acts as an amplifier. In other words, the voltage change was made more significant by placing a strong magnet next to the coils to increase the magnetic flux as the steel passes through the coils. The type of magnet selected was a Rare Earth magnet.

The major goal was to increase the speed of the shot between 150 and 300 meters per second. By decreasing the diameter of the plastic tube, the air velocity was greater, thus propelling the small shot to higher velocities. The inner diameter of the new tube was closer to that of the water-jet. Additional coils were also made with the same outer diameter as the tube. The new coils were more sensitive because of their closer proximity to the shot. The current equipment is capable of measuring four coil signals at once, thus allowing four velocity measurements to be made in one trial.

7. EXPERIMENTAL RESULTS

The particle velocity of the abrasive is measured by various means. The unit described above was tested on different types of waterjet systems, different types of nozzles, different sizes of steel shot and different types of abrasives. The particle velocities obtained are compared between waterjet cutting systems and nozzle designs.

7.1 Velocity and Acceleration Calculations

The coil assembly contains a total of five coils, four coils for actual velocity measurement and a fifth one which acts as a reference. Figure 7 shows the coil arrangement for four basic coils where, S= distance in meters. T= time in seconds. All the calculations were made using this coil arrangement. The average velocity of the steel shot or abrasive from coil 1 to coil 2 is (S1 / T1). Velocity is measured as distance/time. There are three velocities V1=S1/T1, V2=S2/T2, V3=S3/T3 for each experiment.

Acceleration is measured as velocity/time. It is assumed that the acceleration of the steel shot is constant throughout the coil tube.

S1 = uT1 + ½ a (T1^2)
S2 = uT2 + ½ a (T2^2)
Where “u” is the initial velocity of the steel shot at the Coil 1 and “a” is acceleration.

Solving for Acceleration “a”, we get
a1 = (2/ (T1-T2) * [S1/T1 – S2/T2]... for (T1, T2)
Similarly,
a2 for (T1, T3) is
a2 = 2/ ((T1-T3) * [S1/T1 – S3/T3]... for (T1, T3)

7.2 Initial Experiments

The initial experimental arrangement and velocity measuring device are illustrated in Figure 8 and 9. Here, a single air driven steel shot was fired through the coil assembly using an air compressor with a capacity of 9 MPa, and the transit time was determined by means of a transient recorder or Digital Storage Oscilloscope. The signal from the spherical steel shot is shown by the repeated waveform, displaced by the transit time. Figure 10 shows the graph of average velocity measurement for different trials using the smallest steel shot available S70.

The name of the files used in Figure 10 is related to the coil assembly number. CLA2S170 means it is the second coil assembly file tested with steel shot of size S170. Each coil set was tested six times using every available size of steel shot. Therefore, there were a total of 18 trials carried out using each coil set and for three sizes of steel shot. The next step was to test the whole set up on different waterjet systems.

7.3 Experiments made on a Conventional AWJ System

The testing unit was set up in front of a particular nozzle, with a selected abrasive, pressure and steel shot and mounted on the OMAX cutting tank (Figure 11). The figure shows the dual D.C. power supply (ranging from 0 to 25 V) on the right side of the trolley. There is a Lecroy DSO used to show the amplitude-time response from the experiment on the left side of the trolley. The five amplifier unit covered with aluminum shields is on the top of the DSO.

Typical results of the particle velocity measurements are illustrated in Figure 13. Here, the pink trace represents signals from the first coil, while the cyan (sky-blue) trace represents signals from the second coil. The brown trace is for the third coil and blue is for the fourth. The record has been triggered by a particle moving through the first coil at T = 0. This particle, marked “la” in the figure, is recorded by the second coil, marked “lb", 69 microseconds later. This particle has a calculated initial velocity V1 of 434 meters-per-second. Similarly velocities V2 from second to third coil and V3 from third to fourth coil are calculated (Table 5).

7.4 Comparison of Nozzle Performance

The instrument was used with different nozzles to compare their performance. The velocity waveforms obtained in figure 14 was matched with the predicted results for the designated nozzle. The three nozzle patterns are differentiated by giving particular names to each. CW170-1 is the velocity pattern of the first trial taken with only water with nozzle C. Similarly CAG means Nozzle C-Abrasive-Garnet i.e., the trial was carried out with garnet abrasive on C nozzle. BAO is Nozzle B-Abrasive-Olivine and AAG means Nozzle A-Abrasive-Garnet.

The waveform pattern above clearly indicates the best nozzle design. The lowest waveforms are all related to nozzle C. The two patterns are for water only and for a water-abrasive feed test. This nozzle gave a steady performance for increasing pressure but the velocity range obtained was really low when compared with the other two nozzles in this trial. The topmost pattern is the mixture of A and B nozzle tests. The steady wave in the middle is that of nozzle A. Only this nozzle gave almost equal velocities for tests carried out without and with abrasive feed. The total velocity values were the highest when compared to the other two nozzle velocities. The particles were accelerated at a constant rate. The nozzle B when it gave velocities in a higher range than nozzle A produced a totally oscillating pattern. The waveforms were not consistent and it was hard to determine the average velocities and the acceleration. The nozzle A proved to be the best design among all.

7.5 Experiments made on ASJ System

The Abrasive Slurryjet (ASJ) System was found to be a better system over the Conventional Abrasive Waterjet (AWJ) in terms of energy transfer efficiency. It can provide exactly the same cutting performance as an AWJ system but at much lower pressure scale. The velocity measurement unit was tested on the ASJ system at pressures of 140, 350 and 700 MPa. The purpose was to compare the velocity results of both the systems and analyze the performance. Figure 12 shows the setup arranged for ASJ system. The diameter of the nozzle used was 0.75 mm. The abrasive used was garnet. The steel shot used was of the size S170. The comparative graph shows the difference between two cutting systems (Figure 15).

The velocities for the shot were equal to that of the water for the ASJ but only half that for the AWJ and that explains the difference in the cutting performance.

8. CONCLUSIONS

The current AWJ system of mixing abrasive particles with a high velocity water jet stream has limited effectiveness. If the particles could be injected directly in the center of the jet, they should acquire essentially the full jet velocity within two cm or less of travel. This method is used in ASJ system. The particle velocity was found to be nearly equal to the water velocity at higher pressures.

Typically the nozzle length should be at least ten times the diameter in order to ensure that the particles are brought up to full velocity prior to delivery to ambient conditions. In an AWJ system the delivery nozzle is slightly tapered outward from the throat in order to provide additional acceleration for the particles to maximum velocity. These design considerations are somewhat seen in the current ASJ system. That has increased the effectiveness of the total velocity measurement design system.

9. ACKNOWLEDGEMENT

Several UMR students contributed to the development of the equipment used in this work, over and above the graduate students included as authors, that help and the help of the technical and administrative staff in the Rock Mechanics and Explosive Research Center at UMR is gratefully acknowledged.

10. REFERENCES

1. Samir P. Dorle, “Developing the technique for penetrating and inspecting destroyed buildings,” M.S. Thesis, University of Missouri Rolla, May, 2003.

2. R. K. Swanson, M. Kilman, S. Cerwin, and W. Tarver ,Southwest Research Institute, San Antonio, Texas, R. Wellman, U. S. Government, Washington, D. C., “Study of Particle Velocities in Water Driven Abrasive Jet Cutting,” Proceedings of the 4th U.S. Waterjet Conference, August 26-28, 1987, Berkeley, CA.

3. Summers, D. A. (1995), “Waterjetting Technology,” Book, E & FN SPON, ISBN #: 0 419 19660 9, First Edition 1995, 882 pp.

4. Hashish, M., “A Modeling Study of Metal Cutting with Abrasive Water Jets," Trans. ASME, Vol. 106, January, 1984, pp. 88-100.

5. Bitter, J.G.A., “A Study of Erosion Phenomena-Part I," Wear, Vol. 6, 1963, pp. 5-21.

6. Tabitz, Schmidtt, Parsy Abriak, and Thery “Effect of Air on acceleration process in AWJ entrainment system,” 12th ISJCT, Rouen, 1994 p 47 - 58.

7. Galecki, G., Summers, D., “Steel Shot Entrained Ultra High Pressure Waterjet for Cutting and Drilling in Hard Rocks,” 11th International Symposium on Jet Cutting Technology, St. Andrews, Scotland, September 8-10, 1992.

8. Hashish, M. (1984), Hashish, M., "Aspects of Abrasive-Waterjet Performance Optimization," Proceedings of the 8th International Symposium on Jet Cutting Technology, BHRA,Durham, England, September, 1986. pp. 297-308.

9. Hashish, M. (1983), “Experimental Studies of Cutting with Abrasive Water Jets,” Proc. of the 2nd U.S. Water Jet Conference, Rolla, MO, January, l984.

10. Fairhurst, R. M., “Abrasive Water Jet Cutting,” MSc thesis, Cranfield Institute of Technology, January, 1982.

11. See www.pan-abrasives.com

12. See http://engr.smu.edu/rcam/research/waterjet/ProcessParameter/Abrasiveparticles.pdf

13. Hashish, M., “Cutting with High Pressure Abrasive Suspension Jets,” paper 33, 6th American Water Jet Conference, Huston, TX, August, 1991, pp.439-455.

11. GRAPHICS

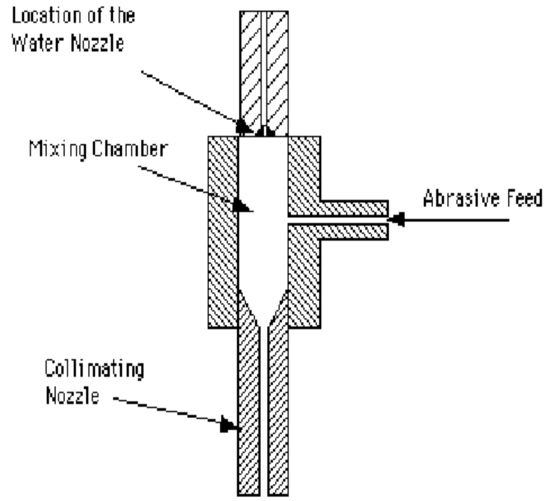

Figure 1. Conventional Method of Abrasive Injection

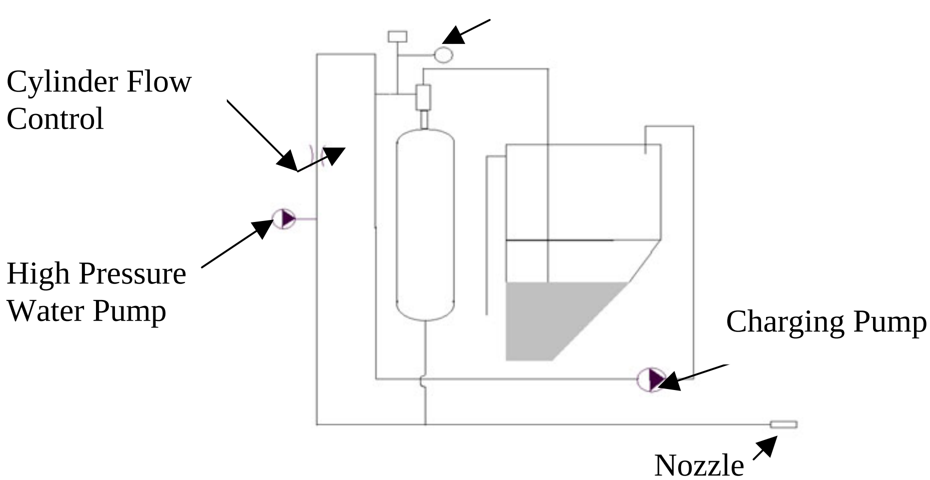

Figure 2. Schematic representation of the DIAjet flow circuit.

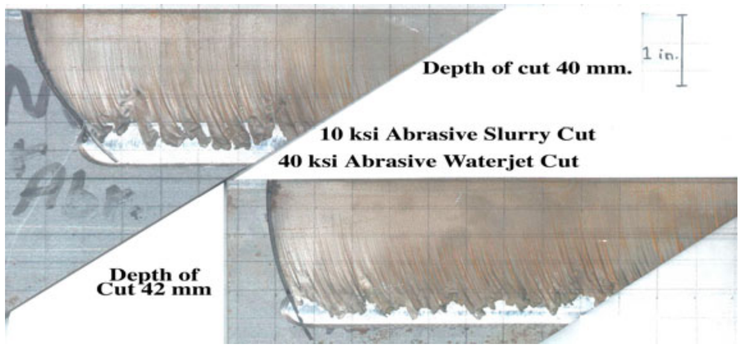

Figure 3. Comparative cuts between the most commonly used AWJ nozzle at 280 Mpa and an ASJ nozzle operated at the same water flow rate at 70 Mpa.

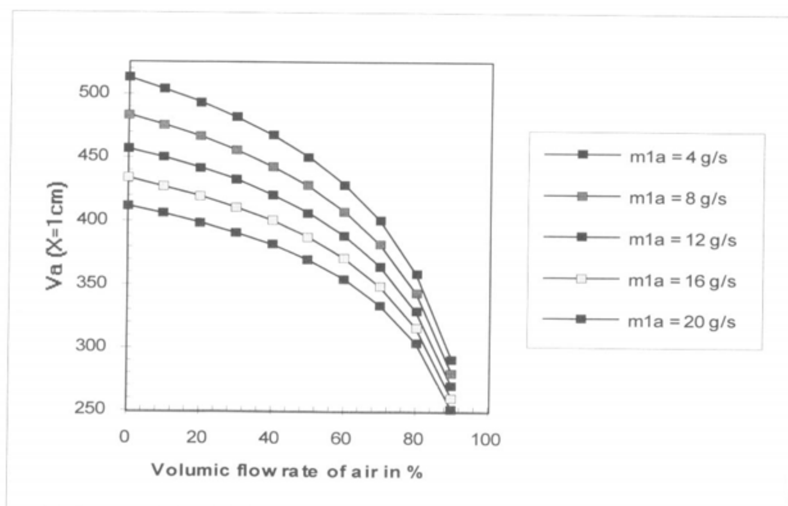

Simulations of the influence of air on the particle velocity.

Figure 4. Effect of air content on abrasive particle velocity (after Tabitz, et al.).

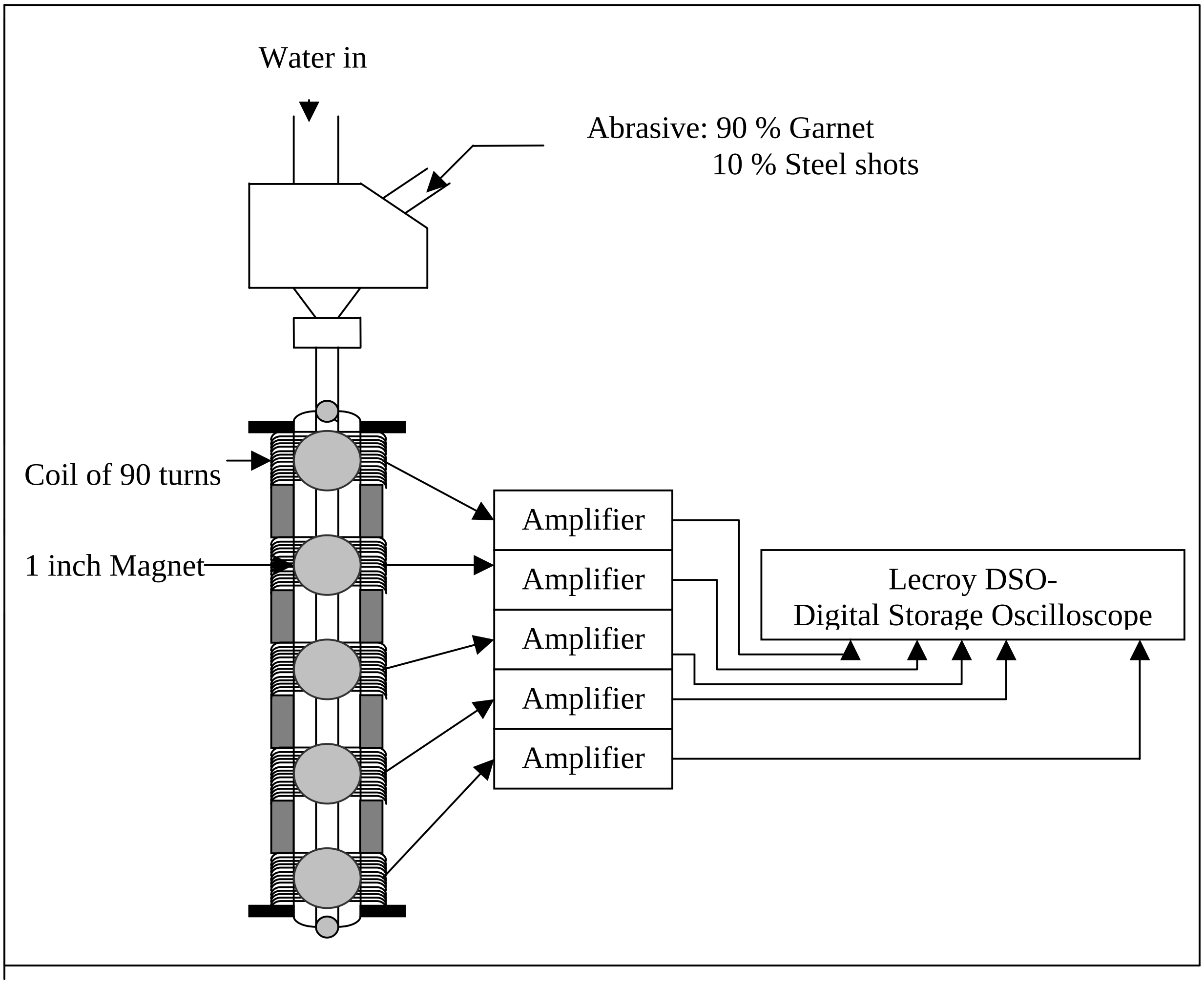

Figure 5. Experimental Setup.

FUNCTIONAL BLOCK DIAGRAM

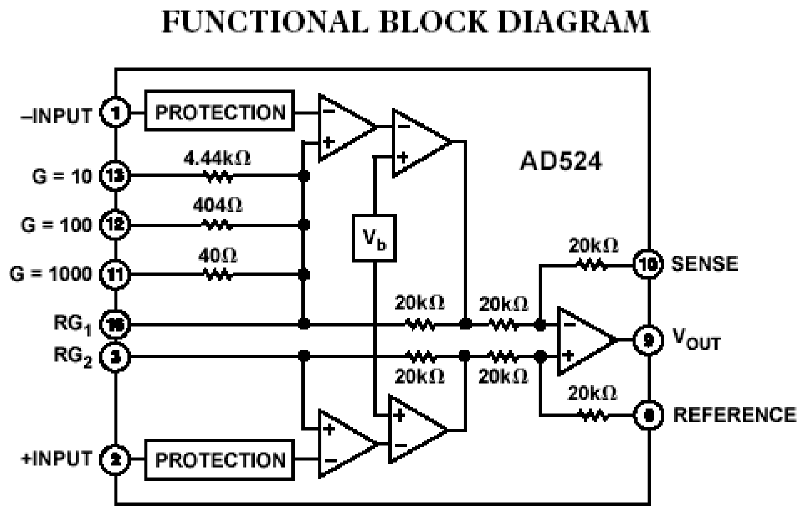

Figure 6. Precision Instrumentation Amplifier.

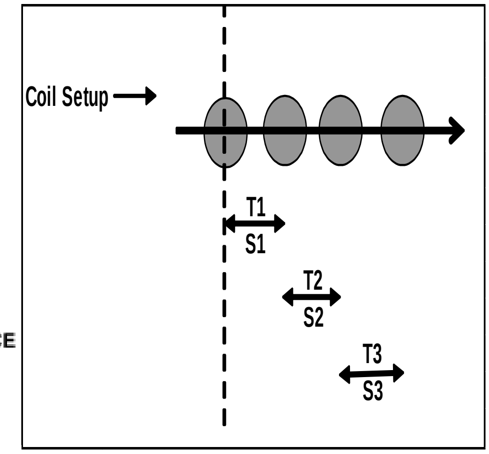

Figure 7. Basic coil arrangement.

Relative velocity Measurement:At constant pressure of ~120psi
Steel shot size S70 ~ Grit size 120 (0.125 to 0.425mm)

Filename	Trial #	V1	V2	V3
CLA2S70	1	210.97	224.21	238.1
	2	109.65	133.33	142.5
	3	185.18	167.79	140.5
	4	185.87	202.43	212.8
	5	199.2	202.44	218.3
	6	150.61	165.02	187.3
CLA3S70	7	114.29	119.05	124.2
	8	121.95	141.84	149.3
	9	124.23	153.85	157.5
	10	192.31	200	210.5
	11	110.49	125.79	133.3
	12	138.89	138.89	126.6
CLA4S70	13	169.5	175.44	181.8
	14	139.85	145.99	175.4
	15	125.78	143.88	165.3
	16	137	153.85	175.4
	17	129.88	147.06	153.9
	18	185.2	194.17	212.8
CLA5S70	19	158.72	158.73	170.9
	20	118.35	128.21	148.2
	21	166.68	175.44	194.2
	22	210.53	222.21	224.7
	23	176.98	173.91	186.9
	24	150.37	162.6	177
CLA6S70	25	177	186.92	188.7
	26	148.16	158.73	170.9
	27	198.02	210.51	200
	28	153.86	158.73	163.9
	29	141.84	163.93	163.9
	30	208.33	224.69	224.7
CLA7S70	31	177	188.68	204.1
	32	144.93	155.04	162.6
	33	165.29	169.49	172.4
	34	168.07	177	177
	35	153.85	166.67	161.3
	36	173.91	183.49	192.3
CLA8S70	37	119.76	115.61	117.7
	38	169.49	194.17	200
	39	183.48	186.92	183.5
	40	165.29	160	158.7
	41	152.67	166.67	169.5
	42	168.07	152.67	149.3

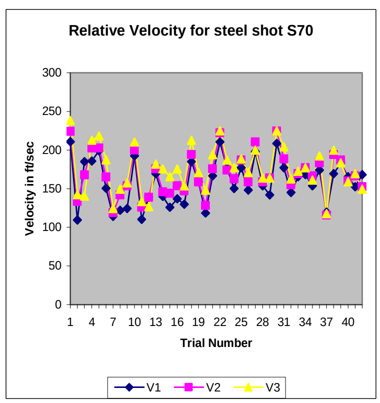

Average Velocity V1	139.1071
Average Velocity V2	143.2402
Average Velocity V3	150.8893

Figure 10. Average velocity measurement for S70.

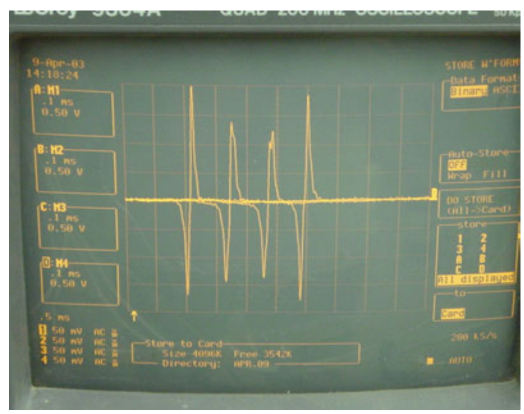

Figure 8. Recording data on DSO.

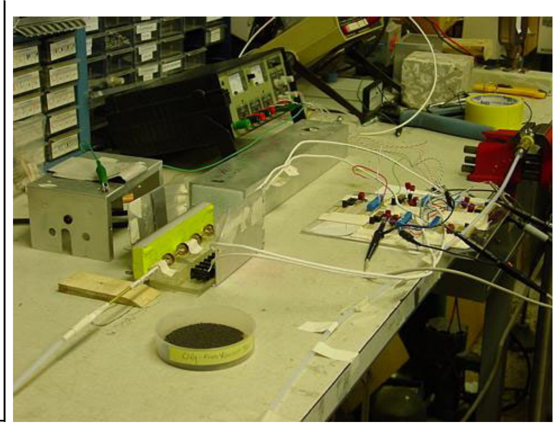

Figure 9. Initial Experimental Setup.

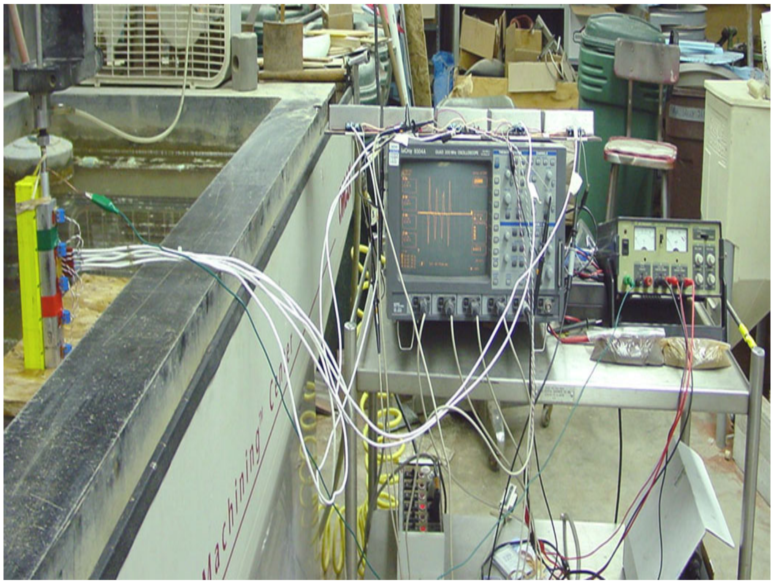

Figure 11. Arrangement of the testing unit on OMAX tank.

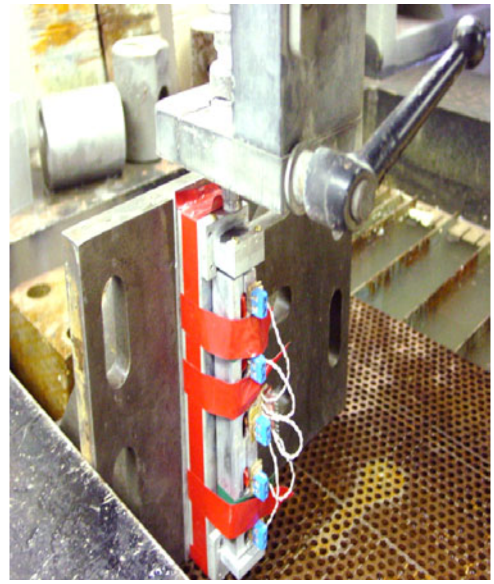

Figure 12. ASJ system set up.

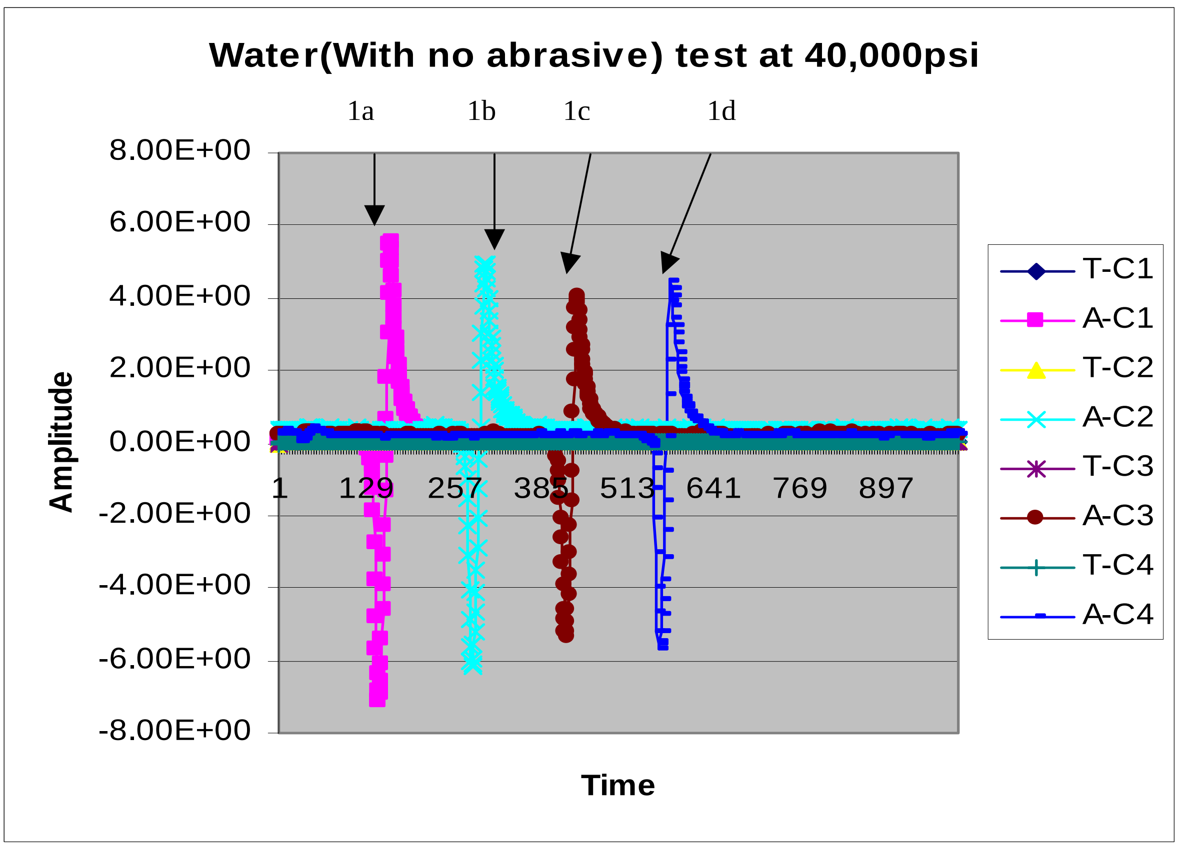

Figure 13. Plot for velocity calculation related to data in Table 5.

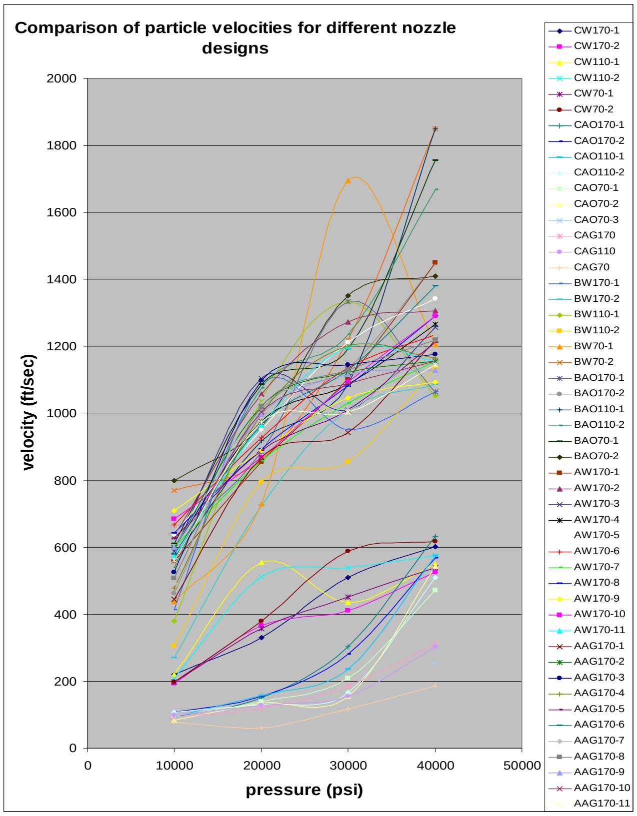

Figure 14. Comparison of velocities for different Nozzle designs.

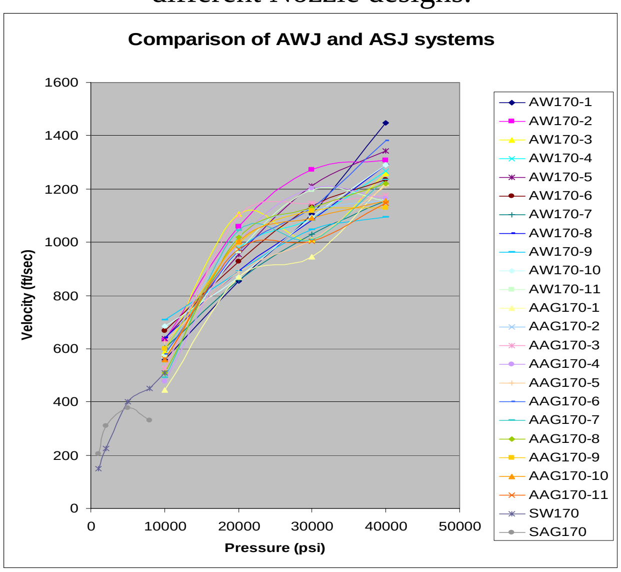

Figure 15. Comparison of accelerations for Different Nozzle designs where SAG170 means Slurry-Abrasive-Garnet-S170 and SW170 is Slurry-Water only-S170 test.

Coil 1(C1)		Coil 2 (C2)		Coil 3(C3)		Coil 4(C4)			
Time	Ampli.	Time	Ampli.	Time	Ampli.	Time	Ampli.	5.5625	Max Amplitude (Max
T-C1	A-C1	T-C2	A-C2	T-C3	A-C3	T-C4	A-C4		
-4.96E-08	0.125	-4.96E-08	0.375	-4.96E-08	0.25	-4.96E-08	0.25	164	Sample no of MaxA1
4.50E-07	0.125	4.50E-07	0.375	4.50E-07	0.25	4.50E-07	0.313	0.00007995	Time for MaxA1 (**t1**)
9.50E-07	0.125	9.50E-07	0.375	9.50E-07	0.25	9.50E-07	0.25		
1.45E-06	0.125	1.45E-06	0.375	1.45E-06	0.25	1.45E-06	0.313	4.9375	Max Amplitude (Max
1.95E-06	0.125	1.95E-06	0.375	1.95E-06	0.25	1.95E-06	0.313	302	Sample no of MaxA2
2.45E-06	0.125	2.45E-06	0.375	2.45E-06	0.25	2.45E-06	0.313	0.00014895	Time for MaxA2 (**t2**)
2.95E-06	0.125	2.95E-06	0.375	2.95E-06	0.25	2.95E-06	0.313		
3.45E-06	0.125	3.45E-06	0.375	3.45E-06	0.188	3.45E-06	0.375	4.0625	Max Amplitude (Max
3.95E-06	0.125	3.95E-06	0.375	3.95E-06	0.188	3.95E-06	0.375	439	Sample no of MaxA3
4.45E-06	0.125	4.45E-06	0.375	4.45E-06	0.188	4.45E-06	0.313	0.00021745	Time for MaxA3 (**t3**)
4.95E-06	0.125	4.95E-06	0.313	4.95E-06	0.25	4.95E-06	0.313		
5.45E-06	0.125	5.45E-06	0.375	5.45E-06	0.25	5.45E-06	0.313	4.4375	Max Amplitude (Max
5.95E-06	0.125	5.95E-06	0.375	5.95E-06	0.25	5.95E-06	0.313	576	Sample no of MaxA4
6.45E-06	0.125	6.45E-06	0.375	6.45E-06	0.25	6.45E-06	0.313	0.00028595	Time for MaxA4 (**t4**)
6.95E-06	0.063	6.95E-06	0.375	6.95E-06	0.188	6.95E-06	0.313		
7.45E-06	0.125	7.45E-06	0.375	7.45E-06	0.25	7.45E-06	0.25	1449.275362	Velocity V1
7.95E-06	0.125	7.95E-06	0.375	7.95E-06	0.188	7.95E-06	0.313	1459.854015	Velocity V2
8.45E-06	0.125	8.45E-06	0.313	8.45E-06	0.188	8.45E-06	0.313	1459.854015	Velocity V3
8.95E-06	0.063	8.95E-06	0.313	8.95E-06	0.188	8.95E-06	0.25		
9.45E-06	0.063	9.45E-06	0.375	9.45E-06	0.188	9.45E-06	0.25	0.000069	**T1** = (t2 -t1)
9.95E-06	0.063	9.95E-06	0.313	9.95E-06	0.188	9.95E-06	0.313	0.0001375	**T2** = (t3 - t1)
1.05E-05	0.125	1.05E-05	0.375	1.05E-05	0.188	1.05E-05	0.25	6.49894E-13	DENOM
1.10E-05	0.125	1.10E-05	0.313	1.10E-05	0.125	1.10E-05	0.25	1E-07	NUMER
1.15E-05	0.063	1.15E-05	0.25	1.15E-05	0.188	1.15E-05	0.25	153871.3059	a1 acceleration (T1,
1.20E-05	0.063	1.20E-05	0.25	1.20E-05	0.188	1.20E-05	0.25		
1.25E-05	0.125	1.25E-05	0.25	1.25E-05	0.125	1.25E-05	0.25	0.000206	**T3** = (t4 - t1)
1.30E-05	0	1.30E-05	0.25	1.30E-05	0.063	1.30E-05	0.188	1.94732E-12	DENOM
1.35E-05	0	1.35E-05	0.25	1.35E-05	0.063	1.35E-05	0.125	2E-07	NUMER
1.40E-05	-0.063	1.40E-05	0.188	1.40E-05	0	1.40E-05	0.063	102705.3619	a2 acceleration (T1,
1.45E-05	-0.063	1.45E-05	0.188	1.45E-05	0.063	1.45E-05	0.063		
1.50E-05	-0.063	1.50E-05	0.188	1.50E-05	0	1.50E-05	0.063	1443.966802	U initial velocity a1
1.55E-05	-0.063	1.55E-05	0.188	1.55E-05	0	1.55E-05	0.125	1443.966802	U initial velocity a2
1.60E-05	-0.063	1.60E-05	0.188	1.60E-05	0.063	1.60E-05	0.125		
1.65E-05	-0.063	1.65E-05	0.188	1.65E-05	0.063	1.65E-05	0.125	1443.966802	U NEW (T1, T2)
1.70E-05	0.063	1.70E-05	0.25	1.70E-05	0.063	1.70E-05	0.125	153871.3059	a1 NEW
1.75E-05	0	1.75E-05	0.25	1.75E-05	0.125	1.75E-05	0.188		
1.80E-05	0.063	1.80E-05	0.25	1.80E-05	0.125	1.80E-05	0.188	1445.732027	U NEW (T1, T3)
1.85E-05	0.063	1.85E-05	0.313	1.85E-05	0.188	1.85E-05	0.25	102705.3619	a2 NEW
1.90E-05	0.063	1.90E-05	0.313	1.90E-05	0.188	1.90E-05	0.25		
1.95E-05	0.125	1.95E-05	0.375	1.95E-05	0.25	1.95E-05	0.25	1451.00212	U NEW (T2, T3)
2.00E-05	0.125	2.00E-05	0.375	2.00E-05	0.313	2.00E-05	0.313	51539.41799	a NEW
2.05E-05	0.125	2.05E-05	0.375	2.05E-05	0.25	2.05E-05	0.313		
2.10E-05	0.125	2.10E-05	0.375	2.10E-05	0.25	2.10E-05	0.375	0.0000685	T4 = (t3 - t2)
2.15E-05	0.125	2.15E-05	0.438	2.15E-05	0.313	2.15E-05	0.313	0.000137	T5 = (t4 - t2)
2.20E-05	0.188	2.20E-05	0.438	2.20E-05	0.313	2.20E-05	0.375		
2.25E-05	0.125	2.25E-05	0.375	2.25E-05	0.313	2.25E-05	0.375	1459.854015	U (T4, T5)
2.30E-05	0.188	2.30E-05	0.438	2.30E-05	0.25	2.30E-05	0.313		
2.35E-05	0.188	2.35E-05	0.438	2.35E-05	0.313	2.35E-05	0.313	1.77456E-08	a1 acceleration (T4,

Figure 16. Data for Nozzle A -Water with no abrasive test at 280 Mpa.

12. TABLES

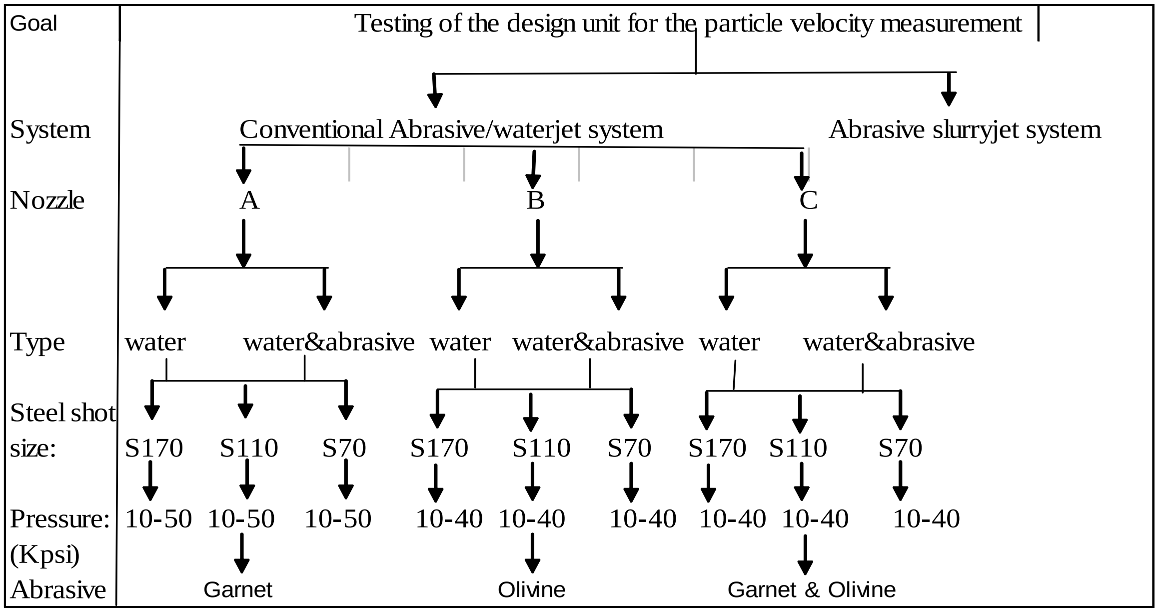

Table 1. Design and Testing Topology.

AFR/ Pressure	30,000 psi	40,000 psi	50,000 psi	Average
0.6 lb/min	72.7	68.3	64.6	68.6
1.0 lb/min	72	67	64.3	67.8
1.5 lb/min	70.5	61.6	59.3	62.4
Average	71.7	65.6	62.7	

Table 2. Percentage of abrasive at 100 µm or greater as an average of the first six nozzles tested and as a function of AFR and pressure.

Mesh/Grit #	Micron(µm)
60	250
80	177
100	150
120	125
140	106
160	75

Table 3. Different sizes of garnet abrasive.

Steel shot size	Millimeter(mm)
S330	0.710 to 1.400 mm
S280	0.600 to 1.180 mm
S230	0.500 to 1.000 mm
S 170	0.355 to 0.850 mm
S 110	0.180 to 0.600 mm
S 70	0.125 to 0.425 mm

Table 4. Different sizes of steel shot.

2003 WJTA American Waterjet Conference
August 17-19, 2003 • Houston, Texas

Paper 3-G

MONITORING OF THE AWJ CUTTING IN THE SUBMERGED CONDITIONS

Andrej Lebar, Bostjan Jurisevic and Mihael Junkar
University of Ljubljana
Faculty of Mechanical Engineering
Ljubljana, Slovenia

ABSTRACT

In this paper a novel approach to the monitoring of the AWJ cutting process in the submerged conditions is presented. To measure the water back-flow force, induced by the jet detection on the cutting front the back-flow pressure sensor was used. The sensor was mounted on the cutting head in the position opposite to the traverse direction of the AWJ cutting head. Electrical signal from the pressure sensor was sampled by A/D converter and stored for off-line processing. The AWJ cutting head traverse velocity was set to five different values with a central value at the separation cutting speed.

Processing of the signals acquired by the pressure sensor showed, that the most informative is a distribution of pressure amplitudes. A beta function was fitted to the distribution of pressure amplitudes, thus reducing the amount of data to two parameters of beta function. It was found out, that parameters of beta function could be used as an AWJ cutting process performance index.

With the experiment presented in this paper it has been shown, that the AWJ cutting process can be monitored on-line by using the pressure sensor which measures the water backflow force behind the AWJ cutting head, even in the case when using the water catcher tank.

1 INTRODUCTION

Surface of the abrasive water jet (AWJ) machined workpiece exhibits random roughness character with superposition of periodic striations which diminishes the AWJ machining effectiveness. In the shop floor there are typicaly few cut and try cycles applied to obtain the near optimal process parameters. In the core of the present state of the art AWJ machines computer control are advanced semi-empirical models as the one obtained by Zeng [1] or Yong and Kovacevic [2, 3] or even expert system as developed by Kovacevic and Kwak [4] or Singh et al. [5].

Optimisation of the AWJ machining based on the computer simulations as presented by Fukunishi et al. [6], Kovacevic et al. [3] or Lebar and Junkar [7] are still far away from the on-line applications, but will be included in the AWJ machining feedback control when the appropriate computer power and proper sensors will be available.

Present approaches to AWJ process results prediction are all based on a priori measurements and posteriori fitting of the data to the relations obtained by means of dimensional analysis or heuristics. In the contrary the computer control of the AWJ cutting makes AWJ very suitable for application in flexible manufacturing system [8], which enables to dynamically adapt the proces parameters to the machining conditions. The control algorithm for automated AWJ machining was developed already in the year 1987 by Mazurkiewicz at al. [9]. The general scheme has been developed by Kovacevic et al. 1997 [10]. Most of the AWJ machine related signals proposed by Kovacevic are already implemented in the up-to date AWJ machines, which is not the case for the signals in the “process sensing system” group. There are several obstacles for the application of the process sensing system as proposed, but we think, that too complex systems are not appropriate for the harsh environment of the AWJ machining systems.

In this paper a novel approach to the monitoring of the AWJ cutting process is presented. It is proposed to use the pressure sensor to measure the water back flow force induced by the jet deflection on the cutting front. This approach is applicable for the systems using water catcher tank. The water catcher tank is less health hazardous option to open catcher tank, due to much lower noise level and lower abrasive particles emission in the air [11].

2 EXPERIMENTAL SETUP

The influence of the AWJ cutting head traverse velocity on the waterjet backflow force was measured on a commercial AWJ cutting system with a water catcher tank. The experimental setup is schematically shown in Figure 1. It consisted of AWJ cutting system (OMAX 2652A), a screen which intercepted the water backflow, pressure sensor and a computer equipped with an A/D acquisition board.

The parameters which were kept constant during the experiment were: water jet pressure p=280 MPa, orifice diameter d_o= 0.3 mm and nozzle diameter d_f = 0.8 mm. Stand-off distance was set to the optimal value for the cutting application h_{so}=2.5 mm. Abrasive was garnet type GMA 80 mesh with mass flow rate set to 0.34 kg/min. Jet angle was set to 90^o. Experiments were performed with three different workpiece thicknesses: 5 mm, 10 mm and 30 mm. The workpiece material was the construction steel St37.

Having in mind that we want a relation between the parameters of the measured pressure signals and the AWJ cutting quality, we have chosen the cutting velocities to be related to a separation cut velocity v_{sc} for the particular workpiece thickness. The separation cut velocity v_{sc} of AWJ cutting is the velocity of AWJ cutting head traverse, at which AWJ separates the workpiece on the bottom of the cut on 98% of the length of the cut. The separation cut velocity was experimentally determined for the 10 mm thick workpiece and calculated for the 5 mm and 30 mm thick workpiece using the Zeng-Kim equation [1]:

$$v_t = \left(\frac{N_m \; p^{\alpha} \; \dot{m}_w^{\beta} \; \dot{m}_a^{\gamma}}{C \, q \, h \, d_j^{\delta}} \right)^{\varepsilon} \tag{1}$$

where N_m is the machinability number, p is the water pressure, $\dot{m}_w$ is the water-mass flow rate, $\dot{m}_a$ is the abrasive-mass flow rate, q is the quality level index, h is the thickness of the material and d_j is the diameter of the jet. Parameters α, β, γ, δ and ε are regression parameters. In the calculation we used only parameter ε, since all other parameters cancel each other when calculating the change of AWJ cutting head traverse velocity for different workpiece thickness. For ε we used ε =1.15 as suggested in the literature [1].

In a cycle of experiments each workpiece was machined with a set of five different velocities calculated as a separation cutting speed multiplied by the factor *f*: $v_t = f \cdot v_{sc}$. The set of factors used in this study was *f*={0.6, 0.8, 1.0, 1.2, 1.4} as presented in the Table 1. Experiment cycles were repeated five times, thus we performed 25 measurements on each workpiece thickness and consequently total of the 75 measurements were included in the processing of measured pressure signals.

A special screen shown in Figure 2 was mounted on the AWJ nozzle. It was made of thick PMMA plate with a milled cavity. Over the cavity a pressure sensor was mounted. It was a Motorola MPX5100 pressure sensor on-chip; temperature compensated and calibrated. It had a pressure measuring range from 0 up to 100 kPa. The sensitivity of the sensor was 45 mV/kPa and the precision 2.5%. The output voltage was fed to a computer equipped with National Instruments PCI-MIO-16E-4 data acquisition board driven by Matlab software. The electrical signal from the pressure sensor was sampled with frequency 20 samples per second and saved for posterior processing.

3 RESULTS AND DISCUSSION

In Figure 3 are shown three typical pressure signals obtained during the cutting of the workpiece of thickness h = 30 mm. Signals correspond to the experiments with cutting head traverse velocity equal to 0.6, 1.0 and 1.4 times separation cutting velocity, which in the case of the workpiece of thickness h = 30 mm equaled to v_{sc} = 1.0 mm/s.

In Figure 3 (a, b and c) three acquired pressure signals are presented. They correspond to the image of the bottom surface of the workpiece in Figure 3 d. The pressure signal (Fig. 3 a) correspond to the cut labelled ”good” and was cut with the traverse velocity of the cutting head equal to 60% of the separation cutting speed, thus $f = 0.6$. Pressure signals with $f = 1.0$ and $f = 1.4$ correspond to the cuts labelled with “separation” and “uncut” on the Figure 3 d.

It is obvious from Figure 3, that the amplitude of the pressure signals can be related to the quality of the cut. Unfortunately can amplitude analysis discriminate only significantly different quality of the cutting. Further on our study showed, that the histogram (distribution) of the pressure signal can be much more informative. In Figure 4 the pressure signal and the corresponding histogram normalized to values between 0 and 1 is shown.

A beta function was fitted to histograms of pressure signals in order to obtain two parameters representing the performance of the AWJ cutting process. In the integral form, beta function B is given with the expression in the following equation:

$$B(a,b) = \int_0^1 x^{a-1} (1-x)^{b-1} \, dx \ . \tag{2}$$

The range of the definition of the beta function is the interval [0, 1], therefore the distribution had to be normalised prior to fitting the beta function to the experimental data. Example of this procedure is also shown in Figure 4.

The results of the presented process performance determination are shown in the Figure 5. Particular measurements are presented as dots in the graph, where are the mean values of the groups of data with the same AWJ cutting head traverse velocity presented with markers.
Results are presented separately for each workpiece thickness. A very similar situation can be observed in Figure 5 a, b or c, regardless the sixfold increase of workpiece thickness. Moreover in the interesting range of AWJ traverse velocities, that is between 60% of the separation cutting velocity (f = 0.6) and separation cutting velocity (v_{sc}) a very good resolution in terms of parameters a and b.

4 CONCLUSIONS

Processing of the signals acquired by the pressure sensor showed, that the most informative is a distribution of pressure amplitudes. A beta function was fitted to the distribution of pressure amplitudes, thus reducing the amount of data to two parameters of beta function. It was found out, that parameters of beta function could be used as an AWJ cutting process performance index.

With the experiment presented in this paper it was shown, that AWJ cutting process can be on-line monitored even in the case when using the water catcher tank by using the pressure sensor which measures the water backflow after the AWJ cutting head.

5 REFERENCES

[1] J. Zeng and T. J. Kim. “Machinability of engineering materials in abrasive water jet machining.” International Journal of Water Jet Technology, p.p. 103-110, Vol.2 (2), 1995.

[2] Z. Yong and R. Kovacevic. “Simulation of chaotic particle motion in particle-laden jet-flow and application to abrasive waterjet machining.” Journal of Fluids Engineering, p.p. 435-442, Vol. 119, June 1997.

[3] Z. Yong and R. Kovacevic. “Modelling of 3D Abrasive Waterjet Machining, part I+II.”, pages 73-89, Jetting Technology, Mechan. Engrs. Publ., London,1996.

[4] R. Mohan, R. Kovacevic, H. S. Kwak: “AE sensing as a tool for understanding the mechanisms of AWJ drilling of difficult-to-machine materials”. Proc. Instn. Mech. Engrs., Journal of Engineering for Manufacturing, 212, Part B:45-58, 1998.

[5] Singh P.J. “Development of a window-based expert system for abrasive water jet cutting”. In T.J.Labus, editor, Proc. 8th Amer. Water Jet Conf., St.Louis, volume 2, pages 717-726. Water Jet Techn. Ass., 1995.

[6] Y. Fukunishi, R.Kobayashi, and Uchida. “Numerical simulation of striation formation on water jet cutting”. In T.J.Labus, editor, Proc. 8th Amer. Water Jet Conf., St.Louis, volume 2, pages 657-670. Water Jet Techn. Ass., 1995.

[7] A. Lebar and M. Junkar. “Simulation of abrasive waterjet machining based on unit event features”. Proc. Instn Mech. Engrs, J. Engineering Manufacture, Vol. 217 Part B, 2003. *in print.*

[8] L. Wang R. Kovacevic and Y.M. Zhang. “Detection of abrasive waterjet nozzle wear using acoustic signature analysis”. In M. Hashish, editor, Water Jet Cutting Technology Ass., volume 1 of Proc. 7th Amer. Water Jet Conf., pages 217-231, St. Louis, 1993.

[9] P. Karlic M. Mazurkiewicz. “Material response during hydroabrasive jet machining (HAJM)”. In Hood M. Dornfeld D., editor, Proc. 4th Amer. Water Jet Conf., pages 159-167, New York, 1987. ASME.

[10] R. Mohan M. Ramulu T.J. Kim E.S. Geskin R. Kovacevic, M. Hashish. “State of the art of research and development in abrasive waterjet machining”. ASME J. Manuf. Sci. and Engng., 119:776-785, 1997.

[11] J. Munoz and I. Kain. “Abrasive waterjet cutting a comparative study between open catcher tank and water catcher tank”. In Edward Wantuch, editor, WJM 2001 : proceedings of 2nd International Conference on Water Jet Machining, pages 101-109, Cracow, Poland, 2001. Institute of Metal Cutting.

6 NOMENCLATURE

h	depth of cut
l_{dr}	jet lag
v_t	AWJ cutting head traverse velocity
h_{sc}	smooth cutting depth
h_{so}	stand off distance
v_{sc}	separation cutting velocity
f	factor used to multiply the v_{sc}
p	water jet pressure
d_o	orifice diameter
d_f	nozzle diameter
N_m	machinability number
$\dot{m}_w$	water mass flow rate
$\dot{m}_a$	abrasive mass flow rate
q	quality level index
$\alpha,\beta,\gamma,\delta,\varepsilon$	regression parameters
B	beta function
a,b	beta function parameters

7 TABLES

Table 1. Plan of experiments. The AWJ traverse velocity values are determined relative to the separation cutting velocity v_{sc}.

	$v_t = f \cdot v_{sc}$				
workpiece thickness [mm]	$f = 0.6$	$f = 0.8$	$f = 1.0$	$f = 1.2$	$f = 1.4$
	v_t [mm/s]	v_t [mm/s]	v_t [mm/s]	v_t [mm/s]	v_t [mm/s]
5	4.8	6.4	8.0	9.6	11.2
10	2.4	3.2	4.0	4.8	5.6
30	0.6	0.8	1.0	1.2	1.4

8 FIGURES

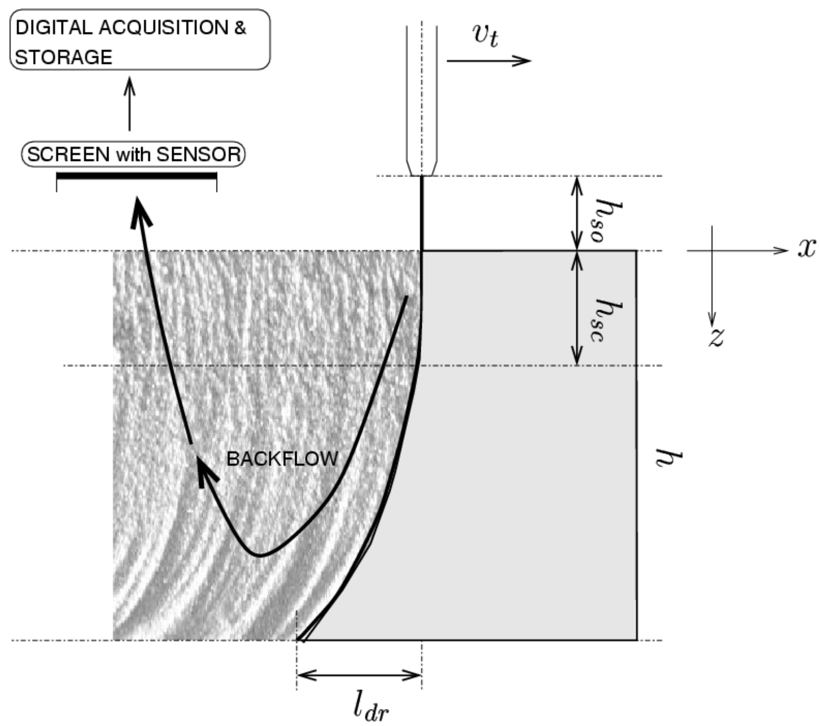

Figure 1. Scheme of the situation in the AWJ cutting. Generation of the water backflow and position of the sensing screen is schematically shown. Depth of the cut h, jet lag l_{dr}, AWJ cutting head traverse speed v_t, smooth cutting depth h_{sc} and stand off distance of the cutting head from the workpiece h_{so}.

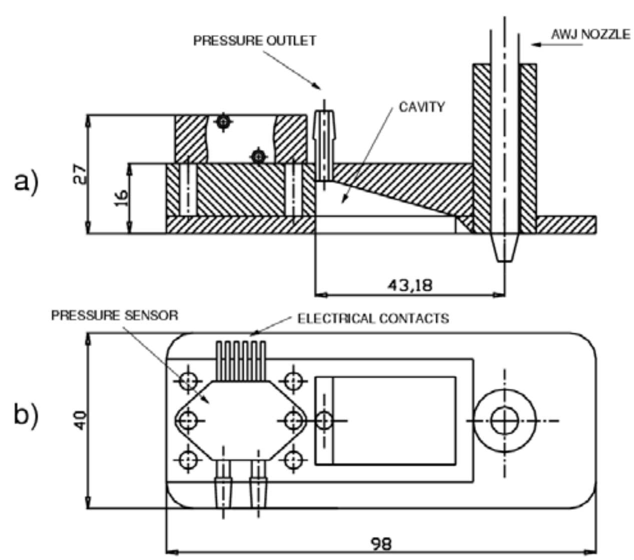

Figure 2. AWJ nozzle with mounted backflow interception screen with pressure sensor; sideview a) and top view b).

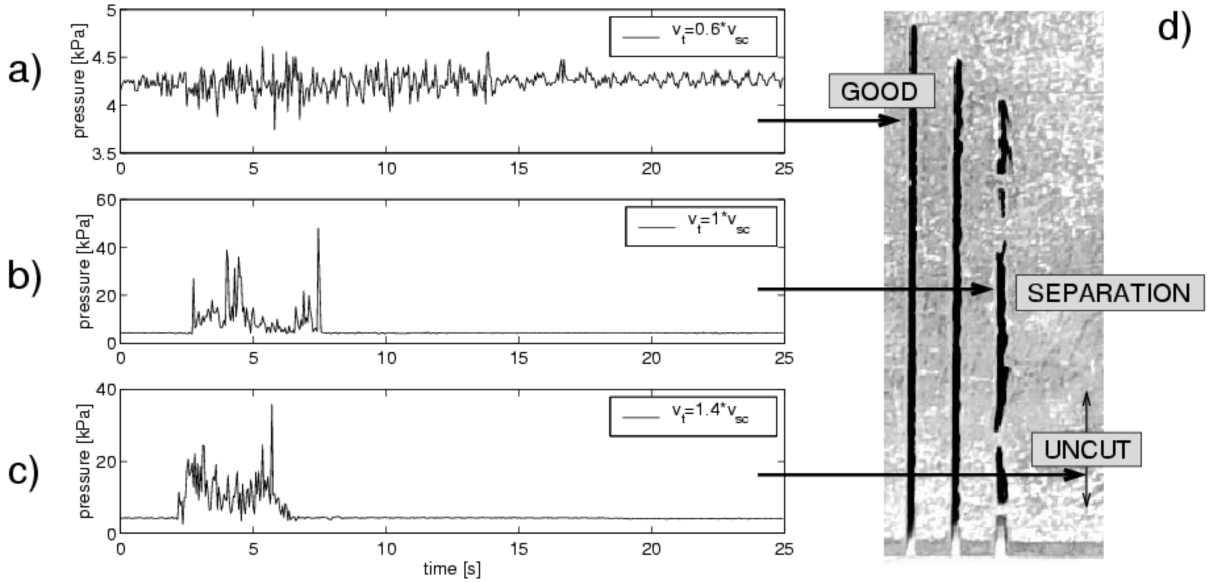

Figure 3. Acquired pressure signals on the workpiece of thickness h=30 mm. The separation cut speed for this workpiece was v_{sc}=1.0 mm/s.

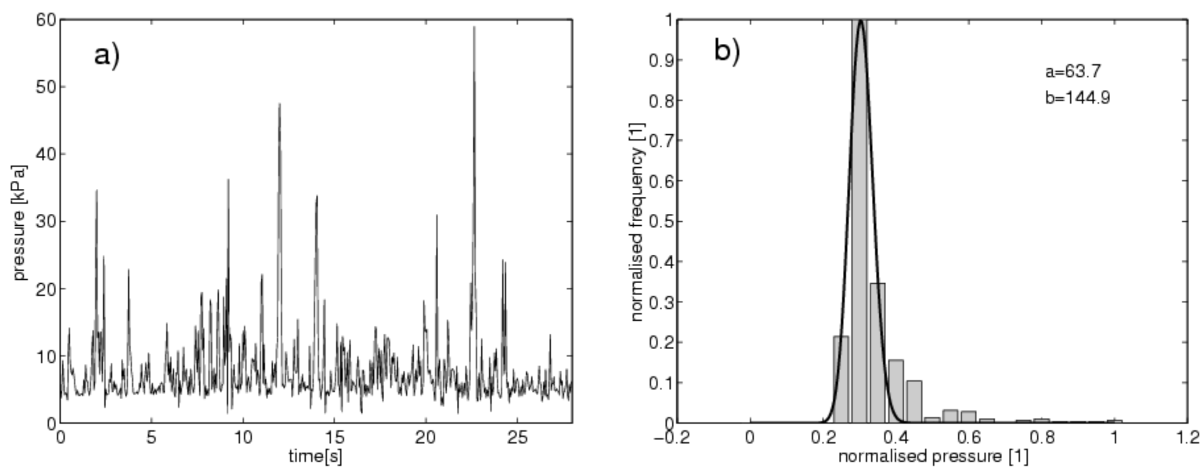

Figure 4. Pressure signal (a) and corresponding histogram (b) with a fitted beta function.

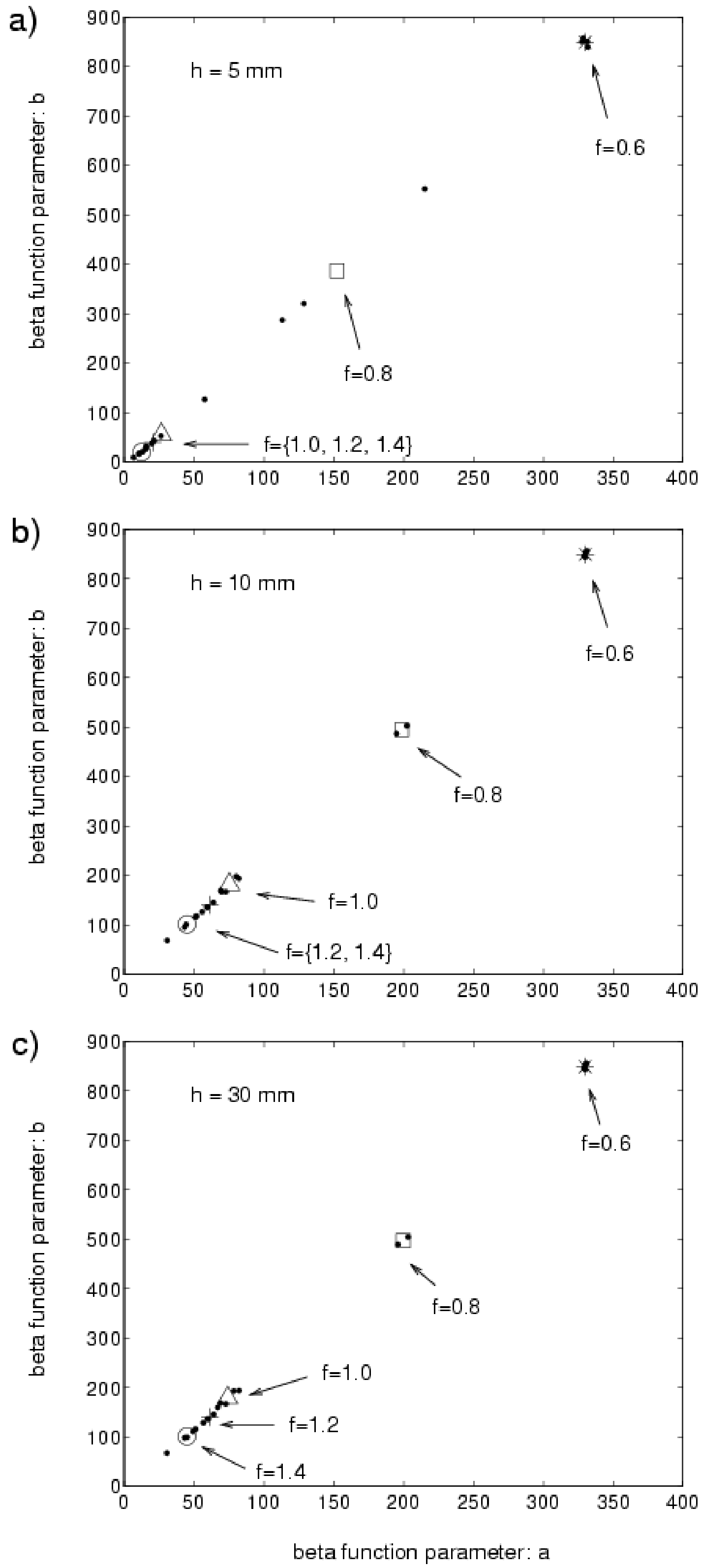

Figure 5. Parameters of beta function: a and b as the AWJ process performance index. Graphs a, b and c correspond to the experiments on workpieces with thickness h = 5, 10 and 30 mm.

2003 WJTA American Waterjet Conference
August 17-19, 2003 • Houston, Texas

Paper 4-G

STUDY OF ICE PARTICLE PRODUCTION USING EXPERIMENTAL AND COMPUTATIONAL FLUID DYNAMIC METHODS

D.K Shanmugam and Y. Morsi
Modeling and Process Simulation Research Group
Industrial Research Institute Swinburne
Swinburne University of Technology
Hawthorn, Victoria, Australia

ABSTRACT

A study was conducted to examine ice particles production using atomized water technique. The specific purpose of this study was to investigate the characteristics of ice particles produced by the utilization of convection heat transfer between the water droplets and a heat sink. A heat exchanger was designed and constructed to facilitate this process and provide a quantitative data of the temperature variation of the formed ice particles.

In the experiments conducted, the water flow rate was varied from 2 to 12 liters/hour while the inlet temperature of the water droplets was varied from 6°C to 18 °C. At these settings, the amplitude of the ultrasonic atomiser was varied from 60 µm to 120 µm. The temperatures of the Liquid Nitrogen (LN2) at the ice particle formation point and at the exit of the heat exchanger were measured for a range of inlet temperature of the liquid nitrogen. In addition, additives namely sodium chloride was introduced along with the inlet water and the temperature readings were recorded so that the melting rate of the particles can be determined. The results show a considerable difference in ice particle temperatures and the rate of melting between the pure water and water with additives. Furthermore, using optimized inlet parameters a controlled production of ice particles is obtained. The paper also discusses the results of our predicted temperature distributions using a numerical technique based on volume fractions and velocity of inlet fluids. In this technique the governing equations (continuity, momentum and energy) were discretized using finite volume approach. Finally the results obtained for ice particles exit temperature were validated using the available experimental data.

1. INTRODUCTION

While abrasive water jet (AWJ) is used in industry for cleaning, paint removing, and for machining a number of engineering materials there are some applications were the use of AWJ is not feasible due to the secondary treatment of the abrasives involved in the process. These processes include processing meat products, medical surgery and cleaning of sensitive surfaces. In these applications Ice jet, which is non-destructive, nonabrasive, residue-free and environment friendly can potentially be used as an alternative. Ice jet can be used for critical and non critical cleaning applications in the semiconductor, disk drive, vacuum technologies, surface science, surface analysis, optical, medical, automotive, analytical instrument, and for other manufacturing applications. However, the technology is still in its infancy and a significant amount of work need to be carried out to make it viable and efficient method. The objective of this research work is to study ice particles formation for use in ice jet machining. To achieve this a numerical and experimental approach is taken with the aim of formulating empirical correlation using process parameters such as ice particle temperature, velocity and the inlet temperatures and to quantify the effects of each of these parameters.

Although the principle of producing ice particles is relatively simple, the method and process of producing it in laboratory conditions are demanding. The obvious difficulty of this technology lies in the fact that many auxiliary systems for production and transportation of ice particles are necessary. Very little work has been done to study the formation process of ice particles and its temperature distribution. However, the applications are quite different from the study proposed in this paper. Hindmarsh and Russell (2003) conducted experiments to measure the temperature within freezing droplets of water for spray crystallization processes. They observed the different stages of freezing process. They also derived a simple heat balance model for every stage of liquid cooling, solid cooling and freezing stages and these were used to solve the internal energy balance of the droplet. They modeled the heat balance using Ranz and Marshall Equation for the application of dual heat and mass transfer from a spherical object at sub-zero temperatures. However, the incorporation of solute techniques would also be necessary for the prediction of the behavior of real fluids.

Satoh and Fushinobu (2002) examined the freezing characteristics of water droplets due to evaporation under evacuation. In their study, the cooling/freezing phenomena of a PCM droplet due to evaporation in an evacuated chamber were experimentally examined in order to investigate the heat transfer dominating the evaporation-freezing. They suspended water droplets by a fine thermocouple to measure the change in temperature of water. The initial temperature of the water droplet was controlled using an infrared (IR) radiation emitted from a filament lamp. However, in this experiment, it was not possible to locate the starting point of the solidification of ice particles.

Kim and Shin (2000) performed a theoretical and experimental study to examine the water spray method of ice slurry production. In their study they considered spherical ice particles of size below 300µm. These were practically obtained by spraying water of ambient temperature into the vacuum chamber where pressure is maintained below freezing point of water. Both theoretical analysis and experiments were carried out to verify the possibility of the water droplets to convert to ice particles, the transportability of ice particles and the conditions needed to form ice particles were also investigated. The conditions for the ice particle formation were theoretically investigated by using a diffusion-controlled evaporation model. But the heat transfer dominating the evaporation-freezing of water droplets sprayed into the evacuated chamber has not been sufficiently clarified by this study, since they neglected temperature distribution in a droplet during the evaporation-freezing, and assumed the droplet to be lumped capacity.

However, the use of ice jet for cleaning, blasting and food processing has been demonstrated under laboratory conditions. Galecki and Vickers (1982) established an experimental setup for cleaning and abrading surfaces with an ice-blasting technique. Ice particles of approximately 3 mm in diameter were produced by mechanically crushing 30 mm of ice cubes that were accelerated by a compressed air jet. These were then transferred to a container having liquid nitrogen where the ice cubes were further cooled. In doing so they used an air/ice venturi nozzle of 1.42 cm in inner diameter. It may be concluded from the experiments that the ice-blasting technique was more effective than both water jets and percussive needle guns, but not as effective as grit blasting. However, the argument states that for cleaning applications where grit blasting could not be tailored, the ice blasting could be a very promising technique.

Geskin et al. (1999) applied ice particles for precision cleaning of sensitive surfaces. Mechanical crushing formed ice particles. For this, FIDAP Computational software package was used to determine the probability of particles survival in the course of the jet formation. The operated nozzle diameter was 5mm and the ice particles were of 2 to 5mm in diameter. A. Hisasue et al. (1994) developed an apparatus for polishing surfaces of an article having a relatively low hardness, such as compound semiconductor and crystalline block. The process involved producing super fine ice particles by mixing liquid nitrogen and atomised water droplets. Geskin et al. (2000) experimented with icejet for decontaminating sensitive surfaces. Various electronic devises were disassembled and their electronic boards were contaminated by grease and metal powder. They then tried to clean it with ice blasting. It was then reassembled in order to study whether it was working normally. The study indicated that at sufficient kinetic energy ice particles could be used for machining of metals, ceramics and composites. Truchot, et al. (1991) conducted a study to develop a cryogenic water jet system for food processing and medical applications. They tried to enhance the cutting efficiency by mixing pellets of crystalline ice into the stream of pure water jets. Several different approaches for entraining the ice pellets into the jet stream were tested in their study. They investigated two methods based on water ice diagrams.

Ahmed (2002) studied the survival of ice particles inside the focus tube of the water jet nozzle. He simulated the impact of different inlet ice particle temperature (-50°C, -40°C, -30°C, -20°C and -10°C) over the ice particle exit temperature. He concluded that water and air temperature plays an important roll for the existence of ice particles at the exit of the focus tube. From his simulation results he predicted that ice particles can survive as ice particles at the exit of the focus tube if the inlet water temperature of the jet is kept at 0°C.

This study is a continuation of the work carried out by Shanmugam (2002) that dealt with the effect of parameters such as the angle of contact between the Liquid Nitrogen transfer tube and the atomized water droplets, the amplitude of the atomizer, the water flow rate into the atomizer probe, the inlet temperature of the inlet water, the temperature of the liquid nitrogen and the inlet velocity of the air. An empirical correlation for the dependency for the exit ice particle diameter was constructed from these results. The ice particle size varied from 90 µm to 110 µm in diameter.

The most important consideration in the production of ice particles is their size, temperature and consistency of formation. Finer and consistent particles are more effective as they result in better surface finish and thus higher surface quality when entrained with high velocity water jet. Both radiative and convective heat transfer were adopted and the pros and cons were calculated in arriving at an efficient heat transfer between them. Direct contact heat transfer between two immiscible liquids associated with the evaporation of one of the fluids has an advantage of eliminating a heat transfer surface and has a higher heat transfer rate and an ability to operate at a small temperature difference. Therefore, the use of convective heat transfer was adopted in this experiment.

2. NUMERICAL ANALYSIS

An analytical prediction was used in developing an actual physical model. A numerical solution of a differential equation consists of a set of numbers from which the distributions of the dependent variables were constructed. The formula for calculating the time required for the water droplets to form into ice particles using lumped capacitance method is

$$t = \frac{\rho V c}{h A_s} \ln \frac{\theta_i}{\theta} \qquad \ldots\ldots\ldots\ldots\ldots\ldots\ldots\ldots\ldots\ldots (1)$$

By this method the time taken for the water droplets to dissipate heat can be calculated theoretically with respect to time. These equations were used in determining the actual physical model of the heat exchanger.

2.1 Governing Equations

The generic scalar advection diffusion equation considered for simulation using simulation was,

$$\frac{\partial}{\partial t}(r_\alpha \rho_\alpha \Phi_\alpha) + \nabla \bullet (r_\alpha(\rho_\alpha \mathbf{U}_\alpha \Phi_\alpha - \Gamma_\alpha \nabla \Phi_\alpha))$$

$$= r_\alpha S_\alpha + \sum_{\beta=1}^{N_P} c_{\alpha\beta}(\Phi_\beta - \Phi_\alpha) + \sum_{\beta=1}^{N_P} (\dot{m}_{\alpha\beta}\Phi_\beta - \dot{m}_{\beta\alpha}\Phi_\alpha) \quad \text{-----------------}6$$

Where,

1. The term $c_{\alpha\beta}$ $(\Phi\beta-\Phi\alpha)$ describes inter-phase transfer of Φ between phase's α and β

2. $c_{\alpha\alpha} = 0$, $c_{\alpha\beta} = c_{\beta\alpha}$. Hence the sum over all phases of all inter-phase transfer terms is zero

3. The term $\dot{m}_{\alpha\beta}\Phi_\beta - m_{\beta\alpha}\Phi_\alpha$ only arises if inter-phase mass transfer takes place. $m_{\alpha\beta}$ is the mass flow rate per unit volume into phase α from phase β. In this case there is no mass transfer and hence it equates to zero.

2.2 Geometry

In this problem, in order to determine the rate of change of temperature, it is very important to construct a model in three dimensions to perform calculations to obtain reliable results on droplets in a surrounding gas flow. With a two-dimensional approach or applying symmetrical planes, erroneous droplet velocity may be obtained on the symmetrical side of the simulated water droplets.

Cartesian coordinate system was used to create the geometry. A two phase flow was considered with the liquid nitrogen flowing through one inlet and the water flowing through the other inlet as shown in Figure 1. Furthermore, air was flown through two inlets provided at the near lower exit of the model. The setting up of a problem in CFX-Meshbuild was done by creating and manipulating objects. Geometric objects (or physical objects) define the physical shape and position of a problem. A physical object is one that has a fixed position in space. The mesh objects define the grid. The fundamental type of mesh object is the block, which defines a piece of computational space. Grid cells are generated only within blocks. The purpose of a grid generator is to relate grid cells (computational space) to physical position in the problem. Within CFX-Meshbuild it is the relationship between the mesh objects and objects in physical space that defines the grid.

The geometry was created using 4 blocks and 4 inlet patches. The outlet was considered as a pressure boundary, and kept at atmospheric pressure. Figure 1 shows a three dimensional model with inlet and outlet patches.

3. EXPERIMENTAL APPARATUS AND METHOD

In this present study, water at different temperature with and without an additive agent was used. The reason for adding additives is to decrease the freezing point of water. It takes more amount of energy to freeze the water droplets in order to form ice particles, but on the other hand, the melting time of the ice particles increases. Another reason for adding additives is to make the ice particles coalescence free. Sodium chloride was used in proper concentration with water. The solubility of the sodium chloride in water was tested for various proportions at various temperatures. It was found that a concentration of 10% sodium chloride by volume is the optimum solubility factor by this addition the melting time of the ice particles can be increased. There has been a concern in developing ice particles of uniform diameter in size. The reason for generating uniform diameter ice particles is to enhance the quality of machining without any variation in surface quality. With the inlet parameters set to the same conditions set forth in using pure water, the readings for temperature were taken. Preliminary experiments show that the heat transfer from Liquid Nitrogen to water droplets is compared to that of the plain water.

Initially, there were number of parameters to be considered, this included the angle of contact between the Liquid Nitrogen transfer tube and the atomized water droplets, the amplitude of the atomizer, the water flow rate into the atomizer probe, the inlet temperature of the inlet water, the temperature of the liquid nitrogen and the inlet velocity of the air. However, all other parameters except inlet water temperature and inlet liquid nitrogen temperature are kept to the optimal level. A schematic diagram of the experimental apparatus for producing ice slurry and observing the characteristics of spray droplets from a nozzle is shown in Figure 2.

The experimental setup consists of a heat exchanger system, an ultrasonic atomizing unit, a liquid nitrogen storage unit, a water storage unit, a chilling unit and an air compression unit. The heat exchanger was the main unit, which was connected to the liquid nitrogen storage unit, and the atomizing unit. The atomizing unit was connected to a water storage unit that in turn was connected to a chiller. The air compression unit was connected to the heat exchanger through two inlets.

In order to make water freeze effectively it is important to reduce the heat flux into the water from the surroundings. Therefore, the heat exchanger was insulated to minimize this heat transfer. The design of the heat exchanger was made in such a way that there is an effective heat transfer between the liquid nitrogen and the water droplets.

Water from the water storage unit was filtered and fed into the ultrasonic atomizer's probe. Liquid nitrogen was stored under pressure in the storage unit and was transferred to the heat exchanger through a transfer tube. An insulated hopper was used to collect the ice particles at this stage of the experiment.

K-type thermocouples were used to measure temperature at various points of the heat transfer process as shown in Figure 2. The thermocouples were connected to a data acquisition system which in turn was connected to a computer to record the readings. These thermocouples read the online variation of temperature at the inlet for the liquid nitrogen, the exit for liquid nitrogen, at the point of ice particle formation and inside the insulated hopper.

Readings were taken with all four thermocouples until the ice particle temperature exiting the heat exchanger tends to be constant. At that stage the inlet water and the liquid nitrogen were stopped. This allowed all the thermocouple to recover to room temperature. In obtaining those readings, the melting rate of the ice particles was also observed from the thermocouple inside the insulated hopper.

In general the accuracy of the results depends on the errors in all the devices. Calibration was made and following errors were recorded

- The temperature of the water was measured using a K-type thermocouple having an accuracy of ± 1%
- The water flow meter has an error of ± 2%
- The atomiser has an error of ± 100Hz for the 40 KHz model used in this experiment
- Each measurement was done after 5 minutes for a period of 20 minutes after opening the liquid nitrogen valve. This was done to bring the liquid nitrogen to atmospheric pressure while flowing out from the storage unit.

5. RESULTS AND DISCUSSION

The results of the experiments that were conducted to measure the temperature transition of the immiscible fluids are shown in Figures 3-15. Figure 3 shows the plot of temperature against time for the liquid nitrogen flow. This was done to observe the phenomenon of liquid nitrogen heat loss from the exit of the storage unit to the exit of the heat exchanger. It is found that the temperature at all the points drops exponentially with time to a certain minimal point. The temperature increases curvilinear after the flow was stopped. It is noted that the thermocouple in the insulated hopper does not show any difference in temperature. The reason for that is the liquid nitrogen does not flow until the exit point of the heat exchanger, but escapes through a relief valve provided at the top of the heat exchanger. It can be concluded that the thermocouple in the insulated hopper is not affected by the liquid nitrogen flowing through the heat exchanger.

Preliminary experiments on temperature versus time helped in determining the temperature step interval of the inlet water temperature. The inlet temperature of the water was varied from 6°C to 18°C in a step interval of 6°C and the readings of all thermocouples were noted. The thermocouple at the transfer tube inlet was neglected as the temperature does not constitute in any variation of the inlet water temperature. All the readings were taken at half a second time interval in order to provide a fast and accurate response to time. Figure 4 shows the rate of temperature change with time. As the Liquid Nitrogen temperature decreases it was observed that the temperature of the ice particles decreases from room temperature to -25°C in 5 minutes. After 5 minutes it was observed that the temperature difference of the ice particle falls and reaches a stable temperature. At that moment the flow of both Liquid Nitrogen and water was stopped and the thermocouples were allowed to recover to the room temperature. The temperature in the ice particle Formation point and at the Liquid Nitrogen Entry point shown in Figure 2, increases after the flow of both the fluids were stopped.

Experiments were repeated for 12°C and 18°C by dropping the inlet liquid nitrogen temperature to -90°C. Figure 5 shows the plot of temperature against time for the 12°C inlet water temperature. The temperature at the ice particles formation point reached -22°C, while the exit temperature reached -17°C. Figure 6 shows the plot of temperature against time for the 18°C inlet water temperature. It is observed that the minimum ice particle temperature is found to vary between -16°C and -18°C. From the observations, it is found that there is a heat loss from the formation point to the exit point of the ice particles flow. This phenomenon is opposed to theoretical calculations. From theoretical calculations the ice particle temperature is found to be optimum at the design length of the heat exchanger considered in this experimentation. The reason for the temperature difference between the Formation and Exit point is caused by the air flow through the two inlets provided near the exit of the heat exchanger. It is observed that the exit ice particle temperature is dependent on both the velocity and temperature of the air at the inlet. When the flow is stopped, the temperature rises except that of the temperature inside the hopper. It is found that the temperature rises slowly in the thermocouple inside the hopper compared to the other thermocouples. The ice particles remain below 0°C for a minimum period of 6 minutes.

Further, experiments were repeated by adding additives to water. The heat transfer phenomena are similar to that of the plain water, except that the heat loss is minimal. Figures 7 to 9 shows the plot of temperature versus time for inlet water with additives. In Figure 7, the ice particle temperature drops to a minimum of -39°C at the formation point and a minimum of -35°C at the Exit point. These show that there is a 65% decrease in temperature compared to that of the pure water. Figure 8 shows the plot for 12°C inlet water temperature. The exit ice particle temperature drops to a minimum of -22°C with the temperature at the formation point dropping to -35°C. Comparing it with the pure water, it is seen that there is a substantial increase, 57%, in the heat transfer. From the Figure 9 it is found that the ice particle temperature drops to a minimum of -30°C. All these plots show that a controlled ice particle production has been achieved with atomized water droplets.

6. VALIDATION OF NUMERICAL RESULTS

The numerical results obtained have to be validated with the experimental data. The inlet variable parameters were kept at the same conditions for both simulation and experiments. However, in simulation the process of decreasing the inlet liquid nitrogen temperature with time differs from that of the experimental conditions. In simulations, the liquid nitrogen temperature is kept at the pre-cooled temperature of -90°C from the 0^{th} second. Figures 10-12 show various plots of temperature versus time for the plain water with liquid nitrogen. In Figure 10, it is seen that the temperature of ice particles reduces to -30°C in 8 seconds with the liquid nitrogen temperature kept at -90°C. Comparing this reading with the experimental observation there is a 5°C variation in temperature. In Figure 11, however, it is noted that the simulation differs by 3°C with the ice particle temperature dropping to -25°C. Furthermore, in the Figure 12, the minimum ice particle temperature differs by 3°C. These comparison studies show that there is a 10 to 20% deviation between the experiments and simulation predictions. The reason is in numerical simulations the atmospheric temperature is kept as the same as the inlet boundary conditions, whereas the atmospheric temperature is much higher in case of experiments. This gives the deviation between the experiment and simulation results.

Another set of simulations were carried out to compare the effect of additives with water. Figures 13-15 show the predictions of temperature variations with time. In Figure 13, the minimum temperature of the ice particles is found to be -42°C and -38°C at the Formation and Exit point respectively. Here, the variation is found to be 3°C compared with that of the experiments. In Figures 14 & 15, the minimum ice particle temperature at the Formation point is found to be -37°C and -33°C respectively. However, the exit ice particle temperature is found to be -31°C and -25°C respectively. In comparison with experimental results, an error of 40% was observed. Except the plot of temperature against time for 12°C and 18°C inlet water temperature using additives, all other results gives a reasonably good results.

7. CONCLUSION

Both theoretical and experimental study shows that at a certain inlet temperature it is possible to produce ice particles. However, the numerical simulations show that by keeping the inlet liquid nitrogen temperature at the same temperature ice particles can be produced instantaneously. Experimentally however, a considerable time is required to allow the liquid nitrogen to reach the required temperature and allow the vapor to flow out. Future work will concentrate on the time difference in reducing the temperature of the Liquid Nitrogen.

The following specific conclusions can be made from this study

1. Controlled ice particle production is possible at a certain temperature and with certain initial time interval
2. Simulation predictions agree with the experiments, but there are exceptions for the 12°C and 18°C water inlet conditions
3. Heat loss can further be reduced by minimizing the liquid nitrogen flow distance. This can be done by decreasing the length of the transfer tube between the storage tank and the heat exchanger.
4. Experiments and simulations can be carried out by further decreasing the liquid nitrogen temperature in order to obtain lower ice particle temperatures

8. ACKNOWLEDGEMENTS

The researchers wish to express their gratitude to the CRC for Intelligent Manufacturing Systems and Technology, for their continuing support. The CRC for Intelligent Manufacturing Systems and Technology was established under the Australian Government's Cooperative Research Centres Scheme.

9. REFERENCES

Ahmed D. H., "Numerical Simulation of Ice Jet and Existence of Ice Particles", Seventh International Conference on Manufacturing & Management, Bangkok, Thailand, pp. 922-927, 2002.

Galecki G., and Vickers G. W., "The development of Ice-Blasting for surface cleaning", *Jet cutting Technology*, pp. 59-79, April 1982.

Geskin E. S., Shishkin D., and Babets K., "Application of ice particles for precision cleaning of sensitive surfaces", *Proceedings of the 10th American Waterjet Conference*, Houston, Texas, Vol. 22, pp. 315-333,1999.

Geskin E. S., Goldenberg B., Shishkin D., Babets and K., Petrenko O., "Ice-based decontamination of sensitive surfaces", *Proceedings of the 15th International conference on Jetting technology*, Sweden, pp. 219-228, 2000.

Hindmarsh J.P., and Russell A. B., "Experimental and Numerical analysis of the temperature transition of a suspended freezing water droplet", *International Journal of Heat and Mass Transfer*, Vol. 46, pp. 1199-1213, 2003.

Hisasue A., Kanno I., and Fukumoto T., "Apparatus for polishing an article with frozen particles", *United States Patent*, No. 5283989, 1994.

Kim B. S., and Shin H. T., "Study on ice slurry production by water spray", *International Journal of Refrigeration*, Vol. 24, pp. 176-184, 2001.

Satoh I., and Fushinobu K., "Freezing of a water droplet due to evaporation-heat transfer dominating the evaporation-freezing phenomena and the effect of boiling on freezing characteristics", *International Journal of Refrigeration*, Vol. 25, pp. 226-234, 2002.

Shanmugam D. K., and Morsi Y., "Study of Ice Particle Formation Process", *Proceedings of the 4th International Conference on Modelling and Simulation*, Melbourne, Australia, pp. 323-327, 2002.

Truchot E. P., Mellinger P., Duchamp R., and Ocampo R., "Development of Cryogenic Waterjet Technique For Biomaterial Processing Applications", *Proceedings of the 6th American Waterjet Conference*, Houston, Texas, pp. 473-480, 1991.

10. NOMENCLATURE

A_s	surface area of the water droplet
c	Inter-phase term
C	specific heat capacity of water
h	convective heat transfer coefficient
H	Total enthalpy or static enthalpy
m	mass flow rate
N_p	Total number of phases
N_u	Nusselt number
r	Radius
t	time taken for the water droplets to form ice particles
T	Temperature
U	Velocity
V	volume of the water droplet
ρ	density of ice particles to be formed
θ_I	temperature difference between the water and liquid nitrogen
θ	temperature difference between ice particles to be formed and liquid nitrogen
λ	Thermal Conductivity

Subscripts

α, β, γ phases

Superscripts

h Heat transfer

11. TABLES

Table1. Simulation Properties

State of Nitrogen	gas and continuous
State of Water	liquid disperse with a mean diameter = $1.000\text{x}10^{-04}$ meters
State of Air	gas and continuous
Inlet boundaries	
Inlet1	Water
V Velocity	3.0 m/sec
Temperature	6°C, 12°C and 18°C
Volume fraction	1.0 i.e., pure Water is flowing through inlet1
Inlet2	Liquid Nitrogen
V Velocity	0.4 m/sec
Temperature	-90°C
Volume fraction	1.0 i.e., pure LN2 is flowing through inlet2
Inlet3	Air
V Velocity	1 m/sec
Temperature	10°C
Volume fraction	1.0 i.e., pure Air is flowing through inlet3

12. FIGURES

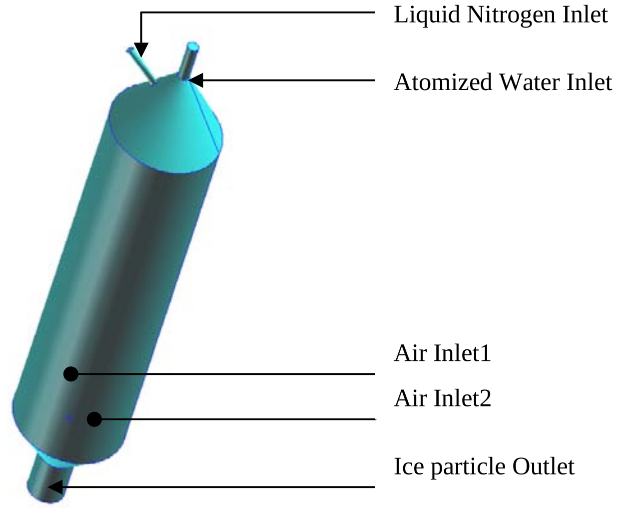

Figure 1 3-D model of the heat exchanger constructed using CFX

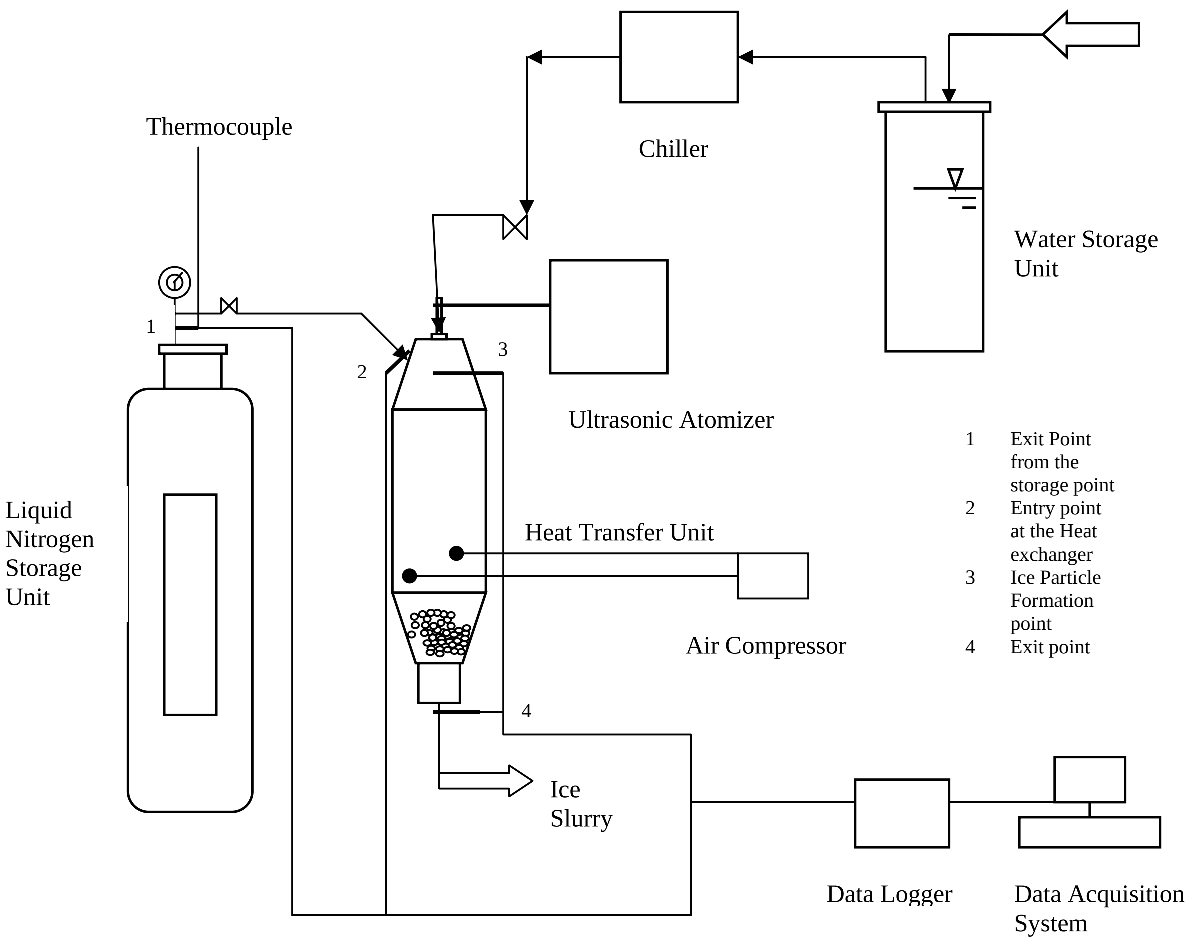

Figure 2 Schematic of the Ice particle formation and temperature measurement

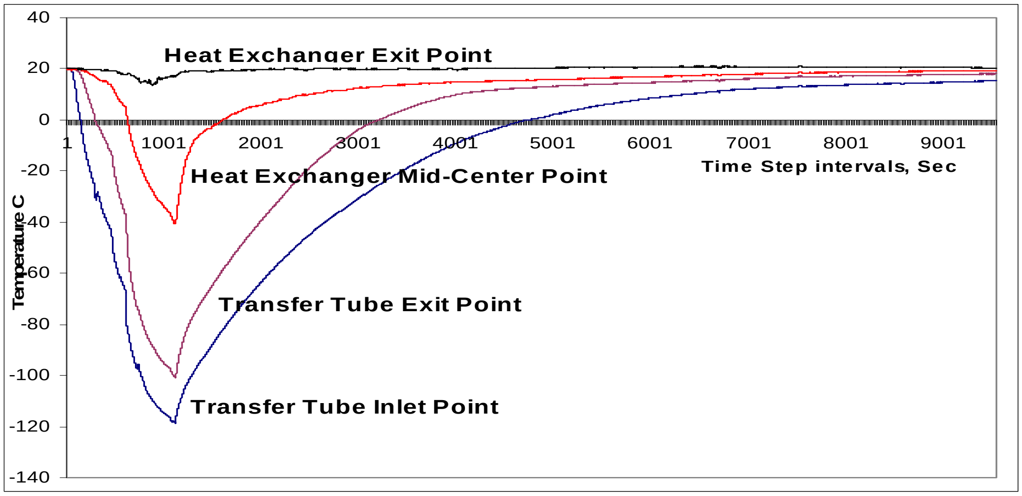

Figure3. Temperature of Liquid Nitrogen

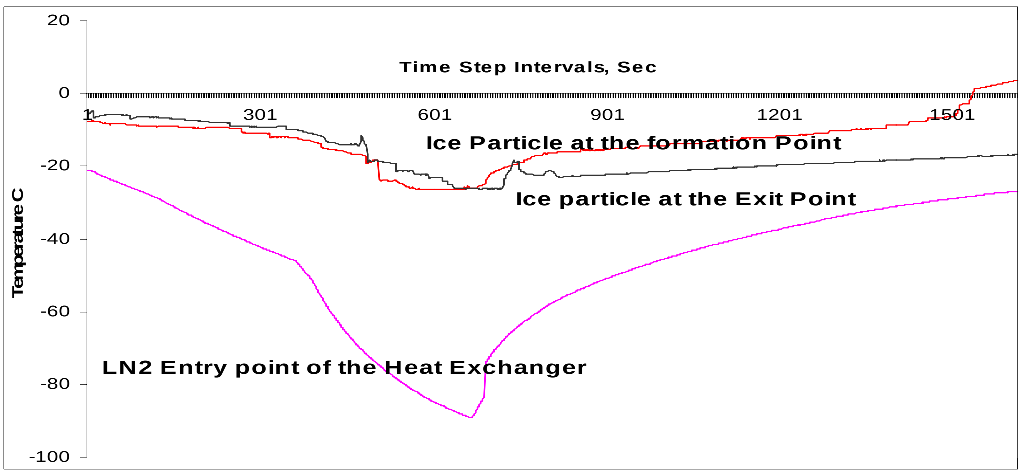

Figure4. Temperature versus time for Inlet Water Temperature 6°C

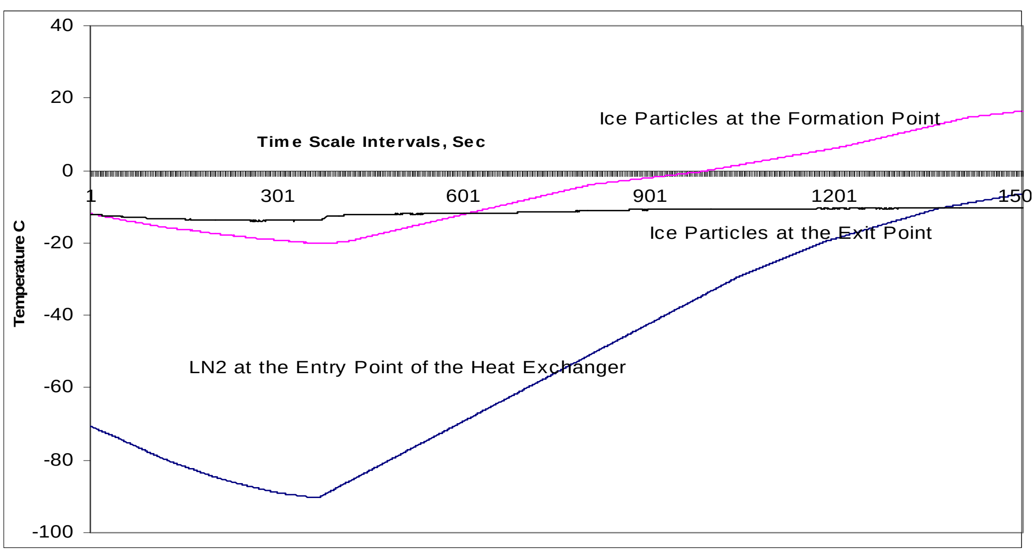

Figure5. Temperature versus time for Inlet Water Temperature 12°C

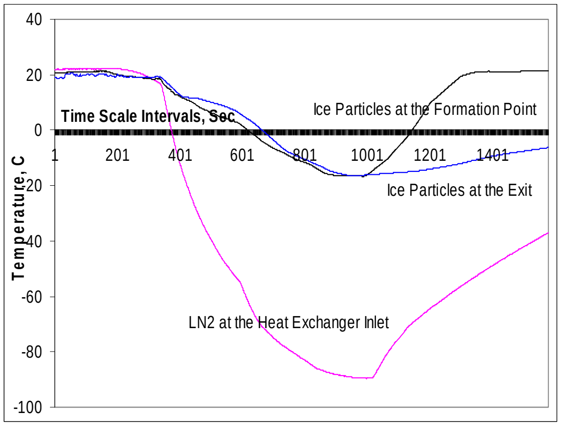

Figure 6. Temperature versus time for Inlet Water Temperature 18°C

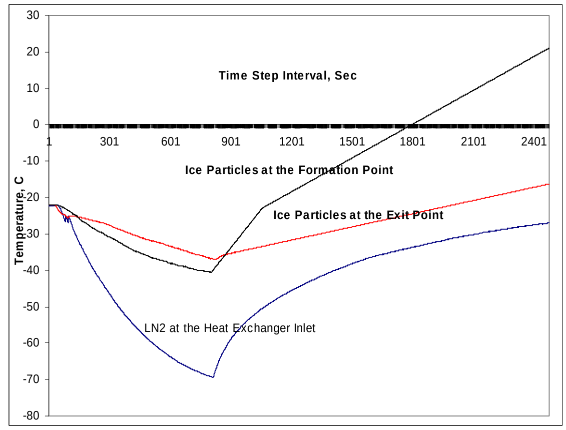

Figure 7. Temperature versus time for Inlet Water Temperature 6°C, with additives

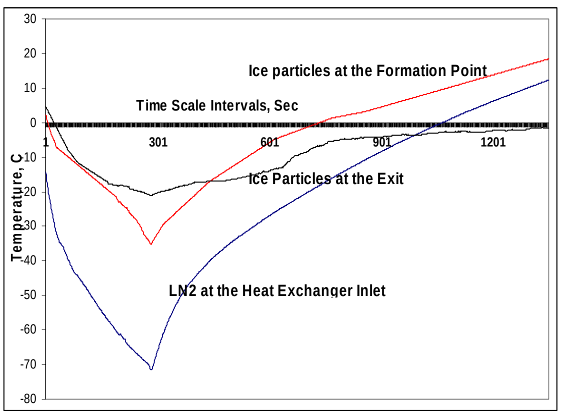

Figure 8. Temperature versus time for Inlet Water Temperature 12°C, with additives

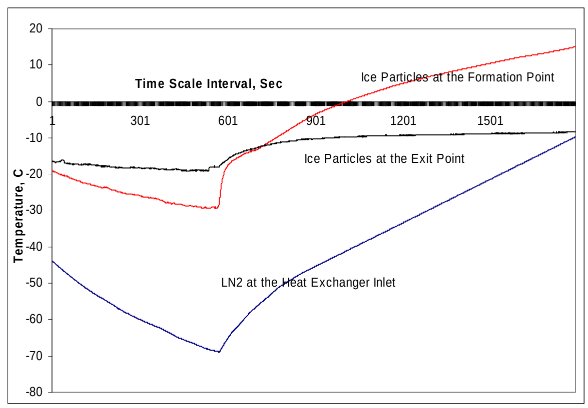

Figure 9. Temperature versus time for Inlet Water Temperature 18°C, with additives

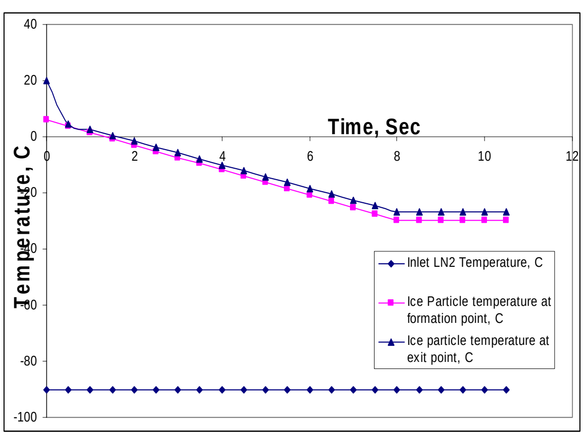

Figure 10. Temperature versus time for Inlet Water Temperature 6°C

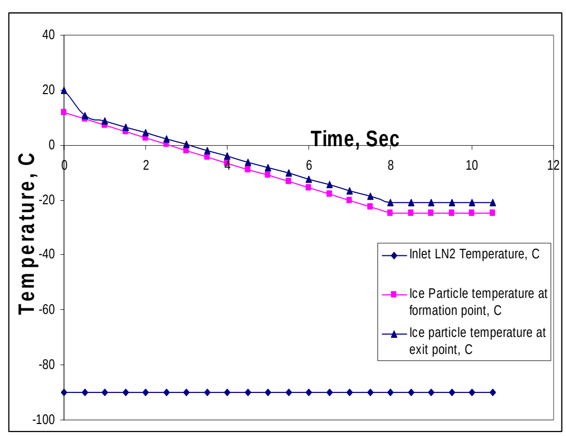

Figure 11. Temperature versus time for Inlet Water Temperature 12°C

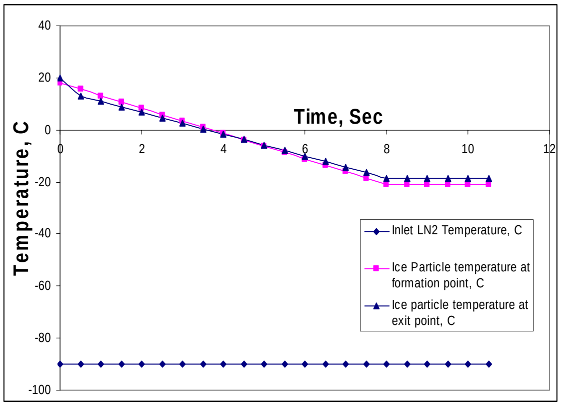

Figure 12. Temperature versus time for Inlet Water Temperature 18°C

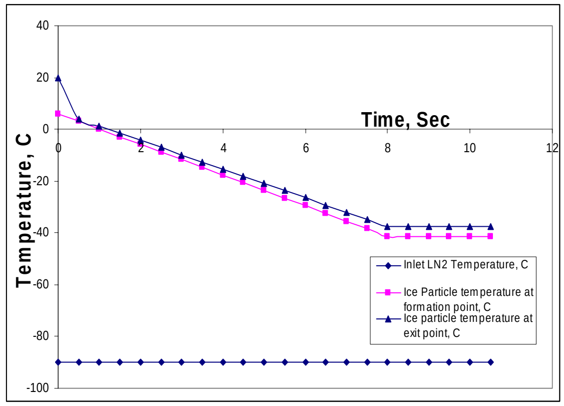

Figure 13. Temperature versus time for Inlet Water Temperature 6°C, with additives

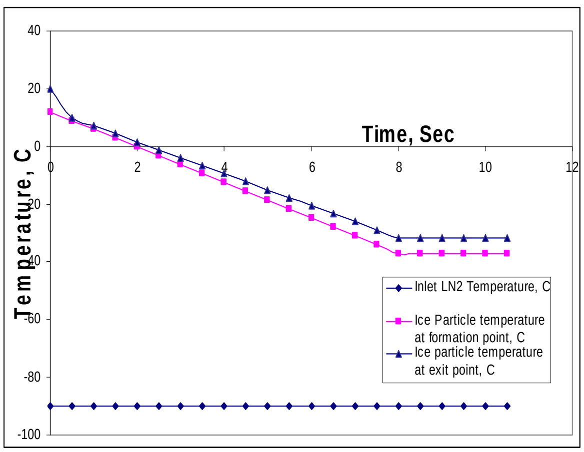

Figure 14. Temperature versus time for Inlet Water Temperature 12°C, with additives

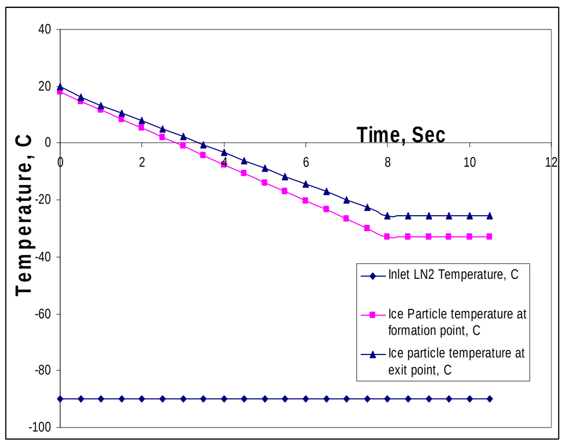

Figure 15. Temperature versus time for Inlet Water Temperature 18°C, with additives

2003 WJTA American Waterjet Conference
August 17-19, 2003 • Houston, Texas

Paper 3-A

MODULATION OF CUTTING OPERATION WITH ABRASIVE WATERJETS

A. Henning, E. Westkämper,

Fraunhofer Institute for Production Engineering and Automation

Nobelstr. 12, 70569 Stuttgart, Germany

henning@ipa.fhg.de

ABSTRACT

Abrasive waterjet cutting has already been established in many fields of industrial production. Yet limited cutting performance and cutting edge quality hinder a wider distribution of abrasive cutting systems. As major limiting factor process immanent step propagation and thus striation formation can be spotted. Better understanding and control of these processes could result in reduction of striation and better cutting performance.

This paper focuses on modulations of the jetting process as a promising possibility of process controlling. Nonlinear phenomena were identified to strongly influence the appearance of striation structures. With adequate control strategies it was proven that these effects could be used to influence the step initiation and the step propagation process. The experiments showed that an improvement of the cutting performance could be achieved by using adequate cutting parameter sets.

In this experimental approach the influence of sub- and superharmonic frequencies was observed. This technique could prove as a promising new way of optimizing both quality and performance of abrasive waterjet cutting, qualifying this brilliant technique for even more innovative applications.

1 INTRODUCTION

Abrasive waterjets have become a most recent tool in mechanical machining. With its great advantages the technology is spreading more and more among industry. Thorough understanding of the relevant processes is essential for achieving the demanded high quality output. With the approach of nonlinear modelling a new sight on the very influences of the process could be gained. In this paper new approaches to modifying the typical structures at the cutting edge utilizing external periodic forces are presented. Suitable process models could so deliver new approaches to improving both quality and performance of the machining outcome.

The usage of new materials in industrial applications sets high requirements for machining processes. High sensitivity regarding mechanical and thermal stress or due to specific material properties makes these ingenious materials hard to machine with conventional processes. To meet these specific requirements, new machining technologies are necessary. Here abrasive waterjets have become a most recent tool in mechanical machining. Due to its geometrical and material flexibility and its ability of cutting hard-to-machine materials, this technology is spreading more and more for two- and three dimensional cutting applications. Applications of waterjet technology can be found in many different fields like the automotive or aerospace industry or for the generation of prototypes (Westkämper, 1998).

With abrasive waterjet cutting a very typical characteristic appearance of the cutting edge can be found. Like in other jetting technologies (laser, plasma etc.) typical striation structures are observed (Ditzinger et.al., 1999). This is commonly understood to be the result of instationary periodic processes within the kerf generation (e.g. Hashish, 1986). Even though these striation structures are a major issue in optimising both quality and performance of the cut most modelling approaches of the abrasive waterjetting process have addressed either the maximum cutting depth or the roughness of the cutting edge in the quality cutting zone (e.g. Kim and Zeng, 1991). Only few have considered the very cutting process as being spatial in three dimensions (Guo, 1994). The analysis of the cutting edge has therefore been mostly limited to two dimensions ignoring spatial characteristics of the process when describing the cutting edge as a surface with randomly distributed structures, i.e. white noise (Zeng, 1997).

When aiming at the optimisation of the cutting process the understanding of the mechanisms and the formation of striation structures is of essential importance. In previous work (Westkämper, 2000 and Henning, 2001) the authors have introduced signal processing methods for the analysis of surface structures. First the existence of two different impact situations within the cutting process (primary and secondary impact) that had been suggested (e.g. Hashish, 1986) and analytically been derived before (Friedrich, 2000) could be experimentally proven (Westkämper, 2000). Also significant factors could be derived that describe both depth and shape of striation structures (Henning, 2001). Introducing these methods the surface of the cutting edge can more thoroughly be analysed and the effect of significant factors (e.g. pumping frequency) on the cutting process could be identified and evaluated (Henning, 2001).

In this paper new methods for deeper analysis of the cutting edge are introduced and the effect of process modulation is evaluated. With this new insights on the process of structure generation could be gained and new approaches to optimising the process and the quality of the cutting surface could be developed.

2 MODULATION OF THE CUTTING PROCESS

The cutting process has been subject to optimization since its invention in the 1970s. Most effort of modeling approaches was laid on gaining understanding of the very processes and formulating the effect of the different parameters in order to increase mainly the cutting depth through higher cutting power. Few attempts have been made so far to analyze the influence of the cutting path and of geometrical cutting parameters like jet oscillation.

When optimizing the outcome of the cutting operation there are several targets that can be set. The maximum cutting depth is one of the most common optimization criteria. With this the rough cutting speed that just barely separates the workpiece is maximized resulting also in increase of performance in the quality cutting zone. The second relevant criteria is the cutting quality, which can be defined by reachable accuracy that highly correlates with striation depth. The third relevant criteria is the extend of the jet lag at a given set of parameters. Depending on the extend of the jetlag the maximum feedrate must be reduced especially at complex contours with small radii. In daily work on the shopfloor all three criteria have to be met. Unfortunately all three cannot be maximized together. So the goal would be to extend the area of high quality surface and to reduce the extend of the jet lag at a given cutting speed.

One approach to utilize mainly the primary cutting zone was cutting in multipath operation. With this the appearance of striation structures could be avoided to a large extend. Cutting performance was reduced though and usability of this strategy is limited (e.g. Wang, 2000). In other studies the path of the cutting head was stabilized using oscillations of the cutting angle resulting in reduction of surface roughness when cutting thin sheet metal (Chen et.al., 2003).

Only Friedrich gave first analytical approaches when deriving a nonlinear partial differential equation for the removal rate of Kuramoto-Sivashinsky type (Friedrich et.al., 2000). In this system instabilities occur at low feedrates resulting in a change of removal mechanism. These instabilities that most likely serve as initiation point for step propagation and thus striation formation are know to be influenced by superposed external frequencies. In earlier studies (Henning, 2001) the influence of pressure fluctuation resulting from plunger movements could be identified to show a non-linear frequency coupling behaviour with the striation frequency at the probe.

2.1 Geometrical Modulation

There are many way of applying periodic external forces to the system. In this paper three different modulations were chosen. With all experiments the cutting parameters were held constant (f=23mm/min, p=300Mpa, mp=300g/min, dd=200µm, df=800µm). During these experiments, the position of the cutting nozzle was influenced, in the case of cutting head oscillation or the abrasive flow was toggled.

In the first experiment the abrasive waterjet oscillated parallel to the cutting direction, by using a pneumatic device (Figure 1a). In the second experiment, the same device was used, to oscillate the abrasive waterjet perpendicular to the cutting direction (Figure 1b). And during the last experiment a toggling device was used in order to influence the abrasive flow (Figure 1c). At the abrasive modulation experiments the average abrasive flow was held constant.

Parallel oscillation $\vec{s} = \begin{pmatrix} a \cdot \sin \omega t \\ 0 \end{pmatrix} + \begin{pmatrix} u_0 \\ 0 \end{pmatrix} \cdot t$

Lateral oscillation $\vec{s} = \begin{pmatrix} 0 \\ a \cdot \sin \omega t \end{pmatrix} + \begin{pmatrix} u_0 \\ 0 \end{pmatrix} \cdot t$

In the first case the normal jet position at steady movement was superimposed with a sine-oscillation. With this movement the average feedrate u and therefore the jet intensity (power per area unit) remains constant. Only the temporal intensity is periodically varied with the feedrate. The resulting geometrical wavelength is $\lambda_G = u / f_G$. For the second case (Figure 1b) the sinus-oscillation takes place in y direction, perpendicular to the cutting direction. In the third sets of experiments the abrasive flow was interrupted within in a defined duration. With the average abrasive flowrate being constant the flow was shut off for a certain proportion of the period[1]. The average flow was held constant by adapting the active flow rate.

3 EXPERIMENTAL RESULTS

The major purpose of jet modulation is to optimize the appearance of surface structures at the cutting edge. Therefore the major factors striation depth and jet lag are analyzed for all three modulation approaches. To compare the outcome of the modulated cuts with a reference cut without modulation the reference is plotted in a dashed red line. This enables the interpretation of the significance and the effect of each modulated cut.

3.1 Jet lag

The curved shape of the cutting front generates curved striations at the cutting edge. With this the exit point of the jet from the cutting edge lags behind for a certain amount. In cutting corners or curved shapes the effect of the jet lag has to be reduced to a minimum by slowing down the cutting speed in order to achieve reasonable cutting edge geometry and to meet requirements of accuracy. With a smaller jet lag the total cutting time can be reduced significantly at complex cutting paths.

In Figure 3b the displacement of striation structures is displayed over the cutting depth by using the first maximum of the cross-correlation function of the surface scan (see Henning, 2001). With accumulation of the displacement the medium shape of the striation shape can be derived.

In Figure 4 the jet lag is plotted for different combinations of oscillation in cutting direction (see Figure 1a). In each subfigure the modulation frequency is the same (as shown above the subfigure). Only the amplitude varies from 0,3mm to 1.2mm. For all combinations the amount of jet lag could be reduced significantly. The reference cut shows a curved jet lag shape almost from the top of the cutting edge. With the modulated cuts the primary impacting zone where no jet lag occurs is enlarged and when rising it shows first a linear shape resulting

---

[1] The proportion 1:4 means that the abrasive flow was shut off for 20% of the length of the period. (frequency 1Hz: 0,8sec on – 0,2sec off)

in less increase in the total amount of jet lag. The curvature of the jet lag in the modulated cut may be larger- the total amount never reaches the amount of the jet lag at the reference cut. It can be seen, that the modulation of the cutting head improves the quality of the cutting edge by reducing the jet lag.

In Figure 5 the effect of lateral oscillation is shown. Similar to the oscillation in cutting direction, the amplitude and the oscillation frequency are varied. The obtained results show, that similar to the parallel oscillation the jet lag is reduced. The effect is not as big as with parallel oscillation. Figure 6 shows the results of the jet lag obtained for on-off-toggling of the abrasive device. For this modulation type certain ratios of the abrasive flow were established. I.e. the ratio of the time when the abrasive flow was on to the time it was off was varied. The abrasive flow mass per minute though remained constant in all cases. One can see, that toggling the abrasive device improves the jet lag slightly for most of the investigated cases. Only at long off-periods (1:2 and 1:4) the magnitude at the reference cut is better. The jet lag being a most important factor in precision cutting proved to be subject to influences of external modulations. In almost all cases the quality of the cut was increased. The largest effect could be seen with oscillation in cutting direction.

3.2 Striation depth

Striations are formed at steps propagating down at the cutting front. The depth of striation structures is here calculated as $ds=6*\sigma$ with a probability of 99,6% of the scan data being in that range (see Figure 2). The appearance of striation structures limits strongly the quality of the cutting edge. First it is very obvious and can be clearly seen by bare eye and secondly precision cutting is not possible with structures on the surface. Therefore in precision cutting only the upper third of the possible cutting depth is used by reducing the feedrate equivalently.

In Figure 7 the striation depth is displayed for oscillation parallel to the cutting direction. The cut without modulation is again displayed with a dashed line as a reference for comparison. Other than with the jet lag the effect does strongly depend on the choice of modulation parameters. The best results are achieved by using small oscillation amplitudes of 0.3 and 0.6 mm. I.e. for these two amplitudes the striation depth is reduced for nearly all used oscillation frequencies. The best results, concerning the modulation frequency, were achieved with oscillation frequencies of 2.5 Hz. With a high oscillation frequency, and more distinct for the last three ones, a reduction of the striation depth could be observed especially in the transition zone.

Figure 8 shows the striation depth obtained through oscillation lateral to the cutting direction. It can be seen, that with this type of modulation the depth of striation is increased. Figure 9 shows the striation depth as a result of the abrasive toggling experiments. Similar to the jet lag, the toggling of the abrasive device reduces striation depth for most of the investigated parameters. Here an optimum was found at a ration of 1:6. All of the investigated modulation approaches showed significant effect on striation depth. The best effect again was achieved with parallel cutting. From these results it can be stated, that modulation techniques can significantly influence the cutting process. In most parameter combinations of modulations a significant improvement of the cutting quality can be achieved. The maximum cutting depth remained the same, though.

4 CONCLUSION

For waterjet cutting the appearance of the cutting edge plays a vital role. Striation structures do not only limit the possible range of applications but also reduce accuracy and quality of the machining outcome. In normal operation the cutting performance is adjusted to reach the desired quality. With the approach of modulating the jet according to different methods both striation depth and jet lag could be positively influenced. The effect of parallel oscillation showed the largest effect. As shown in Figure 10 for all parameter combinations the jet lag could be reduced significantly. The minimum jet lag did occur at lowest modulation frequencies. In Figure 12 the projected area of the striation structure is displayed. With higher modulation frequencies and lower modulation amplitude the area was reduced significantly. For over all optimization low amplitudes at high frequencies can be proposed. Further work is necessary in this field in order to evaluate the influence of cutting parameters on the effect of modulation.

5 ACKNOWLEDGEMENT

We gratefully acknowledge the support of the Volkswagen Foundation in this project.

6 REFERENCES

Ditzinger, T.; Friedrich, R.; Henning, A.; Radons, G. (1999): Non-Linear Dynamics in Modeling of Cutting Edge Geometry. In: Hashish, Mohamed (Hrsg.); Proceedings of the 10th American Waterjet Conference - Vol. I : August 14-17, 1999, Houston, USA, S. 15-32

Friedrich, R., Radons, G., Ditzinger, T., Henning, A. (2000)." Ripple formation through a convective instability from moving and erosion sources", Physical review letters

Friedrich, R.; Ditzinger, T.; Henning, A.; Radons, G. (2000): Mechanisms of the Evolution of Spatio-Temporal Instabilities in Abrasive Water Jet Cutting. In: Proceedings of the 6th Pacific Rim International Conference, 9-11 October, 2000, Sydney, Australia, S. 83-87

Guo, N.S. (1994), Schneidprozess und Schnittqualität beim Wasserabrasivstrahlschneiden. VDI-Fortschritt-Berichte, Reihe 2, Nr. 328,

Hashish, M. (1988), „Visualization of the abrasive waterjet cutting processes,“ Experimental mechanics 45, 159 (1988), pp. 159-169.

Henning, A. (1997). „Computer aided manufacturing for three-dimensional abrasive waterjet machining,“ in Proceedings of the 9th American Waterjet Conference

Henning, A.; Anders, S. (1998): Cutting-edge quality improvements through geometrical modelling. In: Papers presented at the 14th International Conference on Jetting Technology, Brugge, Belgium, 21-23 September 1998, S. 321-328

Henning, A.; Westkämper, E. (2000): Modelling of contour generation in abrasive water-jet cutting. In: Jetting Technology : Papers presented at the 15th International Conference on Jetting Technology, Ronneby, Sweden, 6-8 September 2000, S. 309-320

Westkämper, E.; Henning, A.; Radons, G.; Friedrich, R.; Ditzinger, T. (2000): "Cutting Edge Quality through Process Modeling of the Abrasive Waterjet"In: Teti, Roberto (Hrsg.); CIRP; University of Naples Federico II: Intelligent Computation in Manufacturing Engineering - 2 : Proceedings of 2nd CIRP International,Seminar, June 21-23, 2000, Capri, Italy.Neapel, I, 2000, S. 179-188

Westkämper, E.; Henning, A.; Radons, G.; Friedrich, R.; Ditzinger, T. (1999): Non-linear dynamic modelling of the abrasive waterjet process. In: Investigation of Nonlinear Dynamic Effects in Production Systems : 2nd International Symposium, 25.-26. February 1999, Aachen, S. 1-15

Zeng, J. and Kim, T. (1992). „Development of an abrasive waterjet kerf cutting model for brittle materials,“ in Proceedings of the 11th International Conference on Jet Cutting Technology

Chen, F. L., Siores, E (2003), The effect of cutting jet variation on surface striation formation in abrasive water jet cutting**,** *Journal of Materials Processing Technology*, Volume 135

7 FIGURES

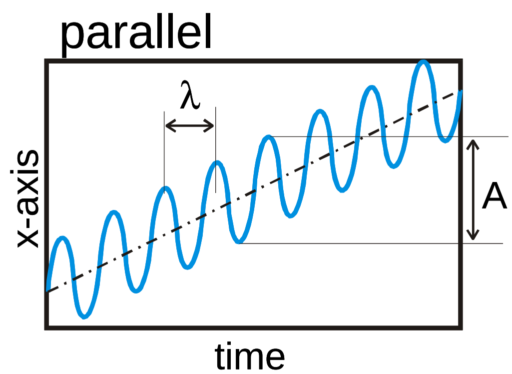

a) Modulation parallel to cutting direction

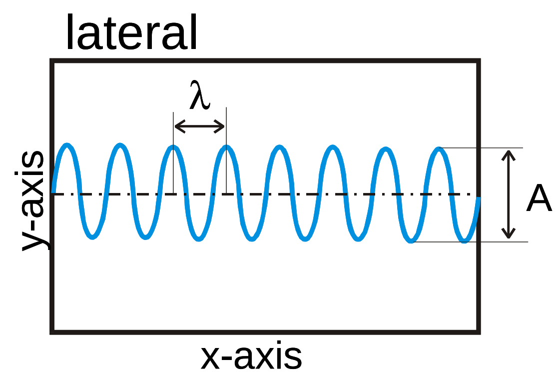

b) Modulation perpendicular to cutting direction

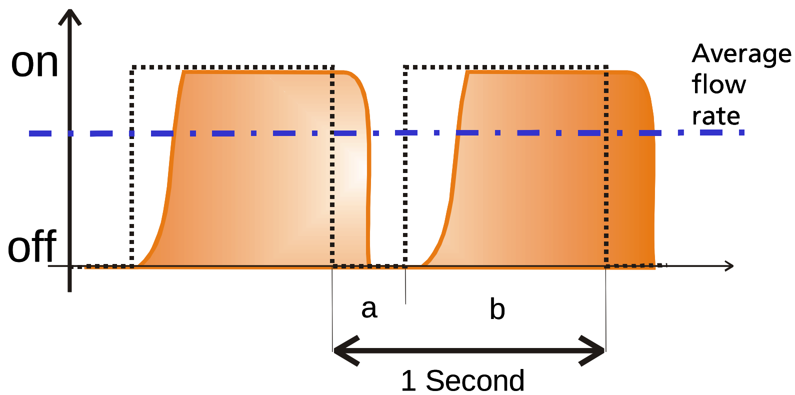

c) toggle device for abrasive flow

Figure 1: Functional principles of modulation

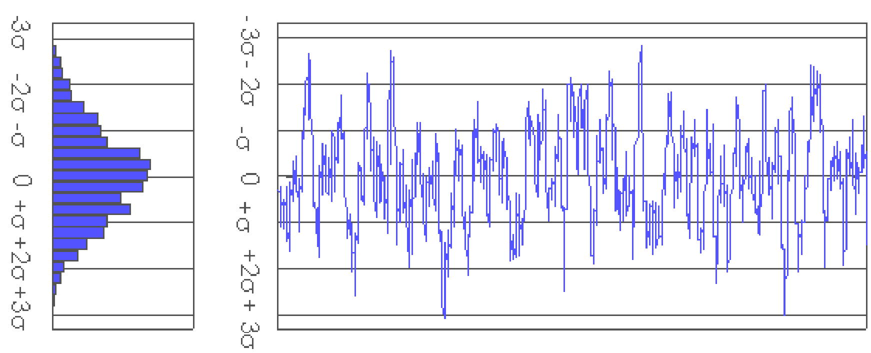

Figure 2: Surface scan line and histogram with corresponding standard deviation σ

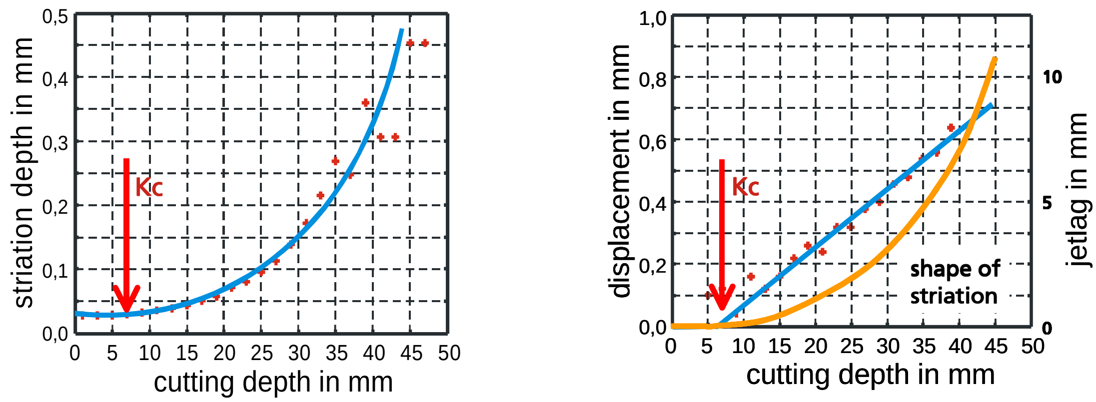

Figure 3: Analysis of striation depth and shape
a) striation depth b) displacement and jet lag

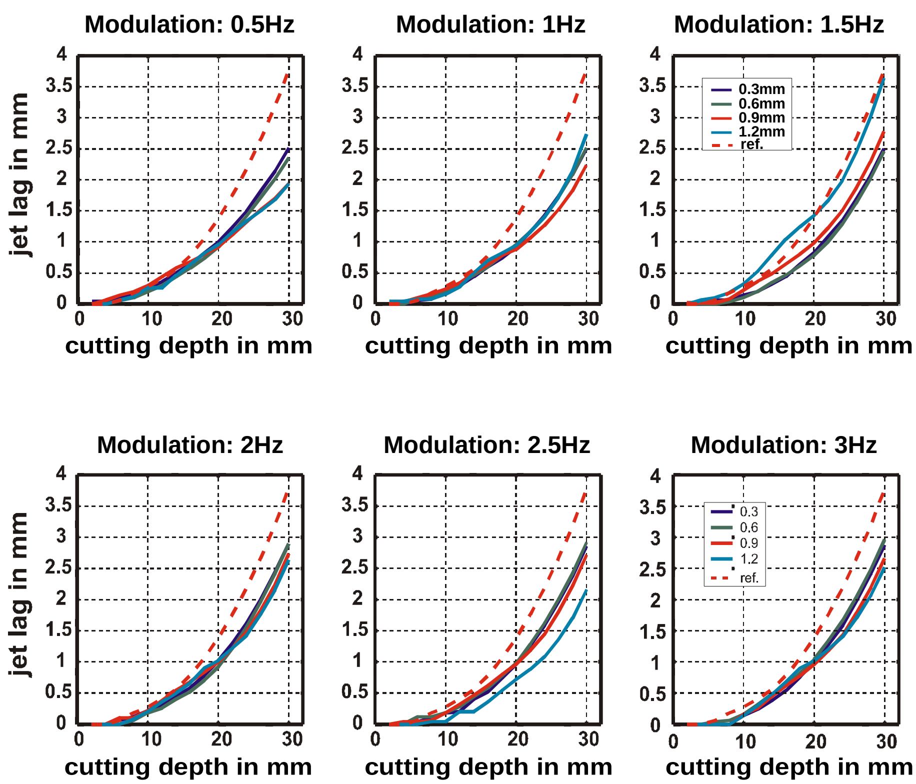

Figure 4: Jet lag for oscillation cuts in cutting direction

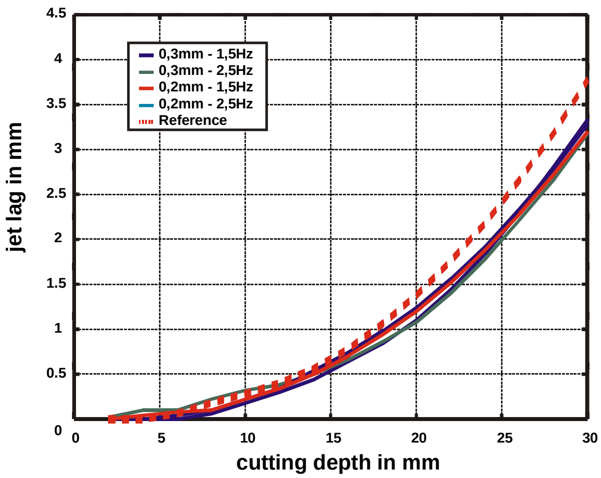

Figure 5: Jet lag for oscillation cuts perpendicular to cutting direction

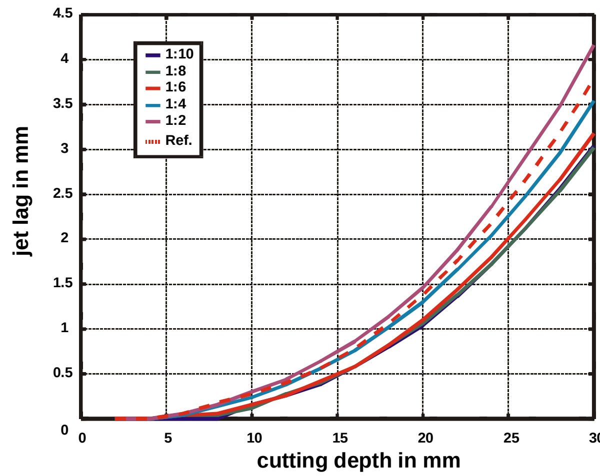

Figure 6: Jet lag for toggling of the abrasive

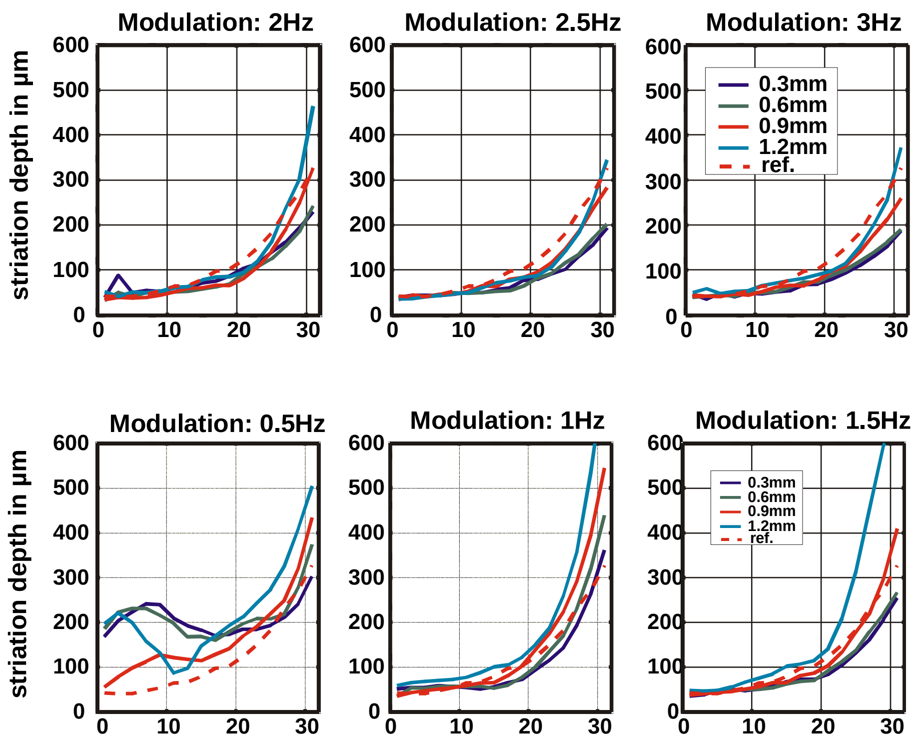

Figure 7: Striation depth for oscillation cuts in cutting direction

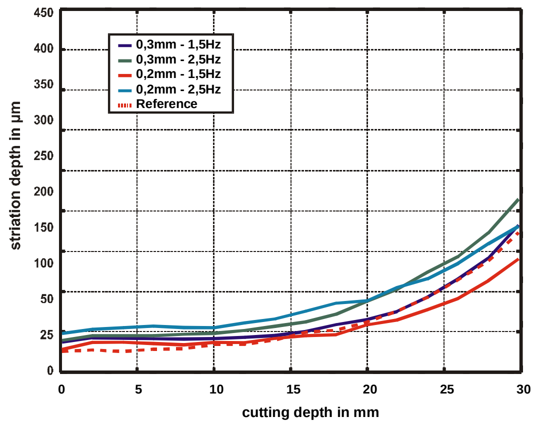

Figure 8: Striation depth for oscillation cuts perpendicular to cutting direction

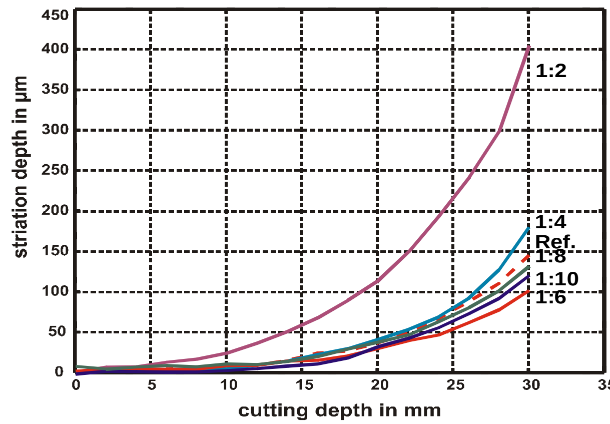

Figure 9: Striation depth for toggling of the abrasive device

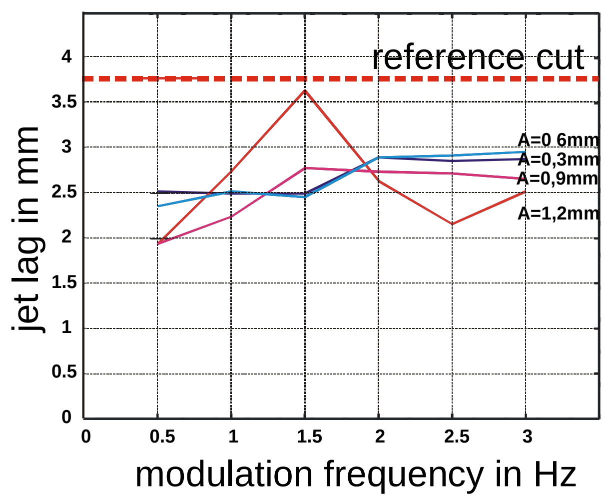

Figure 10: Maximum jet lag at bottom of the cutting edge - Effect of parallel oscillation

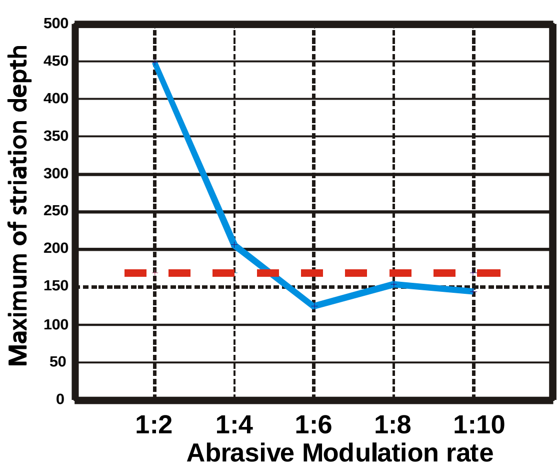

Figure 11: Maximum jet lag for toggling of the abrasive

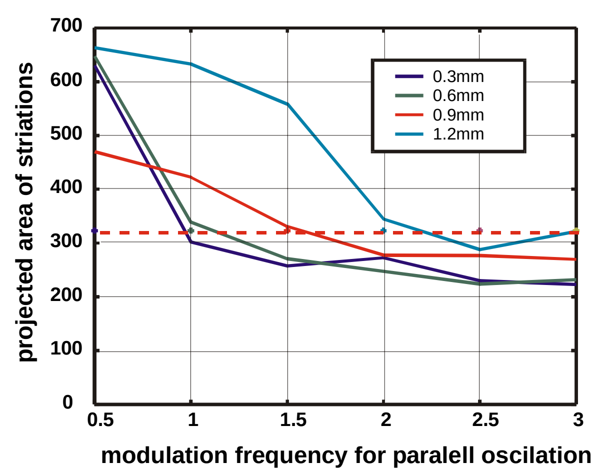

Figure 12: Projected area of striation occurance

2003 WTJA American Waterjet Conference
August 17-19, 2003 • Houston, Texas

Paper 1-H

AN ABRASIVE SUSPENSION WATERJET FOR DRILLING SMALL-DIAMETER HOLES

P.W. Johnson, A.J. Graettinger, and C.H. Sewell
The University of Alabama
Tuscaloosa, Alabama, U.S.A.

ABSTRACT

An abrasive-suspension waterjet tool was developed to demonstrate the feasibility of drilling small-diameter long-reach holes to allow non-destructive inspection of foundation piles. Using a 34 MPa (5,000 psi) pump and a 6.35 mm (1/4 –inch) drill rod, the unit delivers a jet of water, garnet, and SUPER-WATER® that rapidly cuts holes in a variety of materials. In laboratory tests, the unit produced straight, in-gauge holes as little as 9.53 mm (3/8-inch) in diameter to depths up to three feet in pre-cast concrete pilings, brick, concrete masonry units, high-strength reinforced concrete, steel rebar, sandstone, wood, steel casing, and plate glass.

1. INTRODUCTION

This research focused on developing a method to evaluate concrete bridge foundations for scour through direct inspection (Graettinger, et al., 2003). Bridge scour is caused by a river changing course or rising enough to remove soil from around or under bridge foundations or abutments. It is the leading cause of failure of over-water bridges in the United States (FHWA HEC-18 Richardson et al., 1993). Scour often occurs during severe storm events when bridges are the most vital link in a transportation network. Determining a bridge's susceptibility to scour requires an accurate understanding of the existing foundation. For older bridges, as-built foundation drawings may not exist or may be inaccurate, so an in-field testing method is needed to determine foundation length.

It is hypothesized that narrow inspection holes, centered in the piling, would have a negligible effect on strength, yet allow for direct sampling. But to drill such holes, 12.7 mm (1/2–inch) in diameter or smaller and up to 30.5 m (100 ft) long, would require development of new technology. To implement the new method, called Micro-Intrusive Testing (MIT), an abrasive-waterjet drill, designed to drill through concrete, rock, and reinforcing steel, was built and tested at the University of Alabama.

There are three major components of the waterjet: 1) a 34 MPa (5,000 pound-per-square-inch (psi)) pump, 2) an accumulator, and 3) a drill. The pump, a 34 MPa (5,000-psi) off-the-shelf contractor-grade pressure washer, supplies the pressure needed to accelerate water and abrasive suspension at the drill tip so that the stream will cut the target material. The accumulator stores the abrasive suspension and meters it in to the pressurized water upstream of the nozzle. The abrasive suspension is a mixture of water, garnet, and SUPER-WATER®. The drill stand is a small metal lathe turned on end that holds, turns, and advances the drill rod. The drill rod and tip 6.35 mm (1/4 inch) in diameter. The cost of the entire waterjet unit is approximately $14,000.

2. ABRASIVE SUSPENSION WATERJET COMPONENTS

2.1 Accumulators

The accumulators, Figure 1, are designed to hold the abrasive suspension at the operating pressure (34 MPa (5,000 psi)) and continuously release a small amount of the suspension into the fresh water stream. The cart has two accumulators so one can be charged with the abrasive suspension while the other is being employed for drilling. This allows for continuous drilling.

The cart holds two accumulators (A and B) and a paint pot. The two accumulators are inverted so they can be charged with abrasive suspension from the top. A bladder underneath the suspension charge is pressurized by the water pump. That pressure plus the suction from the flow of water across the t-fitting at the top is sufficient to meter the abrasive suspension into the high-pressure water stream. The paint pot holds the abrasive suspension before it is pumped in to the accumulators.

2.2 Drill Stand

The drill stand consists of a cart with a vertically mounted lathe as shown in Figure 2. The lathe is used to hold, rotate, and advance the drill rod into the hole. The lathe is mounted with the crosshead fixed so that the lathe body can travel vertically. A counterweight allows for easy and accurate vertical positioning. Safety shields were added to the front of the cart to prevent the abrasive-waterjet from spraying the lathe and operators.

2.3 Drill Rods And Tips

A drill rod is a steel tube that connects from a swivel on the high-pressure to the drill tip. The drill tip is a tungsten carbide insert that has an orifice diameter of approximately .79 mm (1/32-inch). Experimental drill rods ranged in diameter from 3.18 to 12.7 mm (1/8 to 1/2 inches) and in length from 1.22 to 2.44 m (four to eight feet). All tips were approximately the same size, but were oriented either straight or at a small angle (approximately five degrees) to the axis of the drill rod. Tips were centered in some drill rods and were offset in others. Multiple combinations of rods and tips were fabricated and tested.

2.4 Garnet Suspension

The most efficient garnet suspension, a mixture of tap water, garnet, and SUPER-WATER® to keep the garnet in suspension, was developed by trial and error. The goal was to develop a mix to hold the abrasive in suspension for weeks or even months while maintaining the ability to flow. The abrasive is a crushed garnet with sharp angular particles, a particle size range of 0.125-0.355 mm (125-355 microns), and hardness between 6.5 and 7.5.

The final mix design was five liters (1.32 gallons) of tap water, 100 grams (of SUPER-WATER®, and ten kilograms of garnet. By weight the suspension consisted of 0.66% SUPER-WATER®, 66.22% garnet with a specific gravity of about 4.2 and 33.11% water. The net specific gravity of the suspension was 2.02, and the liquid volume fraction of SUPER-WATER® was 2%. The mixture had good flow characteristics, and an undisturbed sample showed little or no tendency for the garnet to settle out even when held still for over a month.

3. TESTS

Both equipment and the drillability of typical civil engineering materials were tested. These investigations were run in parallel with equipment modifications, specifically testing different drilling rods, tips, and tip orientations, while at the same time drilling different target materials. The results drilling can be seen in Table 1.

4. SAMPLE MATERIALS

Eight different materials were drilled during this research project. The materials drilled and results are as follows:

4.1 Red Brick

A red brick, Figure 4, was drilled while the equipment was being proof tested and operating procedures were being developed. A small hole was cut using pure water with a straight-centered nozzle on a 12.7 mm (1/2-inch) drill rod. The hole was cut in about one minute. The diameter of the hole was too small to allow the 12.7 mm (1/2-inch) rod to penetrate.

4.2 Concrete Masonry Unit

While becoming accustomed to the abrasive-waterjet drilling equipment, numerous runs were made on concrete masonry units (CMU's), commonly called cinderblocks. Cinderblocks are easy to manage, align, and cut very rapidly with pure water or water-abrasive mixtures. The abrasive-waterjet drilled 40.6 cm (16 inches) through a CMU in seven minutes. It was found that cutting occurred up to seven inches in front of the tip.

4.3 Reinforced Quickcrete

Several reinforced quickcrete samples were made to form a pile-like material. Samples were eight inches in diameter and lengths between one and three feet. Although these samples allowed longer drilling runs, samples were improperly compacted and full of voids. The quickcrete samples did, firmly hold the reinforcing steel, which demonstrates that the abrasive waterjet drill would rapidly cut through rebar (Figure 5).

4.4 High-Strength Reinforced Concrete

The high strength reinforced concrete samples were sections of spun-formed light poles. The tested compressive strength was 11,000 psi. The samples had a dense aggregate packing and steel reinforcing cables. The abrasive-waterjet drill penetrated these samples rapidly and effectively.

4.5 Steel Rebar

Numerous holes were drilled through steel rebar and cables. Penetration rates were quite rapid (3.23 cm (1.27 inches) in 40 seconds in one case) and because the tip never touched the target material, there was no tendency for the drill to walk or skip off the steel rebar. While penetration of rebar is not a problem, creating a hole with a large enough diameter for the drill rod to pass through is a problem (Figure 6.). The solution was to use an "offset" tip where the nozzle is aligned to the pipe, but not in the center of the pipe. Such a tip cut a full-sized hole through rebar when the standoff distance was maintained at one to two inches.

4.6 Pottsville Sandstone

A Pottsville Sandstone core (Figure 7), taken from a local coal mining operation, was drilled. The sandstone sample was relatively homogenous when compared to other samples drilled. Because of that, the drilled hole was particularly small and consistent. The hole stayed within gage at about 9.53 mm (3/8-inch) for the full sample length of 17.78 cm (7 inches).

4.7 Creosote Treated Wood Pole

Since some bridge pilings are wood, the abrasive-waterjet drill was tested on a wood pole. The drill cut the wood pole rapidly, but produced long-stringy chips that were hard to clean from the hole.

4.8 3/4-Inch Glass Plate

With 5,000-psi pure water, some penetration was achieved, but the glass cracked. Using abrasive, a hole was cut through the glass almost instantaneously (about 3 seconds), but once again cracked the glass. Cracking is a common problem when cutting glass, and requires pressure control beyond that of the present equipment.

5. OPERATING RESULTS

5.1 Water Rate

For all tests the pump was running at the normal operating pressure of 34 MPa (5,000 psi). Under these conditions, the flow rate is controlled by the pressure losses in the system. Since most of the loss occurs at the tip where the flow energy is converted to velocity, a simple Bernoulli's Law calculation modified for friction loss can be used to estimate the flow rate if the nozzle diameter is known. This method becomes unreliable as the nozzle diameter increases due to wear.

The flow rate was also calculated by weighing the total fluid pumped during a timed period of flow. This calculation matched well with the Bernoulli estimates. Flow rates varied between 0.107 and 0.177 liter per second (1.7 and 2.8 gallons per minute (gpm)). Flow rates were measured for pure water, and not measured with garnet in the flow. It is likely that the total flow rate decreases when garnet is added since the net fluid density increases.

5.2 Abrasive Consumption

To calculate the abrasive suspension consumption, the accumulator cart was weighed before and after drilling. The suspension is injected by displacement with water, so the amount of garnet consumed is calculated as:

$$W_g = \Delta W \, f_g \, S_s / (S_s - 1)$$

5.3 Hole Size

The target hole size for this project was a 91.44 cm (36-inch) long hole in concrete having a diameter of 12.7 mm (1/2-inch). It is expected that such a small diameter will have a negligible effect on a pile's strength. The 6.35 mm (1/4-inch) drilling rods consistently produced holes with diameters between 9.53 to 12.7 mm (3/8 to 1/2-inch), and were used to drill one 91.44 cm (36-inch) hole.

6. DISCUSSION AND CONCLUSIONS

Abrasive waterjet systems cut when the abrasive is accelerated above a critical velocity and the abrasive particles begin to chip out pieces of the target material upon collision. The higher the abrasive velocity, the more effective the cutting becomes. Most abrasive-waterjet systems use an external feed of abrasive. A separate feed of dry abrasive is incorporated into the liquid jet immediately downstream of the nozzle. The advantage of this system is that the mixing occurs at atmospheric pressure. The main drawback of this technology are 1) the requirement for separate liquid and particle streams result in an overly large cutting head, and 2) external mixing of water and abrasive is inefficient at accelerating the abrasive particles. Swanson et al. (1987) have shown that external feeds produce an abrasive velocity of only about 25 percent of the water velocity, so external feed systems require very high water pressures to achieve effective cutting.

The target hole of 12.7 mm (1/2-inch) for this research was too small to allow an external abrasive feed in a deep hole. In addition, the system had to be low-pressure to be economical. The abrasive-waterjet drill designed in this research introduces a polymer-abrasive mix on the high-pressure side of the nozzle downstream of the pump. The system uses an off-the-shelf pressure washer to supply only 34 MPa (5,000 psi). This arrangement results in efficient momentum transfer between the water and the abrasive particles, which allows for drilling that would otherwise require 207 to 276 MPa (30,000 to 40,000) psi.

In addition to the abrasive-waterjet equipment, special drilling rods and tips, between 12.7 and 3.18 mm (1/2 and 1/8-inch) in diameter, were developed. These rods are between 1.22 and 2.44 m (four and eight feet) long and are apparently the smallest diameter currently in use for geological and geotechnical applications. Holes as small as 9.53 mm (3/8-inch) in diameter, and as long as 0.91 m (three feet), were drilled with these rods. An unexpected benefit of these small diameter long rods is that deep cuts can be made by moving the head back and forth while lowering the rod into the cut. This abrasive-waterjet drilling systems rapidly drills long, small diameter holes through concrete, hard aggregate, and steel rebar.

7. REFERENCES

Dickinson, W., R. D. Wilkes, and R. W. Dickinson. "Conical Water Jet Drilling." *Proceedings of the Fourth U.S. Water Jet Conference*. pp. 89-96. 1987.

French, M. A. "Safety in high-pressure water jetting." *Water Jet Applications in Construction Engineering*. pp. 387-397. 1998.

Galecki, G. and M. Mazurkiewicz. "Hydroabrasive Cutting Head – Energy Transfer Efficiency." *Proceedings of the Fourth U.S. Water Jet Conference*. pg. 109-111. 1987.

Graettinger, A. "Foundation Evaluation with Micro Intrusive Testing." *UTCA Report Number 01114*. 2002.

Howells, W. Glenn, "Super-Water® Jetting Applications from 1974-1999." *Proceedings of the 10th American Waterjet Conference*, August 1999, Huston, TX. www.aquaprep.com.au. 1999.

Johnson, P. A. and B. M. Ayyub. "Assessing Time-Variant Bridge Reliability due to Pier Scour." *Journal of Hydraulic Engineering*. Vol. 118, no. 6. pp. 887-903. 1992.

Johnson, P. A. "Fault Tree Analysis of Bridge Failure due to Scour and Channel Instability." *Journal of Infrastructure Systems*. March 1999. pp. 35-41. 1999.

Kolle, J. J. "Water and abrasive jetting, and mechanical techniques expedite hard rock drilling." *Oil and Gas Journal*. April 20, 1998. pp. 90-94. 1998.

Nittinger, R. J. "Hydro Demolition – Technology for Productivity and Profits for America." *Proceedings of the Fourth U.S. Water Jet Conference.* pp. 65-71. 1987.

Peters, H. "Stationary jet cutting of construction engineering materials." *Water Jet Applications in Construction Engineering.* pp. 367-383. 1998.

Richardson, E.V., L.J. Harrison, J.R. Richardson, and S.R. Davis. "Evaluating Scour at Bridges." *FHWA HEC No. 18 (Hec-18) Second edition*, publication FHWA-IP-90-017, Revised April, 1993.

Savanick, G. A. and W. G. Krawza "An Abrasive Water Jet Rock Drill." *Proceedings of the Fourth U.S. Water Jet Conference*. pp. 129-132. 1987.

Swanson, R. K., M. Kilman, S. Cerwin, W. Tarver, and R. Wellman. "Study of Particle Velocities in Water Driven Abrasive Jet Cutting." *Proceedings of the Fourth U.S. Water Jet Conference*. pp. 103-107. 1987.

Szymczak, M., S. Tavoularis, A. Fahim, and M. M. Vijay, "Flow Visualization of High-Speed Water Jets." *Proceedings of the Fourth U.S. Water Jet Conference*. pp. 43-49. 1987.

Wu, W. Z., D. A. Summers, and M. J. Tzeng, “Dynamic Characteristics of Waterjets Generated from Oscillating Systems.” *Proceedings of the Fourth U.S. Water Jet Conference*. pp. 35-41. 1987.

Zeng, J. and T. Kim. “Application of a brittle erosion model for abrasive waterjet cutting of asphalt concrete.” *Water Jet Applications in Construction Engineering*. pp. 149-159. 1998.

8. NOMENCLATURE

f_g = the weight fraction of garnet in the suspension = 0.6622
S_s = the specific gravity of the suspension = 2.02
ΔW = the change in weight of the accumulator cart during drilling
W_g = the weight of garnet consumed

9. TABLES

Table 1. A compendium of results from the drilling tests.

Date	Sample[1]	Rod:tip (mm)	Water (L/sec)	Garnet (g/sec)	Duration (sec)	Rev/sec	Depth (cm)	Hole Dia. (cm)
08/09/02	Brick	12.7:0.79	Small hole, water only, testing equipment					
08/12/02	CMU	12.7:0.79	Small hole, water only, testing equipment					
08/12/02	HSRC	12.7:0.79	Oversize hole, angled tip, testing equipment with garnet					
08/12/02	Wood	12.7:1/32	Oversize hole, angled tip, testing equipment with garnet					
08/20/02	CMU[2]	6.35:0.79	0.11	23.44	354	1	11.2	< 1.27
08/30/02	CMU[3]	6.35:0.79	0.17	8.32	462	1	40.6	< 1.27
08/30/02	HSRC[4]	6.35:0.79	0.17	12.10	228	2	14.2	< 1.27
08/30/02	HSRC	6.35:0.79	0.17	7.56	246	1	11.2	< 1.27
08/30/02	RQ[5]	6.35:0.79	0.17	12.85	234	1		< 0.64
09/05/02	PS	6.35:0.79	demonstration only, no data				15.2	0.95
09/20/02	#10 rebar	6.35:0.79	0.17	59.72	42		3.3	< 1.27
09/20/02	#10 rebar	6.35:0.79	0.17	31.75	510			< 1.27
09/20/02	3/4 Glass	6.35:0.79	0.17		6		2	< 1.27
10/01/02	RQ	6.35:0.79			480	1	91.4	< 1.27

[1] CMU – Concrete Masonry Unit, HSRC High-Strength Reinforced concrete, RQ reinforced quickcrete, PS Pottsville Sandstone

[2] A steel nozzle was used for this test, and the I.d. of the nozzle washed-out from 1/32 to about 1/16 -inch during the test. The water rate is measured from the original tip diameter.

[3] The drill rod penetrated the block about 10 inches.

[4] Drilled through a steel reinforcing cable at the surface, but the hole was too small to pass the drill rod

[5] Drilled through rebar, but hole was too small to pass the drill rod

10. GRAPHICS

Figure 1. The accumulators mounted for field application, along with a “paint pot” for recharging.

Figure 2. The drill stand showing the lathe for rotating and advancing the drill rod, the high-pressure connections, and the counterweight cable.

Figure 3. Various experimental drill rods and tips. The 6.35 mm (1/4-inch) rods were the most successful, and a tip aligned with rod axis but off-center (second from left), proved the best combination of all

Figure 4. A standard red brick drilled with pure water.

Figure 5. An example of a hole cut through rebar in a reinforced quickcrete sample.

Figure 6. A small hole through a piece of #10 rebar. This hole was not large enough to pass the drill rod, but subsequent modifications of the tip allowed for full-size holes that would allow the rod to penetrate.

Figure 7. The Pottsville sandstone core, showing the entry of a straight, in-gage hole.

2003 WJTA American Waterjet Conference
August 17-19, 2003 ● Houston, Texas

Paper 2-H

A METHOD FOR SUPPRESSION OF BUILDING FIRES, WHILE PROVIDING ACCESS FOR INTERROGATIVE EQUIPMENT

Samir Dorle, D.A. Summers, A. Gupta
University of Missouri – Rolla
Rolla, Missouri, USA

ABSTRACT

This paper describes the development of a light-weight tool that can be easily transported to a site where there has been a building collapse or fire (whether natural or man-induced). The tool is a small abrasive slurry waterjet that can drill through all the components of the collapsed building, including steel and concrete beams, so that water can be brought to the center of any fire in the structure and so that microphones and other instruments to detect survivors can also be carried through the channel created to the heart of the structure.

Organized and Sponsored by the Waterjet Technology Association

1. INTRODUCTION

When a building is destroyed due to either a man-made or natural cause one will want to inspect the inside structure to find any survivors in the shortest possible time and without further injuring anyone that has been trapped inside. As of today there is no single method that can create a consistent hole through the different materials that will form the pile of rubble created by such an event. Uniquely it is possible that an abrasive waterjet tool may be one way to do this.

Occupied buildings collapse for a number of reasons: both natural, through fire, flood and earthquake and through man-made events such as war, or terrorist attack. In the collapse of the building the outer walls and part of the roofing structure can cover the central part of the building, which can catch fire, and which frequently contains victims.

Access to the heart of the rubblized building is often difficult to achieve since the blocks are hap hazardously stacked and the inter-layers can contain steel, concrete and other materials. This poses a particular problem in that the tools most effective in cutting concrete (drills, impact breakers and splitting tools) do not work well in cutting steel. Likewise the tools that are most effective in cutting steel (flame torches for example) do not work well in cutting concrete. The problem is exacerbated since rubble piles can be quite unstable and thus high impact forces on the pile can cause movement and increase the risk to any rescuers or trapped victims.

Further, if such a tool is to be developed it must be readily available, be not too expensive or difficult to operate and be operable by people without a high degree of technical skill or training. But, if versatile tools can be developed that have multiple uses, then some of these constraints may no longer apply. Further, if the tools can be made to be relatively inexpensive and lightweight then they can be distributed around the community without great cost. And if they can be developed to have a more normal use in other applications, then their availability at a time of sudden critical need becomes more assured. This then provides a different set of constraints on the development of rescue tools, but one that can be addressed in their evolution. As an example of such a tool this paper will consider the use of an abrasive waterjet system as one of the versatile tools for the rescue professional. It exemplifies a process and approach that may have value in the development of other tools for use in these circumstances.

1.1. The Perceived Need

There are a number of critical problems that arise when a building collapses. In the immediate aftermath of the collapse there is the need to determine if any survivors are trapped within the debris pile. Secondarily, there is often a need to extinguish a burning zone within the structure. Both needs are best served by gaining access to the interior of the remaining structure. However, this structure is usually precariously balanced and made up of randomly oriented layers that can be made from a wide variety of materials. This means that conventional access from outside the zone is difficult because of the presence of these beams and walls and their varied composition. And if a hole were to be drilled, it must be able to penetrate through all the materials that it might encounter. It must be able to do this without disturbing the structure, and without causing an additional threat to any survivors that might be present. The presence of cracks and open voids also make conventional drilling difficult.

2. BACKGROUND

High-pressure waterjets have, in their modern resurgence, had two basic industries that they have developed to serve. The first of these is the cutting application in manufacturing. Water under very high pressure can easily cut through relatively soft materials, such as wood and paper.

The narrow range of applications that are available for plain water use, even at these high pressures has, however, limited the overall application of this tool.

Concurrent with the growth of an industry at the high end of the waterjet spectrum another industry has also developed. This has been the use of high pressure waterjet systems for cleaning surfaces. Initially, these operations were not much more than portable car-wash units, operated at relatively low pressure, and used for cleaning large areal surfaces such as houses and the like. With the passage of time the pumps available have been able to generate higher pressures, and have created a sufficiently large market that more manufacturers have been drawn to the industry. This increased competition has resulted not only in cheaper and more reliable systems, but also systems that operate at higher pressure. In the United States one can obtain a pressure washer that operates at around 10 MPa for a cost of less that $200. Units are also available locally (this in a small Midwestern town) that operate at pressures of up to 50 MPa and at relatively low cost.

In a practical sense, conventional waterjets are limited in applications to cutting and drilling materials that are usually fibrous, porous, granular or soft. Hard and dense materials, such as glass, metals and fired ceramics call for more powerful jets. However, there are practical limits to the operational pressure that can be used for this purpose. This pressure is typically around 100,000 psi and this is often insufficient to effectively cut some of these harder materials (Ref. 1). The use of an abrasive feed into the waterjet stream provides a way of solving this problem. It is possible to enhance the performance of waterjets by changing the structure of the available energy using methods such as the addition of long-chain polymers (Ref. 2), the use of jet pulsation (Ref. 3), and the development of segmented (Ref. 4) and cavitating jets (Ref. 5).

However the most effective of all jets as of today for cutting hard materials, is that wherein the jet contains abrasive, and where fine abrasive particles are injected into the jet stream to aid in cutting. By feeding the high pressure jet through a small chamber and then into a second collimating nozzle, suction is created in the chamber. This can be used to draw a small amount of abrasive into the chamber and to mix it with the water to create an abrasive cutting stream. This combination, known as an Abrasive Water Jet (AWJ) is now sufficiently powerful that it will cut through a wide variety of metals and other materials. Operated at pressures of up to 400 MPa and with roughly 8% abrasive in the stream, this tool has found a growing range of application. The tool has a number of advantages. Because the cut is made by the multitude of very small particles (typically on the order of 150 μm in size) it can be made very precisely and without any impact on the material surrounding the edge of the cut. Since it does not generate significant heat in this process (and the water can dissipate some of that generated) it is known as a cold cutting tool. In addition the reaction force exerted by the jet is small. Labus (Ref. 6) quotes this force as being

$$Thrust(Newtons) = 0.745\, Q \sqrt{P}$$

where Q is the flow rate in liters/min and P is the jet pressure in MPa.

This means two separate but encouraging things for our overall purpose, firstly that the jet will not exert much force on the piece being cut, and secondly that it will not require a lot of force to hold the cutting nozzle in place.

The impact that this new tool had on industry has been steadily growing. The low reaction force required to hold the tool meant that it could be integrated with robotic systems for precise and repetitive cutting of parts. The ability of the tool to precisely cut through as much as 30 cm of glass meant that it became a tool of choice for precise cutting of optical parts, while the cool cutting operation made it also very useful for cutting metals such as titanium. Thus, over the years, a significant number of small cutting shops have developed around the world where these systems are available and are used to cut everything from advanced composites to polished stone for floors and walls.

The development of this tool has therefore gone a considerable way towards the creation of the universal cutting tool that is required for use in cutting through buildings that have collapsed. In its original form, however, it still has a number of disadvantages. The first of these is the expense of the system, pumps that operate at 400 MPa come at a cost that makes them impractical for most common applications. Further the equipment that is available must contain this pressure, and thus all the components require highly precise machining, and considerable skill in maintenance and operation. The waterjet machine tool market, for precision cutting of small metal and composite material parts, has emerged as one of the faster growing market segments, with a growth rate forecast at 9.1 percent for the period [1997-2004].

The idea of adding abrasive to the waterjet before it exits the primary nozzle was developed into a system that has since become known as DIAjet (Direct Injection of Abrasive jet) system. More recently, given the proprietary nature of that name this has been changed to the more generic description of Abrasive Slurry Jetting (ASJ). This design overcomes some of the disadvantages of the conventional method of introducing abrasives into a waterjet stream. Instead of mixing the abrasive in a chamber, following the acceleration of the water, the abrasive is metered into the flow of water from the pressurizing pump to the nozzle. This is achieved by first adding the abrasive to a tank, which can be pressurized to the delivery pressure, and then connecting this tank into a loop attached to the delivery line. The connections are made through valves, and a metering valve controls flow through the loop. In this way the concentration of abrasive feeding into the line can be controlled (Figure 1). The system provides an alternative to the conventional AWJ system, and to differentiate it from that system it has been called the Abrasive Slurry Jet (ASJ).

Subsequent experiments have shown (Ref. 10) that when the water and abrasive are mixed in this way, the jet can cut material (other things being equal) at a quarter, or less, of the pressure required with the AWJ system. Not only does this reduce the power required by 75% but it also has the advantage of bringing the operating pressure of the system down to a range of pressures that can be supplied by the pumps developed for the cleaning industry.

This is an additional advantage because the pumps developed for the cleaning industry are operated in a wide variety of conditions and must be mobile. Factory installed very high pressure systems are usually permanently mounted and thus do not need to be as robust. The cleaning industry, however, requires a system that can be moved rapidly to a site, set up and operated by a workforce that is often casual labor, with little training. Thus, the pumps that have developed are, at this pressure level, already robust, simple to operate and easy to maintain. Further, while rescue operations require that all diligent speed be achieved in carrying out operations, the performance criteria are not as stringent as being able to consistently cut through 2-cm thick titanium sheet at a steady rate for 8 hours leaving a surface edge that is perfectly perpendicular to the facing surface. Rather, cuts do not need to be that precise, time scales are more flexible, and cutting is needed on an intermittent basis.

Thus, (and these conditions will change as the equipment continues to become more popular and developed) while it is possible now, for example, to cut through 8 mm of steel at a rate of 60 cm/min using a system at 70 MPa, the reduced cost, size and increased flexibility of a 35 MPa system suggests that this is currently a better choice for use in an ASJ system application.

At the 15th International Waterjet Symposium in Ronneby in Sweden the company CCS Cobra demonstrated that an abrasive waterjet could cut through the wall of a steel container and extinguish, relatively rapidly, the fire burning within.

It has been known for some years that sending a mist of droplets in the size range of around 150 microns is a very effective way of extinguishing the fire. This is because the droplets have sufficient energy to enter the flames, but are then small enough to vaporize in the fire, creating steam and cutting off the oxygen to the fuel. This can lead to fires being extinguished in as little as 30 seconds and with very little of the water damage which is often the greatest part of the damage resulting from fire. (Ref. 11)

Over the time that this new tool has developed it has been used to cut a very wide range of materials successfully. This is one of the requirements if we are to find a tool that can cut access into the heart of a collapsed building.

3. DEVELOPMENT OF A DISASTER RESCUE TOOL

The conventional use of a mist as an extinguisher has however, not been generally adopted since the mist rapidly attenuates in air, and thus a fire hose must approach the fire quite closely. However, the use of the mist will create a draft around the fireman and this will draw the fire down upon him. The tool has not therefore been adopted. However, if the mist can be delivered through a wall, then the fireman can be protected by that wall, while the mist can be directed into the heart of the fire. Thus, drilling the hole through the wall with the abrasive waterjet has a potentially large benefit.

The potential benefit of using this drill as a tool not only to penetrate the outer wall of a burning building, but also the rubble of a destroyed building is evident. Consider that after the World Trade Center was destroyed on September 11, 2002 there was a residual fire in the ruins for over four months. This is because there was no tool that could easily penetrate the mass of rubble to reach the heart of the fire. The intertwined mass of concrete and steel was not stable, and was largely accessed only by surface exploration. Water applied at the surface encountered the same sort of problems in reaching this flame as was found at a site in Montana (Ref. 12). The structure of the debris was such that channels existed that would carry the water away from the fire zone, and until the area was excavated no clear channel into the fire existed.

The original intent was to develop a small light-weight drilling system that could easily be carried to the site, and that would be small enough and simple enough that it could be used to drill a small diameter, but long straight hole into the rubble pile. By cautiously advancing this tool, which is capable of drilling through all the materials likely to be encountered, a conduit could be created into the pile through which instrumentation (including small video cameras and acoustic sensors) could be moved to give a better search capability within the body of the rubble. The low reaction force should not disturb the rubble pile, while the slow feed forward of the drill, through subsequent layers, with stops to check before penetrating each layer, should allow examination without posing additional risks to any survivors within the pile.

The equipment built has a capacity of delivering 35 MPa at 35 liters/min of water. Included water reservoir has a capacity of 500 liters. The pump, water reservoir, fuel reservoir and basic piping was attached to a support platform. The unit has been designed in such a way that it can be set in back of a pick up truck. The whole system is firmly mounted on a steel plate (size: Length – 2 meter, W – 2 meter). In addition, two cylinders that would hold a pressure of 35 MPa were also included in the assembly so that abrasive could be added to the water before it reached the cutting nozzle. A high-pressure hose carried the abrasive slurry from this platform to the drilling unit. (Figure 2 and Figure 3.)

The first unit built was designed to be light and simple. However, the nozzle at the end of the drilling rod must rotate to ensure that the hole was large enough in size to allow the nozzle assembly to pass. An abrasive jet will normally cut a slot some 3–4 times the width of the nozzle and the nozzle was around 0.75 mm in diameter. The nozzle body is around 4 cm in diameter.

To demonstrate the initial capability of the device it was used to drill through sequential targets that included concrete blocks and steel plates. As a measure of performance the nozzle drilled through a solid concrete wall 30 cm thick in 2 minutes. In order to demonstrate the lack of vibration a glass of water was set on top of one of the lighter construction blocks, and the ASJ system drilled through the block underneath without spilling any water (Figure 4). The speed of advance of the drill had to be controlled to ensure that it maintained hole diameter as it advanced.

During further studies, nozzles were modified so as produce a larger jet from the orifice and to further simplify and lighten the structure of the drill.

4. DEVELOPMENT OF A TOOL WITH WIDESPREAD USE POTENTIAL

Fire services will be the most likely users who will be called to use this tool. The majority of their operations deal with the small-scale disasters that occur in small communities where individual buildings and factories catch fire. The tool developed and marketed by the CCS Cobra Company (Ref. 13) has shown that it is possible to drill through building walls and roofs to gain immediate access to the heart of a fire without going through the normal doors and windows.

This capability has considerable importance, since in conventional fire fighting the most effective water distribution to cool and quench the fire is a very fine mist of water (droplet size above 100 μm) that penetrates to the burning zone (Ref. 11), but then the water vaporizes creating a blanket of steam, and not remaining to create large quantities of water damage. As discussed earlier, however, the use of water mists, while known, is not widely practiced. This is because the mist dissipates under normal delivery conditions quite close to the nozzle. Thus, for a fireman to use this tool the nozzle must be brought close to the fire, and if this requires that the fireman enter the building, then it creates a greater risk of injury. By drilling a hole through the side of the building the mist can be injected closer to the fire and with a reduced risk to the fireman. In the conventional design of the Cobra head, the jet creates a small hole through the side of the building and the nozzle and lance remain outside the building.

Experiments at UMR have shown that a small fire can be extinguished extremely rapidly with this method. Small fires were set within a steel barrel. The abrasive jet cut through 15 cm concrete block and the wall of the barrel (Figure 5) before reaching the fire – which went out as the jet penetrated the barrel wall (Figure 6).

Although this is a very effective way of using the technology, it suffers from a slight disadvantage when the nozzle is not carried into the fire. Because the hole is drilled at 35 MPa, the jet that cuts through into the burning room is moving at a speed of over 200 m/sec. This tends to draw air in with the stream so that any fire not directly in front of the jet, while knocked down, will continue to burn under the air drawn in by the jet velocity. To effectively extinguish the fire, therefore, the jet that cuts through the wall must be capable of being moved into the room, and maneuvered around it to reach the pockets of burning material not accessible from the hole in the wall.

The small size of the pump and delivery system required for fire fighting, with the benefits that it brings to the operation in terms of speed of fire fighting (the finer mist is generally a much faster cooling mechanism that conventional fire hose spray) has two ways in which it can be used. The first is similar to that supplied by CCS Cobra in which the system is mounted in a small mobile vehicle. This can bring a fire fighting capability into regions where access for larger fire fighting vehicles is difficult. For example in fighting a forest fire a Fire Chief may be reluctant to send a large engine down a narrow country road to fight a house fire, if there is the likelihood that the engine would have difficulty withdrawing if the fire spread. A smaller, and more mobile unit may well not have that problem. Similarly in an urban environment, small vehicles can more easily penetrate into the heart of a disaster than larger ones, and if the same fire can be extinguished, or brought under control with considerably less water, then it can be fought more rapidly and effectively.

Fire rescue services are, however, not only called upon to fight fires. In many locales they are the only professionals trained to rescue occupants when motor vehicles crash. In such circumstances rescue can be delayed while parts of the vehicle are severed and removed before access can be gained to the injured. The use of an ASJ system can provide a tool that can cut through the different materials (mainly metal) that trap the victim, and with such a localized cold cutting action that it is possible to achieve the cut without risk to the occupant even in the presence of gas vapors. The ASJ system has been used for cutting on the platforms in the North Sea and abrasive waterjets were used almost exclusively to cut through and remove the destroyed wellheads in Kuwait, after the Gulf War, prior to repair.

5. CONCLUSION

Disasters cannot be predicted and may occur at any point and time. To meet the response that is required, effective rescue tools must be readily available that can provide access to the site and increase the chance for finding and recovering trapped individuals. However, such equipment if large, can be too expensive to provide in sufficient numbers and locations that it can be readily available when needed.

Alternately, if small but effective tools that have other uses in more normal life are available, and with personnel that are trained in their use and use them regularly, then a more rapid and effective response to the disaster can be provided. The development of an abrasive slurry waterjet drill is given as an example of the development of such a tool. Its integration into conventional small-scale rescue can be the basis for providing a tool that can be easily modified to assist in the efforts required in a more major disaster.

Experiments at UMR have shown that the use of a small abrasive slurry waterjet at a pressure of 35 MPa is capable of drilling through both concrete layers over 30 cm thick, and can also cut through more than 25 mm steel. As the jet drilled through a concrete block it did not disturb a full glass of water placed on the top of that block.

Abrasive slurry jets are a relatively new development in cutting, yet their cost is not as great as that of conventional systems and they can be assembled from components, which are more readily available and reliable. The uses to which they can be put, particularly in unconventional applications are only just beginning to be explored, yet they hold the promise of solving some otherwise intractable problems.

6. ACKNOWLEDGEMENTS

Several UMR students contributed to the development of the equipment used in this work, over and above the graduate students included as authors, that help and the help of the technical and administrative staff in the Rock Mechanics and Explosive Research Center at UMR is gratefully acknowledged.

7. REFERENCES

1. Summers, D. A. (1995), "Waterjetting Technology".
2. Hashish, M., "Cutting with High Pressure Abrasive Suspension Jets," paper 33, 6th American Water Jet Conference, Huston, TX, August 1991, pp.439-455.
3. Brook, N., and Summers, D.A., "The Penetration of Rock by High Pressure Water Jets," International Journal of Rock Mechanics and Mining Science, Vol. 6, 1969, pp. 249 – 258.
4. Summers, D.A., "Disintegration of Rock by High Pressure Jets," Ph.D. thesis, Department of Applied Mineral Science, University of Leeds, UK, May, 1968.
5. Johnson, V.E., Kohl, R.E., Thiruvengadam, A., and Conn, A.F., "Tunneling, fracturing drilling and mining with high speed water jets utilizing cavitation damage," paper A3, 1st International Symposium on Jet Cutting Technology, Coventry, UK, April, 1972.
6. Fairhurst, R. M., Abrasive Water Jet Cutting, MSc Thesis, Cranfield Institute of Technology, January, 1982.
9. Fairhurst, R.M., Heron, R.A., and Saunders, D.H., "Diajet" -- A New Abrasive Waterjet Cutting Technique," 8th International Symposium on Jet Cutting Technology, Durham, UK, September, 1986, pp. 395 - 402.10. Lexington demil paper.
11. See http://www.fogtec.com
12. Summers, D.A., Mazurkiewicz, M., Galecki, G., "Horizontal Waterjet Exploration of Burning Coal Seams," 8th International Symposium on Jet Cutting Technology, BHRA, Durham, England, September, 1986.
13. See http://www.ccs-cobra.com/

8. GRAPHICS

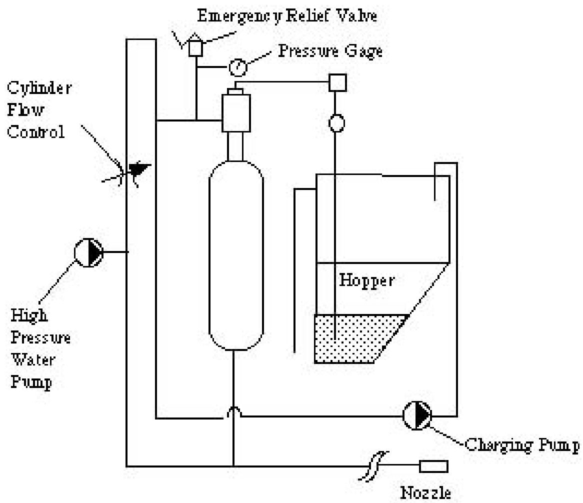

Figure 1. Schematic of the flow circuit of an abrasive slurry jetting system (Ref. 4).

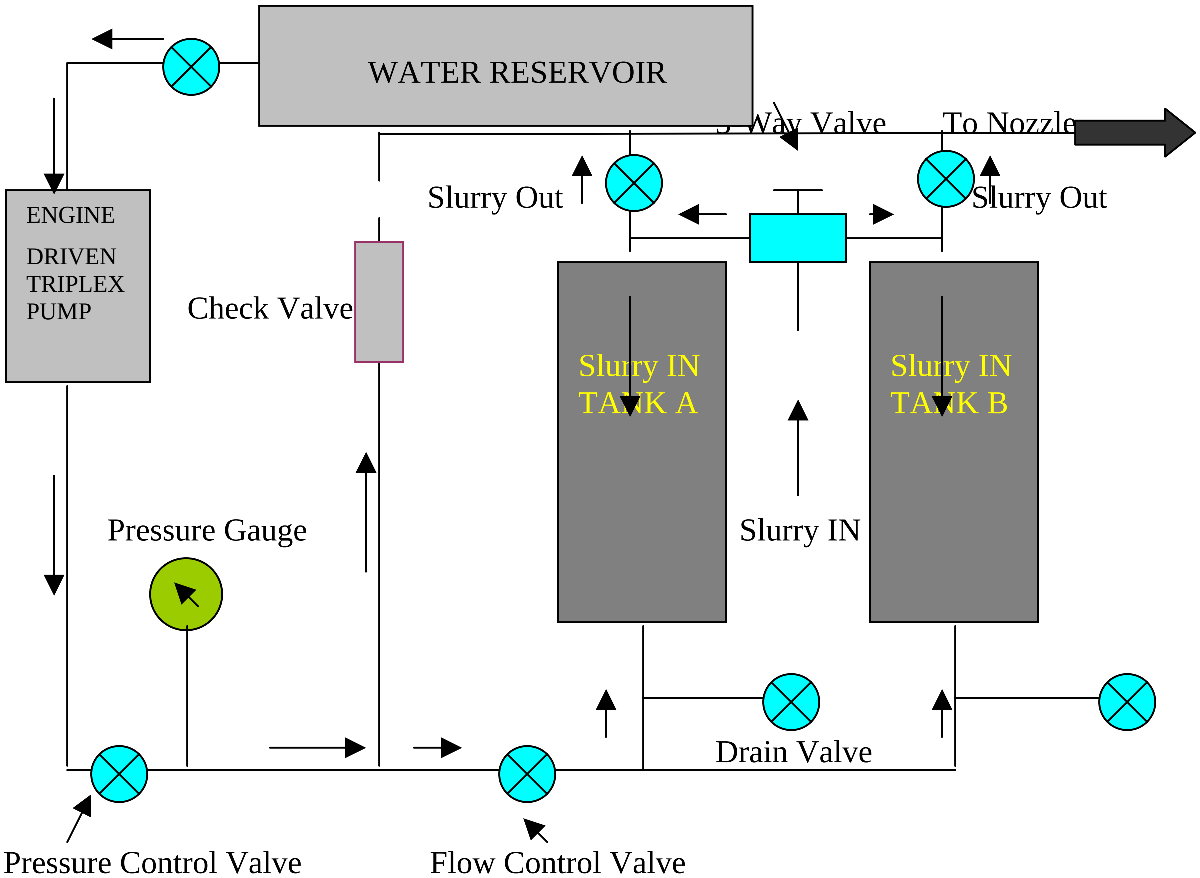

Figure 2. Schematic of Abrasive slurry system.

Figure 3. 35 MPa abrasive slurry system assembled to fit in the bed of a pickup truck.

Figure 4. Hole drilled through concrete and steel, note the glass of water.

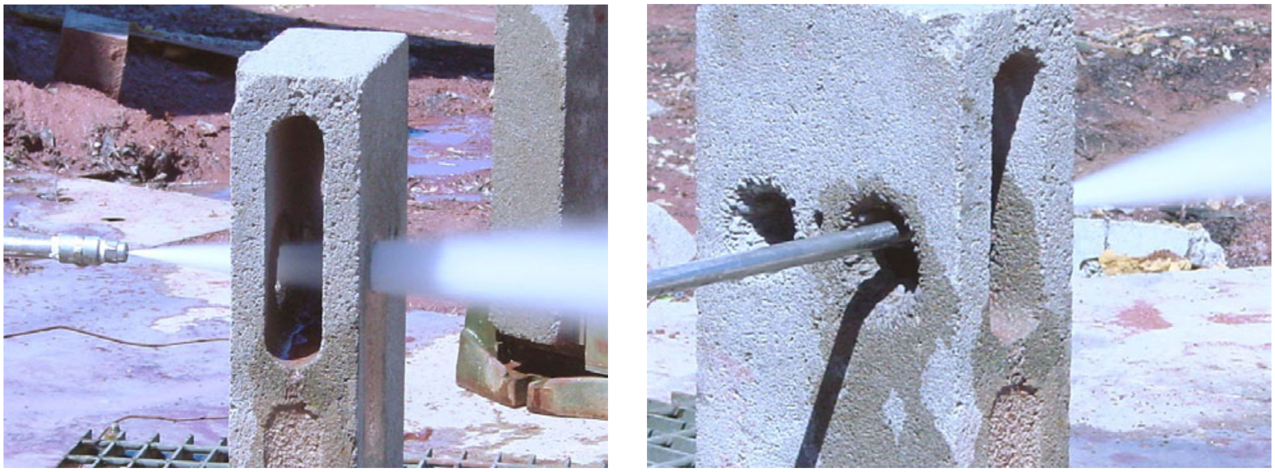

Figure 5. Hole drilled through concrete.

Figure 6. Sequence of frames taken from video of jet penetration into a barrel fire. (The frames are from a sequence so that there is one second between the first and last frames. The jet drill has gone through a concrete construction block and the wall of the barrel.)

2003 WJTA American Waterjet Conference
August 17-19, 2003 • Houston, Texas

Paper 3-H

WJ FORMING: A NEW OPPORTUNITY

E. Grossi, M. Monno and A. Vergari
Dipartimento di Meccanica, Politecnico di Milano, Italy

ABSTRACT

The WJ/AWJ technology has been used, in the recent years, in new applications as rapid prototyping, surface treatments etc.

This paper deals with WJ forming (WJF), a new application of Waterjet technology, that can have promising developments in the field of rapid prototyping. An elastic strain is applied to a low thickness metal sheet, clamping it along its perimeter to a frame having the shape in order to give to the sheet the configuration it has to take after a spring back at the end of the treatment; at this point, regulating the technological parameters to obtain the required energy, the impact of the water jet, following suitable paths, can generate on the slab a sufficient surface plastic strain in order to keep the defined shape also after removing the clamping devices (the process does not require dies). Until now this kind of sheet forming is made by shot peening deformation, where the sheet, clamped to a frame, is over and over again stricken by steel spheroids, carried by high pressure air.

Using the WJ forming technology instead of the shot peen deformation it is possible to avoid the indentation of sheet surface, but the sheet thickness you can deform is about few millimetres.

A preliminary analysis was made to determine factors which influence the process [9].

Then, after selecting the two most important parameters, experimentations have been carried out in order to demonstrate that there exist ranges for these two parameters that allow water jet to deform the sheet without removing material from the sheet surface.

A technological model has been developed for the WJF process, based on water pressure and feed rate of the head.

1 INTRODUCTION

The AWJ/WJ technology has shown, in recent years, a substantial development in the applications and a sensible improvement in the performances. Beside 2D or 3D cutting of a wide range of materials and beside the cleaning process, recent researches propose new applications for the AWJ/WJ technology such as sheet forming process and peening process [1-7].

The aim of water jet forming process is to generate on the slab a sufficient surface plastic strain in order to keep the defined shape also after removing the clamping devices; the aim of water jet peening process is to increase mechanical characteristics of sheet surface [7]. Both water jet forming and water jet peening process induce compressive residual stress on the sheet by the impact of highly coherent water jet on the surface.

The forming application of WJ technology could have promising developments in the field of the rapid prototyping, (fig. 1). An elastic strain is applied to a low thickness metallic slab, clamping it along its perimeter to a frame having the adequate shape in order to give to the sheet the configuration it has to take at the end of the treatment [7].

The sheet, this way bent, is subject to stretch strains that are localized in the upper layer and to compression strains in the lower one. The strain initially applied has to ensure that the sheet is subject to stretch and compression strains within the material elastic strain limit. If there wasn't any constraint, the sheet would lead to regain its original shape, because it has been subject to an elastic strain.

At this point, regulating the technological parameters to obtain the required energy, the water jet, following suitable paths, can generate on the slab a sufficient surface plastic strain to keep the defined shape also after removing the clamping devices (the process does not require dies) [1], also considering a certain spring back effect.

The WJ forming is based on the so called water hammering effect due to the impact, at high speed, of the water drops on the material surface. The action of the water drops causes a compression strain in the external layer, where the water jet impinges. So it is established an equilibrium between the strain induced by the curvature of the sheet and the compression due to the action of the drops on the sheet surface. The compression strains have to compensate the stretch ones, so the spring back is limited as much as possible and to give the sheet the plastic strain that is able to keep it in the required shape.

It is assumed that the effect of the water drops impact on the surface, has a hemispheric distribution and that the range of effect is relevant to the drop diameter. The depth of the plastic boundary that is possible to reach is dependent on the distribution of the water drop dimensions (at the moment under study), that are relevant to the characteristic of the primary nozzle, of the pump and to the physical properties of the water.

The *shot-peen forming* (SPF) is a process able to create metal bent parts starting by metal plane sheets; the shot-peen and the WJ are very similar, but to deform the sheets it makes use of spheroids that are hurled against the sheet surface by an air jet [3][5]. The main characteristics to distinguish the WJ forming from the SPF are the apparent absence of surface texture alterations, the absence of the spheroids (whose control is a critical point in the shot-peen forming) and of the traces they leave on the material. A further aspect is the maximisation of the residual strains on the surface instead of the inner layer.

Compared with traditional shot-peen forming (SPF), WJF is moreover capable of inducing compression residual stress without modifying surface roughness and topography.

The same equipment of the water jet technology can be used for cutting, cleaning, peening and forming, just by a suitable choice of process parameter levels.

The result of the WJF process is in connection with the water jet energy that impacts on sheet surface, then an analysis of water jet energy parameters proposed by literature have been made in order to find the energy parameter which is the most consistent of them with residual deformation of sheet changing the two most important process parameters, chosen before, in the ranges in which water jet deforms the sheet without removing material from the sheet surface.

A technological model has been developed in this paper for the WJF process, based on water pressure and feed rate of the head; the aim is verify if it is possible to control and to forecast the bending of the sheet without removing material from the workpiece surface.

2 PROCESS PARAMETERS FOR THE WATER JET FORMING

A preliminary study of the WJF process [9] outlined the WJF process is in connection with the water jet energy that impacts on sheet surface, but, when the energy increases, an erosion phenomenon and a roughness increasing of sheet surface have been observed in preliminary experiments. When the erosion phenomenon takes place the effect of water jet hammering decreases in terms of compressive residual stress on the treated surfaces.

A similar behaviour was observed for the WJ peening process [2].

The WJF process has been characterised in the preliminary study of WJF and its parameters are [9]:

- Water pressure
- Feed rate
- Lateral step
- Primary nozzle diameter
- Presence or absence of the focuser
- Focuser diameter
- Stand off distance
- Number of treatments (n)
- Water jet head inclination angle

The number of treatments (n), is the number of time the water jet repeats the same path on the specimen surface.

The inclination angle is the angle between the normal to the surface and the direction of the jet in the plane containing the feed rate direction (figg. 2a, 2b).

As it can be observed, among the main advantages of WJF there is the relatively limited number of process parameters that have to be controlled. Indeed, while traditional shot peen forming entails an accurate selection of the characteristics of the spheroids (i.e. material, size, shape and hardness [3][5]), WJF does not require any direct control of the spheroids.

Only the water pressure and feed rate parameters are changed during the experimentation in order to restrict the test number.

The number of treatments (n) has been kept to 1.

The other process parameters have been kept constant to values which maximise the forming effect process (table 1).

The equipment used for forming (fig. 4) consists of a structure, which will be described in the next paragraph and a water jet machining cell using pure water. The cutting table allows a working area of 1600x1900x150 mm with a maximum feed rate (u) of 22500 mm/min. The water pressure (P) can be increased up to 390 MPa by a double effect 37 kW intensifier, while the maximum water flow rate of the cell is 3.2 l/min.

Passing through high-pressure pipes, the water is led to the nozzle (d_n = 0.30 mm).

During the experimental runs the mixing chamber and the focuser, normally used in abrasive water jet, have been mounted on the water jet head. Indeed it has been proved in [4] that this such configuration enhances the compressive residual stress induced on the sheet surface, by enforcing the jet to break-up into drops. Therefore the stand off distance (s.o.d.) will be referred as the distance between the end of the focuser (characterized by a diameter d_l = 1.10 mm) and the workpiece.

The stand off distance influences the drop dimensions, the impact velocity, the jet section and the exposure time [2].

The water flow that comes out of the nozzle, in air, can be split in three regions: the first, close to the nozzle, where the jet remains coherent and continuous, the second, named principal region, characterized by a turbulent behaviour where the water drops are generated, finally in the third region where the flow spreads and diverges. The principal region is where the jet breaks into drops because of the turbulence. This phenomenon permits to deliver on the material surface pressures that are higher than that ones owned by the jet when it is still coherent and the flow is still continuous [8].

The stand off distance value is kept constant at 40 mm: this value is chosen in order to remain in the principal region and to maximise the forming effect process.

The path conferred to the head during the experimentation is composed by a set of parallel linear passes, characterized by a lateral step of 0.5 mm, which has been chosen after SEM observations (kerf width is about 0,50 mm fig. 4c) in order to have a complete covering of sheet surface.

Furthermore, between a linear movement and the adjacent one, the versus of the nozzle feed rate is inverted.

The inclination angle of cutting head is kept constant at 0° in order to maximize the impact energy of water jet on sheet surface.

Only water pressure and feed rate parameters are changed during the experimentation; ranges of these two parameters have to be chosen in order to have a water jet with energy enough lower to avoid erosion phenomenon appears on the sheet surface and enough high to deform the sheet.

The ranges of water pressure and feed rate parameters have been defined in a previous paper by the same authors [9]:

$$80 \text{ MPa} < P < 150 \text{ MPa} \qquad 10000 \text{ mm/min} < u < 20000 \text{ mm/min}$$

The upper limit of feed rate (u = 20000 mm/min) has been chosen close to the maximum feed rate of the water jet machining cell.

The lower limit of water pressure range (P = 80 MPa) has been selected close to the minimum level allowed by the available intensifier.

The upper limit of water pressure and the lower limit of feed rate have been chosen because of at this set (P=150 MPa and u = 10000 mm/min) the erosion phenomenon begins to appear on the treated sheet surface (fig. 3).

Then the values of process parameters which have been used in the experimentation are reported in the table 1.

3 EXPERIMENTATION AIMS

The water jet forming process has been characterised by the preliminary study [9] in which the process parameters of WJF have been found and ranges of water pressure and feed rate parameters have been suggested in order to allow to the water jet to form the sheet without removing material from the sheet surface.

Now it needs more experiments which demonstrate that, changing the water pressure and feed rate in the ranges shown in the table 1, the residual deformation changes; WJF result behaviour has to be found when the two process parameters change in their ranges.

The energy of water drops, impinging the sheet surface, influence the deformation; then a energy index has to be found to connect forming effect process with the water jet energy.

Then a technological model has to be developed to quantify and to forecast the metal sheet residual deformation which you can reach after the WJF changing the two main process parameters, water pressure and feed rate, in the ranges in which water jet deforms the sheet without removing material from the sheet surface.

4 EXPERIMENTATION SETTING AND MAXIMUM RESIDUAL BENDING

Some experiments have been carried out to verify WJF process effectiveness with the values of process parameters shown in the table 1; the water jet has to be able to release a surface layer of plastic deformations (compression) on the sheet surface which allows to keep the defined shape also after removing the clamping devices.

The other constraint which WJF process has to satisfy is to avoid water jet removes material from the sheet surface.

The experimental work has to demonstrate the coherence between residual deformation of the treated sheet and process parameters, with the aim to control bending by the jet energy.

The experimentation has to quantify capability of water jet forming process to release residual deformation of sheet.

Then an experimental plan has been made whose tests are arranged in accordance with factorial plan which has as factors the two chosen process parameters, water pressure and feed rate of head.

Factorial plane has been set to achieve the aims; the plan factors are the two main process parameters, water pressure and feed rate; levels numbers are chosen in order to satisfy two opposite requirements:

- Reduction of tests numbers because of its complexity and lasting
- Increasing of tests number to have high reliability of process results

Then a factorial plan is chosen with two factors and four levels for each factor.

There are three replications for each set of P and u, then tests number are 48 (2^4 x 3 = 48).

Levels of water pressure and feed rate of head, chosen for experimentation, are shown in the table 2.

The WJ machine, used for the experimental runs, doesn't to tilt the cutting head, so it was necessary to develop a specific fixturing system (fig. 4) to control the impact angle normal. Then, during tests the cutting head has gone back and forth along y-axis, which is parallel to specimen short edges; number of linear movements of cutting head has been calculated in order to achieve a perfect covering of sheet surface; between a linear movement and the adjacent one, two gears have shifted the specimen of a lateral step δ along the circular slides which have the same centre of curvature of specimen. Gears movements were obtained with a step motor controlled by computer.

The experimental trials were composed by two different steps: first an elastic deformation has been imposed to the sheet clamping it to a frame with a particular shape and then water jet has to release a thin thickness of compression plastic deformation in order to allow to the sheet to keep its deformed configuration also after removing constrains and after spring back effect.

The sample material is Aluminium 2017 and the dimensions are 400 x 40 x 1 mm.

The curvature, which has been imposed to the specimen, has been calculated in order to apply an elastic strain.

Specimen fibres above neutral fibre are in traction and the ones under neutral fibre are in compression (fig.6). Then stresses can be calculated using the:

$$\sigma = E \cdot \chi \cdot y \quad (1)$$

Where σ is the stress at distance y from the neutral fibre, E is young modulus of aluminium A 2017 (E = 71100 N/mm^2) , χ is the curvature, σ_Y is the yield point (σ_Y = 95 N/mm^2), χ_Y is curvature corresponding to the yield point and "s" is specimen thickness (s = 1mm).

The stress increases, with linear behaviour, coming from neutral fibre up to the specimen surface (1).

The curvature must be lower than one corresponding to the yield point of superficial fibre and then radius of curvature R must be higher than one corresponding to the yield point of superficial fibre ($\frac{1}{\chi_Y}$)

$$.\sigma_Y = E \cdot \chi_Y \cdot \frac{s}{2} \rightarrow \quad \frac{1}{\chi_Y} = \frac{E \cdot s}{2 \cdot \sigma_Y} = 374 \text{ mm} \qquad (2)$$

A radius of curvature "R" = 400 mm was chosen (fig.5); the maximum deflexion "A", corresponding to the radius of curvature "R", is 44 millimetres.

Initial elastic deformation is imposed by using a special frame (fig. 4).

Other theoretical approaches have been used to verify the initial deformation, imposed to the sample is in the elastic field. Anyway, before to start water jet forming process, constraints have been removed to verify that sample come back to initial no-deformated configuration.

The constraints were two hinges and two supports (fig. 4); the two hinges fixed short edges of the sample to the frame; the two supports have been fixed to the fixturing system and their position was the path of cutting head which went back and forth along the y-axis. Then it was possible to suppose that the sample has been fixed to the frame by two cylindrical hinges which were on the two short edges of sample and it had a support which was disposed along two bigger edges of sample.

The use of the supports allowed to avoid sample bending under water jet action, to avoid changing of stand off distance and to avoid part of water jet energy is used to flex sample rather than to release residual stress on sample surface; without the supports the sample begin twisted at high water pressure as you can see in the preliminary study of WJF process, where it was not possible to use texts made at a water pressure of 150 MPa, because samples began twisted[9].

At the end the remaining maximum deflection has been measured, for each experiment, after water jet forming process (figg. 7, 8).

The different system of constraints compared to one of preliminary study [9] has allowed using of high levels of water pressure (the sample didn't twist) and to obtain a higher value of residual deformation of treated sample at the same set of P and u, because water jet energy has been used to release plastic deformation on sample surface and not to inflect sample.

Results of experimentation show it is possible use the water jet technology to form thin sheet without removing material from the sheet surface (figg. 12, 13). WJF process practicability has been demonstrated with the values of process parameters shown in the table 1; the water jet is able to release a layer of plastic deformations of compression on the sheet surface which allows to the sheet to keep the defined shape also after removing the clamping devices, used to give initial elastic deformation to it.

Remaining maximum deflection increases if water pressure increases and if feed rate of head decreases (figg. 7, 8); remaining maximum deflection increases until a saturation region which starts at the set:

$$P = 125 \text{ MPa} \qquad u = 10000 \text{ mm/min}$$

An increase of water jet energy, due to an increase of water pressure parameter (set 150 MPa, 10000 mm/min), cannot determine a further increase of remaining maximum deflection because it is in the saturation area (figg. 7, 8).

Analysis of variance (Anova) has been used to verify result of WJF process is affected by the two parameters, water pressure and feed rate of head. Anova test demonstrates there is statistical evidence two parameters influence WJF process result.

5 ANALYSIS OF WATER JET ENERGY IN WJF PROCESS

The WJF process is relevant to the water jet energy that impacts on the sheet metal surface, then it is possible to verify if there is an energy parameter which is consistent with residual deformation of sheet changing the two process parameters, chosen before, in the ranges in which water jet deforms the sheet without removing material.

Two different water jet energy parameters, proposed in the literature, have been selected. Both indexes have been set for the water jet peening process [2] [10].

One of them is energetic index “E” which is the kinetic energy water jet has at the end of focuser [2]; the E index has been set using the same water jet equipment [2] which is used for WJF process.

The other index has been introduced by Hashish at BHR 2002 conference [10]; this index is the water jet impact pressure on the sheet surface; there was only the primary nozzle in the water jet head, used for peening process [10], while there were not focuser and mixing chamber. Then the impact pressure index has been set with an water jet equipment which is a little bit different from the one used for WJF experiments.

Then the energetic index “E” has to be more consistent than impact pressure index with WJF process results.

By analysis of two index values, which are calculated for each set of P and u (fig. 9), a very similar behaviour of two index and residual maximum bending can be observed (figg. 9, 10, 11). Energetic index is more consistent with residual maximum bending of sample than the water jet impact pressure (figg. 9, 10); in fact there are some difference between behaviours of impact pressure index and sheet residual deformation just next to a little change of residual maximum bending (figg. 9, 10).

Then the possibility to describe water jet capability to form thin sheet is demonstrated; this possibility will be tested in future experimentation.

6 A PREDICTIVE MODEL

An empirical model has been developed to connect sheet residual deformation to the WJF parameters. This model allows to forecast the bending of the specimen at a fixed set of P and u. Model results reliable when P and u change in the ranges chosen before:

$$80<P<150 \text{ MPa} \quad 10000<u<20000 \text{ mm/min}$$

Residual maximum deformation (R M D) depend on water pressure, on feed rate of head and on interaction of two the process parameters:

$$R.M.D. = 73{,}4 - 0{,}00124\,\mathrm{P}^2 - 0{,}517\sqrt{\mathrm{u}} + 0{,}00329\,\mathrm{P}\cdot\sqrt{\mathrm{u}}$$

The empirical model, which is obtained by regression analysis of factorial plane (four levels for each parameter) satisfy statistical hypothesis (fig. 11).

Foreseen values are very close next to the observed (R-Sq = 92.8% fig. 11).

7 CONCLUSIONS AND FURTHER RESEARCH

This study deals with WJ forming process, a new application of WJ technology, that can have promising developments in the field of the rapid prototyping and which could be used to form thin metal sheet without using dies in the future.

New applications of WJF process could be forming processes to obtain wing shape of aircraft or shape of some car body components.

WJF process effectiveness has been verified in this paper; right choose of process parameters allows water jet to release a surface layer of plastic deformations of compression on the sheet surface which allows to the sheet to keep the defined shape also after removing the clamping devices, used to give initial elastic deformation.

The possibility to modify WJF process result with changing process parameters has been demonstrated; residual maximum bending of metal sheet changes if values of process parameters, P and u, change in the ranges in which water jet is able to form without removing material from sheet surface.

The dependence of WJF process results on clamping devices has been demonstrated; the different system of constraints, compared to one of preliminary study [9], allows to obtain a higher value of residual deformation of treated sample at the same set of P and u than with the system of constraints used in the preliminary study [9].

Water jet capability to form low thickness sheet has been quantified; set of P and u has been found when residual maximum bending is about equal to initial elastic bending which has been imposed to the sheet.

An energy index has been found which is consistent with variations of residual maximum bending; this energy index has the same behaviour of residual maximum bending, when process parameters are changed in their ranges.

It needs a further investigations in order to verify if results of WJF process depend on type of WJ head paths (linear, circular,..).

An extension of investigation to other materials is necessary.

An implementation of WJF process, under development, by using finite element method, could be useful to foreseen final shape of specimen, when clamping device and energy and path of water jet are fixed.

8 NOMENCLATURE

P	Water pressure
U	Feed rate
δ	Lateral step
d_n	Primary nozzle diameter
d_f	Focuser diameter
s.o.d.	Stand off distance
n	Number of treatments (n)
α	Water jet head inclination angle
R.M.D.	Residual maximum deformation
E_k	Energy index of water jet
P_{impact}	Water jet impact pressure on the sheet surface

9 REFERENCES

[1] A. Makinouchi, C. Teodosiu, T. Nakagawa: Advance in FEM Simulation and its Related Technologies in Sheet Metal Forming. Annals of the CIRP, 47/2: 641-649. 321/28.

[2] B.M. Colosimo, M. Monno, Q. Semeraro: Process Parameters Control in Water Jet Peening. Vol. 15 - no.1 (January 2000).

[3] Andrews Grasty: Shot Peen Forming finite element prediction of deformated shape. Journal of Engineering manufacture, 1996.

[4] G. Holmqvist and K.M. Ojmertz: Water Jet Peening at Ultra-High Pressures. Proceedings of the 14th ICPR, Osaka, Japan 1997.

[5] Milton Weiner: People in finishing: shot peening. Metal Finishing, May 1995.

[6] D.-F. Walczyk, D.-E. Hardt: Rapid Tooling for Sheet Metal Forming Using Profiled Edge Laminations – Design Principles and Demonstration, Trans. of the ASME 1998.

[7] M. Annoni, M. Monno, A. Vergari: Abrasive Water Jet in Rapid Prototyping. 34th CIRP Seminar for Manufacturing Systems, Athens, May 2001.

[8] Yanaida: Flow characteristics of water jet in air. 5th Int. Symposium on Jet Cutting Technology 1980.

[9] M.Monno, A. Vergari: WJ Forming: a preliminary study Waterjet. 16th International Conference on Water Jetting, Aix En Provence (F), October 2002.

[10] M. Hashish, S. Kunaport, M. Ramulu: finite element analysis of residual stress by ultra high pressure waterjet. 16th International Conference on Water Jetting, Aix En Provence (F), October 2002.

Table 1 Process parameters values

Water pressure “P”	80<P<150 MPa	Focuser diameter “d_f”	1.10 mm
Feed rate “u”	10000<u<20000 mm/min	Nozzle diameter “d_n”	0.30 mm
Stand off distance “s.o.d.”	40 mm	Inclination angle “α”	0°
Lateral step “δ”	0.5 mm	Number of treatments “n”	1

Table 2 Process parameters values

Water pressure “P”	80, 105, 125, 150 MPa	Focuser diameter “d_f”	1.10 mm
Feed rate “u”	10000, 13500, 16500, 20000 mm/min	Nozzle diameter “d_n”	0.30 mm
Stand off distance “s.o.d.”	40 mm	Inclination angle “α”	0°
Lateral step “δ”	0.5 mm	Number of treatments “n”	1

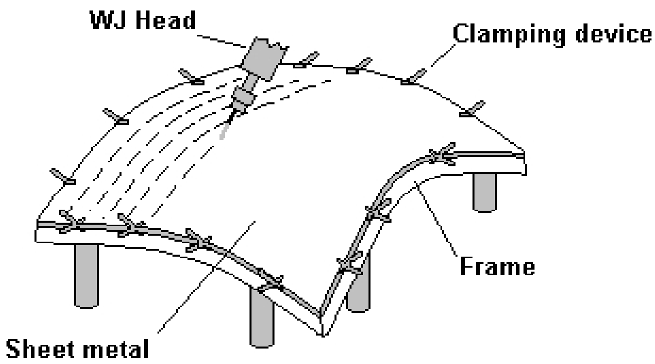

figure 1: Waterjet Forming

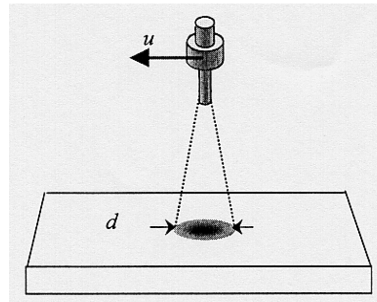

figure 2a: diameter of the impact surface

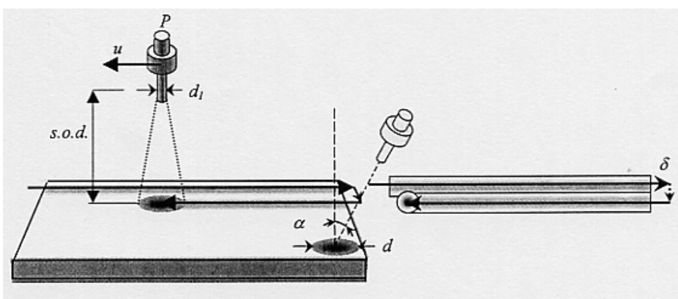

figure 2b: inclination angle of cutting heat

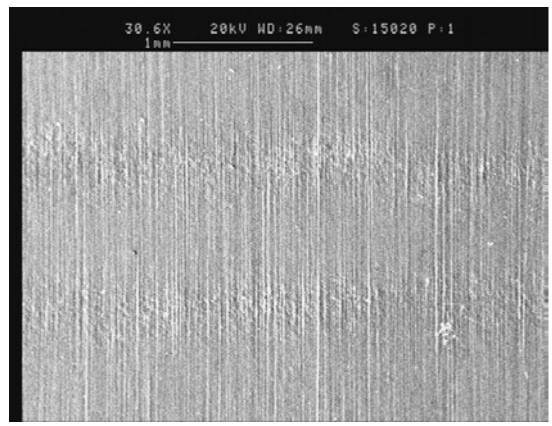

figure 3a: there are no craters on the sheet treated surface (150 MPa 20000 mm/min 30X)

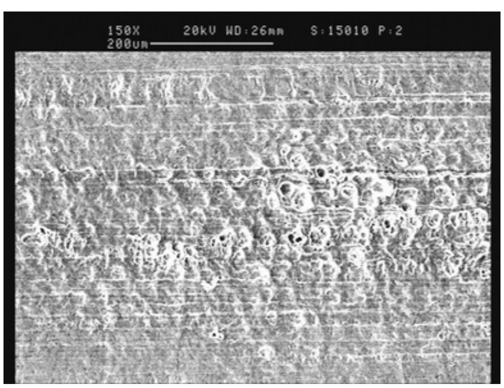

figure 3b: some craters begin to appear on the sheet treated surface (150 MPa 10000 mm/min 200X)

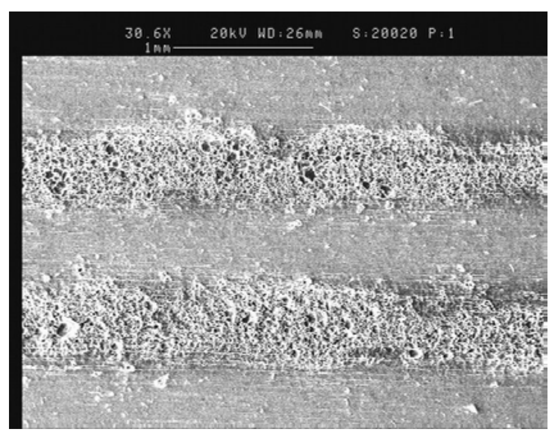

figure 3c: erosion phenomenon take place on the sheet treated surface (200 MPa 20000 mm/min 30X)

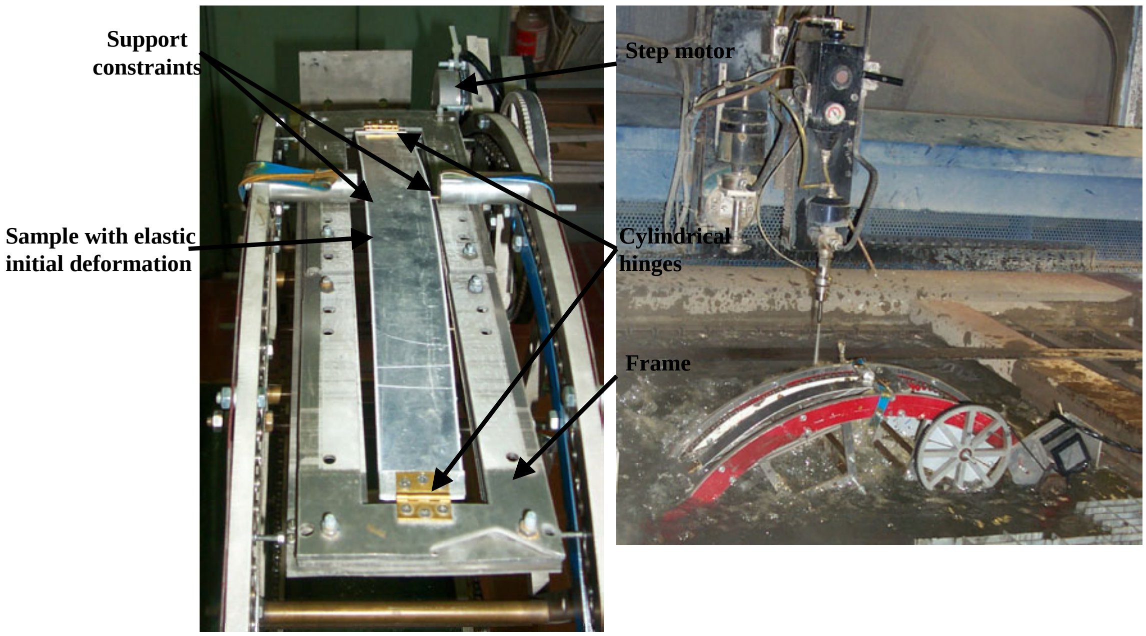

figure 4: fixturing system allowing to keep constant stand off and cutting head inclination angle

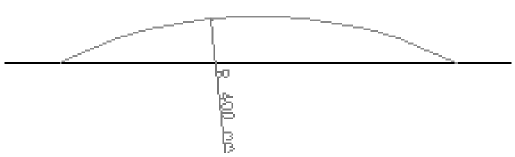

figure 5 initial elastic deformation of specimen

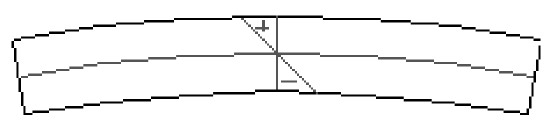

figure 6 stresses due to initial elastic deformation

replications	water pressure [MPa]	feed rate [mm/min]	deflection [mm]
1	80	20000	27,70
2	80	20000	27,48
3	80	20000	27,54
1	80	16500	33,22
2	80	16500	32,96
3	80	16500	32,60
1	80	13500	37,20
2	80	13500	37,82
3	80	13500	37,14
1	80	10000	38,74
2	80	10000	39,38
3	80	10000	38,62
1	105	20000	38,20
2	105	20000	37,64
3	105	20000	37,24
1	105	16500	38,80
2	105	16500	38,50
3	105	16500	38,05
1	105	13500	39,82
2	105	13500	40,48
3	105	13500	40,90
1	105	10000	41,96
2	105	10000	41,72
3	105	10000	41,18

figure 7: Residual maximum deflection at 125 MPa, 150 MPa

replications	water pressure [MPa]	feed rate [mm/min]	deflection [mm]
2	125	20000	38,74
3	125	20000	39,16
1	125	16500	41,36
2	125	16500	40,78
3	125	16500	40,54
1	125	13500	41,52
2	125	13500	41,10
3	125	13500	40,68
1	125	10000	44,22
2	125	10000	43,74
3	125	10000	43,18
1	150	20000	41,42
2	150	20000	40,66
3	150	20000	40,90
1	150	16500	42,30
2	150	16500	42,08
3	150	16500	41,48
1	150	13500	43,72
2	150	13500	43,24
3	150	13500	42,88
1	150	10000	43,22
2	150	10000	44,02
3	150	10000	43,98

figure 8: Residual maximum deflection at 125 MPa, 150 MPa

water pressure [MPa]	feed rate [mm/min]	mean deflection [mm]	energy index [J]	Pimpact [MPa]
80	20000	27,57	3,19	233280
80	16500	32,93	3,87	282764
80	13500	37,39	4,73	345600
105	20000	37,69	4,80	306180
105	16500	38,45	5,82	371127
125	20000	38,87	6,23	364500
80	10000	38,91	6,38	466560
105	13500	40,40	7,11	453600
125	16500	40,89	7,56	441818
150	20000	40,99	8,19	437400
125	13500	41,10	9,24	540000
105	10000	41,62	9,60	612360
150	16500	41,95	9,93	530182
150	13500	43,28	12,14	648000
125	10000	43,71	12,47	729000
150	10000	43,74	16,39	874800

figure 9: energy indexes

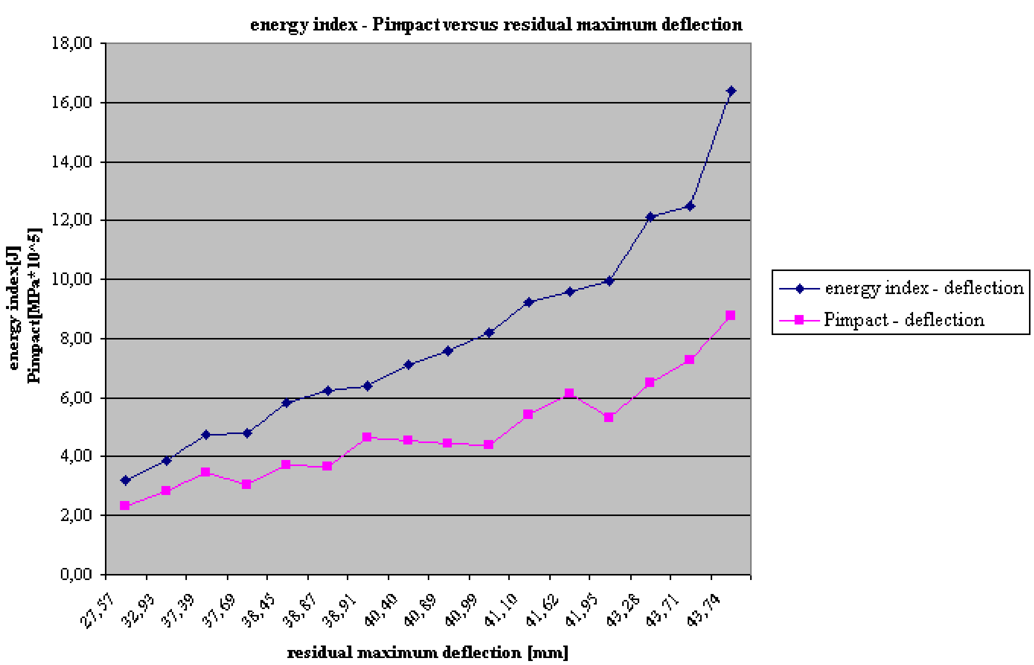

Figure 10 indexes of water jet energy and of water pressure impact versus residual maximum deflection

Regression Analysis: R.M.D. versus P^2; u^(1/2); P*u^(1/2)

```
The regression equation is
R.M.D. = 73,4 - 0,00124 P^2 - 0,517 u^(1/2) + 0,00329 P*u^(1/2)

Predictor        Coef         SE Coef        T        P
Constant        73,428        2,781        26,40    0,000
P               -0,0012397    0,0001765    -7,02    0,000
u^(1/2)         -0,51697      0,03977     -13,00    0,000
P*u^(1/2)        0,0032883    0,0003330     9,87    0,000

S = 1,136       R-Sq = 92,8%      R-Sq(adj) = 92,4%

Analysis of Variance

Source            DF          SS          MS        F        P
Regression         3      736,65      245,55   190,23    0,000
Residual Error    44       56,79        1,29
Total             47      793,45

Source       DF      Seq SS
P             1      394,45
u^(1/2)       1      216,34
P*u^(1/2)     1      125,86
```

Figure 11: predictive model

Figure 12: sample which has been treated at 150 MPa 13500 mm/min

Figure 13: sample which has been treated at 105 MPa 10000 mm/min

2003 WJTA American Waterjet Conference
August 17-19, 2003 Houston, Texas

Paper 4-H

IMPROVEMENTS IN A MULTI-USE WATERJET TOOL FOR HUMANITARIAN DEMINING

R. D. Fossey, D.A.Summers, J.G.Blaine, G.Galecki, S.Dorle
University of Missouri-Rolla
Rolla, Missouri, U.S.A.

ABSTRACT

Safe removal of landmines depends on two separate elements: identification, and neutralization. A multi-disciplinary team from the University of Missouri-Rolla is working on a waterjet tool that can accomplish both elements in a single device. Simplicity and ruggedness are the key components to this dependable, useable device. Identification is accomplished with removal of cover via a "soil sucker" for visual confirmation, and an abrasive jet is used for rapid in-situ neutralization. The design concepts are discussed and the prototypical device described. Preliminary results of field tests will be reported.

Organized and Sponsored by the WaterJet Technology Association

1. INTRODUCTION

Decades of wars and insurrections around the world have left a legacy of landmines to cause the daily maiming or killing of innocents. Many recent efforts at mine clearance have developed into large, sophisticated, and costly systems, as opposed to the traditional method of identification via hand digging and neutralization via blowing. While the recent systemic approach becomes too expensive for deployment on a large scale in all needy areas, it also requires a team of experts for implementation. The traditional method, on the other hand, is quite inexpensive and requires relatively few sophisticated tools. It is, however, potentially deadly.

2. BACKGROUND

The University of Missouri-Rolla began researching the interaction of energetics and high pressure waterjets in 1982 to demilitarize surplus air to air missile warheads. More recently UMR's High Pressure Waterjet Lab began using abrasive entrained waterjets to cut fuses and tracers from 40mm antipersonnel rounds. Even more recently UMR teamed with the U.S. Army and civilian agencies to apply this knowledge to demining strategies; first militarily, then humanitarian.

3. CONCEPT

Initial research was performed to use medium pressure water (10,000 psi) on a robot to perform the two necessary functions. The robot, called the "Pointman" (Figure 1) used the flow to power the soil sucker (Figure 2) and uncover a targeted mine. Following identification of the mine and analysis of the fusing, an abrasive slurry jet (ASJ) was used from the same water source to slice through the mine at the fuse (Figure 3), a point that would render the mine inert for all practical purposes. With the fuse destroyed, the mine could be safely removed to a remote location where it could be treated.

Figure 1. Pointman Robot.

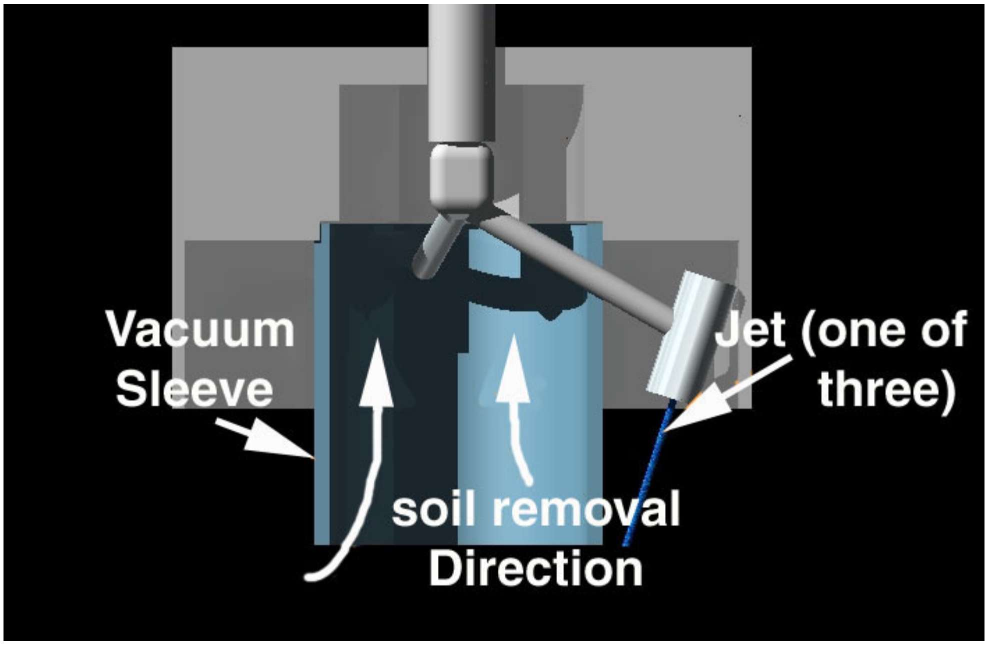

Figure 2. Design of Soil Sucker.

Figure 3. Sectioned Anti-Personnel Mine

In trials for the U.S. Army, several types of live fuses were safely neutralized in this manner. Inert landmines were also cut in-situ after location and identification (Figure 4).

Figure 4. In-situ cutting of Anti-tank Mine

The effectiveness of this system was somewhat reduced when costs and logistics were reviewed. The 10,000 psi pump is expensive and requires a vehicle and/or a trailer by itself. The water container necessitated another vehicle and a trailer was needed for the robot. Many thousands of dollars were required for mine neutralization along with a convoy of vehicles. This expense would greatly reduce the possibility of having such a system available in the remote areas where it is needed. Concurrently, the very sophistication of the system created another drawback whenever maintenance was needed. A specialist (or crew of specialists) would be needed for repair. What is needed is a smaller, simpler, more rugged tool that can accomplish the same objectives and do it in a safe manner with the operator remote from the landmine.

4. APPROACH

The increased efficiency of an ASJ allowed researchers at UMR to cut metal at a lesser pressure than before. Enough less that a commercial pressure washer could be obtained for considerably less money than the cost of a 10,000 psi Pump (Figure 5). The pressure washer develops a pressure of 3,500 psi, which, when applied to an efficient ASJ, is sufficient for cutting the relatively thin steel sheeting used for landmine casings at an acceptable rate. The reduced pressure requirements allow for a drastic reduction not only in expense, but in size and weight as well.

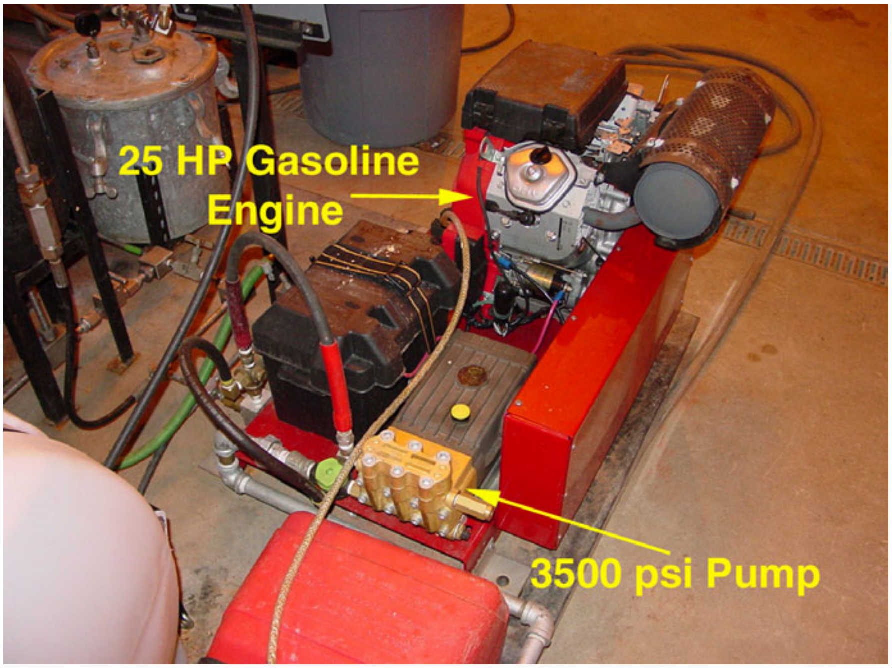

Figure 5. Pressure Washer Pump

The elimination of most of the robotics can further reduce cost and weight for a system, and with the reduction in weight, a person can carry the tools required for identification and neutralization from the delivery vehicle to the potential mine site. The operator can then move out of harms way during the actual operations to maintain safety.

5. COMPONENT PARTS

The identification tool is a lighter weight version of the soil sucker (Figure 6). It uses three jets converging below the vacuum sleeve. The jets rotate as the soil sucker translates across the ground digging a trench with the water as the soil is removed via the vacuum. Rotation is powered by a small 12vdc motor, which can be run from the battery of the support vehicle. Weight of the entire assembly is on the order of 12 kilograms, which can easily be hand carried to the suspected mine area where it is set up and run from a remote distance.

Upon identification of the mine, the second component, the neutralization tool (Figure 7), replaces the soil sucker. The neutralization tool consists of a tripod mounted mini-lance that is driven in either horizontal or vertical direction as needed by a 12 vdc motor for each axis. The operator positions the tripod and lance in the required position for the given mine and retires to the support vehicle where he activates the pump, slurry mixer, and cutting translation motor dictated by the fuse position in the mine. The neutralization tool weighs about the same as the identification tool.

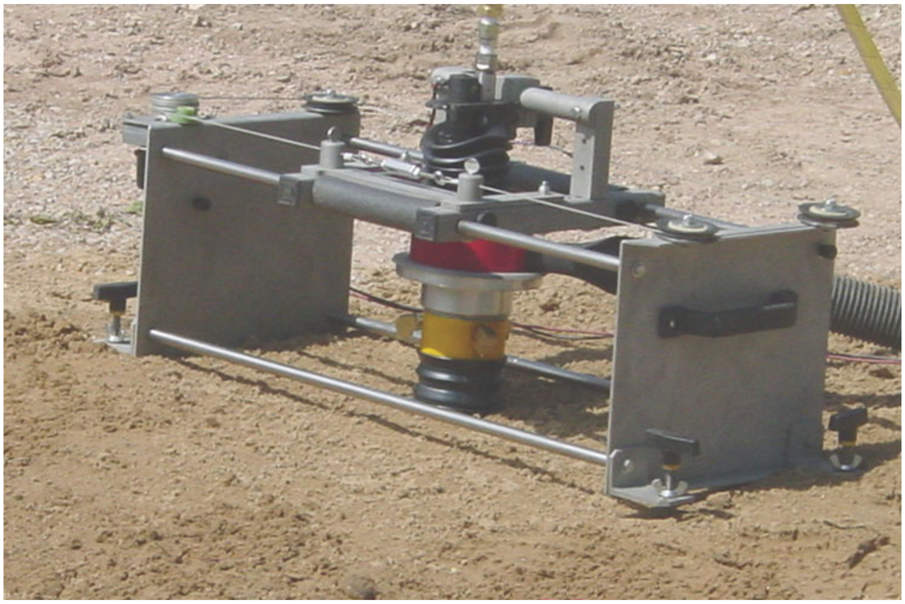

Figure 6. Early Identification Tool.

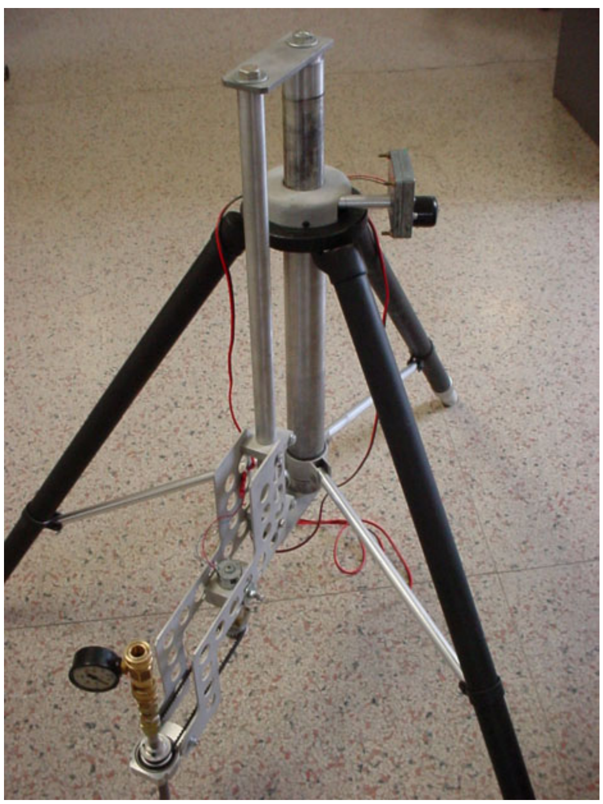

Figure 7. Two Axis Neutralization Tool.

The pump system consists of a 3500 psi commercial pressure washer pump powered by a gasoline engine, a pair of slurry pressure reservoirs, a water supply tank, and a slurry mixing vessel (Figure 8). All components are skid mounted and fit easily in a commercial pickup truck bed (Figure 9). Connections from the pump system to the tools are via lightweight pressure washer hoses, and electrical power for the motors can be transmitted through 18 gauge wires with control switches at the pump.

Figure 8. Pump and Slurry System

Figure 9. Entire System being Deployed.

All components have been designed and fabricated to be as simple and trouble free as possible. Replacement parts can be, in many cases, fabricated from local materials or obtained fairly rapidly from commercial ventures.

6. INITIAL TRIAL RESULTS

Trials of the concept have been successfully carried out at UMR using waterjet pressures of 3,000 to 3,500 psi. Identification of inert mines has been accomplished in a variety of soils with the soil sucker clearing out overburden allowing the operator to see both mine type and orientation. The neutralization tool (Figure 10) then used the 3,500 psi ASJ to slice through the mine at a predetermined zone.

Figure 10. Early Neutralization Tool.

Secondary field trials were conducted at an east coast military reservation which is set up for mine detection and neutralization. With observation from military and civilian agencies, a slightly modified system was tested on actual mines during which location, identification, and neutralization phases were satisfactorily completed (Figures 11, 12, 13, 14).

Figure 11. Field Trial of Early Identification Tool.

Figure 12. Modified Mine Identification Tool with Exposed Mine.

Figure 13. Uncovered Anti-Personnel Mine.

Figure 14. Neutralization Tool Slicing Mine After Identification

7. CONCLUSIONS AND RECOMMENDATIONS

Field trials of the UMR developed de-mining system showed promise in the area of humanitarian de-mining. The ability of a single system to locate, identify, and neutralize landmines has increasing importance in many third-world countries, especially a system that is affordable and robust enough to reliably operate for a prolonged period of time.

8. REFERENCES

R. D. Fossey, D. A. Summers, J. G. Blaine, G. Galecki, S. Dorle "A Multi-use Waterjet Tool for Humanitarian De-mining," 16th International Conference on Water Jetting, Aix-en-Provence, France, October 2002

D.A. Summers, et al., "Mine Neutralization," Interim report to SAIC and NVL, Rolla, Missouri, April 2002.

D.A. Summers, R.D. Fossey, S.J. Thompson "Neutralization of Potential Landmine Hazards by Abrasive Waterjet Use," Detection and Remediation Technologies for Mines and Minelike Targets III, A.C. Dubey, J.F. Harvey, J.T. Broach, Editors Proceedings of SPIE Vol. 3392, pp. 820-828, 1998.

P.L. Miller "Abrasive Waterjets (AWJ) Explosive Safety Tests," 25th DOD Explosive Safety Board Seminar, August 1992.

R.M. Fairhurst, R.A. Heron, D.H. Saunders "DIAjet – A New Abrasive Waterjet Cutting Technique," 8th International Symposium on Jet Cutting Technology, BHRA, Durham, UK, 1986, pp. 395 – 402.

2003 WJTA American Waterjet Conference
August 17-19, 2003 • Houston, Texas

Paper 3-A

A MOBILE WATERJET TRAINING MODULE

Gary W. Toothe
Thompson Industrial Services, Inc.
Sumter, South Carolina, USA

ABSTRACT

Due to the growth of Thompson Industrial Services, the equipment at the corporate training facility was insufficient to support all of the courses being offered. Additionally, the cost of students from regional offices attending the classes was much higher due to travel and per diem expenses. The objective was to produce a facility that would support all of the current training requirements using actual field applications. The facility would also allow the inclusion of additional equipment to support future training requirements and have the ability to be transported to all of the regional offices. The result was the production of a mobile training module that includes equipment identical to that found at customer sites, allowing the "hands on" training in all of the waterjet applications currently being provided. In addition, the training module supports both safety and vacuum training. All levels of personnel, from new hire to superintendents can be trained using the module and annual skills refresher training is fully supported. The module also serves as a test bed for new equipment and jetting techniques, prior to their introduction into the field.

Organized and Sponsored by the WaterJet Technology Association

SECTION 1 INTRODUCTION

Thompson Industrial Services began 17 years ago with a single operating facility located in Sumter, South Carolina. Steady growth, driven in large part by positioning resources convenient to the customer base, has resulted in the Service Division currently operating out of nine (9) regional offices.

Thompson Industrial Services commitment to training has been a tenet of the organization since it's inception. The Training Department within Thompson Industrial Services has always considered the various Thompson Divisions to be their 'customer' and had tried to bring the same levels of service to them as they are expected to provide to their customers.

The corporate facility has both classroom and hands on training equipment for use in waterjet training as well as other required subjects. For many years the use of the central corporate facility was both cost effective and convenient. However, with the geographical expansion driven by growth and customer service considerations the appropriateness and cost effectiveness of a single central location diminished.

Thompson Industrial Services and the Training Group in particular made the determination that a Mobile Training Module coupled with portable classroom materials would allow the training of employees at their work location. This concept would greatly reduce the cost of students traveling to the corporate facility, yet would maintain the integrity and quality of the curriculum by insuring that the instructors and training materials remained constant.

The development, construction, implementation and uses of that Mobile Waterjet Training Module are the subjects of this paper.

SECTION 2 A MOBILE WATERJET TRAINING MODULE

Subsection 1 Identifying the Needs

Training within the Service Division of Thompson Industrial Services traditionally depended on a mixture of classroom instruction, basic hands on training in vacuuming and waterjetting and an apprenticeship within a crew of experienced Service Division personnel. Feedback and site visitations indicated that many New Hires had lengthy apprenticeship times before they were considered to be a 'non-liability' by their coworkers, primarily on production issues. It was not uncommon for some trainees to be told to "stay out of the way we have work to do". Watch and learn was the byword. This not only led to dissatisfaction on the part of some trainees, but also kept the crews in the field from being as productive as possible. The decision was made to train the New Hire's to a standard that would allow them to join a crew in the field with sufficient knowledge and hands on training to insure that not only were they not going to be a liability, but rather be a productive member of their crew.

Interviews with Managers, Superintendents and Crew Leaders form throughout the Company identified a list of tasks that were considered to be essential for a person to be a contributing member of a Service Division work crew. They included:

- Understanding the roles of personnel within the service crew and the Service Division, especially their responsibilities
- Understanding safety on the job site
- Understanding waterjet and vacuum safety
- How to Don, Doff and Decontaminate PPE
- Understanding proper job setup for both waterjetting and vacuuming
- Knowledge of how to tie proper knots for securing and suspending
- Tube lancing with flexible waterjet lances
- Evaporator cleaning with waterjet lances
- Line Moling of piping, primarily 6” in diameter or less
- Vertical and horizontal surface ‘shotgun’ cleaning
- Cleaning ’P-trap’ floor drains
- Vertical and horizontal confined space entry experience

At the time the surveys were being conducted regarding the requirements for new hire skills, many respondents indicated a need to train the current employees of the company as a way of insuring that all employees could perform to an identifiable standard, regardless of which Division they were employed by. Additionally, the need to train current employees was not limited to their particular skill group; rather the requests were made to train each employee to their skill level and all skill levels below their group. Training for advancement was also requested.

With the surveys complete, the Training Group began to search for ways to meet these needs.

Subsection 2 Genesis of the Mobile Training Module

With the desires of the ‘customers’ in hand, the Training Group used a two-fold approach to meeting their expectations. The group began to develop the curriculum for each level of training, including appropriate visual aids, classroom demonstrations, student handouts, tests and the outlines for the hands-on training and testing. Examples of the developed course outlines can be found in Section 5 of this paper.

Concurrent with the course development the search for a means of providing the extensive hands-on training began. Expansion of the existing training facility was considered but rejected due to the difficulty and high cost of current students attending from Regional Offices in other States. Construction of duplicate facilities at other Regional Offices was considered, but this would drastically increase the costs of construction and maintenance and would not guarantee that they would not become just as impractical due to future growth. A mobile training facility on the other hand, would require only one unit, would insure standardization of training and would be able to cover all of the existing Regional Offices, as well as, any future offices added in the future. Therefore it was decided that a transportable training facility would be the best use of Company resources.

Once the decision had been made to develop a transportable training module, the search began for an economical means of constructing such a module. A variety of possibilities were considered, tanker trailers, 40 foot intermodal containers, surplus tanks from customer sites and a company made skid mounted module. While each of these had some benefits, only the tank trailer did not require special equipment for loading or unloading. The tanker trailer itself had some serious drawbacks, primarily overall size and stability. After rejecting the initial possibilities, the start of a boiler cleaning project provided the visual answer to all of our requirements a 21,000-gallon, single step frac tank.

The frac tank was transportable by a tractor, had existing manways and piping, access through a stairway to the roof of the tank and all the room needed to install the training equipment required. Additionally, the use of a frac tank required no equipment for loading or unloading and was extremely stable when uncoupled from the tractor. We solicited quotes for the purchase of a used frac tank that was both roadworthy and in good overall condition. One was secured well within the division's budget and delivered to the corporate facility.

The agreed upon final design for the frac tank based training module included the following components:

1. A horizontal heat exchanger in a cramped confined space
2. A horizontal heat exchanger
3. An evaporator simulator with 1.5" diameter tubes
4. 6" piping with elbows
5. 3" piping with elbows
6. 2" piping with elbows
7. 1.5" piping with elbows
8. A "P-trap" floor drain with run out piping
9. Horizontal surfaces for shotgun cleaning
10. Vertical surfaces for shotgun cleaning
11. Horizontal and vertical confined space entry manways
12. An enclosed area for vacuuming material

Subsection 3 Construction of the Mobile Training Module

Upon delivery the frac tank was thoroughly pressure washed and allowed to dry. Components were secured from customer surplus equipment yards and piping, sheet steel and other required items were ordered.

The initial modification to the frac tank consisted of adding additional folding handrails to the upper roof of the tank, adding gripstrut walkways to the upper roof and adding a 21" domed manway positioned on center, 8' from the front edge of the upper roof. These modifications allowed secure access to all areas on top of the tank and allowed them to be folded down to meet highway maximum height restrictions when in transport.

With the completion of the safety items, modifications began to install the training components. A bulkhead was constructed, using of 3/8" A36 carbon steel plate, in the interior of the tank 6.5 foot from the front of the tank. The bulkhead ran floor to ceiling across the entire width of the tank interior, with small cutouts on the top and bottom edges to allow for drainage and air circulation.

A small heat exchanger was installed in the newly installed bulkhead, centered side to side and 3' off of the tank bottom. With the backside of the heat exchange in the remaining 33.5 feet of the tank interior, the requirements for Components 1& 2 were now complete.

Component 3, the evaporator simulator was constructed by welding 31 pieces of 1.5" diameter carbon steel piping inside a 12" diameter stainless steel pipe. The assembled module was 10' long. A hole was cut in the frac tank roof, 7' from the rear of the tank, and the bundle inserted, resting on a fabricated support welded to the floor of the frac tank. A cover was fabricated for the top of the bundle and the bundle seal welded to the roof.

Components 4, 5, 6 & 7 were constructed using the existing tank mounted vent, fill and drain lines. The 6" and 2" lines were run from the two front side mounted drain valves. The piping ran straight through the 6.5 foot chamber than elbowed both horizontally and vertically within the larger portion of the tank. The 3" line used the existing 3" fill line and the 1.5 " line was installed below the roof accessed vent line.

Component 8, the 'P-trap' floor drain, was purchased commercially in cast iron with carbon steel components. The model selected best reflected the floor drains in the industrial plants most often cleaned as part of routine service. A portion of the loww roof walkway was cut to allow installation of the drain, below the walkway in the roof of the low portion of the tank. The cut was made in such a way that the removed portion could be reinstalled to prevent a trip hazard. A run out pipe was connected to the end of the drain piping and run to the sidewall of the tank to prevent the lance from exiting a short line and becoming hung or presenting a safety hazard.

The construction of components 9, 10, 11 & 12 were realized using the modifications to the tank required for the previous eight components. Horizontal and vertical shotgunable surface were present within both portions of the tank interior. Two horizontal and one vertical manways were present for confined space entry and the vertical manway could be used to put material into the large portion of the tank for vacuum removal.

The Mobile Training Module was now complete.

Subsection 4 Simulating Foulings or Making Messes for Fun & Profit

The ability to remove foulings from customer equipment is the primary reason contractors are in the waterjet business. To have a module where all the students accomplished was the cleaning of already clean surfaces would be a waste of both time and money. Consequently, a simulated fouling needed to be devised so that the students would have an appreciation of, and the experience at, removing the types of materials they could be expected to encounter in the field.

The scrap pieces of 1.5” pipe, used in the construction of the evaporator simulation module, were cut into 6” lengths and sealed at one end. A mixture of coal fly ash and cement powder was mixed in pre-determined ratios and enough water was added to make the mixture pour easily. Each pipe was sealed at the bottom and filled with one of the mixtures, labeled and allowed to dry for one week.

At the conclusion of the drying week, each pipe was secured in a pipe vise and a waterjet instructor attempted to clean the pipe using a shotgun at 10,000 PSI. The instructor measured the ease of cleaning, the dissolution of the material and the time necessary to clean the pipe.

Upon completion of the testing, it was determined that a 3/2 ratio of fly ash to cement powder produced the optimal results.

The fouling is used in the evaporator simulator and on the horizontal and vertical cleaning surfaces for all classes. For New Hire training the fouling is omitted from the horizontal heat exchanger and the pipes. It was felt that learning to work the lance through the pipe elbows would be a sufficient challenge for inexperienced employees. The fouling is added to all of the components for the more advanced classes.

Subsection 5 Utilizing the Training Module

Preparation of the training module is as simple as making sure the tank is level and that the fouling has been applied to the appropriate components. Make sure that Confined Space Entry procedures are followed anytime the tank is entered.

A variety of training can be accomplished using the module. Thompson Industrial Services utilizes the module and it’s components for the following training:

- Confined Space Entry
- Confined Space Rescue
- New Hire Training (see Section 5)
- Technician Skills (see Section 5)
- Operator Skills (see Section 5)
- Crew Leader Skills (see Section 5)
- New waterjet technique training
- New waterjet tool testing and training

Subsection 6 Impact of the Module on Training

The addition of the training module has allowed Thompson Industrial Services to evaluate the skills and potential of all of our employees, or potential employees, as well as teach them the requisite skills required to make them productive members of our work force. Regardless of the skill level or topic to be mastered the module gives us the platform to accomplish the training and the flexibility to add new components as required. The portability has allowed us to significantly reduce the overhead cost associated with training, resulting in a much better use of each training dollar.

By incorporating equipment actually found at customer's sites, coupled with equipment made to simulate the components on customer's sites to large to fit in a portable module, real time job experience can be obtained in a teaching setting. The applied foulings insure that the level of difficulty will match that of actual job situations as well.

Enhanced safety through the use of low student to instructor ratios, typically one instructor for every 5 students, insures that the material is being learned in a safe and efficient manner. Each Division has their own trainers that are required to participate in any training done for that Division. This insures that should the students have any questions or need any additional clarifications after the class has been completed, at least one of the trainers will be a person within their own Division. The use of a foot operated relief valve by the trainer for each trainee regardless of whether the trainee is using a foot operated valve or a hand operated valve is also mandatory. This prevents the trainees from accidentally placing themselves in danger as they may become distracted by the task they are trying to master.

The results at Thompson Industrial Services have been dramatic. The percentage of new hires remaining with the company has increased, the awareness of safety in the existing workforce has risen dramatically and many workers are looking forward to coming to the classes. Although harder to document empirically there is a common feeling that the skill levels throughout the Service Division have increased as well.

Subsection 7 The Future of the Training Module

Thompson Industrial Services intends to increase the utilization of the training module in a variety of ways.

First, the training module can be use in inter-company crew competitions. This would involve crews from throughout the Company competing in simulated job situations with points awarded for: efficiency, safety and quality.

Secondly, the module can be used at Customer sites, or potential customer sites, to highlight the very Safety, efficiency and quality that the crew competitions were designed to measure.

Lastly, as stated previously, any new techniques, tools or job requirements can be added to or tested in the training module.

SECTION 3 CONCLUSION

Many years ago, a Vice President of the company I was with stated: "Anyone can buy the equipment. It's my people that make the difference". With the addition of the Mobile Waterjet Training Module, we have found the means of insuring that our people have the training to make that difference.

SECTION 4 ACKNOWLEDGEMENTS

The author would like to gratefully acknowledge the contributions of the following individuals and organizations, whose support enabled the realization of the Mobile Waterjet Training Module.

• Jose Carrion and Duane Denton	NES Rentals Augusta, GA
• Jimmy Chavis and Donald Day	Voridian, Divison of Eastman Chemical Co.
• Don Gibbons	Wellman, Inc.
• Hugh Barrineau	International Paper, Eastover Mill
• Daniel Boyd	Blue Circle Cement
• Staff of	Santee-Lynches Work Force Investment Board
• Greg Thompson	Thompson Industrial Services
• Chris Niebuhr	Thompson Industrial Services
• Frank Bolyn & Crew	Thompson Industrial Services
• Chris Meldrim	Thompson Industrial Services

SECTION 5 COURSE OUTLINES

Attached are copies of the personnel training courses offered which utilize the Training Module.

NEW HIRE TRAINING SCHOOL

Thompson Industrial Services' New Hire Training School is designed to orient new employees to the expectations and culture of Thompson Industrial Services, as well as, completing the requisite entry material for the Human Resource and Safety Departments and the Introductory Field Skills Training of the Service Division.

The New Hire School lasts for approximately 40 hours over a five day period. Students are given tests to insure knowledge of the classroom training and hands-on testing at the "Thompson Industrial Services' - Service Division Mobile Training Facility" to insure mastery of field skills. An overview of the training follows:

Human Resources Material

- Pre-Employment Testing
- Hire-In Paperwork
- Orientation to Company Policies and Benefits

Safety Department Material

- Teaching of applicable Safety Courses
- Medical Certification and Respirator Fit Testing
- Teaching of applicable Customer Orientation Courses

Service Division Training

- <u>Orientation to Thompson's Policies and Procedures</u>
    - Crew Structure and Responsibilities
    - JSHA – Job Safety Hazard Analysis
    - Applying Safety Training to Field Situations
    - PPE Don/Doff
    - Field Training and Evaluation of Learned Skills
- <u>Orientation to Industrial Vacuuming</u>
    - Principles of Vacuuming
    - Identification and Uses of Vacuum System Components
    - Vacuum Safety
    - Field Training and Evaluation of Learned Skills
- <u>Orientation to Waterblasting</u>
    - Principle of Waterblasting
    - Four Types of Waterblasting at Thompson Industrial Services
        1. Pressure Washing (up to 3,000 psi)
        2. "Standard" Waterblasting (up to 20,000 psi)
        3. "Ultra-High" Waterblasting (greater than 20,000 psi)
        4. "Big Pump" Waterblasting (up to 10,000 psi at very large volumes)
    - Identification and Uses of Waterblast System Components and Tools
    - Waterblast Safety
    - Field Training and Evaluation of Learned Skills

TECHNICIAN SKILLS TRAINING SCHOOL

Thompson Industrial Services' Technician Skills Training School is designed to advance the skills levels of current Thompson Industrial Services employees. The class is offered as both an advanced class to those new employees that have successfully completed their 90-day probationary period, and as a review and upgrade class for current Thompson Industrial Services' Technicians.

The class is scheduled to last for two consecutive 8-hour days. Students are given tests to insure knowledge of the classroom training and hands-on testing at the "Thompson Industrial Services' - Service Division Mobile Training Facility" to insure mastery of field skills.

The class can also be used to teach new techniques, equipment or applications to the Thompson Industrial Services' workforce before they are introduced in Customer applications. An overview of the training follows:

- <u>Review of Technician Job Duties</u>
  - Overview of Technician Job Duties within the Thompson Crew
  - Pre & Post Trip Vehicle Inspections for Support Equipment
  - Inventorying, Loading and Securing Loads on Support Vehicles
  - Inspection, Repair and/or Red-Tagging Equipment and Accessories
  - Proper Vehicle Cleaning Procedures
- <u>Review of Thompson's Policies and Procedures</u>
  - Review of New Procedures and Policies
  - Review of Applicable "Safety Grams" and Accident Investigations
- <u>Industrial Vacuuming Skills</u>
  - Review of New Equipment, Accessories and Techniques
  - Vacuum Safety
  - Advanced Vacuum Theory and Application
  - Evaluation of Job Situations and Solutions
  - Capabilities and Applications for Vacuum Accessories
  - Introduction to Industrial Vacuum Units for the Operator Trainee
  - Field Training and Evaluation of Learned Skills
- <u>Waterblasting Skills</u>
  - Review of New Equipment, Accessories and Techniques
  - Waterblast Safety
  - Advanced Waterblast Theory and Application
  - Evaluation of Job Situations and Solutions
  - Capabilities and Applications for Waterblast Accessories
  - Introduction to Waterblasting Units for the Operator Trainee
  - Field Training and Evaluation of Learned Skills

OPERATOR SKILLS TRAINING SCHOOL

Thompson Industrial Services' Operator Skills Training School is designed to hone the skills of current Operators and to teach the skills of proper equipment operation to those employees that have the ability to drive the equipment. The class is therefore offered as both an advanced class, to those employees that have successfully obtained their CDL but have not yet learned the skills to operate the equipment, and as a review and upgrade class for current Thompson Industrial Services' Operators.

The class is scheduled to last for two consecutive 8-hour days. Students are given test to insure knowledge of the classroom training and hands-on testing at the "Thompson Industrial Services' - Service Division Mobile Training Facility" to insure mastery of field skills.

Those individuals that are not yet Operators will attend an additional one day 8-hour course covering DOT Regulations. This additional day will be scheduled either the day before or the day after the Operator Skills Class. An overview of the training follows:

- <u>Review of Thompson's Policies and Procedures</u>
    - Review of New Procedures and Policies
    - Review of Applicable "Safety Grams" and Accident Investigations
- <u>Industrial Vacuum Unit Skills</u>
    - Review of New Equipment and Accessories
    - Vacuum Safety
    - Advanced Vacuum Theory and Application
    - Evaluation of Job Situations and Solutions
    - Capabilities and Applications for Vacuum Units and Accessories
    - Advanced Industrial Vacuum Unit Operation, Maintenance and Troubleshooting
    - Field Training and Evaluation of Learned Skills
- <u>Waterblasting Skills</u>
    - Review of New Equipment, Accessories and Techniques
    - Waterblast Safety
    - Advanced Waterblast Theory and Application
    - Evaluation of Job Situations and Solutions
    - Capabilities and Applications for Waterblast Units and Accessories
    - Advanced Industrial Waterblast Unit Operation, Maintenance and Troubleshooting
    - Field Training and Evaluation of Learned Skills
- <u>DOT Supplemental Class</u>
    - Review of Applicable DOT Driver Regulations
    - Review of Applicable DOT HAZMAT and Materials-of Trade Regulations
    - Practice for Competency on DOT Paperwork and Inspections

CREW LEADER SKILLS TRAINING SCHOOL

Thompson Industrial Services' Crew Leader Skills Training School is designed to hone the skills of current Crew Leaders and to teach the supervisory skills required to become a successful Crew Leader to those individuals eligible for promotion.

The class is scheduled to last for two consecutive 8-hour days. Students are given tests to insure knowledge of their training. Field Skills tests will be performed at the "Thompson Industrial Services' - Service Division Mobile Training Facility". An overview of the training follows:

- <u>Review of Thompson's Policies and Procedures</u>
    - Review of SOP's
    - Review of New Procedures and Policies
    - Review of Applicable "Safety Grams" and Accident Investigations
- <u>Supervisory Skills</u>
    - Communication Styles
    - Principles of Motivation
    - Interpersonal Skills
    - Safety Responsibilities
    - Effective Discipline
    - Employee Performance Issues
    - Employee Work Habit Issues
    - Handling Employee Complaints
    - Performing Employee Performance Appraisals
    - The Crew Leader as Trainer
- <u>Job Site Skills</u>
    - Pre-Job Planning
    - Job Site Set-Up
    - Completing Required Job Paperwork
- <u>Customer Interaction Skills</u>
    - Task Verification
    - Safety Issues
    - Performance Issues
    - How to Deal with an Irate Customer
- <u>Vacuum and Waterblast Overview for Supervisors</u>
    - Review of New Equipment, Accessories and Techniques
    - Vacuum and Waterblast Safety
    - Advanced Vacuum and Waterblast Theory and Application
    - Evaluation of Job Situations and Solutions
    - Capabilities and Applications for Waterblast Units and Accessories

SECTION 6 GRAPHICS

Views of Frac Tank as Delivered

Training Class at Mobile Waterjet Training Module

Training Module In Use

2003 WJTA American Waterjet Conference
August 17-19, 2003, ● Houston, Texas

Paper 6-H

FORMATION AND APPLICATION OF FINE ICE ABRASIVE

K. Kluz, E.S. Geskin, D.V. Shishkin, B. Goldenberg, O.P. Petrenko
New Jersey Institute of Technology
Newark, NJ, USA

ABSTRACT

A device for formation of fine (5 μm and less) ice particles was designed and constructed. The feasibility to produce the microns level particles was shown and the energy efficiency of the device operation was estimated. The generated ice particles were used for formation of the ice-air jet. The experimental study involved decoating of highly sensitive substrates, such as photo film, coffee cup, CD, etc. The feasibility of damage free pollution free processing of sensitive surfaces was demonstrated.

Organized and Sponsored by the WaterJet Technology Association

1. INTRODUCTION

The water ice particles accelerated by various means (entrainment in a fluid, impact of rotating blades, fluid expansion, etc.) constitute an effective blasting media (Kluz, 2002, Shishkin, 2002, Shishkin et al 2002, 2003, 2003a). In a number of cases the ice can replace the sand blasting and the abrasive waterjet. It is suggested that an ice gun might constitute a new manufacturing tool which will improve technologies of the surface processing (cleaning, decoating, etc.) and machining (drilling, cutting, etc.). A primary advantage of the ice media is almost complete pollution prevention. Ice blasting enables us to eliminate practically both, contamination of the substrate and generation of contaminated waste streams. In addition to the obvious environmental benefits, the use of ice media can improve a number of key techniques, such, for example, as treatment of the sensitive surfaces. Previous studies showed that the potential applications of ice abrasives range from cutting of metals to etching of photo films and precision cleaning of electronic parts

The feasibility of “just-in-time” production of the ice media constitutes an advantage of the ice-based technologies. However the availability of the economically and environmentally acceptable for such a production is a necessary condition of the adoption of the ice blasting by the industry. The absence of such a technique at present is the main reason preventing the practical use of the ice blasting. The NJIT’s Waterjet Laboratory investigated two technologies of ice particles production. The first one involved ice crashing and was suitable for the conditions when solid ice was readily available. The second technology involved generation of ice particles by combining water freezing and decomposition. It was shown that both technologies are suitable for particles production although the their economical aspects were not evaluated.

The objective of this paper is to explore the third candidate technology for ice particles formation which involves direct freezing of water droplets in a cold environment. In our experiments liquid nitrogen was used as a cooling media. Low cost, availability and simplicity of the handling make the use of this media practical. Another objective of this study was investigation of the production and use of fine (micron size) ice particles. The use of these particles as a blasting media will enable us to develop number new technologies, such as processing of very complicated surfaces, removal of coat harder than the underlying substrate surface, treatment of live objects, etc.

This paper discusses the energy efficiency of the suggested ice production technology as well as ways of the use of the fine ice powder. Examples of the powder application are considered.

2. ENERGY ANALYSIS OF THE ICE PARTICLE FORMATION

In the course of performed experiments ice particles were generated as following. Small droplets of water were supplied into a nitrogen bath.. Due to intensive heat exchange caused by the nitrogen boiling the droplets solidified almost instantaneously. The obtained particles were removed from the bath, entrained by an air stream and used as the abrasive in the course of cleaning various samples. In order to estimate process effectiveness, the energy and exergy efficiencies of the device were determined (Gengel, 2001). The input data needed for computations are given in Table 1, which describes the streams shown in Fig. 2. It is assumed that the device is perfectly insulated and ice leaving the device has the temperature equal to the temperature of liquid nitrogen at atmospheric pressure. Water is supplied at the room conditions at the rate of 150 ml/min or 0.00250 kg/s.

The required flow rate of the nitrogen is determined by the energy balance of the process. The supplied nitrogen is needed to solidify the stream of water at the initial temperature of 20°C and to cool the generated ice down to the temperature of liquid nitrogen. Then the energy balance equation has a form

$$\frac{\overset{o}{m}_{nitrogen}}{\overset{o}{m}_{water}} = \frac{h_1 - h_2}{h_4 - h_3} = \frac{83.96 - (-481.83)}{-206.01 - (-405.25)} = 2.84 \tag{1}$$

From Eq. (1) follows that at least 2.84 kg of nitrogen is needed per kilogram of ice produced. The rate of nitrogen supply is

$$\overset{o}{m}_{nitrogen} = 2.84 \cdot \overset{o}{m}_{water} = 2.84 \cdot 0.0025 = 0.0071 \text{ kg/s} \tag{2}$$

The energy balance of the system in question is

$$\overset{o}{E}_1 + \overset{o}{E}_3 = \overset{o}{E}_4 + \overset{o}{E}_2 \tag{3}$$

where:

$\overset{\circ}{E}\, i (i = 1,2,3,4)$ - energy streams

Then

$$\overset{o}{E}_1 = \overset{o}{m}_w \cdot \left(h_1 + \frac{v_1^{\ 2}}{2} + g \cdot z_1 \right) = 0.0025 \cdot (83.96 + 0 + 0) = 0.210 \cdot \text{kW} \tag{4}$$

$$\overset{o}{E}_2 = \overset{o}{m}_w \cdot \left(h_2 + \frac{v_2^{\ 2}}{2} + g \cdot z_2 \right) = 0.0025 \cdot (-481.83 + 0 + 0) = -1.205 \cdot \text{kW} \tag{5}$$

$$\overset{o}{E}_3 = \overset{o}{m}_N \cdot \left(h_3 + \frac{v_3^{\ 2}}{2} + g \cdot z_3 \right) = 0.0071 \cdot (-(-405.25) + 0 + 0) = 2.877 \cdot \text{kW} \tag{6}$$

The energy efficiency of the device is

$$\boldsymbol{\eta_{1st}} = \frac{\overset{o}{\mathbf{E}}_{\mathbf{1}} - \overset{o}{\mathbf{E}}_{\mathbf{2}}}{\overset{o}{\mathbf{E}}_{\mathbf{3}}} \tag{7}$$

or

$$\boldsymbol{\eta}_{\mathbf{1st}} = \frac{\mathbf{0.210 - (-1.205)}}{\mathbf{2.877}} = \mathbf{0.492} \qquad (8)$$

The availability balance of the examined system is

$$\Psi_1 + \Psi_3 + I - \Psi_2 - \Psi_4 = 0 \qquad (9)$$

and

$$\Psi_2 - \Psi_1 = \Delta\Psi_W \qquad (10)$$

Where:

$\Delta\Psi_W$ –change in availability of the water stream

$\Psi_{1,2,3,4}$ – availability streams

I - irreversibility

Then, using Table 1 obtain

$$\Psi_1 = \overset{o}{m}_w \cdot \left[(h_1 - h_0) - T_0 \cdot (s_1 - s_0) + \frac{v_1^{\,2}}{2} + g \cdot z_1 \right] \qquad (11)$$

$$\Psi_2 = \overset{o}{m}_w \cdot \left[(h_2 - h_0) - T_0 \cdot (s_2 - s_0) + \frac{v_2^{\,2}}{2} + g \cdot z_2 \right] \qquad (12)$$

$$\Delta\Psi_w = \overset{\circ}{m}_w \cdot \left[(h_2 - h_1) - T_0 \cdot (s_2 - s_1) + \frac{(v_2 - v_1)^2}{2} + g \cdot (z_2 - z_1) \right] \qquad (13)$$

Since, all the components corresponding to the kinetic and potential energy are very small, they are not included in the calculations. Then

$$\Delta\Psi_w = 0.0025 \cdot \left[(\text{-}481.83 - 83.96) - 298.15 \cdot (-2.851 - 0.297) \right] = 0.932\text{kW} \qquad (14)$$

$$\Psi_3 = \overset{\circ}{m}_N \cdot \left[\left(h_3 - h_0\right) - T_0 \cdot (s_3 - s_0) + \frac{{v_3}^2}{2} + g \cdot z_3 \right] \quad (15)$$

$$\Psi_3 = 0.0071 \cdot \left[\left(-405.25 - 0\right) - 298.15 \cdot (-3.91 - 0)\right] = 5.340\text{kW} \quad (16)$$

The second low efficiency is

$$\eta_{2nd} = \Delta\Psi_W / \Psi_3 \quad (17)$$

and

$$\eta_{2nd} = \frac{\mathbf{0.932}}{\mathbf{5.34}} = \mathbf{0.175} \quad (18)$$

where η_{2nd} – second law efficiency

The performed computations show that it is possible to produce a required amount of small and uniform ice particles at acceptable energy cost. The energy efficiency of the process can be improved still further by the use of the outlet nitrogen flow for cooling of the inlet water.

3. EXPERIMENTAL STUDY OF PARTICLES FORMATION

The objective of the first series of experiments was to demonstrate the feasibility to produce fine ice particles using the device Figs 1 and. 2. The experiments were successful and showed that droplets solidified prior to coalescing. The particle ranging from 25 to 75 μm were generated. (Figs. 3 and 4), however, a small number of large particles were also produced. It was suggested that these particles were formed at the wall of the reactor where water droplets coalesced**.** The objective of the second series of experiments was to investigate the feasibility to increase device productivity. It was found that the particles output can be increased, however, after removal from the reactor ice was wet. The obtained particles had tendency to coalesce. However, in few minutes after removal from the reactor when the residual liquid nitrogen evaporates and ice temperature dropped the particles become loose. Still a few of large granules remained in the mixture.

The objective of the third experiment was to determine conditions, which assure generation of uniform particles. The experiment showed the feasibility of such an operation. As it shown is shown on Figure 5 the uniform particles were produced at the rate of 0.120kg/min. Finally the experiment 4 involved minimization of the particles size. The lamp of such particles (Fig. 6) was generated. The particles size was approximately 5 μm.

4. EXPERIMENTAL STUDY OF ICE BASED PRECISION DECOATINGPRECISION

The objective of these series of experiments was to demonstrate the feasibility of decoating highly sensible surfaces. The fine particles were used for these experiments. The particles were entrained by the air nozzle and formed an ice-air jet (Fig.7). In the course of cleaning the air was supplied at the rate of 7 l/s at the pressure of 500 kPa. The particles size was in the range of 10-20 µm. The particles were produced in the device Figs. 1 and 2 and stored at an insulated box. In the course of operation the particles temperature increased. It was noticed that this increase significantly reduced the rate of surface processing. It was also noticed that at the temperature below -40-50 C the ice particles flow was similar to that of sand and stripping ability of the stream was maximal. The nozzle during experiments was guided manually. The stand off distance was maintained at the range of 25-50 mm.

The first experiments involved stripping of a hard coat from a hard surface. A marker (Figs 8-9) was used in this experiment. The paint at the impact zone was stripped completely with no damage to the underlying surface. The next experiment involved a study of the removal of a hard coat from a brittle surface. The paint was removed from the shell of a boiled egg (Figs 10-11) with no surface damage. Next study involved successful cleaning of a soft porous surface. Precision decoating of a polished surface was investigated in the course of depainting of CD (Figs 12-13). The following experiments involved decoating of soft substrates. The paint was removed from a coffee cup (Figs 14, 15), however in this case minor dimples on the underlying surface were observed. At the same time, removal of the emalsion from the photo film (Figs 16, 17) resulted in the generation of non-damaged surfaces.

5. CONCLUSION

The performed study showed feasibility and effectiveness of the use of fine ice powder as a blasting media. The energy effectiveness of the process is acceptable and the technology is rather simple. A wide range of deposits can be removed using this powder. Process productivity was less than that of other abrasive blasting. However, the principal advantages of the developed technology was its cleanliness and non-damage of a substrate. Thus ice powder should be used for treatment of substrates when the prevention of the surface pollution and damage are the primary process constrains. The proposed technology can be applied for processing of precision mechanical and electronic parts, food processing, laboratory samples preparation, etc. The main expected applications, however, are in medical and biomedical fields. The developed abrasives are the ideal media for skin treatment, wound management, etc.

6. ACKNOWLEDGEMENT.

This study was partially supported by the NJ Center for Micro Fluidic Control.

7. REFERENCES

K. Kluz. Investigation of Heat transfer and Thermodynamics of Ice Particles Formation , MS Thesis, NJIT, 2002

D. Shishkin, Experimental and Analytical Investigation of Ice Particles Formation, Ph.D. Dissertation, NJIT, 2002

D.V. Shishkin, E.S. Geskin, B. Goldenberg, Development of a Technology for Generation of Ice Particles, in Surface Contamination and Cleaning, VI, K.L. Mittal, ed, VSP, Utrecht, 2003, pp. 137-151

D.V. Shishkin, E.S. Geskin, B. Goldenberg,, Practical Applications of Icejet Technology in Surface Processing, , in Surface Contamination and Cleaning, VI, K.L. Mittal, ed, VSP, Utrecht, 2003, pp.193-213

D.V. Shishkin, E.S. Geskin, B. Goldenberg,,Applications of Ice Particles for Precision Cleaning of Sensitive Surfaces in Journal of Electronic Packaging, Dec 2002, pp. 255-262

Y. Gengel and M. Boles, Thermodynamics, McGrow, Fourth Edition, 2001.

8. NOMENCLATURE.

Ei- energy flow
g- gravitatation acceleration-
hi-specific enthalpy
m-mass flow rate
V-velocity
z-elevation
η_{1s}t- energy efficiency
η_{2nd}-exergy efficiency
Ψi-exergy flows

Subscripts

i=1,2,3,4- fluxes Fig. 2
nitrogen
water

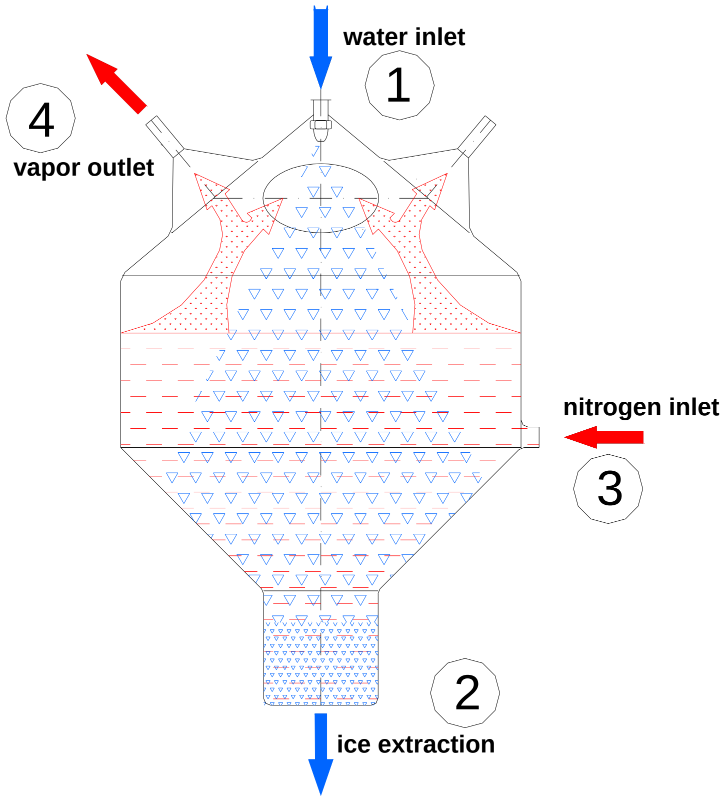

Figure 1. Schematic of ice particle production

Figure 2. The view of the device for ice particle production

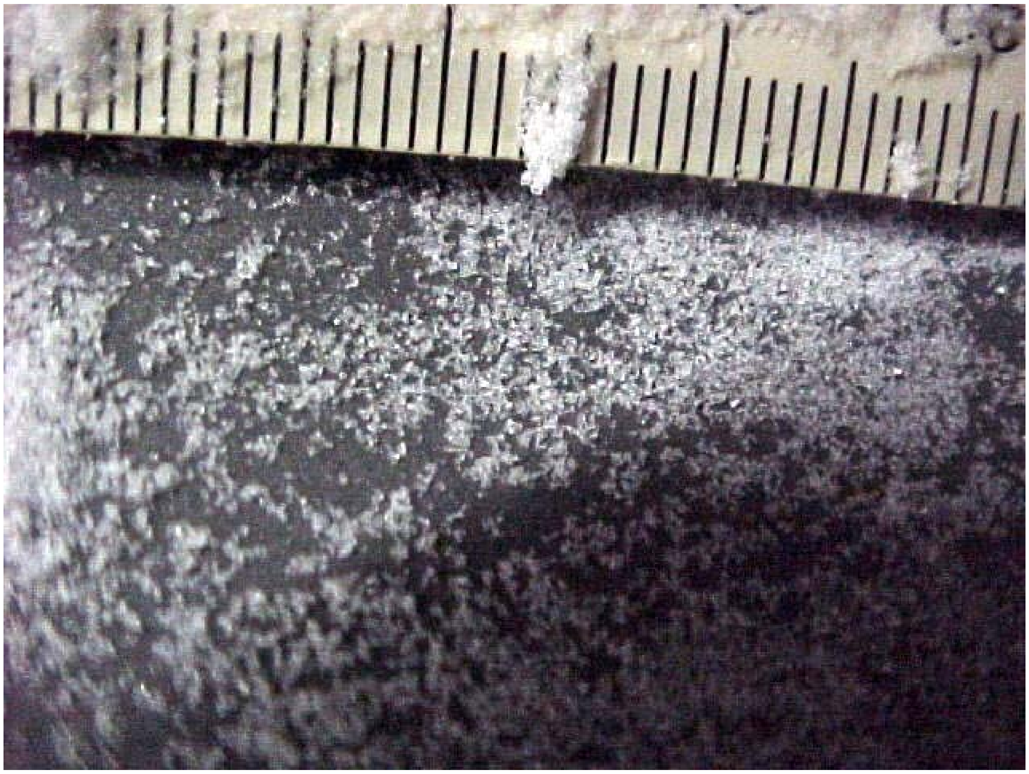

Figure 3. View of a lamp of large (25-75 µk) ice particles.

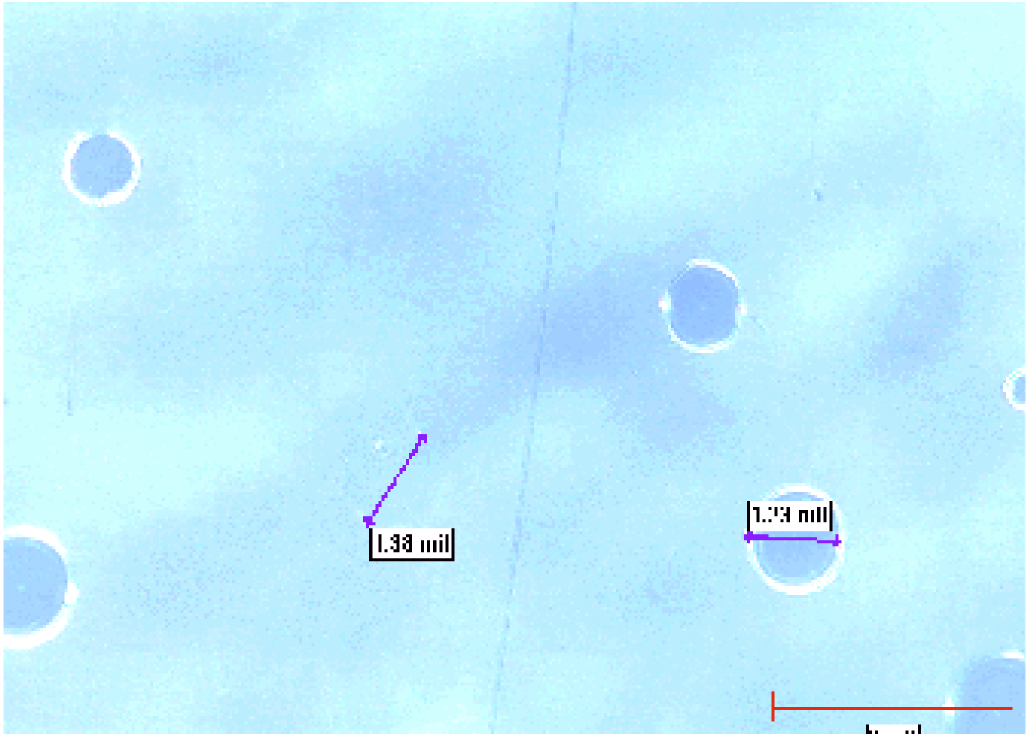

Figure 4. View of ice particles. Numbers are given in thousands of inch.

Figure 5. View of mixture of uniform ice particles prior to nitrogen evaporation.

Figure 6. Figure 6. View of fine (~ 5µk) ice particles after liquid nitrogen evaporated.

Figure 7. View of formation of the ice – air jet.

Figure 8. A marker prior to depainting.

Figure 9. A maker after paint stripping

Figure 10. Boiled egg prior to paint stripping.

Figure 11. A boiled egg after the paint stripping.

Figure 12. A clean CD.

Figure 13. A CD after painting and removal of a part paint.

Figure 14. A coffee cup prior to paint stripping.

Figure 15. A coffee cup after the paint stripping.

Figure 16. Photo film prior to the paint stripping

Figure 17. Photo film after the paint stripping.